SHEAR STRENGTH AND BEARING CAPACITY OF REINFORCED CONCRETE DEEP BEAMS

by

Kam Kau WONG B.Sc.(Eng.)

A thesis presented in fulfilment of the requirements of the Degree of Doctor of Philosophy

at

Department of Civil Engineering
The University of Leeds

August, 1986

ACKNOWLEDGEMENT

The author would like to take this opportunity to express his appreciation and gratitude to all those who in some way have contributed to the research work herein presented. In recognition of their individual contribution to this study the author would additionally like to express a special thanks to:

Professor A.R. Cusens, Head of the Department of Civil Engineering, for granting the author the opportunity to undertake this study and for his supervision, guidance, comments and patience given throughout it;

The Oversea Research Council and Tetley/Lupton for supporting this work through the award of research studentship and scholarship;

Mr. V. Lawton and his technical staff for preparing and arrangement of the experiments;

Mr. R. Duxbury, Miss M.Y.W. Lam and Miss C. Dahl for preparing and processing the photographs;

My brothers Mr. S. Wong, K.H.J. Wong and K.H.H. Wong for developing their own word processing package, COMET - Customers Orientated Mathematical Expression Text-formater, particularly for this dissertation.

Finally, the author would like to thank his parents for their encouragement and supports.

ABSTRACT

Reinforced concrete deep beams with small span/depth ratios usually fail by crushing of concrete in the bearing zone above the supports. In order to increase the load carrying capacity of deep beams, bearing strength around the supports should be enhanced.

The first part of this study involved the investigation of bearing capacity of plain and reinforced concrete blocks. Effects of edge distance, footing to loading area ratios, heights, base friction and size effect are studied with plain concrete blocks. Bearing capacities of reinforced concrete blocks with different forms, diameter and spacing of reinforcement are also investigated. It is found that interlocking stirrups at small spacing are the most effective form of reinforcement. A failure mechanism for a concrete block in bearing is proposed and found to give the best estimate as compared with other models by different researchers.

The second part is concerned with the behaviour of reinforced concrete deep beams with span/depth ratios ranging from 0.7 to 1.1. These beams were tested under uniformly distributed load at the top. It is found that a shear crack is formed along the line joining the inner edge of the support to the third point at the top level of the beam. The concrete block on the outer side of the crack rotates about the centre of pressure in the compression zone. Shear strength is determined by shear in the compression zone, aggregate interlock of the shear crack and dowel action and the components of forces of reinforcement across the crack. Based on these observations, a model of the failure mechanism in shear is proposed which gives excellent results in comparison with other models proposed.

TABLE OF CONTENTS

PRINCIPAL NOTATION

A	Cross-sectional area of the beam.
a	Width of the concrete blocks.
a_1	Width of the loading plates.
A_b	Sectional area below the reference plane.
A_s	Sectional area of main forcement.
A_{wv}	Area of vertical web reinforcement.
A_{wh}	Area of horizontal web reinforement.
b	Breadth of the concrete blocks.
b_1	Breadth of the loading plates.
b_x	Apparent width of the modified end-blocks.
C	Cohesion of concrete.
C_o	Cohesion of concrete at effective pressure, p=0.
D	Diameter of the footing of the concrete blocks.
d	Effective depth.
D_f	Dowel force.
ΔT_s	Loss of tensile force towards the support due to the present of vertical reinforcements.
e_a	Eccentricity of loading along the side width a.
e_b	Eccentricity of loading along the size width b.
f_a	Aggregate interlocking stress.
f_b	bearing strength of the concrete blocks.
f'_c	Cylinder strength of concrete.

$f_{cu(100)}$	Cube strength of concrete obtained from 100 mm cubes.
$f_{cu(150)}$	Cube strength of concrete obtained from 150 mm cubes.
f_t	Tensile strength of concrete estimated by splitting cylinder tests.
$f_{t(pri.)}$	Tensile strength of concrete estimated by rupture tests.
E_c	Young Modulus of concrete.
H	Overall height of the specimens.
h_b	Depth of the section below the reference plane
H_w	$A_{sw}/b \cdot S_h$
f_L	Restraining stress.
f_{xx}	Direct stresses along the direction of the x-axis.
f_{yy}	Direct stresses along the direction of the y-axis.
f_{xy}	Shear stresses.
L	Span.
L_c	Clear span; distance between the inner edges of the supports.
I	Second moment of inertia of the section of the beam.
I_b	Second moment of inertia of the section below the reference
I_e	Influence factor of bearing capacity of concrete block width eccentricity loading.
M	Bending moment at critical section of the beam.
S_h	Spacing of horizontal web reinforcement.
S_v	Spacing of vertical web reinforcement.

T_s Tensile force of the main reinforcement.

V Shear force at the critical section of the beam.

v Shear strength.

v_c Shear strength taken by concrete.

v_s Shear strength taken by steel.

V_u Ultimate shear force.

V_w $A_{sv}/(b \cdot S_v)$

p Effective normal pressure on the shear plane.

P_c Cracking load.

P_h Uniform horizontal pressure along the wedge form below the bearing plate.

P_u Ultimate load.

R Footing to loading area ratio.

W_a Distance of the loading position from the edge of the blocks.

X Shear span.

X_c Clear shear span; clear distances between the outer edge of the bearing plate and the inner edge of the supports.

X_e effective ahear span.

y Depth of the bar, measured from the top of the beam to the point where it interests the line joining the inside edge of the bearing blocks of the supports to the outside edge of that at the loading point.

y_o Depth of the compressive zone from the top of the beam.

z Lever arm at which the reinforcement act.

ε_y	Yield strain of the reinforcement.
ε_{xy}	Shear strain.
T_{xy}	Shear stress.
ψ	Angle of internal friction.
α	Semi-apex angle of the wedge formed beneath the loading plate,
ρ	Volumetric % of lateral steel.
Φ	$A_s \cdot f_y / a \cdot b \cdot f_c$
μ	Coefficient of friction.
σ_{ex}	Applied direct stresses.

1 INTRODUCTION

1.1 GENERAL

A deep beam may be defined as a structural member whose depth is of the same order of magnitude as its span. Various investigators have shown that their elastic behaviour is different from that of the more common flexural mambers. This difference in behaviour is mainly attributed to the significant effects of vertical normal stresses and shear deformations in these members. The strength of deep beams is usually controlled by shear, rather than flexure, provided normal amounts of longitudinal reinforcement are used. On the other hand, the shear strength of deep beams is significantly greater than that predicted using expressions developed for slender beams. As reinforced concrete structural members are nowadays being increasingly designed on the basis of their ultimate strength, there is a need to know the ultimate behaviour and strength of deep beams as well.

Although a clear division between ordinary flexural member and deep beam behaviour does not exist, most literature [45] dealing with this subject recognizes deep beam action at span/depth ratios less than 2.0 and 2.5 for simply supported and continuous members respectively. However, for beams with span/depth ratios less than 1, its load carrying-capacity is

usually determined by the bearing strength in the region above the supports [12,13,53] rather than shear.

In order to investigate the shear strength and behaviour of deep beams with span/depth ratios less than 1, the behaviour of bearing zones above the supports should be understood first. This thesis is divided into two parts for this purpose, the first part deals with the investigation of bearing capacity of concrete blocks and the second part is concerned with the shear strength of deep beams with span/depth ratios less than 1.

1.2 OBJECTIVE

1.2.1 BEARING CAPACITY OF CONCRETE BLOCKS

The behaviour and ultimate strength of bearing capacity of plain and reinforced concrete blocks is studied. Special attention is paid to the following:

(1) Effect of the loading position: position of the loading point from the edge of the block (edge distance).

(2) Effect of footing to loading area ratio, R.

(3) Effect of the height of the concrete block.

(4) Effect of the size of the specimen (scale effect).

(5) Effect of the friction at the base or supporting edge of the concrete block.

(6) Effect of form, diameter and spacing of reinforcement used.

Based on the experimental behaviour a failure mechanism is proposed for the load-bearing concrete blocks.

1.2.2 DEEP BEAMS

Deep beams with span/depth ratios ranging from 0.7 to 1.1 are studied. Attention is focussed on the crushing of concrete above the supports. The investigation is concentrated on the following areas:

(1) Surface crack formation and development of crack width.

(2) Distribution of strain on the concrete surface.

(3) Distribution of strain in the reinforcement.

(4) Vertical and horizontal deformation.

1.3 OUTLINE OF THESIS

The first part of the thesis, concerned with the bearing capacity of concrete blocks, is dealt in Chapters 2 to 4. The second part about the shear strength of reinforced concrete deep beams is covered in Chapters 5 to 7.

For a better understanding and to provide a background knowledge of the subject, a literature review is necessary. Chapters 2 and 5 are respectively the literature review of the bearing capacity of concrete blocks and of the shear strength of reinforced concrete deep beams.

Chapters 3 and 6 are concerned with the manufacture, instrumentation and testing of specimens for bearing capacity of concrete blocks and deep beams respectively.

Results obtained from experiments are detailed in Chapters 4 and 7 together with discussion and a proposed model of failure mechanism both in bearing capacity and shear respectively.

Chapter 8 is a summary of the findings of this investigation with a number of suggestions for further research.

2 LITERATURE REVIEW ON THE BEARING CAPACITY OF CONCRETE BLOCKS

2.1 INTRODUCTION

In the design of a slender beam, its load-carrying capacity is normally determined by its strength in shear and bending. Bearing at the supports and loading points is rarely a matter of concern. However, for a beam having a small span/depth ratio, say less than 2 (i.e. a deep beam), shear force and bending moment are increased by the geometry of the beam and unfortunately, the bearing capacity cannot benefit from it. Thus bearing failure becomes a serious problem when dealing with beams of small span/depth ratio. The problem of bearing failure is more usually considered at anchorage zones of post-tensioned concrete beams, shear keys in composite structures and pile heads.

Normally, the bearing capacity of plain concrete is between 1 and 2 times the cylinder strength f_c'. The CIRIA Guide to the design of deep beams [68] limited the bearing capacity to $0.4f_c'$. This has been shown by many researchers [76,59,65,30] to be too conservative. The recommendation in the ACI code (fig.2.12) seems to be unsafe for low values of R, the ratio of footing area to loading area. It is therefore necessary to have a further investigation of the behaviour of concrete loaded under a limited area and the

way to improve its capacity.

The bearing strength of plain and reinforced concrete has received attention from researchers since 1888. However, elastic analyses are limited in value by the brittle behaviour of concrete and the complexity of stress in the bearing zone. Different researchers have different ways of approaching these problems. The methods used will be discussed below.

2.2 BEARING CAPACITY OF PLAIN CONCRETE

2.2.1 STRESS DISTRIBUTION AROUND THE BEARING ZONE

The state of stress in the bearing zone is of an exceedingly complex three dimensional nature. This stress distribution is due to the very high compressive stress, and is influenced by many factors, such as the relation between the area over which the load is applied and the size and shape of the cross-section of the unit. For the designer, a knowledge of the distribution of stresses in the bearing zone is essential for detailing, to ensure that adequate steel is provided and properly placed to sustain these stresses, as well as any other bearing or shear stresses that may be present.

The first approach to the calculation of stresses in blocks subjected to concentrated loads was based on some tests

preformed by Mörsch in 1924. The following assumptions were made:

<1> The stress due to a concentrated load are uniformly distributed at a distance equal to the width of the prism.

<2> The curvature of the trajectories causes tensile stresses, the latter being distributed according to a parabolic law.

The distribution of the compressive stress trajectories deduced by Mörsch is shown in fig.2.1. According to the figure, compressive stresses are uniform over the loaded area and the remote end of the end-block. It can be seen that

$$Z = P(a-a_1)/4H \qquad (2.1)$$

and if the tensile stresses are distributed according to a parabolic law, then the maximum tensile stress for a rectangular prism of breath b is

$$f_t = 3Z/2ab \qquad (2.2)$$

However, the assumption of a parabolic law is based on the measurements of transverse strain by Kruger [20] but Kruger measured the strains at three positions only, from which he constructed a parabola representing his view of the stress distribution. Since any curve can be drawn through three points, this assumption may not be true. To obtain the cracking load according to the above formula, the actual tensile strength of the material should be found. Mörsch also advises a correction of the depth of block, h, as shown in fig.2.1(c), and he suggests that it is more important to use

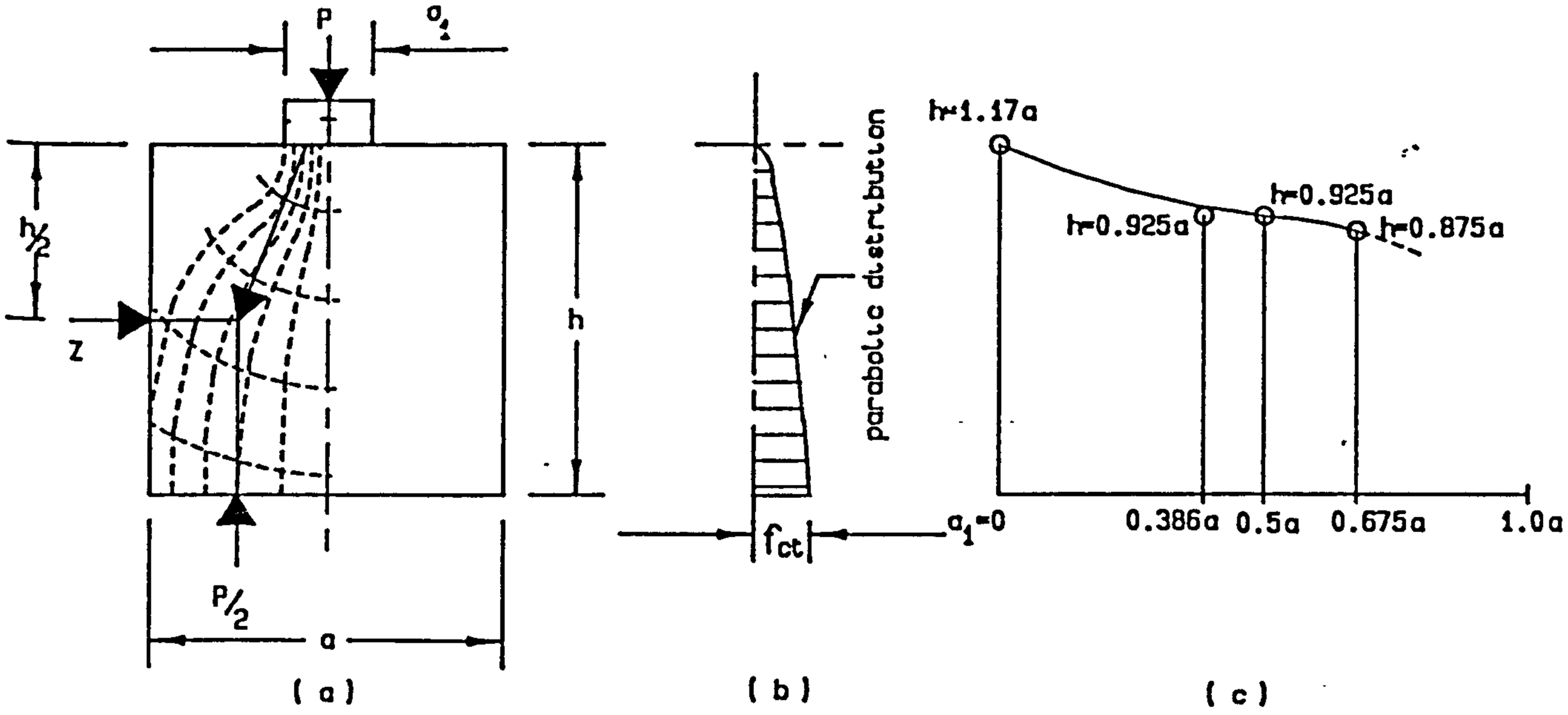

Fig.2.1. (a) Stress trajectories in Morsch's theory.
(b) Tensile stress distribution.
(c) Relation between h and a.

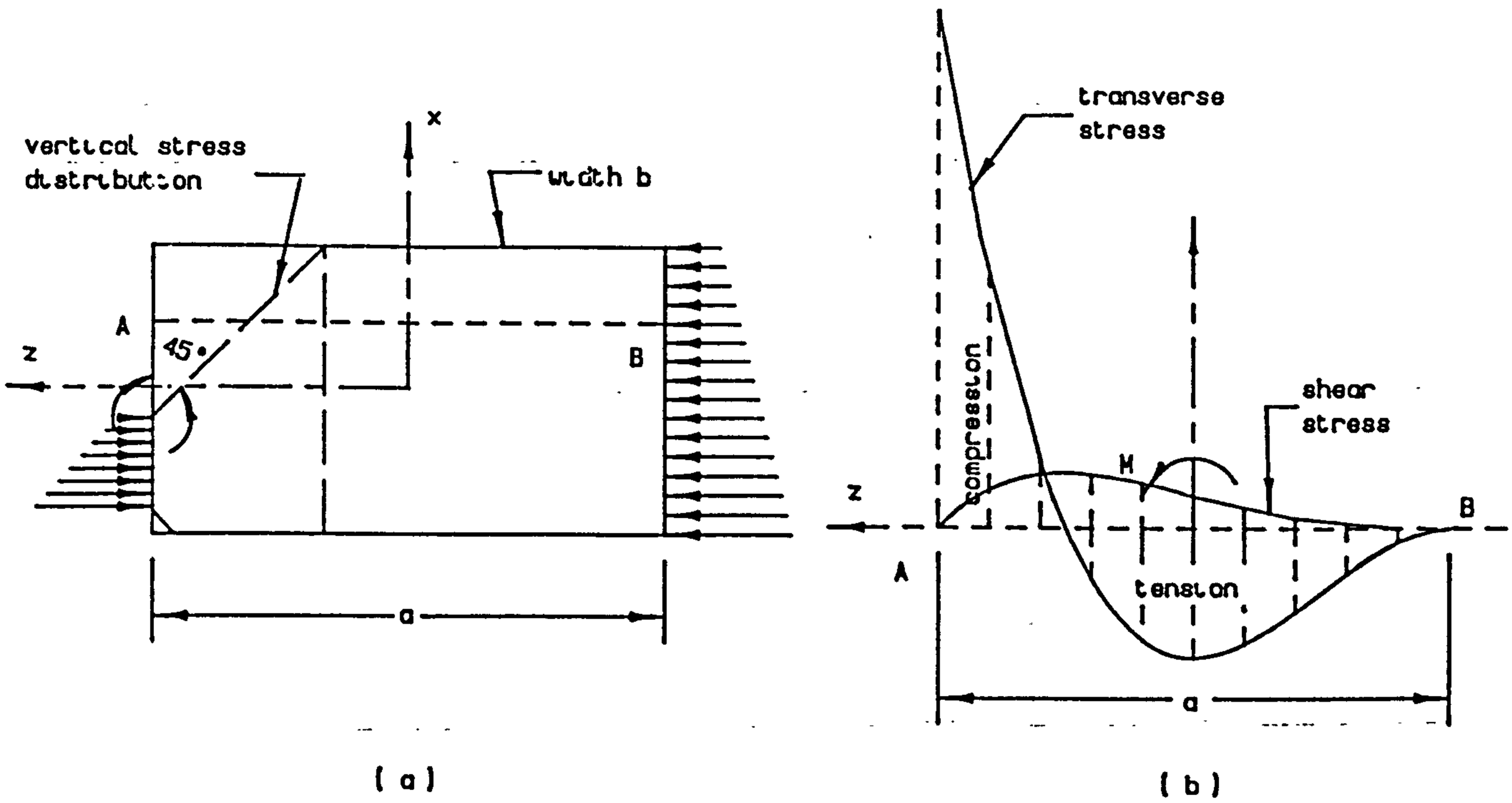

Fig.2.2 (a) Structural model proposed by Magnel.
(b) Transverse and shear stress distributions.

high-strength concrete for the blocks than to employ large amounts of reinforcement.

Another method of computing the principal tensile stresses in the end of a prestressed concrete beam is given by Magnel [55,56] as shown in fig.2.2. He assumed that at a particular reference plane AB, the transverse stress, f_{xx} due to the bending moment M, and shearing force S is distributed in a parabolic curve of the third degree as in fig.2.2(b). By means of the boundary condition, the transverse stress can be calculated and will be a maximum at 0.5a from the contact area. Similarly, the shear stress can be calculated using the appropriate boundary conditions. On the assumption that the pressure under the anchorages of the cables disperses at an angle of 45 degrees into the end of the beam, the distribution of longitudinal stresses can also be calculated. In this way, the principal stresses can be found. The beam will fail in the condition that the principal stress reaches the maximum tensile strength of the concrete. Fig.2.2(b) is an example of the stress distribution of the anchorage block estimated by Magnel.

Bortsch [81,82] made one of the earlier theoretical approaches to the problem of bearing capacity as well as stress distribution in structural units under concentrated loads. He assumed the load distribution on the contact area of the loading plate as a cosine function as shown in fig.2.3. From a stress function analysis, the transverse, longitudinal and

shear stresses can be calculated. The maximum transverse tensile stress f_{yy} occurs at a distance of 0.2 to 0.3a from the contact area which is different from those predicted by Magnel, and it is in a range of 0.38 to 0.45P/a for R between 10 and 20. At a distance of 1.7a from the end of the block, the tensile stress disapear, being 0.055P/a at x/a=1.0 . Bortsch deals with large values of R>20 and does not give any indication as to whether his theory can be used for values of R approaching unity.

Another theoretical approach to the problem of calculating of the stresses in the anchorage zone is by Guyon [26,27]. Fig.2.4 represents the sectional elevation of the end beam with bearing surface AB and plane CD. They are in equilibrium under the action of forces on CD distributed linearly, and the forces on AB, concentrated on small area with P_1 and P_2 as resultants. In addition, the following conditions must be satisfied for equilibrium to be maintained.

<1> According to the St. Venant principle and from experimental verification by photoelasticity that beyond a certain distance from the end of the beam approximately equal to the depth of the beam, the stresses are almost entirely longitudinal, the transverse stresses can be neglected.

<2> The resultant of the stresses f_{yy}, along EF must be zero.

<3> The sum of the moments of the stresses f_{yy} about a point in EF must equal the sum of the moments of the forces acting on EB and FC.

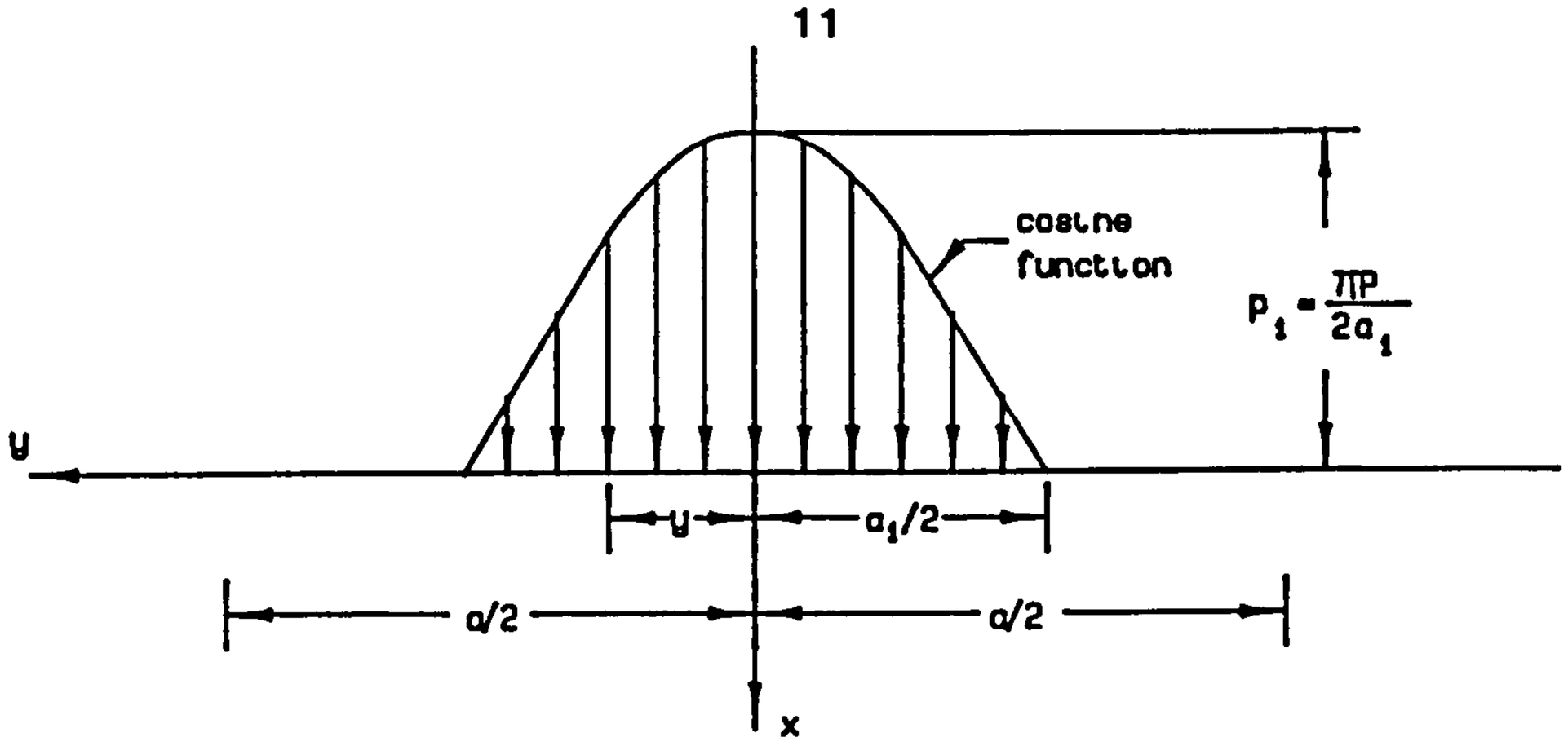

Fig.2.3 Load distribution in Bortsch's theory

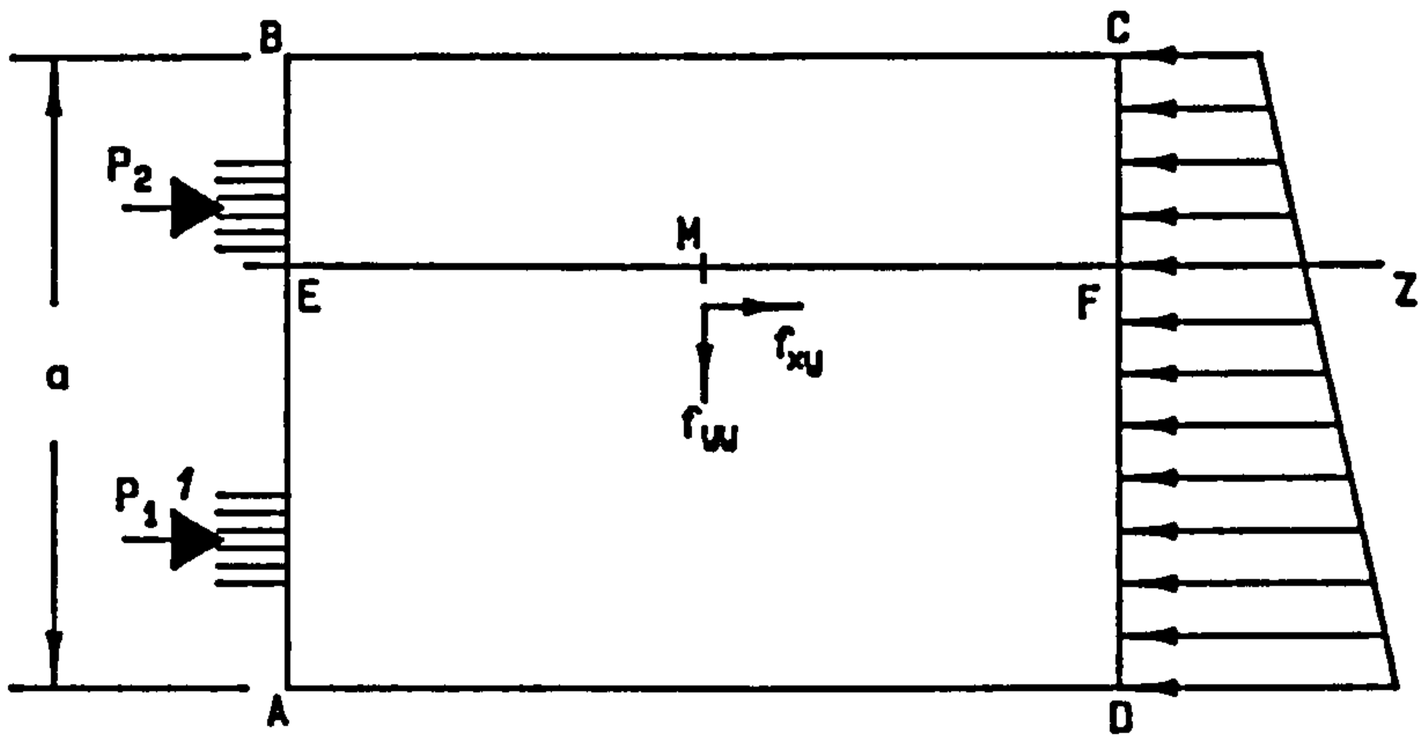

Fig.2.4 Sectional elevation of end beam by Guyon.

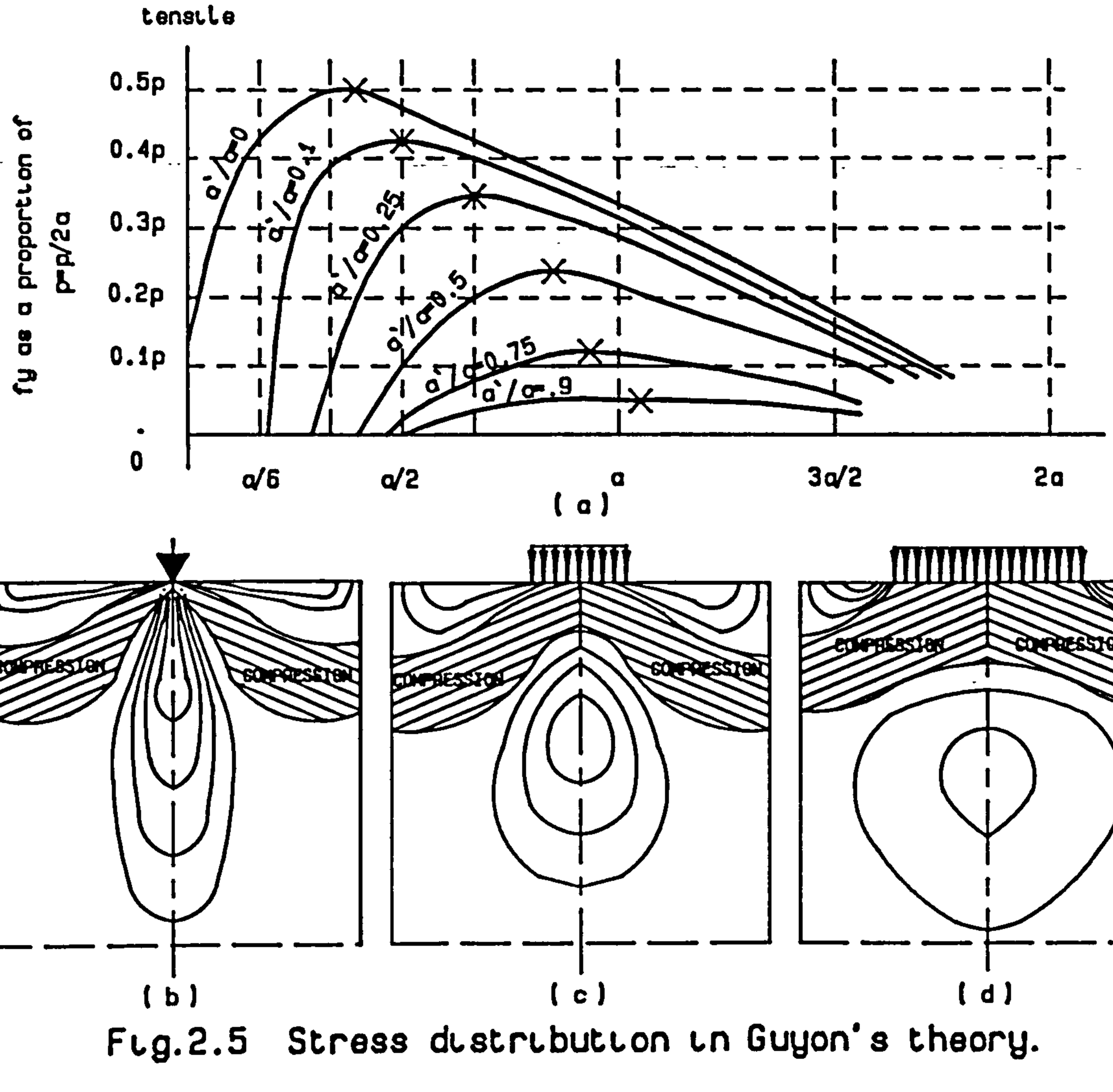

Fig.2.5 Stress distribution in Guyon's theory.

<4> The resultant of the shear stresses, f_{xy} must equal the resultant of the horizontal forces applied to BEFC.

Considering the above boundary conditions by using Fourier series as a stress function, Guyon (5,6) gives six tables for the calculation of stresses f_{yy}, f_{xx} and f_{xy} caused by the forces in the anchorage zone. The variation of f_{yy} along the axis for various value of a_1/a is shown in fig.2.5(a). The tensile stress contours for diffferent degrees of concentration of the applied force are shown in fig.2.5(b) to (d). It is interesting to note that, in addition to the tension produced deep in the block along the line of action of the force, there are tensions near the surface in the two corners; this will be referred to as the spalling zone and the tensile region along the axis as the bursting zone. However, recent photo-elastic tests [83] as well as the tests on concrete units show that Guyon under-estimated the stresses.

Bleich [81,82] made use of an Airy stress function F and considered the boundary conditions. For a two-dimensional problem, he was able to calculate the vertical, horizontal and shear stresses successfully. In the case of the applied load shown in fig.2.6, the tensile stresses calculated are shown in fig.2.7. Sievers [9] presented an approximate formula for the three dimensional condition shown in fig.2.8 which satisfied the boundary condition. He modified the two-dimensional stress distribution developed from Bleich's accurate solution with the

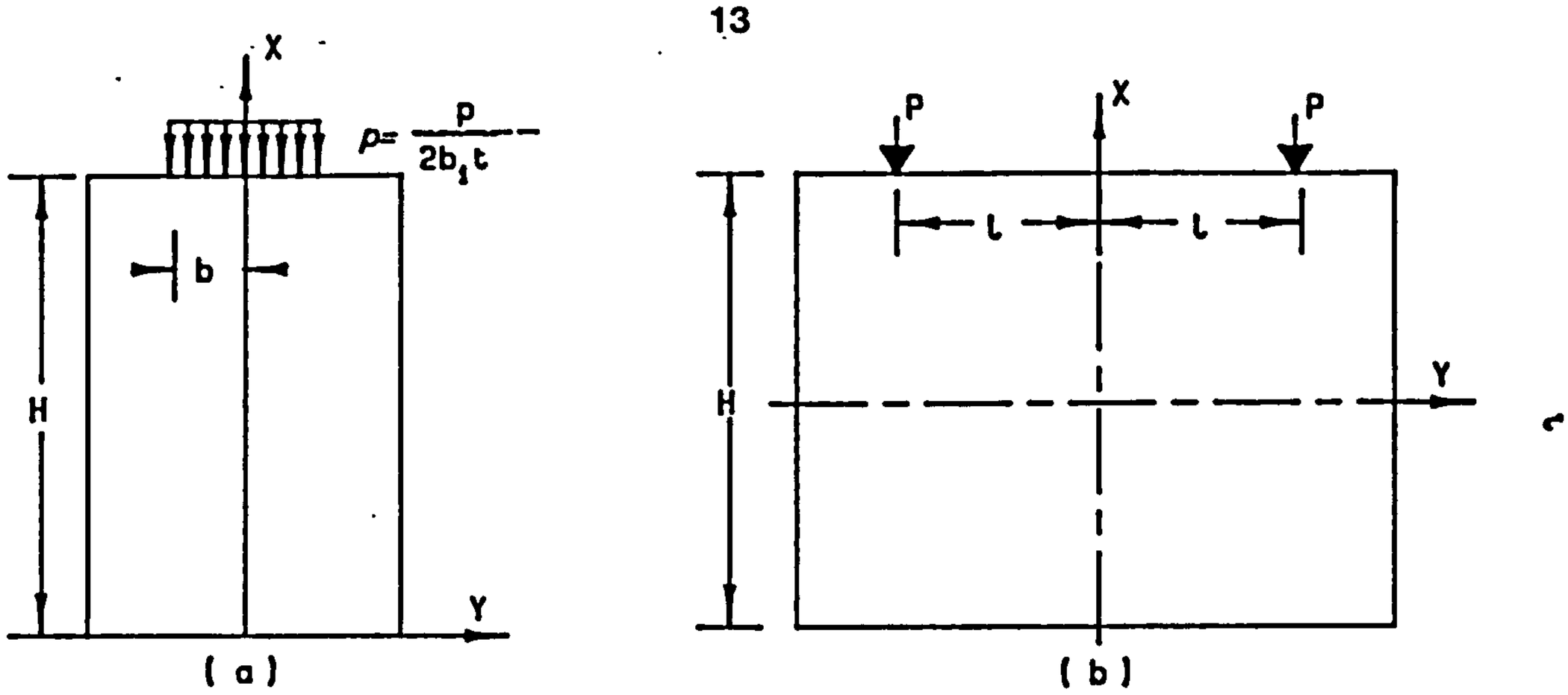

Fig.2.6 Loading condition in Bleich's theory.

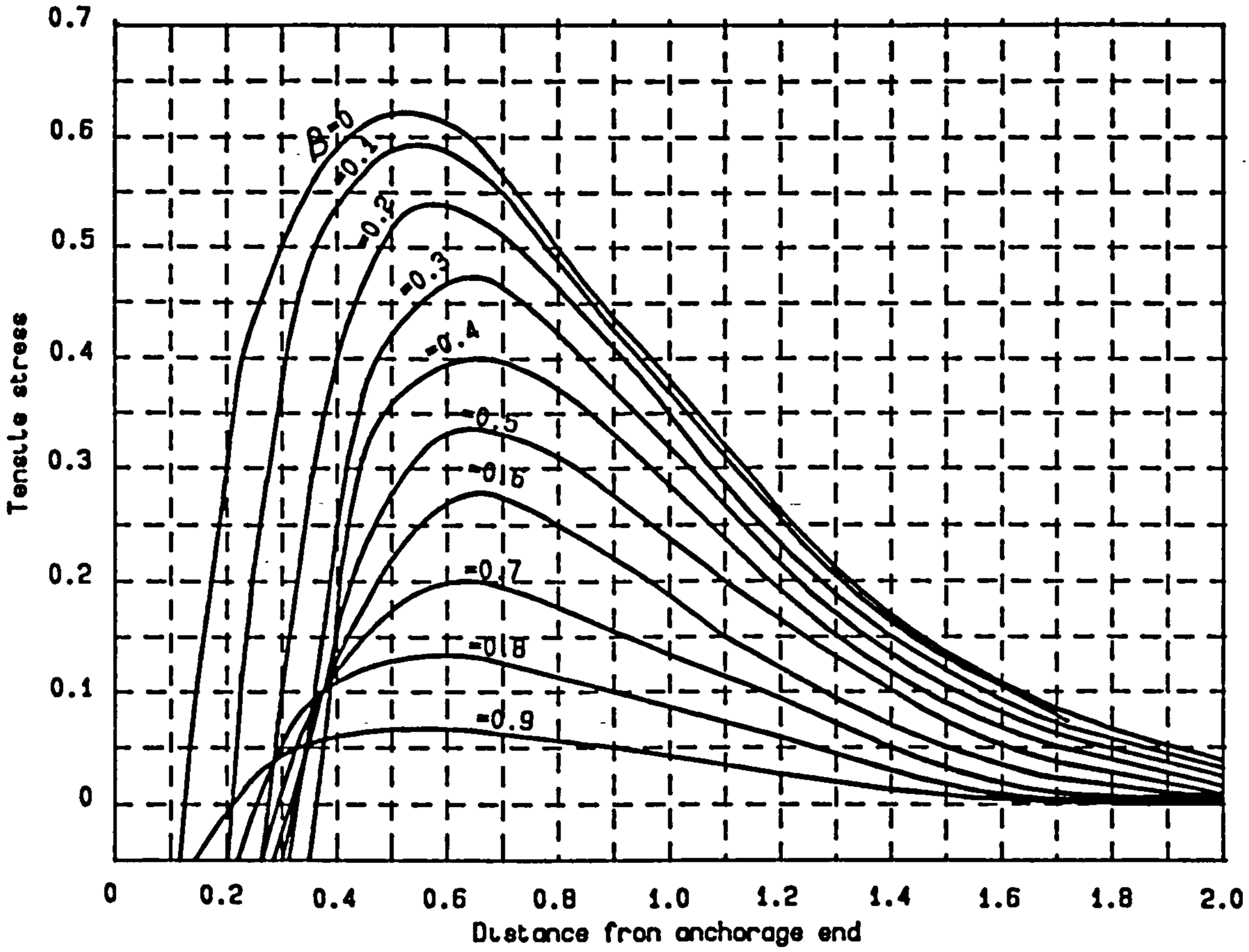

Fig.2.7 Tensile stress distribution by Bleich's Theory.

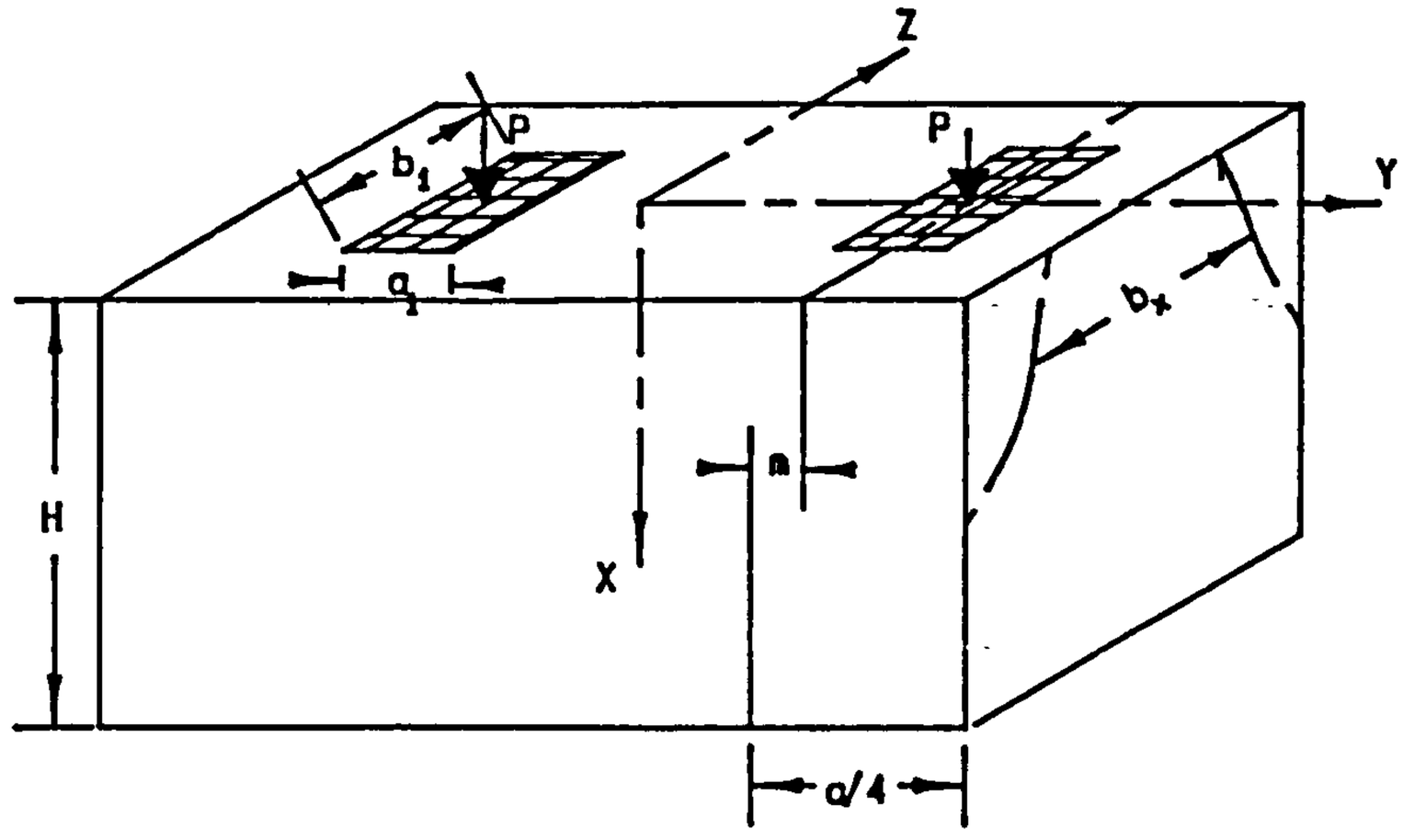

Fig.2.8 Sievers's three dimensional model.

following assumptions:

<1> The actual inner stresses at a distance of (a-x) from the beam end are taken equal to those in a modified end-block having the apparent width of $b=b_x$ obtained by two-dimensional analysis.

<2> The apparent width of the modified end-block is given by

$$b_x = b_1 - (b-b_1)(1+2.5n_q)\, e^{-0.8\pi n_q} \qquad (2.3)$$

<3> The applied load is considered to be uniformly distributed on the area $a_1.b_x$

It has been confirmed by three dimensional photoelastic tests that this formula agrees fairly well with the experimental distribution.

2.2.2 INTERNAL FRICTION THEORY OF SLIDING FAILURE

A number of tests have been carried out by Meyerhof [59, 1953] to investigate the bearing strength of concrete and rock. The results indicate that the material generally fails, depending on the magnitude of the confining pressure, by splitting or shear along one or several rupture surfaces. The failure condition can approximately be represented by the relation for the shearing strength C, of the material.

$$C = C_o + p\cdot\tan\varphi \qquad (2.4)$$

where C_o = shear resistance per unit area for p=0.

p = effective normal pressure on the shear plane.
ψ = angle of internal friction.

Consider a strip load of width a_1 acting concentrically on a concrete block as shown in fig.2.9. On failure, a wedge of material is found immediately beneath the footing with a semi-apex angle equal to α, fig.2.9(b). By considering the equilibrium of half of the wedge and assuming that the horizontal pressure, P_h causing the splitting of the block is uniformly distributed along the wedge. The horizontal splitting pressure can be obtained as

$$P_h = f_b^2 \cdot \tan^2\alpha - 2 \cdot C_o \cdot \tan\alpha, \qquad (2.5)$$

assuming a triangular distribution of tensile stresses to resist the bending moment produced by the horizontal splitting pressure, fig.2.9(a). Substituting in Eq.2.5, the unconfined prism strength is

$$f_c' = 2C_o \cdot \cot\alpha \qquad (2.6)$$

which can be simplified to obtain the ultimate bearing stress, f_b

$$\frac{f_b}{f_c'} = 1 + \frac{2H/a_1 - \cot^2\alpha \cdot f_t \cdot \cot\alpha}{(8H/a_1 - \cot\alpha) \cdot f_c'} \qquad (2.7)$$

For large ratios of H/a_1

$$f_b/f_c' = 1 + f_t \cdot H/(4C_o \cdot a_1) \qquad (2.8)$$

By differentiating Eq.2.7 with respect to α, the minimum value

of f_b/f_c' can be obtained as

$$f_b/f_c' = 1 + 0.15H \cdot f_t/(a_1 \cdot f_c') \qquad (2.9)$$

which is the lower bound for bearing strength to cylinder strength ratio. It can be seen that the bearing capacity of surface footings is directly proportional to the ratio of block thickness to footing width H/a_1. Moreover, experimental results show that the bearing capacity of the mass blocks is somewhat greater than the theoretical estimates for a small ratio of block thickness to footing diameter (H/D); this difference may be explained by the lateral confinement of the material due to frictional restraint on the base of the blocks, which had been rejected in the analysis. For large ratios of H/D, the ratio of the bearing capacity to the prism strength (f_b/f_c'), tends to a limiting value of 7 which is given by the present analysis for shearing failure with φ=45 degree. If the width is increased the bearing capacity of the mass blocks is less than the theoretical estimate on account of premature failure by splitting. Where splitting of the material is prevented, the bearing capacity can be estimated from the theory. It increases rapidly with the size of the block and approaches the limiting value of 24 times the cylinder strength for a footing on a semi-infinite solid. However, tests carried out by Muguruma [62] and Niyogi [65] indicate the opposite result: bearing capacity decreases as the height of the block increases, particularly for those with small values of the

ratio R (footing area/loading area). Probably this is due to the non-linear distribution of tensile stresses, P_h as the height of the block increase.

Tests were conducted by Tung Au [6,7, 1960] to determine the bearing capacity of concrete blocks with R ranging from 2 to 16 and with depth equals to either full (series A) or half (series B) width of the block. It was found that, in series A at failure, a vertical crack which started at the top of the block progressed downward indicating splitting due to sliding failure. The maximum load was reached after the formation of an inverted pyramid. For those in series B, the blocks were split radially and in most cases, no clear-cut pyramids were observed. Cracks usually appeared first at the bottom of the sides and progressed upward. This indicate that splitting was caused by radial pressure resulting from large deformation of concrete under the base plate and the depth of the block is not enough for the formation of an inverted pyramid. He assumes that the block will split diagonally as it is loaded with a square plate, fig.2.10. Based on Meyerhof's proposal, Eq.2.5 can be obtained. Again, with the assumption of the uniform horizontal pressure P_h along the wedge, the horizontal splitting force F can be calculated. This force produces combined direct tension and bending in the concrete block with a stress distribution as shown in fig.2.10(e). The maximum tensile stress at the top of the block can be computed as

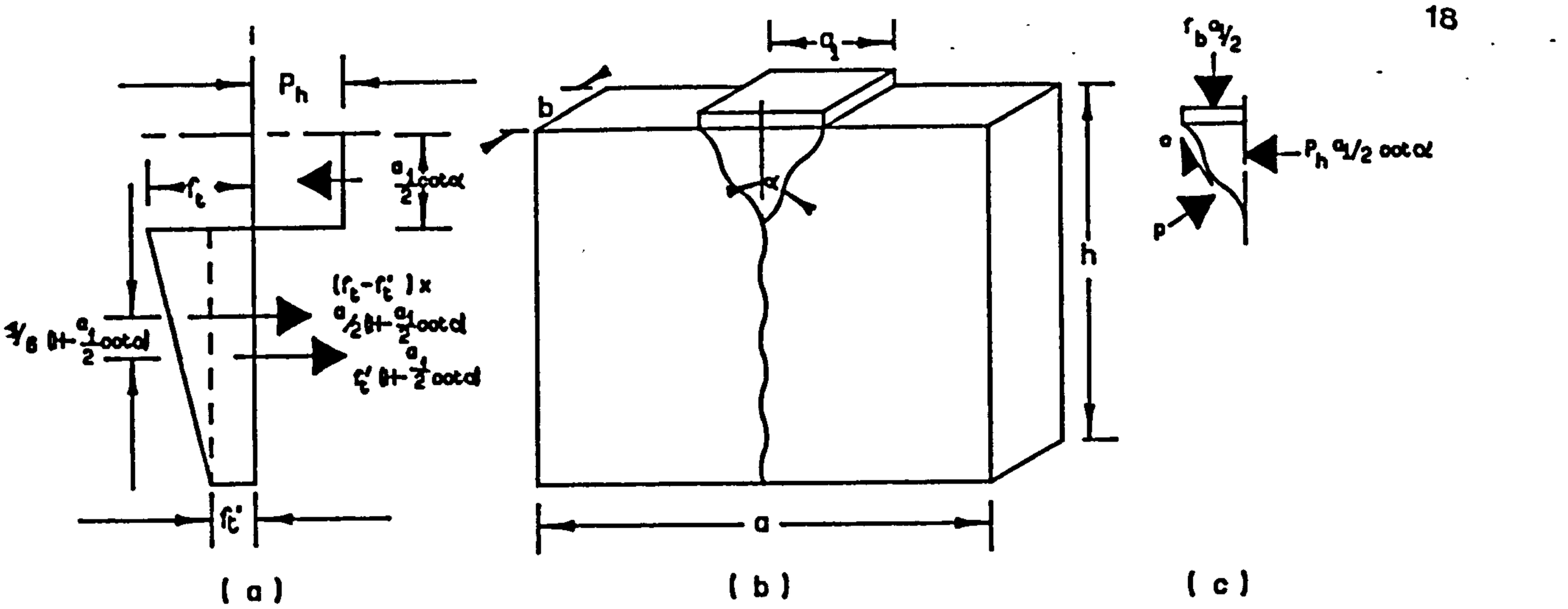

Fig.2.9 Structural model proposed by Myerhof.

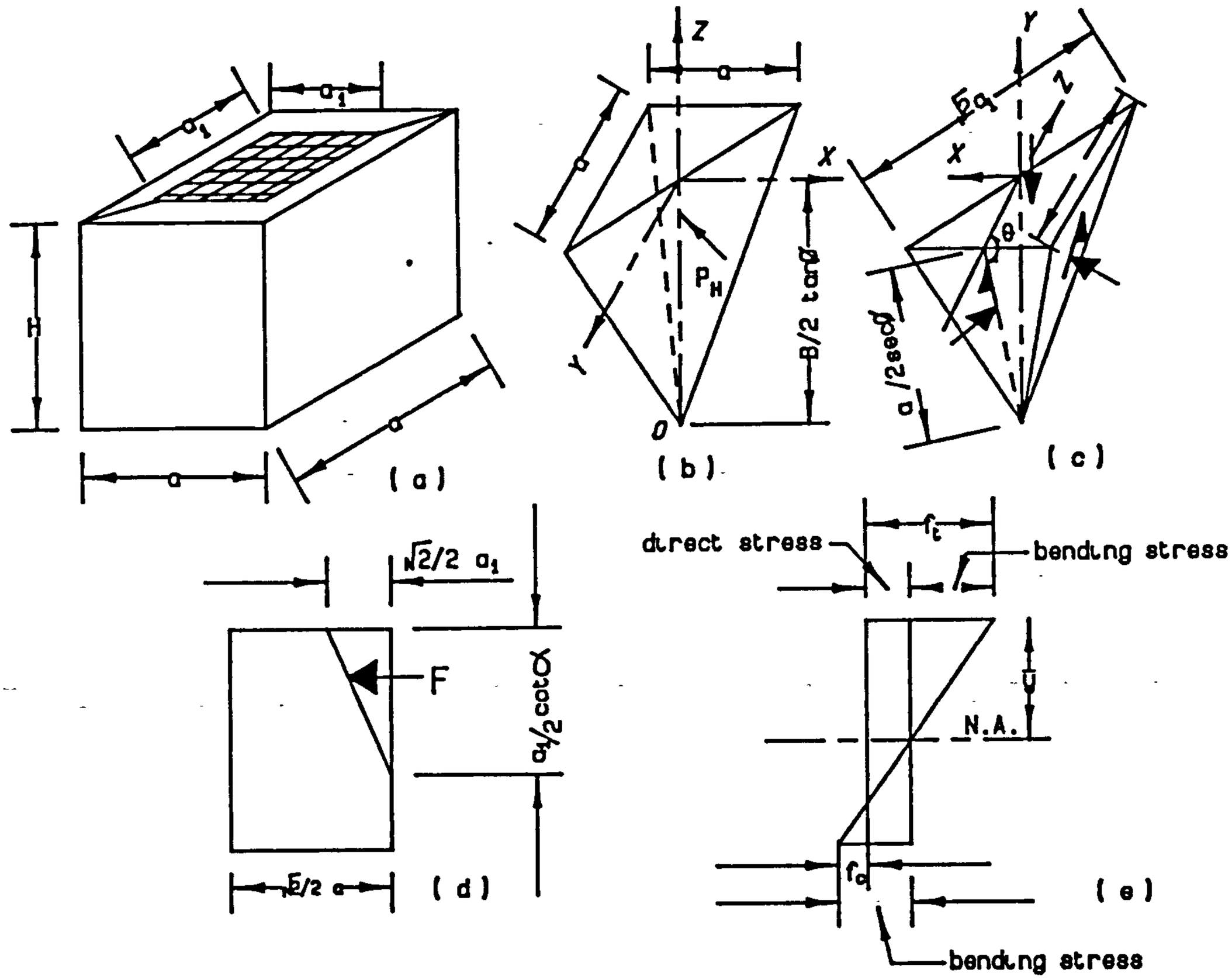

Fig.2.10 Structural model proposed by Tung Au.

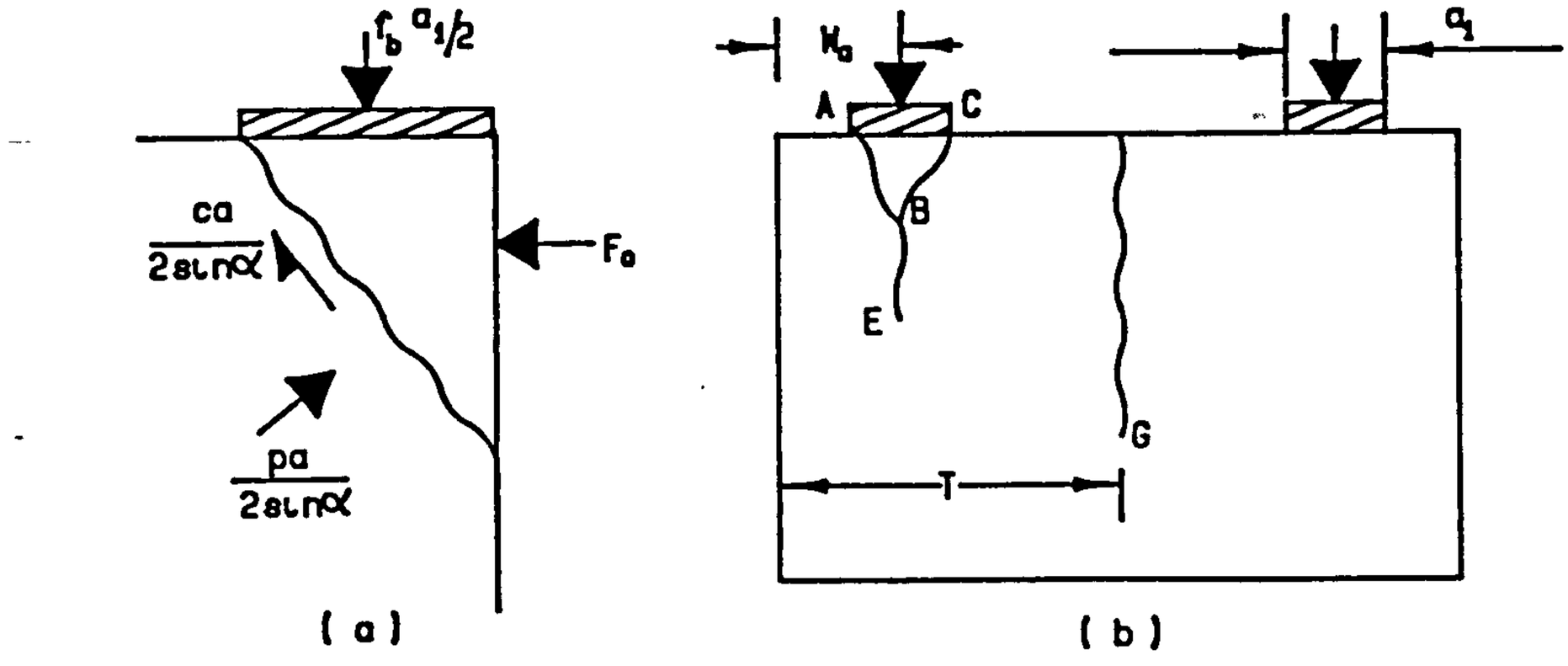

Fig.2.11 Structural model proposed by Hawkins.

$$f_t = P_h/K \cdot \cot\alpha \qquad (2.10)$$

where

$$\frac{1}{K} = \frac{\sqrt{2}\ a_1^{\,2}}{4}\left(\frac{1}{A} + \frac{\bar{y} - a_1/6\cdot\cot\alpha}{I}\,\bar{y}\right) \qquad (2.11)$$

and A = area of the diagonal section of the block except the wedge,

$\bar{y}$ = position of the neutral axis from the top,

I = second moment of inertia of area A about the neutral axis.

By substituting in Eqs.2.9 and 2.5, the bearing strength to cylinder strength ratio can be obtained as

$$f_b/f_c' = \left(2C_o/f_c' + K\cdot f_t/f_c'\right)\cdot\cot\alpha \qquad (2.12)$$

It was found from experiment that the half apex angle α varies from 19 to 25 degs. approximately. As both $\cot\alpha$ and K are sensitive to small changes in the value of α, the results from Eq.2.12 are too scattered to justify. Moreover, at high pressure, the stress distribution along the depth of the block becomes non-linear and Eq.2.10 no longer applies. Therefore, Eq.2.12 only gives an approximate solution. Nevertheless, it provides a rational basis for relating the empirical constants.

A dual failure criterion for concrete is adopted by Hawkins [30-32]. For regions subject essentially to tension, the governing factor is assumed to be maximum tensile stress. For regions subject essentially to compression, failure is assumed to be due to sliding along planes inclined to the direction of principal stress. The limiting stress on the

failure plane is again taken as

$$C = C_o + p \cdot \tan\nu \qquad (2.4)$$

Consider a specimen of rectangular section loaded as shown in fig.2.11. A failure wedge ABC is formed and punched down into the crack. For the equilibrium of the wedge

$$f_b = f_c' + 2F_o \cdot \cot\alpha / a_1 \qquad (2.13)$$

The force F_o depends upon the resistance offered by the block to the penetration of the crack. Lenschow and Sozen [52] assume that

$$F_o = \frac{2.41 f_t \cdot W_a + 11.8 M_o / W_a}{11.8 L / W_a + 7.84} \qquad (2.14)$$

where L is the measure of the crack length shown in fig.2.11(b). M_o is the moment about the crack line DE. The magnitude of M_o depends on the position of spalling crack FG. M_o is approximately given by

$$M_o = f_b \cdot a_1 \cdot W_a^{\,2} / 2H - f_b \cdot a_1^{\,2} / 8 \qquad (2.15)$$

By substituting Eq.2.14, 2.15 into 2.13 gives

$$f_b = f_c' + \frac{1}{a_1} \left[\frac{2.41 f_t \cdot W_a + 5.9 a_1 \cdot W_a \cdot f_c' / T - 1.48 a_1^{\,2} \cdot f_c' / W_a}{(11.8L/W_a + 7.84)\tan\alpha/2 - 5.9 W_a / T + 1.48 a_1 / W_a} \right] \qquad (2.16)$$

At collapse the rate of change in the force F_o with increase in length L equals the tensile strength f_t. Differentiation of Eq.2.13 gives

$$\frac{d(f_b)}{d(L)} = \frac{2}{a_1}\tan\alpha \cdot \frac{d(F_o)}{d(L)} = \frac{2f_t}{a_1}\tan\alpha \qquad (2.17)$$

Differentiation of Eq.2.16 w.r.t. L and substitution into Eq.2.17 give a quadratic expression for L/W_a for which the positive root is

$$\frac{L}{W_a} = \frac{W_a}{T\cdot\tan\alpha} - \frac{0.25a_1}{W_a\cdot\tan\alpha}$$

$$+ 0.29\left[\,2.41+5.91\frac{a_1\cdot f_c'}{T\cdot f_t} - 1.48\left(\frac{a_1}{W_a}\right)^2\,\right]^{0.5} - 0.664 \qquad (2.18)$$

The value of T can estimated by

$$\text{For sym. load .... } T = \begin{cases} 3W_a \text{ —— } W_a < a/6 \\ a/2 \text{ —— } W_a > a/6 \end{cases}$$

$$\text{ecc. load .... } T = \begin{cases} 3W_a \text{ —— } W_a < a/3 \\ a \text{ —— } W_a > a/3 \end{cases} \qquad (2.19)$$

2.2.3 EMPIRICAL FORMULA

Shelson [76] has carried out tests on twenty-one 8in. cubes loaded through a mild steel base 1/4 in. thick and 1.0, 1.41, 2.0, 2.83 and 3 in. square respectively. He found that the maximum bearing pressure increased as the ratio of footing area to loading area increased as shown in fig.2.12. For a relatively low value of R, the bearing capacity increases

considerably as the ratio R incrased. As R becomes larger the ratio of bearing capacity to the compressive strength tends to have a limit of 5, which corresponds to the case of loading of a semi-infinte footing. Fig.2.12 has been plotted together with a comparable curve obtained from the specifications of the ACI Code with a factor of safety of 4. It indicates that the Code provides a more than ample margin of safety at the higher ratio of R, but for low values of R, which are more common in practice, the margin of safety is not good enough. A more reasonable design formula has been proposed by Shelson [76] as (fig.2.12)

$$f_b/f_c' = 0.25\ R^{0.3} \qquad (2.20)$$

It follows the actual failure curve more closely than the ACI Code requirement. At the lower end, this curve provides a permissible stress in accordance with the Code and for higher values of R, the curve remains quite conservative but certainly represents an improvement.

Tests have been carried out by Kriz [49], through 38 plain concrete specimens loaded with different edge distances and plate sizes. He found that the bearing strength was proportional to the square root of f_c' which in turn is related to the concrete tensile strength. Bearing strength was influenced by the width of the bearing plates and by the distance of the bearing plates from the edge of the specimen (edge distance, W_a). Splitting failure occurred when the

distance was more than 40 mm., otherwise there was shear failure along an inclined plane extending outward from the inner edge of the bearing plate. For plain concrete specimens, a proposed formula was used to calculate the bearing strength as

$$f_b = 5.73\, f_c'^{0.5}\, (W_a/a_1)^{1/3} \qquad (2.21)$$

To investigate the effect of height of concrete block upon bearing capacity, concentrated loading tests were carried out in two series by Muguruma [62]. Series I had rectangular section 250 x 150 mm, with three different heights of 500, 250 and 150 mm. Specimens having 200 x 200 mm section were adopted with five different heights, from 100 to 400 mm, in series II. Series I specimens were loaded with a rectangular plate so that load was distributed uniformly throughout the thickness of the block b, while in series II a square plate was used for applying concentrated load. An empirical formula was derived from the results of these tests,

$$f_b = \left(1/(6.67H/a-2.91) + 0.71 \right) \cdot f_t \cdot R^{\frac{7.61H/a-3.54}{16.44H/a-6.65}} \qquad (2.22)$$

This empirical equation is applicable to the prediction of the bearing capacity of concrete of relatively high compressive strength about 40N/mm^2. It was noted that the effect of height becomes important as the value of R become smaller.

It is suggested by Niyogi [65,66] that the bearing

capacity of a specimen is influenced by

<1> The geometry of the block and loading condition,
    (a) the dimensions of the loaded surface of specimen relative to those of bearing plate,
    (b) relative height of specimen defined as ratio H/a,
    (c) eccentricities of loading, expressed as e/a and e/b,
<2> The bearing area,
<3> Mix proportions and strength of concrete,
<4> Size of the specimen.

Tests of over 100 blocks with dimensions varied from 0.5x8x4 to 24x8x24ins, under strip load and eccentric load, with rectangular and square bearing plates, were conducted. The effect of eccentricity on bearing capacity of the concrete block was also investigated by loading the concrete block with unaxial and biaxial eccentric load. As a result of the tests, it is seen that the cube-root formula considerably underestimates the bearing strength for square loading and somewhat overestimates the strength for strip loading. Fig.2.13 gives a plot of results of the experiment. It can be seen that for R less than 8 the bearing strength decreased with increasing height of the specimens. This was probably due to

<1> The reduced influence of base friction as the height of the specimen increased and,
<2> the size effect.

But with R greater than 8, shallow blocks had lower bearing strength. This reduction was perhaps caused by increased concentration of vertical reaction at the bottom of specimens, leading to an equivalent localized loading condition from both top and bottom. Finally, the ratio of the bearing

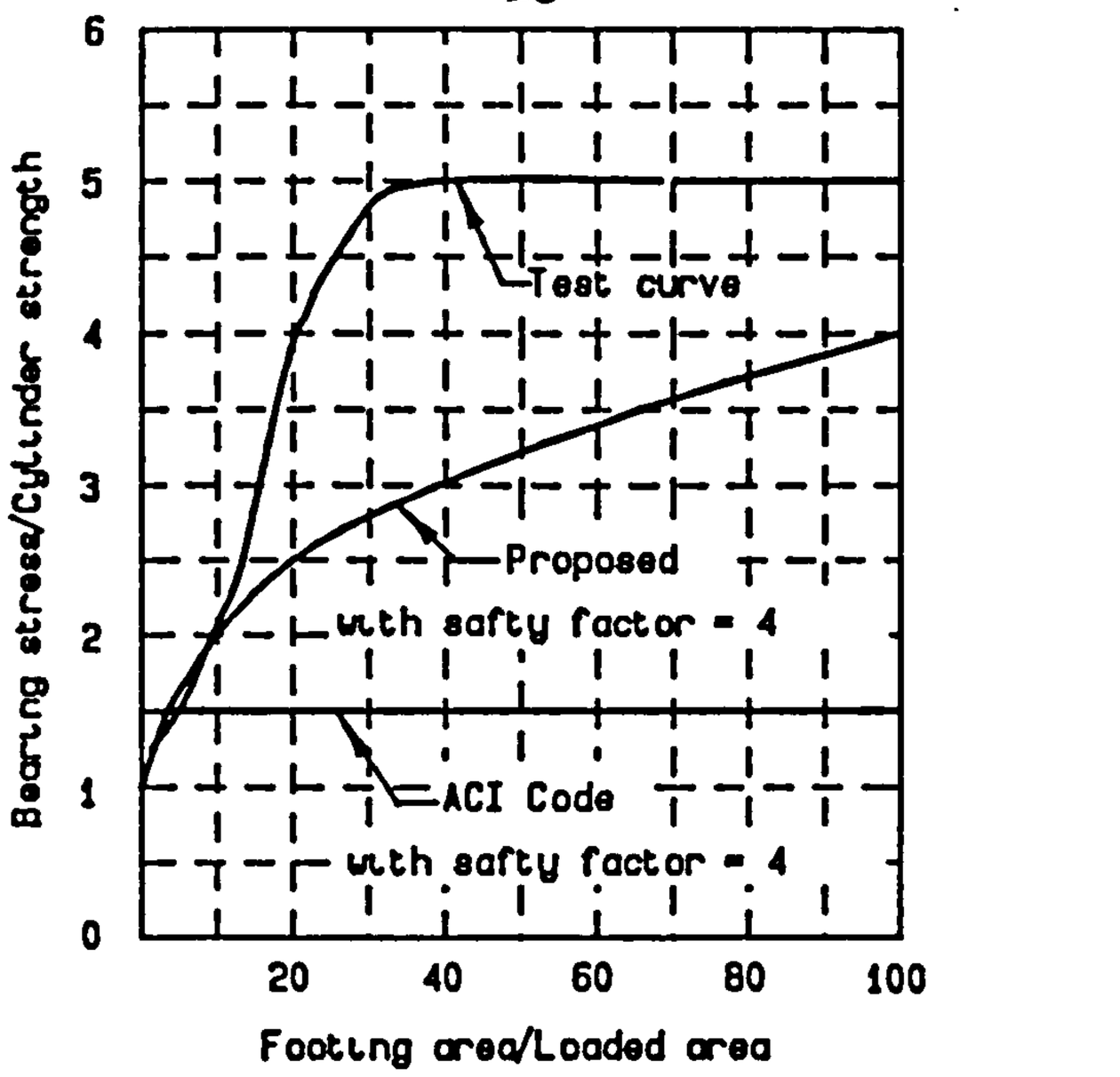

Fig.2.12 Bearing strength to area ratio, Shelson.

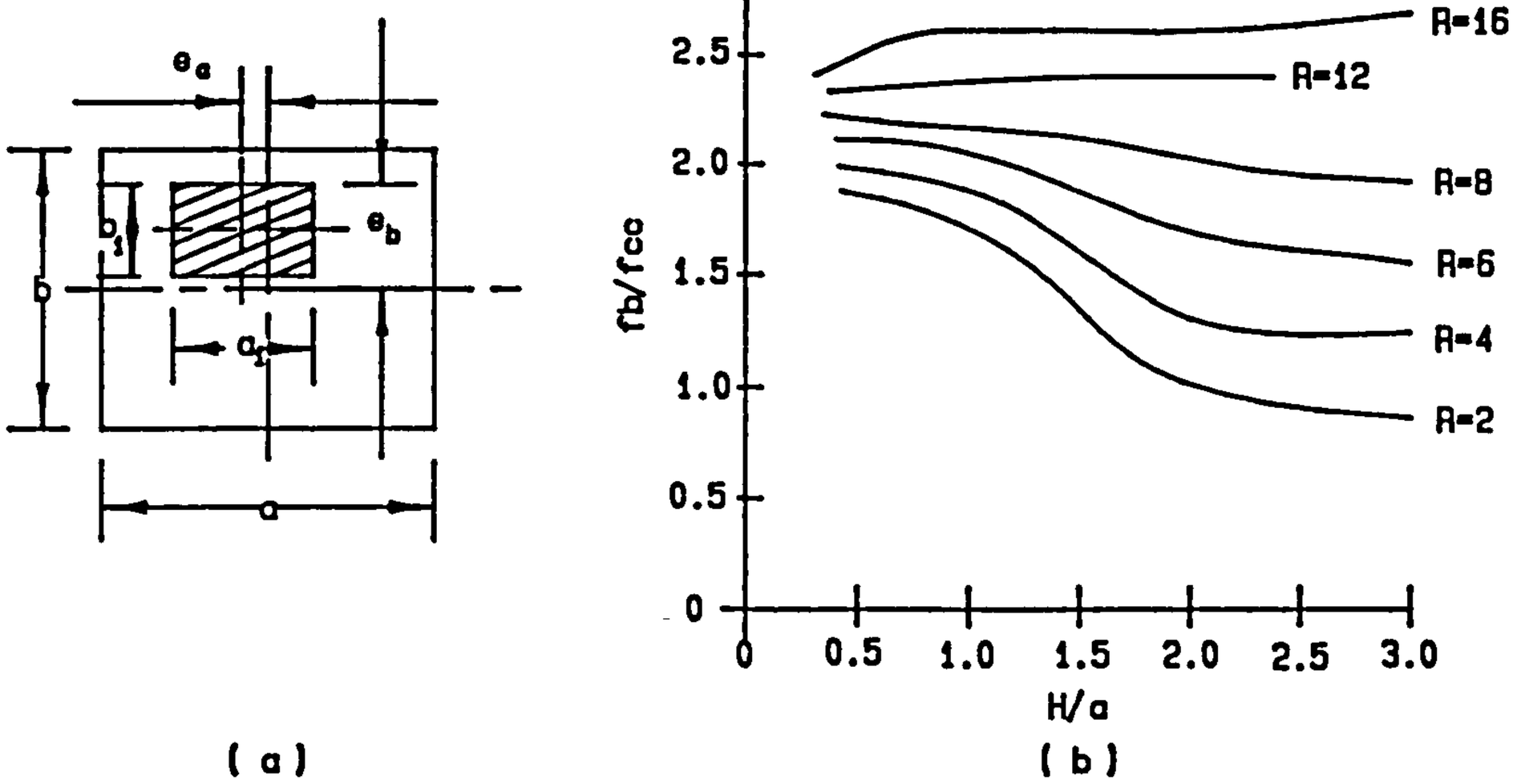

Fig.2.13 Influence of bearing strength by the height of the specimen, Niyogi.

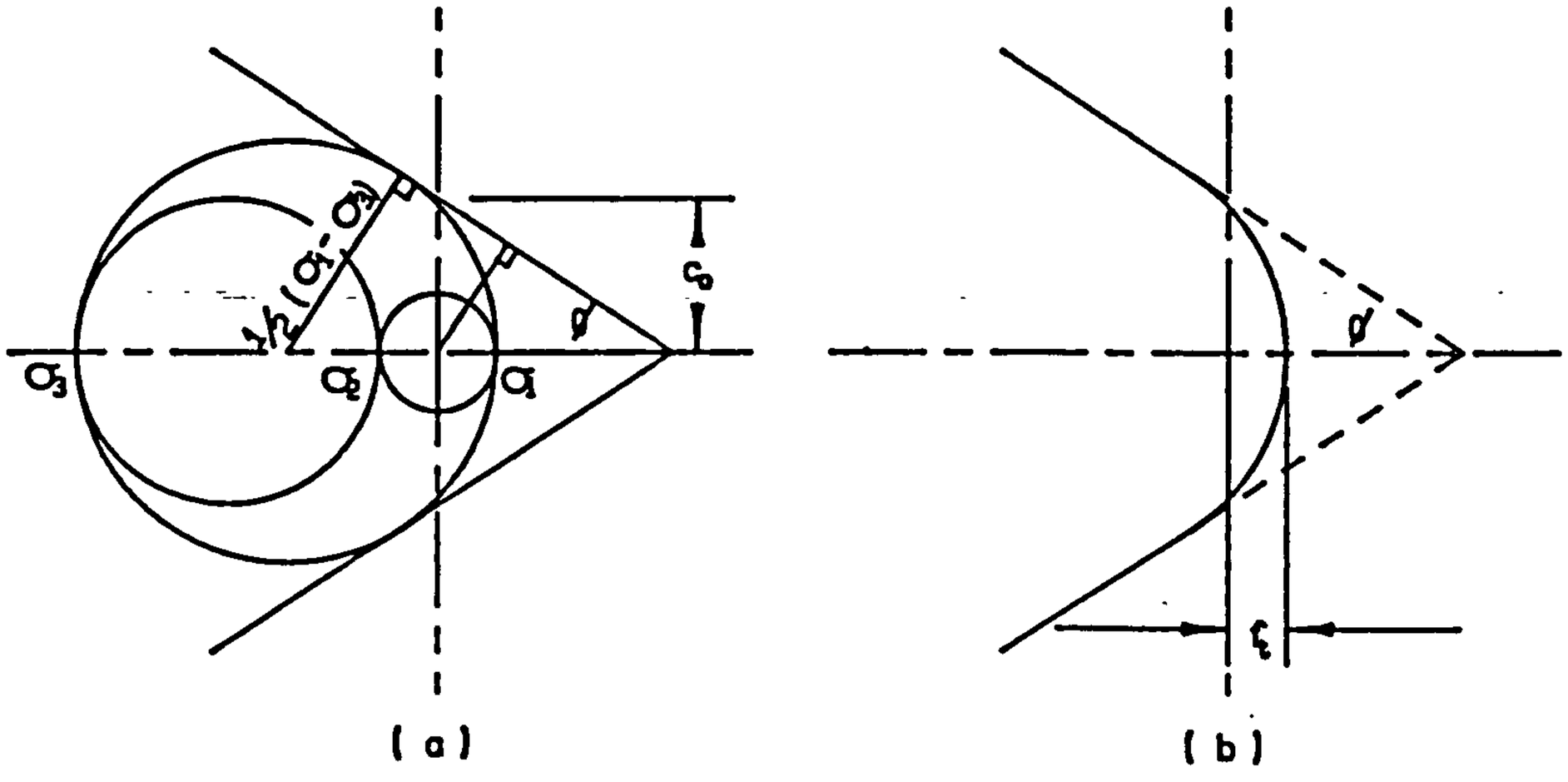

Fig.2.14 Coulomb's failure hypothesis.

capacity to the compressive cylinder strength of a concentric load concrete block can be estimated by

$$\frac{f_b}{f'_c} = 0.42\left[\frac{a}{a_1} + \frac{b}{b_1} + 1\right] - 0.29\left[\left(\frac{a}{a_1} - \frac{b}{b_1}\right) + 5.06\right]^{0.5} \qquad (2.23)$$

The influence of eccentricity on the bearing capacity of the concrete block can be represented by the influence factor I_e

$$I_e = 2.36\left[0.83 - \left(\frac{e_a}{a} - \frac{e_b}{b}\right)^2\right]^{0.5} - 0.94\left(\frac{e_a}{a} + \frac{e_b}{b}\right) - 1.15 \qquad (2.24)$$

2.2.4 PLASTIC ANALYSIS

Coulomb's failure hypothesis was presented in 1773, in which it was assumed that the internal cohesion is constant and the internal friction is proportional to the normal pressure on the sliding surface [21]. This assumption was formulated mathematically by Mohr (1882) as

$$C = C_o - p\cdot\tan\Psi \qquad (2.25)$$

and can be represented diagrammatically as shown in fig.2.14(a)

For uniaxial compression

$$f'_c = 2C_o\cdot\cot\Psi \qquad \text{where } \alpha = 45-\Psi/2 \qquad (2.26)$$

Coulomb's failure hypothesis can be supplemented by another hypothesis (the separation failure hypothesis) in which, the failure surfaces move away from each other perpendicular to the failure section, provided the biggest tensile stress is equal

to the separating resistance f_t, i.e. $\sigma_1=f_t$. This hypothesis can also be represented diagrammatically in fig.2.14(b).

Consider a plane homogeneous deformation field occurring in a narrow zone of height Δ between two rigid parts, marked I and II in fig.2.15. Part II moves V in relation to part I making an angle β to the direction of crack. The internal work per unit length along the line of discontinuity is

$$W = \begin{cases} f_c' \cdot V(1-\sin\beta)/2 \ldots\ldots\ldots\ldots\ldots\ldots\ldots & \alpha<\theta \\ f_c' \cdot V(1-\sin\beta)/2 + f_t \cdot V \cdot \dfrac{\sin\alpha-\sin\theta}{1-\sin\theta} \ldots\ldots & \alpha>\theta \end{cases} \qquad (2.27)$$

A block is loaded with strip load as shown in fig.2.16(a). A wedge of material with an apex angle 2α is formed beneath the loading surface, it fails by sliding along the surface. Splitting failure is found along the vertical crack.

The internal work corresponding to the

wedge is $$W_{iw} = f_c' \cdot V \cdot a_1(1-\sin\psi)/2 \qquad (2.28)$$

vert. crack is $$W_{ic} = 2f_c' \cdot V(H-a_1 \cdot \cot\alpha/2) \cdot \sin(\beta+\psi) \qquad (2.29)$$

External work done by the load is

$$W_e = f_b \cdot a_1 \cdot V \cdot \cos(\alpha+\psi) \qquad (2.30)$$

By equating the internal and external work we find

$$f_b = \frac{f_c'\left[1-\sin\psi\right]/2 + f_t \cdot \sin(\alpha+\psi)\left[2H \cdot \sin\alpha/a_1-\cos\alpha\right]}{\sin\alpha \cdot \cos(\alpha+\psi)} \qquad (2.31)$$

For minimum f_b

$$\cot\alpha = \tan\alpha + \sec\alpha\left[1 + \frac{2H\cdot\cos\psi/a_1}{f_c'(1-\sin\alpha)/2f_t - \sin\psi}\right]^{0.5}$$

$$f_{b_{(min)}} = f_t(2H\cdot\tan(2\beta+\psi)/a_1 - 1) \qquad (2.32)$$

If the loading plate is too near to the edge of the specimen it fails by shearing off the corner as shown in fig.2.16(b). Similarly, by considering internal and external work, we obtain

$$f_{b_{(min)}} = f_c'\cdot(2W_a+a_1)/2a_1 \qquad (2.33)$$

2.3 BEARING CAPACITY OF REINFORCED CONCRETE

Shizuo Ban [9] has performed tests of eighteen specimens to investigate the effect of transverse reinforcement upon the cracking and ultimate loads. He used mortar blocks 20.8 ins. in length and 7.1 by 4.75 ins. in cross-section, loaded with an anchorage plate of 0.5 ins. thick from 2x2 to 6x4 inches in plan. The permissible stress for concrete in tension was assumed as 1/3 of its tensile strength determined by tensile splitting tests of 6x12 ins. cylinders. Spiral reinforcement was arranged in the tensile overstress region based on Bleich's two-dimensional solution. It was found that spiral reinforcement was the most effective way to increase the bearing capacity of concrete particularly as the size of anchorage plate becomes larger. The initial cracking load (not the ultimate load) was approximately proportional to the

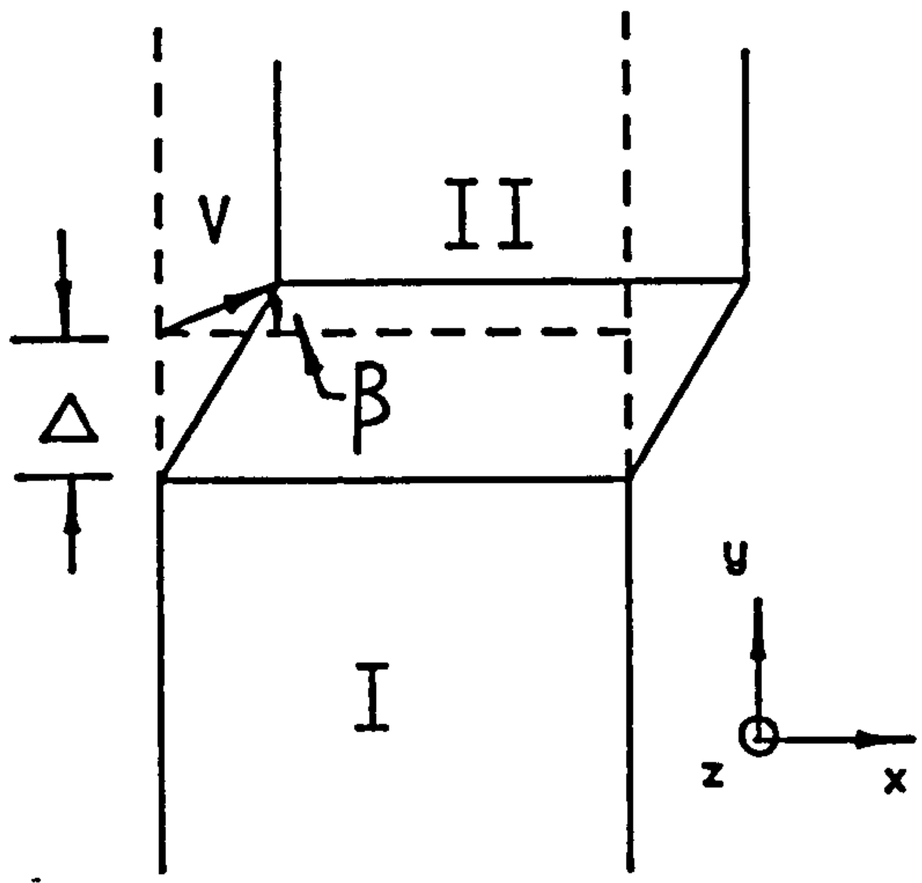

Fig.2.15 Deformation field in plastic analysis.

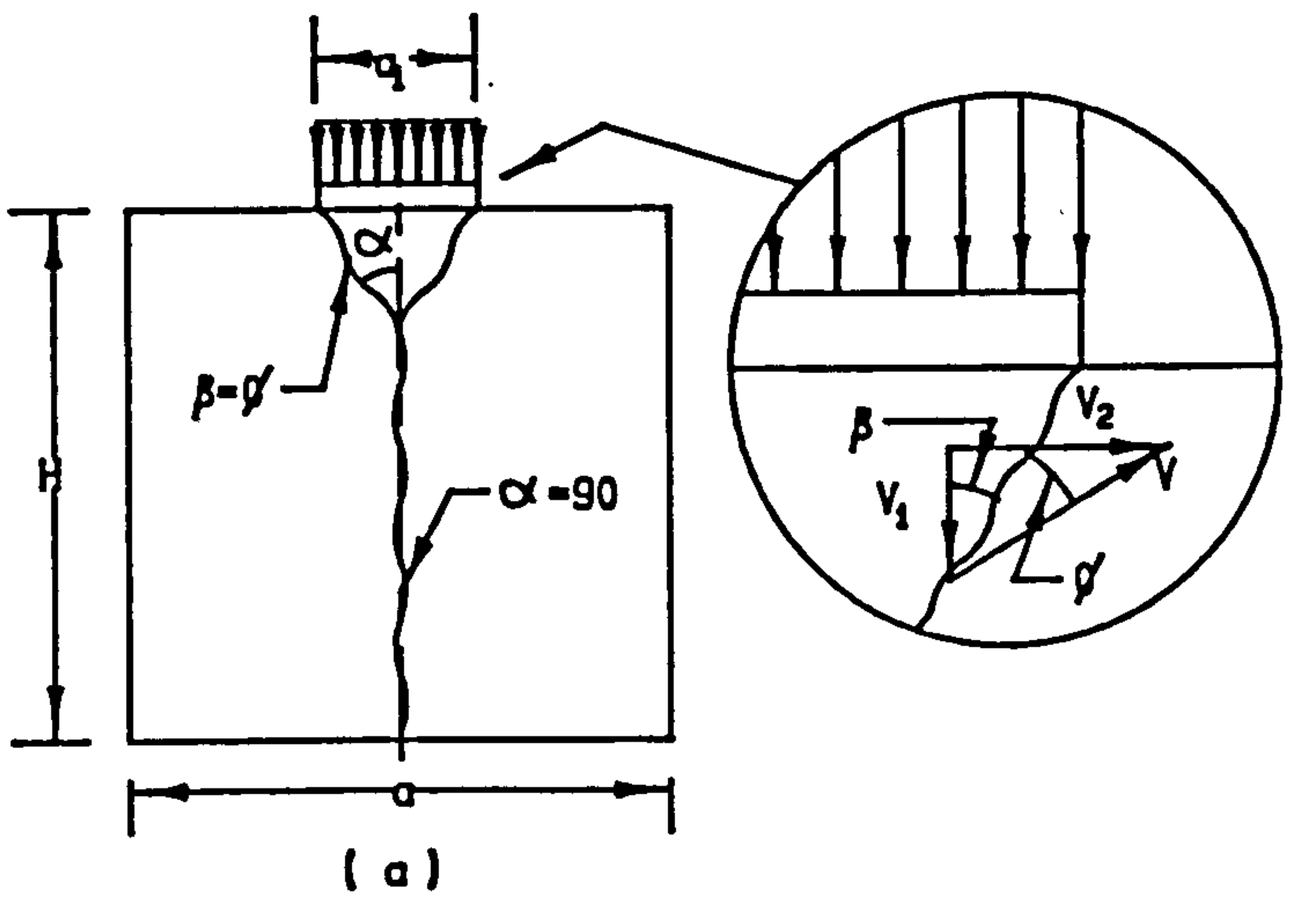

Fig.2.16 Loading condition in plastic analysis.

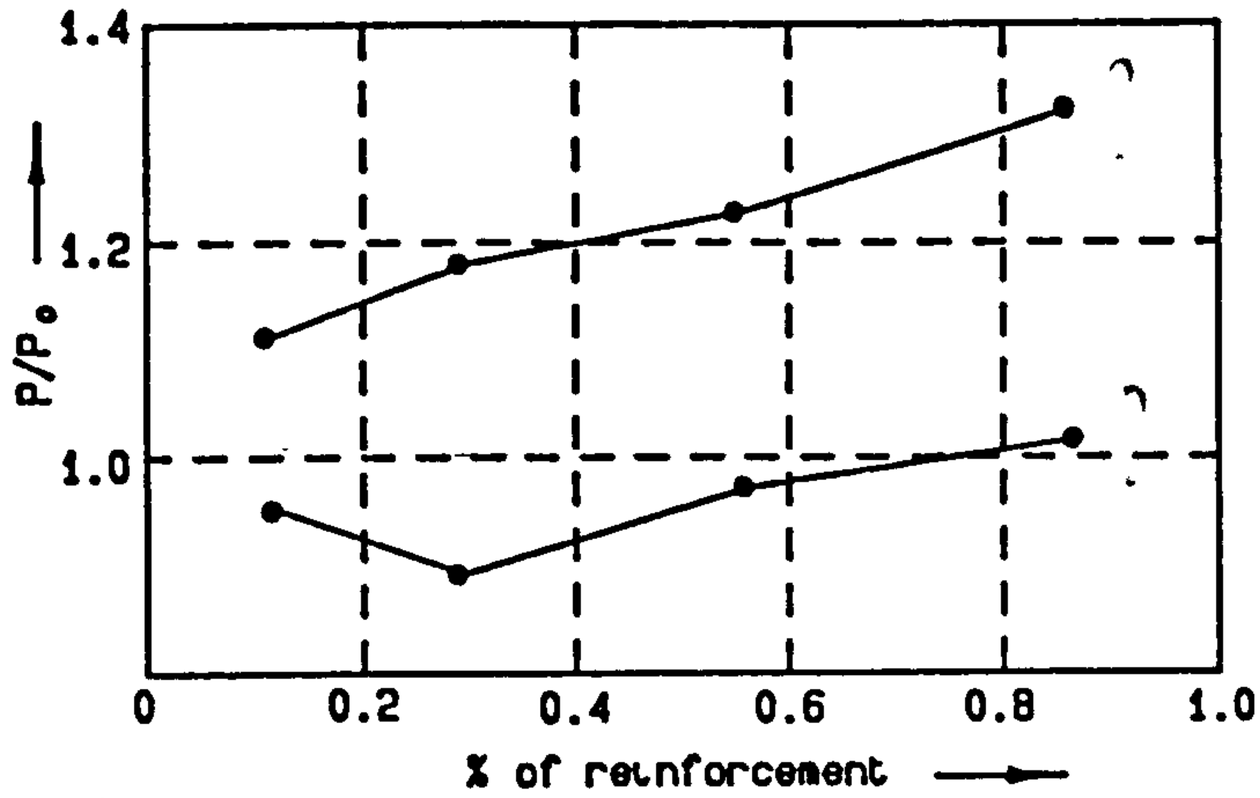

Fig.2.17 Effect of reinforcement on bearing strength, Muguruma.

cylinder strength f_c of concrete.

For the purpose of obtaining the effects of spiral reinforcement on the bearing capacity of concrete block, concentrated loading tests on the 200mm cube specimens having different percentages of spiral reinforcement were tested by Muguruma [62]. The ultimate bearing capacity became larger with increase of spiral diameter of reinforcement but there was no obvious increase in the initial cracking load. However, when the loading area A' became smaller in comparison with the concrete sectional area A'' inside the spiral reinforcement little increase of bearing capacity was to be expected, because sliding failure would take place or there would be shear failure of the concrete just under the base plate. The ultimate bearing capacity increased in proportion to the percentage of reinforcement as shown in fig.2.17. The use of spiral reinforcement with a smaller diameter of steel was more effective in increasing the ultimate load capacity as well as the initial cracking load. Moreover, circular spiral reinforcement was more effective than square spiral reinforcement to resist bearing and cracking.

Niyogi [67] also performed tests in reinforced concrete blocks. All tests were with 8 in. concrete cubes which were reinforced with either spiral steel or reinforcing mesh. Two spiral sizes were used of large and small diameter extending to full or part depth of the cubes. The numbers of turns for the

spirals were varied. Nominal vertical reinforcement was provided to hold the lateral steel. The percentage of lateral steel for the specimens was calculated on the basis of total volume of the lateral steel against the volume of the cubic specimen. Different types of reinforcement are shown in the diagram below, fig.2.18. It is noted that the cracking strength in general improved with the provision of reinforcement. Large spiral (B,BH) appeared to be more effective against cracking than other forms. Spiral of small diameter (S,SH) did not increase the resistance of the specimens against initial cracking. Cracking loads of specimens with larger bearing plates were influenced to a lesser extent by the provision of reinforcement than with smaller plates. In general, the higher the volumetric percentage of lateral steel the greater was the increase in bearing capacity by reinforcement for a particular ratio R. The increase in the bearing strength was probably the result of the effective spreading of the concentrated load over the concrete. With spiral reinforcement the increase was due to the increase in compressive strength of the confined core of concrete induced by the lateral steel under load. Thus, the bearing strength of spirally reinforced concrete compared to that of plain concrete of similar quality may be expressed as

$$n_{(reinft)}/n_{(plain)} = 1 + K \cdot \rho \qquad (2.34)$$

where ρ = volumetric % of lateral steel,
K may be taken as 55 for all variation of R.

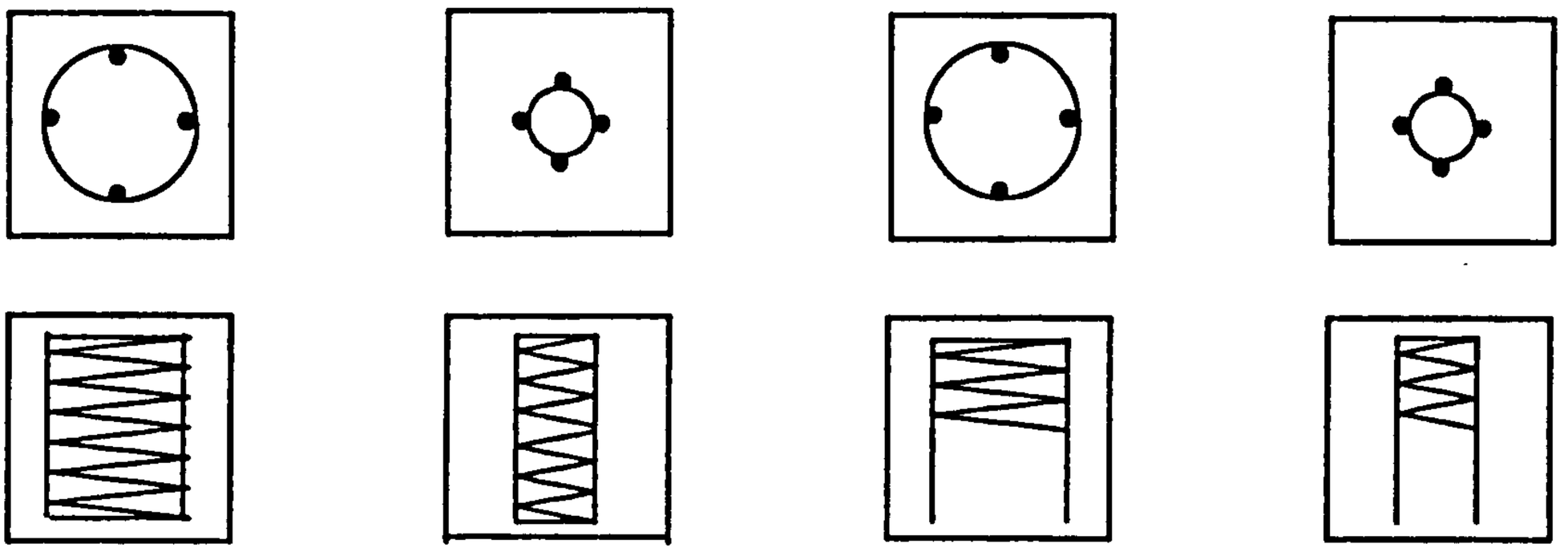

Fig.2.18 Forms of reinforcement tested by Niyogi.

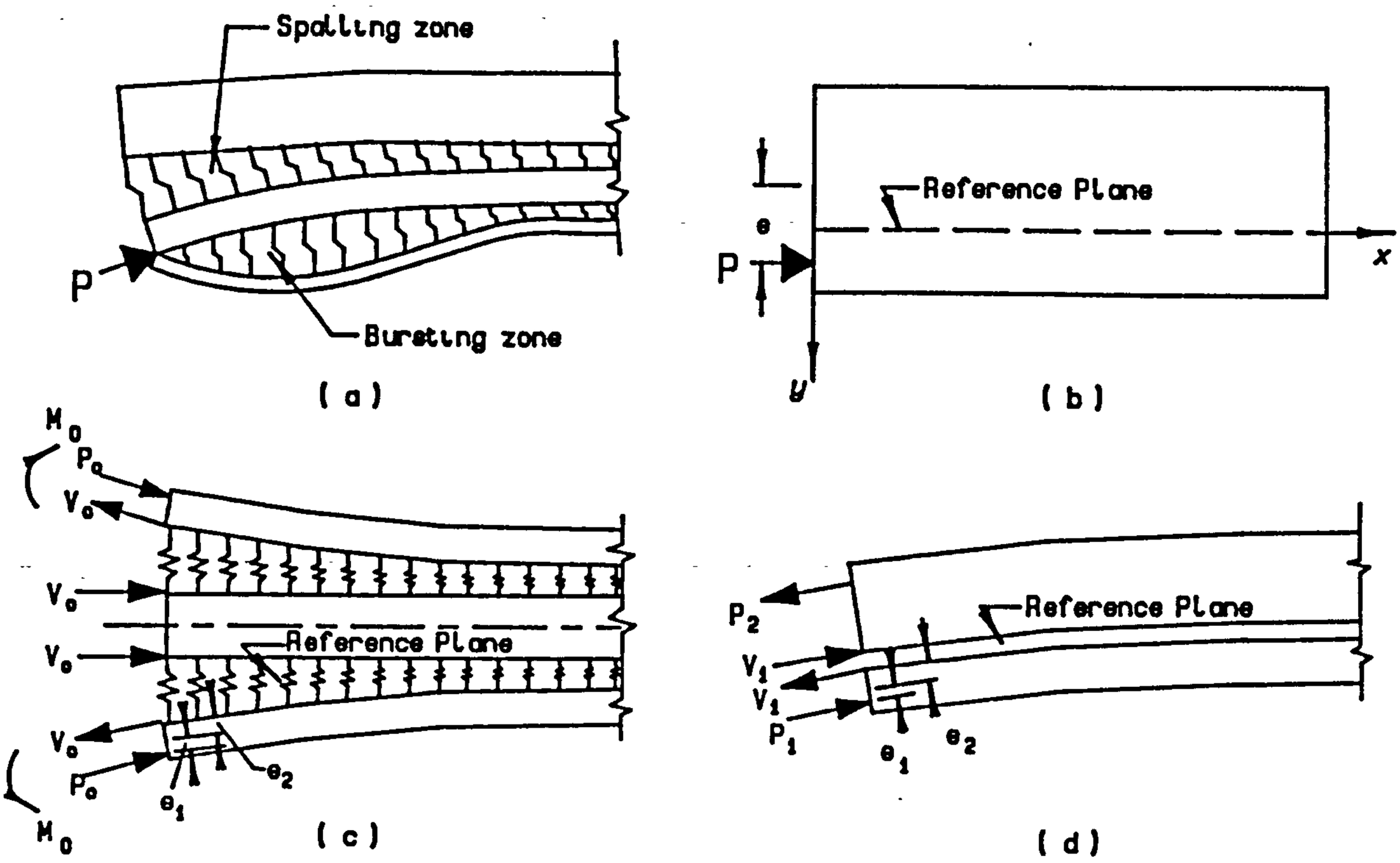

Fig.2.19 Failure mechanism of concrete loading bearing block by Lenshow.

Lenschow [52] proposed a failure mechanism for the concrete block subjected to concentrated load. The distribution of transverse stress in the anchorage zone of a beam subjected to a concentrated load acting parallel to the longitudinal axis is pictured in fig.2.19(a). The deflections of fictitious springs inserted across the longitudinal cuts in the beam were related to the transverse stresses. The transverse tensile stress across the axis of the load was referred to as the 'bursting stress' while the transverse tensile stress across any other longitudinal plane was called the 'spalling stress'. The physical analogue for the anchorage zone of a beam is shown in fig.2.19(b) to (d). The prismatic beam shown in fig.2.19(b) is subjected to a concentrated load P and could be represented by the beams in figs.2.19(c) and (d). Fictitious springs inserted represented the concrete and resisted the deflection of the outer parts of the beam. According to the physical analogue, the maximum spalling stress for a rectangular section is

$$f_s = -2 \cdot \sqrt{6} \cdot M_o / b \cdot h_b^2 \qquad (2.35)$$

and the maximum bursting stress is

$$f_{bc} = M_o / b \cdot h_b^2 \qquad (2.36)$$

The force of a single concentration of transverse reinforcement at the surface of the spalling zone with tensile strength of the concrete neglected was expressed as

$$F_o = -M_o \left[\frac{1}{9E_c \cdot I_b \cdot \gamma / A_b \cdot G - 3W/M_o} \right] \qquad (2.37)$$

where E_c = Young Modulus of concrete,
I_b = Second moment of inertia of the section below the reference plane,
A_b = Sectional area below the reference plane,
h_b = depth of the section below the reference plane.

The effect of the concrete tensile strength can be recognized by modifying F_o as

$$F_1 = F_o \left[1 - E_c \cdot I_b / K \cdot (b \cdot f_t / M_o)^2 \right] \qquad (2.38)$$

The effect of transverse reinforcement on the bursting crack varies drastically with the position of the reinforcement. It is advisable to use light stirrups at close spacing. The force in the reinforcement in terms of force per unit length f_o, can be expressed as

$$f_o = M_o (1 - f_t / f_b) / h_b^2 \qquad (2.39)$$

Jensen [36] has considered the problem of an upper bound plastic solution using a failure mechanism. This type of failure is frequently observed in lightly reinforced blocks and known as splitting failure. He made a number of tests on 200 x 200 x 400 mm blocks with reinforcement perpendicular to the direction of the load as in fig.2.20. A sliding failure occurred along the sides of the wedge and a separation failure along the vertical line. By considering the external work done

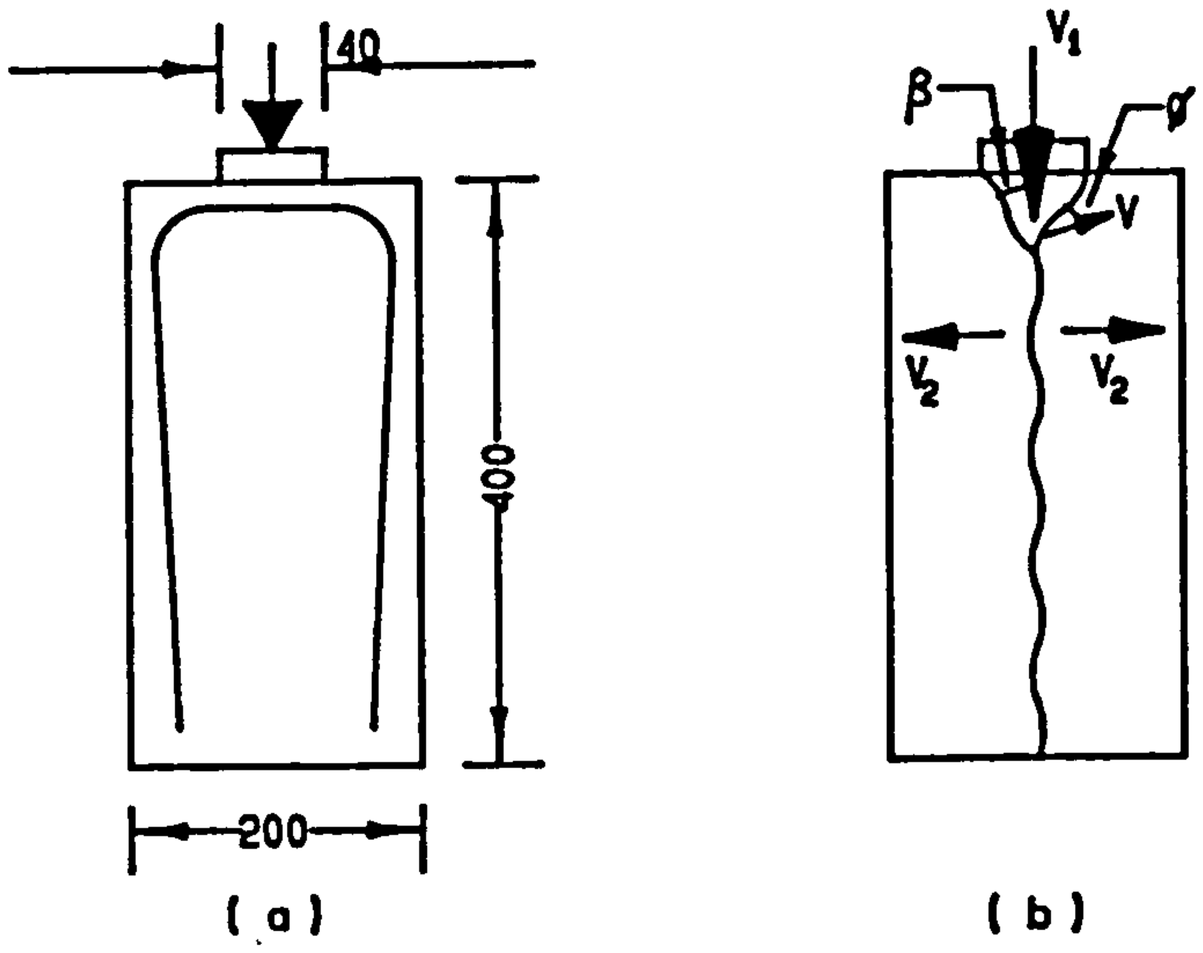

Fig.2.20 Sliding and separation failure mechanism by Jensen.

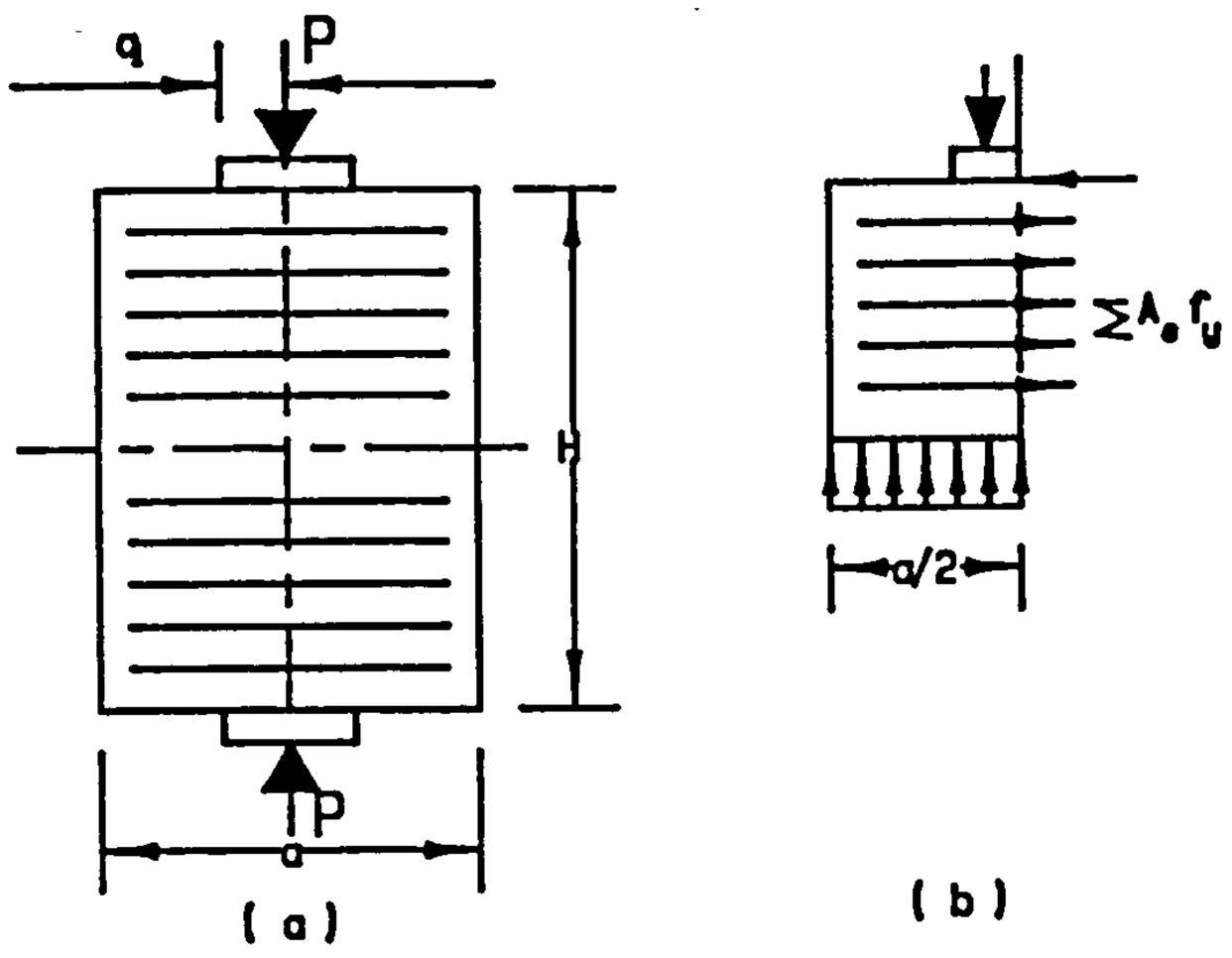

Fig.2.21 Nielsen's failure mechanism for reinforced concrete blocks.

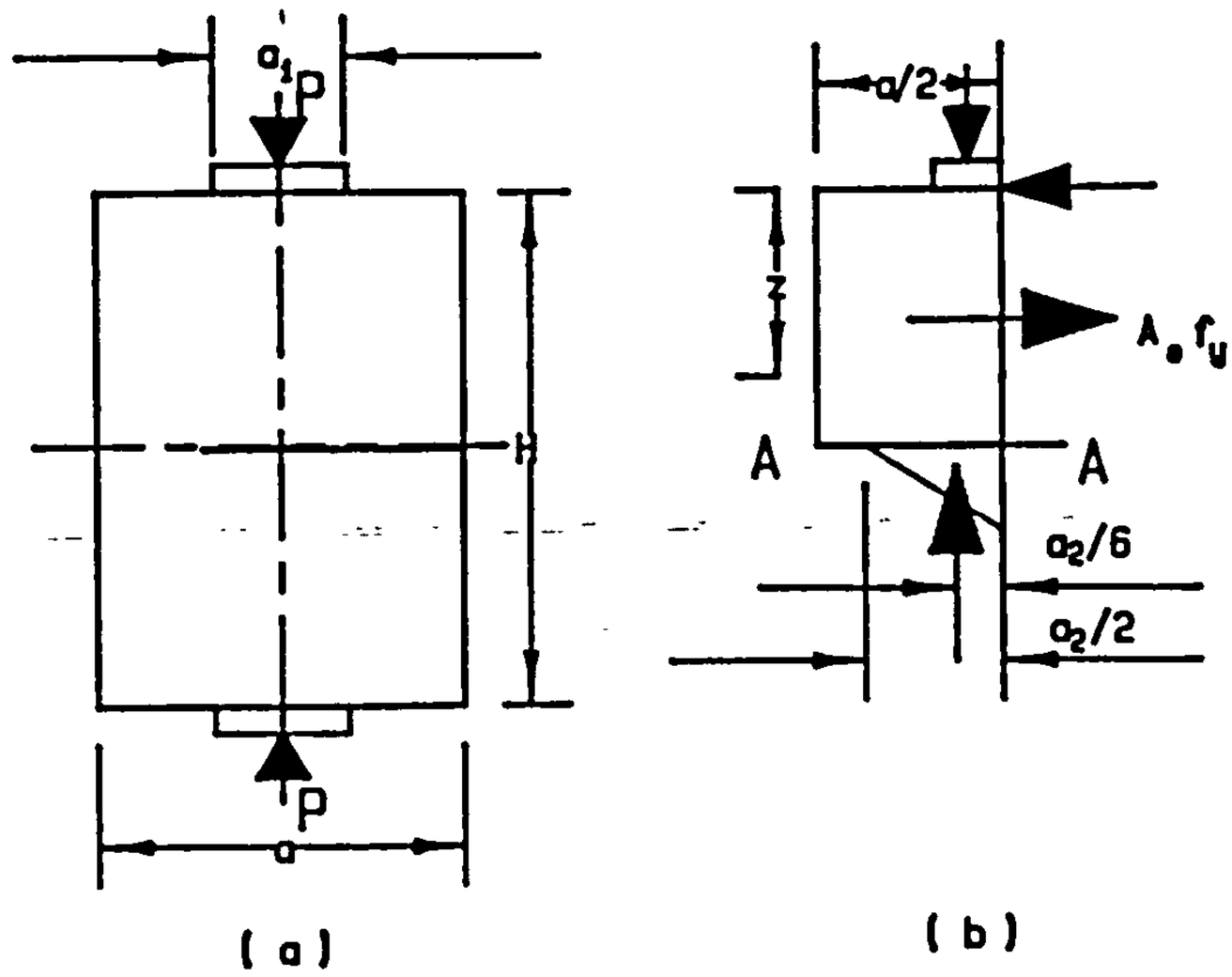

Fig.2.22 Al-Najjim's failure mechanism for reinforced concrete blocks.

by the load and the internal work by the concrete and reinforcement, the bearing capacity of the reinforced block could be expressed in terms of the degree of reinforcement Φ and the angle of internal friction ψ as

$$\frac{f_b}{f_c'} = \frac{4\cdot\Phi\cdot\sin(\beta+\psi)\cdot\sin\beta + (1-\sin\psi)}{2\cos(\beta+\psi)\cdot\sin\beta} \qquad (2.40)$$

where

$$\tan\beta = \frac{[1 + 4\cdot\Phi\cdot\cos\psi/(1-\sin\psi) - \sin\psi]^{0.5}}{4\cdot\Phi/(1-\sin\psi) + \cos\psi} \qquad (2.41)$$

For high Φ the above equation can be estimated by a straight line

$$f_b/f_c' = 2.6\cdot\Phi + 1.2 \qquad (2.42)$$

Nielsen [64] considered the rotational equilibrium of a quarter block acted on by vertical load and uniformly distributed reaction at mid-height of the original block, and maintained in equilibrium by horizontal compression near the load and tensile forces in the transverse steel as in fig.2.21. It can be calculated that the ultimate load can be expressed as

$$P_u = t\cdot b_1\cdot h_1/(a-a_1)^2 \quad \text{where} \quad t = 2A_s\cdot f_y/b_1\cdot h_1 \qquad (2.43)$$

He concluded that with the light reinforcement provided, the carrying capacity depended on the compressive strength and not the tensile strength of the concrete.

Al-Nijjam [63] proposed a model based on Nielsen's model with some modifications. Fig.2.22(b) shows the state of

internal forces assumed as an equilibrium system with the vertical load at the top and a triangular stress distribution on AA at mid-height of the original block, instead of the uniform distribution stress proposed by Nielsen. When the block was heavily reinforced, an upper limit of the bearing capacity could be expressed as

$$f_b/f'_c = (a/a_1)^{1/3} \qquad (2.44)$$

When the reinforcement was lighter, the equilibrium conditions of fig.2.22(b) could be maintained with $a_2<a$ and for these cases the bearing capacity could be related to the reduced dimensions

$$f_b/f'_c = (a/a_2)^{1/3} \qquad (2.45)$$

Referring to fig.2.22.

$$\cot\theta = e/z = (a_2/6-a_1/4)/z \qquad (2.46)$$

and also $$\cot\theta = 2A_s \cdot f_y/P_u \qquad (2.47)$$

Equating these, $$a_2 = 12z \cdot A_s \cdot f_y/P_u + 3a_1/2 \qquad (2.48)$$

By substituting in Eq.2.45

$$f_b/f'_c = \left[12z \cdot A_s \cdot f_y/(a_1^2 \cdot b_1 \cdot f_b) + 3/2\right]^{1/3} \qquad (2.49)$$

Therefore the bearing capacity can be expressed in form of a 4th degree polynomial.

$$(f_b/f'_c)^4 - 3f_b/2f'_c = \Phi(12z/a_1) \qquad (2.50)$$

with the limitation $$f_b/f'_c < [a/a_1]^{1/3} \qquad (2.51)$$

It is noted that the influence of reinforcement at a distance

greater than a/2 from a load is very small and may be neglected from the calculation.

Tests by Kriz [49] were made of 185 reinforced columns subjected to loads distributed across their width through steel bearing plates. The specimens were divided into seven groups with different forms of reinforcement.

Group I ——Specimens were reinforced with 4 no.5 bars of intermediate grade. The vertical reinforcement was tied with no.2 ties spaced 8 ins. centre to centre. The lateral reinforcement at the top of the column consisted of a welded grill with two cross bar and 2,3,4 or 5 lateral bars as shown in fig.2.23(a).

Group II ——Vertical colum reinforcement consisted of 4 no.11 bars with f_y = 90,000psi.

Group III —Ties were omitted.

Group IV ——Both vertical column reinforcement and ties were omitted.

Group V ——Two to three layer of lateral reinforcement were provided with spacing of 2 ins., fig.2.23(b).

Group VI ——Ties and bars are bent as in fig.2.23(c).

Group VII —Specimens were reinforced laterally by 5 no.4 deformed bars welded to two bearing plate as in fig.2.23(d).

Specimens with bearing plates at the edge of the column failed along an inclined plane similar to those observed in plain concrete specimens. Group II to VI failed by crushing of concrete under the bearing plates. The modifications made in the reinforcement in group II and VI had only a small effect on the behaviour of the specimen. Omitting of ties or vertical

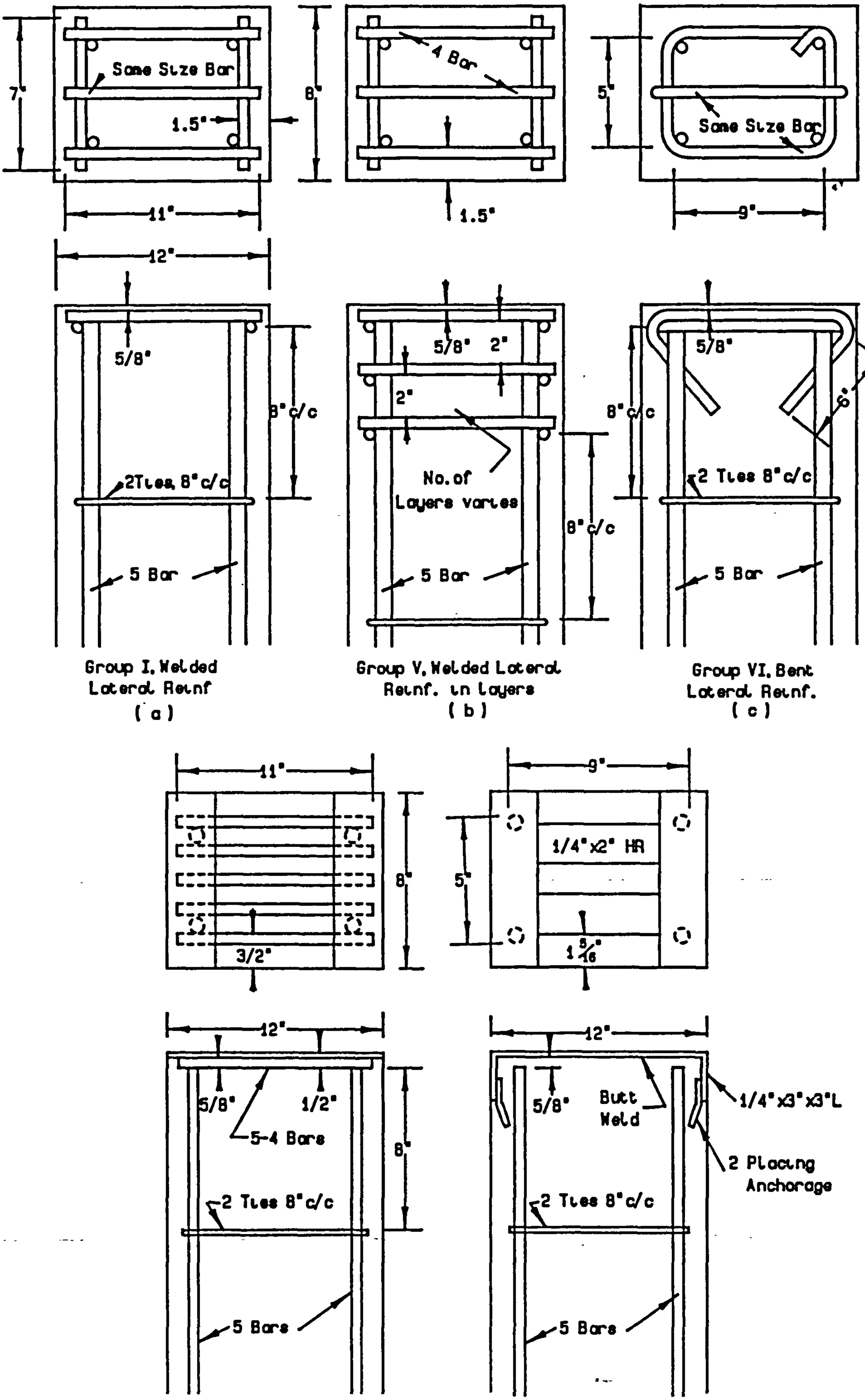

Group I. Welded Lateral Reinf (a)

Group V. Welded Lateral Reinf. in Layers (b)

Group VI. Bent Lateral Reinf. (c)

Group VII Lateral Reinft. Welded to plates (d)

Group VIII Welded Angle & Flat Bar Lateral Reinft. (e)

Fig.2.23 Forms of reinforcement tested by Kriz.

bars resulted in increased propagation of cracks, while additional layers of lateral reinforcement contained the cracking in the top of the columns. The lateral reinforcement apparently had no effect on the bearing strength when the edge distance was less than 40 mm. Empirical formulae were derived from the tests to be

$$f_b = 5.73 f_c'^{0.5} \cdot (W_a/a_1)^{1/3} \cdot [1+0.198 C_1 (A_{sl}/b)^{H/V}](1/16) \quad (2.52)$$

where

$$C_1 = \begin{cases} 0 & \text{..... } W_a < 40\text{mm.} \\ 2.5 & \text{..... } W_a > 40\text{mm.} \end{cases}$$

H = Horizontal force,
V = Vertical force,
A_{sl} = Cross-section area of lateral steel.

This agreed with the experimental results with a slight under-estimation.

2.4 SUMMARY

(1) Magnel [55,56] found that the stress distribution of an anchorage block in the direction of the anchorage force was as shown in fig.2.2b.

(2) Bortsch [81] assumed a cosine function of load distribution on the loading plate and found that the maximum transverse tensile stress occurred at a distance of 0.2 to 0.3a from the loading surface. Tensile stress

gradually diminished further away from the loading plate.

(3) Guyon [26,27] made use of Fourier series to obtain a stress distribution of the anchorage zone as shown in fig.2.5a. He also constructed six tables for the calculation of stress under different loading conditions.

(4) Bleich [82] used Airy stress functions to find the distribution of anchorage stress in fig.2.7. By introducing an apparent width (Eq.2.3), Sievers modified Bleich's two-dimensional solution for three-dimensional used.

(5) Based on the shear strength of concrete, Eq.2.4 and the assumption of uniform distributed horizontal splitting pressure along the wedge, Meyerhof [59] and Tung Au [6,7] worked out their failure model of reinforced concrete bearing blocks (Eqs.2.7 and 2.10 respectively). Meyerhof stated that experimental bearing strength was greater than theoretical estimates, especially in blocks with small H/a ratios, due to the presence of base friction which had been neglected in the analysis. From his calculations, bearing capacity is directly proportional to height/width ratio, however tests carried out by Muguruma and Niyogi indicated the opposite result; this is probably due to the non-uniform distribution of tensile stress P_h.

(6) Tung Au's [6,7] formula only gives approximate bearing

strength of concrete blocks, because of the variation of α.

(7) A Dual failure mode of tensile separation and shear sliding was adopted by Hawkins [30-32]. Bearing strengths of concrete block can be estimated by Eq.2.16.

(8) Empirical solutions were used by Shelson [76], Kriz [49], Muguruma [62] and Niyogi [65,66]. Muguruma's formula is the only one which takes account of the height of the specimens.

(9) Plastic analysis can be used to find the bearing strength of concrete by equating the internal energy and external work, Eqs.2.32 and 2.33.

(10) Shizuo Ban [9] and Niyogi [65-67] stated that spiral reinforcement is the most effective way to increase the bearing capacity of concrete blocks.

(11) Myguruma [62] suggested that spiral reinforcement with smaller diameter of steel and with comparable area inside the reinforcement to the loading area is an effective way to improve bearing capacity.

(12) Lenschow [52] proposed a failure mechanism for concrete blocks subjected to concentrated load and arrived at a solution for the maximum spalling and bursting stresses to be calculated by Eqs.2.35 and 2.36 respectively. Forces

on the transverse reinforcement are given by Eqs.2.37 and 2.38.

(13) Nielson [64] and Al-Nijjam [63] proposed a model based on the equilibrium of internal stresses in the bearing blocks.

(14) Kriz's [49] empirical solution (Eq.2.52) is based on the tests of a large number of specimens with different forms and amount of reinforcement.

3 EXPERIMENTAL INVESTIGATION OF THE BEARING CAPACITY OF CONCRETE BLOCKS

3.1 INTRODUCTION

In this investigation, an attempt has been made to study experimentally the factors affecting the bearing capacity of concrete blocks. Experiments comprised two phases; plain and reinforced concrete blocks.

3.2 PLAIN CONCRETE BLOCKS

The bearing capacity of plain concrete blocks is mainly dependent on:

(1) The distance of the load to the nearest edge of the block (edge distance, W_a),
(2) The ratio of the footing area to the loaded area, R,
(3) The height to width ratio of the blocks, H/a,
(4) Size of the blocks,
(5) Effect of base friction, and
(6) Strength of the concrete.

The effect of the strength of the concrete on the bearing capacity of the blocks was not specially investigated in these experiments. Twenty six concrete blocks were subjected to concentrated load applied over their full breadth by a steel bearing plate. The block tests were divided into four groups. The first (series E) was designed to investigate the effect of edge distance. In the second group (series R-H), specimens

were used to explore the relationships between the ratio R and H/a and the bearing capacity of the blocks. The effects of size and base friction were studied by the third (series S) and the fourth group (series B) respectively.

3.2.1 SERIES E

This series consisted of three blocks with constant dimensions, 100 mm. thickness, 1000 mm. depth, and 1260 mm. overall length. They were placed vertically and loaded with a steel bearing plate of 50.8 mm. width, 100 mm. long, and 50 mm. thick. Each block was loaded twice, once on each edge of the block. Edge distance, W_a varied from 30 to 280 mm.

3.2.2 SERIES R-H

Sixteen blocks with constant width 400 mm. and thickness 100 mm. were cast. Their heights were varied with 200, 400, 800, and 1000 mm., which corresponded to H/a ratios of 0.5, 1.0, 2.0, and 2.5. They were loaded concentrically with 4 different sizes of steel bearing plate across their full breadth. The widths of the bearing plates were 6.35, 25.3, 50.8 and 101.6 mm. which give values of R as 62.99, 15.81, 7.87 and 3.94 respectively.

3.2.3 SERIES S

Concrete blocks of 3 different sizes were included in this series of tests. They varied from 100 mm. to 200 mm. square with corresponding thicknesses from 12.5 to 50 mm. They were loaded concentrically with a bearing plate size from 12.7 to 25.4 mm. so as to give a constant ratio R equal to 7.87. For each size of the specimen, three blocks were tested and the average of their ultimate load was taken.

3.2.4 SERIES B

The effect of the base upon the ultimate bearing strength is believed to depend on (1) the footing to loading area ratio, (2) the height of the blocks. These effects were demonstrated by the testing of 4 blocks. They had constant width, 400 mm. and thickness 100 mm. but with two different heights of 1000 mm. and 200 mm. They were loaded with two sizes of bearing plate 101.6 mm. and 6.35 mm. width. The friction at the base was reduced by using a sheet of 2.4 mm. thick PTFE placed at the bottom of the specimen when it was tested.

3.3 REINFORCED CONCRETE BLOCKS—SERIES R

A series of 8 blocks with dimensions 1260 x 1000 x 100 mm. were cast. They were reinforced at two corners with different

forms of reinforcement. Each corner of the block was loaded separately, with a steel plate 101.6 x 100 x 50 mm., one after the other. Blocks were denoted as R1 to R8 as shown in fig.3.1. In order to distinguish between each end, R1/1 and R1/2 were used to represent block R1 with END 1 and END 2 repestively. A similar arrangement was used for the other 7 blocks.

R1/1, R1/2 and R2/1 were reinforced in such a way as to investigate the effect of the diameter of the stirrups on the bearing capacity of the concrete. R2/2 showed how the block behaved if the reinforcement was placed closer to the surface. R3/1 and R3/2 had almost the same cross-sectional area of steel as in R2/1. They were reinforced with closely spaced thinner steel and were used to study how the spacing of the reinforcement affected the bearing capacity of the blocks. Forms of the stirrups were studied in R4/1 and R4/2. The effect of the spread of reinforcement was investigated by R5/1 and R5/2.

The eccentricity of loading did affect the bearing strength of concrete. For plain concrete, experiments had already been done with blocks E1 to E3. For reinforced concrete, it was investigated by blocks R6 to R8. R8/1 was unreinforced in order to gain an idea of the effectiveness of the reinforcement.

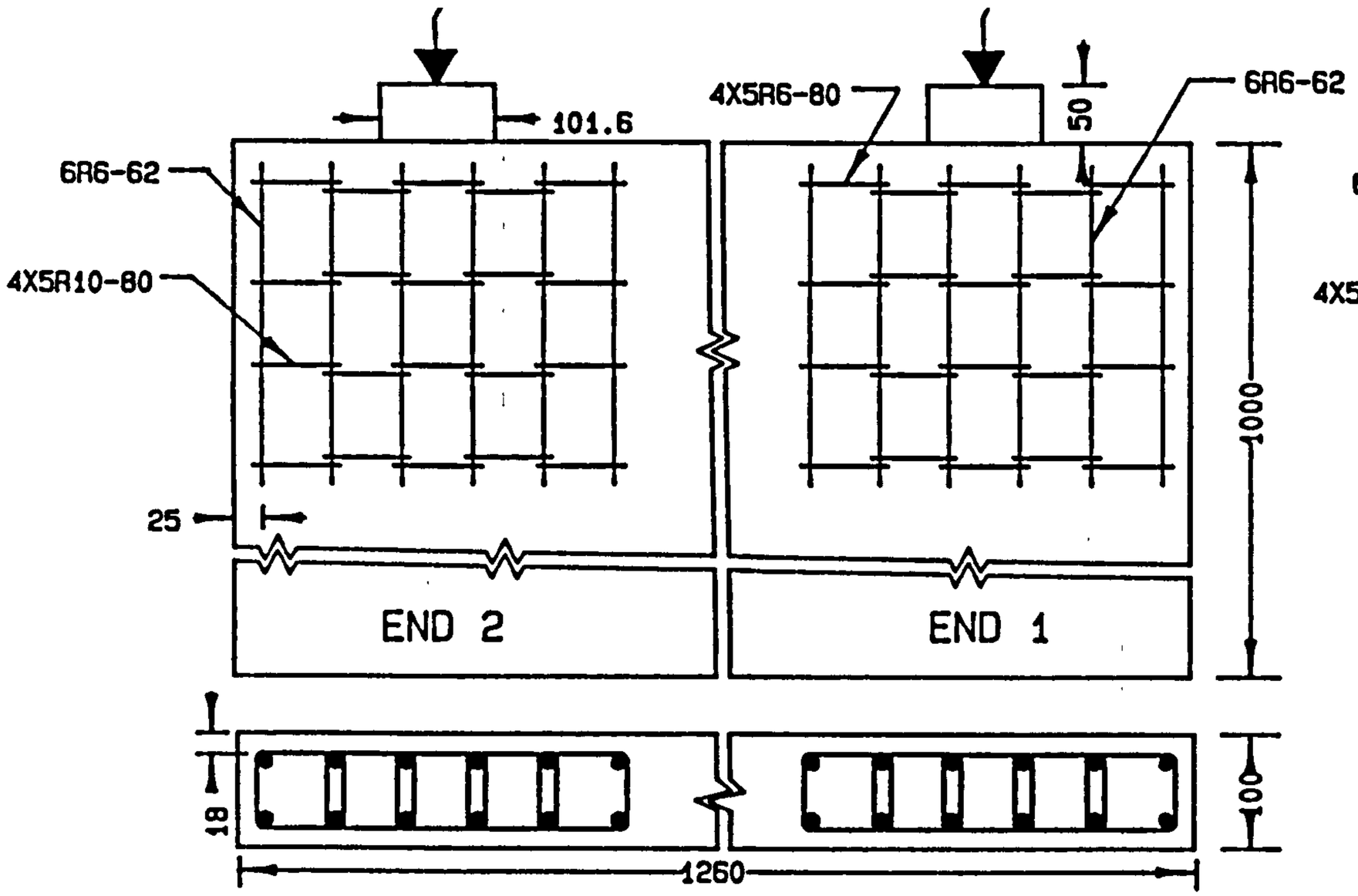

R1

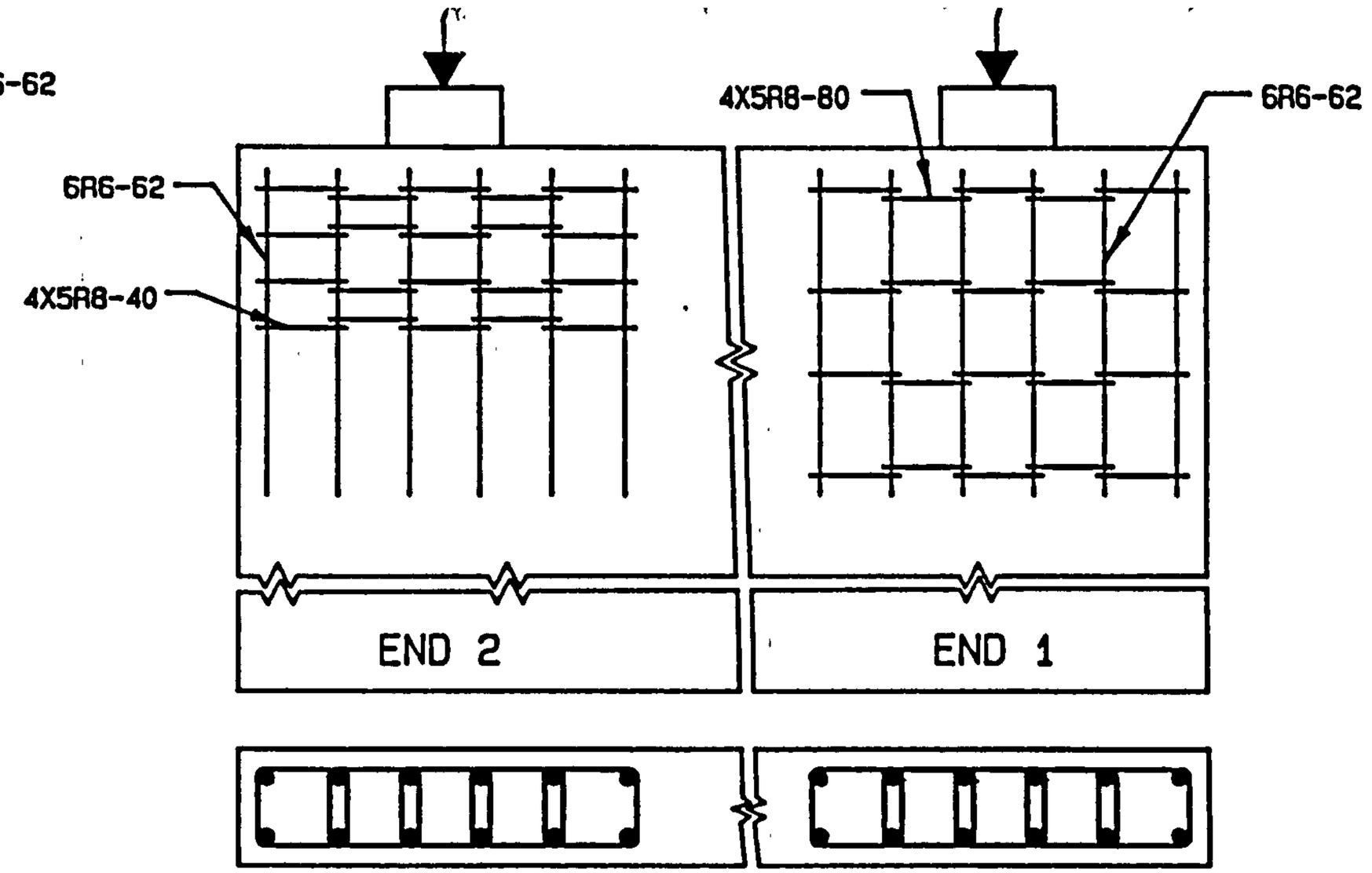

R2

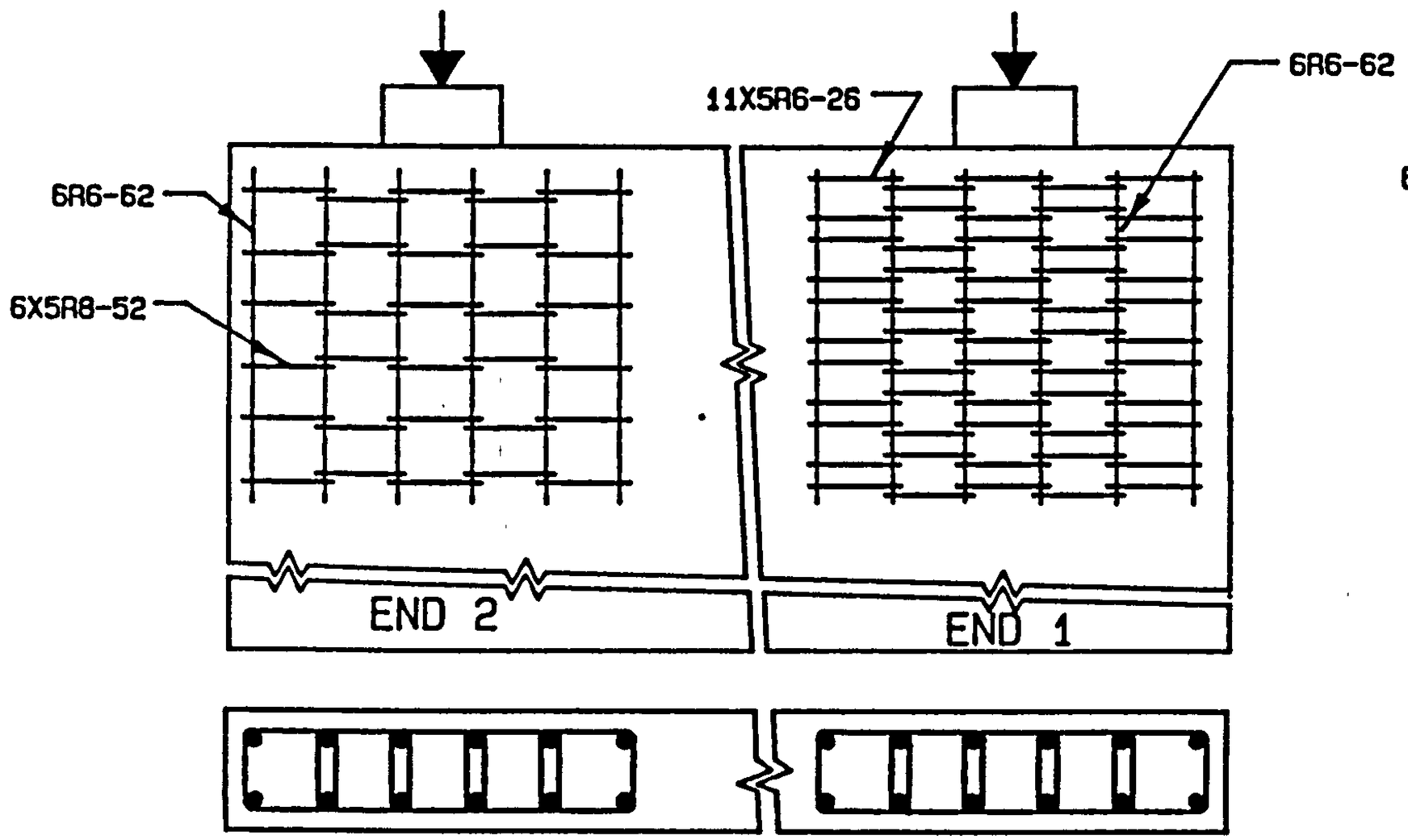

R3

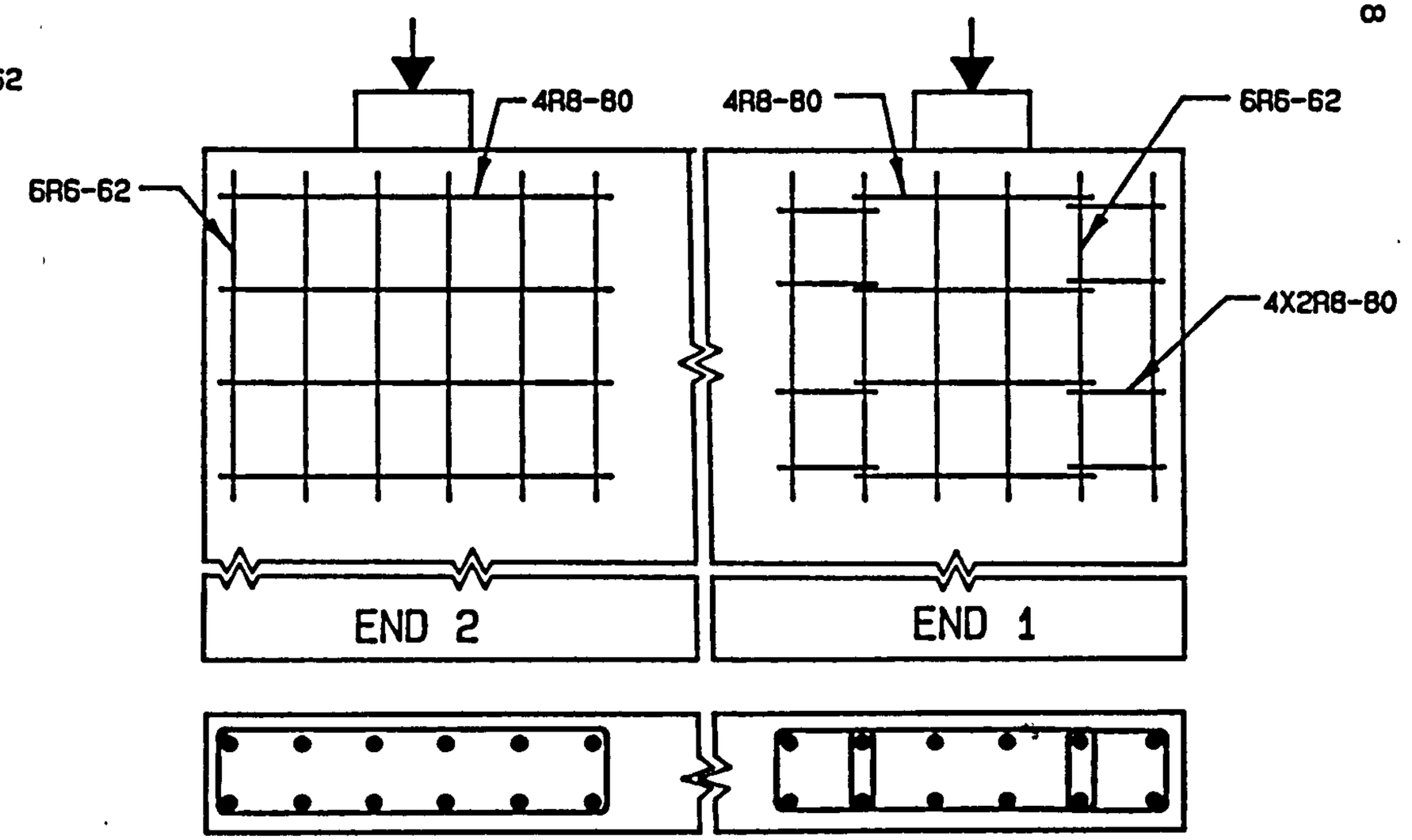

R4

Fig.3.1a. Forms of Reinforcement in Series R.

TEXT BOUND INTO

THE SPINE

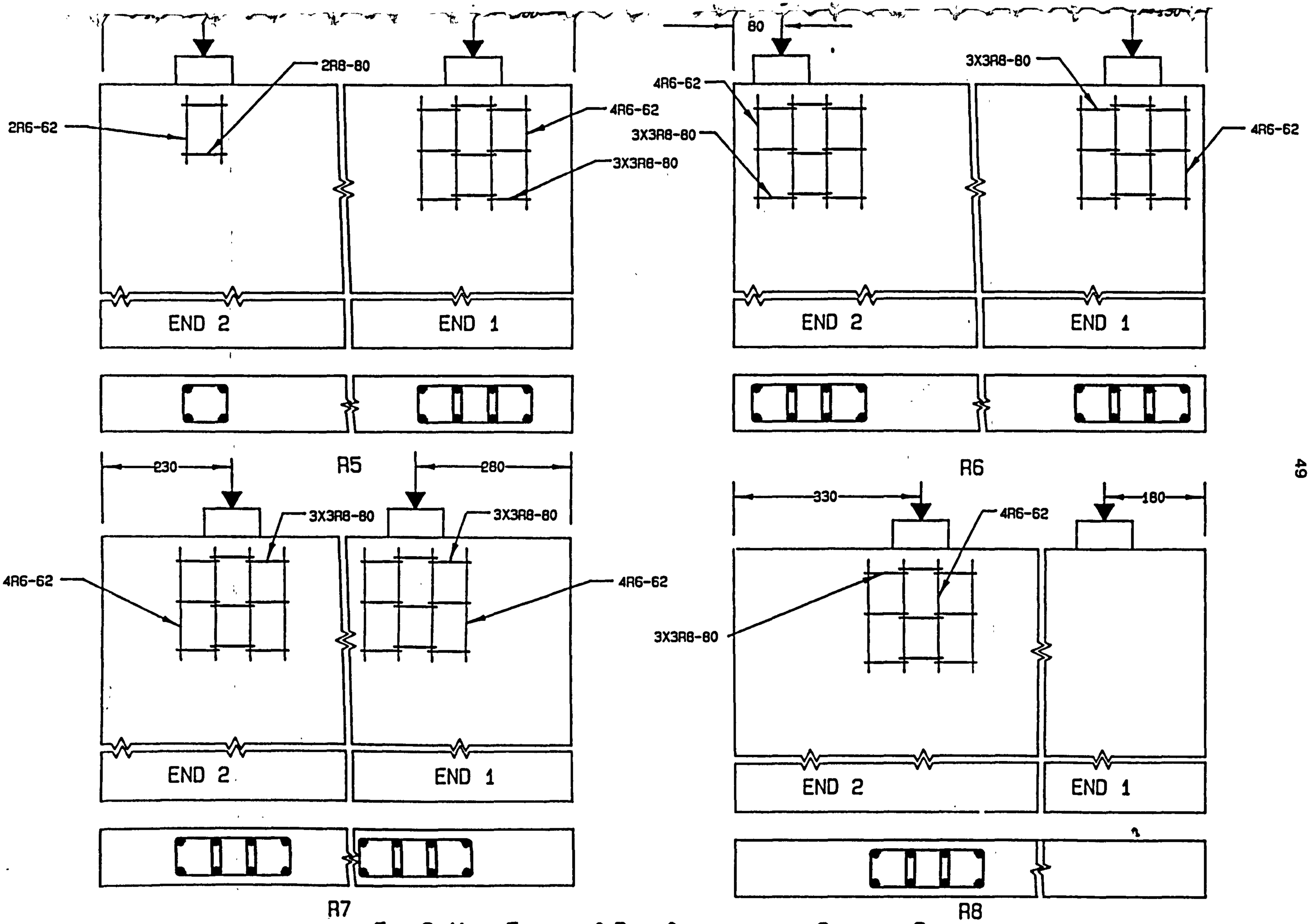

Fig.3.1b. Forms of Reinforcement in Series R.

3.4 MATERIALS & THEIR PROPERTIES

3.4.1 MATERIALS

Cement ——— Ordinary Portland cement conforming to the British Specification was used throughout.

Coarse Aggregate —— North Notts quartzite gravel with a maximum size of 10 mm., 'irregular' shape and 'smooth' surface texture as classified by British Standard, BS 812.

Fine Aggregate ——— Air-dried sand from the same quarry as the coarse aggregate was used. It was classified zone 3 according to BS 882.

The grading curve for the fine and coarse aggregates are shown in Fig.3.2.

Reinforcement ——— Although deformed bars were commonly used in practice, plain round mild steel bars were chosen as their strain can be measured easily and more accurately. If deformed bar is used instead of plain bars, a safer structure will be resulted. A typical stress-strain curve and strength properties are shown in fig.3.3.

3.4.2 MIX DETAIL

The first specimen, E1 was cast using mix proportions by weight 1 : 2.68 : 3.85 with water/cement ratio of 0.65. This gave 20 mm. slump, a V-B time of 4 secs. and a compacting factor value of 0.885. The rest of the specimens were cast using mix proportions by weight 1 : 1.96 : 2.83 with a water/cement ratio of 0.54. Average values of 125 mm. slump,

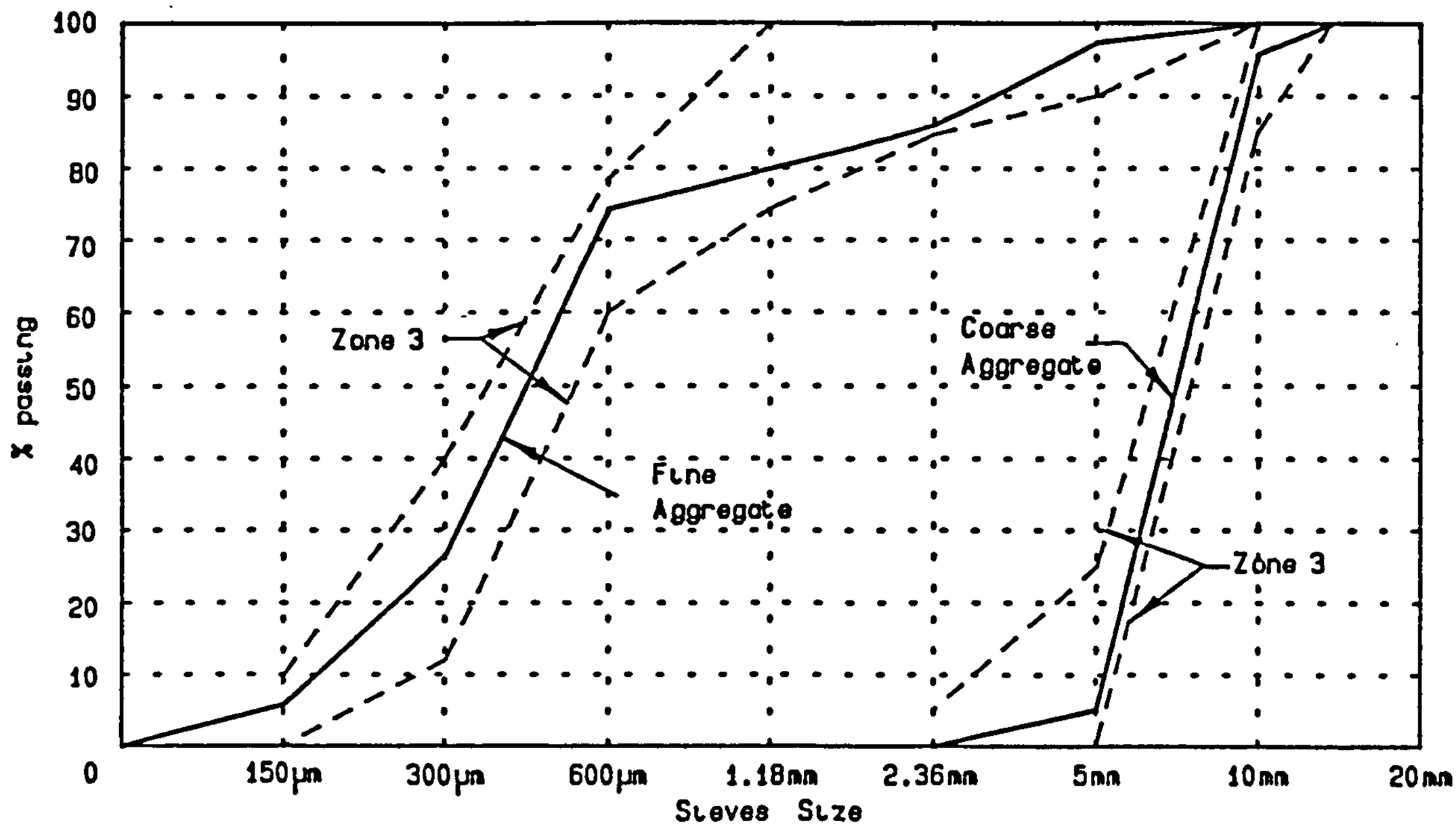

Fig.3.2 Grading curve for fine and coarse aggregates.

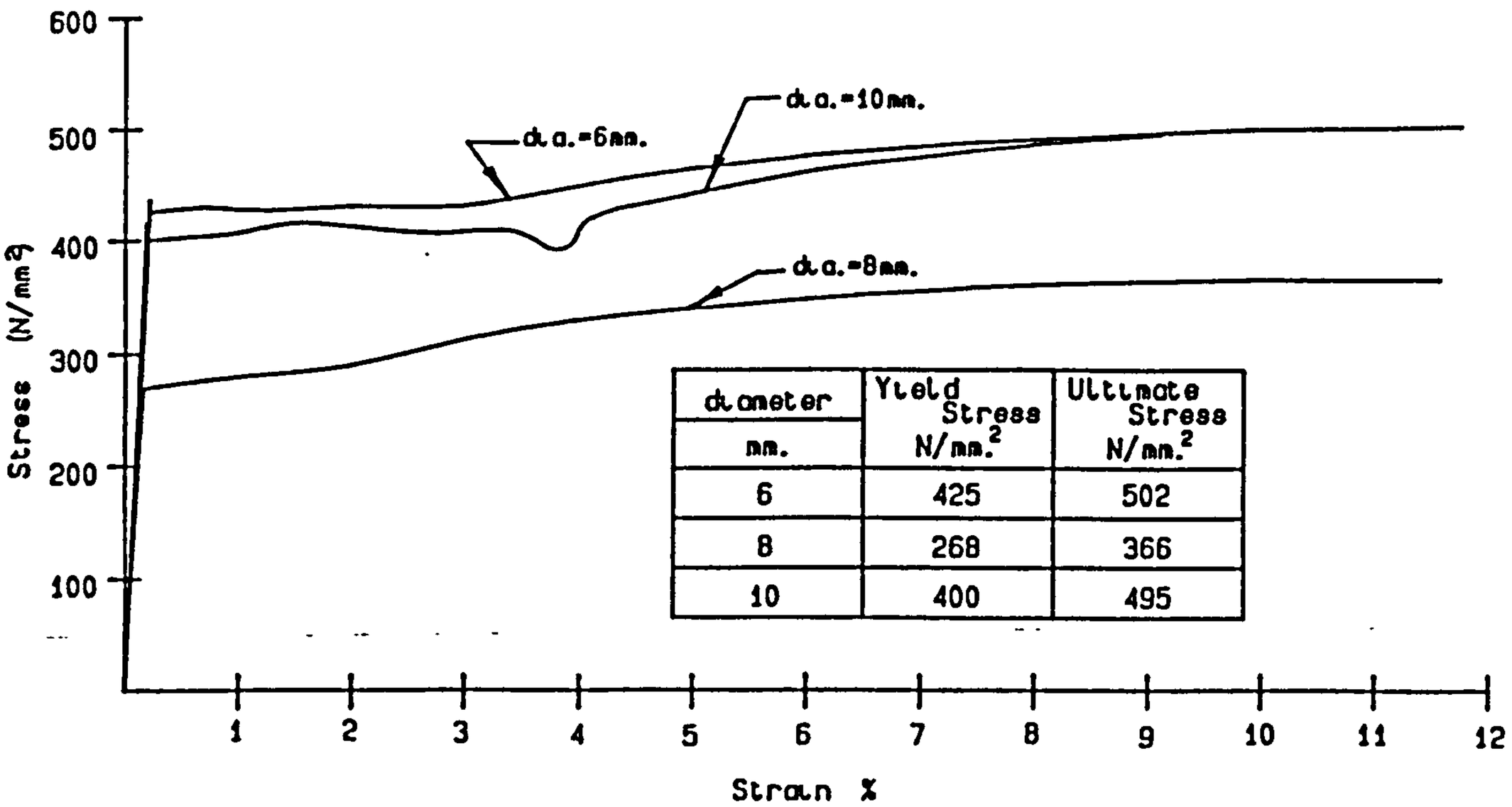

diameter mm.	Yield Stress N/mm.^{2}	Ultimate Stress N/mm.^{2}
6	425	502
8	268	366
10	400	495

Fig.3.3 Stress-strain curve for the reinft.

V-B time less than 1 second and compacting factor of 0.96 were obtained.

3.5 CASTING AND CURING

In order to avoid the variation of strength of concrete along the height of the specimen (Besser 1983, (24)), all the test specimens were cast horizontally. An oiled steel mould 1260 x 1000 x 100 mm. was used throughout. Smaller specimens were obtained by partitioning the mould with wooden blocks which were held firmly by clamps. All the specimens were compacted on a vibrating table.

Control specimens were cast with each mix and also compacted on a vibrating table. They were stripped from the moulds and placed in the curing room at 20 degs. C., relative humidity of 95-100 percent, 24 hours after casting. The test specimens were covered with damp hessian for 3 days, watered constantly and then transferred to the curing room.

3.6 CONTROL SPECIMENS

Control specimens consisted of five 100 mm cubes, five 150 mm. cubes, six 300 x 150 mm. cylinders and three 100 x 100 x 500 mm. prisms. Compressive strength of concrete was provided by 100 mm. cubes, 150 mm. cubes and three

cylinders while the tensile strength of concrete was given by splitting tests of the three cylinders and rupture tests of two prisms. One of the prisms was also used to obtain the Young's Modulus and Poisson's ratio of the concrete. The concrete properties of each specimens are listed in Table.3.1

In order to have a better indication of the strength of concrete in the test specimens from tests on the control specimens, the same procedure was applied for casting and curing on both. The control tests were made at the time when the relevant blocks were tested.

Control specimens were tested in accordance with BS 1881.

3.7 INSTRUMENTS AND TEST PROCEDURE

Strains on the surface of the concrete were measured by Demec gauges. For specimens in series E, in order to obtain the local strain around the compression zone of the test blocks, Demec gauges with 50 mm. gauge length were used and they were more concentrated under the bearing plate. At each position, 6 Demec points were fixed to create a rectangular rosette of 45 degrees.

For test specimens in series R-H, S and B, only the transverse strain along the line of loading and the compressive stains at mid-height of the specimen were measured. In

Spec. no.	Spec. Dimension a	b	h	Bearing Size a_1	Edge Distance Wa	Reinft.	Compressive Strength			Tensile Strength		E-Mod.	Poisson Ratio	Crack Load P_c	Ult. Load P_u	f_b / f_c
						Asl.	$f_{cu\ (100)}$	$f_{cu\ (150)}$	f_c	$f_{t\ (cyl)}$	$f_{t\ (prl)}$	E	ν			
	mm.	mm.	mm.	mm.	mm.	mm^2	N/mm^2	N/mm^2	N/mm^2	N/mm^2	N/mm^2	kN/mm^2		kN	kN	ratio
Series E																
E1/1	1260	100	1000	50.8	80	-	40.6	45.7	41.1	3.28	6.04	35.3	0.161	-	270	1.29
E1/2	1260	100	1000	50.8	230	-	40.6	45.7	41.1	3.28	6.04	35.3	0.161	-	350	1.68
E2/2	1260	100	1000	50.8	130	-	49.1	46.2	34.9	2.99	3.82	29.5	0.146	-	260	1.47
E2/2	1260	100	1000	50.8	180	-	-	44.1	37.2	3.05	3.82	31.6	0.146	-	300	1.59
E3/1	1260	100	1000	50.8	280	-	61.0	51.9	40.9	3.49	4.67	32.1	0.167	-	380	1.83
E3/2	1260	100	1000	50.8	30	-	57.8	47.5	39.4	3.30	4.41	31.7	0.151	-	166	0.83
Series R-H																
R1-H1	400	100	1000	101.6	200	-	52.0	47.2	36.7	3.05	3.66	31.4	0.144	-	433	1.16
R1-H2	400	100	800	101.6	200	-	66.2	58.7	39.7	3.36	3.86	33.0	0.171	-	512	1.27
R1-H3	400	100	400	101.6	200	-	53.8	51.0	39.2	3.24	3.78	31.7	0.179	-	525	1.32
R1-H4	400	100	200	101.6	200	-	63.7	57.3	44.9	3.88	5.53	33.3	0.152	550 B	762	1.67
R2-H1	400	100	1000	50.8	200	-	45.0	45.0	36.5	2.68	4.01	28.1	0.169	-	322	1.73
R2-H2	400	100	800	50.8	200	-	59.0	55.7	42.9	3.26	3.93	32.6	0.177	-	370	1.70
R2-H3	400	100	400	50.8	200	-	53.8	51.0	39.2	3.24	3.78	31.7	0.179	250 T	350	1.76
R2-H4	400	100	200	50.8	200	-	63.7	57.3	44.9	3.88	5.53	33.3	0.152	300 B	535	2.34
R3-H1	400	100	1000	25.3	200	-	44.8	44.3	36.9	3.11	4.37	28.1	0.169	-	245	2.62
R3-H2	400	100	800	25.3	200	-	59.0	55.7	42.9	3.26	3.93	32.6	0.177	-	293	2.70
R3-H3	400	100	400	25.3	200	-	53.8	51.0	39.2	3.24	3.78	31.7	0.179	225 T	300	3.03
R3-H4	400	100	200	25.3	200	-	57.5	54.7	42.3	3.11	5.53	33.3	0.152	180 B	328	3.06
R4-H1	400	100	1000	6.35	200	-	52.0	47.2	36.7	3.05	3.66	31.4	0.144	-	145	6.22
R4-H2	400	100	800	6.35	200	-	66.2	58.7	39.8	3.36	3.86	33.0	0.171	-	168	6.66
R4-H3	400	100	400	6.35	200	-	53.8	51.0	39.2	3.24	3.78	31.7	0.179	-	464	6.59
R4-H4	400	100	200	6.35	200	-	57.5	54.7	42.3	3.11	5.53	33.3	0.152	-	226	8.41

Table 3.1a Concrete Properties of the Bearing Capacity Specimens.

Spec. no.	Spec. Dimension			Bearing Size	Edge Distance	Reinft.	Compressive Strength			Tensile Strength		E-Mod.	Poisson Ratio	Crack	Ult.	f_b / f_c
	a	b	h	a_1	Wa	A_{st}	$f_{cu\ (100)}$	$f_{cu\ (150)}$	f_c	$f_{t\ (cyl)}$	$f_{t\ (pri)}$	E	ν	P_c Load	P_u Load	ratio
	mm.	mm.	mm.	mm.	mm.	$mm.^2$	N/mm^2	N/mm^2	N/mm^2	N/mm^2	N/mm^2	kN/mm		kN	kN	
Series S																
S1	200	50	200	25.4	100	-	60.2	57.7	46.9	4.00	4.10	33.0	0.166	-	117	1.97
S2	150	37.5	150	19.05	75	-	60.2	57.7	46.9	4.00	4.10	33.0	0.166	-	71.6	2.14
S3	100	25	100	12.7	50	-	60.2	57.7	46.9	4.00	4.10	33.0	0.166	-	39.4	2.65
Series B																
B1	400	100	200	101.6	200	-	63.7	57.3	44.9	3.88	5.53	33.3	0.152	200	592	1.30
B2	400	100	200	6.35	200	-	57.5	54.7	42.3	3.11	5.53	33.3	0.152	-	200	7.45
B3	400	100	1000	101.6	200	-	59.4	54.7	41.3	3.10	3.85	33.4	0.186	-	411	0.98
B4	400	100	1000	6.35	200	-	59.4	54.7	41.3	3.10	3.85	33.4	0.186	-	150	5.72
Series R																
R1/1	1260	100	1000	101.6	180	226	70.8	58.9	45.3	3.37	6.07	29.4	0.152	550	600	1.30
R1/2	1260	100	1000	101.6	180	628	69.8	63.0	46.6	3.63	6.07	29.4	0.152	400	590	1.25
R2/1	1260	100	1000	101.6	180	402	64.6	58.8	46.0	3.70	4.04	32.1	0.201	450	620	1.33
R2/2	1260	100	1000	101.6	180	402	64.6	58.8	46.0	3.70	4.04	32.1	0.201	400	590	1.26
R3/1	1260	100	1000	101.6	180	622	61.2	53.4	43.4	3.50	4.00	32.8	0.169	650	770	1.75
R3/2	1260	100	1000	101.6	180	603	61.2	53.4	43.4	3.50	4.00	32.8	0.169	520	643	1.46
R4/1	1260	100	1000	101.6	180	402	59.4	57.6	47.0	3.45	4.20	35.3	0.174	550	680	1.42
R4/2	1260	100	1000	101.6	180	402	59.4	57.6	47.0	3.45	4.20	35.3	0.174	600	660	1.38
R5/1	1260	100	1000	101.6	180	301	66.0	61.8	45.9	3.77	4.13	32.5	0.136	620	650	1.39
R5/2	1260	100	1000	101.6	180	301	66.0	61.8	45.9	3.77	4.13	32.5	0.136	600	640	1.37
R6/1	1260	100	1000	101.6	130	301	58.0	53.8	39.5	3.29	4.30	33.0	0.157	450	530	1.32
R6/2	1260	100	1000	101.6	80	301	58.0	53.8	39.5	3.29	4.30	33.0	0.157	400	520	1.30
R7/1	1260	100	1000	101.6	280	301	59.2	57.5	45.3	3.36	4.16	34.6	0.173	-	750	1.63
R7/2	1260	100	1000	101.6	230	301	59.2	57.5	45.3	3.36	4.16	34.6	0.173	700	720	1.56
R8/1	1260	100	1000	101.6	180	-	66.1	60.4	46.3	3.29	4.48	36.5	0.173	-	550	1.17
R8/2	1260	100	1000	101.6	330	301	66.1	60.4	46.3	3.29	4.48	36.5	0.173	-	820	1.74

Table 3.1b Concrete Properties of the Bearing Capacity Specimens.

general, a 50 mm. gauge length was used for the transverse strain while a 100 mm. gauge length was used for vertical strain.

For reinforced blocks, strain of the steel was measured by electrical resistance gauges and recorded by a data-logger, while strain on the concrete surface was measured by Demec gauges. Load was increased in 50kN increments and at each stage of loading, cracks were observed by means of a hand magnifying glass and marked with ink.

When the specimen was ready for test, it was taken out from the curing room and a thin coat of white emulsion was painted on the surface after it had dried. Demec points were fixed into position. A layer of plaster of paris was introduced in the bottom of the specimen and between the bearing plate and concrete. These allowed a good contact area between steel and concrete. The specimen was then checked for position vertically and loads were applied in steps of 50 or 100 KN. Strain measurements were made at each increment of load. The mechanism of loading is shown in Fig.3.4.

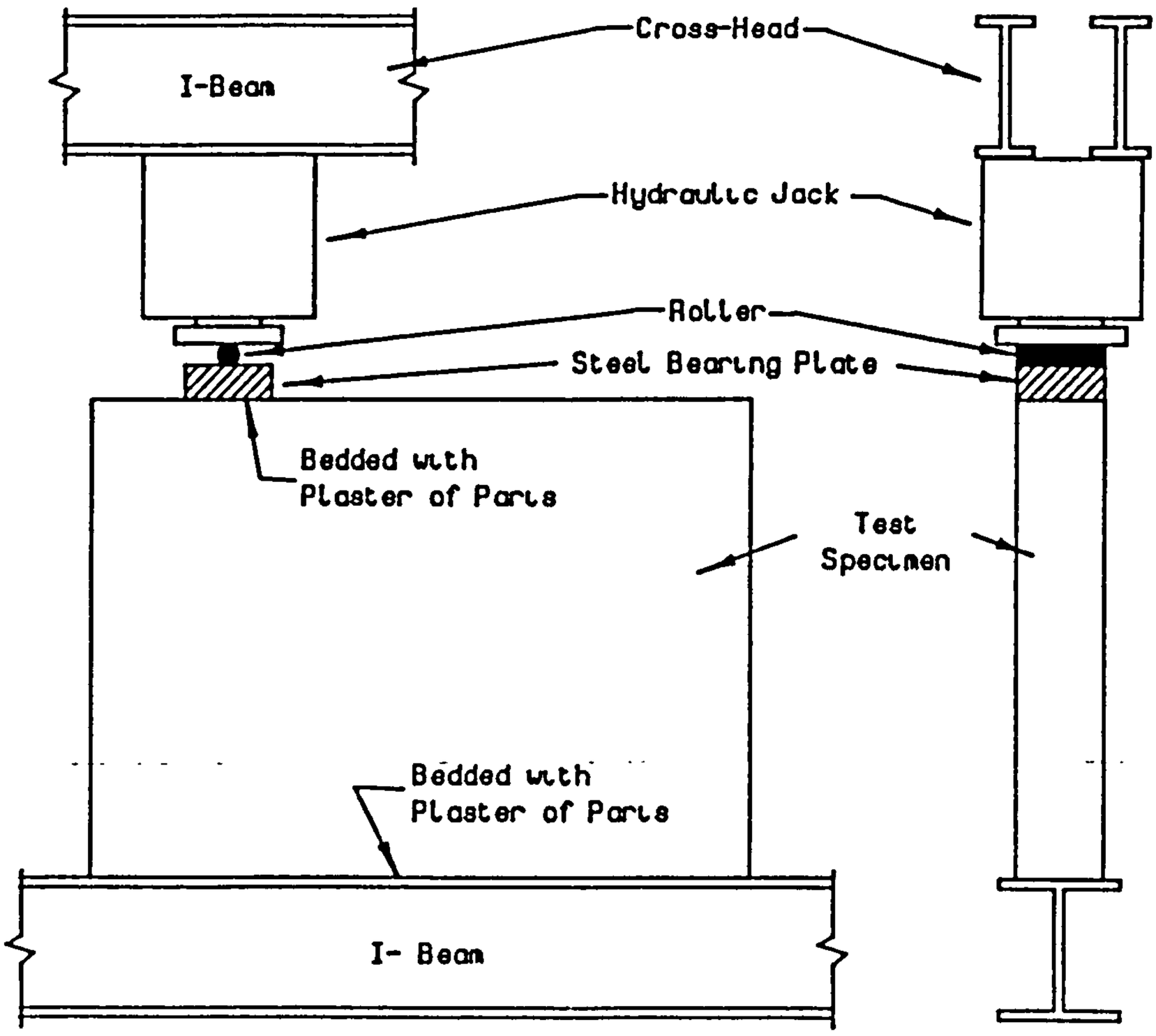

Fig.3.4 Loading Mechanism for Bearing Capacity Expt.

3.8 BEHAVIOR OF TEST

3.8.1 GENERAL

The behaviour of a majority of the unreinforced specimens was characterized by the suddenness and explosive nature of their failure which was often accompanied by an audible report. A wedge was formed beneath the bearing plate with an apex-angle

ranging from 30 to 40 degrees.

Reinforced specimens behaved in a more controlled manner; they usually cracked along the line of load and then failed by subsequent widening of the cracks.

3.8.2 SERIES E

The general patterns of cracks and modes of failure are shown in Fig.3.5. With the exception of block E3/2, the specimens split vertically into two halves along the axis of the bearing plate. For loads with small edge distance W_a, the block was lifted up beyond the point which is about 3 times the edge distance (Fig.3.5.(a)).

In block E3/2, failure was by shearing off the corner, with vertical cracks penetrating almost to the bottom of the specimen. As load was increased to 100kN, a crack was observed at the top of the specimen, 100 mm. from the loading edge. This propagated at an angle 80 degs. to the horizontal as the load was increased (Fig.3.5.(c)).

These failure wedges formed below the loaded area were pyramid-shaped with an apex angle ranging from 30 to 40 degs. All the specimens failed audibly immediately after the formation of vertical cracks below the loaded surface. This originated at about 80mm from the top.

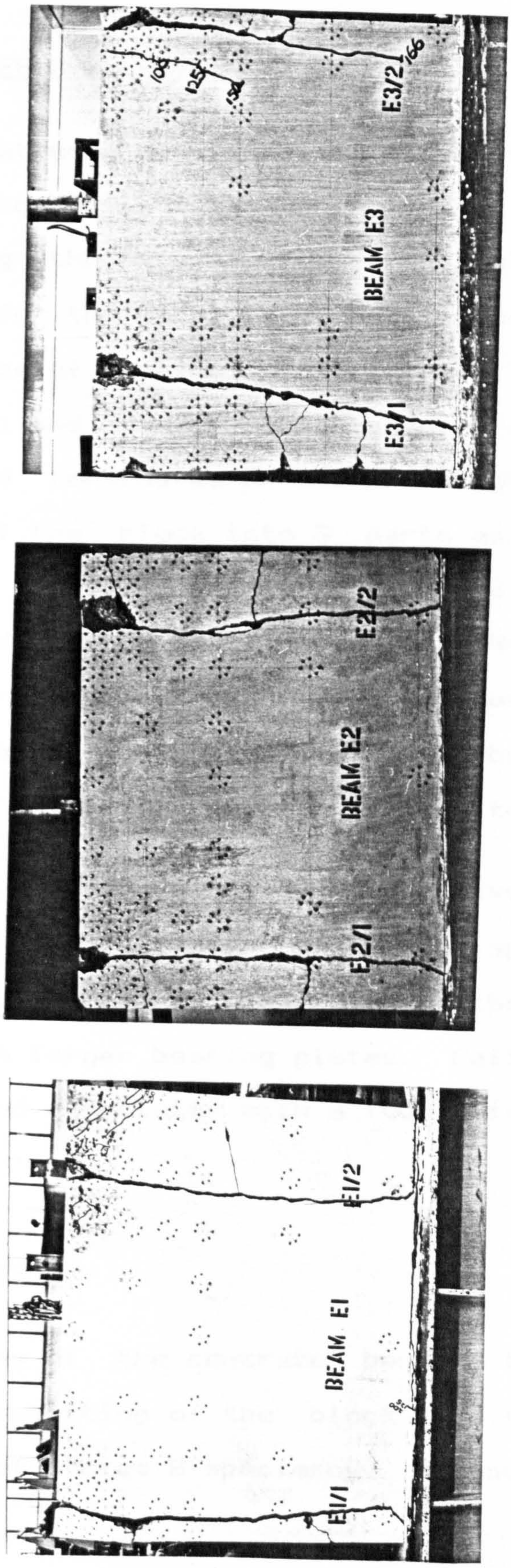

(a) (b) (c)

Fig.3.5 Appearance after failure of blocks in series E.
(a) Block E1, (b) Block E2, (c) Block E3.

3.8.3 SERIES R-H

The patterns of cracks and modes of failure are shown in figs.3.6. to 3.9. Vertical splitting of the blocks into 2 halves along the axis of the bearing plate was the usual mode of failure for the majority of specimens. However, for a small relative size of bearing plates, i.e. large and deep blocks, R4-H1, R3-H1 and R4-H2, splitting occurred from the top of the specimen and terminated on their two sides, resulting in the splitting of the block into 3 parts as shown in figs.3.6(c), 3.6(d) and 3.7(d). On the other hand, for shallow blocks, $h/a<0.5$ and larger bearing plates, $R<63$, splitting usually occurred from the bottom. This is due to settlement of the supporting beam at high loads creating bending of this slender block which initiated cracks at the bottom.

Except for loading over comparatively shallow specimens, cracking and failure of the specimens took place simultaneously. Cracks originated further away from the loaded surface with larger bearing plates. Failure of these specimens is sudden and associated with a loud noise.

3.8.4 SERIES S

Crushing of the concrete beneath the bearing plate and subsequent splitting of the block into two halves was the mode of failure of Series S specimens. Although failure took place

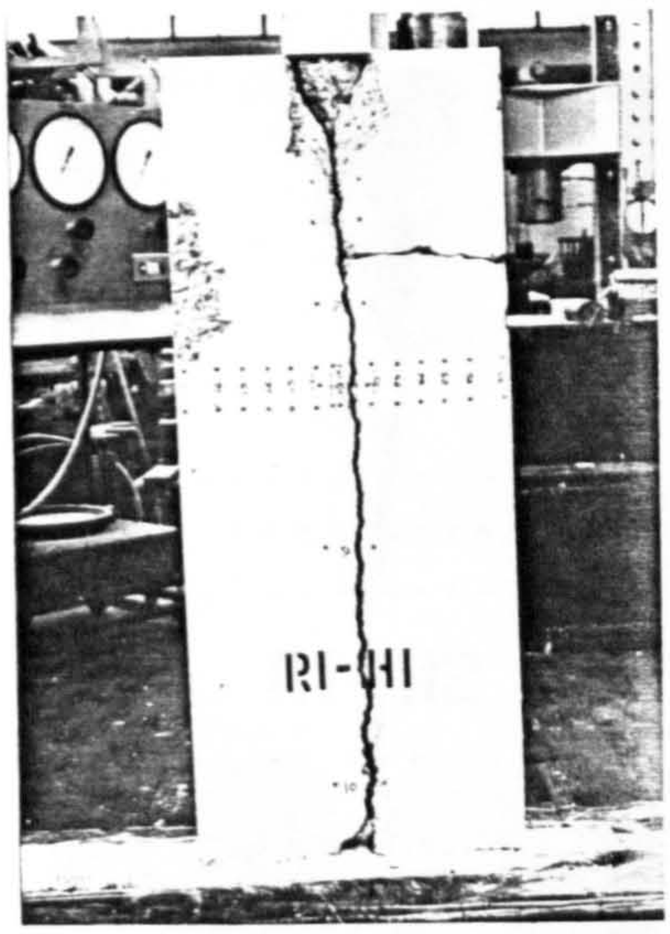

(a)

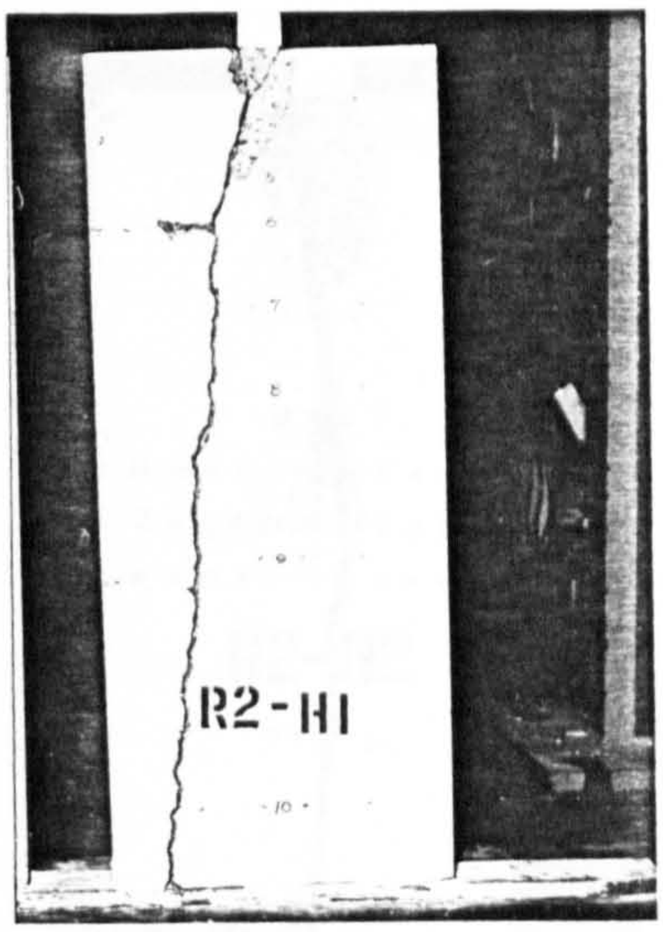

(b)

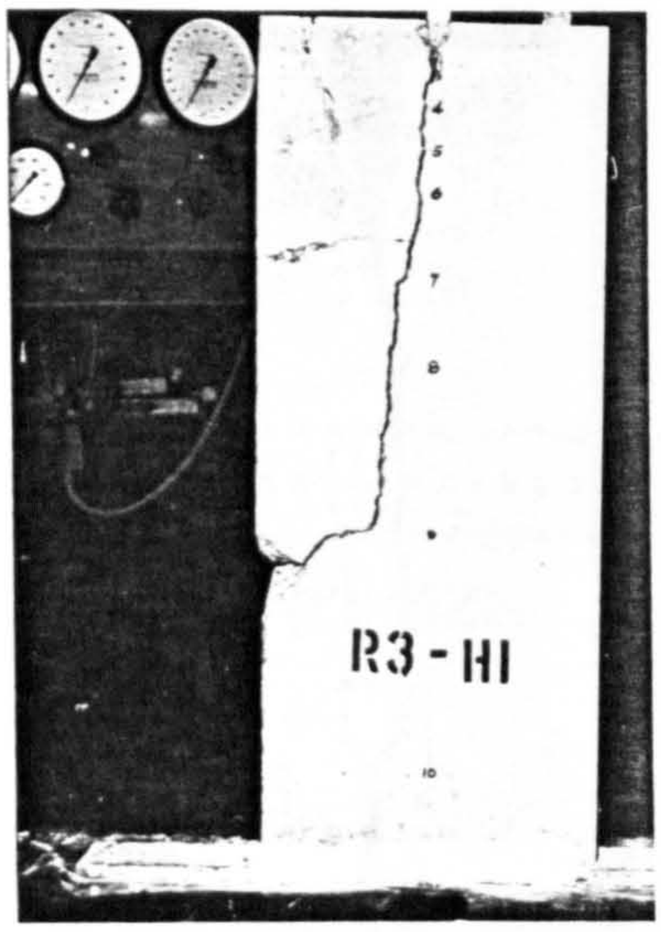

(c)

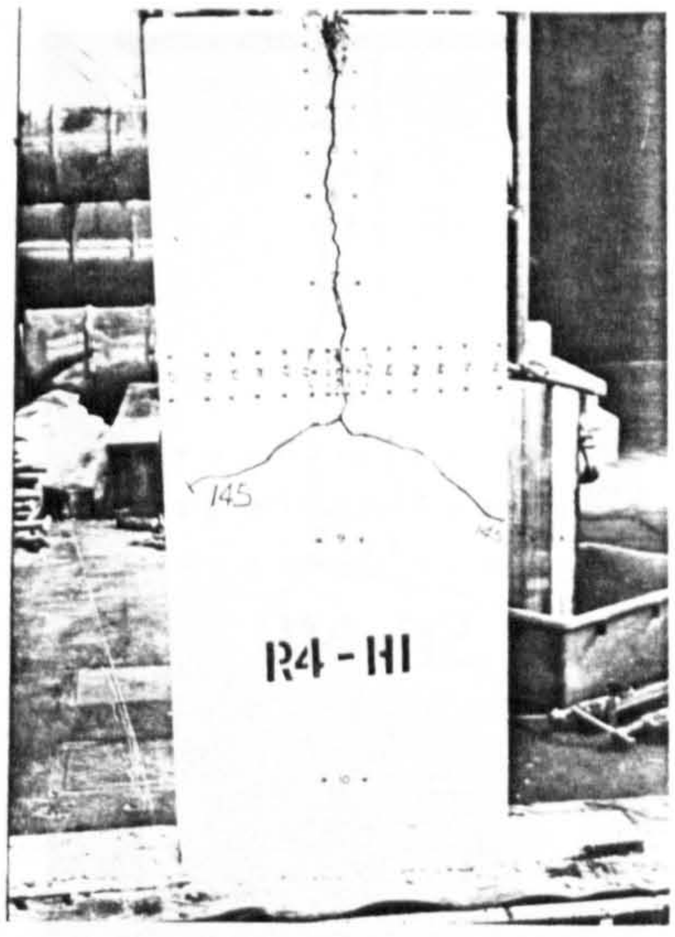

(d)

Fig.3.6 Appearance after failure of blocks in series R-H with heigh = 1000mm.
(a) R1-H1, (b) R2-H1,
(c) R3-H1, (d) R4-H1.

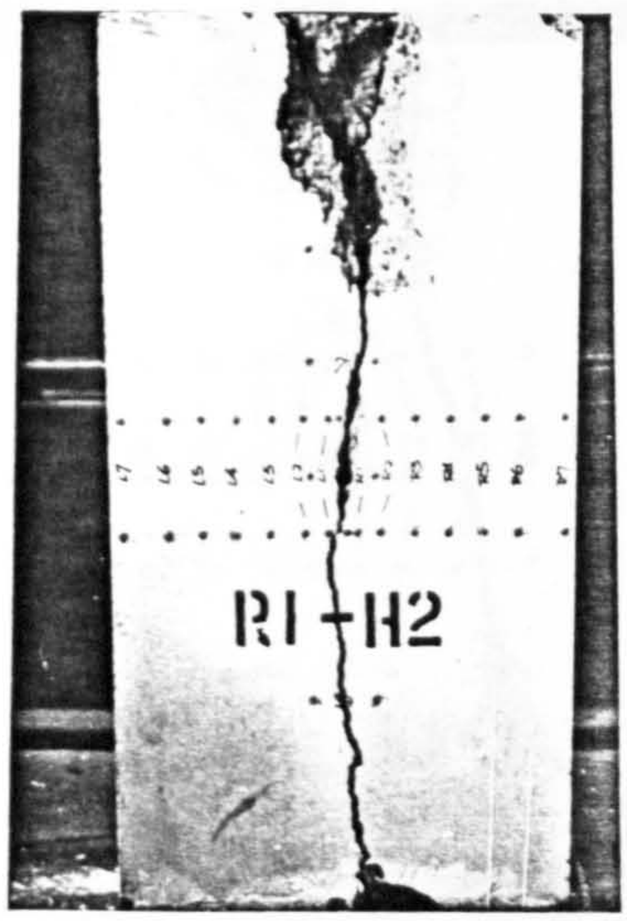

(a)

(b)

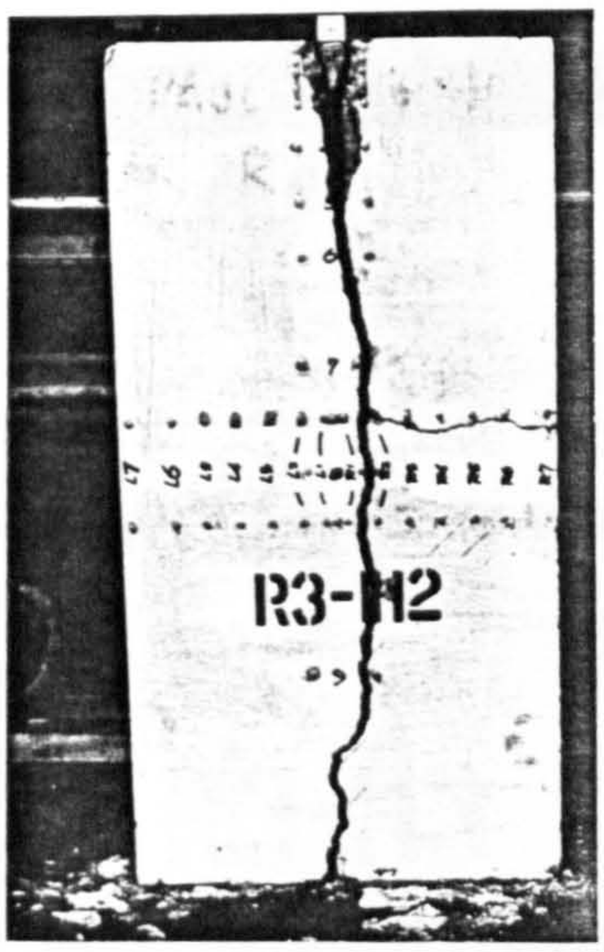

(c)

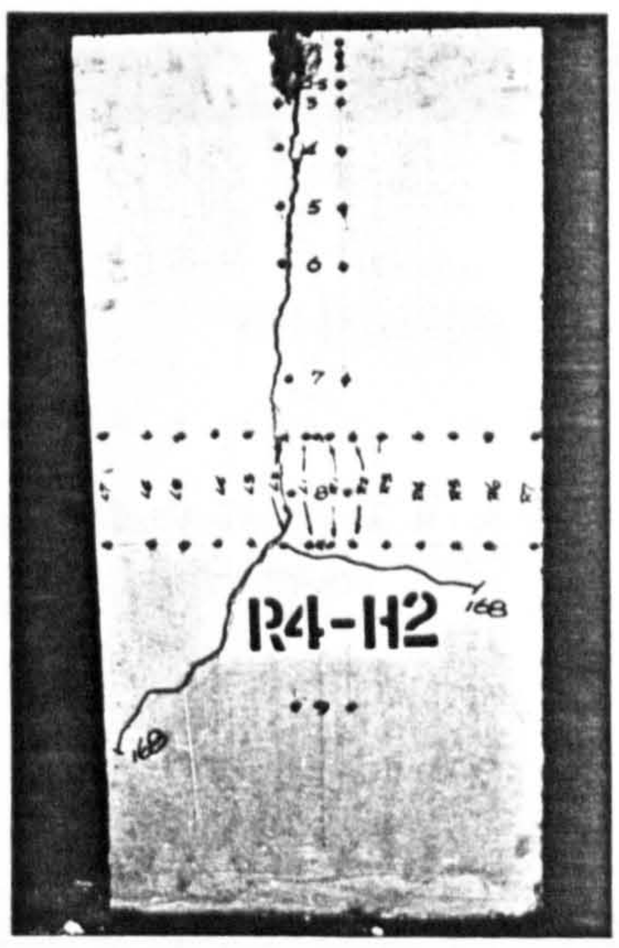

(d)

Fig.3.7 Appearance after failure of blocks in series R-H with heigh = 800mm.
(a) R1-H2, (b) R2-H2,
(c) R3-H2, (d) R4-H2.

(a)

(b)

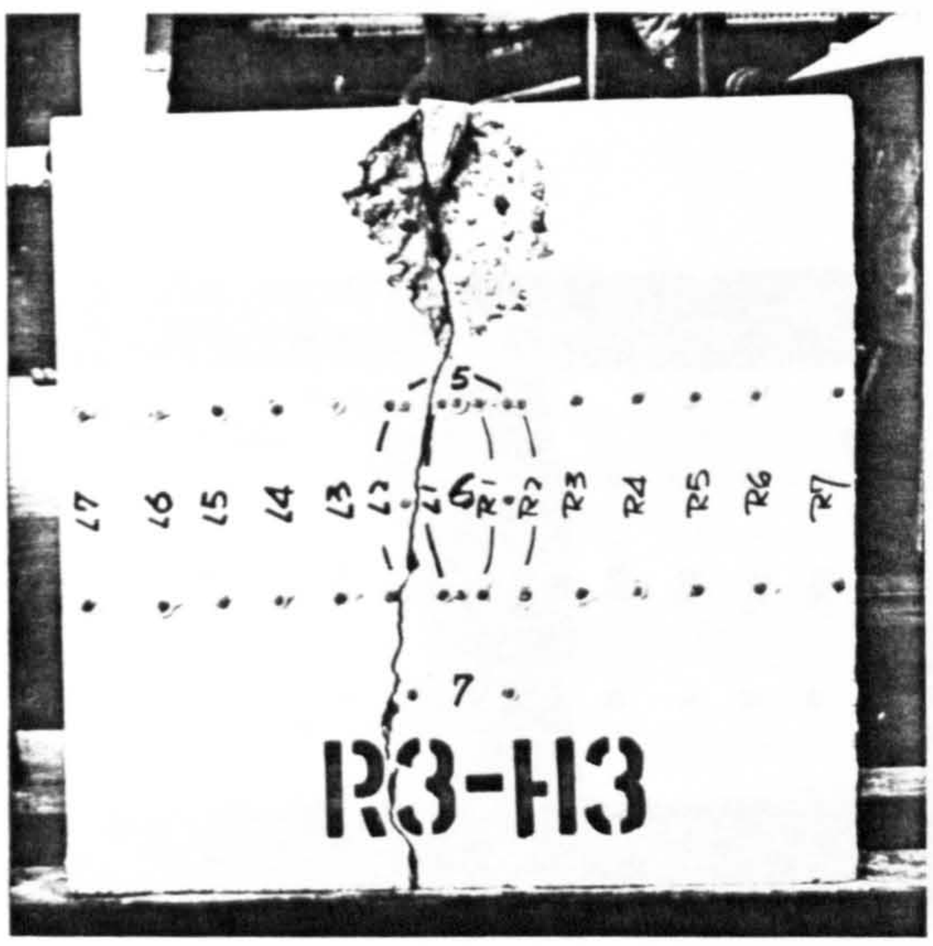

(c)

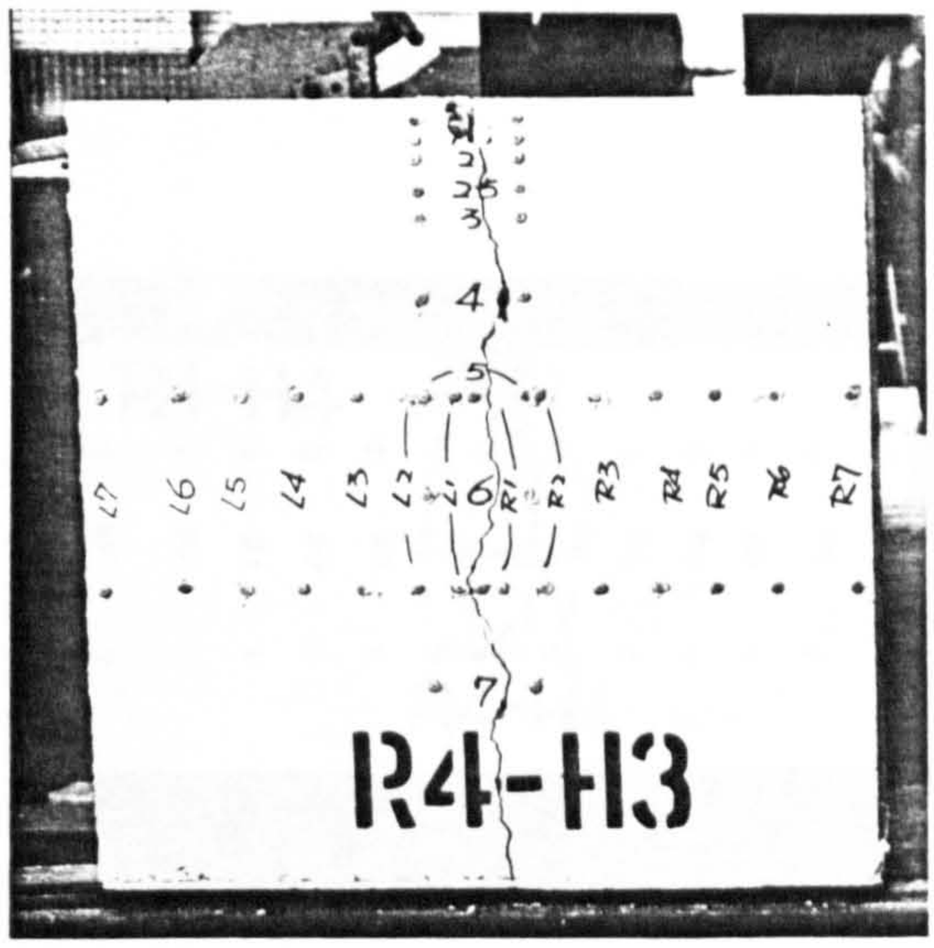

(d)

Fig.3.8 Appearance after failure of blocks in series R-H with heigh = 400mm.
(a) R1-H3, (b) R2-H3,
(c) R3-H3, (d) R4-H3.

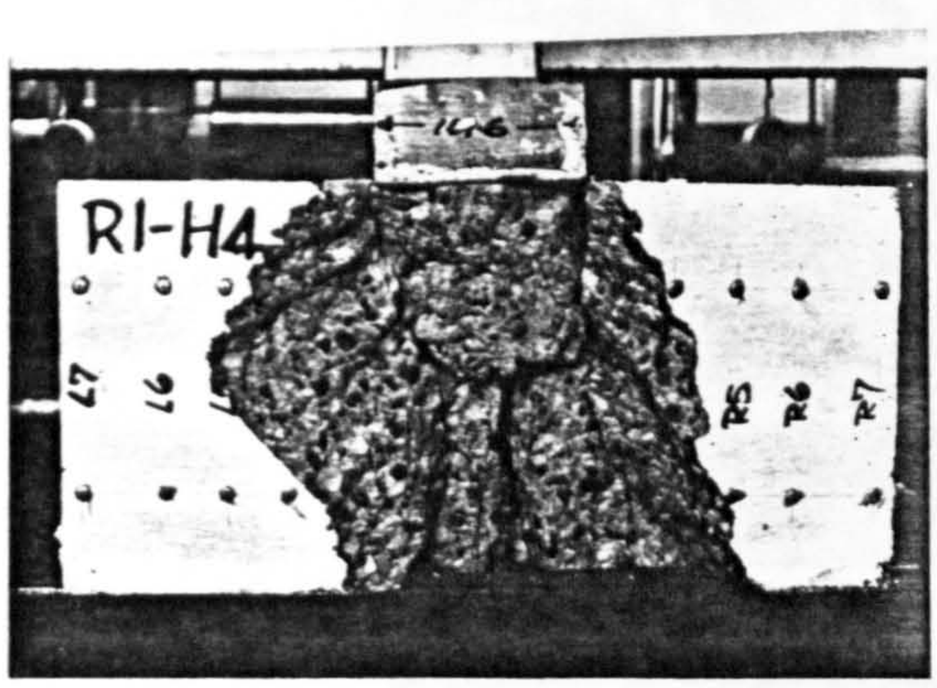

(a)

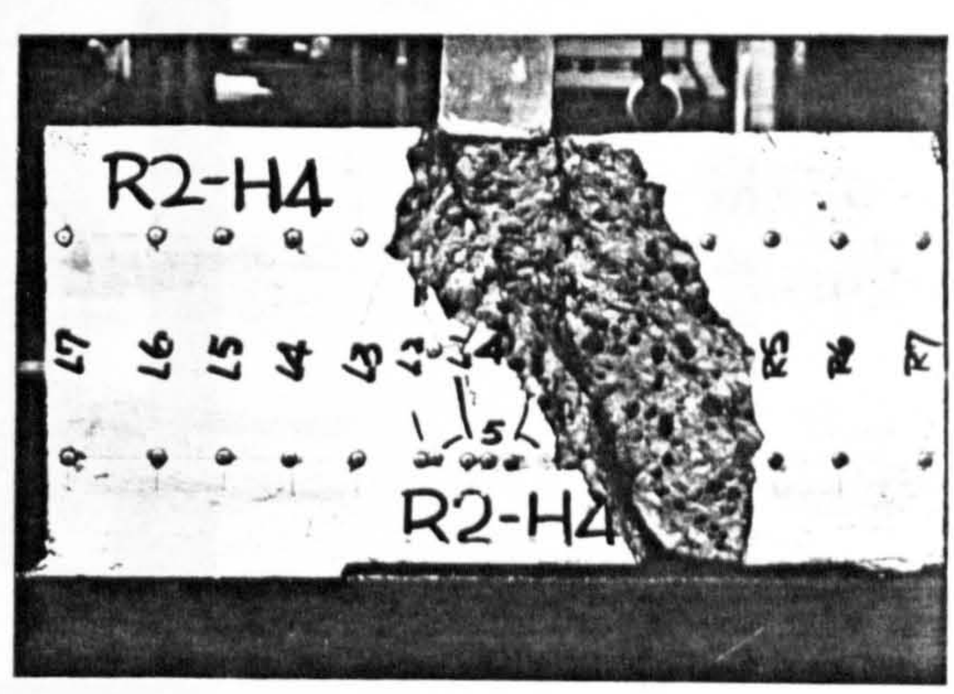

(b)

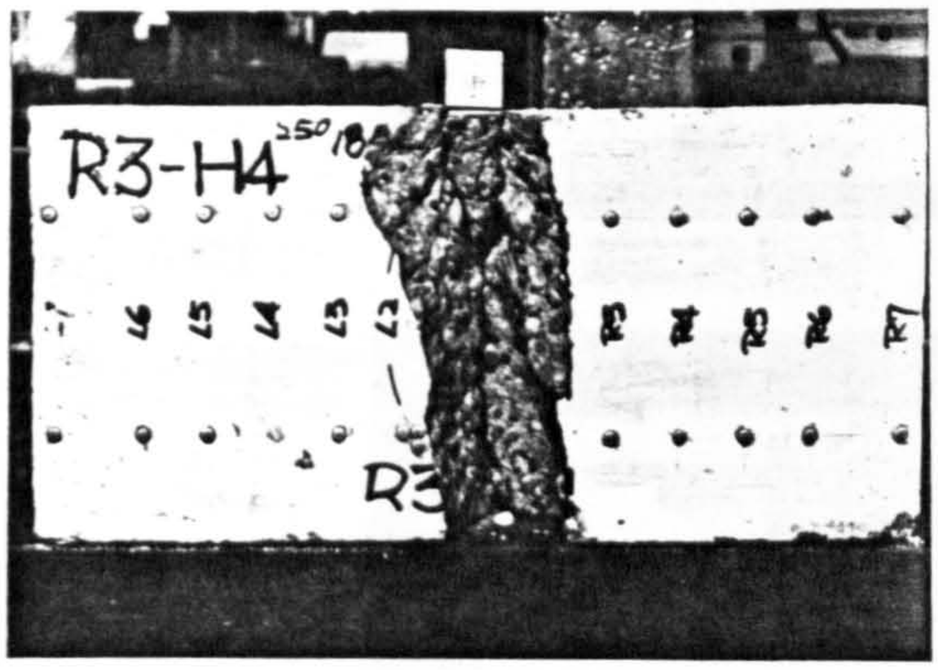

(c)

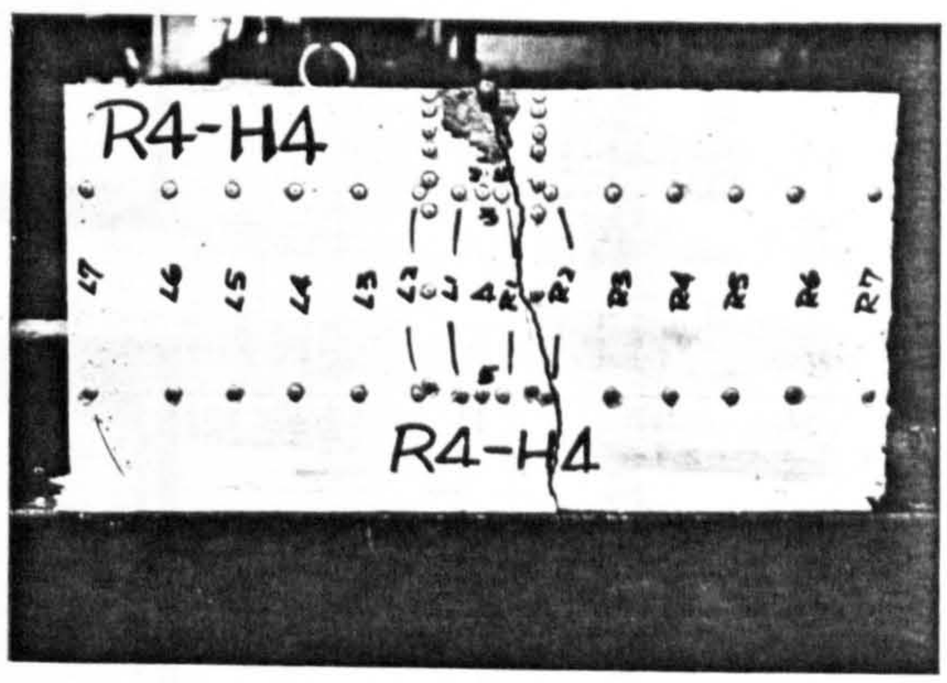

(d)

Fig.3.9 Appearance after failure of blocks in series R-H with heigh = 200mm.
(a) R1-H4, (b) R2-H4,
(c) R3-H4, (d) R4-H4.

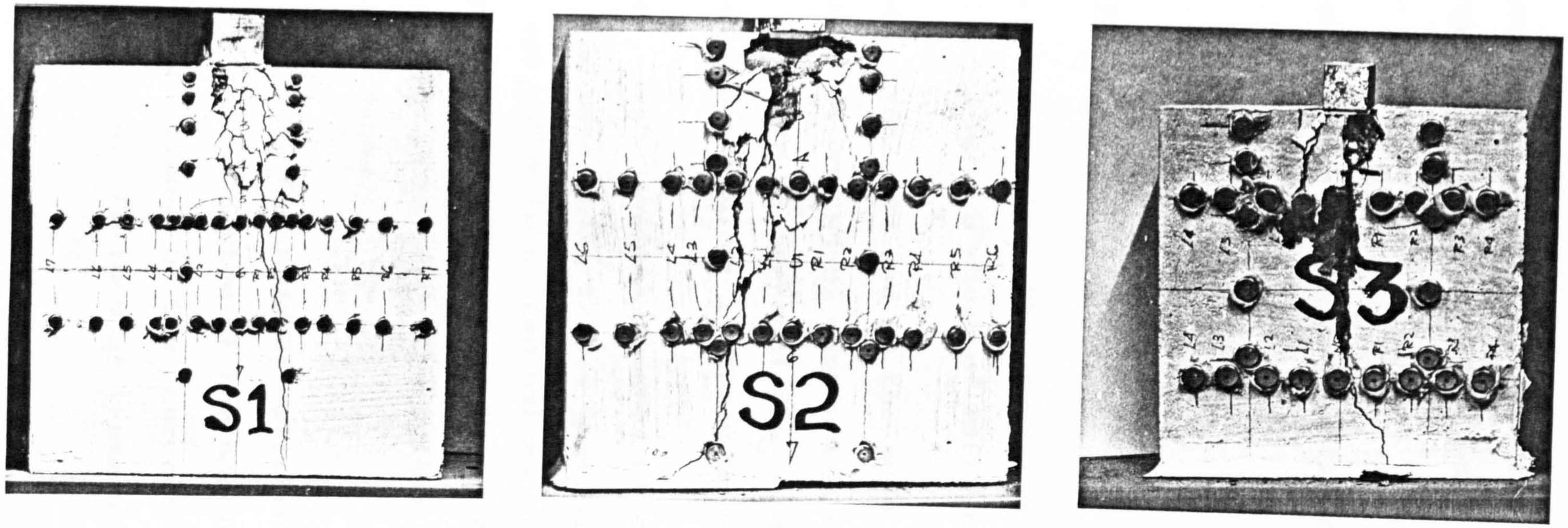

(a) (b) (c)

Fig.3.10 Appearance after failure of blocks in series S.
(a) Block S1, (b) Block S2, (c) Block S3.

almost immediately after the formation of vertical cracks, a more controlled failure was observed. They failed without a loud noise.

The patterns of cracks and failure mode are shown in Fig 3.10.

3.8.5 SERIES B

Fig.3.11 indicates the type of failure of Series B specimens tested with a sheet of PTFE under them.

For deep blocks B3 and B4 the mode of failure was similar to those in R1-H1 and R4-H1 respectively (Fig.3.11(c) and (d)). These show that the presence of the sheet of PTFE had little or no effect on the behaviour of these specimens.

However, with shallow blocks, B1 and B2, a different mode of failure was observed. It was obvious with specimen B1, that the block was split into two halves without crushing of the concrete under the bearing plate (Fig.3.11(a)). For specimen B2, splitting occurred from the bottom instead of from the top as in specimen R4-H4.

Fig.3.12 shows the mode of splitting for specimens B1 and B2. The PTFE at the bottom of the specimen was acting as a tie while the two halves of the concrete block behaved as two compressive struts. Failure of these blocks were taking place

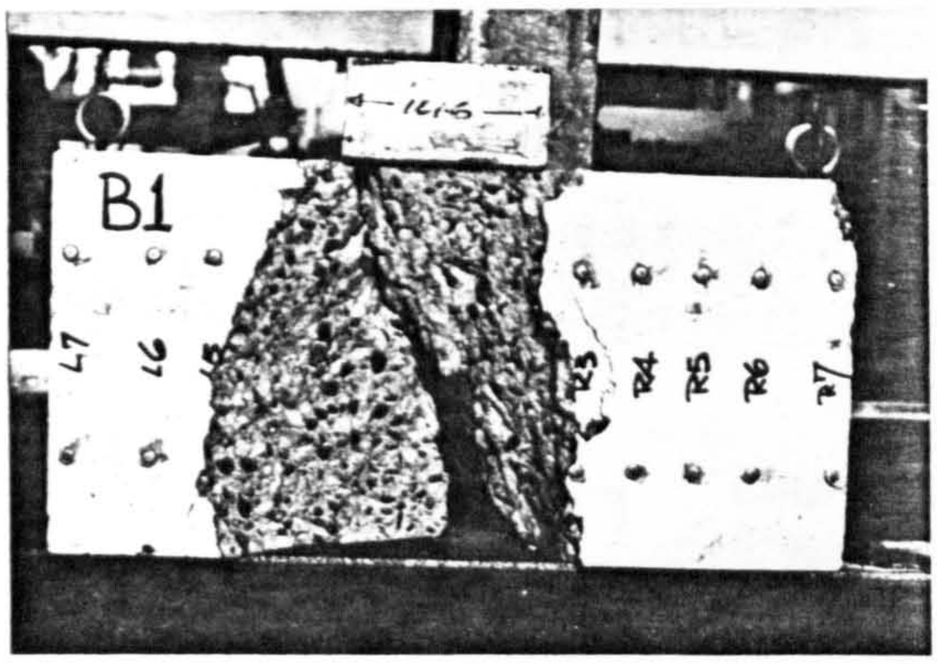

(a)

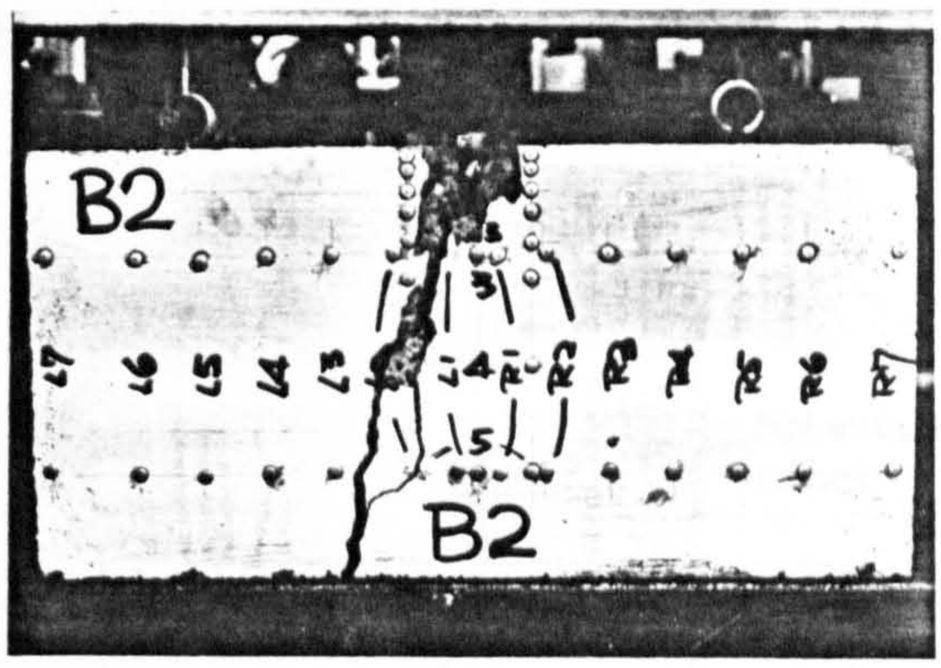

(b)

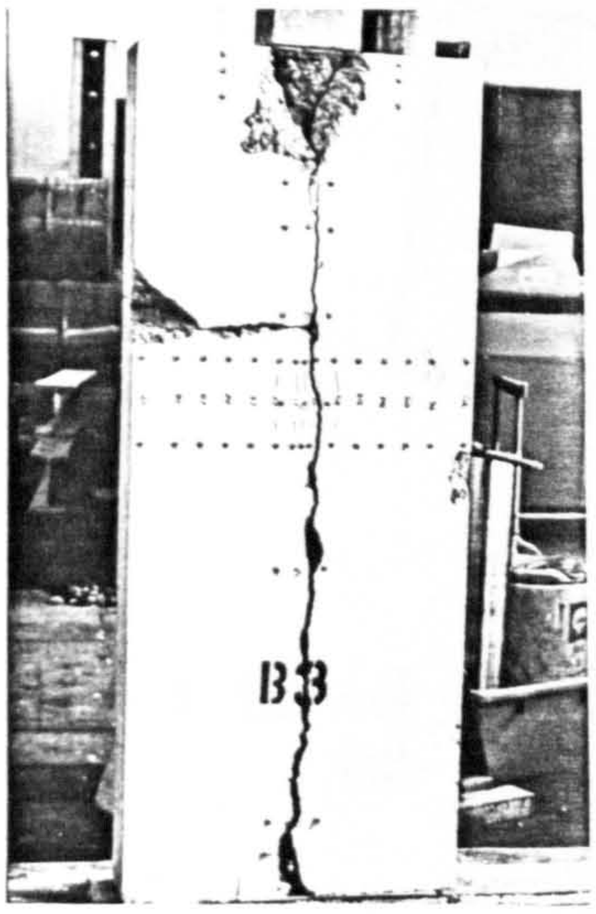

(c)

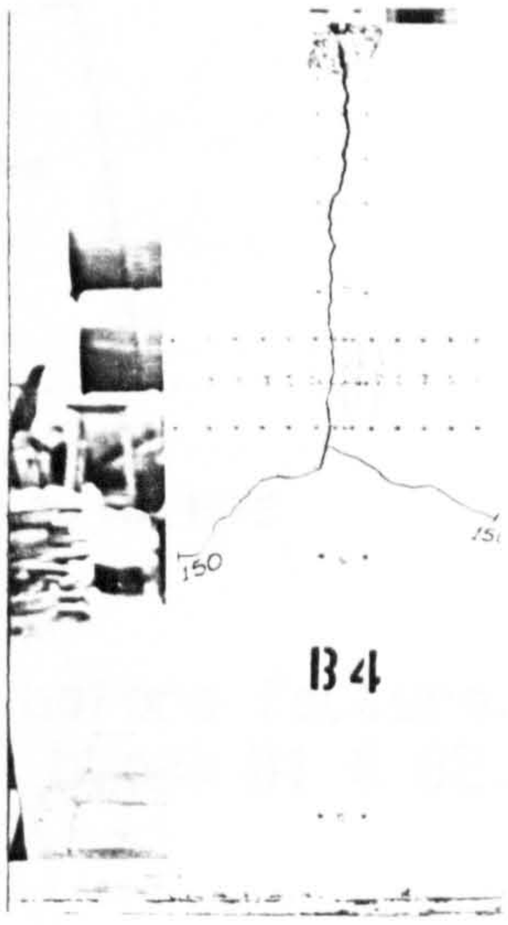

(d)

Fig.3.11 Appearance after failure of blocks in series B.
(a) B1, (b) B2, (c) B3, (d) B4.

as the tie ceased functioning, either by breaking the PTFE into two pieces (block B1) or by the sliding of the struts on the surface of it (block B2). The mechanism of the failure is shown in fig.3.12(c). All the specimens in this series failed with a loud noise.

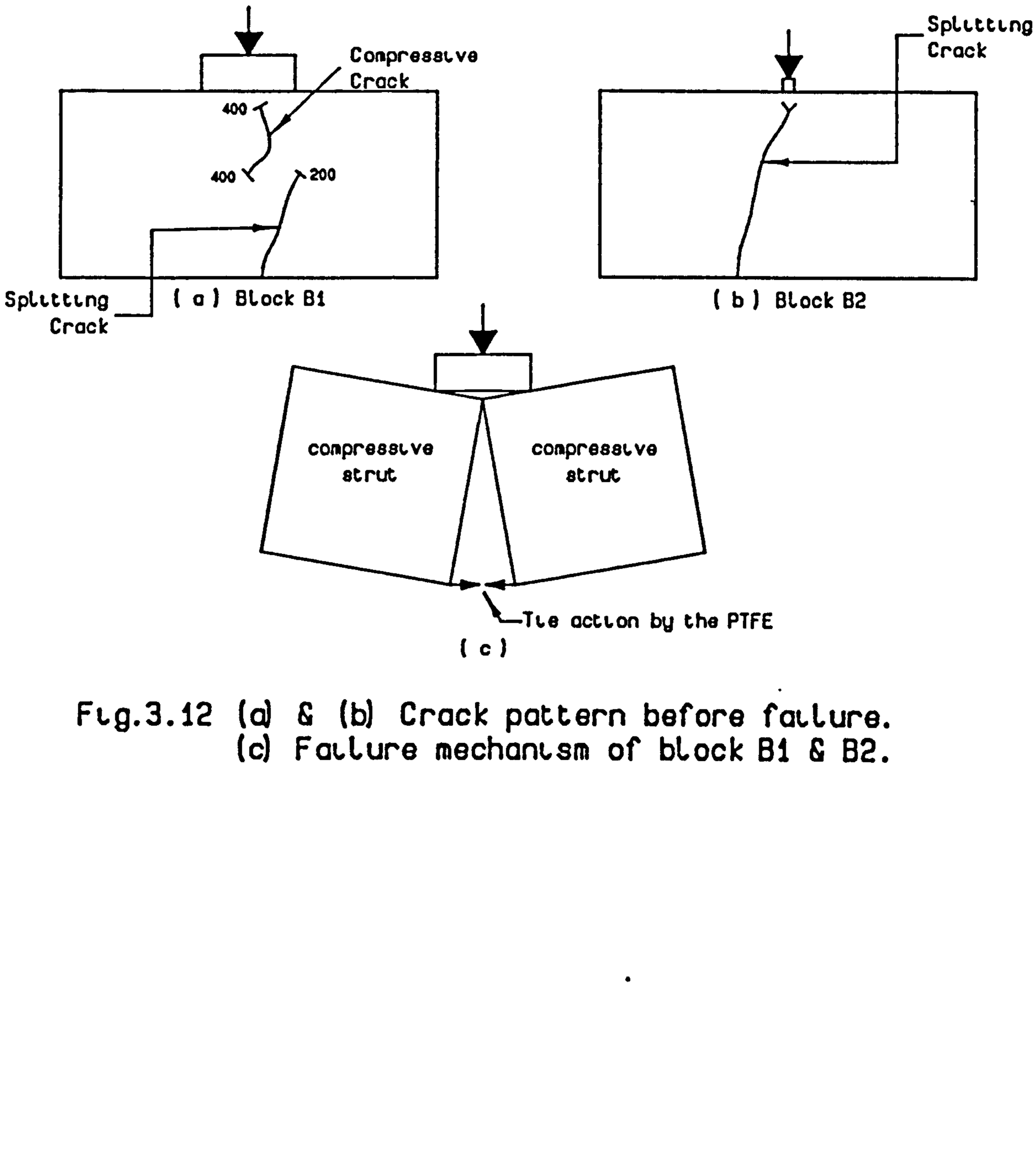

Fig.3.12 (a) & (b) Crack pattern before failure.
(c) Failure mechanism of block B1 & B2.

3.8.6 REINFORCED CONCRETE BLOCK — SERIES R

All of the reinforced blocks (Series R) failed in local bearing at the concentrated load. The presence of the reinforcement gave the block ductility as it failed.

Fig.3.13 shows the crack patterns for all the specimens in this series. Despite the differences in the form and amount of reinforcement used, their crack patterns were similar. The first crack which appeared was in the centre of the bearing plate and originated at about 100 mm. from the loading edge. This crack propagated downward as the load was increased. Occasionally, spalling cracks appeared around 150 mm. from the inner edge of the bearing plate and extended downward at an angle of approximately 70 degrees to the horizontal.

At higher loads, radial cracks appeared, which originated from the edge of the bearing plate and radiated downward as the load increased. Finally, failure was predominantly by local compression with flakes of concrete spalling off below the loading plates, as can be seen in the photographs in fig.3.14.

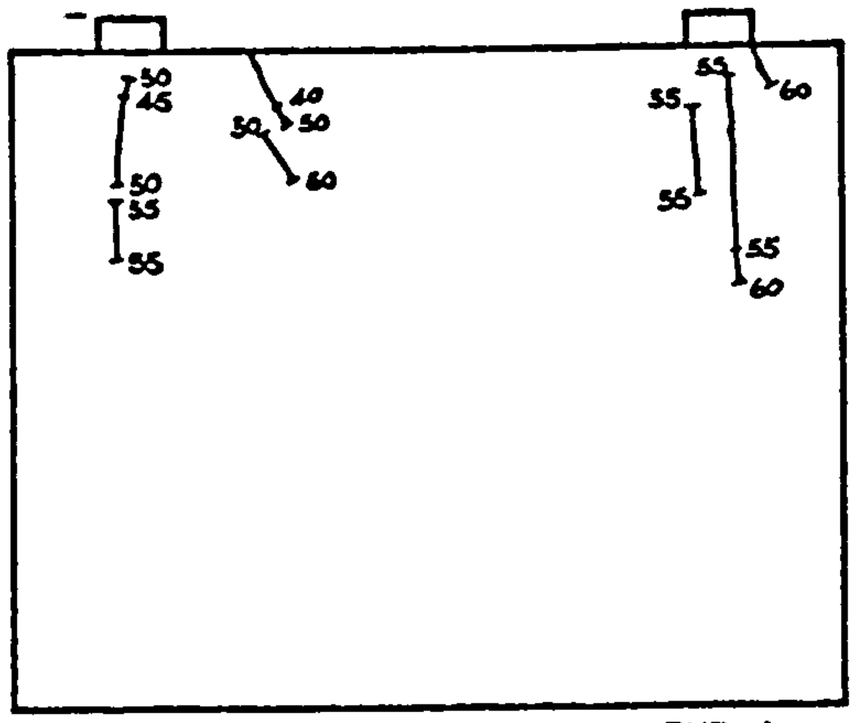

Block R1

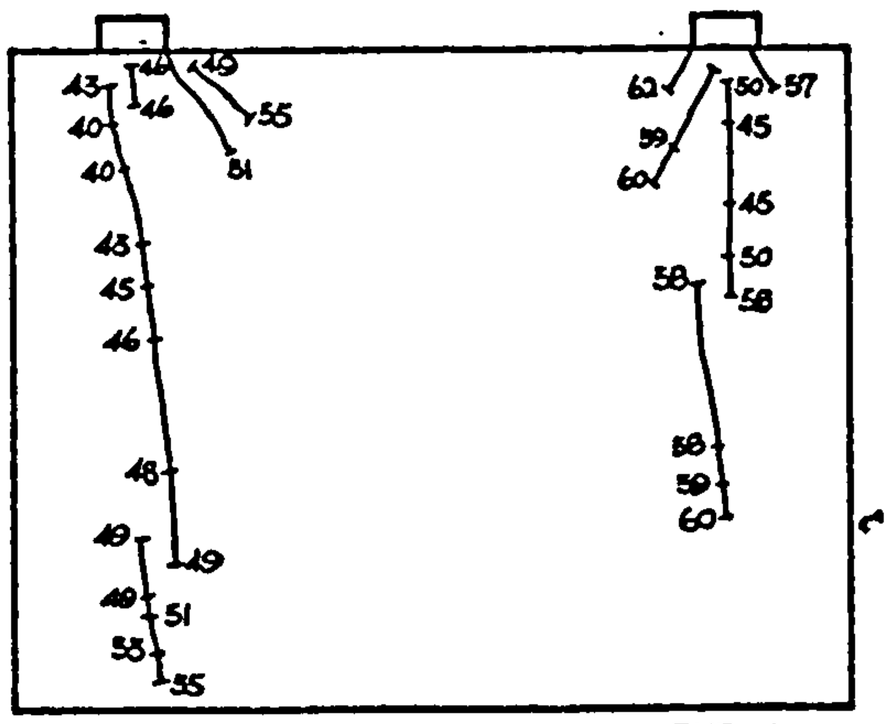

Block R2

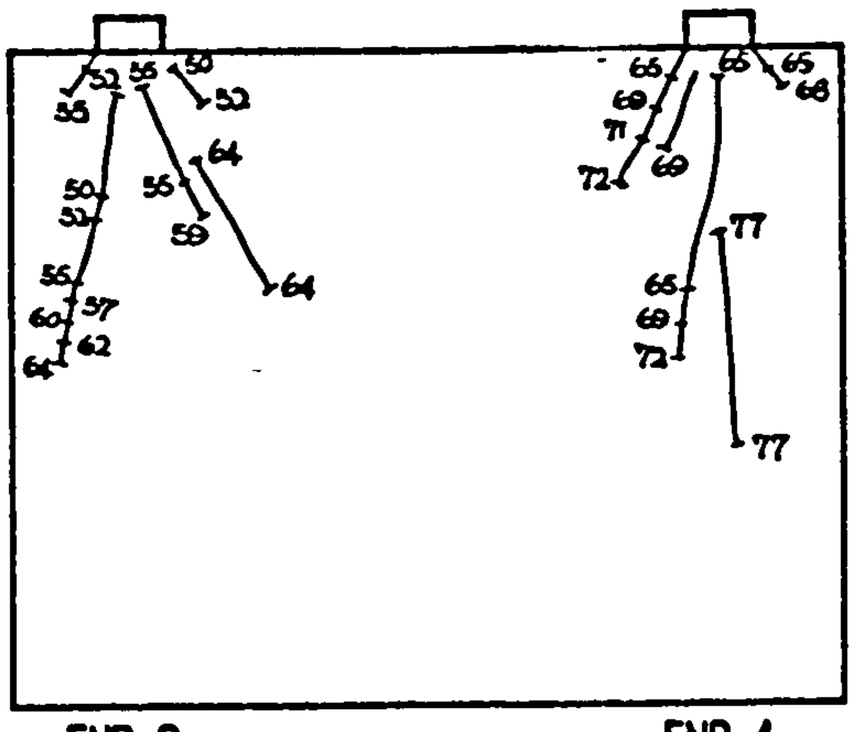

Block R3

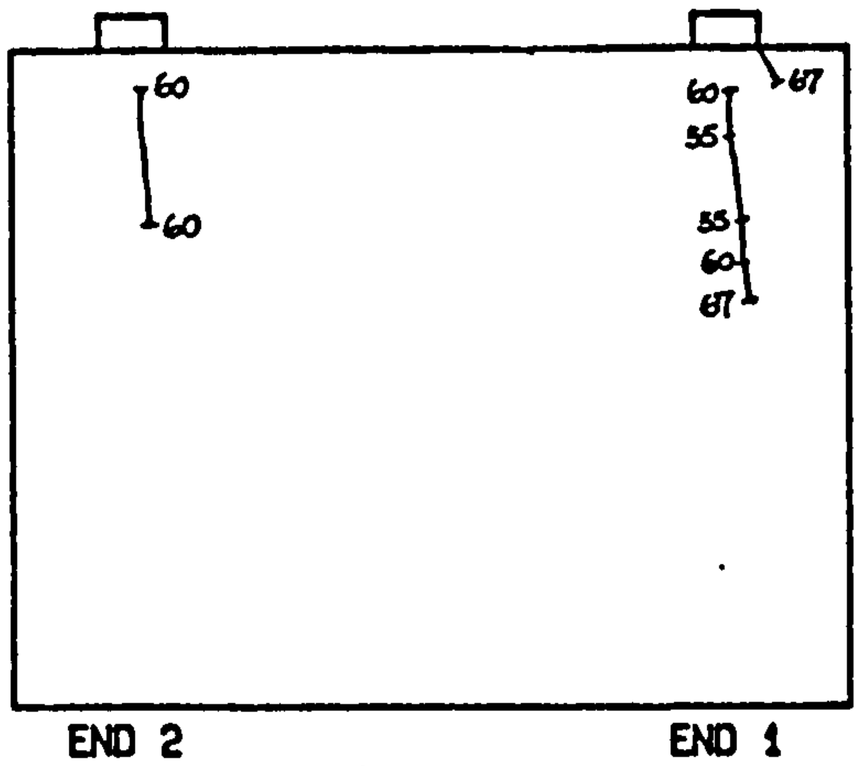

Block R4

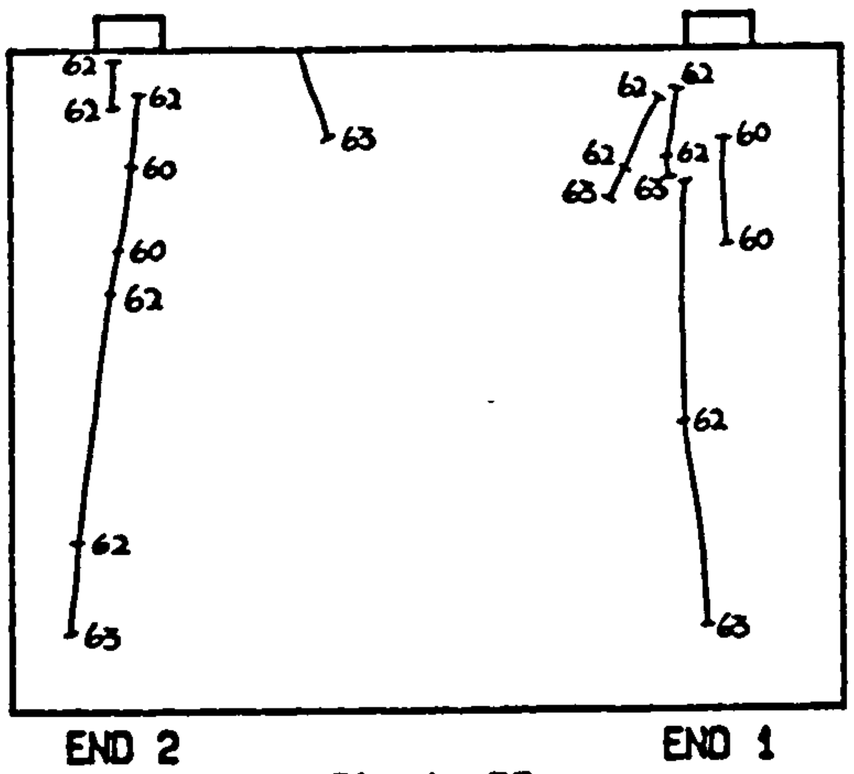

Block R5

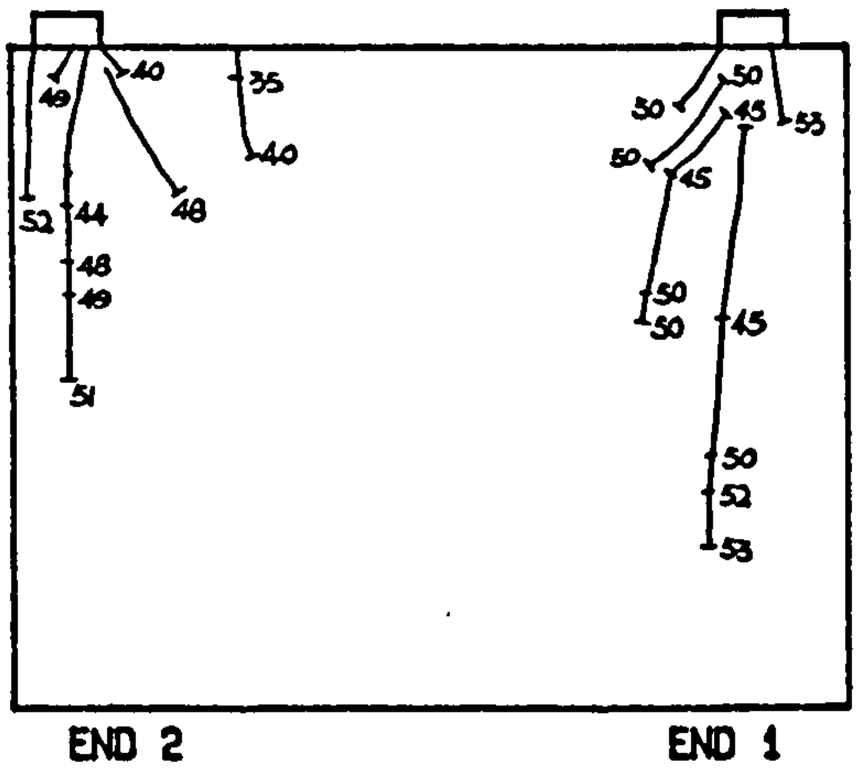

Block R6

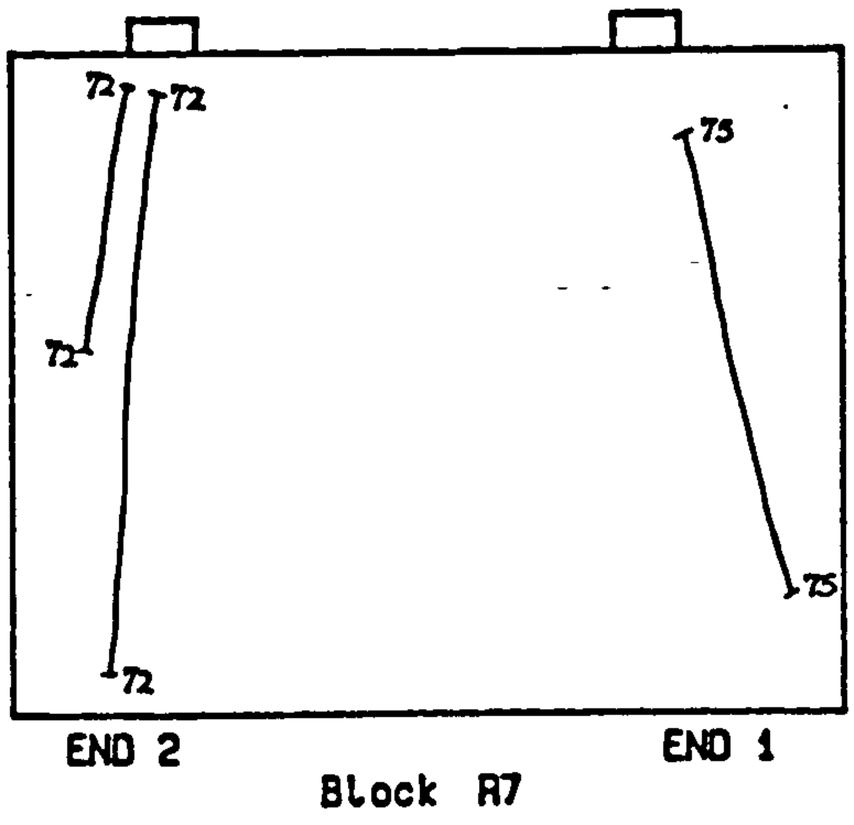

Block R7

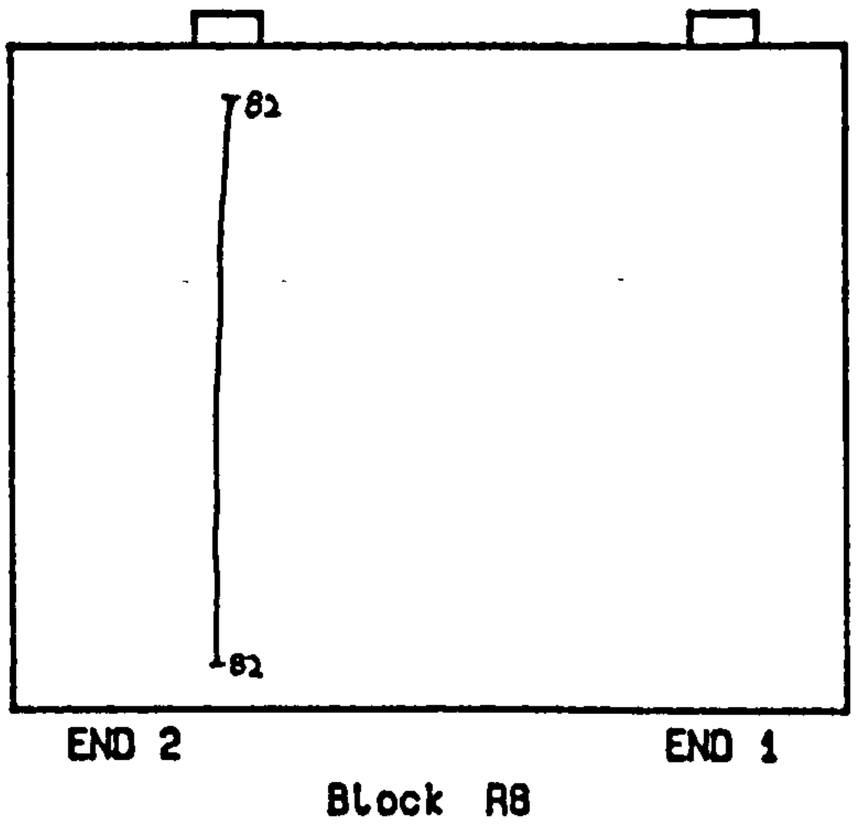

Block R8

FIG.3.13a Crack pattern of series R.

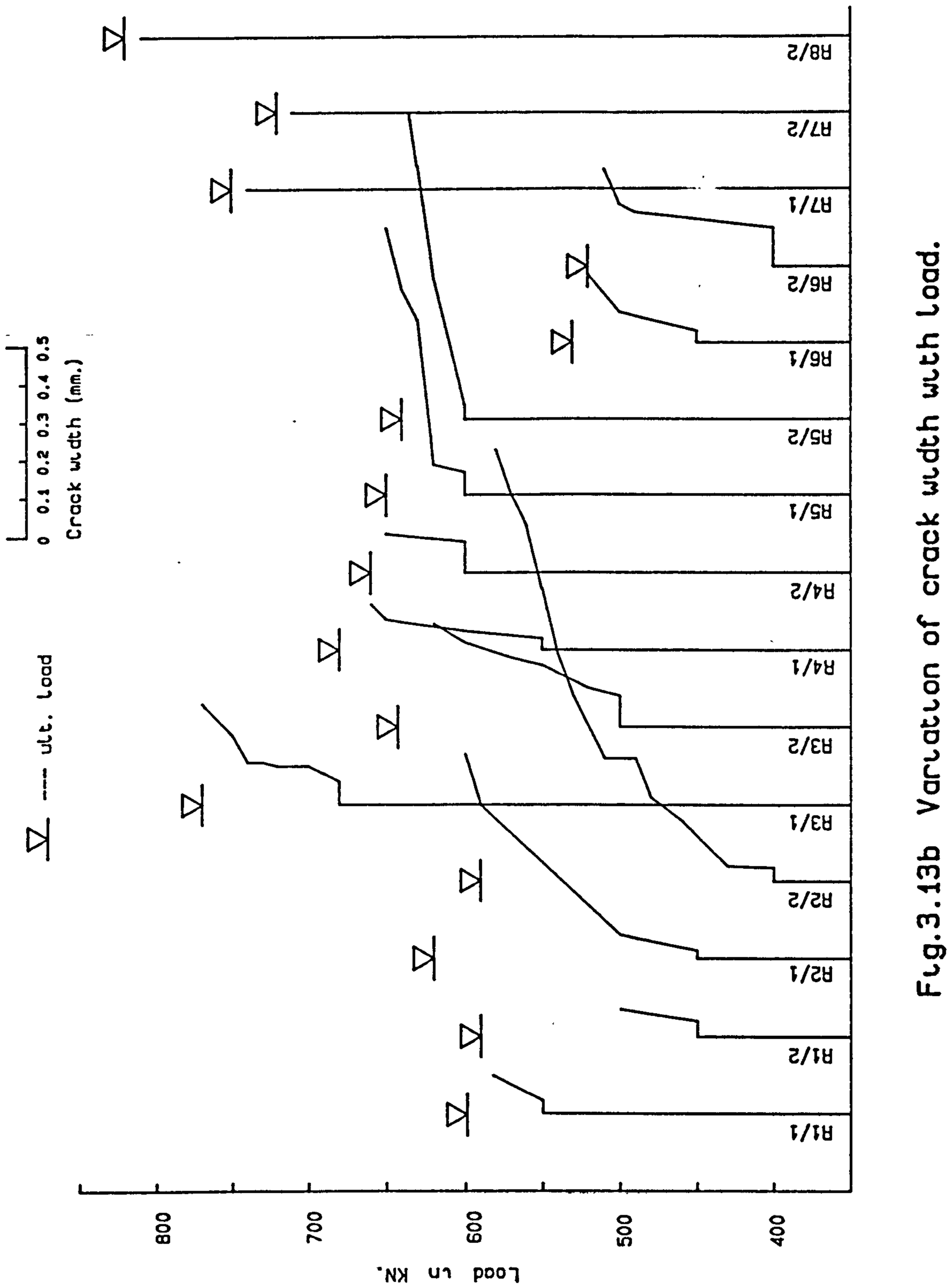

Fig.3.13b Variation of crack width with Load.

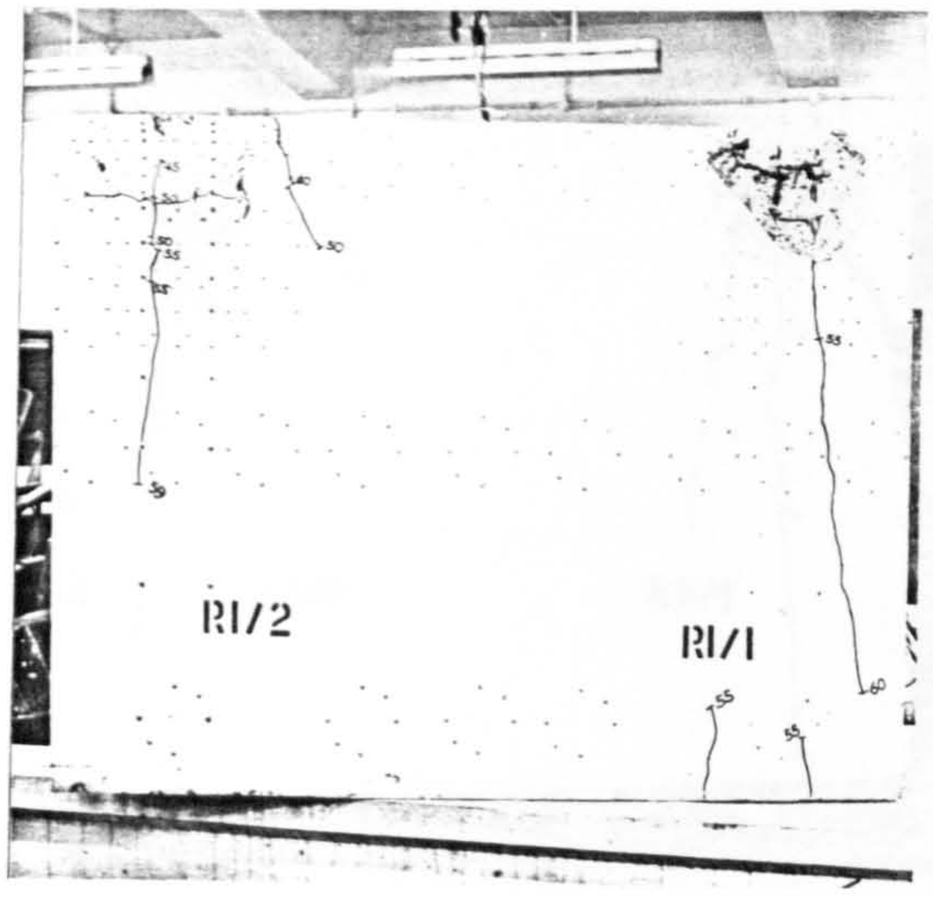

(a)

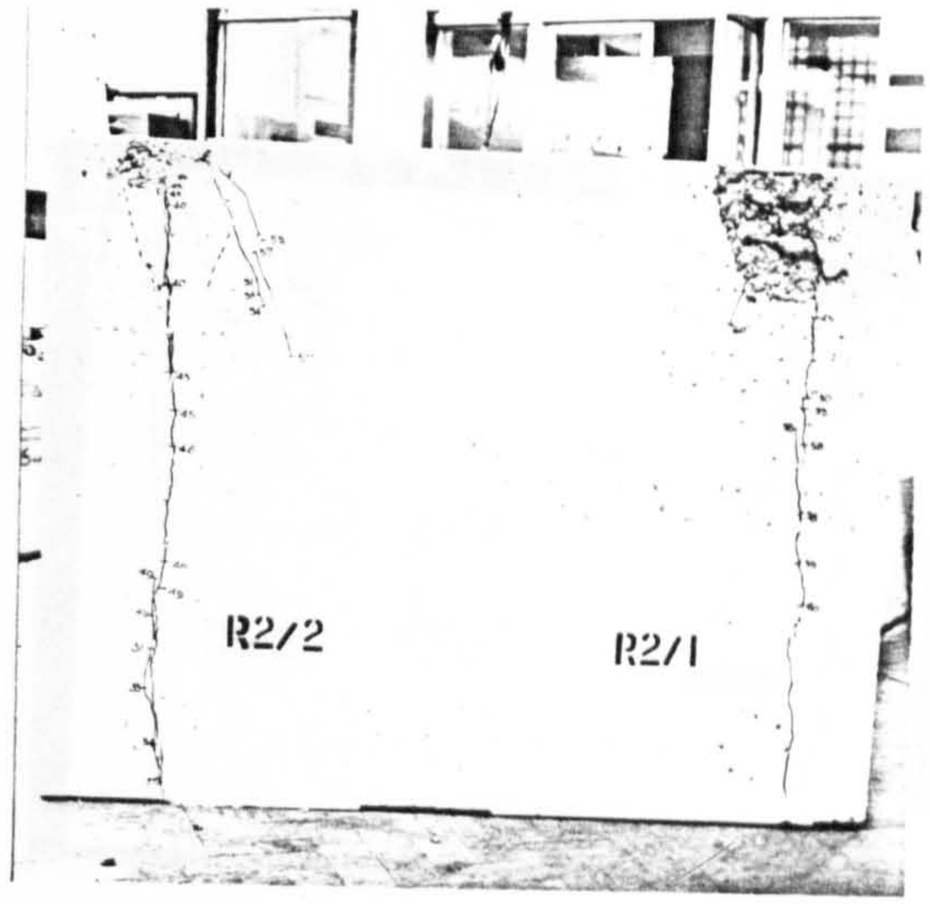

(b)

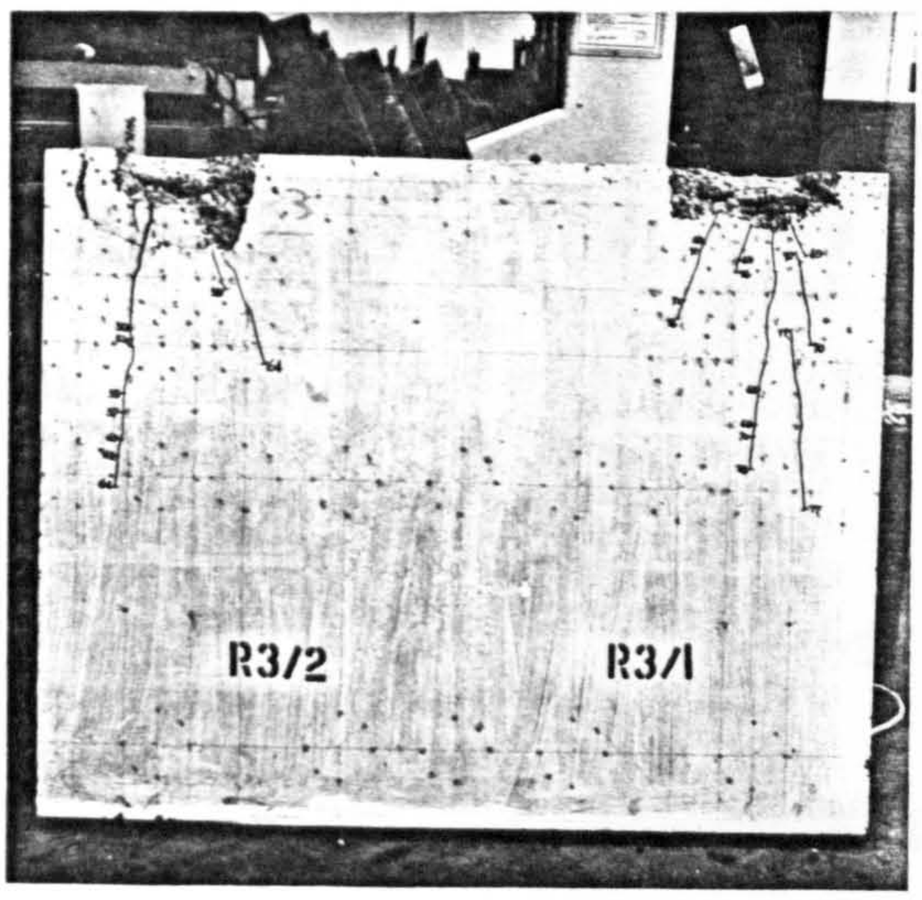

(c)

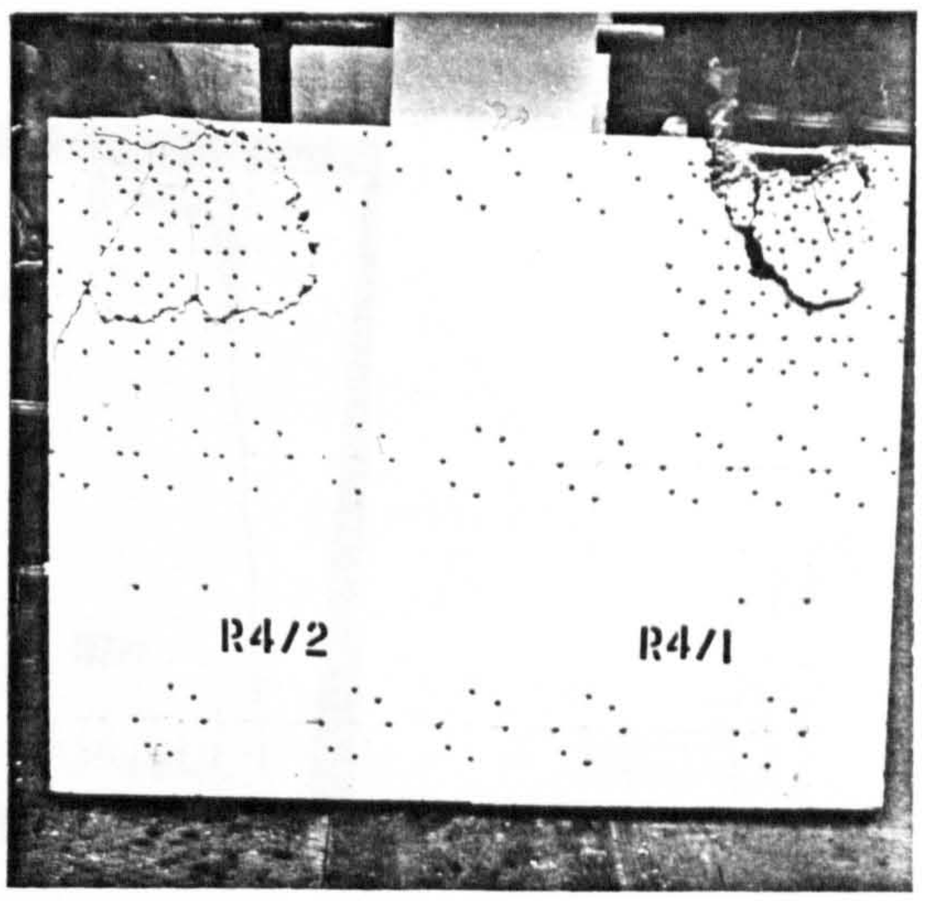

(d)

Fig.3.14 Crack pattern after failure for block in series R.
(a) R1, (b) R2, (c) R3, (d) R4.

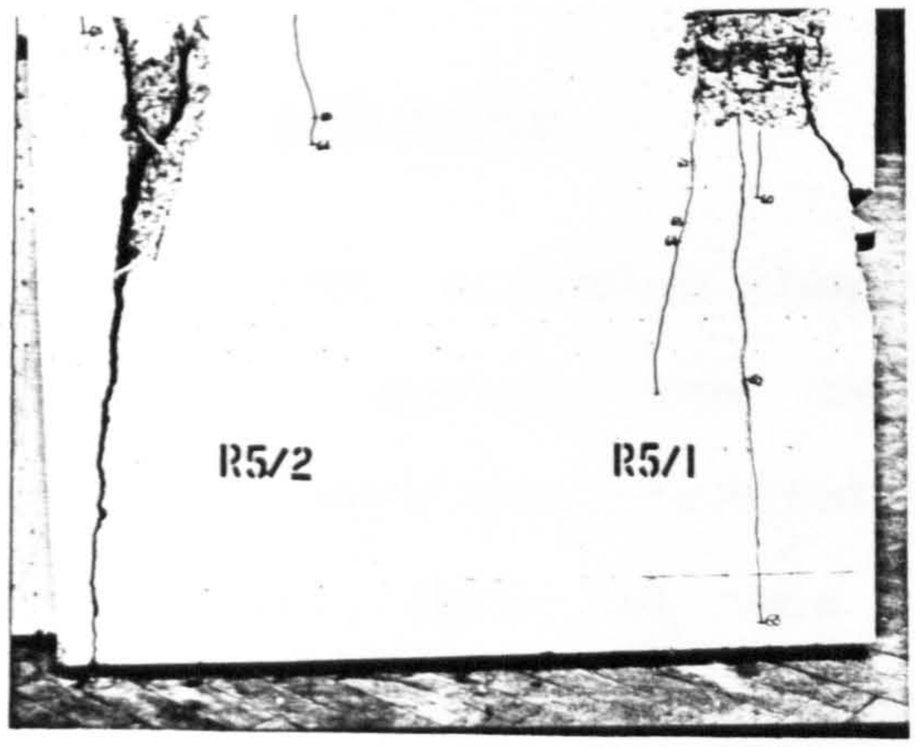

(a)

(b)

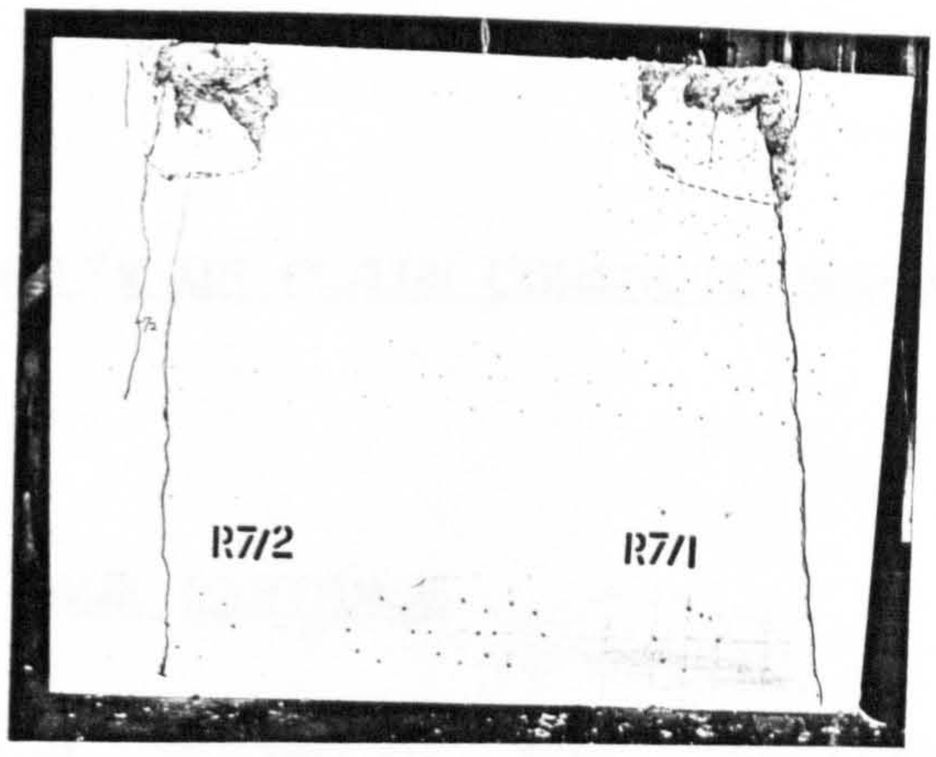

(c)

Fig.3.15 Crack pattern after failure for block in series R.
(a) R5, (b) R6, (c) R7.

4 EXPERIMENTAL RESULTS — BEARING CAPACITY OF CONCRETE BLOCKS

4.1 INTRODUCTION

In the previous chapter, the general behaviour of the specimens during the tests has been described. In this chapter, more experimental results will be shown and discussed in detail, such as the stress and strain distributions in concrete and steel, and the factors affecting specimen behaviour will be analysed. Finally, a proposed model of failure is drawn up and compared with existing theories.

The values of cracking load P_c, and ultimate load P_u are tabulated together with the dimensions and material properties of the specimens in table 3.1.

4.2 BEARING CAPACITY OF PLAIN CONCRETE BLOCKS

4.2.1 EFFECT OF EDGE DISTANCE

The deflected shapes of the specimens analysed by the finite element method (FEM) with edge distances of 30 and 280 mm. are given in fig.4.1(a) and (b) respectively. It can be seen that the specimen with concentrated load near the edge failed by shearing off the corner as a result of less

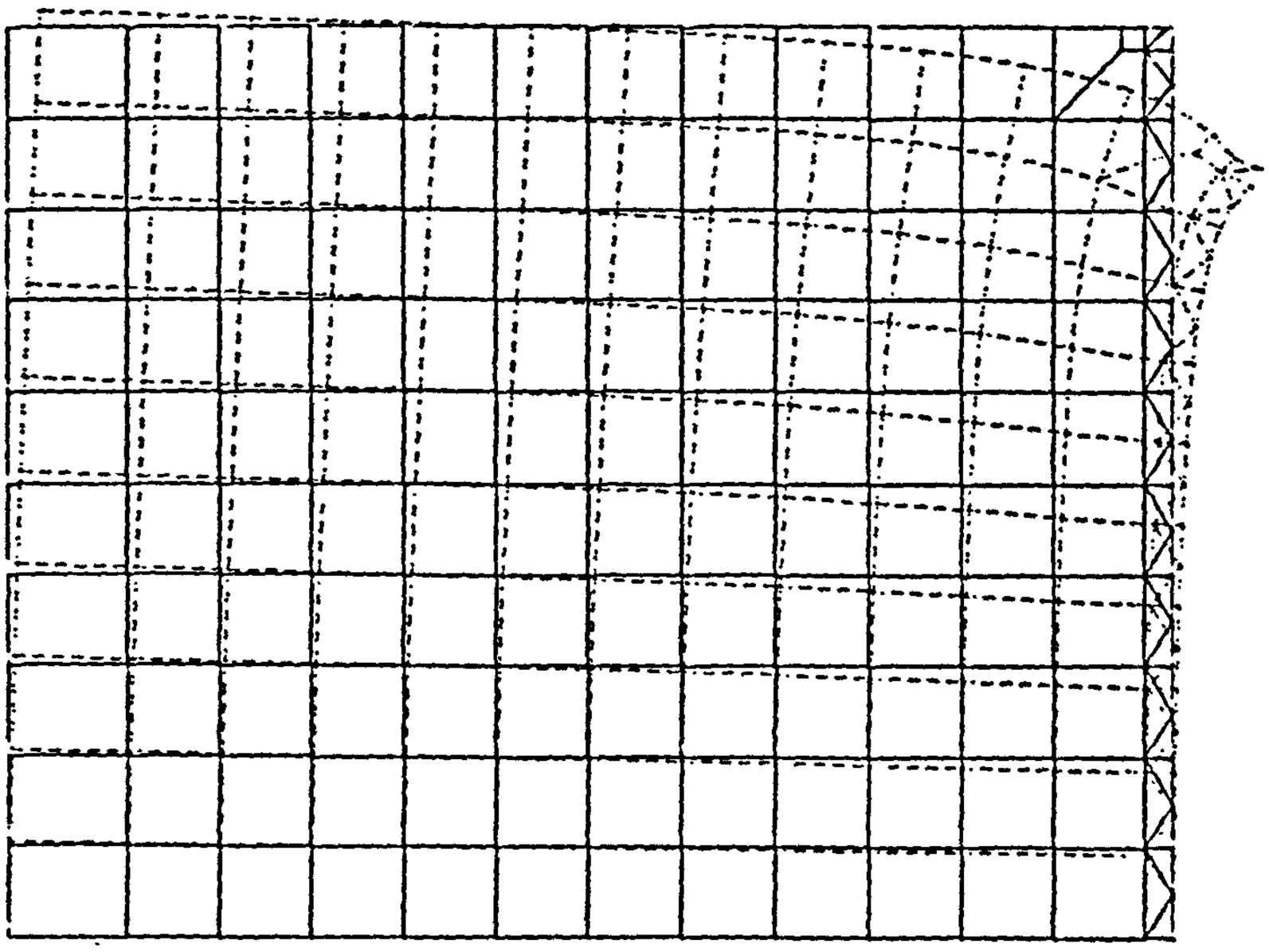

Fig.4.1a Deflected shape of blocks with edge distance = 30mm.

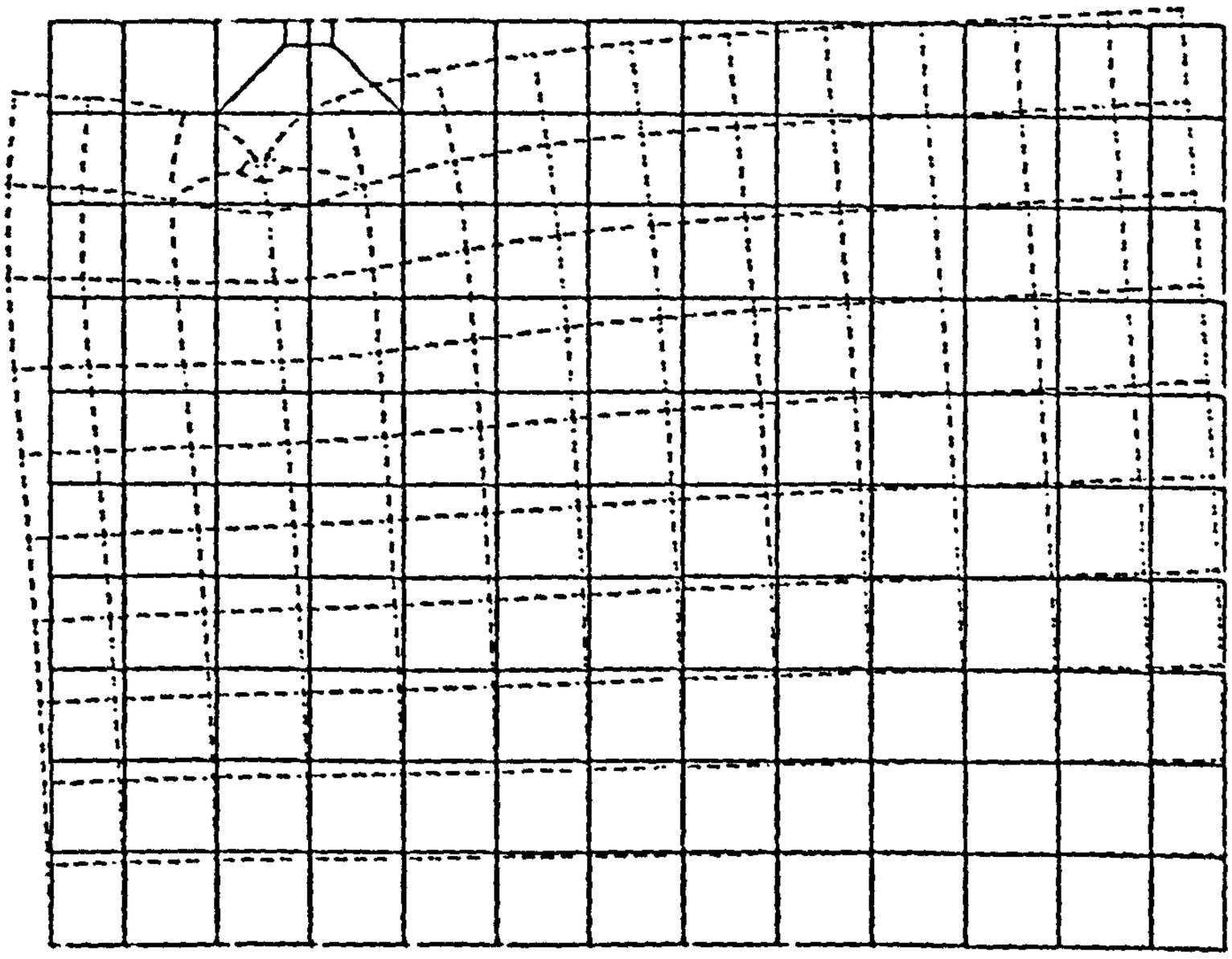

Fig.4.1b Deflected shape of blocks with edge distance = 280mm.

confinement on one side by the concrete near the edge. However, specimens with a larger edge distance failed by splitting the concrete block into two halves.

The variation of transverse stress with depth along the loaded line in blocks E1 to E3 is given in fig.A.1-3. The experimental stresses are plotted together with the stresses analysed by FEM. It can be seen that the general trends of the stress distributions are similar in all three blocks, each contains a high compression zone near to the loaded surface, followed by a tension zone which causes the splitting of the blocks. The depth of the tension zone varies with edge distance, loads further away from the edge creating a larger and deeper tensile zone. The maximum transverse tensile stress occurs at around 30 mm below the loaded surface in blocks with a small edge distance of 30 mm. but at 130 mm in a block with a large edge distance of 280 mm.

From fig.A.1-3 indicate that stresses obtained from the tests tend to fluctuate. This is probably due to the use of the Demec gauge with 50 mm gauge length, which is not sensitive enough to detect small strains. However, the experimental stress distributions still follow the stresses given by the FEM with three discrepancies. High compressive stresses were not recorded in blocks E2 and E3 due to the difficulties in putting Demec points close to the loaded surface. At high loads, tensile stresses obtained experimentally are higher than those

estimated by FEM. This can be explained by the presence of micro-cracks which are not considered in the FEM analysis. Stresses at the bottom of the blocks were recorded as tension during the experiment while compression is suggested by FEM analysis. The tensile stresses in the experiment are generated by the deflection of the supporting beam which is assumed to be fixed in the FEM analysis.

Fig.4.2 shows the variation of the bearing strength of the concrete block with edge distance; the values are plotted as two dimensionless ratios: f_b/f_c' against $W_a/0.5a_1$. It can be seen that the graph is composed of two straight lines, they meet each other at $W_a/0.5a_1=3.5$ which corresponds to the edge distance of 90 mm. It is suggested that with edge distances smaller than 90 mm, decrease in edge distance will result in a dramatic loss of confinement by the surrounding concrete which leads to a large decrease in the bearing strength of the concrete block. On the other hand, with edge distances greater than 90 mm, the increase in edge distance will steadily increase the confinement by the surrounding concrete and a higher bearing strength is obtained. The bearing capacity of the concrete block under concentrated strip load can be estimated by

$$\frac{f_b}{f_c'} = \begin{cases} 0.12W_a/a_1 + 1.16 & \text{—— } W_a/0.5a_1 > 3.5 \\ 0.47W_a/a_1 + 0.55 & \text{—— } W_a/0.5a_1 < 3.5 \end{cases} \qquad (4.1)$$

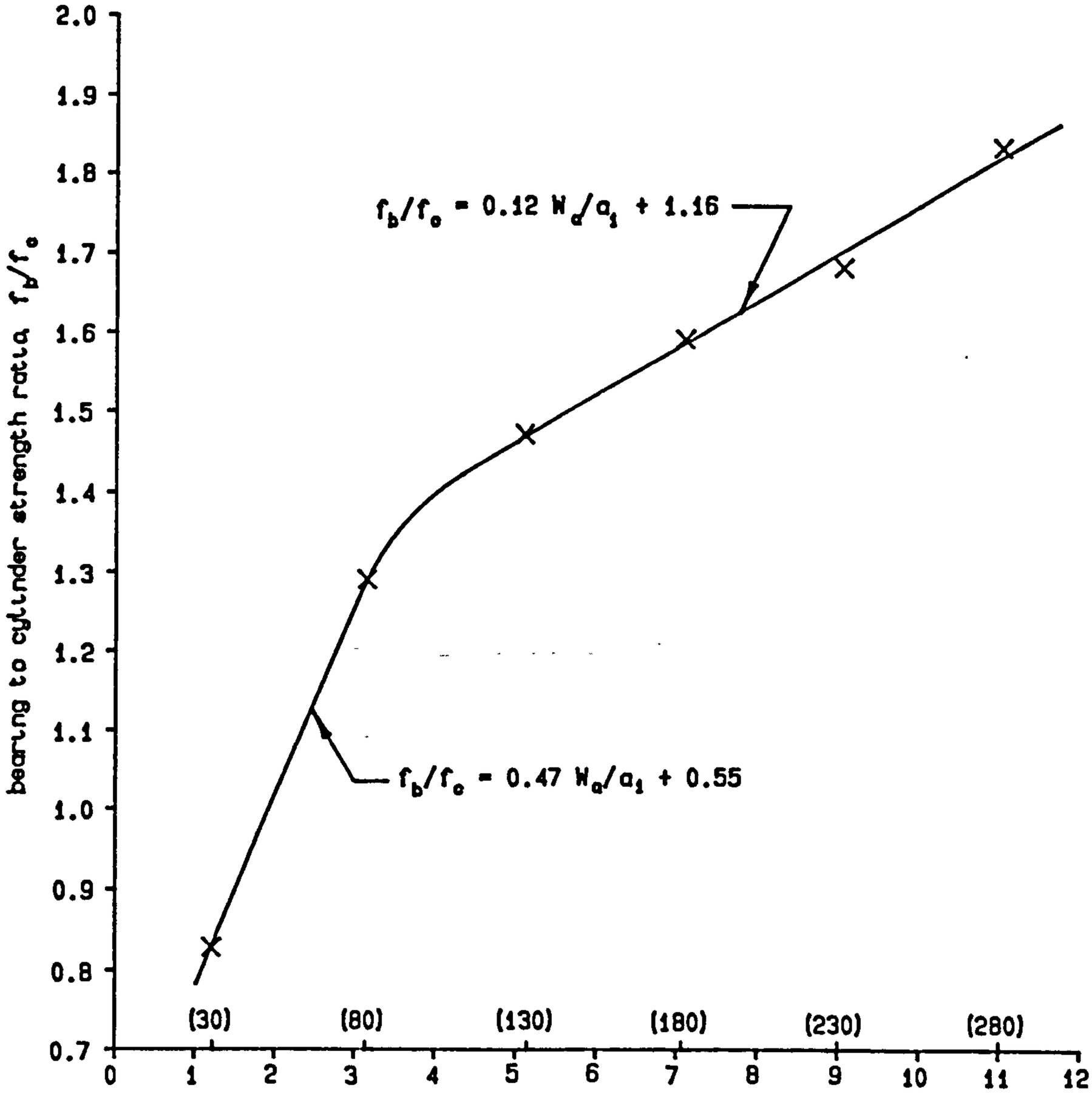

FIG.4.2 Effect of edge distance in blocks of series E.

H (mm.)	R = 3.94	R = 7.87	R = 15.7	R = 63.0
H = 1000	0.96	0.96	0.95	0.96
H = 800	0.95	0.95	0.95	0.95
H = 400	0.97	0.98	0.98	0.98
H = 200	1.57	1.62	1.64	1.64

Table 4.1 Ratio of compressive stress at loaded line to average stress at the bottom of the blocks.

4.2.2 EFFECT OF HEIGHT AND LOADING AREA RATIO

Fig.A.4-19 show both the transverse strain distributions along the loaded line and the vertical strains across the mid-height of the specimen. They are plotted together with the values obtained by FEM analysis.

In general, the experimental data agrees well with the theoretical values and with less fluctuation because a Demec gauge of larger gauge length, 100 mm is used thus increasing the sensitivity. Again, in observing the figures, it can be seen that all the specimens have a compression zone at the top immediately below the loading plate. Their sizes vary with the size of the bearing plate. Below this compression zone is a region of tension, usually described as the bursting zone. Again, the size depends on the size of the bearing plate; maximum tensile strain occurs at 100, 50, 25, and 10 mm below the loading surface when loaded respectively with 101.6, 50.8, 25.3 and 6.35 mm width bearing plates. This bursting zone extended to a depth of 350 mm below the loaded surface for specimens with large bearing plates and 300 mm for those with smaller bearing plates. Nevertheless, below this bursting zone, is a virtually unstressed region especially for high specimens. For shallow specimens, tensile strains are recorded at the bottom of the specimens. These are believed to come from two sources. Firstly, they are actually the tail of the bursting zone; this is particularly important for specimens

with large bearing plates, as the bursting zone for these specimens extends to a greater depth. Secondly, they are caused by the settlement of the supporting beam, this creating a bending moment at the bottom and consequent tensile stresses and strains. Settlement is increased with the magnitude of the load; large bearing plates usually takes more load thus producing a larger tensile zone at the bottom of the specimens, fig.A.16-18.

Compressive strain at mid-height agrees well with that obtained by FEM analysis with a few exceptions according to fig.A.4-19. In some circumstances, fig.A.12-15, the experimental compressive strains tend to be smaller than those estimated by FEM. This is probably due to the estimation of Young's Modulus of the specimen. Blocks R1-H3, R2-H3, R3-H3 and R4-H3 exhibit this discrepancy as they were cast from the same batch of concrete. Apart from this, R1-H4 recorded a particularly high compressive strain around the middle of the specimen, this is in fact due to the presence of a crack across a pair of demec points. This should be ignored in reading this figure.

As shown in fig.A.4-7, compressive strain was almost uniform at mid-height for high specimens with 1000 mm height. As the height of the specimen decreases, compressive strain is increasingly more concentrated below the load position. This is obvious in specimens with 200 or 400 mm height

(fig.A.12-19). Moreover, within the two specimens of equal height, the one loaded with a smaller bearing plate had a higher concentration of compressive strain than the others. Table 4.1 tabulates the ratios of the vertical stress at loaded line to the average compressive stress for all the sixteen specimens.

The ratio of bearing strength to cylinder crushing strength is plotted against the footing to loaded area ratio in fig.4.3. It is noted that results for all the specimens with height other than 200 mm come very close to each other. Shorter specimens have higher bearing strength but this is not very significant. Thus for specimens with 200 mm in height, there is a 30% increase in strength in comparison with others of similar loading condition but greater in height. This is probably due to the disturbance of the tension zone by the base of the specimen. The restraint at the bottom of the specimen by the base contributes a compressive force which delays the splitting of the specimen along the loaded line and thus a higher bearing strength results. The bearing strength ratios estimated by Shelson [2] and Kriz [18] are shown on the same graph in fig.4.3. It can be recognized that Kriz's estimates are conservative for all values of loaded area ratio while Shelson's estimates are conservative for a high loading area ratio, R but become unsafe as the values of R falls below 13.

Fig.4.4 shows how the ratio of bearing to cylinder

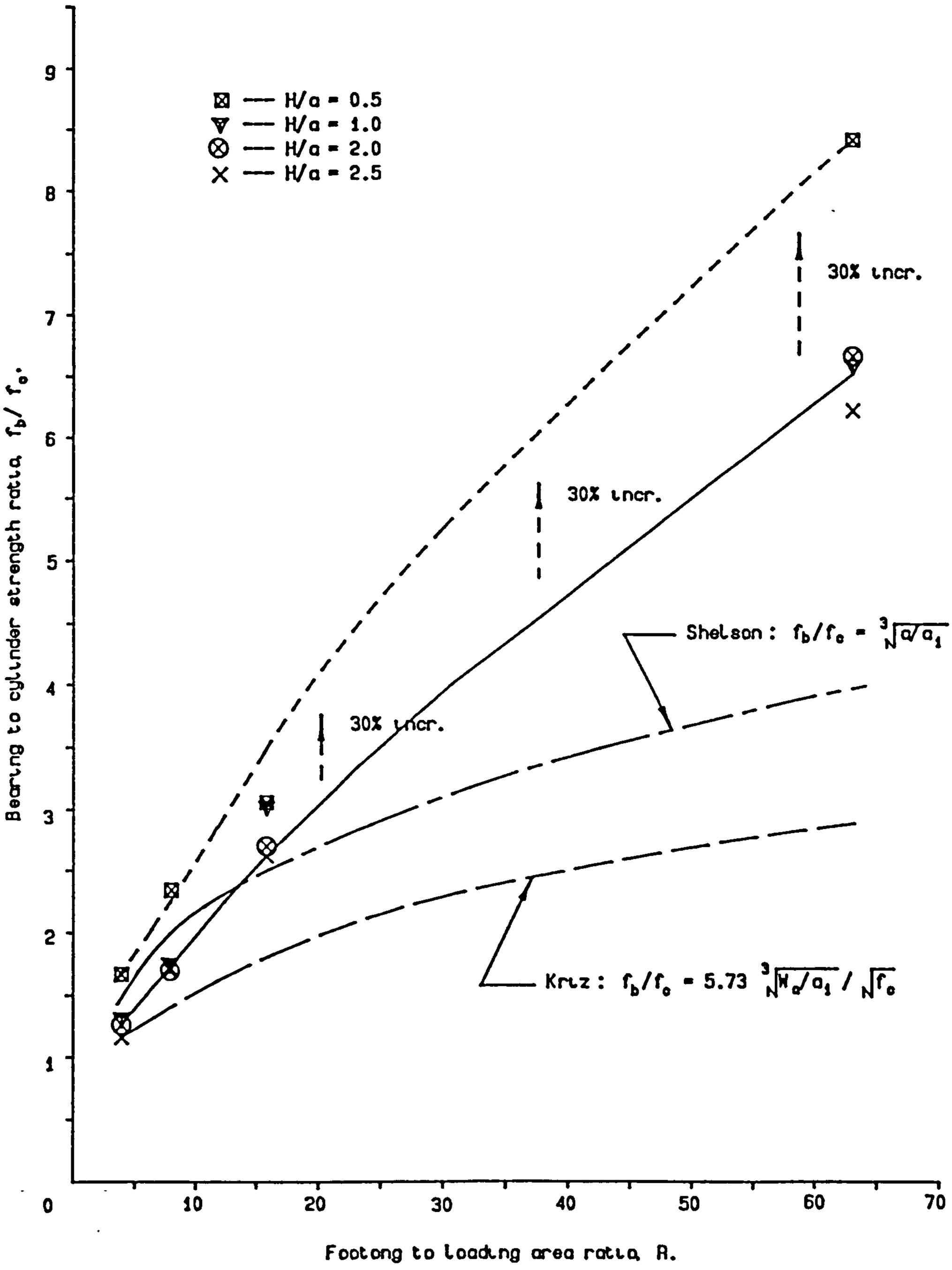

Fig.4.3 Bearing strength ratio vs loading area ratio.

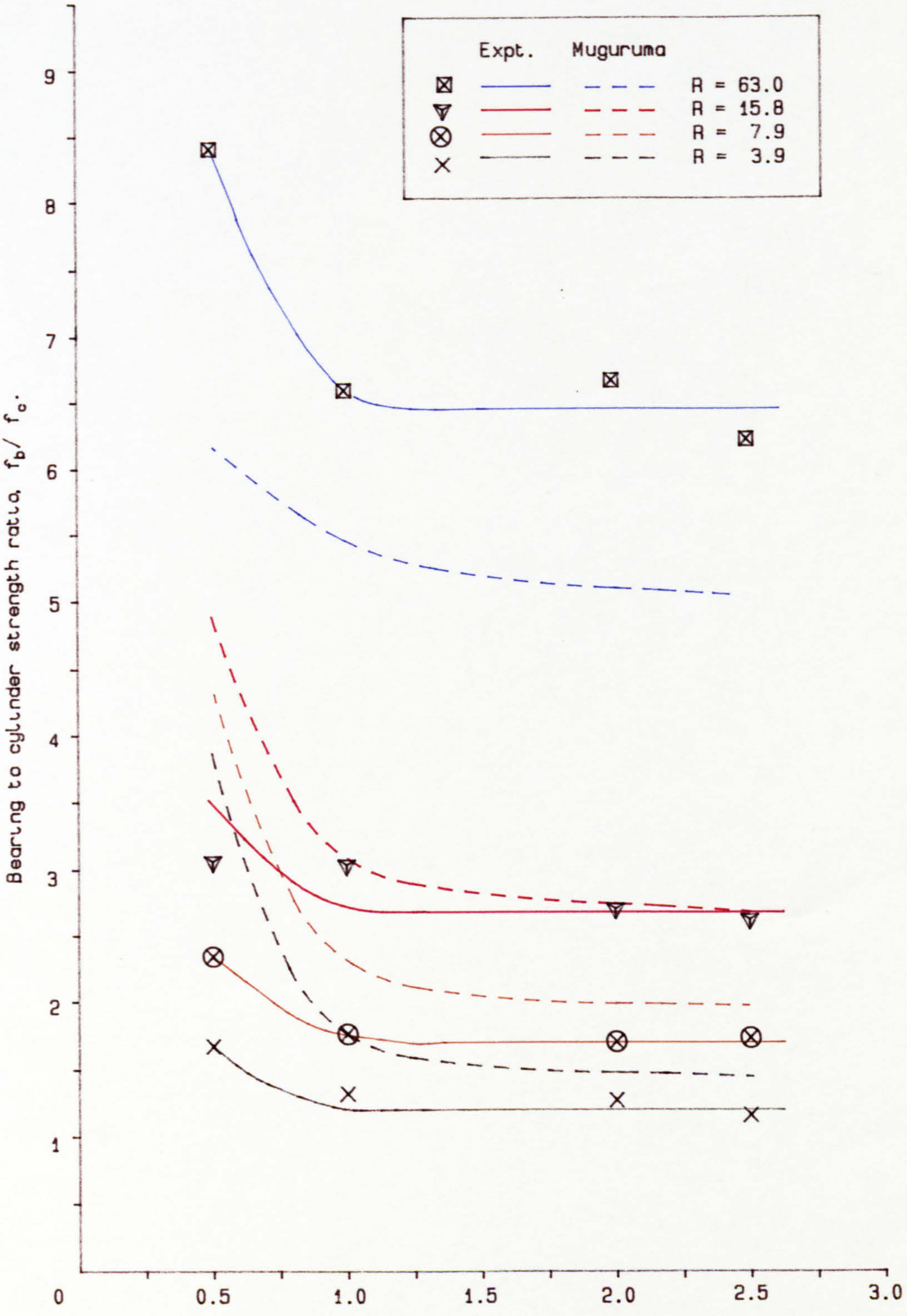

Fig.4.4 Bearing strength ratio vs height to width ratio.

strength varies with the height of the specimens. It can be seen that the bearing to cylinder strength ratio is unchanged with height for specimens higher than 600 mm. Below this height the bearing strength begins to increase slowly and then more rapidly at heights less than 400 mm. This is coincident with the way that compressive force is concentrated at the bottom of the specimen (table 4.1). The values of bearing to cylinder strength ratio estimated by Muguruma [8] are also shown in fig.4.4. Muguruma also gives a similar trend of increase in strength with short specimens as found in the experiments. However, he appears to over-estimate the ratio for the specimens with a bearing area ratio less than 16 and under-estimating those greater than 63.

4.2.3 SIZE EFFECT

The distributions of transverse and vertical strain of blocks S1-S3 are very similar to those in series R-H (fig.A.20-22). They agree well with those obtained by FEM analysis.

The size effect was first introduced by Niyogi [(1974),(19)]. He stated that the bearing strength falls as the size of the specimen is increased. If the loading area ratio, R remained constant, the bearing capacity would decrease with the increase in size according to table 4.2. Al-Nijjam

[(1981),(23)] stated that the bearing strength of concrete is dependent on a factor of

$$(a'/a)^{1/4} \qquad (4.2)$$

where a' = width of the original specimen

according to his test results.

Fig.4.5 shows how bearing strength varies with the size of the specimens. It was found that as the size of the specimens decreases, their strength increases in an exponential nature.

On the same figure (fig.4.5) the way in which bearing strength increases with the decrease in size as suggested by Al-Nijjam, is plotted along with what obtained in this investigation. Al-Nijjam's estimation has a more gentle increase in bearing strength as the size decreases. It is in fact more suitable for larger specimens. For this range of scale phenomena there is adequate aggreement with the following expression

$$f_b/f_c' = k \left[1.45\, e^{-a/80} + 0.9\right] \qquad (4.3)$$

where a = the width of the specimen measured in mm.
k = proportional constant.

4.2.4 EFFECT OF BASE FRICTION

In the presence of a sheet of PTFE at the bottom of the specimen, the mode of failure for blocks B1 and B2 changed. As has been described in chapter 3, splitting occurs from the

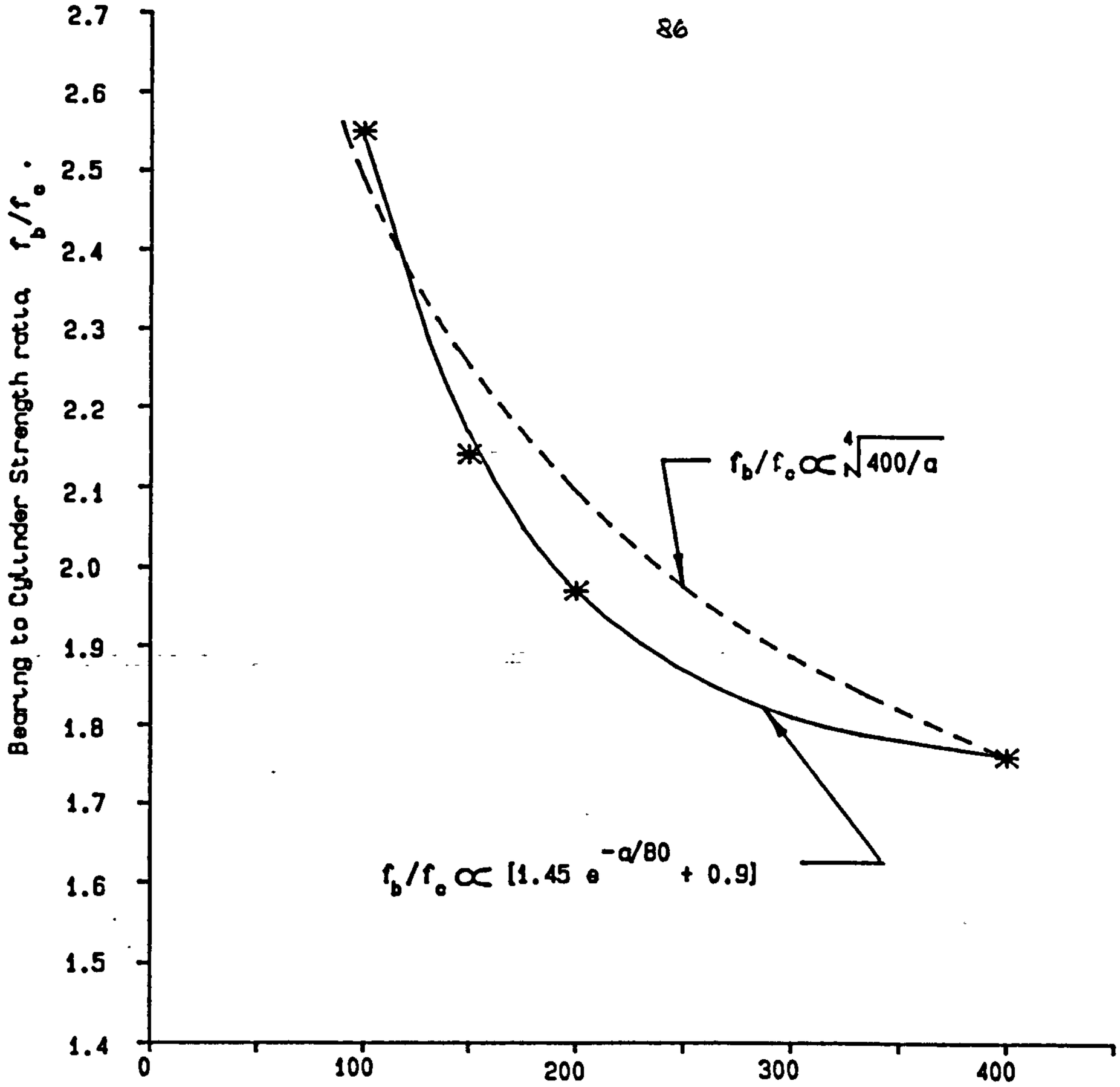

Fig.4.5 f_b/f_c vs size of the blocks a.

% of size increase	% of decrease in bearing strength
3.0	25
2.0	15
1.5	12
1.3	4

Table.4.2 Size effect suggested by Niyogi (19).

bottom of the specimen and failure of these specimens took place without actually crushing the concrete below the bearing plate. This is confirmed by fig.A.23. The tensile strain recorded in block B1 was very much larger than expected. In fact, it was not purely tensile strain, because a crack occurring at the early stage of the experiment, coming from the bottom of the specimen is included. Moreover, the settlement of the support becomes more dominant with the presence of a layer of softer material (PTFE) at the base, thus adversely affecting the cracking of the specimen from the bottom. Apart from this discrepancy, the tensile strain distribution agrees well with the theoretical value by FEM analysis (fig.A.23-26). It is interesting to note that the theoretical transverse strain is not zero at the bottom of th specimen. Tensile strains at the base indicate that tension force is needed in order to restrain the base.

Table 4.3 shows how PTFE affects the bearing strength of the concrete blocks. It can be seen that the bearing strength decreases with a reduction of the base friction. This reduction is (22%) for a short specimen loaded with a large plate,(block B1). This is understandable in that short specimens depend on base friction to gain their bearing strength, especially when loaded with large bearing plates, because the tension zone is more likely to extend to the base. A larger bearing plate means that a higher value of load is needed for failure; high loads can produce larger settlement of

the supporting beam and thus further reduction in the bearing strength. Blocks B2 and B3 show similar reductions in strength of 14 and 16% respectively, because block B2, although short, is loaded with a small bearing plate and block B3 is high but loaded with a larger bearing plate. The smallest reduction in strength is in block B4, only 8%. This is bcause it has the height and is also loaded with a small bearing plate so that the tension zone can hardly reach the bottom, and there is not much bending of the block with a small bearing plate.

4.3 REINFORCED CONCRETE BLOCKS

The crack patterns for all the reinforced concrete blocks had been shown in the previous chapter, fig.3.13a. Fig.3.13b gives an idea of how the maximum crack width varies with load. In this section, the behaviour of each test, the crack patterns, crack widths and strain distributions in concrete and steel will be discussed and compared with each others in detail.

Blocks R1/1, R1/2 and R2/1 are reinforced with steel of similar arrangement but with different diameters of transverse steel of 6, 10 and 8 mm respectively. These three specimens failed with similar load of 600, 590 and 620 kN respectively, (table 3.1b). Although their crack loads are quite different from each other, they are believed to come from two sources:

<1> differences in concrete properties and <2> the recognition of the presence of cracks during the test. They have similar crack patterns, the most vital crack is the one along the loaded line. Blocks R1/1 and R1/2 have a more brittle behaviour than R2/1 which is again considered to be dependent on the concrete properties rather than the reinforcement. The distributions of transverse concrete strain along the loaded line for these specimens are shown in fig.A.27-28. They have similar distributions of strain, a large compressive strain at the top immediately below the loading plate and then followed by a tension zone extending to around 300 mm below the loading surface. Below this tension zone is an unstressed region, but occasionally, tension is recorded at the bottom indicated a bending of the supporting beam. Strains in the reinforcement are shown in fig.A.35-37. Apart from the yielding of one particular stirrup in Block R2/1, the remainder have not yielded even after failure of the specimen. This suggested the ineffectiveness of this form of reinforcement. In fact, these specimens failed by buckling of the vertical steel between two transverse reinforcing bars owing to the lack of restraint. This can be improved by reducing the spacing between the transverse steel.

Block R2/2 employs the idea of pushing the transverse steel upward so that it has stronger reinforcement in the higher tension region. However, the result is not encouraging: it has a lower ultimate load at 590 kN than 620 kN in R2/1.

R2/2 has a larger crack width, up to 1.12 mm at 580 kN. It has a central crack extending from the top to the bottom of the specimen. At low load the distributions of transverse strain are similar to Block R2/1. At high load, (larger than 400 kN), transverse strain is not confined to the top region but extends to the bottom of the specimen, fig.A.28. Most of the reinforcement along the loaded line does yield, fig.A.38, this suggested that the effectiveness of the transverse reinforcement depends on its spacing. The transverse reinforcement in R2/2 has been placed too high, and although it has an effective confinement at the top, an unreinforced region is left below, which is still within the tension zone. Therefore, a large crack width and lower ultimate load has resulted.

Blocks R3/1 and R3/2 have similar amounts of transverse reinforcement in terms of cross-sectional area of steel as in R1/2. They use smaller diameter steel but closer spacing. R3/1 used stirrups of 6 mm diameter and 26 mm spacing, while R3/2 used stirrups of 8 mm diameter and 52 mm spacing. Block R3/1 has a crack load and ultimate load of 650 and 770 kN while R3/2 has crack and ultimate load of 520 and 643 kN respectively, which is much higher than the corresponding values of 400 and 590 kN in block R1/2. The use of smaller diameter steel and closer spacing increases the ductility as the specimen fails, fig.3.13b. Cracks in these two specimens are spread more radially rather than concentrated along the

loading line and have smaller crack width. This indicates that the reinforcement is effective in distributing the stresses to the whole reinforced area rather than concentrated in the line of loading. As shown in fig.A.29, distribution of strain on the concrete surface is similar to block R1/2 but is lesser in magnitude especially in the tension zone in block R3/1. Fig.A.39-40 shows that most of the stirrups in block R3/1 and R3/2 along the loading line, especially those at the top, yielded. Those at the bottom and next to the loading line have been stressed quite significantly. Above all these phenomema suggested that reinforcing with thinner and more closely spaced steel is an effective way of increasing the bearing capacity of the concrete block. Moreover, failure of block R3/1 is in fact not by splitting of the block into two halves, but by sliding of the bearing plate towards the rear of the block, because of setting up errors. Strictly speaking, block R3/1 should withstand a higher load than 770 kN.

Block R4/1 and R4/2 have different forms of reinforcements, fig.3.1. Block R4/2 has long stirrups which enclosed all the vertical stirrups while R4/1 has smaller ones further away from the loaded line enclosing two vertical stirrups and has larger stirrups below the loading position enclosing four vertical stirrups. They were designed to compare their performance with block R2/1 which has only small stirrups each of which enclosed two vertical stirrups. As shown in fig.3.13, their crack patterns are slightly different

from each other. Block R4/2 has the simplest crack pattern, only a single crack along the loading line. As the stirrups decrease in size, in blocks R4/1 and R2/1, more cracks are formed and they radiate from the loading plate. Strain in the steel, fig.A.37, 41-42 indicate that when the small loop stirrups are used higher stress is generated in the steel, this suggested that this form of stirrup is more effective in resisting bearing stresses. The ultimate load of block R4/1, 680 kN is greater than that of block R4/2, 600 kN, confirming this idea. However, block R2/1 has a rather low ultimate load 620 kN, and this may be due to the difference in the properties of the concrete. If the differences of ultimate load and crack load P_u-P_c are considered, it can be found that block R2/1 has the largest difference, P_u-P_c=170 kN, and this becomes smaller in block R4/1, 130 kN and smallest in block R4/2, 60 kN. Therefore, it can be concluded that small stirrups are more effective in resisting bearing stress than large stirrups. This can be explained as more lateral restraint can be provided by smaller stirrups.

Blocks R5/1 and R5/2 were designed to compare the bearing strength with the distribution of the reinforcement, fig.3.13. Block R5/2 has the simplest form of arrangement; two vertical and two horizontal stirrups. Block R5/1 has one more bay of reinforcement, one on each side of the loading line and one more row of reinforcement at the bottom. They are used to

compare their performance with block R2/1 which has one further bay of reinforcement on each side of the loading line and one more row of reinforcement than block R5/1. From fig.A.31 and 28 it can be seen that the distribution of strain on the concrete surface is very similar in blocks R5/1, R5/2 and R2/1. The strains in the reinforcement, figs.A.37, 44-45, are again similar, except that yielding of one stirrup is found in block R2/1. All the others had not reached yield point before the concrete block failed. However, as their crack patterns are considered, there is a difference in mode of failure found in block R5/2, which had its load transferred to the bottom of the reinforcing matrix and failed as if load is applied at the bottom horizontal stirrup in a block of plain concrete. Failure was due to the formation of a wedge of concrete below the reinforcing matrix, followed by the separation of the block along the loading line. It failed with the characteristic of all the plain concrete blocks, —— a brittle mode of failure. It is therefore recommended that the matrix of reinforcement should have a width at least as wide as the loading plate. As far as the ultimate load is concerned, there is only a slight different in magnitude between blocks R5/1, R5/2 and R2/1. It is therefore difficult to decide whether a wider spread of reinforcement do increase the bearing capacity of the concrete block at this stage.

Blocks R5/1, R6/1, R6/2, R7/1, R7/2 and R8/2 were reinforced with the same amount and form of reinforcement but

with different edge distances varying from 80 to 330 mm. They were designed to investigate the effect of edge distance on the reinforced concrete blocks. Figs.A.32-34 show the distribution of transverse strain on the concrete surface along the loaded line. In general, the experimental and theoretical values agree with each other at low load except near the bottom of the block. Higher tensile strain recorded at the bottom of the block during the tests is due to the bending of the supporting beam which is assumed rigid during FEM analysis. At high load, the experimantal strains are greater than those given by FEM analysis due to the presence of cracks. This discrepancy happens at lower loads as the edge distances decrease. Similar to plain concrete blocks, the depth of the tension zone below the loading plate increases as the edge distance increases. More cracks are developed for blocks with small edge distances, fig.3.13. This is because of the earlier formation of cracks with blocks with small edge distances. Fig.4.6 is plotted to show the relation between the difference between ultimate and crack load (P_u-P_c) and the edge distance W_a of the blocks. It can be seen that smaller edge distance exhibit a larger (P_u-P_c) value for blocks with edge distance smaller than 180 mm which correspond to $W_a/0.5a_1=3.5$. Blocks with edge distances larger than this failed as soon as the block cracked. Therefore, it can be said that reinforcement is more effective with a block of small edge distance as it can prevent the block from shearing at the corners to cause failure. Strains in the

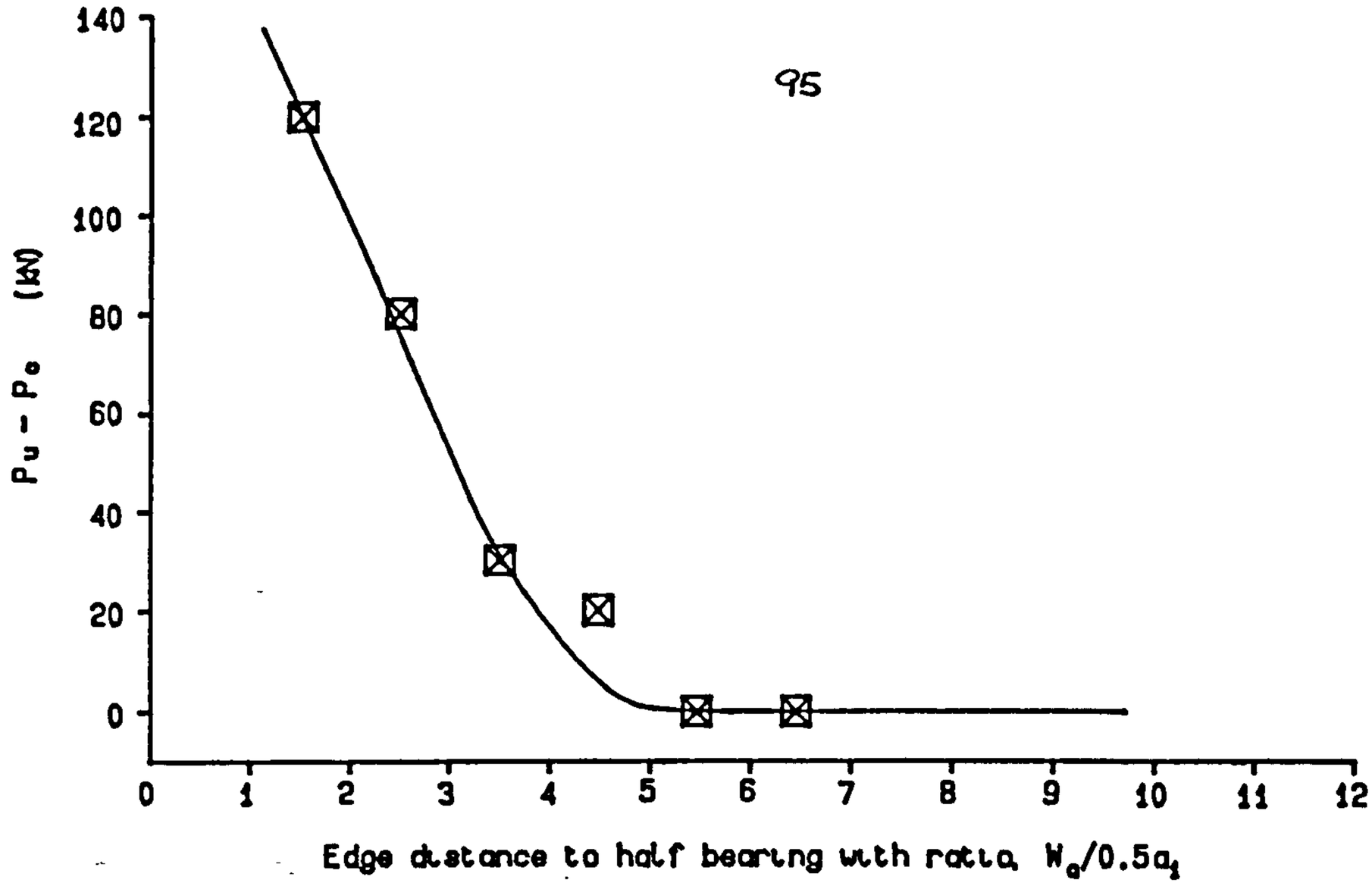

Fig.4.6 $P_u - P_o$ vs edge distance W_e.

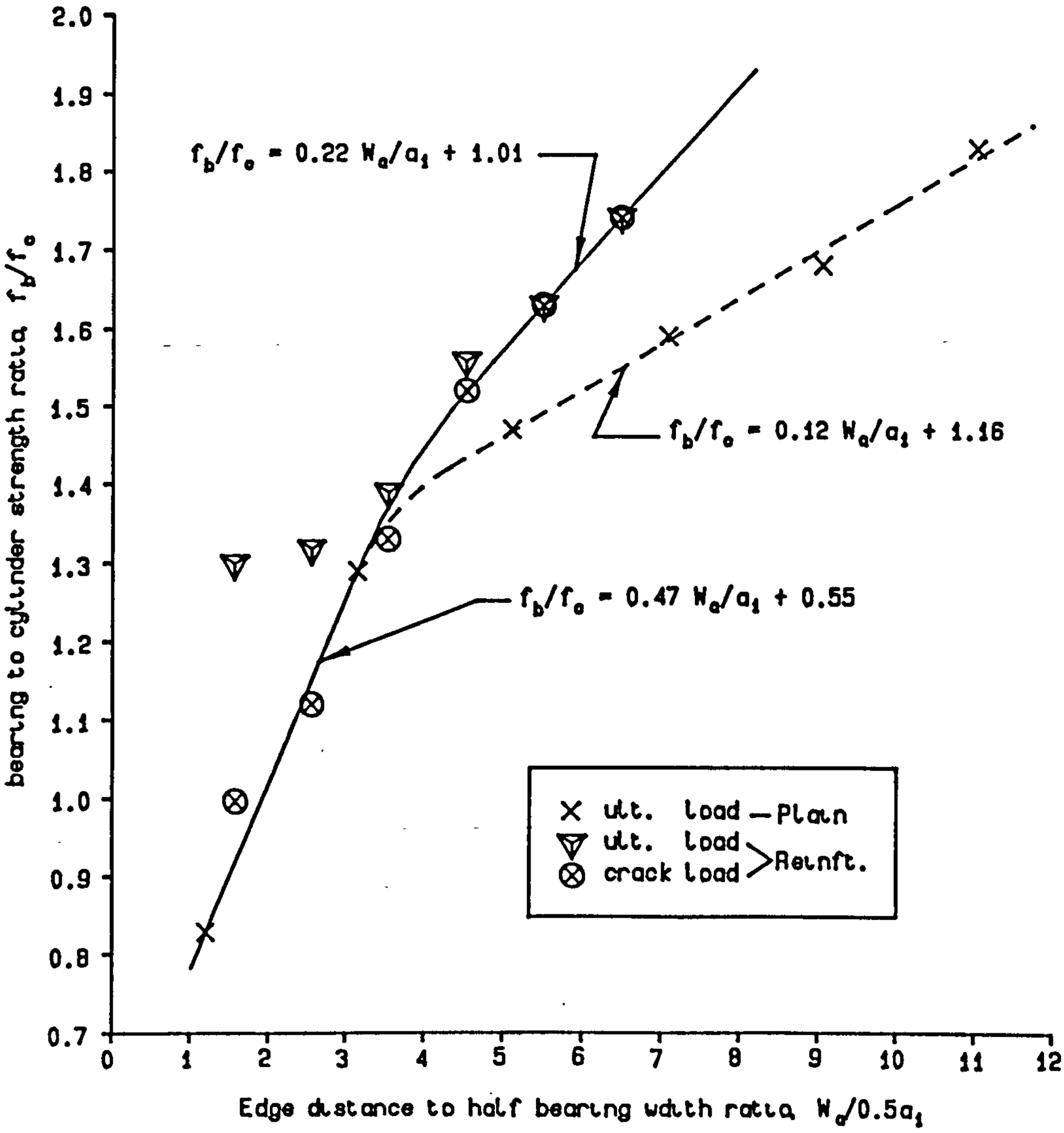

FIG.4.7 Effect of edge distance in blocks.

reinforcement are shown in figs.A.43, 45-49. Fig.4.7 is plotted of cracking to cylinder strength ratio against edge distance to half bearing width ratio. It can be seen that for $W_a/0.5a_1<3.5$, the cracking strength agrees well with Eq.4.1, and the concrete block cracks as soon as its corresponding plain concrete block fails. For $W_a/0.5a_1>3.5$, the cracking strength is higher than that estimated by Eq.4.1. In conclusion, the cracking strength of a concrete block can be estimated by

$$f_b/f_c' = \begin{cases} 0.47W_a/a_1 + 0.55 & \text{——————} \quad W_a/0.5a_1<3.5 \\ \left.\begin{array}{ll} 0.12W_a/a_1 + 1.16 & \text{— plain} \\ 0.22W_a/a_1 + 1.01 & \text{— reft.} \end{array}\right\} & W_a/0.5a_1>3.5 \end{cases} \tag{4.4}$$

4.4 CONCLUSION

The behaviour of concrete blocks under bearing pressure can be summarized by the following:

(A) PLAIN CONCRETE BLOCKS

<1> Specimens with concentrated load near the edge $W_a/0.5a_1<3.5$, failed by shearing off the corner while specimens with a larger edge distance $W_a/0.5a_1>3.5$ failed by spliting the concrete block into two halves.

<2> The depth of the tension zone below the loading plate increased as the edge distance increased.

<3> The bearing capacity of plain concrete blocks under concentrated strip load can be estimated by

$$f_b/f_c' = \begin{cases} 0.12\ W_a/a_1 + 1.16 \quad \text{——} \quad W_a/0.5a_1 > 3.5 \\ 0.47\ W_a/a_1 + 0.55 \quad \text{——} \quad W_a/0.5a_1 < 3.5 \end{cases} \qquad (4.1)$$

<4> When a concrete block is loaded with a bearing plate, a compression zone is generated at the top immediately below the loading plate. Below this compression zone is a region of tension (bursting zone). Both the size of the compression zone and the bursting zone increase with increase in size of the bearing plate.

<5> Specimens with heights shorter than 300 mm have their tension zone confined by the restraint at the bottom of the specimen. This contributes a compressive force which delays the splitting of the specimen. The bearing strength of specimens 200 mm in height is 30% higher than corresponding specimens of similar condition but greater in height.

<6> Muguruma [59] describes a similar trend of increase in bearing strength with short specimens but he appears to over-estimte the strength for specimens with a bearing area ratio less than 16 and to under-estimete those greater than 63.

<7> Kriz's estimates [49] are conservative for all the values of loaded area ratio while Shelson's estimates [76] are conservative for a high loading area ratio, R but become unsafe as the value of R falls below 13.

<8> Reducing the size of the specimen can increase its bearing strength and this is known as the size effect (or scale effect). Al-Nijjam [63] has stated that the bearing strength of the concrete is increased by a factor of

$$(a'/a)^{1/4} \qquad (4.2)$$

<9> Al-Nijjam's estimation [63] has a more gentle increase in bearing strength as the size increases and is more suitable for larger specimens. From the present experiments, the bearing capacity is found to be proportional to the following expression

$$f_b/f_c' = 1.45\ e^{-a/80} + 0.9 \qquad (4.3)$$

<10> Bearing strength decreases with a reduction of the base friction. The largest reduction (22%) is found with short specimens loaded with a large plate (block B1) while the smallest reduction (8%) corresponded to high blocks loaded with a small plate (block B4).

(B) <u>REINFORCED CONCRETE BLOCKS</u>

<1> Similar strain distributions are obtained in reinforced

concrete blocks as in plain concrete blocks.

<2> The bearing capacity of the reinforced concrete block is not dependent on the diameter of the reinforcement.

<3> Reinforcement should be maintained in the whole of the tension zone. Lack of reinforcement in any part of the tension zone may result in large crack widths and lower strength.

<4> Closely spaced smaller diameter reinforcement is much more effective in resisting bearing force than widely spaced thick reinforcement. With this form of reinforcement more restraint can be provided to the vertical reinforcement by horizontal stirrups. This can prevent the buckling of the vertical steel at early stages and provide a better spread of tensile stress to the surrounding block. Radial cracks with small crack widths are found in place of a single vertical crack with large crack width.

<5> The use of small interlocking stirrups is more effective than using a single long stirrup, because more lateral restraint can be provided by small interlocking stirrups.

<6> From the present tests, it is difficult to tell whether the distribution of reinforcement has any effect on the bearing capacity of the blocks. It is recommended that the matrix of reinforcement should have its width at least as wide as the loading plate to prevent brittle failure of

the block below the reinforcement.

<7> Reinforcement is more effective with blocks of small edge distance, $W_a/0.5a_1<3.5$ as it can prevent blocks from shearing off the corners.

<8> The cracking strength of the reinforced concrete block with $W_a/0.5a_1<3.5$ can be estimated by the bearing strength of plain concrete block using Eq.4.1.

<9> In general, the cracking strength of reinforced concrete blocks and the bearing strength of plain concrete blocks can be estimated by

$$f_b/f_c' = \begin{cases} 0.47W_a/a_1 + 0.55 \text{ ——————} & 2W_a/a_1<3.5 \\ \left.\begin{matrix} 0.12W_a/a_1 + 1.16 \quad \text{(plain)} \\ 0.22W_a/a_1 + 1.01 \quad \text{(reinft.)} \end{matrix}\right\} & 2W_a/a_1>3.5 \end{cases} \tag{4.4}$$

Block no.	f_b / f_o	% of reduction in strength
B1	1.30	22 %
R1-H4	1.67	
B2	7.45	14 %
R4-H4	8.41	
B3	0.98	16 %
R1-H1	1.16	
B4	5.72	8 %
R4-H1	6.22	

Table 4.3 Reduction in strength with PTFE at the bottom of the blocks.

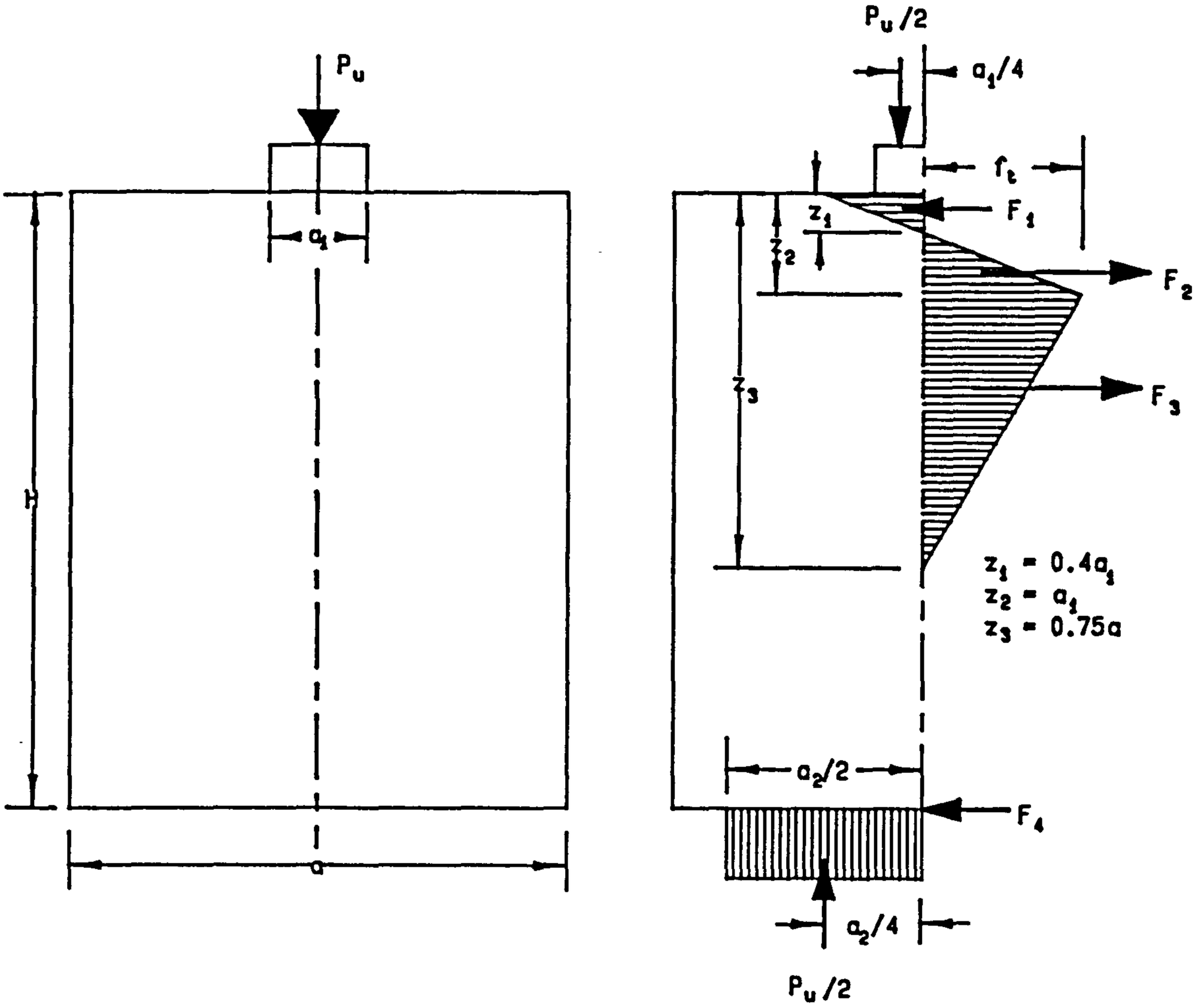

Fig.4.8 Structural model of a concrete block subjected to concentrated load.

4.5 PROPOSED SOLUTION

Consider a plain concrete block (axbxH) as shown in fig.4.8a subjected to a vertical compressive force along its centre line at its top surface through a steel plate, width a_1 and across the full thickness b of the concrete block. At the bottom, the concrete block is supported over its entire surface.

Fig.4.8b shows the concrete block split into two halves and its internal forces are considered. First of all, it is assumed that the bearing plate is thick and rigid enough to have a rectangular stress distribution immediately below the steel bearing plate. Therefore, after splitting there is a resultant force $P_u/2$ acting at a distance $a_1/4$ from the line of splitting. Along the line of splitting, the distribution of stresses is rather complex and assumptions are made according to observations made during the experiments. It is observed that there is a compression zone at the top of the block immediately below the bearing plate followed by a region of tension and then an unstressed region at the bottom. For reasons of simplicity, they are assumed to be linearly distributed along the splitting line. As described in section 4.2.2, it is noted that the depth of the compression zone is dependent on the width of the bearing plate. According to the graphs showing the experimental transverse stress distributions, figs.A.4-19, it is reasonable to assume that the

compression zone ends at a depth of $0.4a_1$ from the loaded surface. Below this compression zone is a region of tension, and similarly the position of the maximum tensile stress is dependent on the width of the bearing plate. With the help of figs.A.4-19, it is assumed that this maximum tensile stress occurs at a depth a_1 below the loading surface. The position where this tension zone ends is not distinct and it is rather difficult to determine as there is usually a long tail of small stress before it finally become zero. However, it is assumed that the tension zone effectively ends at a distance 0.75a below the loading surface.

At the moment, only higher blocks H/a>0.75 are considered and for high blocks, compressive stress is distributed uniformly along the base, figs.A.4-11. A rectangular distribution of compressive stress is therefore asumed at the bottom of the block. As demonstrated by blocks B3 and B4, where the friction at the base of the blocks was released, behaviour was similar to their counterparts R1-H1 and R4-H1, This suggests that the friction at the base for high blocks is negligible and therefore, can be ignored in this model. Furthermore, the concrete block is assumed to fail as soon as the maximum tensile stress reaches the tensile strength of concrete as estimated by splitting cylinder test.

Fig.4.8b shows the proposed model and the assumed stress distribution. The resultant forces and their centres of action

have been calculated based on a unit thickness of the concrete block and they are as follows:

$$\begin{aligned} F_1 &= F_2 + F_3 - F_4 & z_1 &= 0.4a_1 \\ F_2 &= f_t\cdot(z_2-z_1)/2 & z_2 &= a_1 \\ F_3 &= f_t\cdot(z_3-z_2)/2 & z_3 &= 0.75a \\ F_4 &= 0 & z_4 &= H \end{aligned} \qquad (4.5)$$

By taking moments at the position of the resultant force F_1 and considering the free body diagram in fig.4.8b

$$P_u\cdot(a_2-a_1)/8 = \left[2z_2\cdot F_2 + (z_3-z_1+2z_2)F_3\right]/3$$

$$\therefore \quad a_2 = 4\left[4z_2\cdot F_2 + 2(z_3-z_1+2z_2)F_3\right]/3P_u + a_1 \qquad (4.6)$$

Although many researchers [6,7,32,49,76] adopted the cube root formula

$$f_b/f_c' = R^{1/3} \qquad (4.7)$$

this has been demonstrated to be conservative especially for large values of R (fig.4.3). It appears that

$$f_b/f_c' = R^{1/2} \qquad (4.8)$$

would be a more appropriate formula for the estimation of the bearing capacity of the concrete block. The ratio R is the footing to the loading area ratio a/a_1 and in this case it should be related to the reduced dimensions (or effective block size), a_2 for $a_2<a$. Therefore,

$$f_b/f_c' = (a_2/a_1)^{1/2} \qquad (4.9)$$

Substituting Eq.4.9 into 4.6,

$$(f_b/f_c')^2 = \left[16z_2 \cdot F_2 + 8(z_3 - z_1 + 2z_2) \cdot F_3\right]/3P_u \cdot a_1 + 1 \quad (4.10)$$

since $P_u = a_1 \cdot f_b$ and let $r = f_b/f_c'$, therefore,

$$r^2 = \left[16z_2 \cdot F_2 + 8(z_3 - z_1 + 2z_2) \cdot F_3\right]/3a_1^2 \cdot f_b + f_b/f_c'$$

$$r^3 - r - \left[16z_2 \cdot F_2 + 8(z_3 - z_1 + 2z_2) \cdot F_3\right]/3a_1^2 \cdot f_c' = 0 \quad (4.11)$$

By solving the cubic equation (Eq.4.11) the ratio of bearing strength to cylinder splitting strength can be obtained.

For blocks with height to width ratio less than 0.75, the calculation is based on the assumption that the tension zone ends at the bottom of the specimen. Moreover, for blocks with eccentric loading, the near edge side has a similar amount of confinement as the corresponding concentrically loaded block with a width equal to twice as the edge distance. Therefore, by using $a = 2W_a$, Eq.4.11 can also be used for the estimation of the bearing strength in eccentrically loaded concrete blocks.

4.6 COMPARISON WITH TEST RESULT

4.6.1 PLAIN CONCRETE BLOCKS

All the test results available from various sources

[32,49,62,65] are analysed in the light of the proposed method and also compared with the method given by Meyerhof [62], Hawkins [32], Shelson [76], Kriz [49], Muguruma [62], Niyogi [65] and Jensen [36]. The results are presented in table 4.4 for all concentrically loaded specimens and table 4.5 for all eccentrically loaded specimen. For easy comparison, ratios of the values of bearing capacity obtained from the experiment to the corresponding values obtained by calculation are tabulated together with the mean and standard deviation for each group of data with the same height to width ratio. Fig.4.10-18 are plotted with the ratios of bearing to cylinder strength obtained from experiment to those from the calculation with different formulae. They can be read in conjunction with table 4.4 and 4.5, so as to gain an idea of how the data are distributed about the diagonal line, on which experimental values would be equal to the calculated values of bearing strength. Furthermore, an overall mean and standard deviation are shown at the end of each table. In the calculation with Hawkins's and Meyerhof's formulae the values of α is assumed to be 27.5 degs. which is suggested by Hawkins (14). The internal angle of friction, φ is assumed to be 37 degs. as is recommendated in the literature [6,7,36] when calculated with Jensen's model.

It can be seen from fig.4.10 and table 4.4d that Meyerhof's equation can give a fairly good value of the mean, 0.98 for all the specimens with height to width ratio greater

than 1 but values are rather scattered around the diagonal line with a large value of standard deviation of 0.24. However, the deviation is reasonable for each group of specimens with the same height to width ratio (table 4.4), for instance, it has a standard deviation of only 0.04 and 0.08 for the specimens with H/a = 2 using Muguruma's and Niyogi's data respectively. Meyerhof tends to over-estimate the strength of high blocks and under-estimate for lower ones. This phenomenon becomes obvious for a block with height less than its width (table 4.4b and fig.4.10). It has an overall mean for all the specimens of 1.224 and standard deviation of 0.406. Meyerhof has considered the effect of height on the bearing capacity of the concrete block but gives the wrong trend. With his method of calculation bearing strength decrease with the decreasing height of the blocks but in fact, bearing strength is increased with decreasing height except for very short blocks H/a<0.33. Generally, Meyerhof's formula is not accurate for the estimation of bearing strength of the concrete block especially with specimens which have their height less than the width.

Hawkins gives better result in comparison with those calculated by Meyerhof. Although the mean for all specimens with H/a>1 of 0.888 is not as good as the 0.98 given by Meyerhof, the standard deviation is much smaller at 0.101 for specimens with H/a>1 and 0.158 for all specimens. Moreover, the mean for all specimens is good with only 5.4% under-estimated. With Hawkins' formula the results are similar

to those obtained from Meyerhof's formula, in that there is a trend of increasing under-estimation as the height to width ratio decreases. However, with H/a<0.33 a sudden decrease in bearing strength is recorded with Niyogi's data (mean test to calculated bearing strength equal to 0.81). This is probably due to the restraining force, which has increased to its maximum as the height decreases. Further reduction in height of the specimens may result in the weakening of the splitting strength of the specimen as the cross-sectional area is decreasing with height. Hawkins equation represents an improvement in the estimation of the bearing strength of concrete blocks in comparison with Meyerhof's estimation. It is an acceptable means of estimation, but it should be borne in mind that there is a certain percentage of over-estimation.

Shelson, Kriz, Muguruma and Niyogi developed empirical formulae. Amongst these four formulae, Shelson gives the best result with an overall mean of 1.005 and a standard deviation of 0.242, although there is obvious scatter on the graph (fig.4.12). The result is improved somewhat if only blocks with H/a>1 are considered: the formula has a slightly over-estimating mean of 0.958 and smaller deviation of 0.208. Kriz's empirical formula gives the safest estimate which has over 20% of under-estimation for specimens with H/a>1 and 25% for all specimens. His result is even more scattered than those with Shelson's formula; it has an overall standard deviation of 0.387 and 0.325 for all the specimens with H/a>1.

Muguruma's formula is the only empirical formula which considers the effect of height on the bearing capacity of the concrete blocks. This gives reasonably good results (mean = 0.915, deviation = 0.121), for specimens with H/a>1. However, his formula fails to gives a reasonable estimate for specimens with H/a<1, and his estimation of bearing capacity becomes negative, for a block with H/a = 0.33 (table 4.4b), which is not acceptable. Fig.4.14 shows that his equation over-estimates the strength of nearly all the specimens particularly for specimens with H/a<1. The overall mean and standard deviation are 0.751 and 0.368 respectively.

Niyogi's formula is another one which over-estimates the bearing capacity of the concrete block with a large standard deviation. He seriously over-estimates for concrete blocks with H/a>1, mean = 0.889 and with a good standard deviation, 0.244. The mean is improved at, 0.946 when all specimens, including those with H/a<1, are considered but the deviation becomes worse at, 0.329. In general, Muguruma's formula is good for the estimation of the bearing capacity of concrete blocks with H/a>1 but it cannot be used for blocks with H/a<1. Shelson gives a reasonably good estimate for all specimens including those with H/a<1. Kriz's formula is the safest estimator even for specimens with H/a<1 and it can be used as an upper bound bearing capacity.

Jensen's model is based on the equilibrium of internal

energy and external work. With his method of calculation, he seriously over-estimates the bearing strength of the concrete blocks with H/a>1 and with a large standard deviation (mean = 0.643, deviation = 0.205). Fig.4.16 shows that he has more or less over-estimated the strength of all the specimen with H/a>1 and under-estimated all those with H/a<1. In general, his formula gives scattered results with an overall mean and standard deviation are 0.884 and 0.374 respectively.

The proposed model gives excellent results for all the specimens with H/a>1; it has a mean of 1.005, which represents an under-estimate of only 0.5% and a small deviation of 0.098 (see fig.4.17). However, if specimens with H/a<1 are also considered, the result is not so good. The overall mean and standard deviation are 1.072 and 0.181 respectively. Moreover, the under-estimate seems to increase with the decrease in H/a ratio. Fig.4.9 plots the mean of the ratio of bearing capacity obtained in the tests to values obtained by the proposed model for each group of data against its corresponding height to width ratio. The number beside each symbol is the number of blocks involved in the relevant group. This shows that the under-estimate increases exponentially as H/a decreases. Regression analysis leads to the following equation:

$$f_{b(test)}/f_{b(cal.)} = 0.657\, e^{-1.15H/a} + 0.9 \qquad (4.12)$$

The increase in bearing strength for shorter blocks is believed to come from three sources:

<1> As the blocks become shorter, the end of the tension zone is disturbed and the transverse tensile stress will not be zero at the bottom of the block. These restraining forces will increase the bearing strength of the concrete block.

<2> The vertical compressive stress at the base of the block will not be distributed linearly. It will change to a triangular or even trapezoidal distribution of stresses.

<3> With the rearrangement of vertical compressive stress at the base of the block, the horizontal restraining force which had been ignored in high blocks becomes dominant and this will increase the bearing strength of the concrete block.

The proposed model can be improved for shorter blocks by solving the above three problems. However, due to the complexity of stress in the tension zone and the variable source of the restraining force, it is quite difficult to analyse systemtically. However, the proposed model can still be improved by means of Eq.4.12. Using this equation to modify the bearing capacity calculated by the proposed model, the result will be improved considerably.

This modified proposed model, gives a mean and standard deviation of 0.984 and 0.085 for all the specimens with H/a>1 respectively. Moreover, it improves the overall mean and standard deviation from 1.072 to 1.010 and 0.181 to 0.137

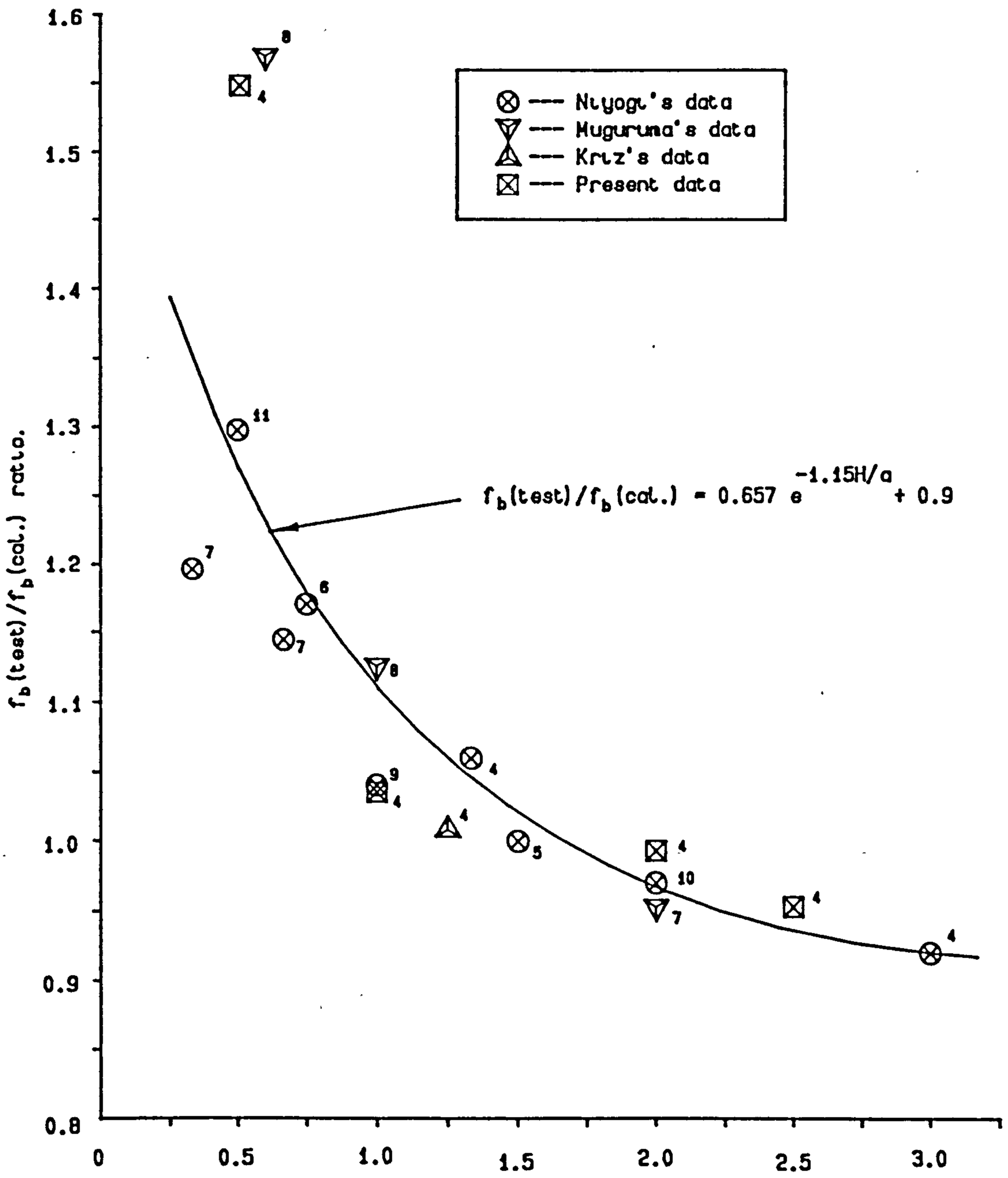

Fig.4.9 Effect of height on the bearing capacity of concrete blocks.
(Calculated by the proposed model)

a mm.	a_1 mm.	H mm.	H/a	f_c N/mm²	f_{ct} N/mm²	f_b/f_c (test)	Bearing strength ratio f_b(test)/f_b(cal.)																	
							Meyerhof Eq.2.7		Hawkins Eq.2.16		Shelson Eq.2.20		Kriz Eq.2.21		Muguruma Eq.2.22		Niyogi Eq.2.23		Jensen Eq.2.31-2		Proposed Eq.4.11		Proposed Eq.4.12	
Niyogi (1973)																								
203.2	12.7	609.6	H/a = 3.0	31.0	1.90	2.62	0.70	x = 0.62 σ = 0.10	1.04	x = 0.77 σ = 0.16	1.04	x = 0.77 σ = 0.16	1.27	x = 0.96 σ = 0.22	0.97	x = 0.81 σ = 0.10	0.76	x = 0.70 σ = 0.06	0.35	x = 0.38 σ = 0.03	1.07	x = 0.92 σ = 0.11	1.16	x = 1.00 σ = 0.12
203.2	25.4	609.6		28.4	1.85	1.62	0.68		0.81		0.81		0.95		0.82		0.69		0.36		0.94		1.02	
203.2	33.8	609.6		27.7	1.83	1.30	0.64		0.72		0.71		0.83		0.75		0.64		0.37		0.86		0.93	
203.2	50.8	609.6		28.2	1.88	1.06	0.64		0.67		0.67		0.78		0.74		0.64		0.42		0.81		0.88	
203.2	101.6	609.6		10.0	1.91	0.79	0.44		*0.51		0.63		*0.44		0.75		0.77		*0.53		*0.63		*0.68	
101.6	12.7	203.2	H/a = 2.0	24.8	1.86	2.00	0.98	x = 0.89 σ = 0.08	0.97	x = 0.84 σ = 0.10	1.00	x = 0.83 σ = 0.12	1.09	x = 0.97 σ = 0.15	0.98	x = 0.86 σ = 0.03	0.85	x = 0.97 σ = 0.09	0.53	x = 0.54 σ = 0.05	1.12	x = 0.97 σ = 0.11	1.16	x = 1.00 σ = 0.11
101.6	17.0	203.2		26.4	1.76	1.68	1.01		0.94		0.93		1.05		0.94		0.83		0.57		1.11		1.15	
101.6	25.4	203.2		25.4	1.64	1.21	0.87		0.77		0.76		0.84		0.81		0.73		0.53		0.93		0.96	
101.6	33.8	203.2		25.1	1.74	1.12	0.87		0.77		0.78		0.86		0.85		0.81		0.56		0.93		0.96	
101.6	50.8	203.2		23.3	1.52	0.97	0.84		0.77		0.77		0.82		0.88		0.94		0.65		0.88		0.91	
203.2	12.7	406.4		32.7	2.02	2.57	0.92		1.01		1.02		1.28		0.93		0.75		0.47		1.04		1.08	
203.2	25.4	406.4		31.2	1.97	1.71	0.91		0.87		0.86		1.05		0.84		0.73		0.50		1.00		1.04	
203.2	33.8	406.4		27.8	1.83	1.50	0.91		0.84		0.82		0.96		0.84		0.74		0.51		0.99		1.02	
203.2	50.8	406.4		31.2	1.98	1.14	0.82		0.73		0.72		0.88		0.76		0.69		0.51		0.88		0.91	
203.2	101.6	406.4		30.0	1.94	0.86	0.75		0.68		0.68		0.82		0.78		0.84		0.55		0.78		0.81	
203.2	12.7	304.8	H/a = 1.5	30.0	1.92	2.48	1.04	x = 1.04 σ = 0.07	0.96	x = 0.88 σ = 0.07	0.98	x = 0.88 σ = 0.07	1.18	x = 1.06 σ = 0.12	0.87	x = 0.88 σ = 0.05	0.72	x = 0.81 σ = 0.13	0.54	x = 0.85 σ = 0.09	1.00	x = 1.00 σ = 0.05	0.98	x = 0.98 σ = 0.05
203.2	25.4	304.8		31.9	1.99	1.75	1.08		0.90		0.88		1.09		0.83		0.75		0.62		1.02		1.00	
203.2	33.8	304.8		31.1	1.94	1.62	1.12		0.91		0.89		1.09		0.87		0.80		0.68		1.08		1.06	
203.2	50.8	304.8		25.1	1.74	1.24	0.96		0.78		0.78		0.86		0.79		0.75		0.62		0.94		0.92	
203.2	101.6	304.8		34.2	2.12	1.07	0.98		0.85		0.85		1.09		0.93		1.04		0.78		0.97		0.95	
152.4	12.7	203.2	H/a=1.33	26.3	1.69	2.33	1.24	x = 1.14 σ = 0.09	1.02	x = 0.93 σ = 0.07	1.02	x = 0.92 σ = 0.07	1.15	x = 1.08 σ = 0.02	0.91	x = 0.90 σ = 0.04	0.80	x = 0.90 σ = 0.14	0.67	x = 0.75 σ = 0.07	1.10	x = 1.08 σ = 0.05	1.06	x = 1.02 σ = 0.05
152.4	25.4	203.2		28.7	1.79	1.65	1.19		0.93		0.91		1.07		0.87		0.81		0.74		1.10		1.06	
152.4	50.8	203.2		23.3	1.52	1.23	1.07		0.86		0.85		0.91		0.87		0.89		0.78		1.02		0.98	
152.4	76.2	203.2		30.9	1.92	1.12	1.05		0.89		0.89		1.09		0.95		1.09		0.85		1.02		0.98	
203.2	12.7	203.2	H/a = 1.0	32.1	1.99	2.52	1.36	x = 1.21 σ = 0.14	0.99	x = 0.92 σ = 0.04	1.00	x = 0.92 σ = 0.05	1.25	x = 1.11 σ = 0.07	0.82	x = 0.83 σ = 0.06	0.73	x = 0.85 σ = 0.32	0.74	x = 0.86 σ = 0.08	1.02	x = 1.04 σ = 0.05	0.92	x = 0.94 σ = 0.04
203.2	17.0	203.2		30.6	2.00	2.18	1.32		0.95		0.95		1.16		0.80		0.75		0.75		1.03		0.93	
203.2	25.4	203.2		31.3	2.04	1.87	1.34		0.95		0.93		1.15		0.81		0.80		0.82		1.09		0.98	
203.2	33.8	203.2		26.9	1.70	1.64	1.29		0.92		0.90		1.03		0.80		0.81		0.85		1.09		0.98	
203.2	50.8	203.2		28.6	1.80	1.38	1.20		0.89		0.87		1.02		0.79		0.84		0.88		1.07		0.97	
203.2	63.5	203.2		31.1	2.05	1.31	1.18		0.89		0.89		1.09		0.83		0.91		0.91		1.07		0.97	
203.2	67.8	203.2		31.3	2.04	1.26	1.15		0.88		0.87		1.08		0.82		0.91		0.91		1.05		0.95	
203.2	101.6	203.2		31.6	1.99	1.10	1.06		0.87		0.87		1.08		0.84		1.07		0.93		1.00		0.90	
203.2	203.2	203.2		28.9	1.77	0.96	0.96		0.95		0.96		1.13		0.98		1.76		0.98		0.94		0.85	

Table 4.4a f_b(test)/f_b(cal.) calculated by various researchers.
(Concentric loading)

a mm.	a_1 mm.	H mm.	H/a	f_c N/mm²	f_t N/mm²	f_b/f_c (test)	Bearing strength ratio f_b(test)/f_b(cal.)															
							Meyerhof Eq.2.7		Hawkins Eq.2.16		Shelson Eq.2.20		Kriz Eq.2.21		Muguruma Eq.2.22		Niyogi Eq.2.23		Jensen Eq.2.31-2		Proposed Eq.4.11		Proposed Eq.4.12	
Niyogi (1973) (cont')																						
203.2	12.7	152.4	H/a = 0.75	26.7	1.75	2.56	1.55	x = 1.48 σ = 0.12	0.99	x = 1.02 σ = 0.02	1.02	x = 1.02 σ = 0.02	1.16	x = 1.15 σ = 0.04	0.75	x = 0.79 σ = 0.04	0.74	x = 0.97 σ = 0.19	0.88	x = 1.09 σ = 0.12	1.02	x = 1.17 σ = 0.07	0.87	x = 1.00 σ = 0.06
203.2	25.4	152.4		26.0	1.67	2.04	1.60		1.04		1.02		1.14		0.78		0.87		1.06		1.19		1.01	
203.2	33.8	152.4		29.7	1.87	1.81	1.54		1.02		1.00		1.19		0.77		0.89		1.09		1.21		1.03	
203.2	50.8	152.4		25.1	1.80	1.58	1.43		0.99		1.00		1.10		0.78		0.96		1.11		1.20		1.02	
203.2	76.2	152.4		25.1	1.61	1.39	1.34		1.01		1.00		1.10		0.80		1.09		1.17		1.20		1.02	
203.2	101.6	152.4		25.9	1.77	1.33	1.31		1.04		1.06		1.18		0.86		1.29		1.22		1.20		1.02	
304.8	25.4	203.2	H/a = 0.67	25.4	1.72	2.06	1.46	x = 1.42 σ = 0.09	0.88	x = 0.88 σ = 0.05	0.90	x = 0.94 σ = 0.08	1.00	x = 1.10 σ = 0.08	0.63	x = 0.67 σ = 0.04	0.71	x = 0.88 σ = 0.19	0.89	x = 1.07 σ = 0.12	1.02	x = 1.14 σ = 0.07	0.85	x = 0.95 σ = 0.06
304.8	33.8	203.2		30.3	1.74	1.87	1.50		0.94		0.90		1.09		0.63		0.75		1.01		1.11		0.92	
304.8	38.1	203.2		27.9	1.81	1.83	1.48		0.93		0.91		1.06		0.64		0.78		1.01		1.12		0.93	
304.8	50.8	203.2		25.4	1.72	1.69	1.46		0.94		0.93		1.03		0.66		0.83		1.06		1.16		0.96	
304.8	76.2	203.2		27.3	1.75	1.56	1.45		1.00		0.98		1.13		0.70		0.95		1.18		1.24		1.03	
304.8	101.6	203.2		29.1	1.80	1.36	1.31		0.96		0.94		1.12		0.68		0.98		1.15		1.17		0.97	
304.8	152.4	203.2		31.2	1.90	1.28	1.27		1.02		1.02		1.25		0.74		1.25		1.22		1.19		0.99	
406.4	12.7	203.2	H/a = 0.5	26.2	1.66	2.09	1.51	x = 1.58 σ = 0.18	0.82	x = 1.01 σ = 0.14	0.83	x = 1.00 σ = 0.14	0.93	x = 1.15 σ = 0.17	0.43	x = 0.43 σ = 0.04	0.61	x = 0.86 σ = 0.28	0.93	x = 1.27 σ = 0.23	0.71	x = 1.30 σ = 0.28	0.56	x = 1.02 σ = 0.20
406.4	33.8	203.2		27.0	1.78	1.92	1.50		0.83		0.84		0.96		0.41		0.66		0.99		1.11		0.87	
406.4	50.8	203.2		26.2	1.65	1.72	1.50		0.88		0.86		0.97		0.40		0.73		1.10		1.20		0.95	
406.4	101.6	203.2		27.7	1.72	1.54	1.49		0.99		0.97		1.12		0.40		0.93		1.30		1.48		1.17	
406.4	203.2	203.2		33.2	1.90	1.25	1.25		1.00		0.99		1.26		0.36		1.22		1.27		1.20		0.95	
203.2	12.7	101.6		23.1	1.54	2.34	1.66		0.89		0.93		0.98		0.48		0.68		1.02		1.17		0.92	
203.2	25.4	101.6		27.9	1.74	2.01	1.75		1.03		1.01		1.17		0.46		0.86		1.29		1.41		1.11	
203.2	33.8	101.6		29.4	1.87	1.93	1.77		1.08		1.06		1.26		0.47		0.95		1.39		1.49		1.17	
203.2	50.4	101.6		26.0	1.74	1.80	1.73		1.14		1.13		1.27		0.47		1.09		1.50		1.54		1.21	
203.2	67.2	101.6		25.8	1.81	1.68	1.67		1.20		1.21		1.35		0.46		1.31		1.59		1.51		1.19	
203.2	101.6	101.6		27.2	1.83	1.52	1.52		1.19		1.21		1.38		0.44		1.48		1.56		1.45		1.14	
609.6	25.4	203.2	H/a = 0.33	29.3	1.89	2.01	1.44	x = 1.42 σ = 0.09	0.65	x = 0.81 σ = 0.13	0.70	x = 0.81 σ = 0.11	0.83	x = 0.96 σ = 0.15	-		0.45	x = 0.72 σ = 0.28	0.89	x = 1.17 σ = 0.19	1.01	x = 1.20 σ = 0.11	0.75	x = 0.88 σ = 0.10
609.6	38.1	203.2		27.7	1.73	1.89	1.54		0.74		0.75		0.87		-		0.55		1.05		1.17		0.87	
609.6	50.8	203.2		25.7	1.73	1.63	1.41		0.70		0.71		0.79		-		0.56		1.02		1.12		0.83	
609.6	76.2	203.2		26.6	1.77	1.59	1.48		0.80		0.80		0.90		-		0.68		1.19		1.21		0.90	
609.6	101.6	203.2		31.5	1.81	1.49	1.44		0.86		0.82		1.01		-		0.73		1.27		1.30		0.96	
609.6	152.4	203.2		31.4	1.94	1.43	1.42		0.92		0.90		1.11		-		0.87		1.36		1.32		0.98	
609.6	304.8	203.2		29.1	1.81	1.26	1.24		1.00		1.00		1.19		-		1.23		1.39		1.24		0.92	

Table 4.4b f_b(test)/f_b(cal.) calculated by various researchers.
(Concentric loading)

a mm.	a_1 mm.	H mm.	H/a	f_c N/mm^2	f_t N/mm^2	f_b/f_c (test)	Bearing strength ratio f_b(test)/f_b(cal.) Meyerhof Eq.2.7	Hawkins Eq.2.16	Shelson Eq.2.20	Kriz Eq.2.21	Muguruma Eq.2.22	Niyogi Eq.2.23	Jensen Eq.2.31-2	Proposed Eq.4.11	Proposed Eq.4.12
Muguruma (Series I)															
250	10	500	H/a = 2.0	41.8	3.67	4.40	0.87	*1.18	*1.50	*2.14	*1.30	0.95	0.44	*1.23	*1.27
250	25	500		41.8	3.67	2.20	0.86	0.92	1.02	1.45	0.98	0.84	0.45	1.05	1.09
250	50	500		41.8	3.67	1.63	0.96	0.90	0.95	1.36	0.99	0.88	0.54	1.09	1.13
250	75	500		41.8	3.67	1.28	0.90	0.81	0.86	1.22	0.93	0.86	0.59	0.99	1.02
250	100	500		41.8	3.67	1.11	0.86	0.78	0.82	1.16	0.92	0.91	0.63	0.93	0.96
250	150	500		41.8	3.67	0.96	0.83	0.78	0.81	1.15	0.95	1.09	0.72	0.87	0.90
250	200	500		41.8	3.67	0.92	0.85	0.83	0.85	1.21	1.03	1.36	0.82	0.88	0.91
250	250	500		41.8	3.67	0.89	0.85	0.88	0.89	1.27	1.10	1.63	0.98	0.86	0.89
250	10	250	H/a = 1.0	40.7	3.50	4.43	1.51	1.20	1.52	2.13	1.19	0.96	0.78	1.24	1.12
250	25	250		40.7	3.50	2.41	1.42	1.02	1.12	1.57	0.95	0.92	0.81	1.16	1.05
250	50	250		40.7	3.50	1.85	1.44	1.02	1.08	1.52	0.97	1.00	0.95	1.24	1.12
250	75	250		40.7	3.50	1.52	1.32	0.97	1.02	1.43	0.94	1.03	0.97	1.18	1.06
250	100	250		40.7	3.50	1.37	1.26	0.96	1.01	1.42	0.96	1.12	1.01	1.15	1.04
250	150	250		40.7	3.50	1.23	1.20	1.00	1.04	1.46	1.02	1.40	1.07	1.13	1.02
250	200	250		40.7	3.50	1.04	1.03	0.94	0.97	1.35	0.97	1.54	1.01	0.99	0.89
250	250	250		40.7	3.50	0.94	0.94	0.93	0.94	1.32	0.96	1.72	0.98	0.91	0.82
250	10	150	H/a = 0.6	38.5	3.60	4.85	2.21	1.26	1.66	2.26	1.07	1.05	1.18	1.52	1.24
250	25	150		38.5	3.60	2.92	2.09	1.20	1.36	1.85	0.86	1.11	1.31	1.54	1.25
250	50	150		38.5	3.60	2.46	2.17	1.33	1.44	1.96	0.91	1.33	1.63	1.77	1.44
250	75	150		38.5	3.60	2.13	2.02	1.33	1.43	1.95	0.89	1.44	1.71	1.74	1.42
250	100	150		38.5	3.60	1.85	1.81	1.28	1.36	1.86	0.85	1.51	1.67	1.62	1.32
250	150	150		38.5	3.60	1.67	1.67	1.34	1.41	1.92	0.87	1.90	1.74	1.56	1.27
250	200	150		38.5	3.60	1.55	1.54	1.39	1.44	1.96	0.89	2.29	1.76	1.50	1.22
250	250	150		38.5	3.60	1.33	1.29	1.31	1.33	1.81	0.82	2.44	1.60	1.30	1.06

Table 4.4c f_b(test)/f_b(cal.) calculated by various researchers. (concentric loading)

Spec. no.	a mm.	a_1 mm.	H mm.	H/a	f_{c2} N/mm²	f_t N/mm²	f_b/f_c (test)	Bearing strength ratio f_b(test)/f_b(cal.) Meyerhof Eq.2.7		Hawkins Eq.2.16		Shelson Eq.2.20		Kriz Eq.2.21		Muguruma Eq.2.22		Niyogi Eq.2.23		Jensen Eq.2.31-2		Proposed Eq.4.11		Proposed Eq.4.12	
Present investigation																									
R1-H1	400	101.6	1000	H/a=2.5	36.7	3.05	1.16	0.70	x̄ = 0.64 σ = 0.15	0.70	x̄ = 0.86 σ = 0.11	0.74	x̄ = 1.05 σ = 0.36	0.98	x̄ = 1.41 σ = 0.48	0.80	x̄ = 0.97 σ = 0.19	0.71	x̄ = 0.72 σ = 0.53	0.47	x̄ = 0.36 σ = 0.10	0.86	x̄ = 0.95 σ = 0.06	0.92	x̄ = 1.02 σ = 0.07
R2-H1	400	50.8	1000		36.5	2.68	1.73	0.76		0.85		0.87		1.16		0.88		0.75		0.40		0.99		1.06	
R3-H1	400	25.3	1000		36.9	3.11	2.62	0.65		0.91		1.04		1.40		0.97		0.77		0.33		0.98		1.05	
R4-H1	400	6.35	1000		36.7	3.05	6.22	0.46		0.96		1.56		2.08		1.24		0.65		0.24		0.98		1.05	
R1-H2	400	101.6	800	H/a=2.0	39.7	3.36	1.27	0.84	x̄ = 0.78 σ = 0.12	0.77	x̄ = 0.90 σ = 0.12	0.80	x̄ = 1.10 σ = 0.40	1.11	x̄ = 1.55 σ = 0.54	0.85	x̄ = 1.00 σ = 0.22	0.78	x̄ = 0.75 σ = 0.05	0.51	x̄ = 0.43 σ = 0.09	0.94	x̄ = 0.99 σ = 0.06	0.97	x̄ = 1.03 σ = 0.06
R2-H2	400	50.8	800		42.9	3.26	1.70	0.84		0.82		0.85		1.23		0.84		0.73		0.45		0.95		0.98	
R3-H2	400	25.3	800		42.9	3.26	2.70	0.85		0.98		1.07		1.55		0.98		0.79		0.43		1.04		1.08	
R4-H2	400	6.35	800		39.8	3.36	6.66	0.60		1.01		1.67		2.32		1.31		0.69		0.31		1.04		1.08	
R1-H3	400	101.6	400	H/a=1.0	39.2	3.24	1.32	1.11	x̄ = 1.21 σ = 0.14	0.80	x̄ = 0.93 σ = 0.13	0.84	x̄ = 1.15 σ = 0.38	1.15	x̄ = 1.58 σ = 0.52	0.76	x̄ = 0.93 σ = 0.22	0.81	x̄ = 0.79 σ = 0.08	0.78	x̄ = 0.70 σ = 0.10	0.98	x̄ = 1.03 σ = 0.08	0.88	x̄ = 0.93 σ = 0.07
R2-H3	400	50.8	400		39.2	3.24	1.76	1.17		0.83		0.88		1.22		0.76		0.76		0.70		0.97		0.88	
R3-H3	400	25.3	400		39.2	3.24	3.03	1.42		1.06		1.21		1.66		0.98		0.88		0.76		1.14		1.03	
R4-H3	400	6.35	400		39.2	3.24	6.59	1.12		1.02		1.66		2.28		1.21		0.69		0.57		1.04		0.94	
R1-H4	400	101.6	200	H/a=0.5	44.9	3.88	1.67	1.59	x̄ = 2.09 σ = 0.47	1.00	x̄ = 1.16 σ = 0.18	1.06	x̄ = 1.39 σ = 0.48	1.56	x̄ = 2.02 σ = 0.67	0.43	x̄ = 0.74 σ = 0.42	1.02	x̄ = 0.95 σ = 0.07	1.36	x̄ = 1.35 σ = 0.04	1.39	x̄ = 1.55 σ = 0.17	1.09	x̄ = 1.22 σ = 0.14
R2-H4	400	50.8	200		44.9	3.88	2.34	1.96		1.09		1.18		1.74		0.54		1.01		1.38		1.53		1.21	
R3-H4	400	25.3	200		42.3	3.11	3.06	2.12		1.13		1.22		1.75		0.63		0.90		1.29		1.49		1.17	
R4-H4	400	6.35	200		42.3	3.11	8.41	2.71		1.41		2.11		3.02		1.37		0.88		1.37		1.79		1.41	
Kriz (1963)																									
11	203	25.4	762	3.8	28.0	Estimated by $f_t = 0.66\sqrt{f_{c2}}$	1.75	0.53		0.82		0.88		1.02		0.90		0.75		0.39		0.95		1.05	
29	914	50.8	1219	1.33	19.4		2.63	0.83	x̄=0.88 σ=0.08	0.79	x̄=0.81 σ=0.02	1.00	x̄=1.12 σ=0.16	0.97	x̄=0.96 σ=0.01	0.86	x̄=1.02 σ=0.22	0.71	x̄=0.74 σ=0.04	0.43	x̄=0.47 σ=0.05	0.86	x̄=0.90 σ=0.05	0.83	x̄=0.86 σ=0.04
37	914	76.2	1219		19.8		2.23	0.94		0.82		1.23		0.95		1.17		0.77		0.50		0.93		0.89	
15	610	25.4	762	H/a=1.25	19.0		3.53	0.94	x̄ = 1.04 σ = 0.07	0.89	x̄ = 0.88 σ = 0.04	1.22	x̄ = 1.11 σ = 0.11	1.17	x̄ = 1.02 σ = 0.11	1.01	x̄ = 0.97 σ = 0.06	0.78	x̄ = 0.85 σ = 0.06	0.48	x̄ = 0.56 σ = 0.03	0.96	x̄ = 1.01 σ = 0.05	0.91	x̄ = 0.96 σ = 0.05
27	610	50.8	762		15.7		1.41	1.10		0.94		1.17		1.02		1.03		0.93		0.59		1.08		1.02	
28	610	50.8	762		19.0		2.69	1.03		0.86		1.04		0.99		0.91		0.82		0.55		0.98		0.93	
36	610	76.2	762		17.4		1.98	1.07		0.85		0.99		0.91		0.91		0.85		0.60		1.01		0.96	

For all specimens with H/a ≥ 1.0	mean	0.980	0.888	0.958	1.200	0.915	0.889	0.643	1.005	0.984
	deviation	0.240	0.101	0.208	0.325	0.121	0.244	0.205	0.098	0.085
For all specimens shown above.	mean	1.224	0.946	1.005	1.254	0.751	0.946	0.884	1.072	1.010
	deviation	0.406	0.158	0.242	0.387	0.368	0.329	0.374	0.181	0.137

Table 4.4d f_b(test)/f_b(cal.) calculated by various researchers.
(concentric loading)

Spec. no.	a mm.	a_1 mm.	H mm.	W_a mm.	f_c N/mm²	f_t N/mm²	f_b/f_c (test)	Bearing strength ratio f_b(test)/f_b(cal.) Meyerhof Eq.2.7	Hawkins Eq.2.16	Shelson Eq.2.20	Kriz Eq.2.21	Muguruma Eq.2.22	Niyogi Eq.2.23	Jensen Eq.2.31-2	Proposed Eq.4.11
Kriz (1963)															
1	305	25.4	762	12.7	19.7		0.90	0.24	1.08	0.90	0.88	1.15	1.12	0.90	0.87
2	203	25.4	762	12.7	27.7		0.71	0.22	0.84	0.71	0.82	0.94	0.93	0.71	0.69
3	305	25.4	762	25.4	19.7		1.34	0.36	1.14	1.06	1.04	1.25	1.24	0.89	1.17
4	203	25.4	762	38.1	27.2		1.24	0.37	0.92	0.86	0.99	1.00	0.92	0.62	1.00
5	305	25.4	762	38.1	22.3		1.40	0.39	1.02	0.97	1.01	1.09	1.05	0.70	1.11
6	203	25.4	762	38.1	27.6		1.10	0.33	0.82	0.76	0.88	0.88	0.82	0.55	0.89
7	203	25.4	762	63.5	27.6		1.38	0.42	0.85	0.60	0.93	0.59	0.76	0.46	0.93
8	305	25.4	762	63.5	19.2		1.44	0.38	0.84	0.84	0.81	0.89	0.81	0.48	0.93
9	305	25.4	762	63.5	19.4		1.77	0.47	1.04	1.04	1.00	1.10	0.99	0.59	1.15
10	305	25.4	762	63.5	46.1		1.11	0.40	0.73	0.65	0.97	0.69	0.62	0.37	0.79
12	305	25.4	762	101.6	21.9		2.26	0.63	1.11	1.13	1.16	1.13	0.96	0.50	1.19
13	610	25.4	762	203.2	20.0		2.72	0.74	0.95	1.08	1.06	0.92	0.75	0.38	0.96
14	610	25.4	762	279.4	20.3		2.52	0.68	0.69	0.90	0.89	0.75	0.58	0.35	0.73
16	305	50.8	762	25.4	20.9		1.16	0.52	1.38	1.16	1.17	1.48	1.54	1.16	1.12
17	305	50.8	762	25.4	21.4		1.06	0.48	1.26	1.06	1.08	1.35	1.41	1.06	1.02
18	203	50.8	762	25.4	27.7		0.78	0.37	0.92	0.78	0.90	1.03	1.04	0.78	0.76
19	305	50.8	762	38.1	22.3		1.27	0.58	1.23	1.11	1.15	1.35	1.37	1.02	1.17
20	203	50.8	762	50.8	27.6		1.03	0.49	0.89	0.82	0.94	1.00	0.92	0.69	0.91
21	305	50.8	762	63.5	19.2		1.35	0.59	1.04	0.99	0.96	1.14	1.09	0.77	1.11
22	305	50.8	762	63.5	21.4		1.23	0.55	0.96	0.91	0.92	1.04	0.99	0.70	1.02
23	305	50.8	762	63.5	44.8		0.92	0.50	0.75	0.68	1.00	0.78	0.74	0.53	0.80
24	305	50.8	762	63.5	44.8		1.01	0.55	0.83	0.74	1.09	0.85	0.81	0.58	0.88
25	305	50.8	762	101.6	20.5		1.43	0.63	0.92	0.90	0.90	0.98	0.87	0.57	1.02
26	305	50.8	762	101.6	24.8		4.41	0.66	0.93	0.89	0.97	0.97	0.86	0.56	1.02
30	305	76.2	762	38.1	19.4		1.11	0.61	1.33	1.11	1.08	1.42	1.47	1.11	1.07
31	305	76.2	762	38.1	20.9		1.10	0.62	1.31	1.10	1.11	1.41	1.46	1.10	1.06
32	305	76.2	762	57.2	24.3		1.17	0.68	1.13	1.02	1.11	1.25	1.23	0.94	1.08
33	305	76.2	762	63.5	21.9		1.25	0.71	1.15	1.05	1.08	1.27	1.24	0.94	1.13
34	305	76.2	762	63.5	46.1		1.84	0.55	0.79	0.71	1.06	0.85	0.83	0.63	0.78
35	305	76.2	762	101.6	20.5		1.27	0.71	0.96	0.92	0.91	1.04	0.96	0.69	1.03
							mean	0.514	0.994	0.942	1.038	1.035	1.013	0.711	0.980
							standard deviation	0.142	0.186	0.208	0.207	0.225	0.257	0.233	0.144

Estimated by $f_t = 0.66\sqrt{f_c}$

Table 4.5a f_b(test)/f_b(cal.) calculated by various researchers.
(Eccentric loading)

Spec. no.	a mm.	a_1 mm.	H mm.	W_o mm.	f_{co} N/mm²	f_t N/mm²	f_b/f_o (test)	Bearing strength ratio f_b (test)/f_b (cal.) Meyerhof Eq.2.7	Hawkins Eq.2.16	Sheleon Eq.2.20	Kriz Eq.2.21	Muguruma Eq.2.22	Niyogi Eq.2.23	Jensen Eq.2.31-2	Proposed Eq.4.11
Hawkins (1970)															
	381	19	721	19	27.9	Estimated by $f_t = 0.66\sqrt{f_{co}}$	1.22	0.23	1.00	0.97	1.12	1.10	1.03	0.81	1.04
	381	19	721	38	27.9		1.57	0.29	0.95	0.99	1.15	1.04	0.97	0.63	1.06
	381	19	721	57	27.9		1.87	0.35	0.95	1.03	1.20	1.04	0.93	0.53	1.06
	381	19	721	76	27.9		2.12	0.40	0.94	1.06	1.23	1.04	0.89	0.47	1.04
	381	19	721	95	27.9		2.29	0.43	0.91	1.06	1.23	1.01	0.84	0.42	0.99
	381	25.4	721	19	84.5		-	-	-	-	-	-	-	-	-
	381	25.4	721	38	84.5		0.96	0.34	0.73	0.67	1.35	0.73	0.71	0.48	0.79
	381	25.4	721	57	84.5		1.03	0.36	0.69	0.62	1.26	0.65	0.62	0.38	0.75
	381	25.4	721	76	84.5		1.12	0.39	0.67	0.62	1.25	0.62	0.57	0.32	0.72
	381	25.4	721	95	84.5		1.15	0.40	0.64	0.59	1.19	0.58	0.51	0.27	0.67
	457	25.4	1015	38	48.1		1.11	0.25	0.81	0.77	1.17	0.86	0.81	0.56	0.88
	457	25.4	1015	76	46.8		1.62	0.36	0.90	0.89	1.34	0.92	0.81	0.46	0.98
	457	25.4	1015	127	46.8		2.02	0.44	0.90	0.94	1.41	0.91	0.75	0.37	0.94
	457	25.4	1015	229	31.5		2.71	0.51	0.75	1.03	1.28	0.94	0.73	0.28	0.84
	457	50.8	1015	76	40.9		0.95	0.34	0.68	0.66	0.93	0.73	0.71	0.48	0.74
	457	50.8	1015	38	40.9		0.95	0.34	0.91	0.83	1.17	0.99	1.03	0.76	0.87
							mean	0.362	0.829	0.849	1.219	0.877	0.794	0.481	0.891
							standard deviation	0.072	0.123	0.178	0.113	0.172	0.159	0.159	0.135
Present investigation															
E1/1	1260	50.8	1000	80	41.1	$f_t = 0.66\sqrt{f_{co}}$	1.29	0.54	0.95	0.44	1.24	0.33	0.86	0.62	1.04
E1/2	1260	50.8	1000	230	41.1		1.68	0.70	0.83	0.57	1.13	0.42	0.64	0.33	0.87
E2/1	1260	50.8	1000	130	34.9		1.47	0.59	0.89	0.50	1.10	0.37	0.77	0.48	0.97
E2/2	1260	50.8	1000	180	37.2		1.59	0.66	0.86	0.54	1.11	0.40	0.70	0.39	0.92
E3/1	1260	50.8	1000	280	40.9		1.83	0.74	0.82	0.63	1.16	0.46	0.62	0.38	0.84
E3/2	1260	50.8	1000	30	39.4		0.83	0.34	0.92	0.28	1.08	0.21	0.76	0.76	0.79
							mean	0.595	0.875	0.493	1.137	0.365	0.725	0.493	0.905
							standard deviation	0.144	0.048	0.123	0.058	0.088	0.090	0.166	0.091
For all the eccentric loaded specimens.							mean	0.479	0.931	0.862	1.078	0.920	0.915	0.618[1]	0.945
							standard deviation	0.147	0.174	0.236	0.142	0.294	0.246	0.232	0.140

Table 4.5b f_b (test)/f_b (cal.) calculated by various researchers.
(Eccentric loading)

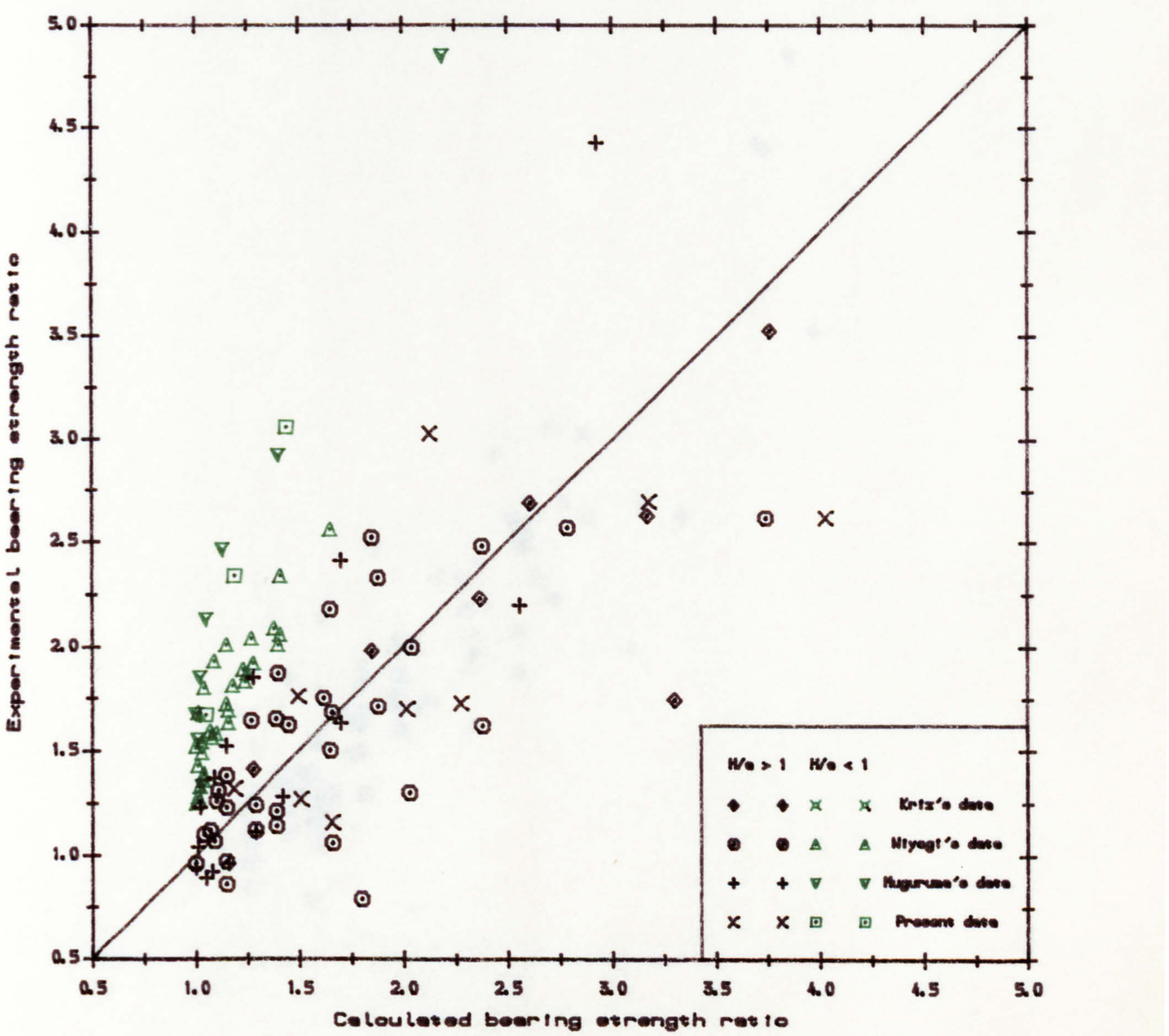

Fig. 4.10. Expt. vs calculated bearing strength. (Meyerhof's formula)

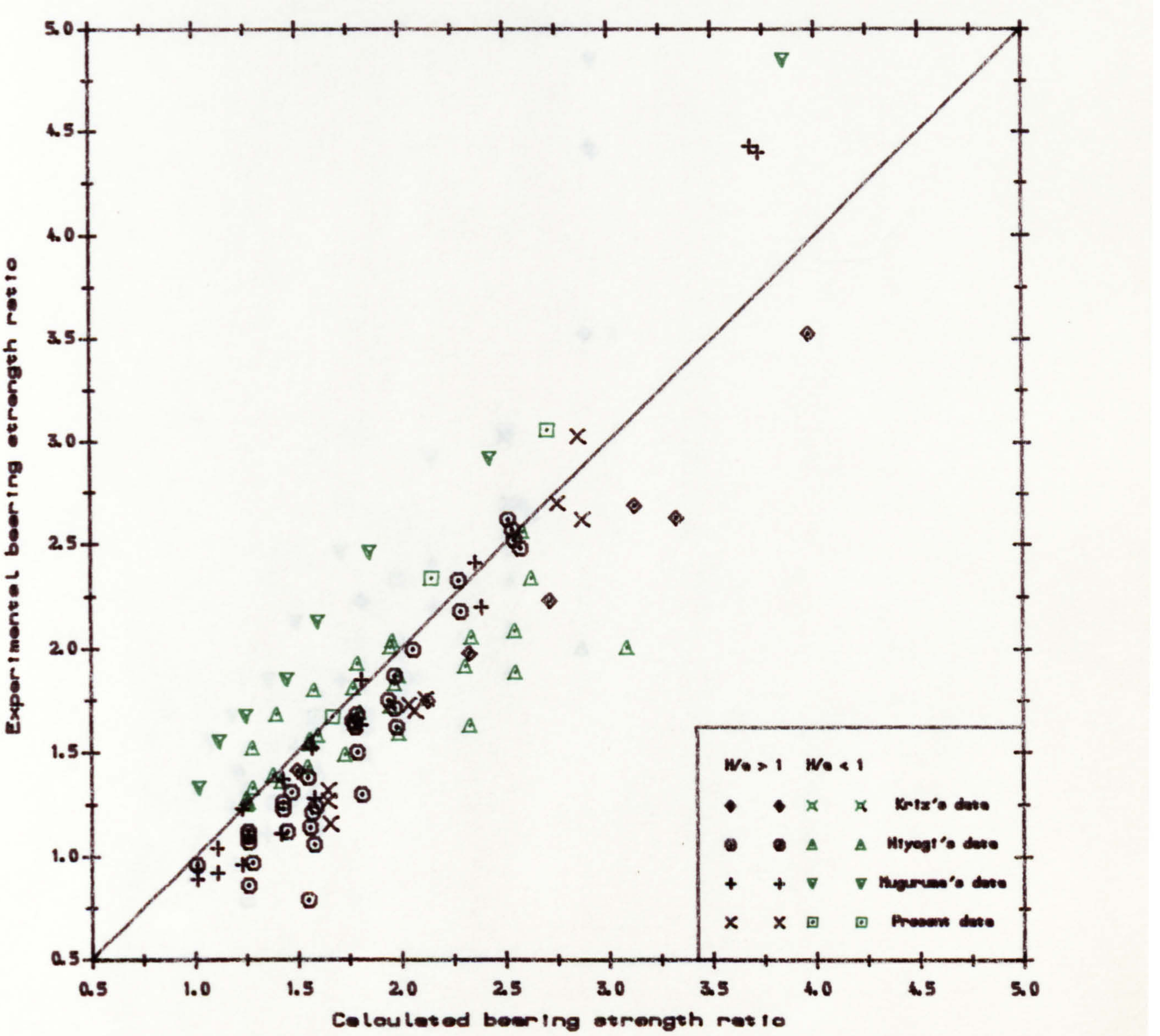

Fig. 4.11. Expt. vs calculated bearing strength. (Hawkins' formula)

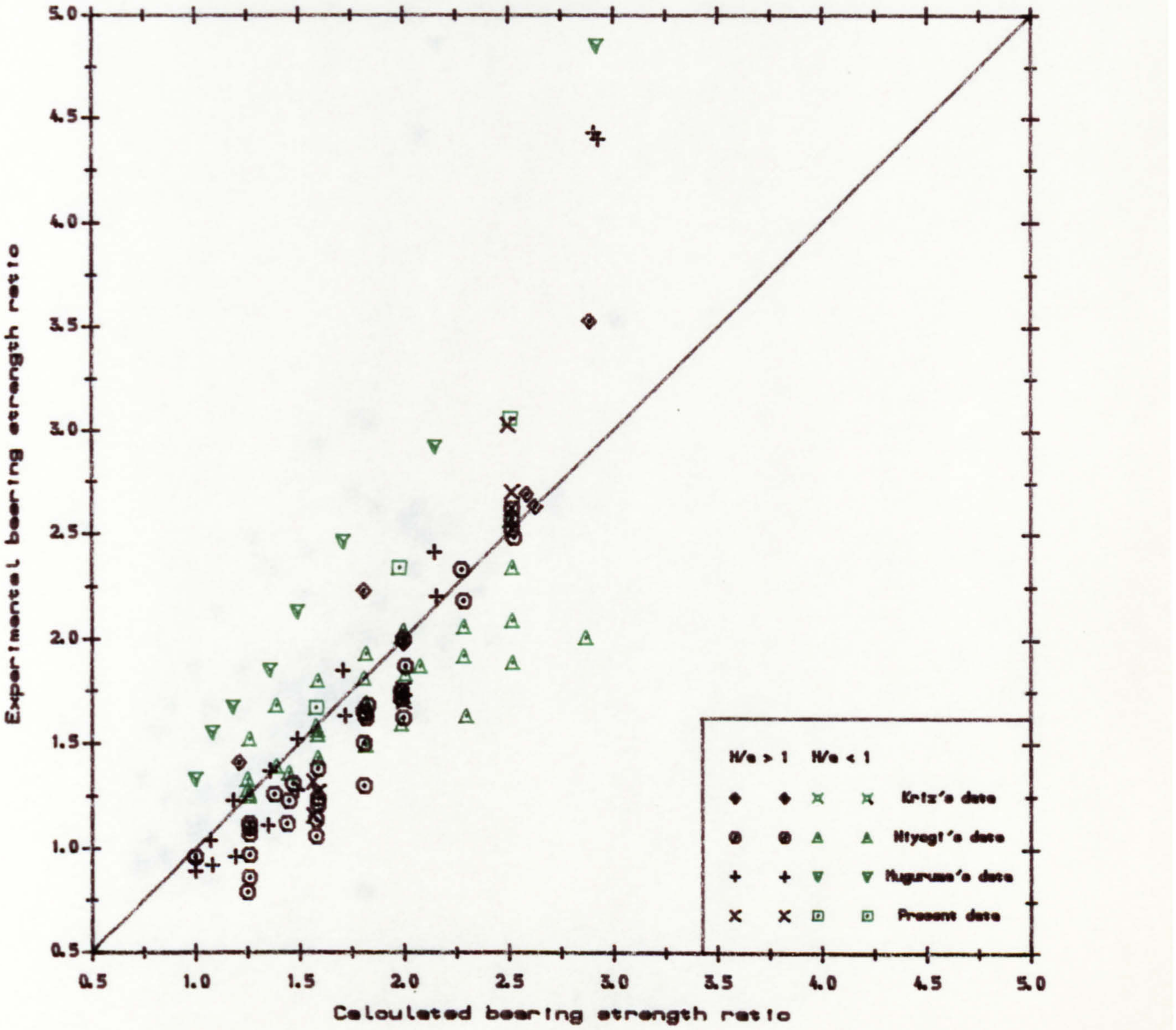

Fig. 4.12. Expt. vs calculated bearing strength. (Shelson's formula)

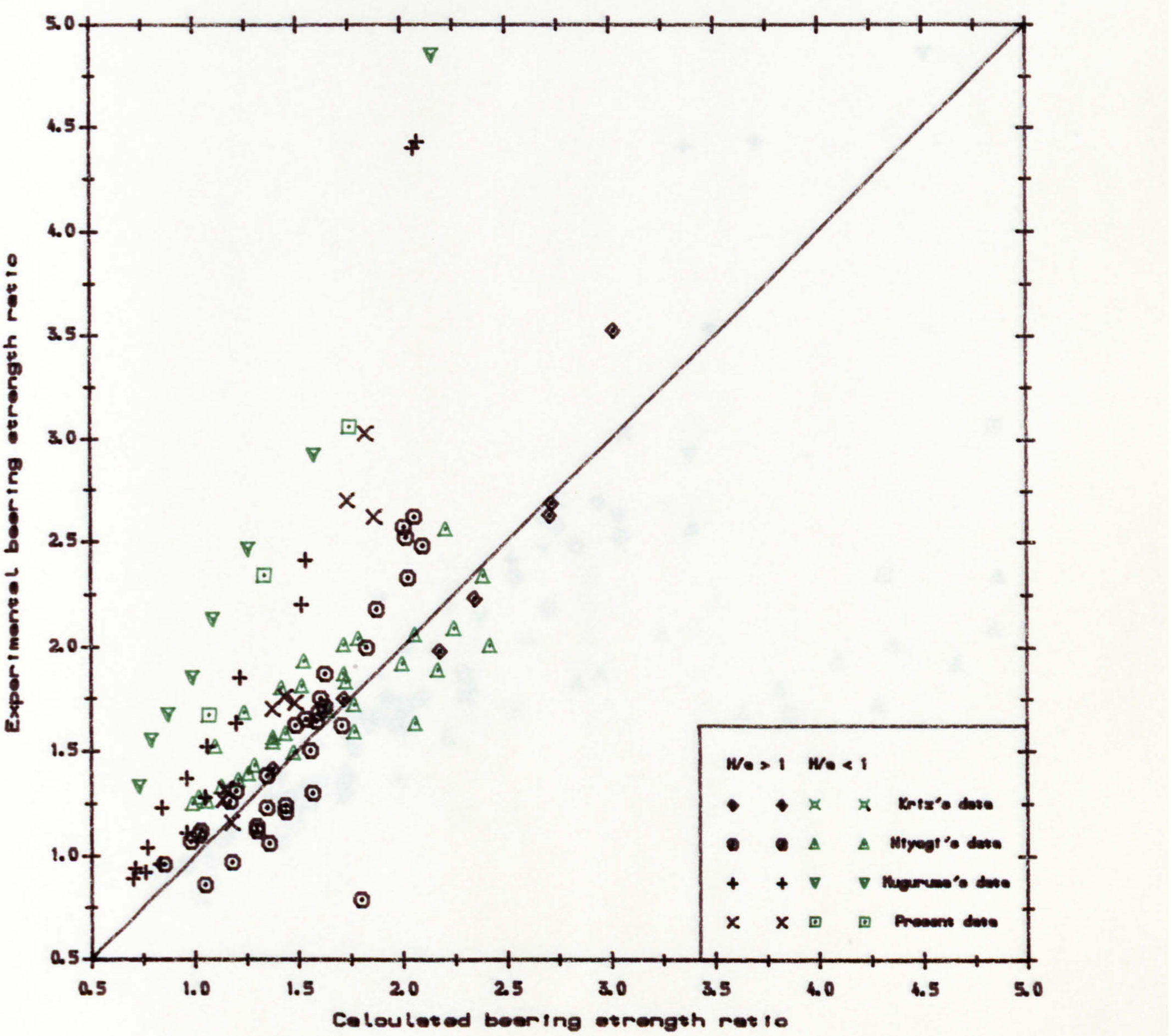

Fig. 4. 13. Expt. vs calculated bearing strength.
(Kriz's formula)

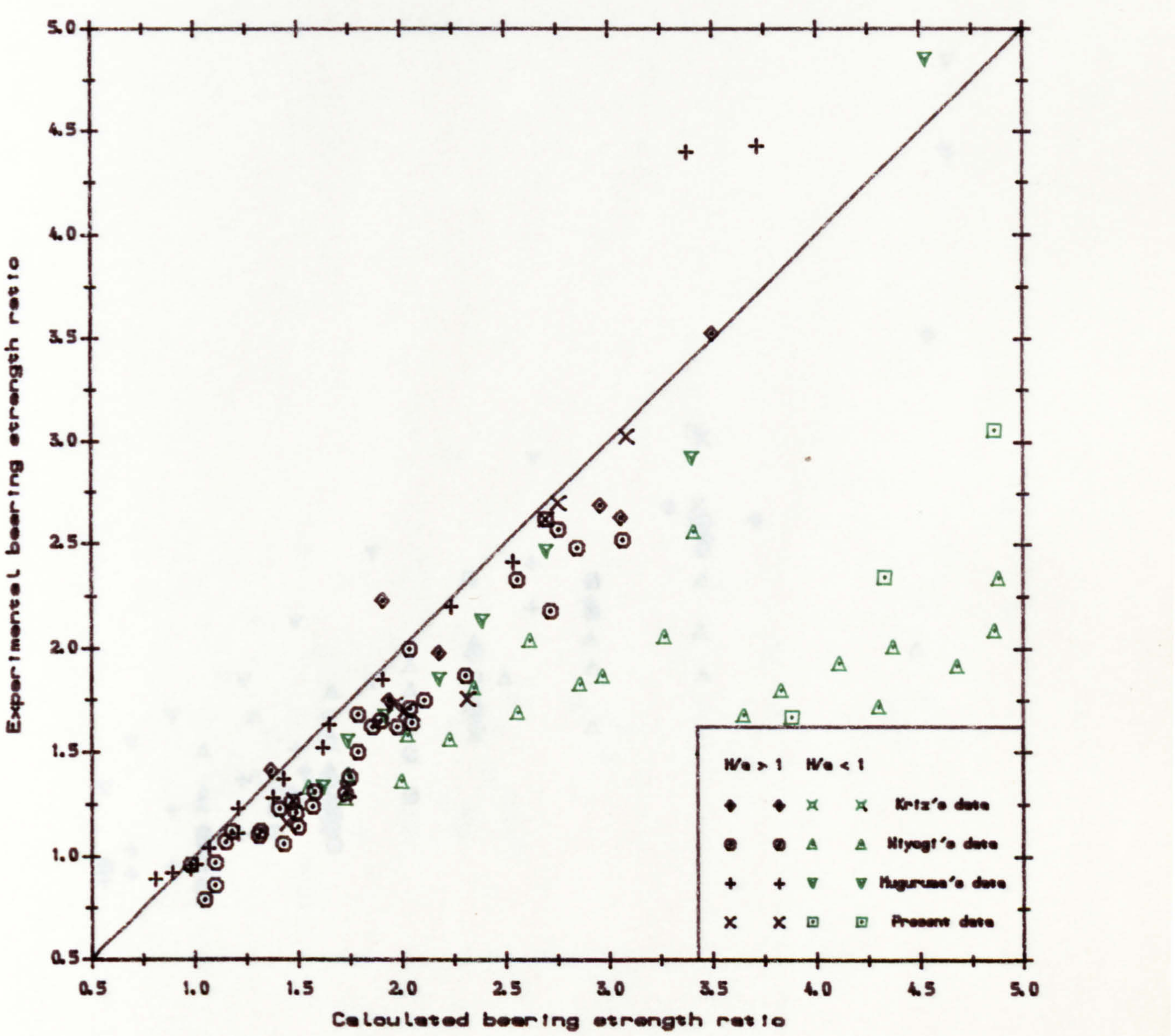

Fig. 4. 14. Expt. vs calculated bearing strength.
(Mugurumа's formula)

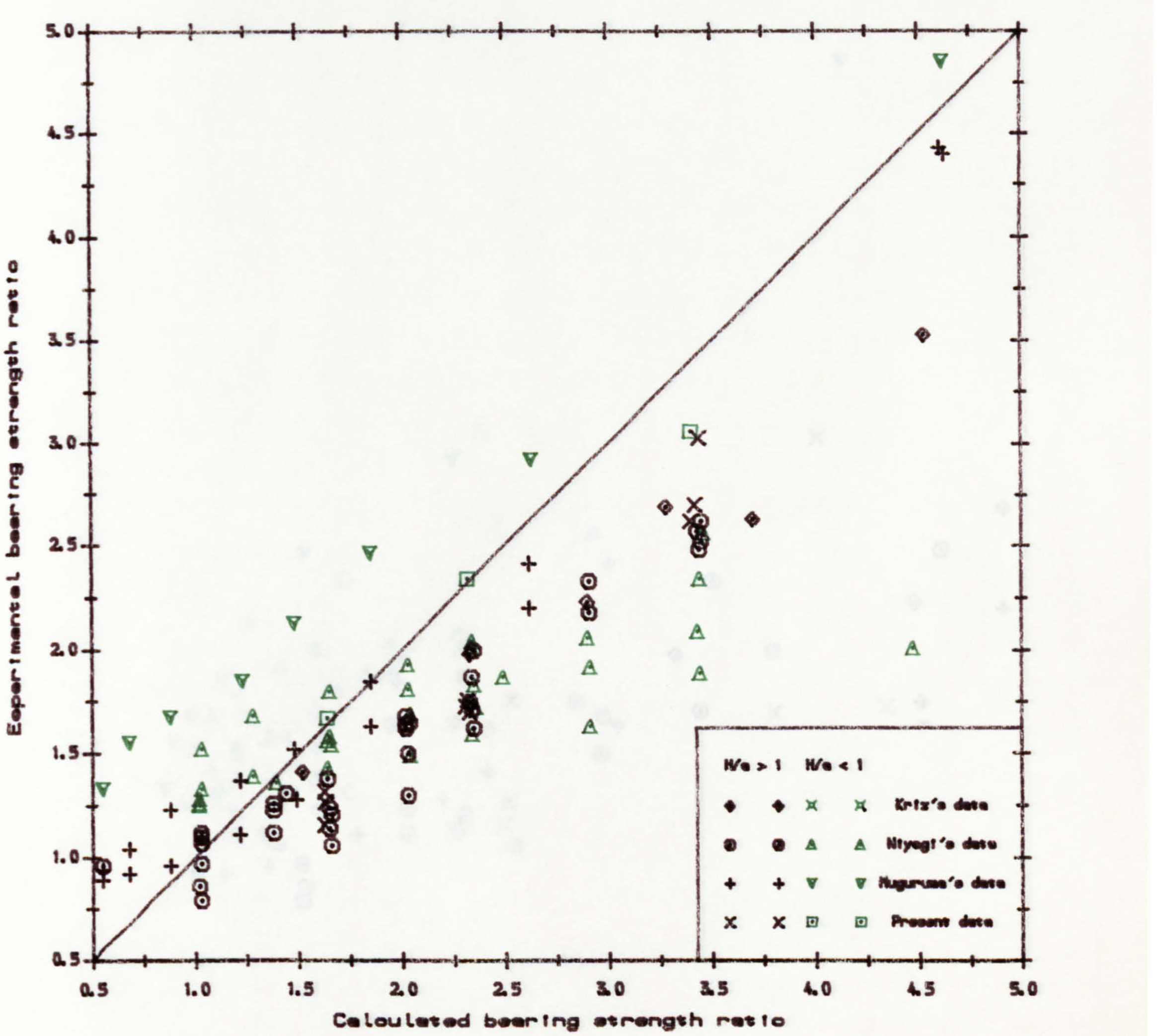

Fig. 4.15. Expt. vs calculated bearing strength. (Niyogi's formula)

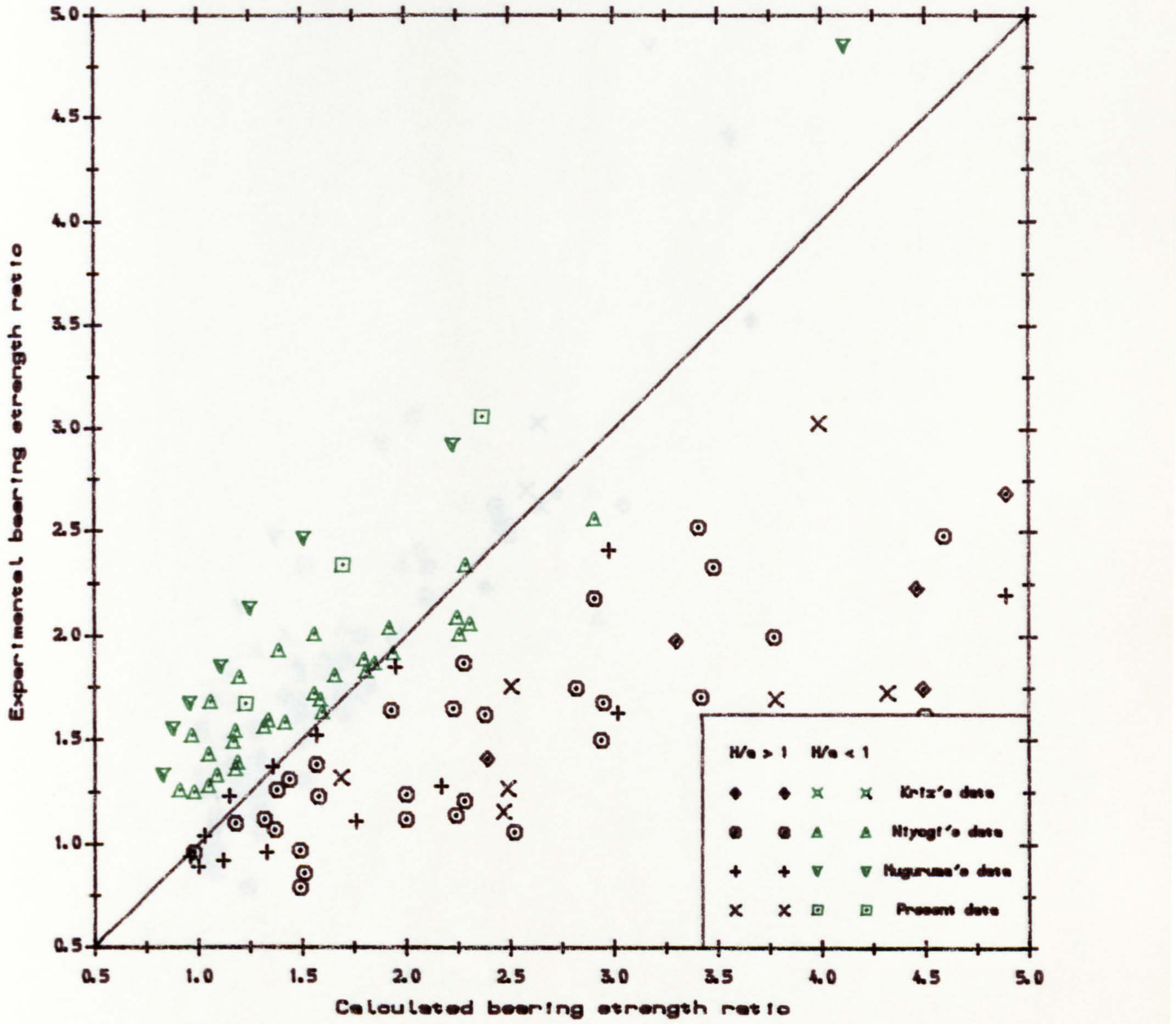

Fig. 4.16. Expt. vs calculated bearing strength. (Jensen's model)

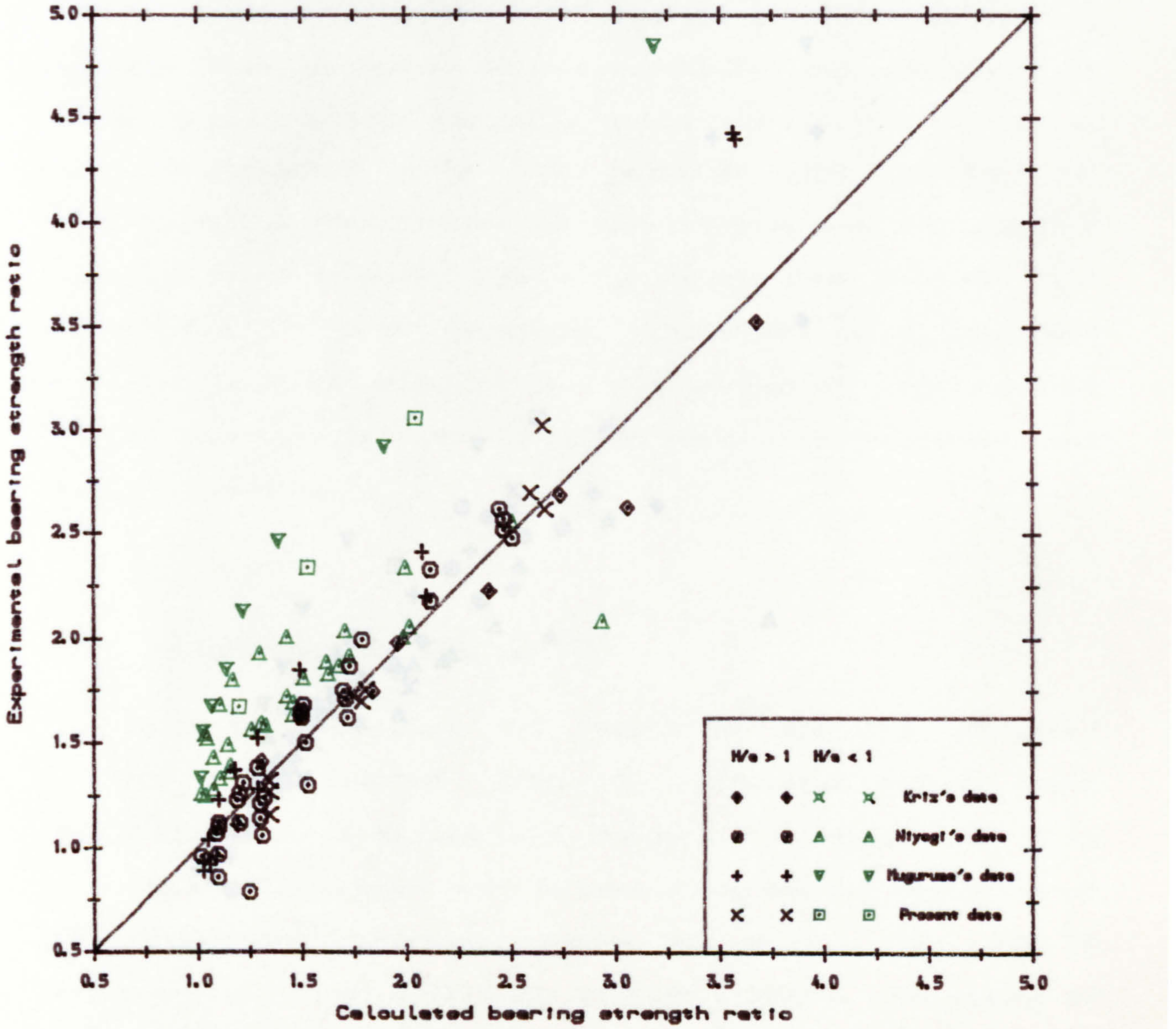

Fig. 4.17. Expt. vs calculated bearing strength. (Proposed model)

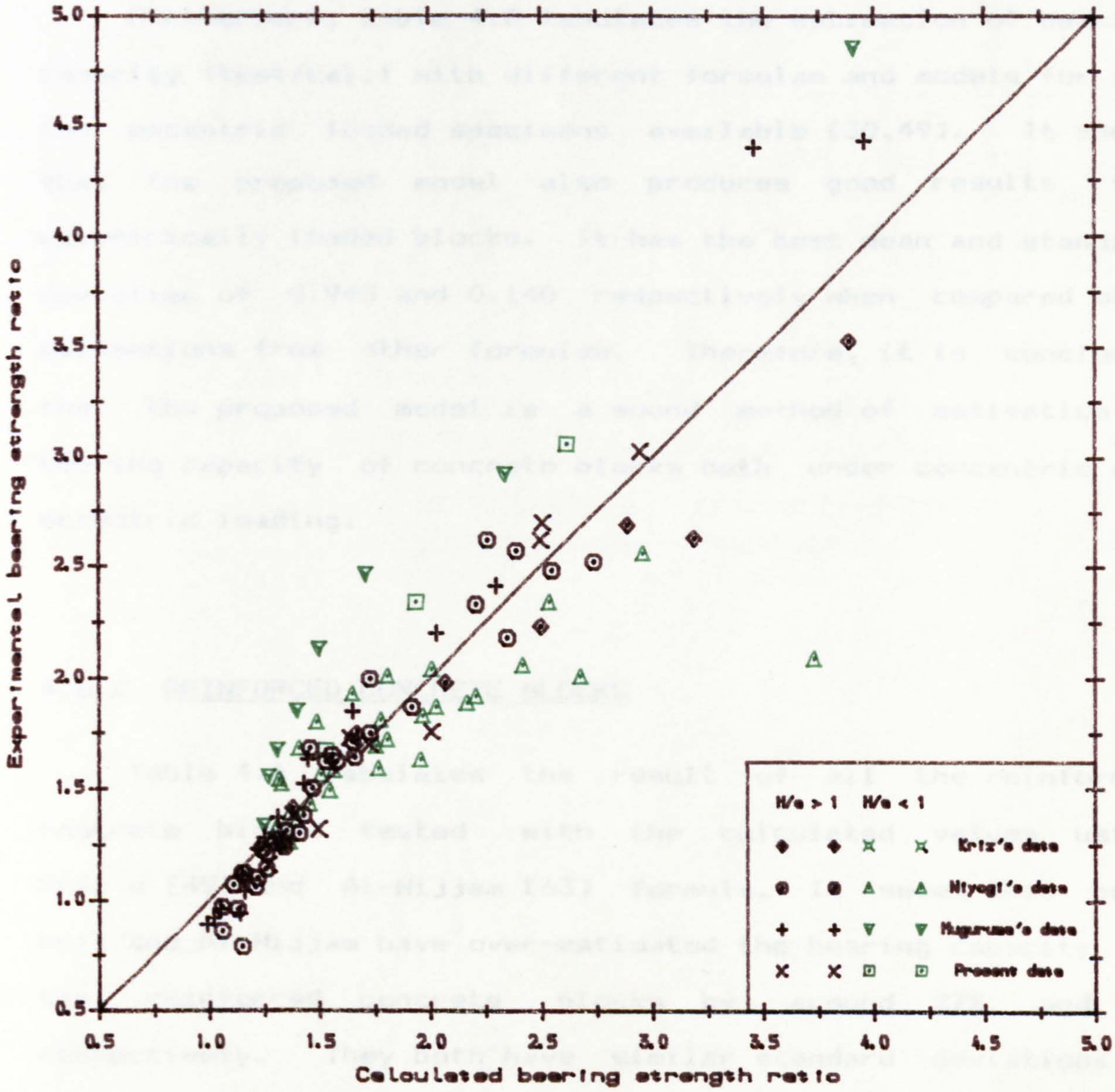

Fig. 4. 18. Expt. vs calculated bearing strength.
(Modified proposed model)

respectively. Fig.4.18 shows that after multiplication by the factor in Eq.4.12, most of the data are congested around the diagonal line.

Furthermore, table 4.5 tabulates the estimation of bearing capacity (test/cal.) with different formulae and models for all the eccentric loaded specimens available [30,49]. It shows that the proposed model also produces good results for eccentrically loaded blocks. It has the best mean and standard deviation of 0.945 and 0.140 respectively when compared with estimations from other formulae. Therefore, it is concluded that the proposed model is a sound method of estimation of bearing capacity of concrete blocks both under concentric and eccentric loading.

4.6.2 REINFORCED CONCRETE BLOCKS

Table 4.6 tabulates the result of all the reinforced concrete blocks tested with the calculated values using Kriz's [49] and Al-Nijjam [63] formula. It seems that both Kriz and Al-Nijjam have over-estimated the bearing capacity of the reinforced concrete blocks by around 27% and 7% respectively. They both have similar standard deviations of around 0.130 and 0.129 respectively. However, over-estimation of the strength of the reinforced concrete block may not be due to the theory itself, it is possibly due to the ineffectiveness

Spec. no.	Wa (mm.)	Asl (mm.)	f_c (N/mm²)	f_t (N/mm²)	Kriz Eq.2.54		Al-Nuijjan Eq.2.50		Proposed Eq.4.12	
					f_b/f_c	test/cal.	f_b/f_c	test/cal.	f_b/f_c	test/cal.
R1/1	180	226	45.3	3.37	1.80	0.72	1.59	0.82	1.22	1.07
R1/2	180	628	46.6	3.63	2.28	0.55	1.89	0.66	1.14	1.10
R2/1	180	402	46.0	3.70	2.04	0.65	1.61	0.83	1.21	1.10
R2/2	180	402	46.0	3.70	2.04	0.62	1.44	0.88	1.21	1.04
R3/1	180	622	43.4	3.50	2.35	0.74	1.77	0.99	1.21	1.45
R3/2	180	603	43.4	3.50	2.33	0.63	1.76	0.83	1.21	1.21
R4/1	180	402	47.0	3.45	2.02	0.70	1.61	0.88	1.19	1.19
R4/2	180	402	47.0	3.45	2.02	0.68	1.61	0.86	1.19	1.16
R5/1	180	301	45.9	3.77	1.90	0.73	1.47	0.95	1.21	1.15
R5/2	180	301	45.9	3.77	1.90	0.72	1.39	0.99	1.21	1.13
R6/1	130	301	39.5	3.29	1.84	0.72	1.50	0.88	1.08	1.22
R6/2	80	301	39.5	3.29	1.56	0.83	1.50	0.87	0.97	1.34
R7/1	280	301	45.3	3.36	2.22	0.73	1.47	1.11	1.48	1.10
R7/2	230	301	45.3	3.36	2.08	0.75	1.47	1.06	1.33	1.17
R8/1	180	-	463	3.29	1.02	1.15	1.14	1.03	1.27	0.99
R8/2	330	301	463	3.29	2.32	0.75	1.47	1.18	1.60	1.07
mean						0.729		0.926		
standard deviation						0.130		0.129		

Table 4.6 f_b/f_c calculated by various researchers for reinforced concrete blocks.

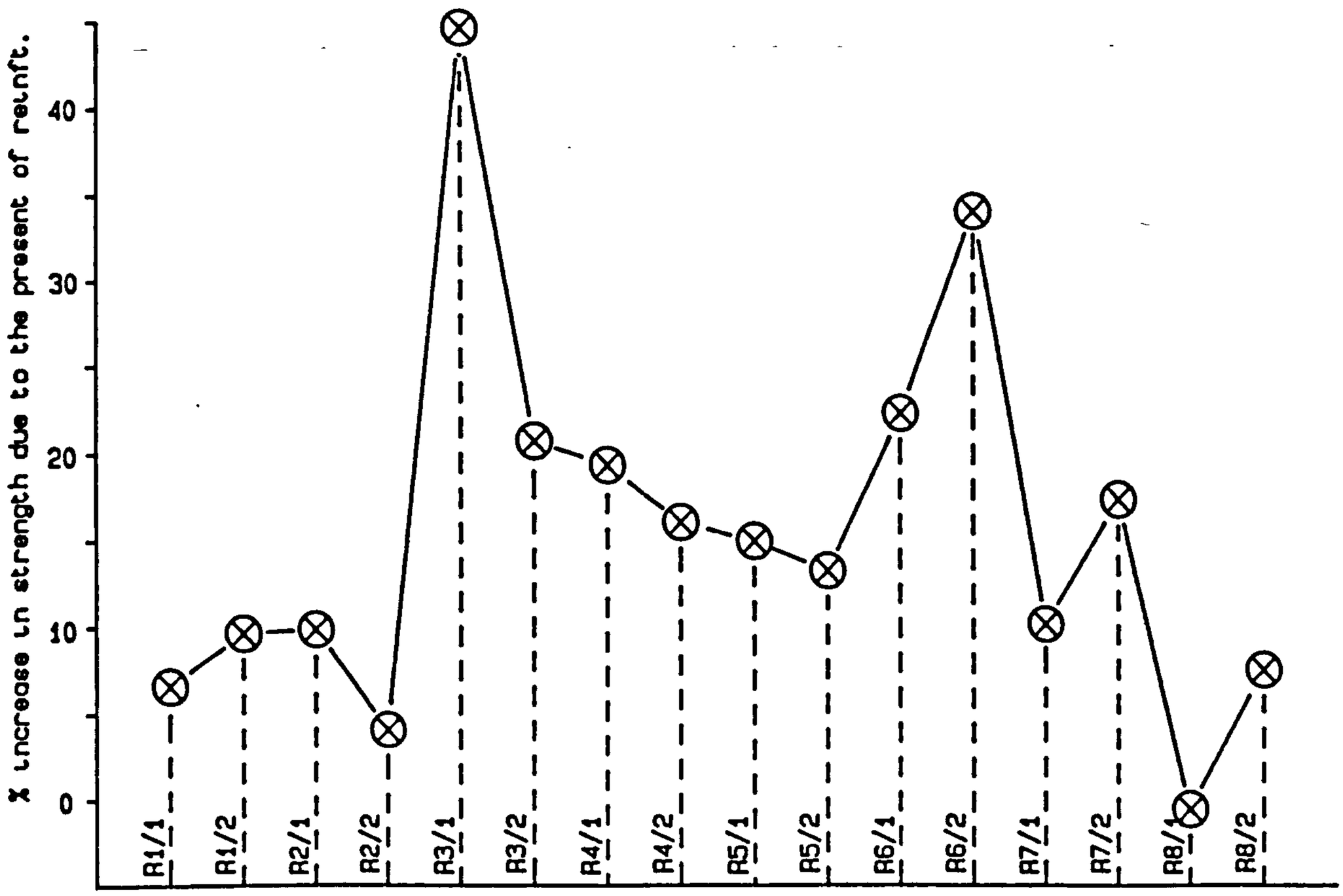

Fig.4.19 Percentage increase in strength for various forms of reinforcement.

of some forms of reinforcement. For instance, Al-Nijjam's formula successfully estimates the bearing strength of block R3/1 which may be said to have effective reinforcement, with a test to calculated bearing capacity of 0.99 which is a good result. On the other hand, a test to calculated bearing capacity ratio of 0.66 is obtained for block R1/2, which is consisered to have ineffective reinforcement. Therefore, at this stage it cannot be concluded whether Kriz's or Al-Nijjam model can be used generally as a means of calculation for reinforced concrete blocks.

Table 4.6 also tabulates the bearing capacity estimated by the modified proposed model as if they were plain concrete blocks. The ratio of the test to calculated values of bearing capacity is also tabulsted on the table. This can give an indication of the effectiveness of each form of reinforcement, and it is found that there are mostly 10 to 20% increases in bearing strength due to the presence of reinforcement. The most extra-ordinary one is block R3/1, which has more than 45% increase in strength with the presence of reinforcement. Fig.4.19 gives a plot of the percentage increase in strength with reinforcement for all the specimens in the present investigation.

5 LITERATURE REVIEW ON THE SHEAR STRENGTH OF REINFORCED CONCRETE DEEP BEAMS

5.1 INTRODUCTION

Nowadays, short span reinforced concrete panels are often used as structural members in civil engineering works and are referred to as deep beams. They can be defined as beams whose depth is of the same order of magnitude as span. The stresses in a deep beam differ radically from stresses predicted by ordinary beam theory because simple beam theory does not account for the vertical normal stresses induced by the applied loads and supports nor for the shearing deformations. The shear strength of a deep beam is significantly greater than predicted using expresions derived from simple beams. As increasingly design is carried out on a basis of ultimate strength, there is a need to understand the ultimate behaviour and strength of deep beams.

The investigation of the stresses and ultimate strength of deep beam is not a new subject. Different researchers have different techniques of investigation and have arrived at various results. In this chapter, an overall review of previous research on deep beams is presented.

5.2 ELASTIC SOLUTION

Dischinger [22,1932] was the first researcher looking into the stress distribution in deep beams with periodic loading represented by Fourier series and he constructed a stress function to satisfy the boundary condition. His results were later published graphically in a pamphlet by the Portland Cement Association [72]. In 1951, Chow [18] undertook the investigation of a single span deep beam by superimposing two stress functions. He used the stress function of the continuous deep beam that satisfied all but one of the boundary conditions and then constructed another stress function by the principle of virtual work to elimate the normal stress left at the vertical edges from the first stress function. He solved the differential equation by the method of finite differences and presented the results in graphical and tubular form for direct use in design. However, Chow could not produce accurate results at all cross-sections of the beam. Uhlman [80,1952] was another researcher of that period to investigate a single span deep beam. He solved the governing differential equations using Richardson's method of successive approximations and computed the stress trajectories for a number of loading cases. His solution can give some guidelines for the design of reinforced concrete deep beams with discussion of the effect of the presence of web openings. In 1954, Caswell [16] made use of photoelastic analysis to investigate the stress distribution in a simply supported deep beams. In comparing the fringe

patterns from photoelastic analysis with theoretical estimates, a close estimate of stress in deep beams subjected to simple loading was obtained. Kaar [37,38] performed experiments on small deep beams of aluminium and steel in 1957. He recognized the gradual departure from the simple linear flexure relationship to a highly non-linear stress state in a very deep beam. Archer and Kitchen [4,1956] constructed a stress function directly by means of virtual work. Their solution of bending stress agreed well with the results of Chow, but their shear stresses were not in good agreement. Later, Archer and Kitchen summerized the solutions of eight loading cases on deep beams with span/depth ratio equal to 1 together with correction factors for deep beams with span/depth ratios equal to 1.5 and 2.0 respectively. They presented these in tabular form for the purpose of design in the later paper [3]. Geer [25,1960] also used the method of finite differences to solve the differential equation but with a much finer computational grid than Chow. He discovered that the greatest tensile stress occurred not at the mid-span but near the face of the support. In 1961, Saad and Hendry [74,75] reported the results of a series of photoelastic tests on simply supported deep beams with either central load or gravitational load. In the latter case, they used a large centrifuge to simulate the gravitational loading. They summarized the results in figures showing the magnitude and direction of the principal stress. Holmes and Mason [34] made use of virtual work to present a method in solving the

problems of a single span deep beam supported by a parabolic shearing forces applied at the vertical edges. Since, this loading condition does not create a high bearing pressure around the supports, their results did not differ from the results obtained by shallow beam theory by as much as might be expected for beams of deep proportions. In 1973, Bhatt [11] generated a general procedure for solving continuous deep beams in statically indeterminate supports. The magnitudes of the reactions were determined by imposing the condition of displacements at the support. His solution comprised a power series and a series of hyperbolic functions. However, his results of stress distribution for deep beams with three spans differed little from those obtained by elementary beam theory. Recently, (1983), Barry and Ainso [10] applied the multiple Fourier technique to a simply supported deep beams under uniform loading at either top edge or bottom edge. They superimposed three stress functions in order to have all boundary conditions safisfied. Contour maps of the stress field were presented and illustrated the apearance of regions of pure tension and pure compression in the stress fields.

Previous elastic analyses fall within the three categories: (1) Fourier series technique, (2) Method of finite differences and (3) Photoelastic technique. However, with the invention of computer, the above mentioned elastic analyses have lost some value and have been replaced by the powerful method of finite element analysis (FEM), fig.5.1 shows the

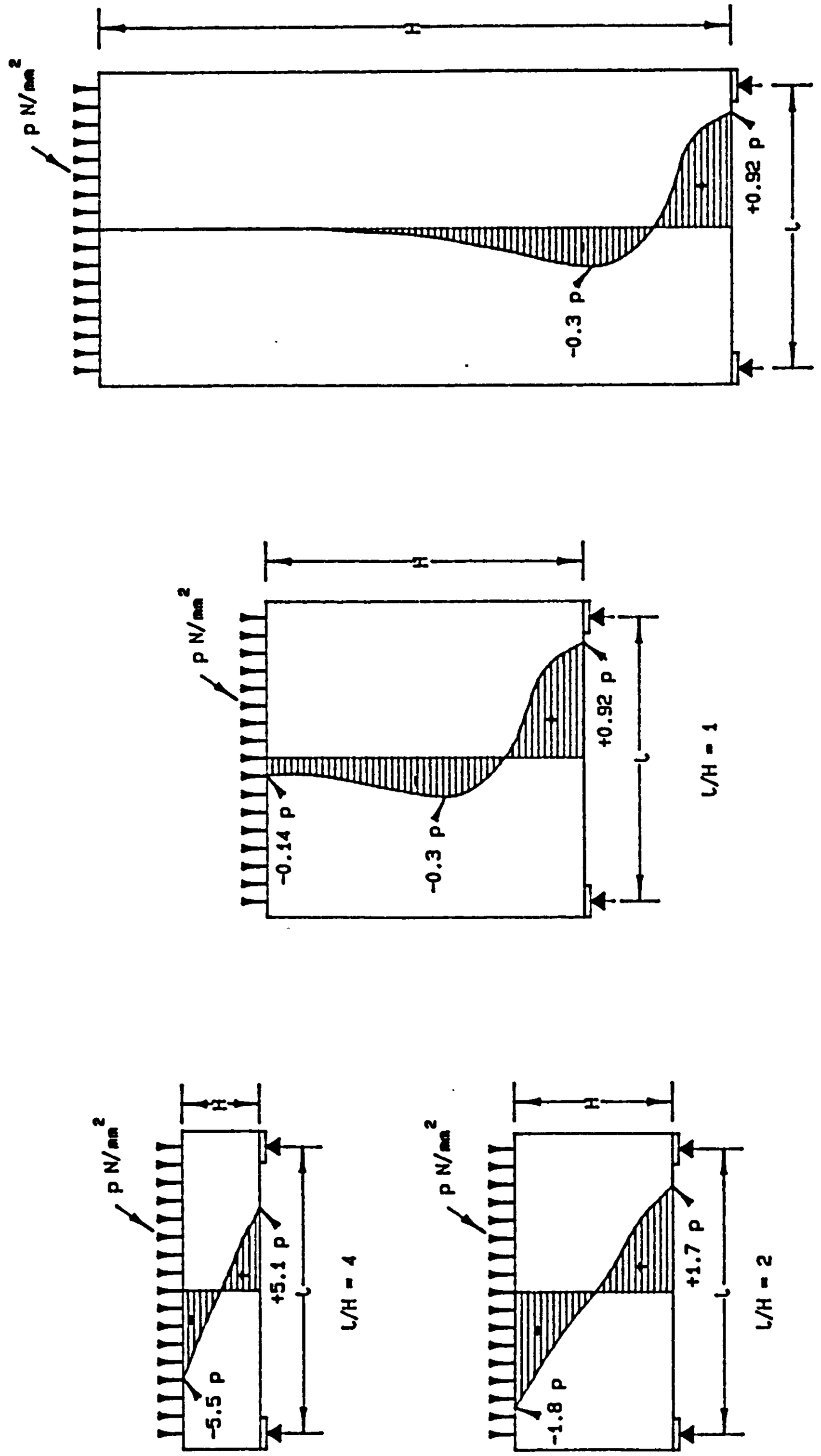

Fig.5.1 Stress distribution by FEM analysis with different L/H ratios.

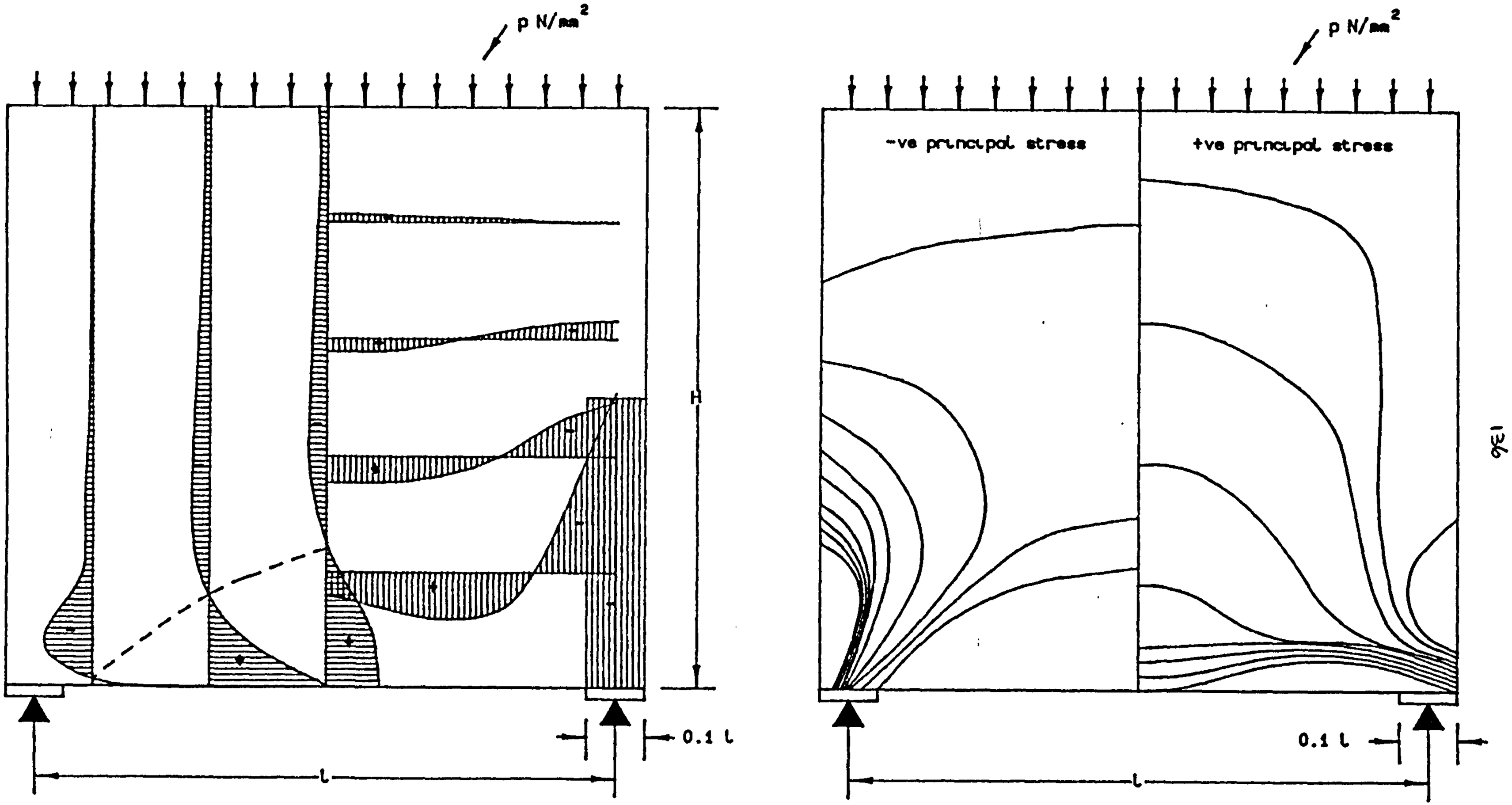

Fig.5.2 Stress distribution by FEM analysis for beams with l/H=1.

horizontal stress distributions at the centre of a simply supported beam with span/depth ratio from 0.5 to 4.0, analysis by FEM. It illustrates clearly how the stress dirtribution deviates from elementary beam theory as the span/depth ratio decreases. Fig.5.2 is also the result of FEM analysis; it gives the vertical and horizontal stress distribution at various sections along a beam (fig.5.2) with a span/depth ratio equal to one, together with the stress contours of the principal tension and compression stresses (fig.5.2b).

5.3 EXPERIMENTAL ANALYSIS OF REINFORCED CONCRETE DEEP BEAMS

The gradual introduction of limit state analysis into most national codes implies that elastic analysis is no longer of prime importance in design. It only gives information of stress distributions in reinforced concrete deep beams up to the onset of cracking and also it sheds no light on the modes of failure which are important in design. For the above reasons, extensive experiments have been carried on reinforced concrete deep beams for the past two decades. Some of these tests are summarized in this section.

Paiva and Siess [69,1965] were early researchers investigating the shear strength and behaviour of moderately (span/depth ratios from 2 to 6) deep reinforced concrete deep beams. The main variables involved in the study were the

amount of main and web reinforcement, concrete strength and the span to depth ratios. All the beams were 711 mm long and supported on a span of 610 mm. The depth was varied from 178 to 330 mm with three effective span/depth ratios of 4, 3 and 2 respectively. The widths of the beams were varied in such a way to give a constant cross-sectional area. The bearing plate at load points and reactions were 101 mm long and it was loaded at the third points. Fig.5.3 indicates the dimensions of the specimens and types of reinforcement used. From the results of the tests, they concluded that an increase in the concrete strength of the beam particularly at low span/depth ratios. has no effect on the beam failing in flexure but increases the shear strength The presence of web reinforcement had no effect on the cracking load for the shear capacity of a beam with shear span to effective depth ratio (x/d) greater than 3. However, for x/d smaller than this value, there is a large increase in shear capacity beyond the cracking load. Web reinforcement tended to reduce the deflection at ultimate load.

Leonhardt [53,54,1966] reported the tests of five simply supported deep beams with span/depth ratio of 0.9. They were 1600 mm square and 100 mm thick. The bearing length was 1600 mm, leaving a span of 1440 mm. All specimens were tested under uniformly distributed top load; dimensions and reinforcement details are shown in fig.5.4. In one of these beams (WT4), the bearing area was increased by a transverse strip up to a height of 600 mm from the bottom. It was found from the tests that tensile stresses in the main reinforcement

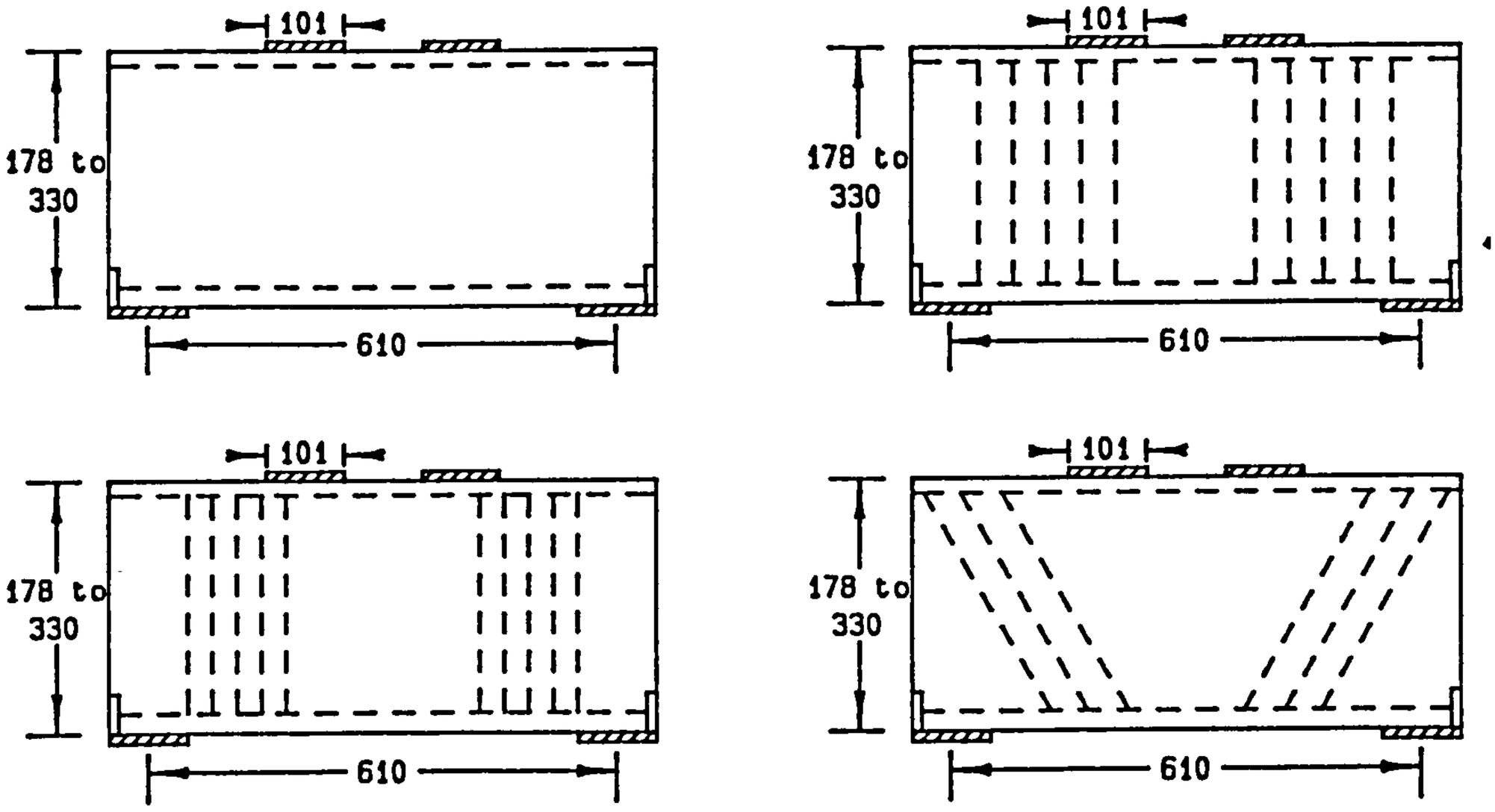

Fig.5.3. Test specimens of Paiva and Siess (1965).

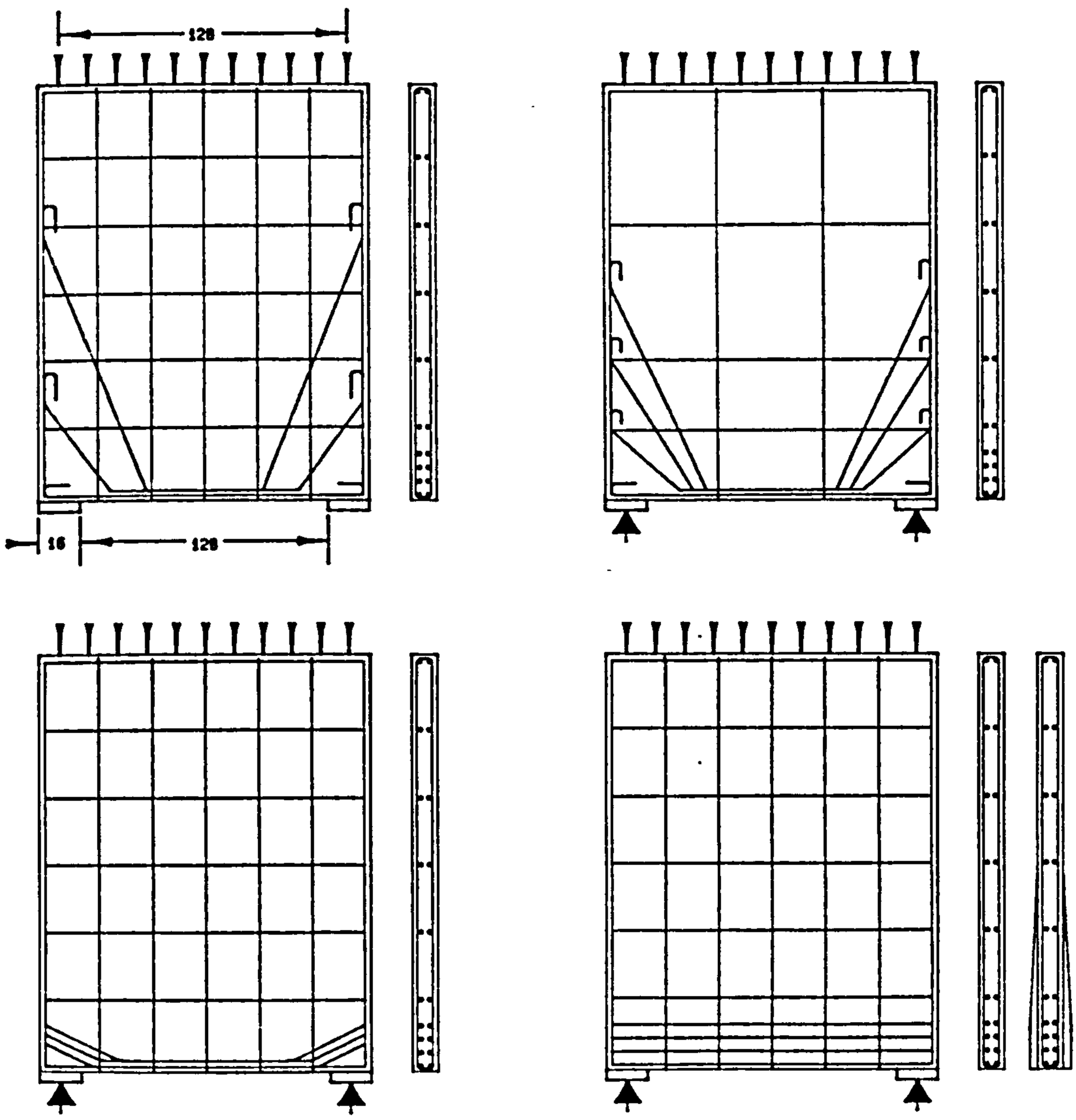

FIG.5.4. Test specimens of Leonhardt (1966).

do not decrease towards the support as in ordinary slender beams but remains constant almost to the supports. In order to provide anchorage of the main reinforcement, Leonhardt suggested that long horizontal hook loops should be used in the main reinforcement at the supports. He stressed that bent up bars from the main reinforcement mainly received compressive stresses and therefore serve no purpose. On the other hand, the weakening of the main reinforcement through bent up rods reduced the fracture load. In 1968, Ramakrishnan and Ananthanarayana [73] presented experiments on 26 single span rectangular deep beams having span/depth ratios of 1 to 2. They were tested under concentrated (at a single point and two points) and distributed loads. All specimens have a constant span of 686 mm and height varied from 381 to 762 mm. Plain mild steel round bars were used as reinforcement in all beams. Details of the dimensions and reinforcement of the beams are shown in fig.5.5. Different modes of shear failure were reported in their investigation. They were classified as follows;

(1) Diagonal tension failure — characterized by a clean and sudden fracture. For concentrated loads, it occurs along a line joining the support and the loading point. For uniformly distributed loads, it is along a line joining either support with the nearest third span point.

(2) Diagonal compression failure — involved with the formation of two cracks. The first one, developed nearly along the line joining the support and load points. The second one is formed parallel to the first one but closer to the support. Failure of the beam was by the destruction of the portion of concrete between these two cracks.

(3) Splitting of the compression zone — characterized by the clear vertical fracture of the compression zone at the top of the inclined crack.

(4) Flexure-shear failure — Although the tensile steel of the beam had considerably yielded but before the beam could fail in flexure, suddenly diagonal tension cracks developed and caused the collapse of the beam.

Kong et al [39-47] carried out major tests on reinforced concrete deep beams. This included experiments with normal weight and lightweight concrete and with different forms of web reinforcement. In 1970 and 1972, Kong et al [29,44] presented an experimental study on the effectiveness of different web reinforcement in 45 normal weight concrete deep beams. The types of web reinforcement used are shown in fig.5.6. Each of the specimens had an overall length, 915 mm, 762 mm span and 76 mm width. They were tested with span/depth ratios varying from 1 to 3 and loaded with two point loads at their third span. The bearing length of both the support or loading point

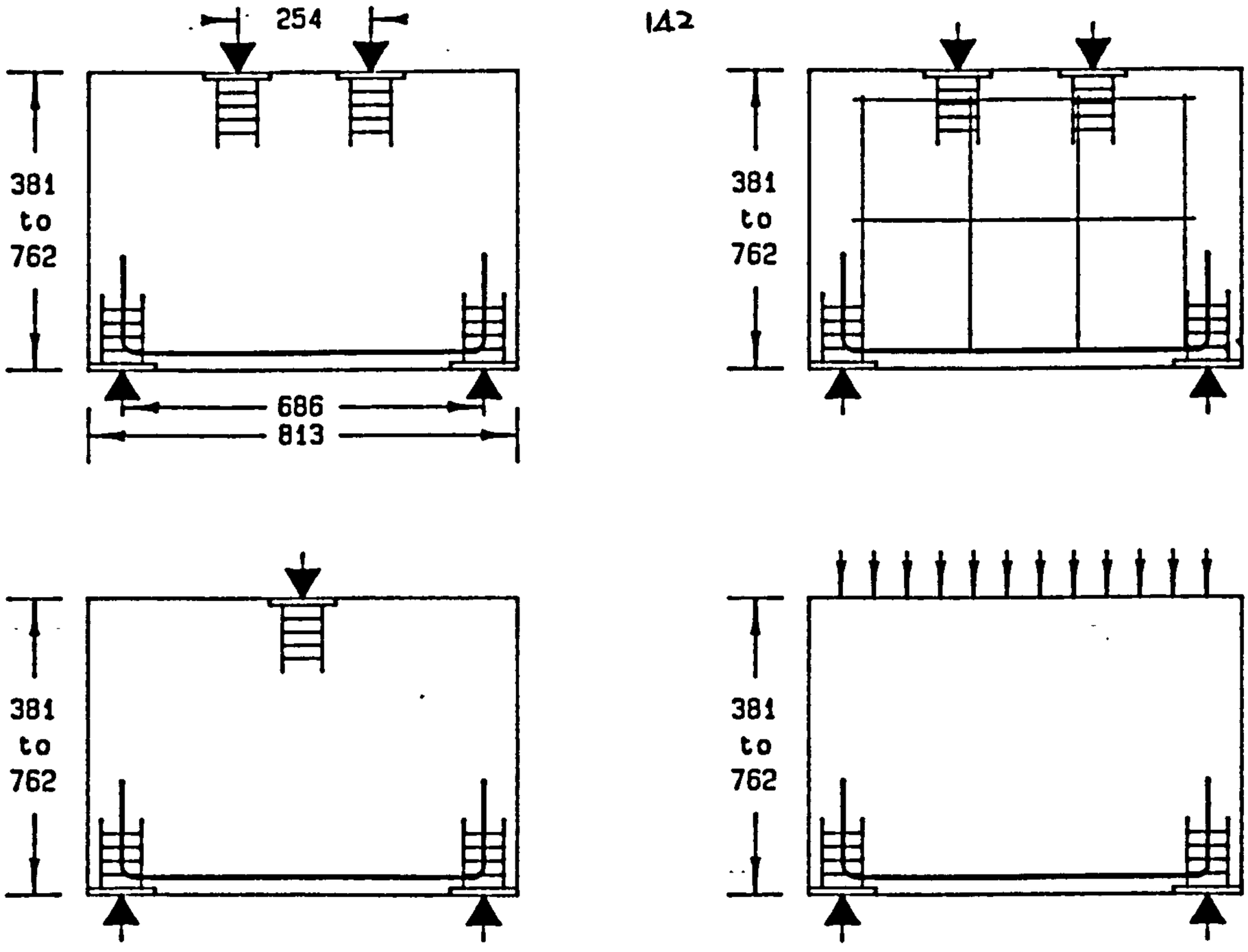

Fig.5.5 Test specimens of Ramakrishnan & Anathanarayana (1968).

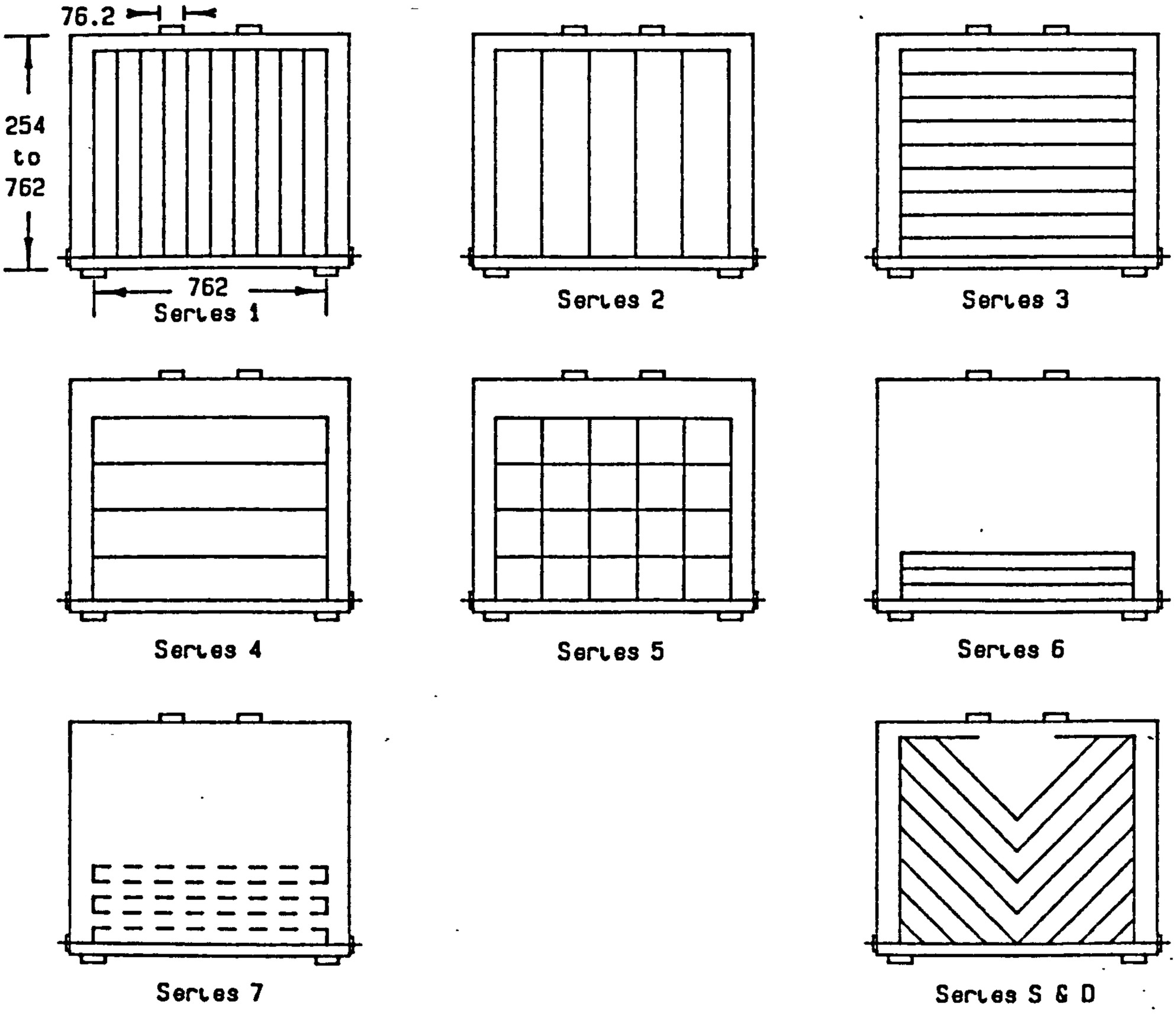

Fig.5.6 Test specimens of Kong (1972).

was 76 mm. Anchorage of the main reinforcement was provided by steel blocks at the ends of the beams. It was found that the strength, deflection and crack widths were dependent on the depth (L/H) and clear span to depth (X_c/H) ratios. For low L/H and X_c/H ratios, only horizontal web reinforcement near the bottom of the specimen was effective while for higher L/H (>3) and X_c/H (>0.7) vertical web reinforcement was more preferable than others. Inclined web reinforcement was the best in controlling crack widths and deflection, and could also increase the ultimate strength of the beams. However, they pointed out that inclined web reinforcement may be uneconomical in construction.

Kong and Robins [42] reported tests on simply supported lightweight concrete deep beams with dimensions and types of reinforcement similar to those with normal weight concrete beams [39,44] except deformed bars were used for reinforcement. They arrived with similar conclusions as for normal weight concrete deep beams in that inclined web reinforcement was the most effective form of reinforcement in controlling crack widths and deflection and produced higher strength as well. It was found that the formulae for normal weight concrete deep beams were not necessarily suitable for lightweight concrete beams.

Further investigation on lightweight concrete deep beams has been carried out by Kong and Singh [47]. Results were

obtained for 45 rectangular deep beams with constant depth, 508 mm, but varying span from 508 to 1524 mm. They were tested with L/H ratios ranged from 1 to 3 and X_c/H ratios from 0.23 to 0.7. Different types and amounts of web reinforcement were used as shown in fig.5.7. It was reported that the X_c/H ratio critically affected the crack and ultimate load of the beams. Inclined web reinforcement was the most effective form of reinforcement for all ranges of X_c/H ratio tested. For low X_c/H ratio, the next most effective reinforcement was horizontal reinforcement placed close to the bottom of the beam but for higher X_c/H ratios it was vertical web reinforcement. Generally, The de Paiva and Siess's formula could be used to estimate the ultimate strength of lightweight concrete deep beams, but was not so accurate as for normal weight concrete beams.

Reinforced concrete deep beams subjected to repeated loadings were also tested by Kong et al [48]. All the beams tested were 76 mm thickness, 1524 mm span and had two different heights of 508 and 762 mm (span/depth ratios were 3 and 2 respectively). They were loaded with 3 clear shear span/depth ratios (X_c/H = 0.25, 0.4 and 0.55). It was found that inclined diagonal web reinforcement was still the most effective in controlling crack width, reducing deflection and increase shear strength of the beam. de Paiva and Siess design formula was

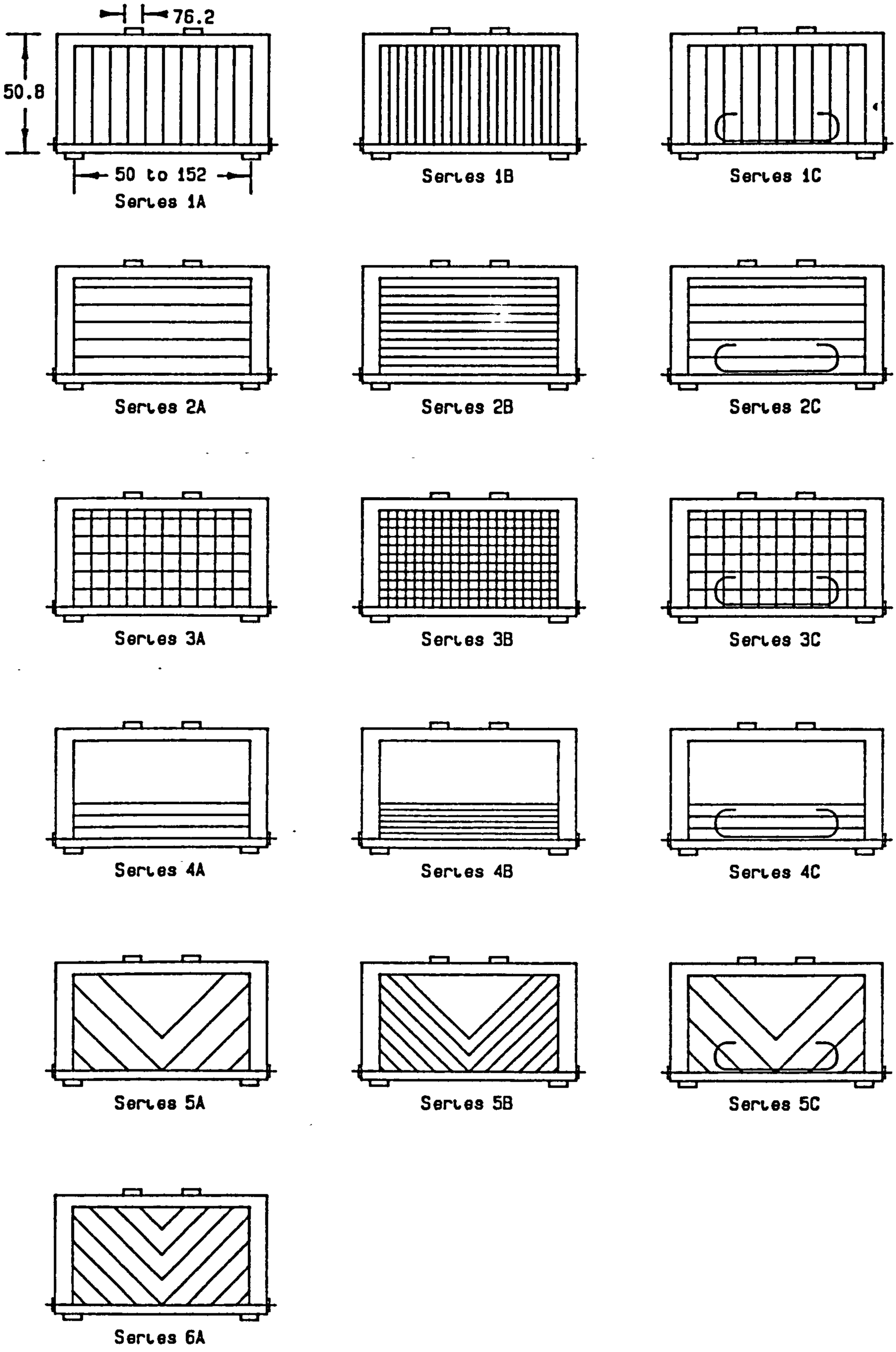

Fig.5.7 Test specimens of Kong (1972).

more accurate for deep beams with a repeated loading history. Repeated load (within the tested range, mean level of load and number of cycles) had no overall effect on the ultimate shear strength of the reinforced concrete deep beams.

Amongst all the deep beams tested by Kong [39-47] four principal modes of failure were reported. They are as follows (1) Splitting of the beam into two by a diagonal crack. (2) Crushing of the concrete between two diagonal cracks. (3) Penetration of a diagonal crack into the concrete compression zone near a bearing plate and failure of the beam resulting from by the crushing of the concrete in the reduced compression zone. (4) Crushing of the concrete at a load bearing block (true crushing failure mode).

Al-Najjim [63] reported tests of 24 simple supported beams, of which 6 had no web reinforcement, and the others were reinforced with different forms of reinforcement; horizontal, vertical, orthogonal and inclined web reinforcement. Amongst the tested beams, 8 had vertical stiffening ribs to prevent failure due to bearing at the supports. In fact, with the exception of the specimens with stiffened ribs, most of them failed by crushing of concrete above the supports: However, he arrived a conclusion similar to Kong et al [47] in that for small clear span/depth ratios, horizontal and diagonal web reinforcement were more effective while vertical web reinforcement was suitable for beams with larger clear

span/depth ratios.

Smith and Vantsiotis [77] presented tests on 52 deep reinforced concrete beams under two point loading. All the beams tested had a constant depth of 356 mm, 102 mm thickness and varying lengths from 1420 to 2080 mm. They were tested with spans varying from 813 to 1470 mm in 4 clear span/depth ratios (X_c/H) of 0.77, 1.01, 1.34 and 2.01 respectively. Five of the beams had no web reinforcement, the rest of them having horizontal and vertical web reinforcement percentages ranging from 0.23 to 0.91% and from 0.31 to 1.25% respectively. The forms of reinforcement used are shown in fig.5.9. It was reported that failure of the beams was caused by crushing of concrete in the reduced compression zone at the head of the inclined crack or by fracture of concrete along the inclined crack. Beams with web reinforcement has smaller cracks and less damage at failure. Increasing the ratio X_c/H could increase the deflection and reduce the ultimate load of the beam. It was also found that the effectiveness of the vertical reinforcement diminished and the influence of horizontal web reinforcement increased as X_c/H decreased. Concrete strength played an important parts in the ultimate shear strength of deep beams exceptionally at low clear shear span/depth ratios.

Besser [12,13] carried out tests on 7 deep reinforced concrete panels with depth ranging from 720 to 2880 mm corresponding to span/depth ratios from 0.25 to 1.0. All the

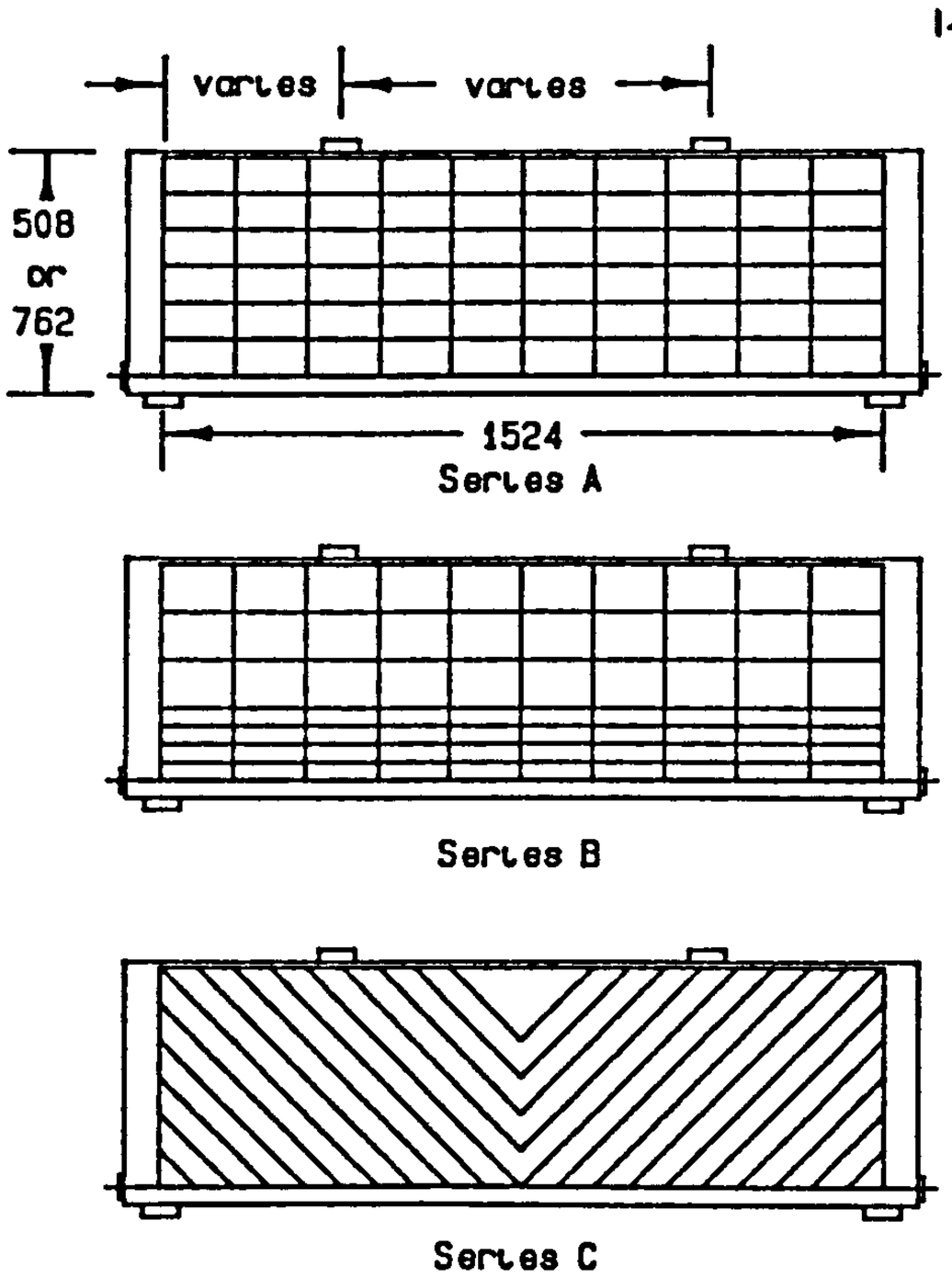

6mm nomtal dta. stirrups
Hortzontal spactng 152 mm.
Vertical spactng 76 mm.

6 mm nomtal dta. stirrups.
Hortzontal spactng 152 mm.
Vertical spactng 38 mm & 108 mm.

6 mm nomtal dta. tnclined stirrup.
at 45 degs. to hortzontal, at 76 mm
spactng hortzontally.

Fta.5.8 Test spectmens by Kong (1974).

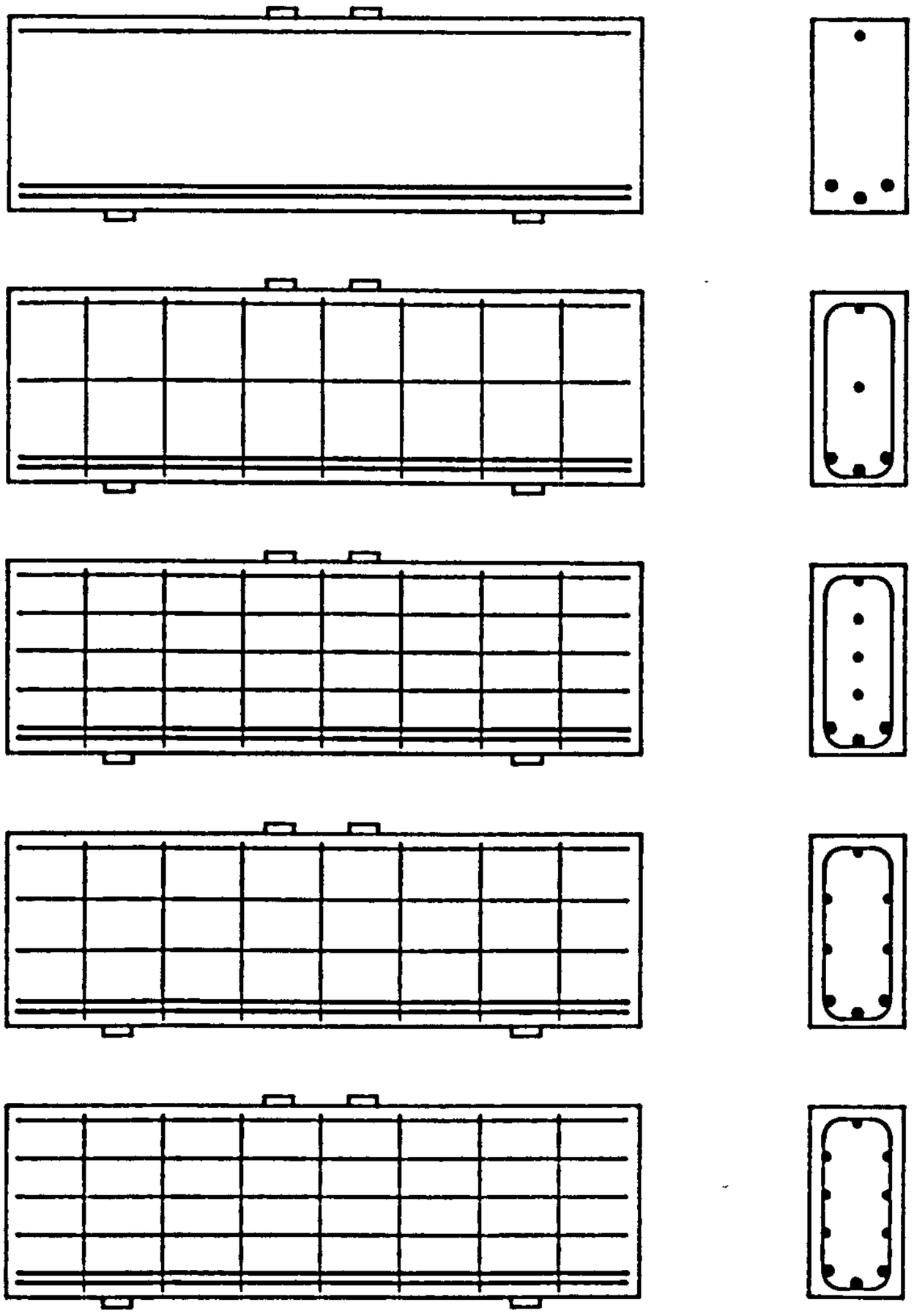

Fta.5.9 Type of retnforcement used by Smtth et al (1982).

specimens had span 720 mm, overall length 872 mm and 72 mm thickness, the depth/thickness ratios varied from 10 to 40. They were reinforced with four 10 mm diameter bars as main reinforcement which were anchored by external steel blocks at the ends of the panel. Web reinforcement was orthogonal arranged with 5.3 mm plain mild steel bars. Detail of the dimension and reinforcement of the specimen is shown in fig.5.9. It was reported that the diagonal crack loads were increased as span/depth ratio decreased from 1 to 1/3 and thereafter they were unaffected by the depth of the panel. For a specimen with span/depth ratio equal to 1, failure was by shearing along the line joining the load and support points. Bearing failure at the support was dominant in the specimens with span/depth ratios ranging from 0.28 to 0.67. However, failure by buckling of the specimen was reported with span/depth ratios equal to 0.25 (height/thickness ratio equal to 40).

5.4 RECOMMENDATIONS FOR THE DESIGN OF REINFORCED CONCRETE DEEP BEAMS

A brief summary of various documents providing guidance for the design of reinforced concrete deep beams follows;

5.4.1 PORTLAND CEMENT ASSOCIATION [72,1946]

This is a design method based on the elastic analysis and not on the results of ultimate load tests. It is applicable to reinforced concrete deep beams with the span/depth ratio (L/H) not exceeding 1.25 for simply supported beams and 2.5 for continuous beams. Design charts are used as a method of design and it is based on two parameters: the height to span ratios (β=H/L) and ther ratios of the support width to span (ϵ=a_1/L). They can be calculated according to the loading and supporting conditions as follows;

$$\epsilon = \begin{cases} a_1/L & \text{—— continuous beams} \\ 0.5 & \text{—— U.D.L. (simple beam)} \\ a_1/2L & \text{—— point load (simple beam)} \end{cases} \qquad (5.1a)$$

$$\beta = \begin{cases} H/L & \text{—— continuous beam} \\ H/2L & \text{—— simple beam} \end{cases} \qquad (5.1b)$$

After obtaining the values of ϵ and β from eq.5.1, tensile force T in terms of total load can be found from a design chart. Thus, the area of the main longitudinal steel can be calculated by

$$A_{sl} = T/f_s \qquad (5.2)$$

where f_s is the allowable working stress in steel. It was suggested that the main longitudinal reinforcement should be placed as close as possible to the lower edge of the beam.

Shear stress in the beam should be limited by

$$v = 8V/7b\cdot d < (1+5H/L)v_c/3 \qquad (5.3)$$

where v = shear stress of the beam

V = applied shear force
v_c = allowable shear stress for slender beams.

5.4.2 DE PAIVA AND SIESS [69,1965]

Previously, Laupa [51] had derived an expression for the shear strength of reinforced concrete beams;

$$v = V/b \cdot H = 200 + 0.188f'_c + 21300P_t \qquad (5.4)$$

where v = nominal shear strength, psi.
V = shear force, lb.
f'_c = cylinder compressive strength of concrete, psi.
H = depth of the beam, inches
b = thickness of the beam, inches.

and

$$P_t = A_s(1 + \sin\alpha)/b \cdot H \qquad (5.5)$$

in which A_s = Total sectional area of steel crossing a vertical section between the load point and support.
α = Angle of inclination of reinforcement to the axis of the beam and should not be greater than 62.7 degress.

Using De Paiva's experimental data to calculate shear strength by Eq.5.4, a linear relationship was found between experimental and calculated values. It varied with the clear shear span/depth ratio in such a way that

$$V_{(expt.)}/V_{(cal.)} = 0.8(1-0.6X_c/H) \qquad (5.6)$$

and is valid for X_c/H between 0 and 1. Therefore, an expression for computing the ultimate load of reinforced concrete deep beams was obtained as follows.

$$P_u = 2 \cdot b \cdot H \cdot v = 1.6(200+0.188f_c'+21300P_t)(1-0.6X_c/H) \quad (5.7)$$

5.4.3 RAMAKRISHNAN AND ANANTHANARAYANA [73]

According to the results of their experiments, it was found that most beams failed in a diagonal tension mode. This mode of failure was similar to that of a cylinder splitting test, and therefore, equations were developed to predict the ultimate shear strength of reinforced concrete deep beams based on the equations for the evaluation of splitting strength of concrete. The splitting strength of the concrete ft can be expressed as;

$$f_t = F/K \cdot A \quad (5.8)$$

where F = Maximum splitting force.
A = Area resisting the splitting force.
K = 1.57 for cylinder splitting test.

Consider an eccentric single point load acting at the top of the beam as shown in fig.5.10a and resolve it according to the figure. It can be seen that the splitting force of the failure strut will be equal to

$$F = P_u \cdot \cos\phi/\sin(\theta+\phi) \quad (5.9)$$

where $\phi > \theta$

The area resisting the splitting force is

$$A = b \cdot H \cdot \mathrm{cosec}\phi \quad (5.10)$$

By substituting Eq.5.8-10, the ultimate load of the reinforced concrete deep beams failed in diagonal tension will be

$$P_u = K(1 + \tan\theta \cdot \cot\phi) \cdot f_t \cdot b \cdot H \qquad (5.11)$$

For a central concentrated load $\theta=\phi$, thus the ultimate diagonal tension failureload will be

$$P_u = 2K \cdot f_t \cdot b \cdot H \qquad (5.12)$$

For a two-point loaded deep beam as shown in fig.5.10b, the splitting force, F is

$$F = P_u \cdot \operatorname{cosec}\theta/2 \qquad (5.13)$$

and the area resisting the splitting force is

$$A = b \cdot H \cdot \operatorname{cosec}\theta \qquad (5.14)$$

Therefore, the ultimate load for a deep beam with two-point load is

$$P_u = 2 \cdot b \cdot H \cdot K \cdot f_t \qquad (5.15)$$

For uniformly distributed load on the top of the beam (fig.5.10c), the ultimate load can be found by considering it as a superimposition of a series of point loads and integrating it throughout the span of the beam. The splitting force reached a maximum when the diagonal crack plan was defined by

$$\tan\theta = 3H/L \qquad (5.16)$$

and the total ultimate load Pu on the beam is given by

$$P_u = 2K \cdot f_t \cdot b \cdot H \qquad (5.17)$$

The value of K can lie between 1.0 and 1.57 depending on the method used for accessing the tensile splitting strength of concrete. Generally, a value of 1.12 is a reasonable lower bound for all the tested beams. Moreover, during the derivation of the above expression, the effect of web

reinforcement has been neglected and tests carried out by the author had little or no web reinforcement. Therefore, no conclusion can be made as to whether these equations can be used for beams with web reinforcement. However, it provided a tool to estimate the cracking strength of a reinforced concrete deep beam.

5.4.4 COMITE' EUROPEEN DU BETON — FIP [17]

CEB-FIP recommended that beams with span-depth ratios less than 2 and 2.5 for simply supported beams and continuous beams respectively should be designed as deep beams. In this section only simply supported deep beams with top load are discussed. The area of main reinforcement should be calculated from the largest bending moment in the span, using the lever arm, z defined as follows:

$$z = \begin{cases} 0.2(L + 2H) & 1 < L/H < 2 \\ 0.6L & L/H < 1 \end{cases} \qquad (5.18)$$

The main reinforcement should be extended without reduction from one support to the others and anchored with a force equal to 0.8 times the maximum force calculated. It should also be distributed uniformly over a depth 0.25H-0.05L (<0.2L), measured from the lower face of the deep beam. In order to facilitate anchorage at the support and limit the development of cracks and crack width, small diameter bars should be employed. Anchorage by means of vertical hooks is not

recommended as it tends to promote cracking in the anchorage zone.

For top loaded deep beams, CEB-FIP proposes the use of orthogonal reinforcement in the web, consisting of vertical stirrup and horizontal bars on both faces of the beam. The area of the reinforcement is given by 0.0025b.s for a smooth round bar or 0.002b.s for a high-bond bar, where b is the thickness of the beam and s is the spacing between bars. It is interest to note that most of the CEB-FIP recommendations are based on the findings of Leonhardt and Walther [53,54].

5.4.5 ACI COMMITTEE 318

The proposed revision of ACI 318-63: Building Code Requirements for Reinforced Concrete [2] has a section of recommendations on the design of deep beams and they will be discussed briefly here.

The revised ACI Code is applicable to mambers with clear span to effective depth ratio (L_o/d) less than 5 and loaded at top or compression face when designed for shear. The shear strength of the reinforced concrete deep beams, v is believed to be composed of the nominal shear strength provided by concrete, v_c, and the nominal shear strength provided by shear reinforcement, v_s, so that

$$v = v_c + v_s \tag{5.19}$$

Regardless of the amount of web reinforcement, the nominal shear strength, v is limited by the following expressions

$$v = k \cdot v_u \tag{5.20}$$

and
$$v_u = \begin{cases} 8 \cdot f_c'^{0.5} \quad \text{——————} \quad L_o/d < 2 \\ \\ 2(10+L_o/d) f_c'^{0.5}/3 \quad \text{——} \quad 2 < L_o/d < 5 \end{cases} \tag{5.21}$$

where k = the capacity reduction factor and is taken as 0.85

The nominal shear stress, v_c carried by concrete is calculated by

$$v_c = (3.5-2.5M/V \cdot d)(1.9f_c'^{0.5}+2500\rho \cdot V \cdot d/M)$$

$$< 2.5(1.9f_c'^{0.5}+2500\rho \cdot V \cdot d/M) \tag{5.22}$$

$$< 6f_c'^{0.5}$$

where M,V = the design bending moment and shear force at the critical setion respectively.
ρ = the ratio of main reinforcement A_s to the area bxd of the concrete section.
f_c' = compressive cylinder strength, psi.

The remaining shear stress is carried by the web reinforcement and it can be calculated by

$$v_s = v - v_c$$
$$= f_y \cdot A_{wv}(1+L_o/d)/(12S_v \cdot b) + f_y \cdot A_{wh}(11-L_o/d)/12S_h \cdot b) \tag{5.23}$$

where A_{wv} = area of vertical shear reinforcement within a distance, S_v.
A_{wh} = area of horizontal shear reinforcement within a distance S_h.
f_y = specified yield strength of reinforcement, psi.

However, irrespective of the values of shear stress, the cross-sectional areas of vertical and horizontal reinforcement should not be less than 0.15%B.L and 0.25%b.d respectively.

5.4.6 KONG [40,45]

Kong has proposed a design formula to calculate the ultimate shear strength of reinforced concrete deep beams for both normal and lightweight concrete. The formula can be used for beams with span/depth ratio not greater than 3 if the clear span/depth ratio does not depart widely from the range 0.23 to 0.7. The formula is as follows:

$$P_u = 2\left[C_1(1-0.35X_c/H)f_t \cdot b \cdot H + C_2\Sigma A_s \cdot y \cdot \sin^2\alpha/H\right] \quad (5.24a)$$

where P_u = ultimate load of the deep beam.
C_1 = coefficient equal to 1.4 for normal weight concrete and 1.0 for lightweight concrete.
C_2 = coefficient equal to 130 and 300 N/mm^2 for plain round bars and deformed bars respectively.
f_t = cylinder splitting strength, N/mm_2.
b = thickness of the beam, mm.
H = overall depth of beam, mm.
y = depth of bar, measured from top of beam to the point where it interests the line joining the inside edge of the bearing blocks at the support to the outside edge of that at the loading point.
α = angles between bars and the line described above.
n = numbers of bars, including the main reinforcement that cross the line between support and loading block.

Recommendations have also been made for the design of flexural reinforcement. Longitudinal main reinforcement should be added so that the bending moment will not exceed.

$$M < 0.6A_s \cdot f_y \cdot H/\gamma_m \quad \text{or} \quad 0.6A_s \cdot f_y \cdot L/\gamma_m \qquad (5.24b)$$

Since the amount of flexural reinforcement required in deep beams is small and main reinforcement can also act as web reinforcement, although the above formula gives conservative results, it does not lead to wasteful use of reinforcement.

5.4.7 CIRIA GUIDE 2 [68,1977]

This is the most comprehensive set of rules and recommendations available for the design of deep flexural members. It can be used for beams with span/depth ratios less than 2 for single span or less than 2.5 for continuous supports. A brief summary of the design method is listed below.

(a) Design for flexure

The area of main reinforcement can be calculated by

$$A_s = M/0.87f_y \cdot z \qquad (5.25)$$

where M = Design bending moment.
f_y = yield strength of the reinforcement.
z = lever arm at which the reinforcement acts and is given by

$$z = \begin{cases} 0.2L + 0.4H \text{ —— single span } L/H < 2 \\ 0.2L + 0.3H \text{ —— continuous } L/H < 2.5 \end{cases} \qquad (5.26)$$

For a simply supported single span deep beam, the main reinforcement should be distributed uniformly over a depth of

0.2H at the bottom of the beam. Reinforcement is not curtailed in the span and must be anchored to develop 80% of maximum ultimate force beyond the face of the support. Twenty percent of bars should anchor beyond a point 0.21 from support.

(b) Design for shear

For top loaded beams, the effective clear span X_e is defined as either the clear shear span for a load which contributes more than 50% of shear or 0.25L for uniformly distributed load. In the case of more than one load but none has more than 50% of the total shear, the weighted average of clear span should be taken as the effective clear shear span, X_e. The shear strength for top loaded reinforced concrete deep beams can be estimated by

$$V_u = \gamma_1 \cdot b \cdot H(1-0.35X_e/H) \cdot f_{cu} + \gamma_2 \cdot \Sigma 100A_s \cdot y \cdot \sin^2\alpha/H \quad (5.27)$$

$$< 1.3b \cdot H \cdot \gamma_1 \cdot f_{cu}$$

where
$$\gamma_1 = \begin{cases} 0.44 & \text{for normal weight concrete} \\ 0.32 & \text{for light weight concrete} \end{cases}$$

$$\gamma_2 = \begin{cases} 1.95\ N/mm^2 & \text{for deformed bars} \\ 0.85\ N/mm^2 & \text{for plain bars} \end{cases}$$

(c) Bearing capacity

CIRIA Guide limited the maximum bearing stress to $0.4f'_c$ and the bearing length is regarded as the lesser of the actual bearing length a_1 and $0.2L_c$.

5.4.8 AL-NAJJIM [63]

Al-Najjim proposed a structural model of failure of reinforced concrete deep beams with and without web reinforcement. There are a numbers of assumptions and they are listed below:

(1) Steel is assumed to be properly anchored so as to develop a tie and strut action.

(2) Steel is assumed to be perfectly plastic and has a yield stress, f_y in tension.

(3) Steel is assumed to carry only uni-axial stress along the original bar direction.

(4) The size of the compressive strut is determined either by the yield resistance of the tension steel or by local conditiona at supports.

(5) The struts between loads and suports are deflected by the presence of web reinforcement. For uniform web steel, the deflected strut is in parabolic form.

(6) The force in the main steel decreases towards the supports and this is due to the presence of vertical stirrups.

Al-Najjim [63] presented his model in many loading conditions (single point, two point and uniformly distributed load) and with different types of web reinforcement. To be brief, only

beams with uniformly distributed orthogonal web steel and under two-point load are discussed here. Fig.5.12 shows the dimenmsions of the beam, notation and the forces to maintain equilibrium. There are two modes of failure as follows:

(A) Failure of the tie

By taking moments at the intersecting point of the centre of the strut with the direction of the load (point A) and considering the horizontal equilibrium of one of the struts, the following equatons are obtained.

$$V_u = (T_s \cdot z + 0.9d \cdot Z_w \cdot H_w - \Delta T_s)/X \qquad (5.28)$$

and $$y_o = (T_s + 0.9d \cdot H_w - \Delta T_s)/(b \cdot \beta_2 \cdot f_c') \qquad (5.29)$$

where $$z = d - y_o/2 \quad \& \quad Z_w = 0.45d - y_o/2 \qquad (5.30)$$

and $H_w = A_{sw}/b \cdot S_h$

$V_w = A_{sv}/b \cdot S_v$

T_s = Tensile force of the main reinforcement.

ΔT_s = Loss of tensile force towards the support due to the presence of vertical reinforcement.

y_o = Depth of the compressive zone at the top of the beam.

Combining Eqs.5.28-30, the shear strength of the deep beam with the yielding of the tie is

$$V_u = T_s(d-K')/X + 0.9d \cdot H_w(0.45d-K')/X \qquad (5.31)$$

where $$K' = (T_s - 0.9d \cdot H_w - \Delta T_s)/2b \cdot \beta_2 \cdot f_c'$$

(B) Failure of the strut

Consider the equilibrium at one of the support.

Vert.: $$V_u = w_o \cdot b \cdot \beta_2 \cdot f_c' \cdot \sin\theta = K \cdot b \cdot \beta_2 \cdot f_c' \cdot \sin^2\theta \quad (5.32)$$

Hor.: $$T_s - \Delta T_s = w_o \cdot b \cdot \beta_2 \cdot f_c' \cdot \cos\theta = K \cdot b \cdot \beta_2 \cdot f_c' \cdot \sin(2\theta)/2 \quad (5.33)$$

since $$\sin^2\theta = \left[1 - (1-\sin^2(2\theta)\right]^{0.5} \quad (5.34)$$

By substituting Eqs.5.32, 5.33 into 5.34, the magnitude of the tensile force in the main reinforcement T_s' can be found by solving the equation below.

$$A \cdot T_s'^2 + B \cdot T_s' + C = 0 \quad (5.35)$$

where $A = 0.81d^2/X^2 + 1$

$$B = 0.73H_w \cdot d^3/X^2 - 0.9K \cdot d \cdot b \cdot \beta_2 \cdot f_c'/X - 2d \cdot T_s$$

$$C = \Delta T_s^2 + 0.16d^4 \cdot H_w^2/X^2 - 0.41d^2 \cdot H_w \cdot K \cdot b \cdot \beta_2 \cdot f_c'/X$$

After getting the values of T_s', the shear strength of the beam can be found by substituting back into Eq.5.28, thus

$$V_u = \left(T_s' \cdot z + 0.9H_w \cdot Z_w \cdot d\right)/X \quad (5.36)$$

It is noted that the value of ΔT_s (decrease in tension force of the main reinforcement from mid-span to the support) can be determined by assuming that both main and web reinforcement yield, taking moments at A (fig.5.12) and considering all forces from mid-span to the support. Integrating it along the main reinforcement and ΔT_s can be found by solving the equation

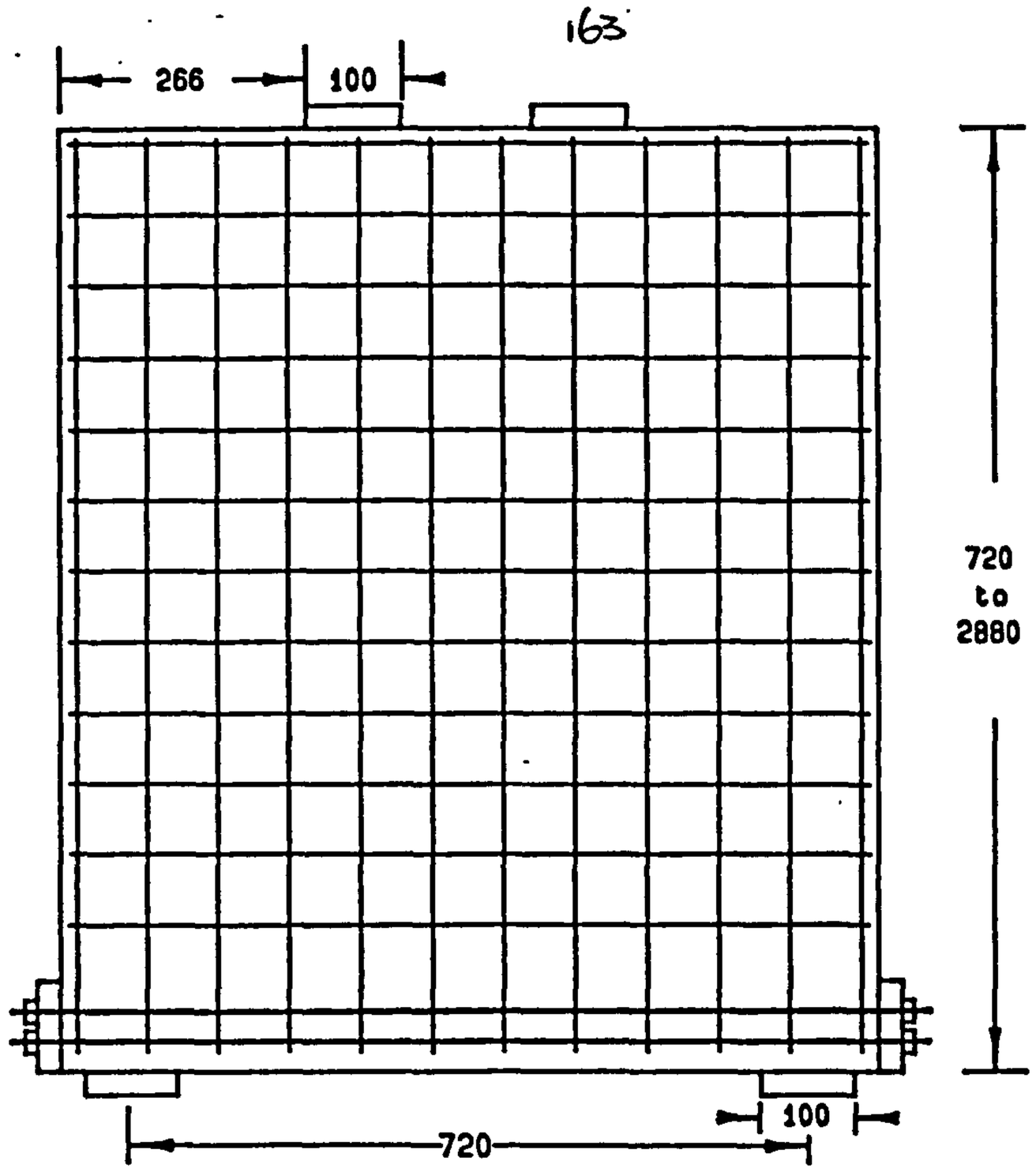

Fig.5.10 Test specimens of Besser (1984).

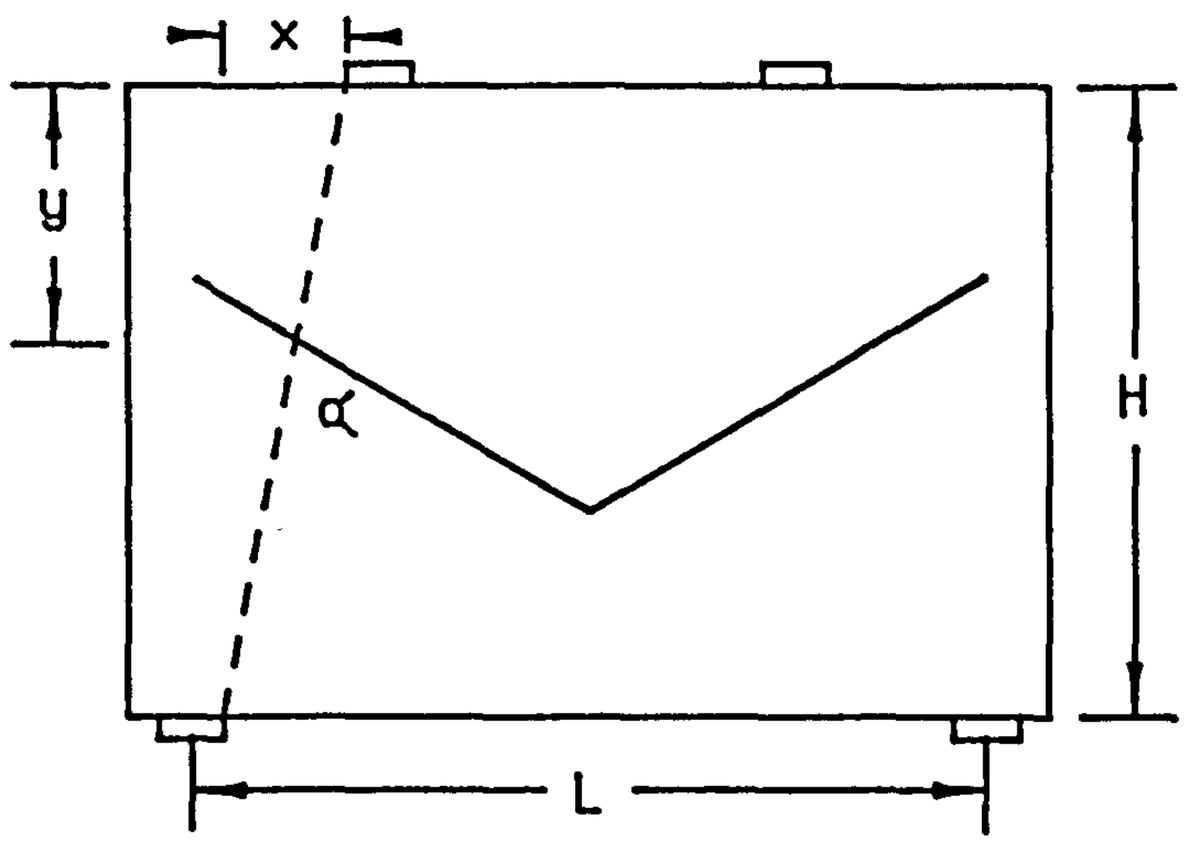

Fig.5.12 Structural model proposed by Kong (1972).

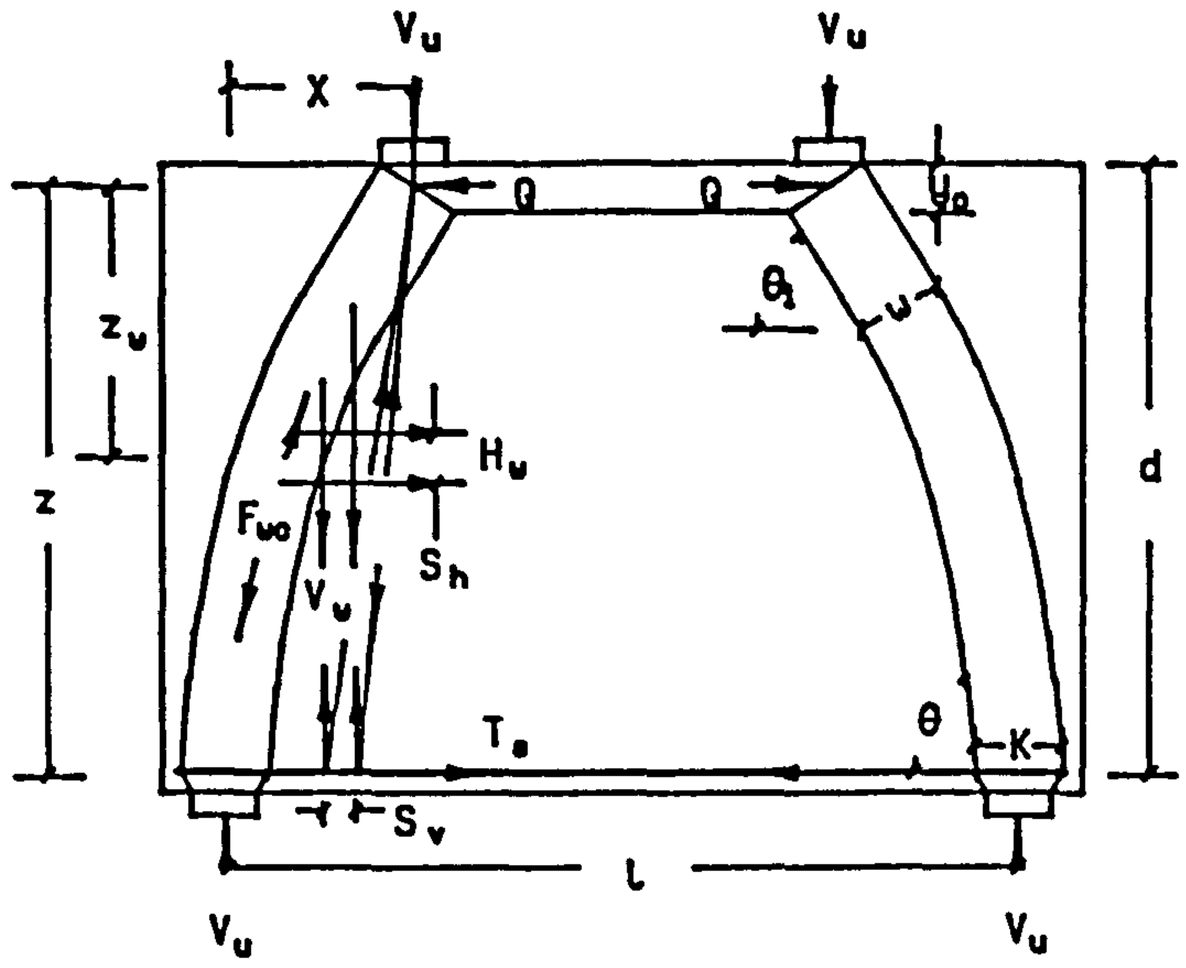

Fig.5.13 Structural model proposed by Al-Najjim (1981).

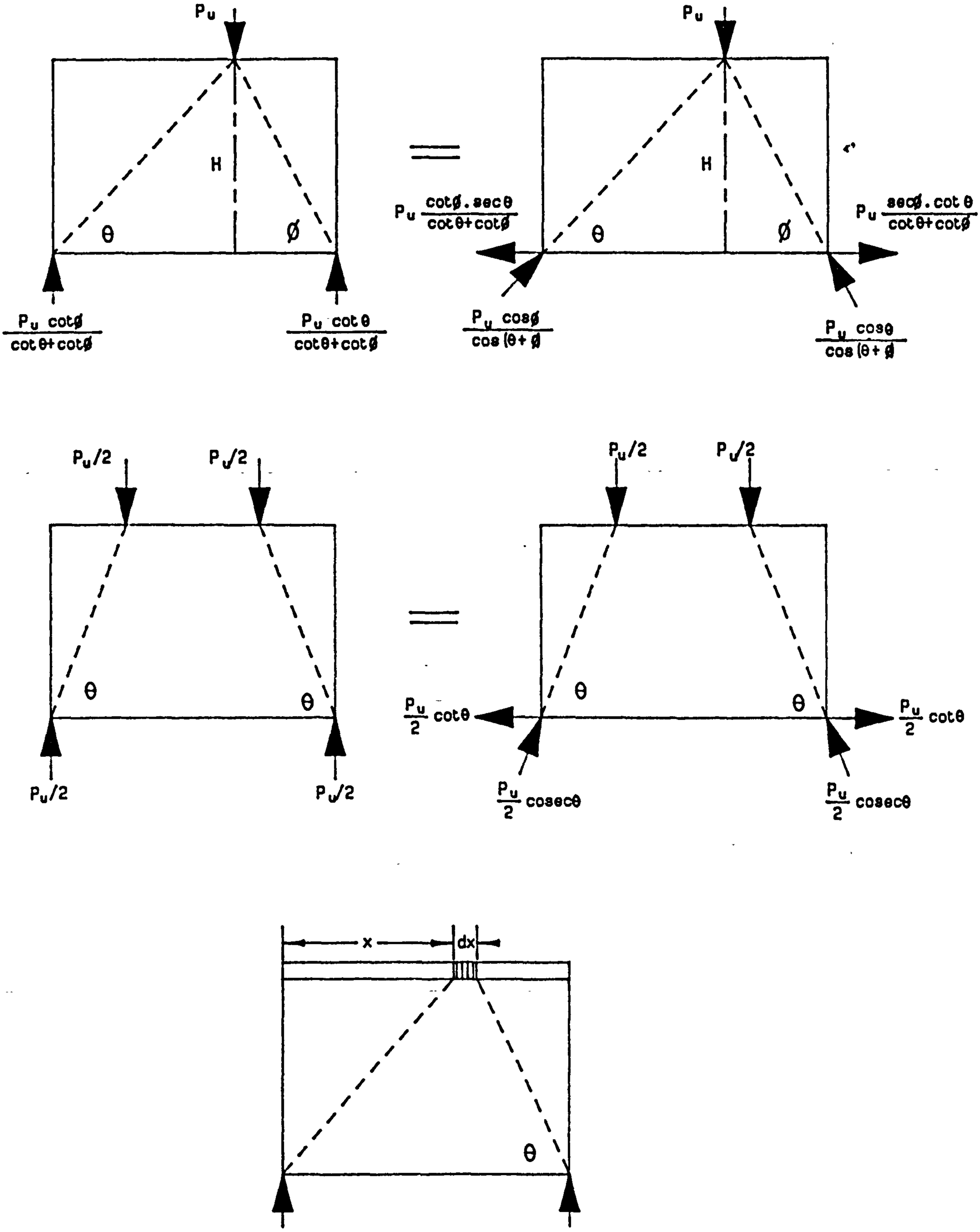

Fig.5.11 Effect of load in deep beam by Ramakrishnan and Ananthanarayana(1968).

below.

$$\Delta T_s^2+\left(2b\cdot d\cdot\beta_2\cdot f_c'-T_s-0.9d\cdot H_w\right)\Delta T_s-b\cdot\beta_2\cdot f_c'\cdot V_w\cdot X^2 = 0 \quad (5.37)$$

5.5 SUMMARY

(1) Early research on deep beams concentrated on finding the distribution of stresses within the structures and falls into three categories (1) Fourier series technique, (2) method of finite differences and (3) photoelastic technique.

(2) With the invention of the computer, the finite element method of analysis has been introduced and virtually replaced all the above mentioned techniques.

(3) The introduction of limit state design and the non-linear behaviour of concrete in the presence of cracks has limited the value of elastic analysis. This has lead to extensive experimental analysis on reinforced concrete deep beams during the past two decades.

(4) Paiva and Siess [69] concluded from their experiments that web reinforcement had no effect on cracking strength of deep beams with large clear span/depth ratios (>3) but increases strength with smaller clear span/depth ratios. Concrete strength increases the shear capacity slightly with low span/depth ratio but flexural strength is

unaffected.

(5) Leonhardt found that tensile stresses in the main reinforcement do not decrease towards the suport as in ordinary slender beams. He also stressed that anchorage of the main reinforcement is very important, any weakening owing to bent-up bars may lead to the failure of the strut and tie system of the beam.

(6) Ramakrishnan and Ananthanaarayana [73] observed four different modes of failure and they were (1) diagonal tension failure, (2) diagonal compression failure, (3) splitting of the compression zone and (4) flexural-shear failure. However, the diagonal tension mode was the most common in their tests and they constructed a failure model able to estimate the ultimate failure load as

$$P_u = 2K \cdot f_t \cdot b \cdot H \qquad (5.12)$$

(7) Kong [39-47] found that the shear strength, deflection and crack widths were dependent on the clear span/depth ratios. He also pointed out that inclined web reinforcement was the most effective form of reinforcement and horizontal web reinforcement was more effective than vertical for low span/depth ratios. Four different modes of failure were reported; (1) splitting along the diagonal crack, (2) crushing of concrete along the diagonal cracks, (3) crushing of concrete in the compression zone and

(4) crushing of concrete in the bearing zone. Based on the experimental data, empirical formula was drawn up for the estimation of ultimate loads for reinforced concrete deep beams.

$$P_u = 2\left[C_1(1-0.35X_c/H)f_t \cdot b \cdot H + C_2\Sigma A_s \cdot y \cdot \sin^2\alpha/H\right] \quad (5.24a)$$

(8) Al-Najjim [63] arrived at the conclusion that inclined and horizontal web reinforcement were more suitable for beams with small clear span/depth ratios. Structural models of the failure mechanism were proposed based on (1) failure of the strut and tie system in which its shear strength can be found by Eq.5.31, and (2) compression failure of the strut where its shear strength can be found by Eq.5.36 after obtained the value of T_s' by Eq.5.35. The predicted ultimate shear strength will be the lesser of those obtained by the above two methods.

(9) Smith and Vantsiottis [77] arrived at conclusions similar to Kong's suggestion. They added that concrete strength can affect the ultimate shear strength of deep beams especially at low clear span/depth ratios.

(10) With the exception of one specimen (L/H=1), which failed by shearing along the diagonal crack, all the others (L/H<1) tested by Besser [12,13] were dominated by crushing of concrete above the supports. Buckling of the specimen was only observed with specimen having L/H=0.25

and height to thickness ratio equal to 40.

(11) Recommendations for the design of reinforced concretre deep beams by Portland Cement Association [72] were based on elastic analysis. They involved the estimation of the amount of tensile steel required with the help of design charts and limited the shear stress by Eq.5.3.

$$v = 8V/7b\cdot d < (1+5H/L)v_c/3 \qquad (5.3)$$

(12) CEB-FIP recommended that the area of main reinforcement should be calculated from the largest bending moment in the span with lever arm, z defined by Eq.5.18. Shear is controlled by orthogonal web reinforcement with cross-sectional area equal to $0.0025b\cdot s$ and $0.002b\cdot s$ for plain and deformed bars respectively.

(13) ACI Code limited the maximum shear stress by Eq.5.21 and evaluated the shear stress taken up by concrete to be calculated by Eq.5.22. The contribution of shear by reinforcement can be obtained by Eq.5.23.

(14) CIRIA Guide is the most comprehensive set of rules for the design of deep beams. The area of main reinforcement can be calculated by

$$A_s = M/0.87f_y\cdot z$$

where z is the lever arm and is given by Eq.5.26. Shear force is limited by Eq.5.27 and bearing and bearing stress is not recommended to exceed $0.4f'_c$.

6 EXPERIMENTAL INVESTIGATION OF THE SHEAR STRENGTH OF REINFORCED CONCRETE DEEP BEAM

6.1 INTRODUCTION

In order to cater for large spans in buildings, new structural systems consisting of frames and deep beams have evolved. Because of their proportions in depth and span, the strength of deep beams is usually controlled by shear, rather than flexure, provided that normal amounts of longitudinal reinforcement are used. On the other hand, the deep beam's shear strength is significantly greater than that predicted using the expression for slender beams, because of its special capacity to redistribute internal force before failure.

Investigation has been made of the shear strength of deep beams with different span/depth ratios (0.7 to 1.1) with a uniformly distributed load on top. In particular, for beams with low span/depth ratios, bearing failure usually takes place around the supports. Special forms of reinforcement (chapter 3) are put into this region to prevent it from failing in this mode.

6.2 DESCRIPTION OF TEST SPECIMENS

The test specimens consisted of 6 beams with different

spans varying from 700 to 1100 mm. All had the same dimensions 1260 x 1000 x 100 mm except for a step of 5 mm which varied in length according to the span of the beam (fig.6.1), leaving a central section over which uniformly distributed load was to be applied.

All beams were reinforced with a similar amount of steel. Main longitudinal reinforcement consisted of 8 plain mild steel bars with 10 mm nominal diameter. This reinforcement was placed in 4 layers, consisting of 4 closed stirrups, at 50 mm spacing. The web reinforcement was provided by an orthogonal arrangement of bars on both faces of the beam. They were 6 mm diameter plain mild steel bars, with 100 mm centre to centre spacing. Vertical reinforcement above each support was four plain mild steel stirrups, 6 mm in diameter at 66.7 mm spacing. Beams DB2 to DB6 had additional stirrups in the bearing zone above the supports of the beams so as to resist bearing stresses. They were plain mild steel bars, 6 mm nominal diameter and were placed alternatively around the horizontal reinforcement (fig.6.1). In order to avoid the anchorage problems, particularly for main reinforcement, all stirrups were welded to form a closed link.

6.3 MATERIAL AND MIX DETAIL

Basically similar materials were used as for the bearing

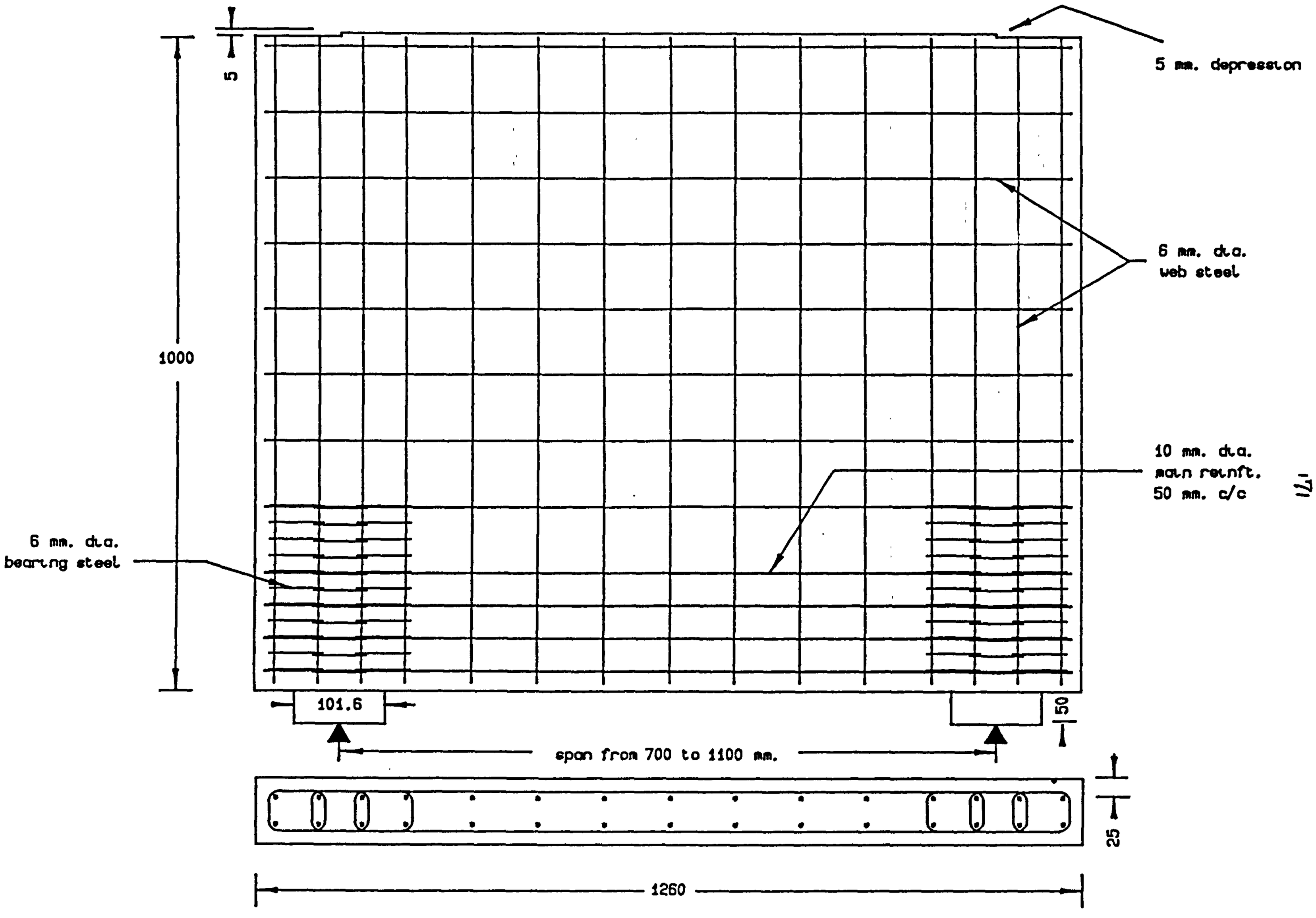

Fig.6.1 Geometric shape & reinforcement detail of test beams DB1 to DB6.

capacity blocks. Ordinary Portland cement confirming to British Specification was used throughout. Coarse aggregate was North Notts quartzite gravel with maximum size of 10 mm, 'irregular' shape and 'smooth' surface texture as classified by BS 812. Air-dried sand from the same quarry as the coarse aggregate was used and it was classified as zone 3 according to BS 882. The grading curves for the fine and coarse aggregatea are shown in fig.3.2.

Reinforcement was plain round mild steel bars and a typical stress-strain curve and strength properties are shown in fig.3.3.

The concrete mix used was identical for all the six specimens, in order to obtain similar strengths of concrete. The mix proportions by weight were 1 : 1.96 : 2.83, with a water/cement ratio of 0.54. It was designed to give a more workable mix so that concrete can get through the congested steel in the bearing zone. Workability tests gave average values of 120 mm slump, V-B time less than 1 sec. and compacting factor of 0.95.

6.4 CASTING AND CURING

The reinforcing cage was prepared as shown in fig.6.1 and 6.2, placed in position on the mould and adjusted to give the designed cover for the reinforcement. An oiled steel mould

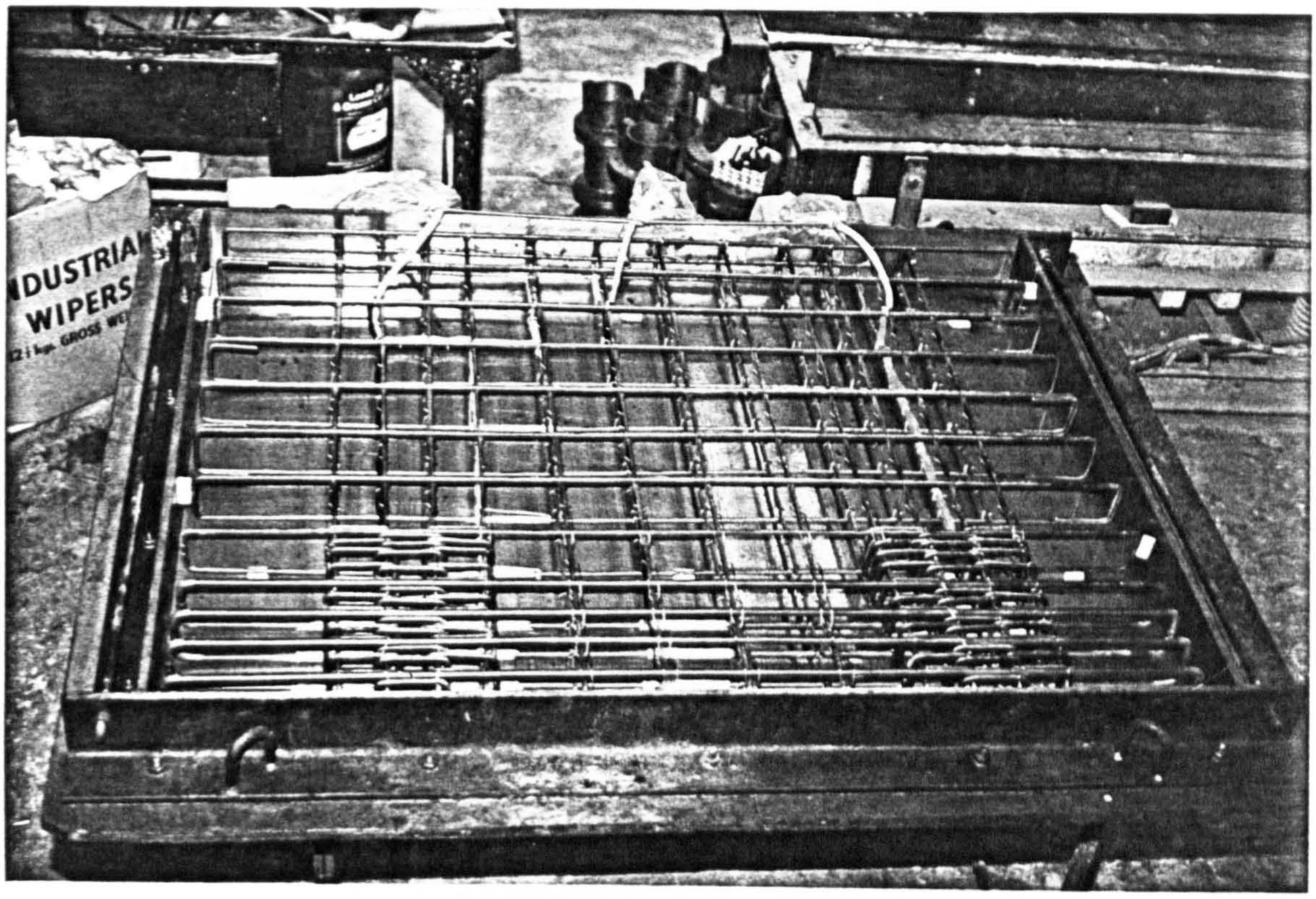

Fig.6.2 Typical cage reinforcement for deep beams.

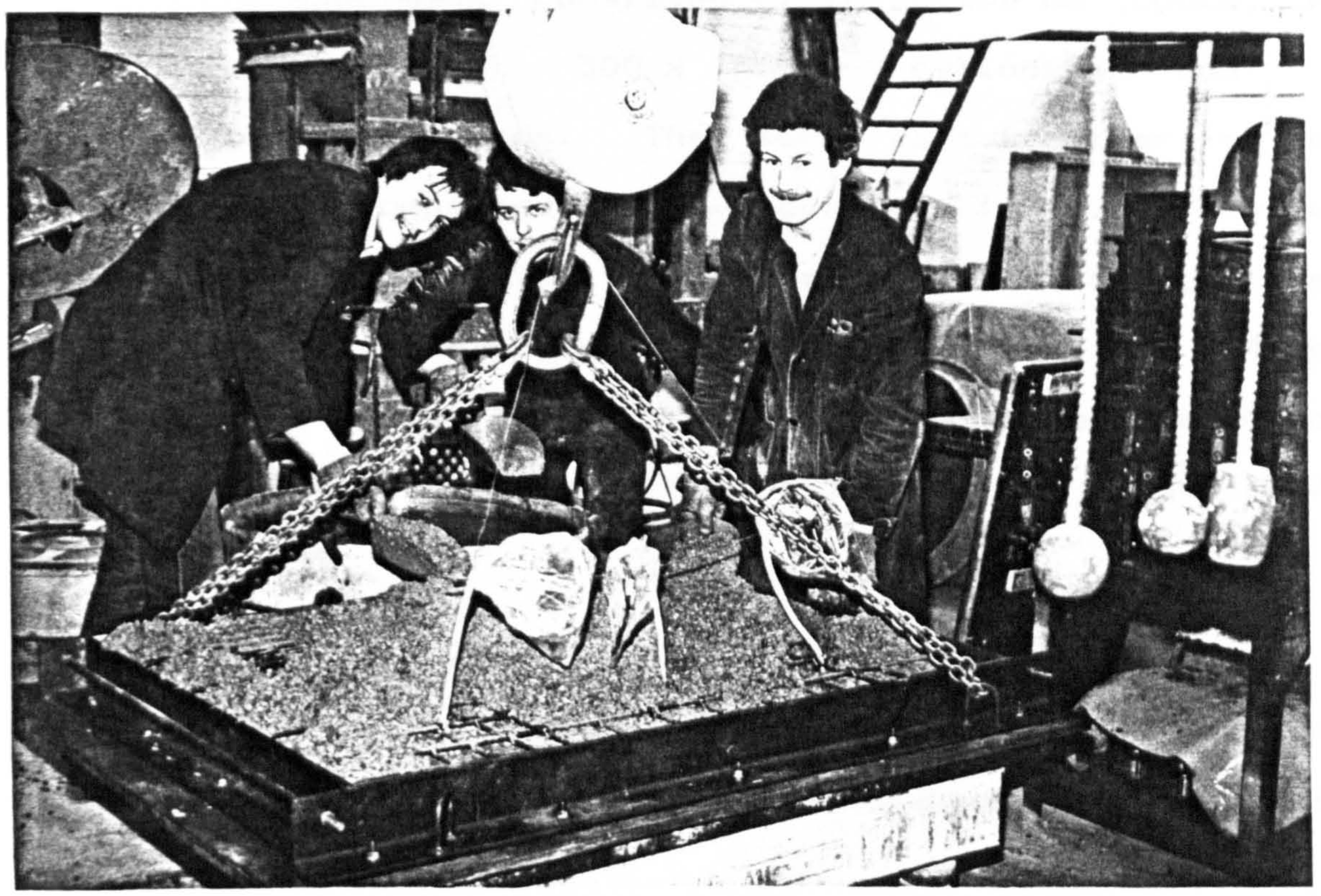

Fig.6.3 Deep beams cast horizontally on a vibration table.

1260 x 1000 x 100 was used throughout. The depressions of 5 mm on each side of the beam were provided by attaching a 5 mm thick plastic strip on the mould. In order to avoid the variation of strength of concrete with height of the specimen [63], all the test specimens were cast horizontally (fig.6.3).

For each mix, all the constituent materials were weighed in the required proportions before being fed into a mixer of 350 kN dry weight capacity. The materials were turned over for about 15 secs. before the addition of the required quantity of water. The materials were mixed for 3 minutes in order to ensure a unform workable mix. It was then poured into the mould and compacted in two layers on a vibrating table.

Control specimens consisted of three 100 mm cubes, three 150 mm cubes, eight 300 x 150 mm cylinders and two 100 x 100 x 500 mm prisms. They were cast together for each mix and also compacted on a vibrating table. They were stripped from the moulds and placed in the curing room at 20 degs. C., relatively humidity of 95-100 percent, 24 hours after casting. The test specimens were covered with damp hessian for 3 days, watered constantly and then transferred to the curing room.

Compressive strengths were obtained by three 100 and 150 mm cubes and four 100 x 150 mm cylinders. Tensile strength was assessed from four 100 x 150 mm cylinders by the splitting

cylinder test and from one 100 x 100 x 500 mm prism by the modulus of rupture test. The remaining prism was used to obtain the Young's Modulus and Poisson's ratio of the concrete. Similar procedures were applied for casting and curing of the tests and control specimens so as to have a better indication of the strength of concrete in the test specimen. The control tests were made at the time when relevant beams were tested and were according to BS 1881. The properties of each specimen are listed in table 6.1.

6.5 INSTRUMENTS AND TEST PROCEDURE

Strains on the surface of the concrete were measured by Demec gauges with 100 mm gauge length except near the edge where space is not available for a 100 mm gauge length, a 50 mm Demec gauge was used. Strains were measured on twelve particular sections of the beam (fig.6.4). Section 1 was a vertical section along the centre line of the support, and measurements were made at the level of the reinforcement both vertically and horizontally so as to obtain the vertical and horizontal strains. Sections 2 and 3 were vertical sections similar to section 1 except that they were 200 mm from section 1 and of the centre of the beam respectively. Sections 4 and 5 were horizontal sections 20 mm below the top and 10 mm above the bottom of the beam respectively. They were chosen to measure the horizontal strains at the top and bottom

Spec. no.	Span (mm.)	Span/depth ratio	Compressive $f_{cu(100)}$ N/mm^2	Compressive $f_{cu(150)}$ N/mm^2	Compressive f_c N/mm^2	Tensile f_t(cyl.) N/mm^2	Tensile f_t(pri.) N/mm^2	Young's Modulus kN/mm^2	Posson ratio ν	P_u kN
Present investigation										
DB1	1000	1.0	67.5	62.7	46.9	3.57	4.06	34.2	0.149	1415
DB2	1100	1.1	70.1	58.8	45.4	3.36	3.98	31.3	0.150	1400
DB3	1000	1.0	74.6	66.2	50.9	3.57	4.06	34.9	0.169	1700
DB4	900	0.9	69.9	59.4	50.2	4.03	4.53	34.9	0.175	1960
DB5	800	0.8	71.4	62.8	47.5	3.82	4.24	35.4	0.173	1975
DB6	700	0.7	68.1	65.6	49.8	3.77	5.62	32.5	0.158	1980

Notes: For all the specimens, a = 1260mm, b = 100mm, h = 1000mm.

Table 6.1 Concrete propreties of the test beams (DB1-DB6).

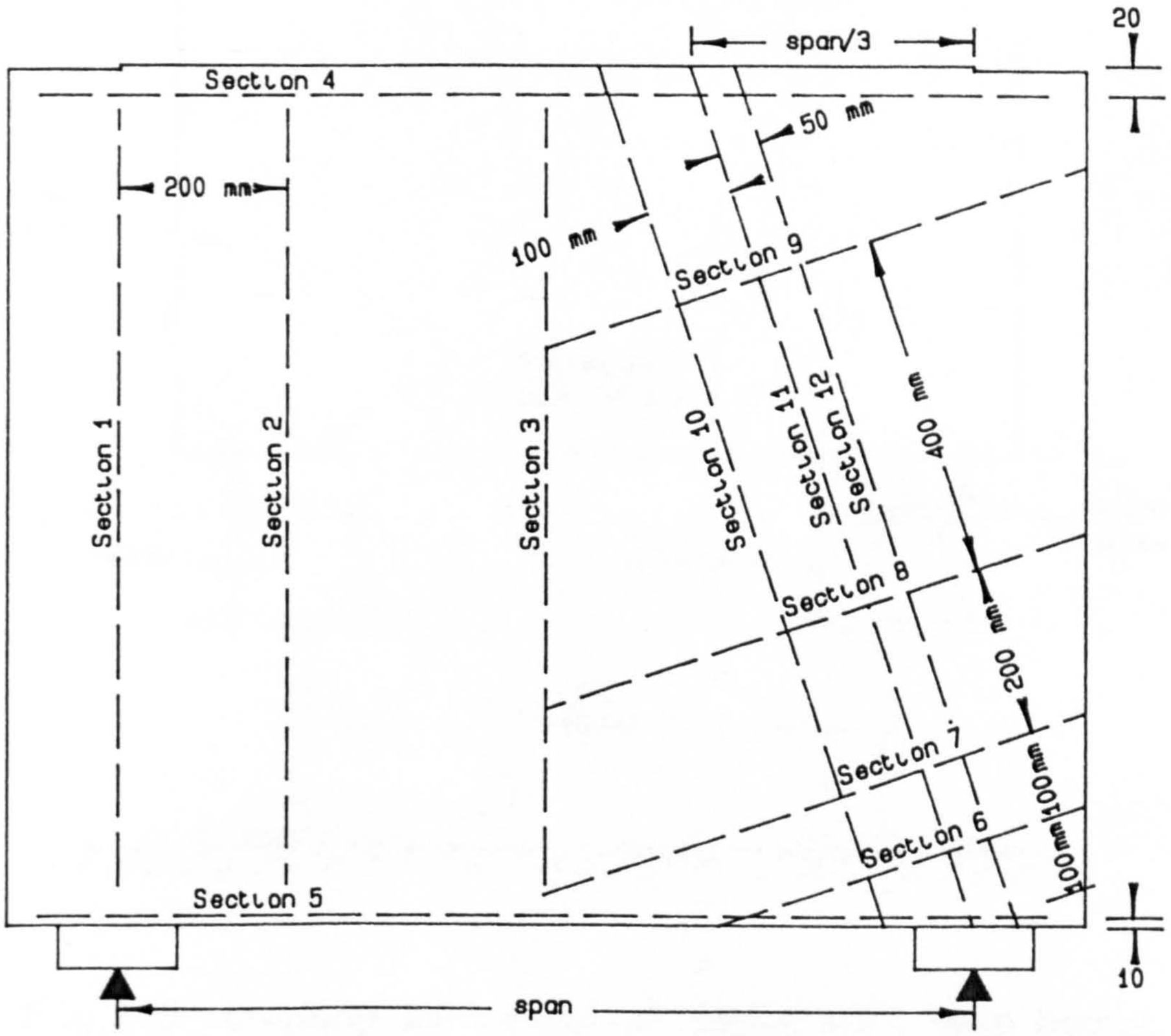

Fig.6.4 Sections on the surface of the beam where strains were measured.

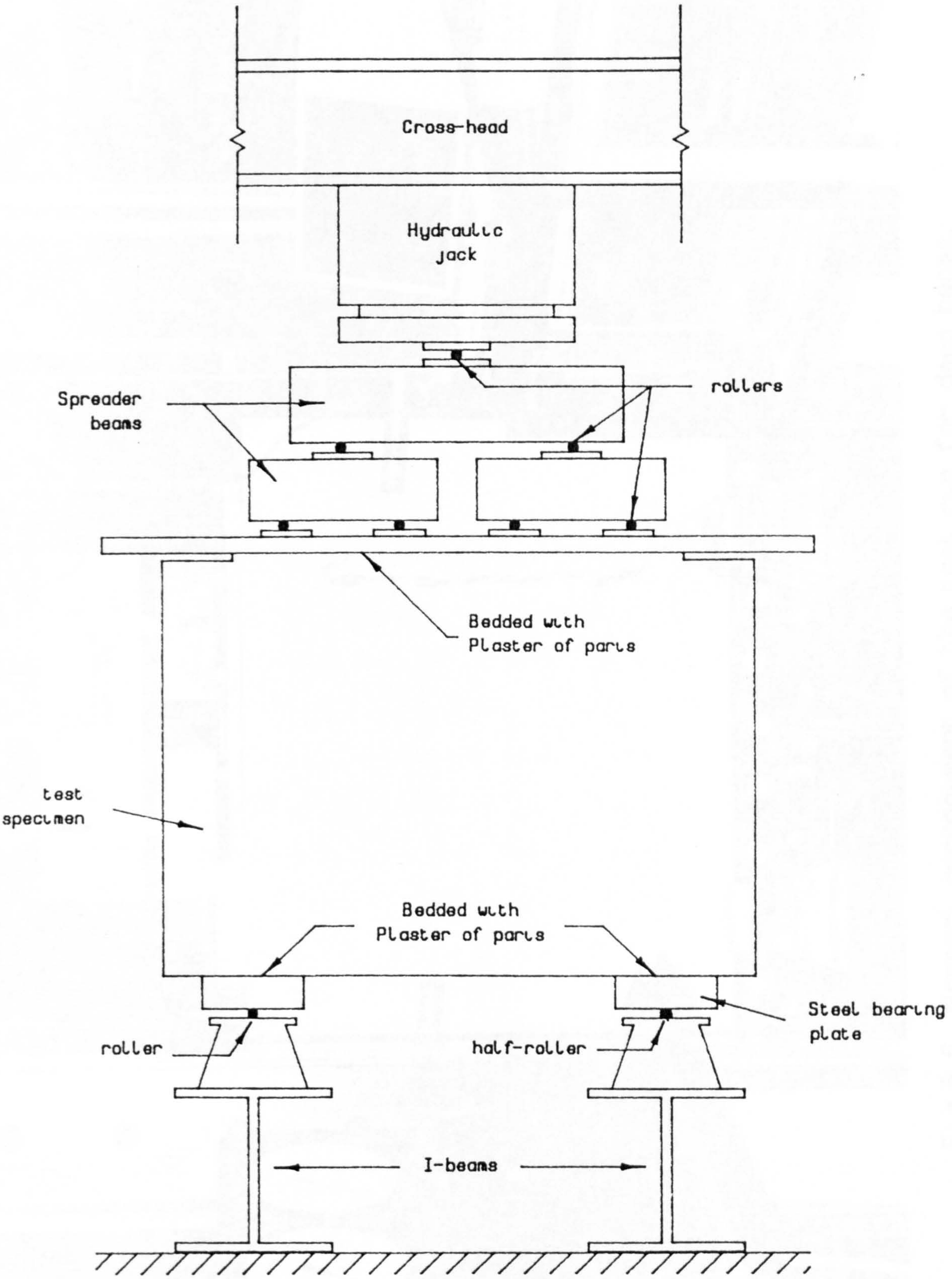

Fig.6.5 Loading mechanism of tests with deep beams.

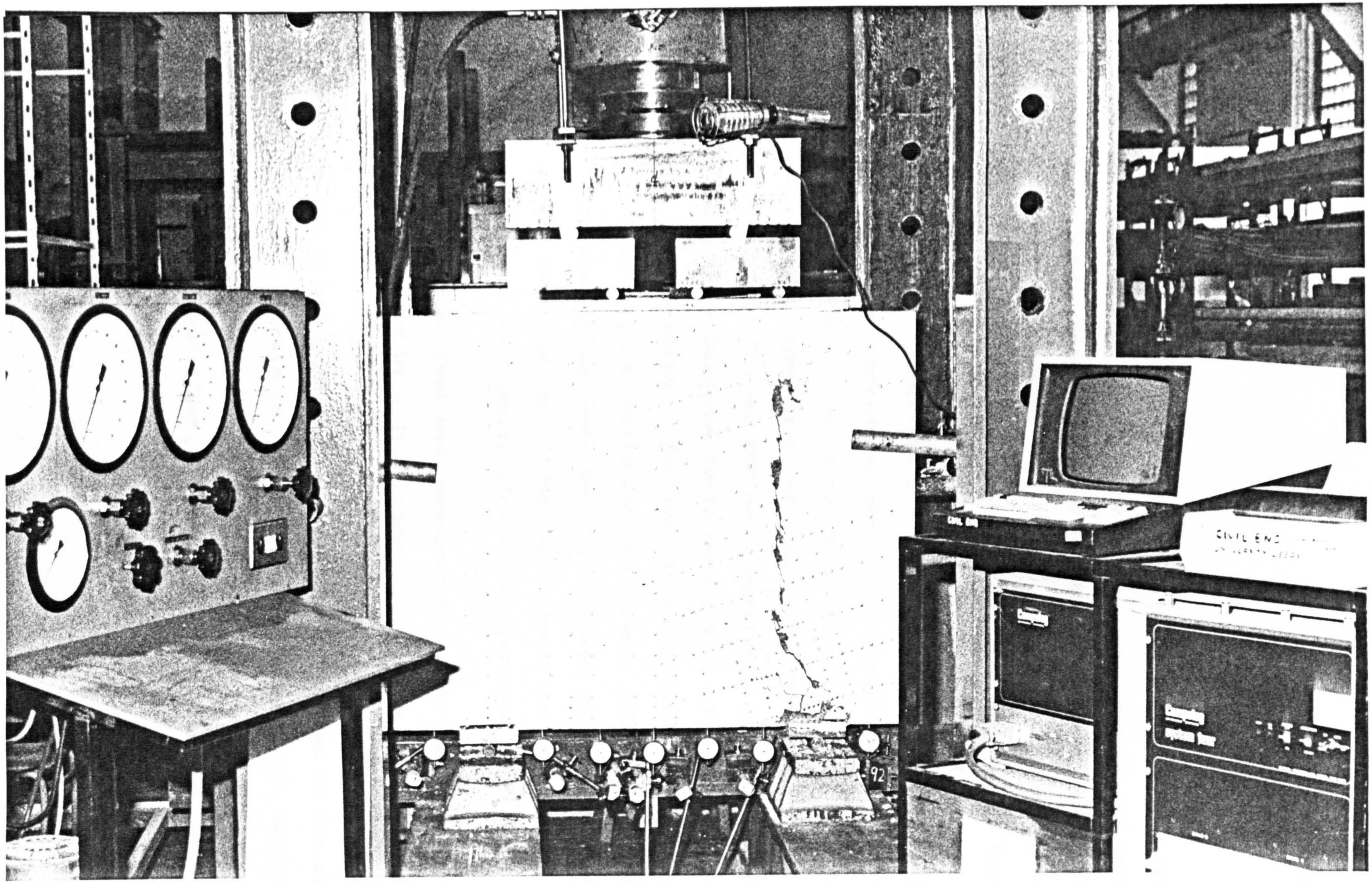

Fig.6.6 General arrangement of the test rig for deep beams.

of the specimens.

It was pointed out by Ramakrishnan [73] and Al-Nijjam [63] that failures of deep beams were in fact failures of the strut and tie system. Ramkrishnan had suggested that for uniformly distributed loaded beams, the strut lies on the line between the support and a third span point on the top of the beam. Strain measurements on sections 6-12 were specially designed to investigate this. Sections 6-9 were perpendicular to the direction of this compressive strut and strains were measured along the direction of the strut so as to give an idea of the distribution of compressive strain. Sections 6, 7, 8 and 9 were at 100, 200, 400 and 800 mm respectively from the centre of the support. Sections 10-12 were lying parallel to the direction of the strut. Section 11 was passed through the centre of the support while section 10 was 100 mm inside and section 12 was 50 mm outside the centre of the support. Strains were measured both along and across the strut so as to give compressive and tensile strains at different positions.

Strain of the steel was measured by electrical resistance gauges and recorded by a data-logger. Strain in the main steel was measured in three positions; along the centre line, along the centre of the compressive strut and at the end of the main reinforcement. Strain in the web reinforcement was measured along the centre-line of the compressive strut. For those beams with bearing steel, strain was also measured at the

appropriate positions. Detailed positions of the strain measurements are shown individually in chapter 7.

When a specimen was ready for test, it was taken out from the curing room together with the control specimens. A thin coat of white emulsion was applied. Demec points were fixed into positions. The specimen was then carefully placed on to the testing rig. Two bearing plates, each 140 x 100 x 50 mm, were placed in an appropriate position to give the correct span of the beam. A roller and a half roller were put underneath the bearing plates and they were supported by two I-section beams placed on the floor. A spreader beam was put on the top of the specimen to obtain an uniformly distributed load. In order to have a better contact between steel and concrete, plaster of paris was applied on the surfaces between the spreader beam and the specimen and on the two bearing plates and concrete. The mechanism of loading is shown in figs.6.5-6.

The beam was then checked for position, vertically verified and dial gauges were placed and adjusted both under the base and at the back of the beam for measuring deflection and horizontal movement respectively. After taking the initial readings of all the gauges, load was applied in constant increments of 100 kN. At each stage of loading, gauge readings were recorded, cracks were marked on the surface and the load at which it was observed was noted at the end of the crack. The widths of the cracks were measured by a hand microscope

with a magnification of 40 and graduation in the eyepiece scale of the microscope corresponded to a crack width of 0.02 mm. This procedure was repeated until the specimen failed, it was then removed from the test rig and photographed to record the final crack pattern. The control specimens were tested on the same day.

6.6 BEHAVIOUR DURING TESTS

The appearance of the test specimens and their crack patterns after failure are shown in figs.6.7-12. The numbers shown at the ends of the cracks should be multiplied by 10 in order to obtain the load in kN. Fig.6.13 shows the development of crack width with load for three types of crack; flexural, shear and bearing.

In beam DB1, fig.6.7, the first crack to appear was a flexural crack around the middle bottom section of the beam at 400 kN. As load increased to 500 kN, more flexural cracks were observed in the bottom of the beam. They extended upwards, to a height of 500 mm above the bottom edge of the specimen, and cracks widened gradually as load was increased. Cracks in the middle of the beam extended more quickly than those near the supports. At 900 kN, a diagonal crack was observed above the right hand support extending at an angle of 68 degs. which agrees well with the direction of the imaginary compressive

strut with the horizontal. It extended its length and widened rapidly, finally coming to a point 200 mm below the top of the specimen at 1300 kN. At 1000 kN, a similar diagonal crack was formed above the left hand support. As load was further increased to 1300 kN, vertical cracks (bearing cracks) were formed above the two supports. Their length extended slowly but the crack width increased even more rapidly than the diagonal cracks. Finally, failure of the beam took place as the vertical cracks widened so much that pieces of concrete fell away from the right hand support which could not substain more load. The beam failed with an audible report and this was considered as a bearing failure.

Beam DB2 behaved similarly to DB1 in the first stages of loading. A flexural crack formed at around 500 kN at the bottom of the beam and extended to 550 mm above the bottom of the specimen. At 900 kN, a vertical bearing crack was found at the right hand support and this increased its width vigorously as shown in fig.6.13. Shear cracking was found at 1000 kN. This formed at the end of a flexural crack near the support and began to extend its length at an angle of 70 degs., which is again in the direction of the predicted compressive strut, and stopped when it reached a height of 600 mm above the support.

In the presence of bearing steel, less vertical cracks were found above the support, as shown in fig.6.8. However, the support in this specimen was too near to the edge of the beam and bearing cracks near the edge were uncontrolled. These

bearing cracks were widening so quickly that at 1400 kN, the bearing zone is totally distorted and affecting the stability of the beam. Beam DB2 had not actually failed but it slid off the testing rig and test was abandoned.

Beam DB3 was identical to DB1 except that reinforcement was added in beam DB3 near the support in the bearing zone. It behaved rather similarly to DB1 with the formation of flexural cracks at 400 kN. Again, these extended upward to a height of 700 mm above the bottom edge of the specimen and widened gradually as the load was increased. The formation of flexural and shear cracks was observed at loads of 400 kN and 900 kN respectively, as in beam DB1. The shear cracking was inclined at an angle of 70 degs. with the horizontal and agreed well with the direction of the predicted compressive strut by Ramakrishnan [73]. It extended almost to the full height of the specimen. However, the behaviour of the bearing cracks was the major difference between DB1 and DB3, (fig.6.9). Beam DB3 had more controlled bearing cracks. They occurred at more or less the same load as in beam DB1 but crack widths remained approximately constant (0.04 mm) in beam DB3 whereas extensive widening up to 0.27 mm at 1300kN took place in beam DB1 (fig.6.13). Moreover, the bearing cracks in beam DB3 remained short and concentrated in the region of 100 mm above the support while those in beam DB1 were more widely spread to 200 mm above the support. This shows the effectiveness of the form of bearing steel used. With this reinforcement, the

bearing zone above the support was held as one unit and beam DB3 was prevented from failing in bearing, (fig.6.9b). Loads could then be increased beyond 1415 kN and finally, failure of this specimen was by shearing of the concrete along the crack in the centre of the compressive strut, with the buckling of vertical steel above the support, together with the dowel failure of main reinforcement at 1700 kN.

Despite differences in span, beams DB4, DB5 and DB6 behaved very similarly to each other. In general, the first crack which appeared was a flexural crack in the bottom middle section of the beam at around 500 to 600 kN. The length and width of these flexural cracks decreased with the span of the beam, (fig.6.10-13). Shear cracks appeared at 700 to 1000 kN and they were inclined approximately in the direction of the suggested inclined compressive strut, rising to a height of 900 mm above the bottom of the specimen. As load was increased, the crack width increased gradually. Around 1200 to 1600 kN, bearing cracks emerged but crack widths did not increase with load and remained at 0.02 mm until the beam failed. At later stages of the test, around 1800 to 1900 kN, a new vertical crack was formed. This was vertically above the inner edge of the support, originating at a height 600 mm above the support and extending in both directions until the beams failed by vertically shearing of the two concrete blocks on either side of the crack, as shown in fig.6.10-12. Beams DB4, DB5 and DB6 failed with similar loads of 1960, 1975 and 1980 kN

respectively. With the exception of beams DB1 and DB2, all specimens failed quite gently with a reasonably audible report.

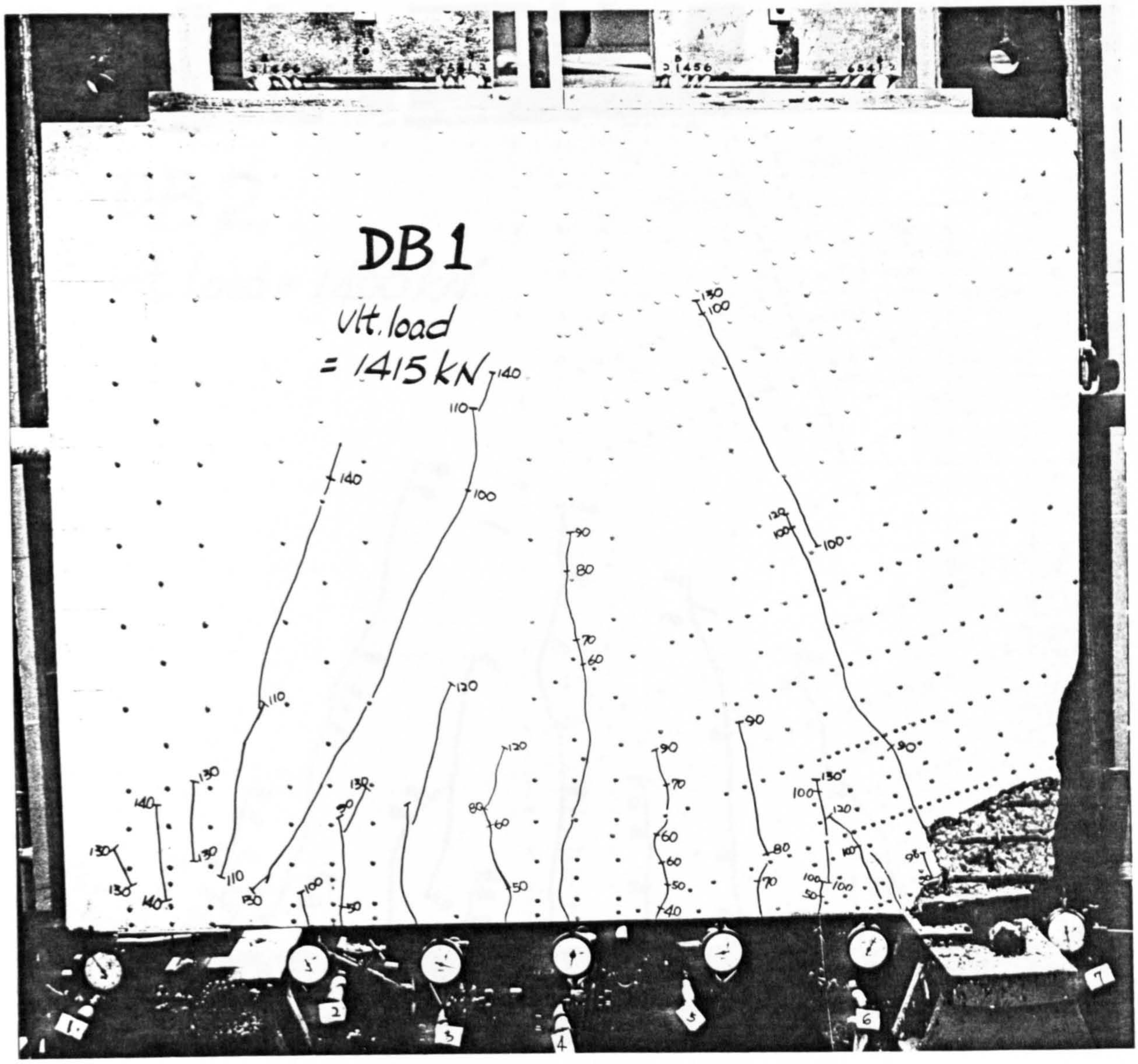

Fig.6.7 Crack pattern of beam DB1.

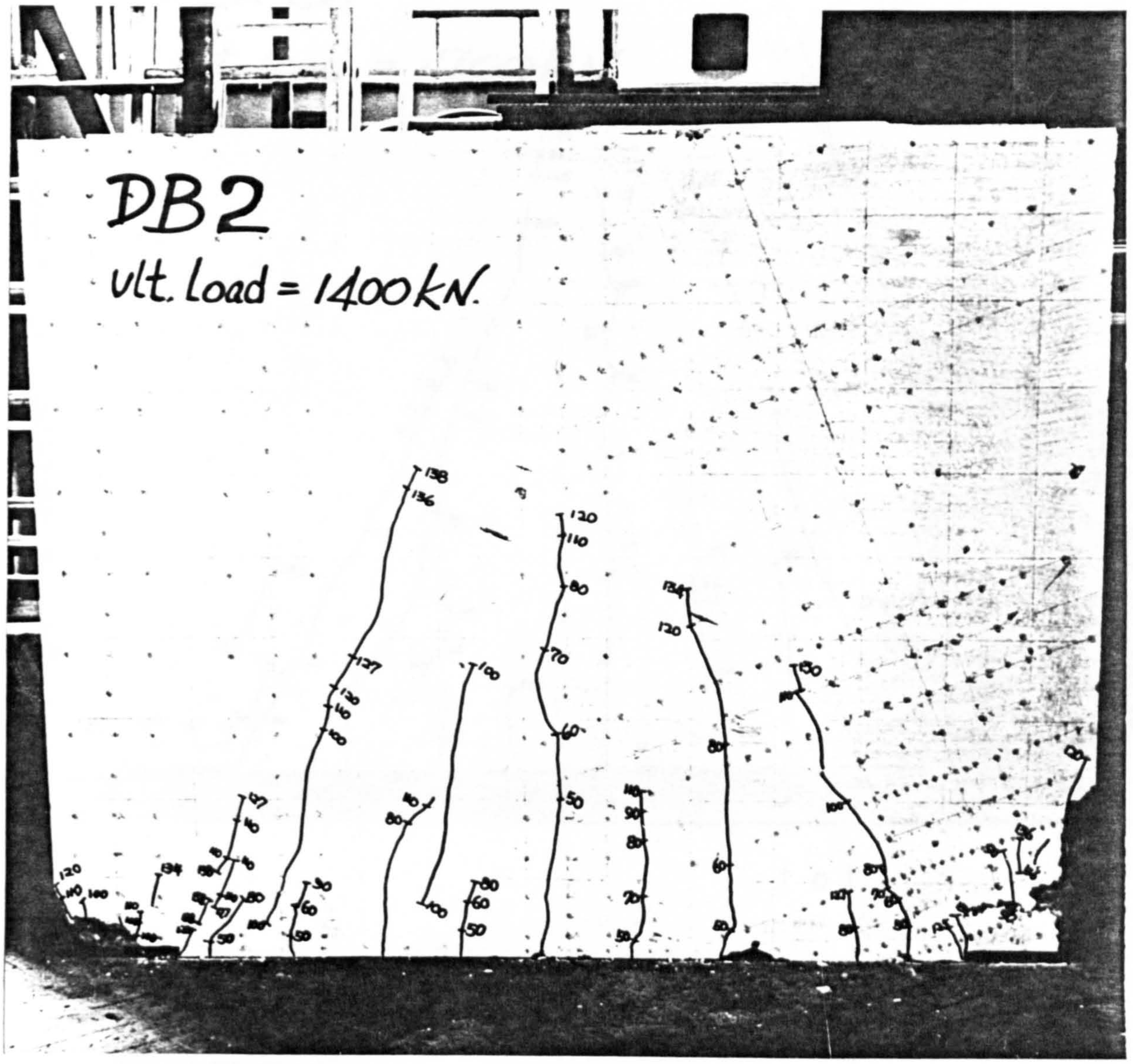

Fig.6.8 Crack pattern of beam DB2.

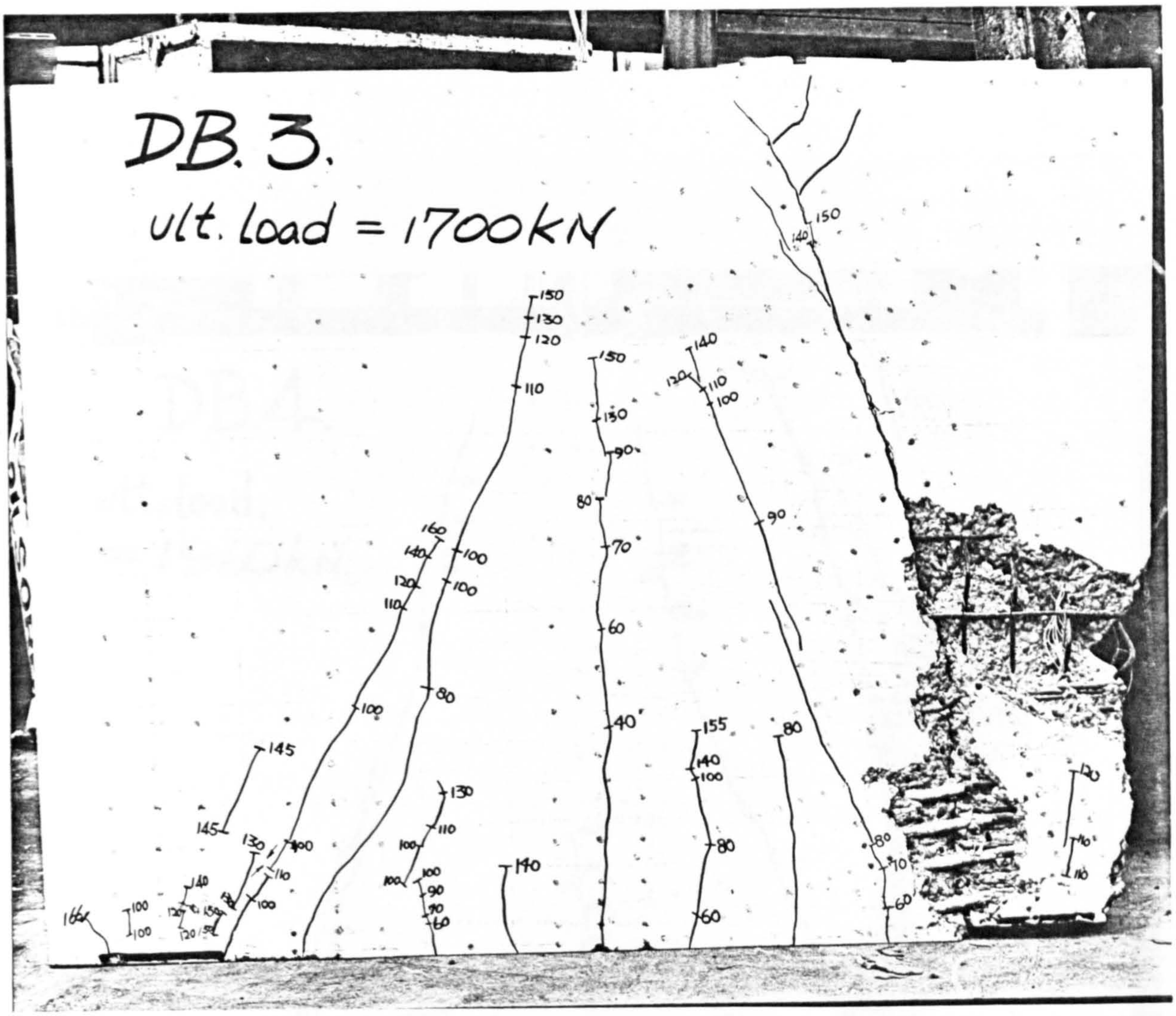

(a)

(b)

Fig.6.9 Crack pattern of beam DB3.

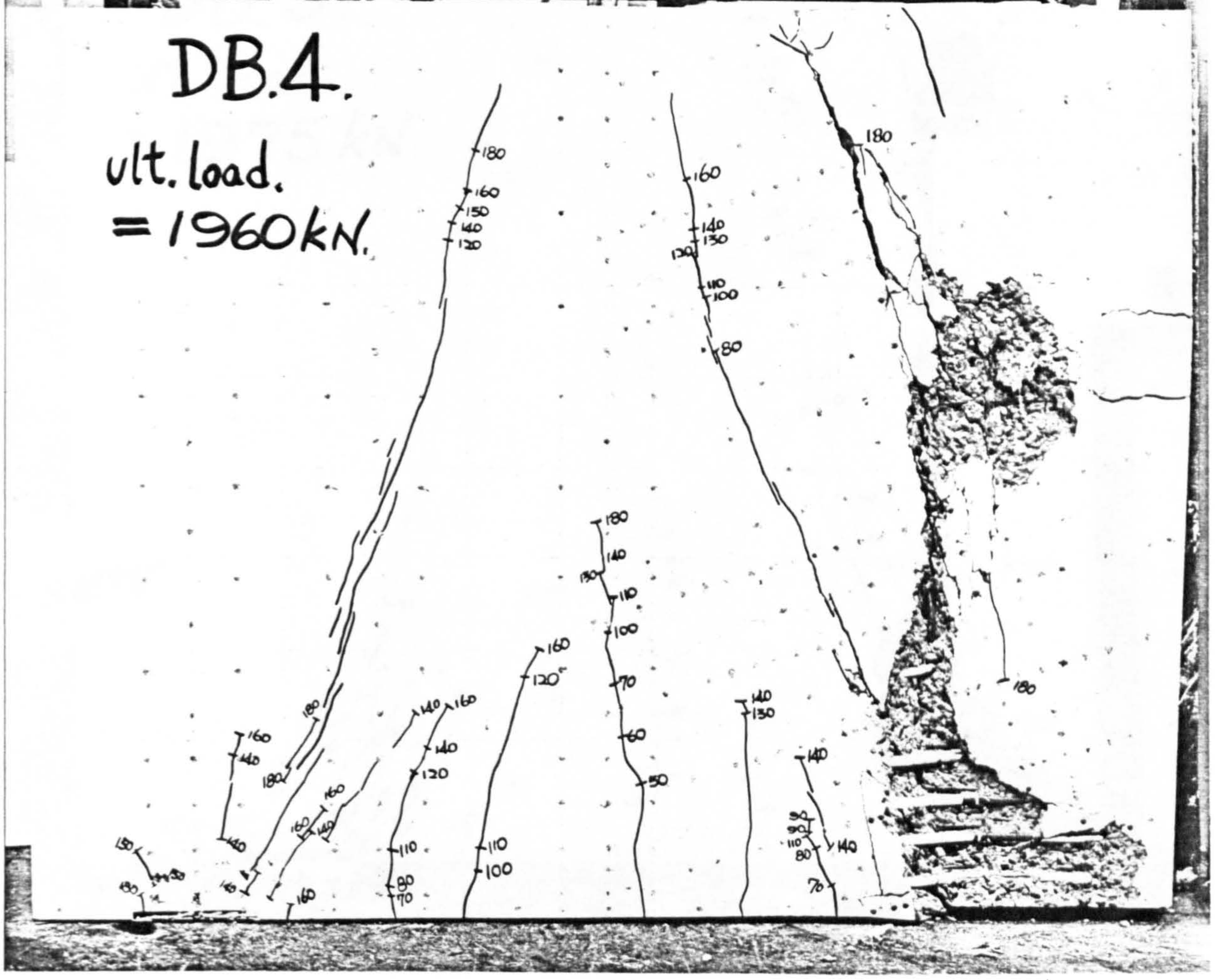

Fig.6.10 Crack pattern of beam DB4.

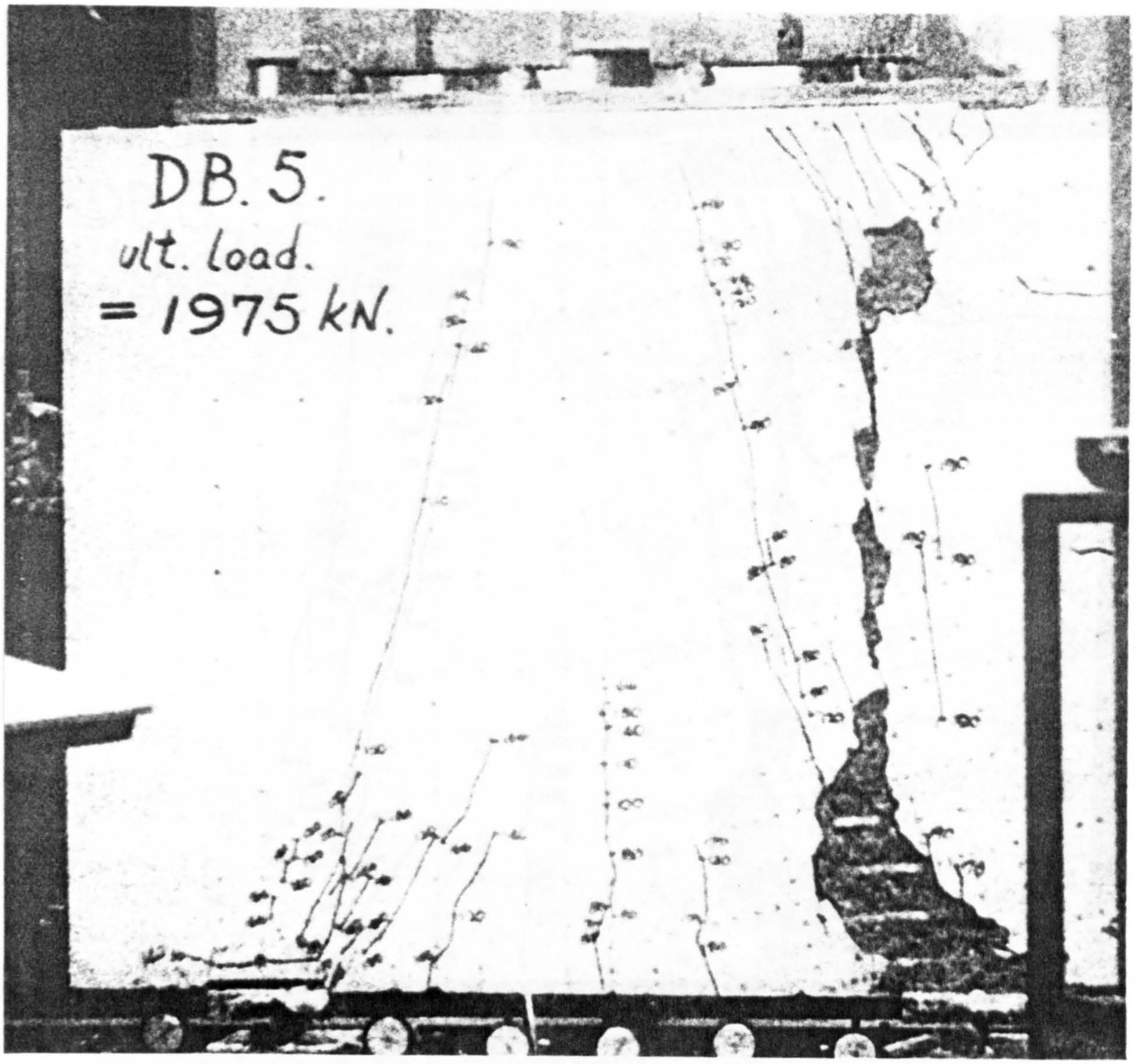

Fig.6.11 Crack pattern of beam DB5.

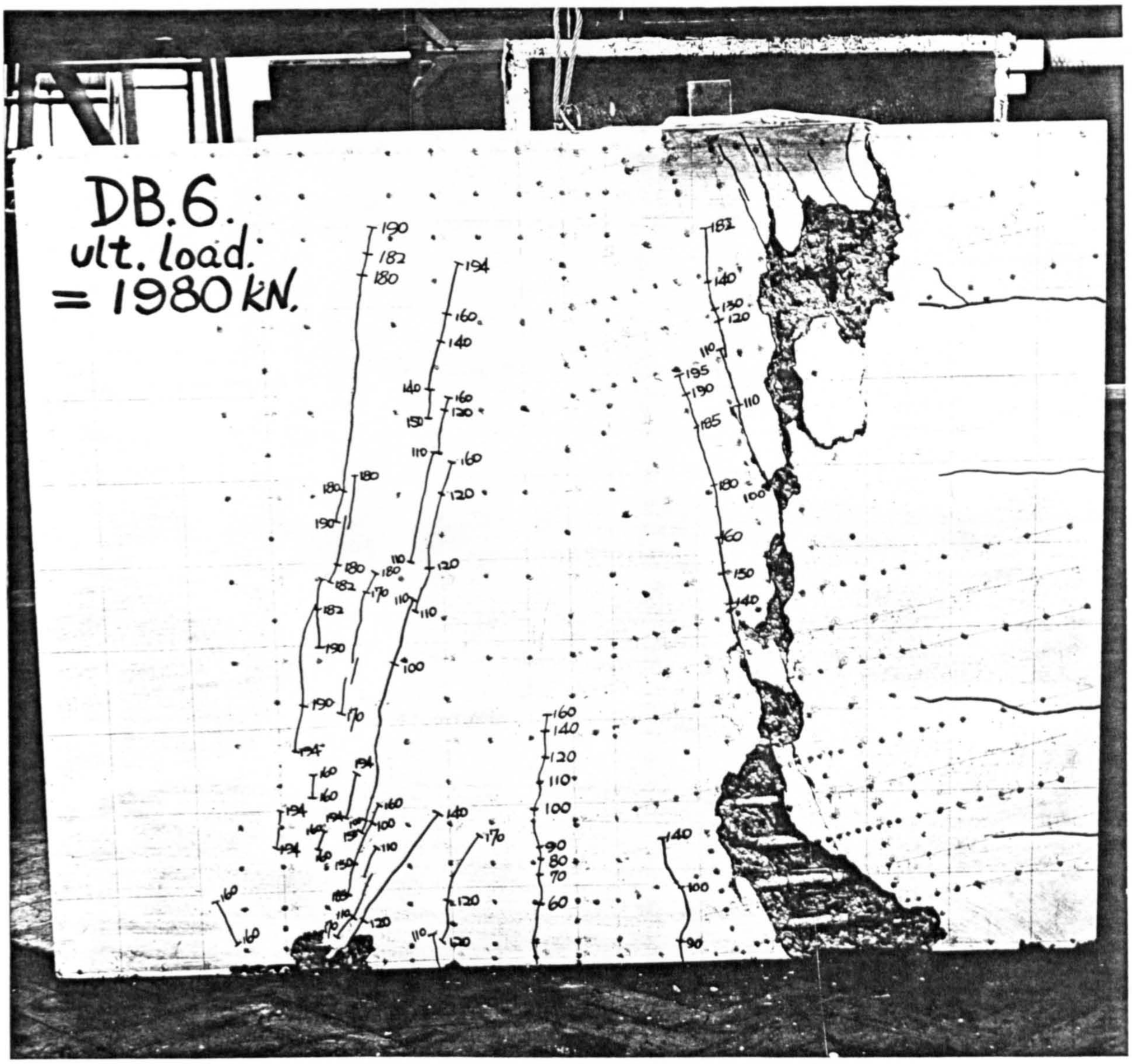

Fig.6.12 Crack pattern of beam DB6.

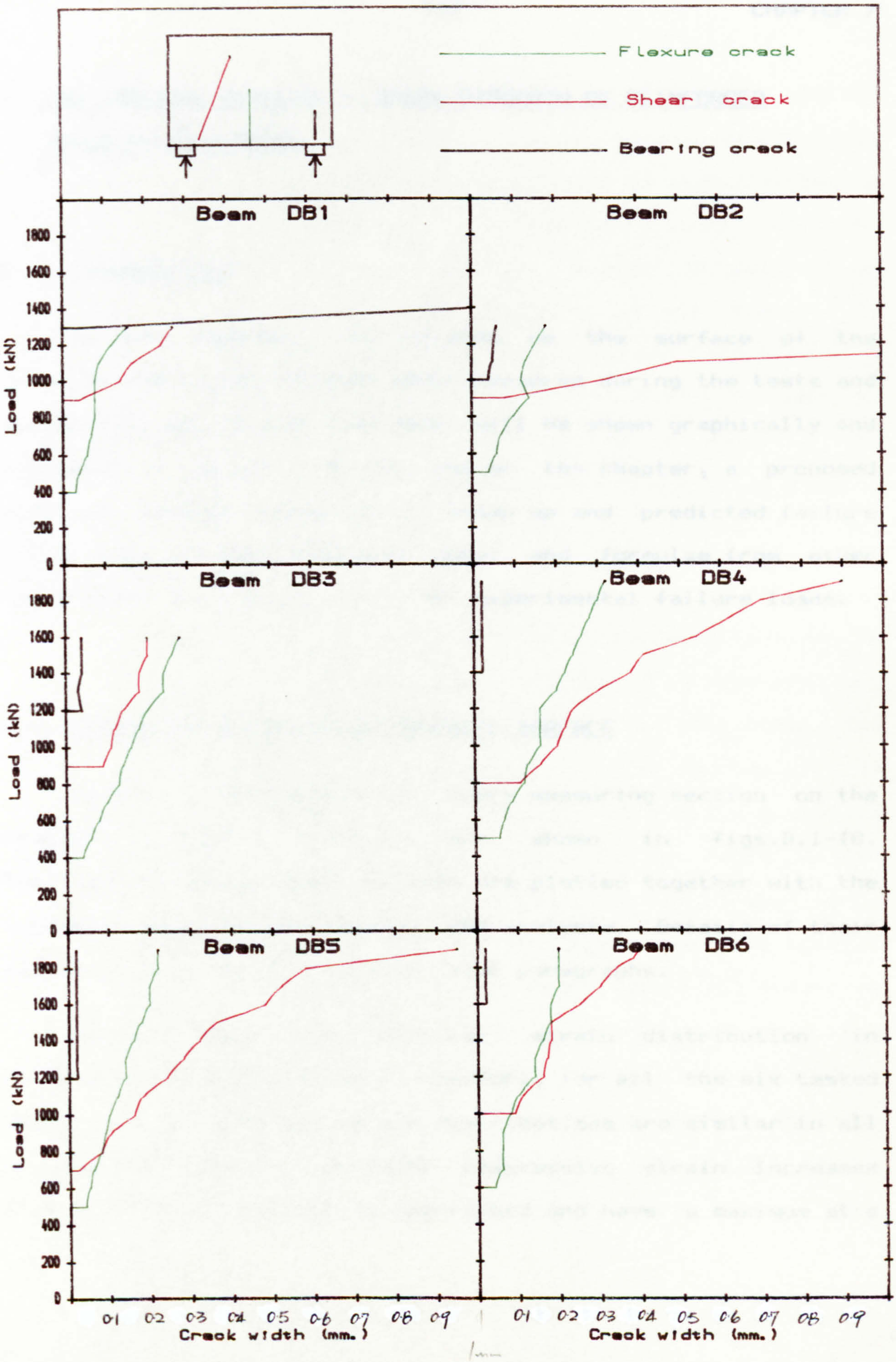

Fig. 6. 13. Load against crack width in beams DB1-DB6

7 EXPERIMENTAL RESULTS — SHEAR STRENGTH OF REINFORCED CONCRETE DEEP BEAMS

7.1 INTRODUCTION

In this chapter, the strains on the surface of the concrete and in the reinforcement measured during the tests and the deflections of the specimens will be shown graphically and discussed in detail. At the end of the chapter, a proposed model of failure mechanism is drawn up and predicted failure loads both by the proposed model and formulae from other researchers are compared with the experimental failure loads.

7.2 STRAIN DISTRIBUTION ON CONCRETE SURFACE

Strain distributions for every measuring section on the concrete surface (fig.6.4) are shown in figs.B.1-18. Experimental strain distributions are plotted together with the theoretical values obtained by FEM analysis. Details of their behaviour will be discussed in later paragraphs.

Fig.B.1 shows the vertical strain distribution in section 1 (fig.6.4), above the support, for all the six tested beams. In general, the strain distributions are similar in all the tested beams. Vertical compressive strain increases gradually as the support is approached and have a maximum at a

point 100 mm above the bearing plate. Below this maximum point, the vertical compressive strain decreases slightly. Strains obtained by FEM analysis are plotted in dotted lines on the same figure (fig.B.1). It can be seen that the experimental and theoretical values agree well for small loads (less than 800 kN) on the upper section of the beams. At higher loads, the experimental strain is larger than predicted by FEM analysis particularly in the regions near the supports. This is probably due to the formation of a wedge in the concrete above the bearing plate and large compressive strains correspond to the action of this wedge of concrete on the concrete block.

Figs.B.2 and B.3 show the vertical strain distributions in sections 2 and 3 respectively. Strain distributions are similar in these two sections and with all the test beams, but they are different from the distribution in section 1. In sections 2 and 3, the vertical compressive strain has a maximum at the top and decreases gradually towards the depth of the beam. At a position 100-200 mm from the bottom of the beam, the vertical strain becomes zero, and their vertical tensile strain emerges and increases in magnitude towards the bottom of the beam. Occasionally, maximum vertical tensile strains were recorded at 100 mm above the bottom of the beam (DB3 and DB6). Analysis from FEM shows similar results, a maximum vertical compressive strain occurs at the top of the beam, it is constant over the top 200 mm and then decreases more or less

linearly with the depth of the beam. In section 2, the vertical compressive strain decreases more rapidly at the position 200 mm from the bottom until a point 100 mm from the bottom of the beam. Thereafter, the vertical compressive stress becomes constant. In section 3, the position at which the compressive strain becomes constant depends on the span of the beam. Larger spans have a larger constant region which varies from 250 to 100 mm from the bottom of the beam.

The horizontal strain distributions in sections 1-3 are shown in figs.B.4-6 respectively. The horizontal strain distribution in section 1 (fig.B.4) is very similar to the transverse strain distribution along the loading line of the bearing concrete blocks which has been discussed in chapter 4 (fig.A.27-34). It has a high compression region close to the bearing plate and then a tension zone with maximum tensile strain occurring at 100 mm from the loaded surface. This agrees well with the assumption that maximum tensile strain occurs at a distance a_1 from the loading surface. The tensile strain gradually diminishes and comes to zero at 900 mm from the bearing plate. Theoretical analyses with FEM have identical results except that the maximum tensile strain is not so high as the experimental values. This is again due to the formation of cracks and a wedge in the bearing zone. It can be seen from fig.B.5 that at low load (less than 800 kN) the horizontal strains in section 2 are very small and approach zero for the region 200 mm above the bottom and 100 mm below the top of the beam. For the section below this region, tensile strains were

recorded and for the section above, compressive strains measured. This is due to the flexural behaviour of the beams. However, at higher loads intercept the strain-measuring line creating large strains which correspond to large strain in the middle section section of the beam. In section 3, large tensile strains were recorded at the bottom of the beam for loads greater than 800 kN. The presence of these tensile strains is due to the formation of flexural cracks at the bottom of the beams. Therefore the magnitude of these tensile strain and the affected region is dependent on the span of the beam. At the top of the beam, small compressive strains were recorded. In general, theoretical and experimental horizontal strain distributions in section 1-3 agree well for the region which is not affected by cracks.

Fig.B.7 shows the distribution of horizontal strain across the top of the beams (section 4). It can be seen that compressive strain was found in all six beams between the two supports. There is a parabolic distribution of compressive strain with a maximum at the centre of the beam. Slight tensile strains were found over the supports. However analytical results from FEM produce a flatter distribution of horizontal compressive strains between the supports and a rapid increase in tensile strain over the supports. In most beams experimental compressive strains between the supports are larger than the predicted values while the experimental tensile strains over the supports are smaller than the corresponding

theoretical values.

Horizontal strain at the bottom of the beam (section 5) is shown in fig.B.8. At small loads (less than 400 kN), experimental tensile strain between the supports has a magnitude similar to the analytical values by FEM. At higher load (greater than 800 kN), the experimental strain distribution fluctuates due to the existence of flexural cracks. Therefore, comparison cannot be made between experimental and analytical values at higher loads. However, rapid changes in strain around the support are recorded by FEM analysis which seem to be unreasonable in practice.

It was suggested by Ramaskrishnam [73] that failure of deep beams was in fact failure of a strut and tie system. Sections 6-12 were specially designed to investigate the behaviour of this compressive strut. Sections 6-9 are perpendicular to this strut, transverse strains being measured at positions 100, 200, 400 and 800 mm from the support (fig.6.4). Fig.B.9-12 show the compressive strain across this compressive strut in section 6-9 respectively. It can be seen that the magnitude of the compressive strain falls dramatically at sections further away from the support. In section 6, maximum compressive strain is found in the centre of the strut and gradually falls to zero at 150 mm from the centre. In beams DB4-6, a sudden decrease in compressive strain is found at 50 mm to the left of the strut; this is believed to be

affected by the presence of shear cracks. Section 7 has a similar distribution of strains as in section 6 but with smaller magnitude. Again the maximum strain is found at the centre of the strut and becomes zero at 100 mm to the left of the strut. Similar to section 6, a sharp decrease in compressive strain, affected by shear cracking, is found at 100 mm to the left of the strut in beams DB3-5. It is interesting to note that to the right of the shear crack high compressive strains are found but little or no strain was recorded to the left of it. Therefore, the shear crack is actually the dividing line of the compressive strut with the beam. Sections 8 and 9 have similar magnitudes of compressive strain, these are much less than in sections 6 and 7. The distribution of strain is comparatively uniform and occasionally, depressions are present due to the presence of shear cracks.

Figs.B.13-15 show the distributions of longitudinal strain in sections 10-12 respectively (fig.6.4). In section 10 uniform compressive strain was recorded along the section. Compression is small in magnitude, around 700 micro-strain, even at 1600 kN. Sections 11-12 have a distribution of strains similar to section 1 but with larger magnitudes (fig.B.1). An increase of compressive strain occurs as the support is approached and there is a maximum at 100 mm from the support. Below this point compressive strains begin to decrease. Transverse strain distributions in sections 10-12 are shown in

figs.B.16-18. Compressive strains are found at the top for all three sections. These compressive strains decrease slowly and become zero at 900 mm from support. Transverse tensile strains begin to emerge below this point. Rapid increases in tensile strain are recorded in section 10 with loads greater than 800 kN. It increases linearly to a point 300 mm from the support and then decreases. This rapid increase in strain actually indicates a rotational movement of the concrete block from the shear crack. The decrease of transverse strain below 300 mm from the support is due to the presence of four main steel bars of larger diameter which help to hold back the concrete block. Only small strains were recorded in sections 11-12 showing that the concrete block is not rotating along these sections but rotating in section 10.

7.3 STRAIN DISTRIBUTION IN REINFORCEMENTS

The distributions of strain in main and web steel are shown in figs.B.19-24. The strains in the bearing steel are given by figs.B.25-29. On each figure, reinforcement details are drawn; the position and direction of every strain gauge is marked on the reinforcement and numbered beside it. It is drawn together with the variation of strain in each gauge with loads.

Gauges 1-4 were mounted on the reinforcement in the centre

of the beam. As load is increased, strain increased linearly. At around 400 to 1000 kN, depending on the span of the beam, strain increased at a faster rate. This indicates the flexural cracking of the beam at that load. In the presence of flexural cracks, of course, strain increases more rapidly remains at this rate until failure of the beam. It is noted that none of the gauges shows yielding of the main reinforcement in this position. Gauges 5-8 were placed along the direction of the imaginary compressive strut. They again increase in strain at two rates, before and after the formation of shear cracks at 800-1000 kN. With the exception of beams DB1 and DB2, which did not fail in shear, all gauges show yielding of the reinforcement in this position. In most beams, except DB2, the upper main steel exhibits larger strains. With the exception of beam DB2, gauges 9-12 are placed on the main reinforcement above the outer edge of the bearing plate. These four gauges have similar strains and they all have demonstrated an enhanced rate of increase in strain with loads. In beam DB2, gauges 9-12 were actually in the main reinforcement above the bearing plate. They had different characteristics to those in beams DB3-6. Gauge 11 recorded the highest strain, it yielded at an early stage (400 kN) but gauge 10 is virtually unstrained. This outstanding characteristic is believed to stem from the small edge distance from the support. Gauge 34 is at the end of the bottom main reinforcement, it is designed to monitor the anchorage problem of the main reinforcement.

Strain in this gauge is low, therefore, it is accepted that there is good anchorage of the main reinforcement. Gauges 13-17 were in the horizontal web reinforcement in the direction of the suggested compressive strut. It is found that with the exception of gauge 13, all gauges show tensile strain in the reinforcement. Compressive strain in gauge 13 shows a constant increase in strain with load while all the others show two stages of increase before and after the formation of shear cracking. In beam DB2, gauges 14-17 are virtually unstrained as DB2 has not failed in shear and no shear crack is found. In beams DB1 and DB3-6, only small strains are found in gauges 14-17 at loads below 700-900 kN, at higher loads, rapid increase in strain is taking place. Generally, web steel near the bottom has larger strain and yield occurs before the specimen fails. This suggests that shear cracking originates at a point above the main reinforcement but below the web steel. Gauges 18-20 were installed in the vertical web steel and again along the direction of the imaginary shear crack. Compression found in this reinforcement and higher compression was recorded at the reinforcement near the bearing plate.

Bearing steel in the form of small interlocking stirrups is inserted in beams DB2-6 to prevent bearing failure above the supports (figs.B.25-29). Gauges 21-26 are placed on the centre stirrup above the support while gauges 27-29 and 30-32 are on either side of the central stirrups. In beam DB2, only small strains are recorded in the gauges, especially for

gauges 10-12. This shows the ineffectiveness of the bearing steel and beam DB2 fails by sliding of the bearing plate off the corner of the beam because the supporting position is too close to the corner. Gauges in beams DB3-6 have larger strains and usually show yielding of one or more stirrups in the first or secondary layer of bearing steel. This indicates that bearing steel can in fact prevent premature failure of the beam by crushing of the concrete around the support.

7.4 DEFLECTION

Deflections at the bottom of the beams are shown in fig.B.30. Due to the failure of some of the dial gauges during the tests of beams DB1 and DB2, no experimental results are shown for these two beams. Theoretical results by FEM analysis are shown in dotted lines on the same figure. Both experimental and theoretical results show similar deflection patterns. The larger span has larger deflection at the middle of the beam.

Horizontal movement recorded along the centre line of the beams, is shown in fig.B.31. No measurement was taken in beam DB1. Beam DB2 has extensive horizontal movement due to the distortion around the bearing zone above the support. This beam as described in chapter 6, did not fail in shear but slid off the test rig. Limited horizontal movement is recorded in

beams DB3-6 and no buckling was observed for these depth to thickness ratios.

7.5 SHEAR TRANSFER BY AGGREGATE INTERLOCK AND DOWEL ACTION

From the behaviour in failure of deep beams in this investigation, it is believed that the shear strength of deep beams is determined by aggregate interlock and dowel action. A review of past researches in this area is discussed in the following paragraphs.

Shear forces can be transmitted across a crack by the interaction between two rough surfaces of the crack (aggregate interlock) or by the dowel action of tensile reinforcement (dowel action). However, aggregate interlock and dowel action are interdependent and not easy to separate. During the initial stage of crack formation, aggregate interlock plays an important parts in shear resistance. As external shear force is increased the diagonal crack is widened and lengthened by the rotation and shear displacement of the beam. When the crack meets tensile reinforcement, part of the shear resistance is taken up by the dowel action of the reinforcement. This leads to splitting of the concrete at the level of the reinforcement and increases the crack width at a higher rate. Therefore, the shear force taken up by aggregate interlock is further reduced. Houde and Mirza [35] stated that for a beam

without web reinforcement and after cracking, shear carried by aggregate interlock, concrete in the compressive zone and dowel action of the main steel was 50, 30 and 20% respectively. They are distributed as shown in fig.7.1, [79].

Some attempts had been made to separate the action of aggregate interlock and dowel action and then investigate the effect of them with various parameters. Houde and Mirza [35] eliminated dowel action with the absence of reinforcement across the crack. A tensile crack was introduced by applying direct tensile force on either ends of the block and a predetermined crack width was maintained by restraining the specimen as shown in fig.7.2. Shear force was applied across the crack and shear displacement was measured. It was found that the shear stress carried by aggregate interlock ranged from 0.5 to 1.2 N/mm^2. The magnitude of the stress was mainly dependent on the crack width and was proportional to the square root of the cylinder strength of concrete. However, it was independent of the size of aggregate used in the concrete. Twenty seven tests of aggregate interlock was carried out by Paulay and Loebar [70] with constant and variable crack widths under constant or variable restraining forces. The test specimen is shown in fig.7.3. They arrived at similar conclusions to Houde et al in that the aggregate size, shape, hardness and cement mortor had no noticeable effect on the shear carried by aggregate interlock. The largest single factor affecting shear resistance was the width of a crack

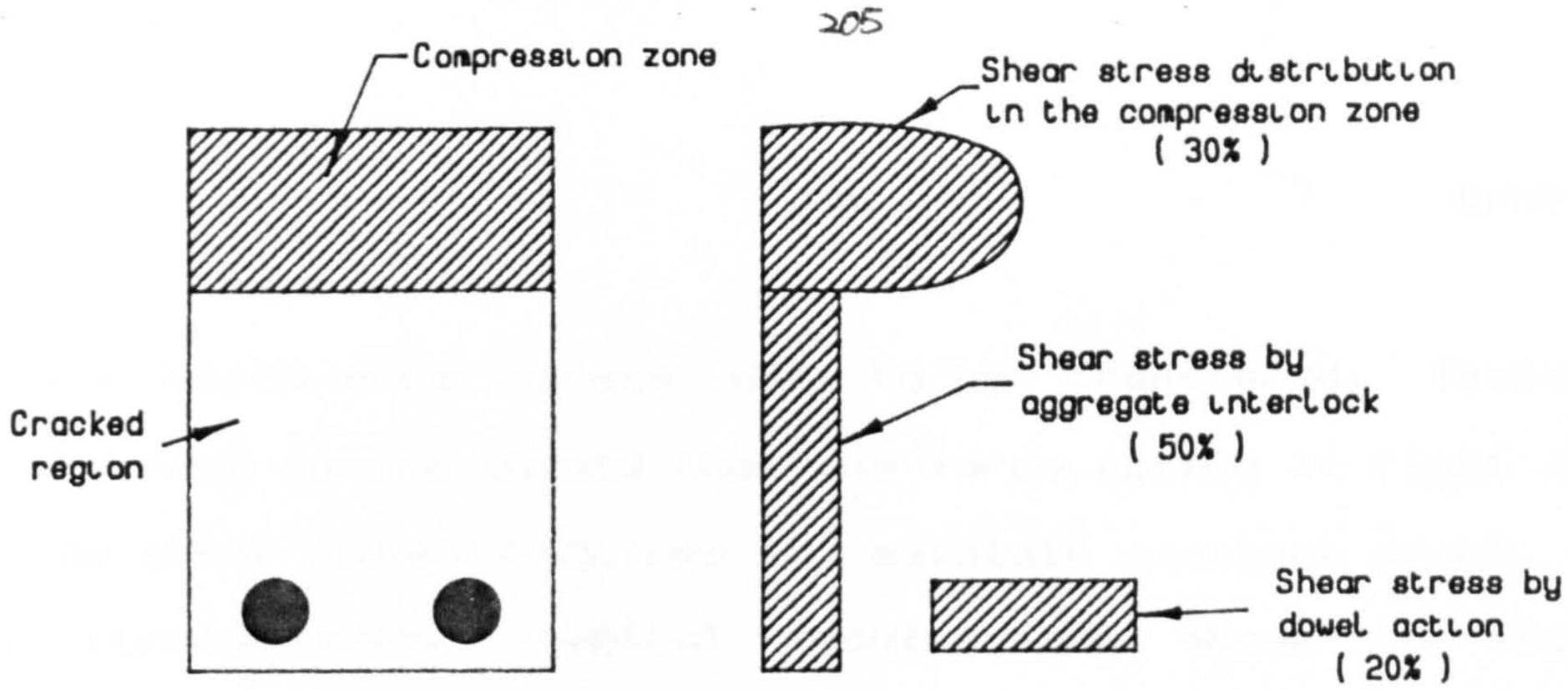

Fig.7.1 Distribution of shear stress along a shear crack.

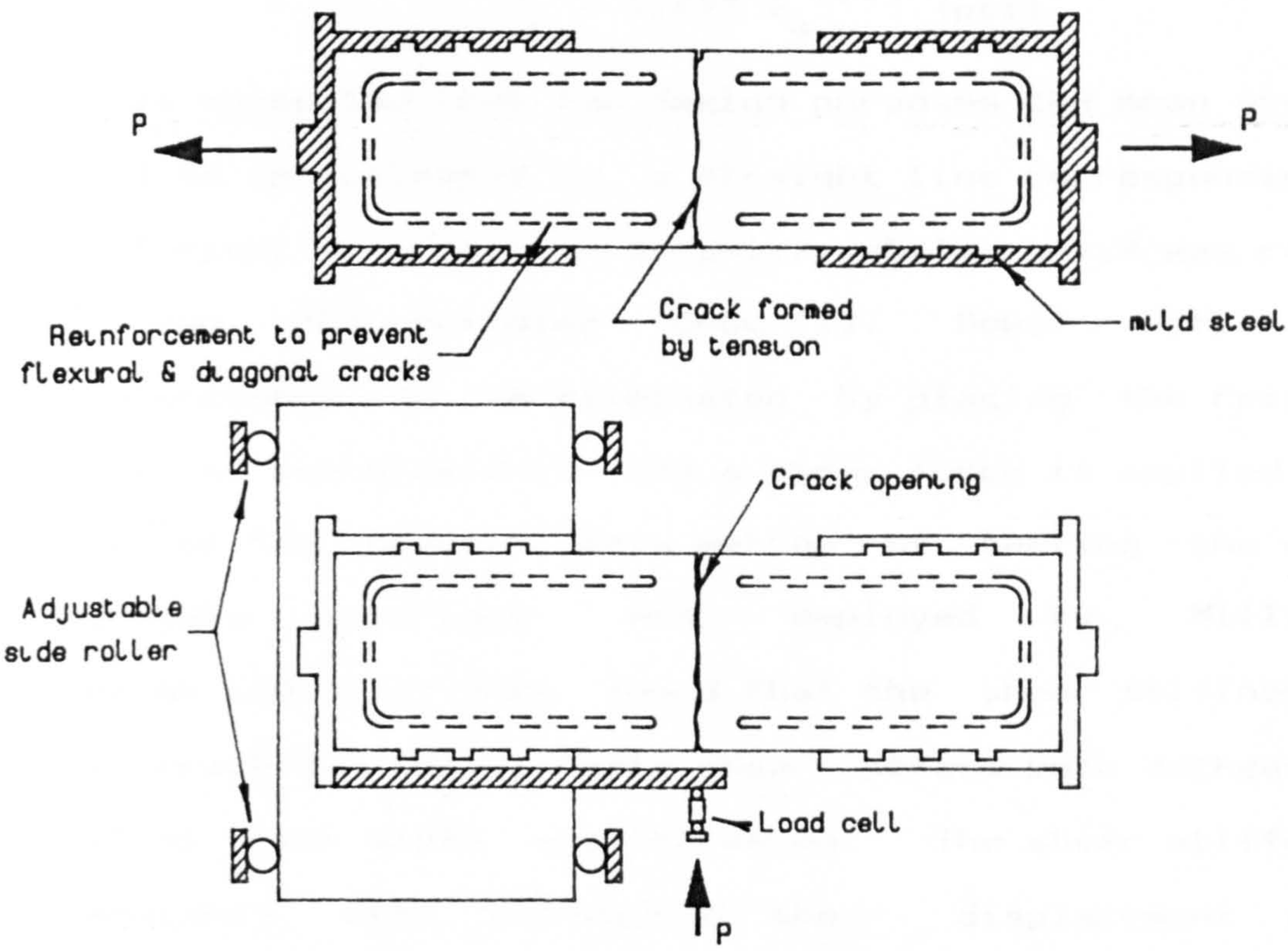

Fig.7.2 Aggregate interlock test by Houde and Mirza.

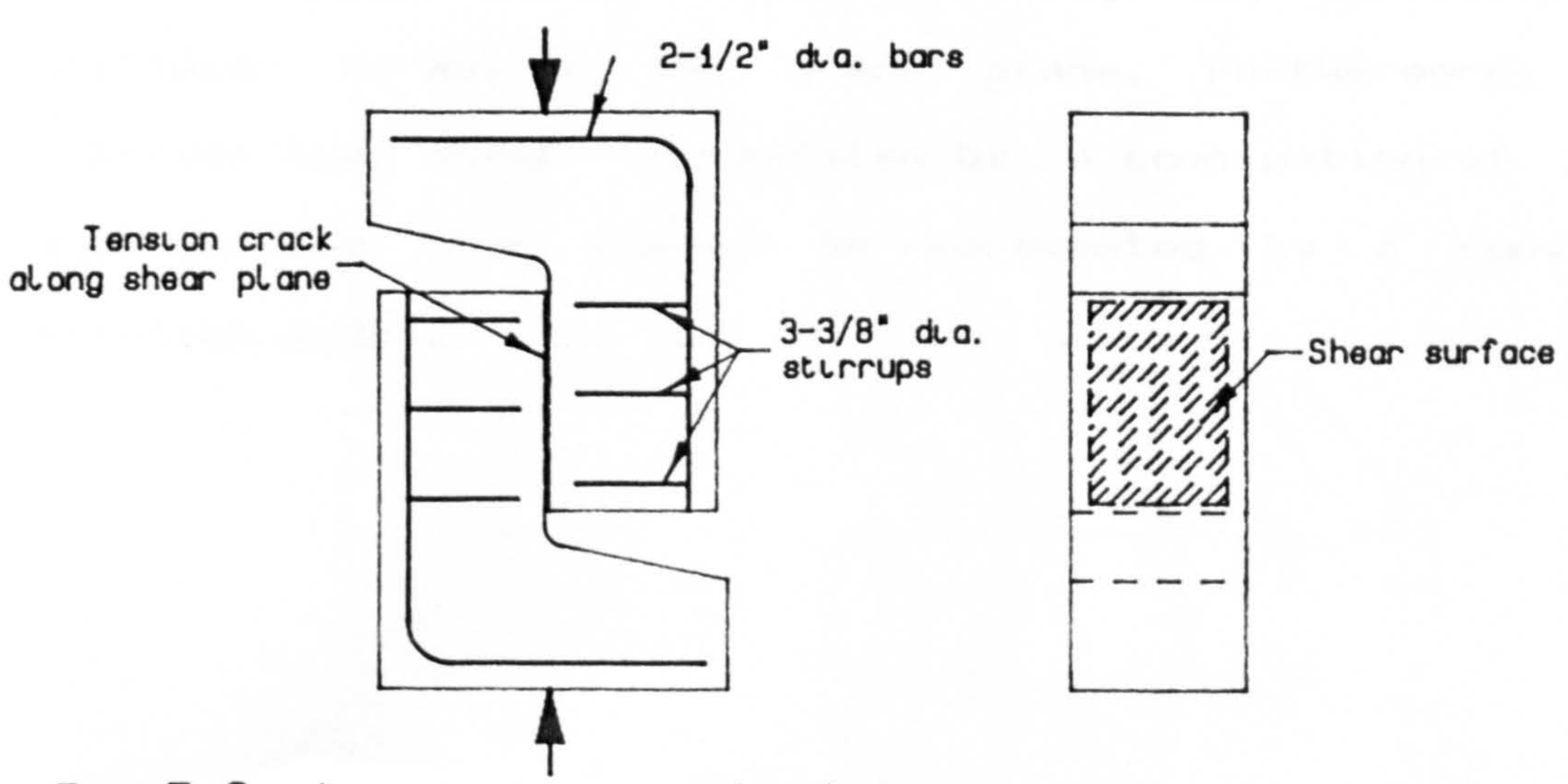

Fig.7.3 Aggregate interlock test specimens of Paulay.

across which shear stress were to be transfered. Tests with restraining forces showed that the force acting at right angles to the shear plane required to maintain constant crack width was considerable. Typical results are shown in fig.7.4. Logarithmic regression analysis was performed and the following relationship obtained.

$$f_L = 0.473\ f_a^{1.03}\ \text{(psi)} \qquad (7.1)$$

It was suggested that for design purposes the mean shear stress could be approximated by a straight line corresponding with a coefficient of friction of μ=1.7, while μ=1.4 was recommended by the ACI Building Code [1]. Dowel action of the reinforcement can be eliminated by placing the reinforcement within an oversize duct and a shear force is applied on either side of the crack. This method of testing the effect of aggregate interlock was employed by Millard and Johnson [60,61]. They found that the shear stiffness across the crack and the ultimate shear stress both decreased as the initial crack width was increased. The shear stiffness also diminished with increasing shear displacement which was associated with crack-widening regardless of the size of the initial crack width. Crack-widening was sensitive to the stiffness normal to the crack plane. Furthermore, it was believed that shear is resisted by a combination of crushing and sliding that cannot be represented by a conventional friction model.

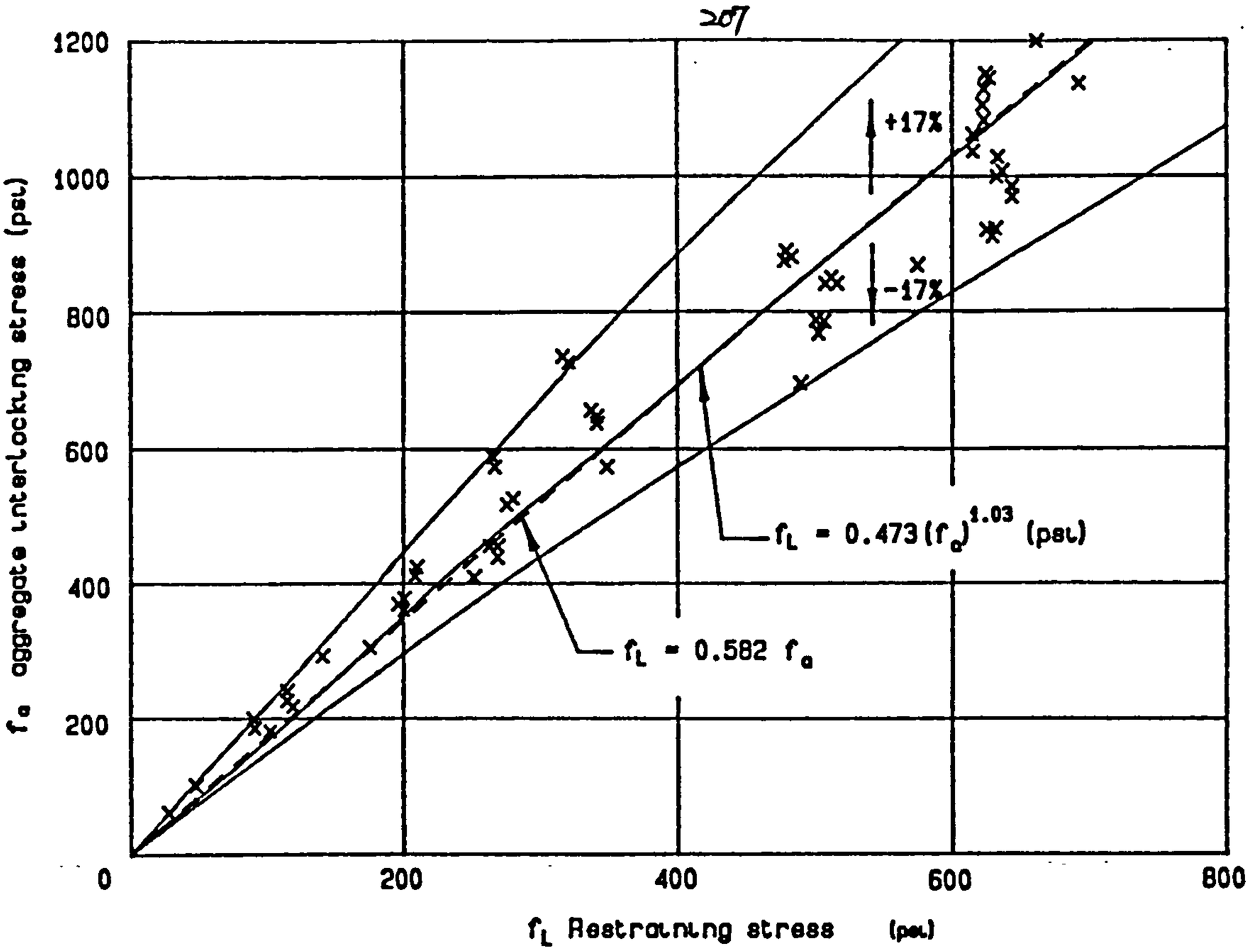

Fig.7.4 Shear vs restraining stress by Paulay.

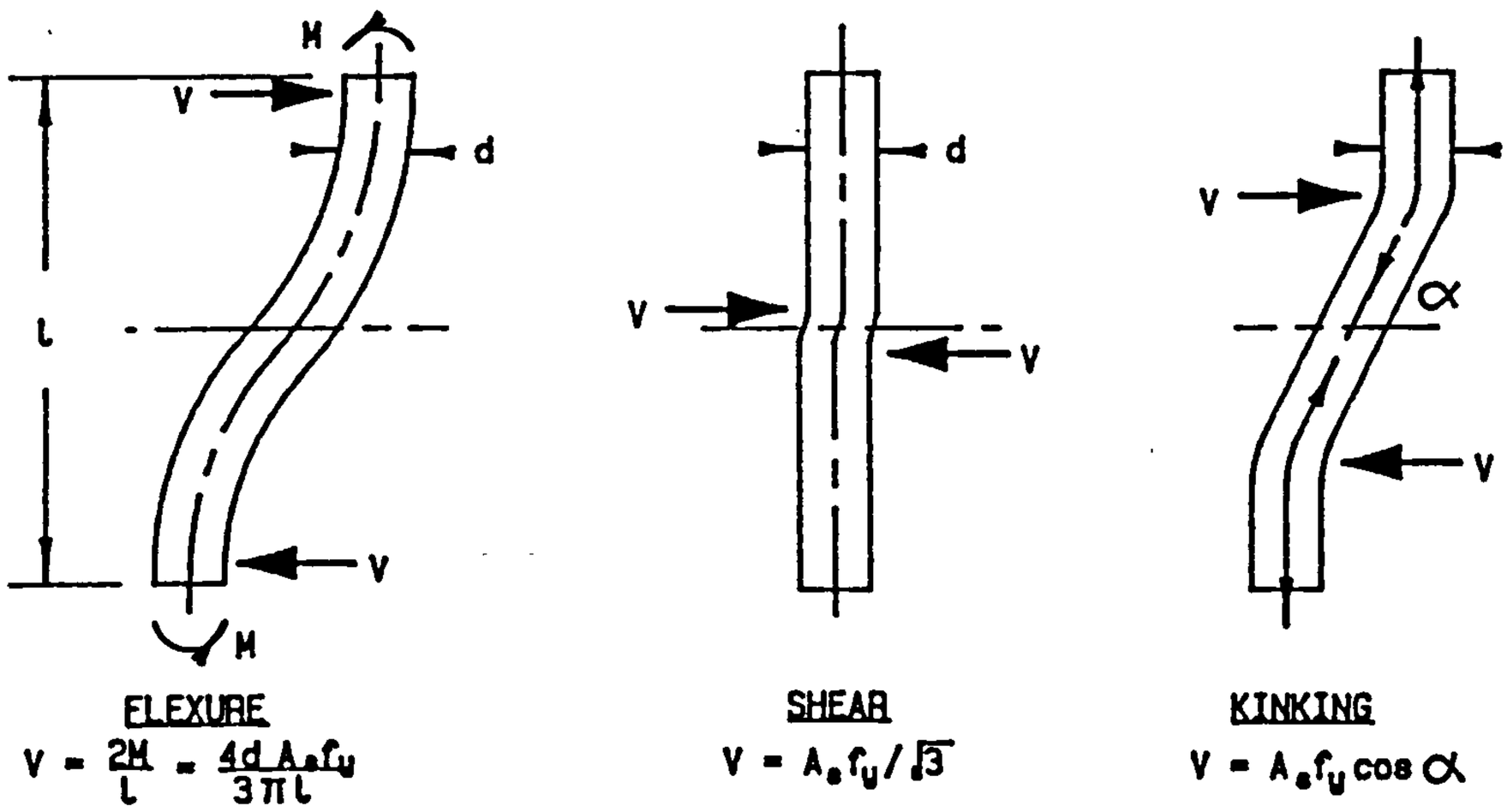

Fig.7.5 The mechanism of dowel action.

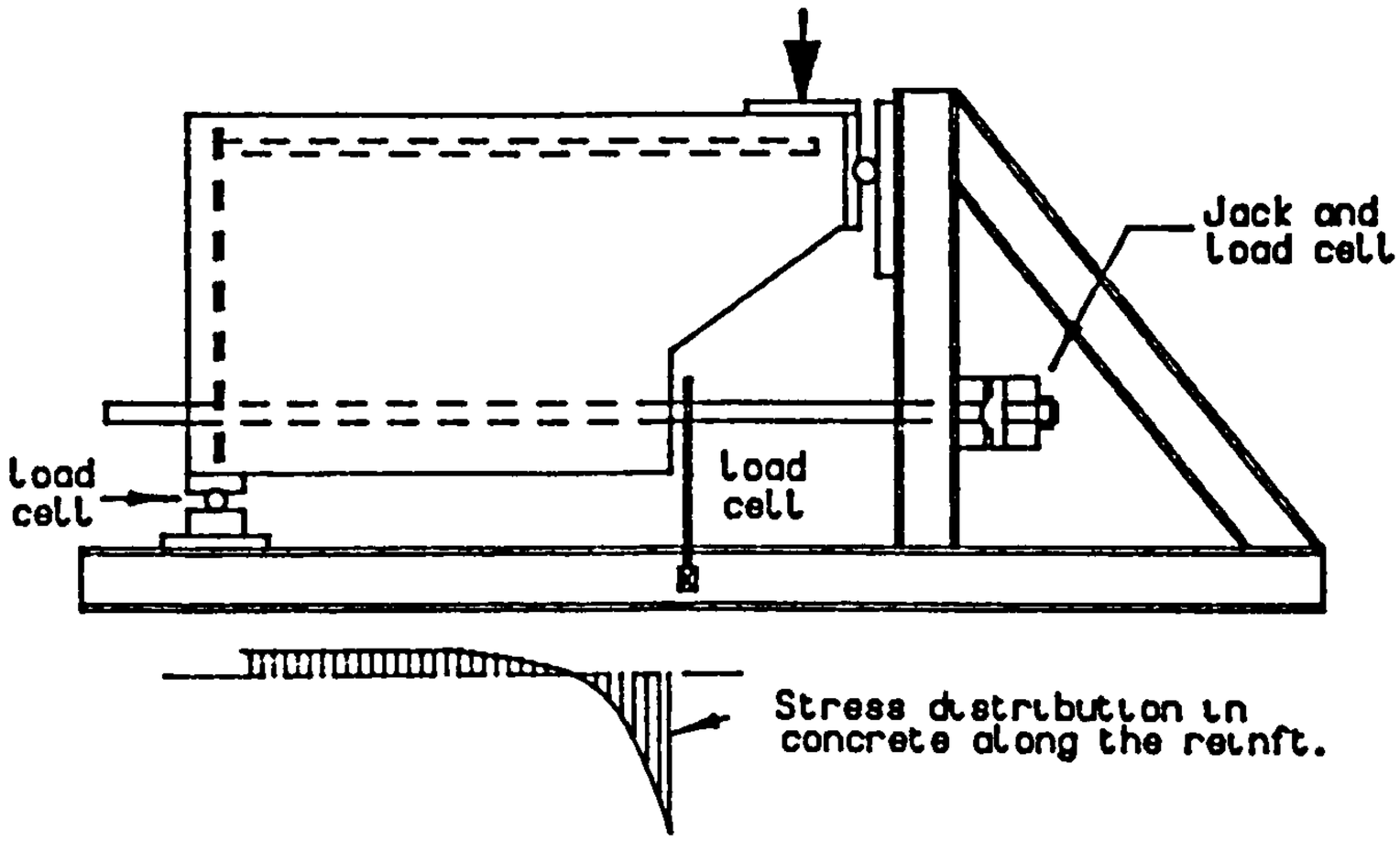

Fig.7.6 Dowel action test by Houde and Mirza.

Dowel action is believed to be come from three sources:

(1) the flexure of the reinforcement,
(2) the shear across the bars, and
(3) the kinking of the reinforcement.

These shear mechanisms are illustrated in fig.7.5 associated with the shear strength expressed in terms of the diameter of the bar and its strength. However, when the dowels are large the shear capacity of a dowel is determined by the strength of the surrounding concrete rather than the yield strength of the reinforcement. Thirty push-off type specimens were tested by Pauley [61] with varied surface preparation from smooth to keyed surface and three different amounts of reinforcement across the shearing surfaces. It was found that the dowel force is proportional to the total steel area (square of the diameter of the reinforcement). This infers that shear and kinking are the principal mechanisms of dowel action as the dowel force produced by flexure of the reinforcement is proportional to the cube of the diameter of the reinforcement. Thirty two beam-end specimens shown in fig.7.6 were tested by Houde and Mirza [35] to determine the ultimate dowel strength under dowel acting alone or dowel action combined with predetermined pull-out forces. Dowel cracking loads were found to be directly dependent on the beam width and the concrete tensile strength. The bar size and the embedment length did not have any influence on the dowel cracking load. This contradict with Pauley's finding in which dowel force is proportional to the total area of steel. The pull-out forces

had no effect on the dowel capacity which did not exceed 20% of the shear capacity of the beam. The dowel cracking load may be expressed by

$$D_f = 40 \cdot b \cdot f_c'^{1/3} \qquad (7.2)$$

Similar specimens were used by Millard and Johnson [60] in aggregate interlock tests, except that this time no duct was surrounding the reinforcement. The shearing surfaces were smoothed by casting each specimen in two stages and separating them with two layers of thin polythene sheeting. The experimental results show that increasing the diameter of the reinforcement resulted in a higher shear stiffness and ultimate stress. It also increased the tendency for the smooth crack to widen. An increase in the strength of the concrete had only a small effect on the behaviour but an increase in axial force in the reinforcement resulted in a lower shear stiffness and ultimate shear stress together with an increased tendency for crack widening. This is due to some localized damage and softening of the concrete by the axial tension force.

However, interaction between aggregate interlock and dowel action makes the combined effect in reinforced concrete more complex than if considered separately. For instance, in dowel action tests, elimination of aggregate interlock by artificially smooth cracks also suppressed the tendency for crack faces to override which causes widening of the crack, increase in axial tension force in the reinforcement and

reduction in the shear stiffness of the dowel action. In aggregate interlock tests, elimination of dowel action by means of an oversize duct also removed the local bond between reinforcement and concrete. This could lower the axial stiffness and thus underestimate the shear stiffness provided by aggregate interlock. Also the internal crack widths are dissimilar for two specimens with the same surface crack width but with bonded and unbonded reinforcement. Crack width is a prime factor of aggregate interlock; therefore these two specimens cannot be expected to have similar shear stiffness.

Hofbeck et al and Mattock [33,57] have presented some tests on the combined effect of aggregate interlock and dowel action. Their test apecimens included orthogonal, inclined or parallel reinforcement of initially cracked or uncracked concrete along the shear plane in fig.7.7. It is found that the spacing and diameter of the reinforcement did not affect the linear relationship between $\rho.f_y$ and the ultimate shear force V_u. Reinforcement with high yield strength and a small yield plateau give higher shear resistance. A structural model was constructed according to the observed mode of failure shown in fig.7.8, with the following assumptions:

(1) The stress in the reinforecment, f_s is proportional to the component of relative displacement of concrete on the two sides of the shear plane in the direction of the reinforcement.

(2) The relative displacement at ultimate, δ_u is constant and

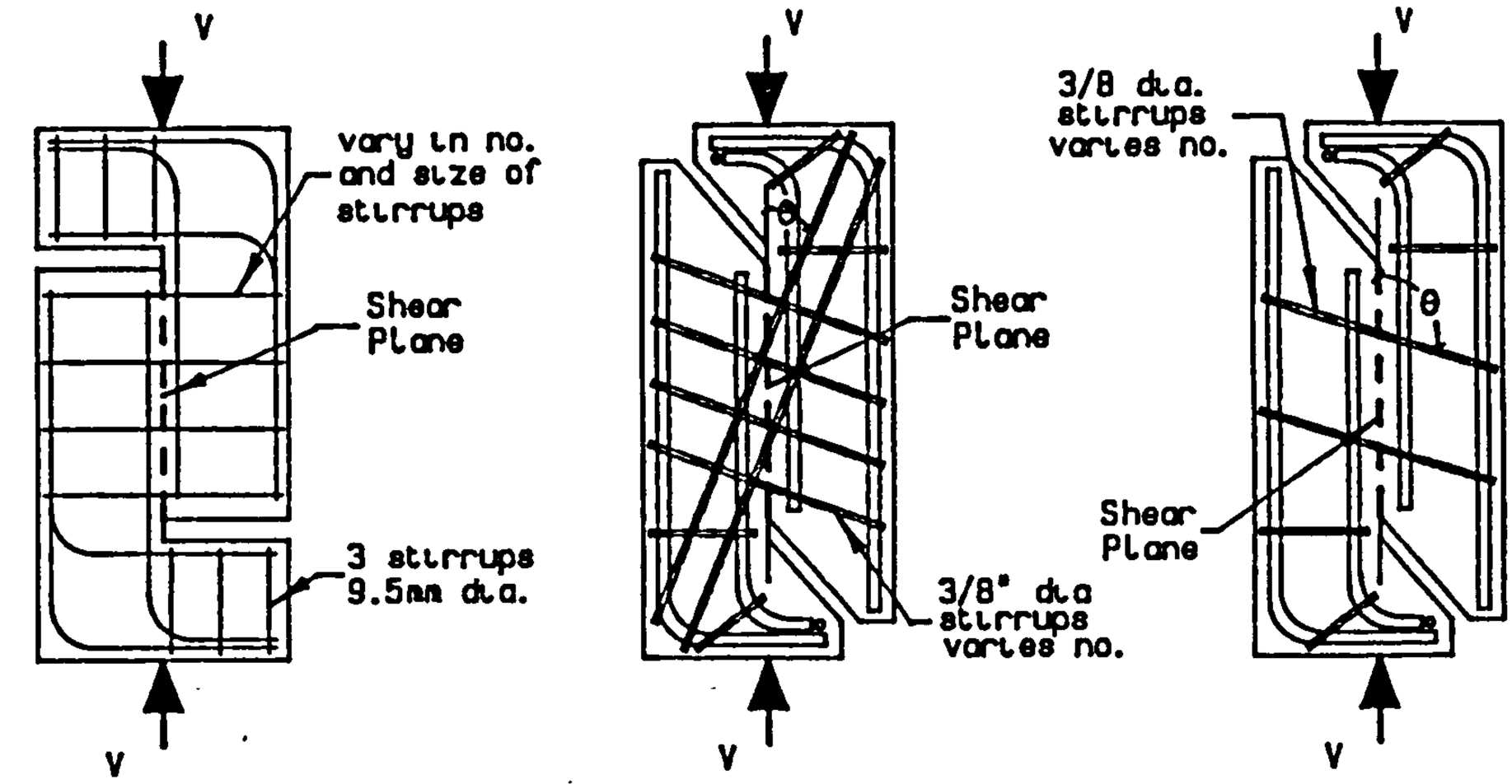

Fig.7.7 Push-off test by Mattock and Hofbeck.

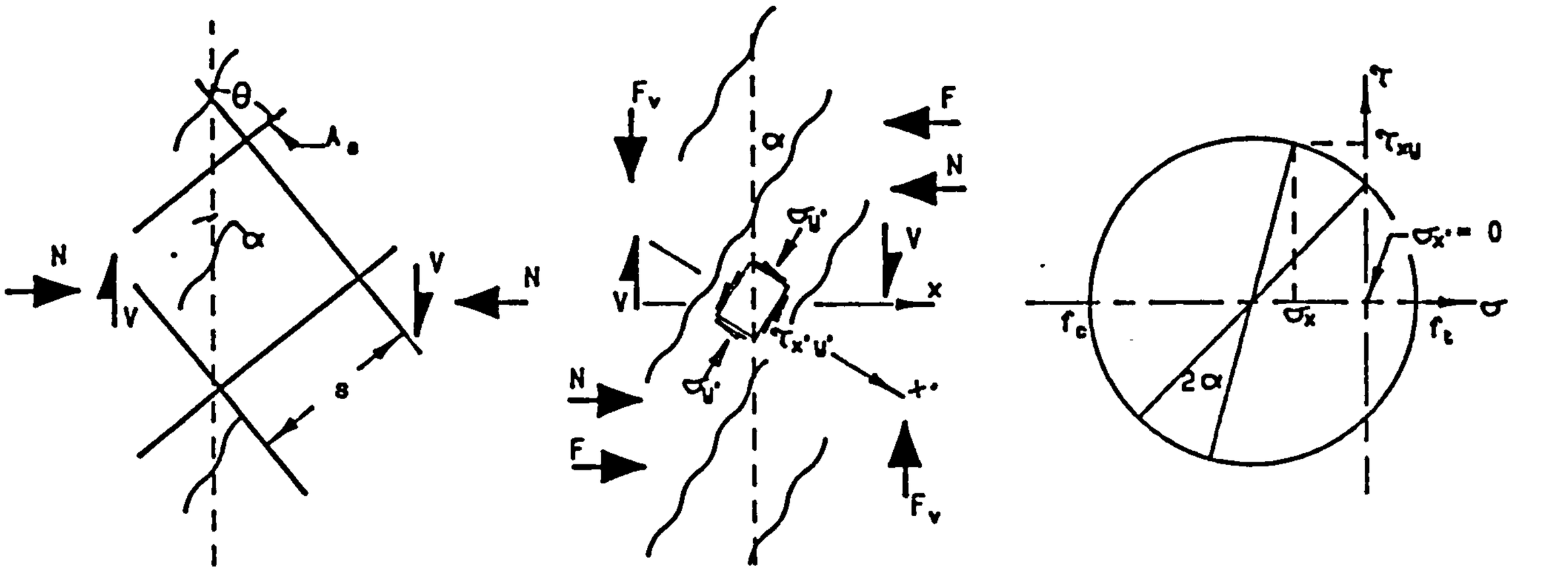

Fig.7.8 Shear model of initial uncracked specimen by Mattock.

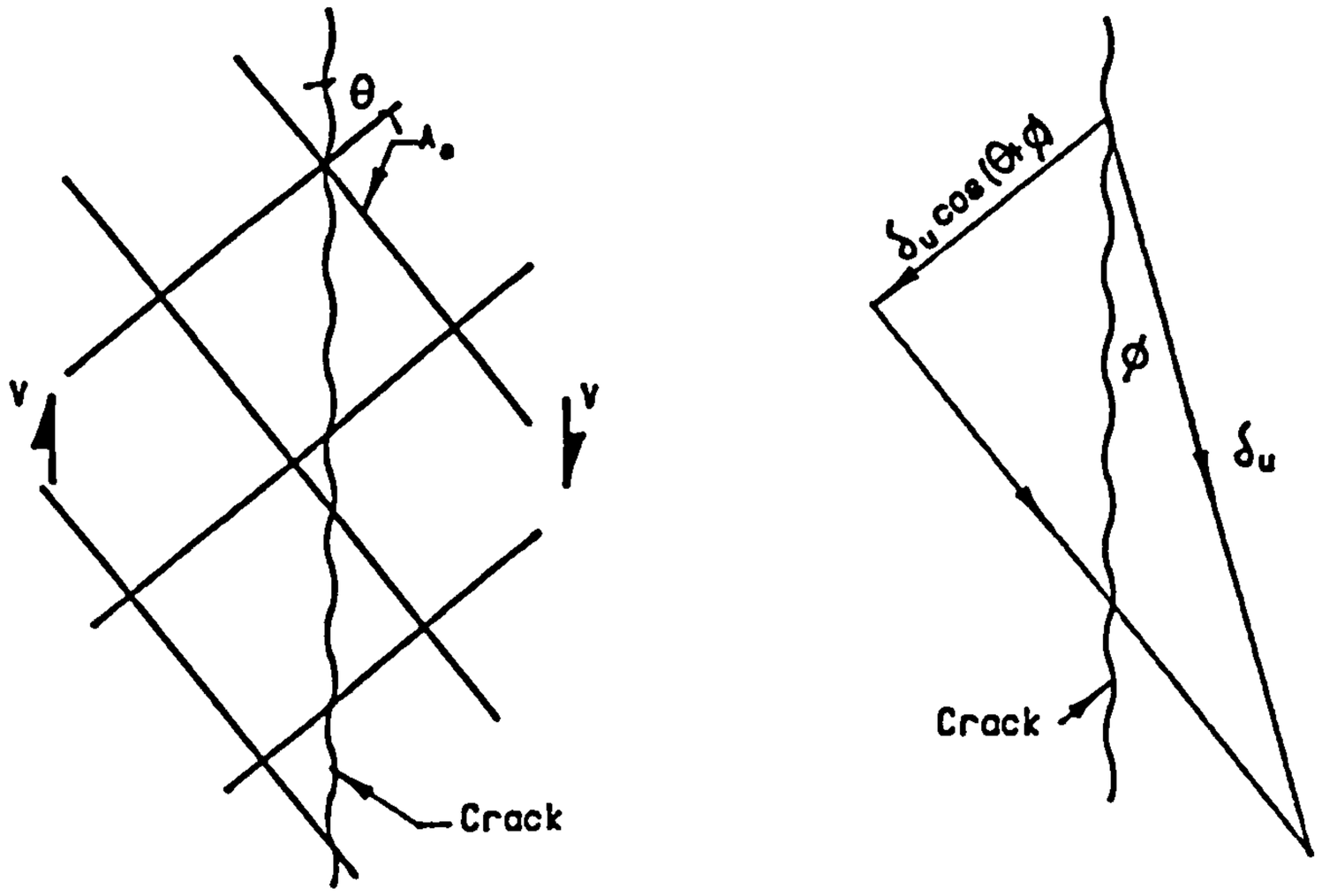

Fig.7.9 Shear model of initial cracked specimen by Mattock.

equal to that necessary to produce a strain ϵ_y in the reinforcement in the shear plane.

During the tests on initially uncracked specimens, diagonal cracks at short intervals were formed across the shear plane. Movement of the two halves of the specimen relative to one another occurs by rotation of the concrete strut between the diagonal cracks. Therefore, the strain ϵ_s in reinforcement at angle θ to the shear plane is

$$\epsilon_s = C \cdot \delta_u \cdot \cos(90+\alpha-\theta) \tag{7.3}$$

where C = constant and when $\theta+90$, $\epsilon_s=\epsilon_y$

therefore

$$\epsilon_s = \epsilon_y \cdot \sec\alpha \cdot \cos(90+\alpha-\theta) \tag{7.4}$$

stress f_s can be expressed as:

$$f_s = \begin{cases} -f_y & 0<\theta<2\alpha-90 \\ f_y \cdot \sec\alpha \cdot \cos(90+\alpha-\theta) & 2\alpha-90<\theta<90 \\ f_y & 90<\theta<180 \end{cases} \tag{7.5}$$

Total steel force perpendicular and parallel to the crack are respectively

$$F = A_s \cdot f_s \cdot \sin^2\theta / S_b \tag{7.6}$$

$$F_v = A_s \cdot f_s \cdot \sin(2\theta) \tag{7.7}$$

At failure, the direct stress σ_x acting across the shear plane as a result of the stresses in the reinforcement and any externally direct stress σ_{ex} is

$$\sigma_x = F/b \cdot d + \sigma_{ex} \tag{7.8}$$

where b = width of the shear plane
d = length of the shear plane.

Thus T_{xy} can be found by the Mohr circle (fig.7.8) with a given compressive and tensile strength of concrete. The ultimate shear force can be estimated as

$$V_u = F_v + K \cdot T_{xy} \qquad (7.9)$$

where K may be taken as 0.84

For initially cracked specimens, movement of the two halves of the specimen was along the crack (shear plane). The faces of the crack was rough, and hence when slip occurs, the crack faces were forced to separate. The relative displacement δ_u which takes place is assumed to be in a direction at angle ψ to the crack,

where $\psi = \arctan\mu$ (7.10)
μ = coef. of friction between crack faces, taken as 0.8 (μ=38.7)

Thus using the foregoing assumptions, the strain at ultimate ϵ_s in reinforcement at an angle θ to the crack is given by

$$\epsilon_s = C_2 \cdot \delta_u \cdot \cos(\theta+\psi) \qquad (7.11)$$

similarly the stress at ultimate of the reinforcement at angle θ to the crack is

$$f_s = \begin{cases} -f_y & 0<\theta<90-2\psi \\ -f_y \cdot \mathrm{cosec}\psi \cdot \cos(\theta+\psi) & 90-2\psi<\theta<90 \\ f_y & 90<\theta<180 \end{cases} \qquad (7.12)$$

It has been proposed [58] that for the case of reinforcement crossing a crack at right angle to the ultimate shear transfer strength may, for the purpose of design, be taken as

$$v_u = 200 + 0.8\rho \cdot f_y < 0.3f_c' \qquad (7.13)$$

The first term in Eq.7.13 represent the shear transfer by dowel action of the reinforcement. But this gives the lower bound value for design purpose. Since, shear force along the crack is resisted by dowel force perpendicular to the reinforcement, therefore shear force is proportional to sine times the dowel force perpendicular to the reinforcemment (i.e.)

$$V_u = k \cdot D_f \cdot \sin\theta \qquad (7.14)$$

Dowel force is produced by steel stress in the direction perpendicular to the crack, thus dowel force is proportional to sine times steel stress (i.e.)

$$D_f = k \cdot \sin\theta \cdot f_s \qquad (7.15)$$

Combining Eqs.7.14 and 7.15,

$$V_u = k \cdot \sin^2\theta \cdot f_s \qquad (7.16)$$

Therefore, Eq.7.13 is modified to give the mean value of shear strength as

$$V_u = 400b \cdot h \cdot \sin^2\theta + 0.8F + F_v \qquad (7.17)$$

where $F = A_s \cdot h \cdot f_s \cdot \sin^2\theta$ & $F_v = -A_s \cdot h \cdot f_s \cdot \sin(2\theta)$

7.6 PROPOSED FAILURE MECHANISM OF REINFORCED CONCRETE DEEP BEAMS

Consider a reinforced concrete deep beam with orthogonal reinforcement subjected to two point loading as shown in fig.7.10a. It had been observed from experiments that the shear crack was usually formed along the line joining the inner edge of the support and the outer edge of the loading plate. Equilibrium of the forces along the crack were maintained by the shear in the compression zone, aggregate interlock, stresses of any reinforcement across the crack and the tensile strength of concrete. Various forces acting along the crack are shown by the free body diagram in fig.7.10b. For the purpose of analysis, certain assumptions have been made and they are as follows:

(1) A crack is formed along the line joining the inner edge of the supporting plate and the outer edge of the loading plate.

(2) Movement of the concrete block is by the rotation about the centre of forces in the compression zone (point A) and movement of each point along the crack is perpendicular to the direction of the crack.

(3) Strain in the reinforcement across the crack, ϵ_s is proportional to the displacement of the concrete, δ_u along the direction of the reinforcement.

(4) Ultimate displacement between two concrete surface, δ_u is equal to that neccessary to produce yielding of the reinforcement.

(5) A reinforced concrete deep beam is said to fail when the ultimate displacement, δ_u has taken place at the bottom-most of the main reinforcement.

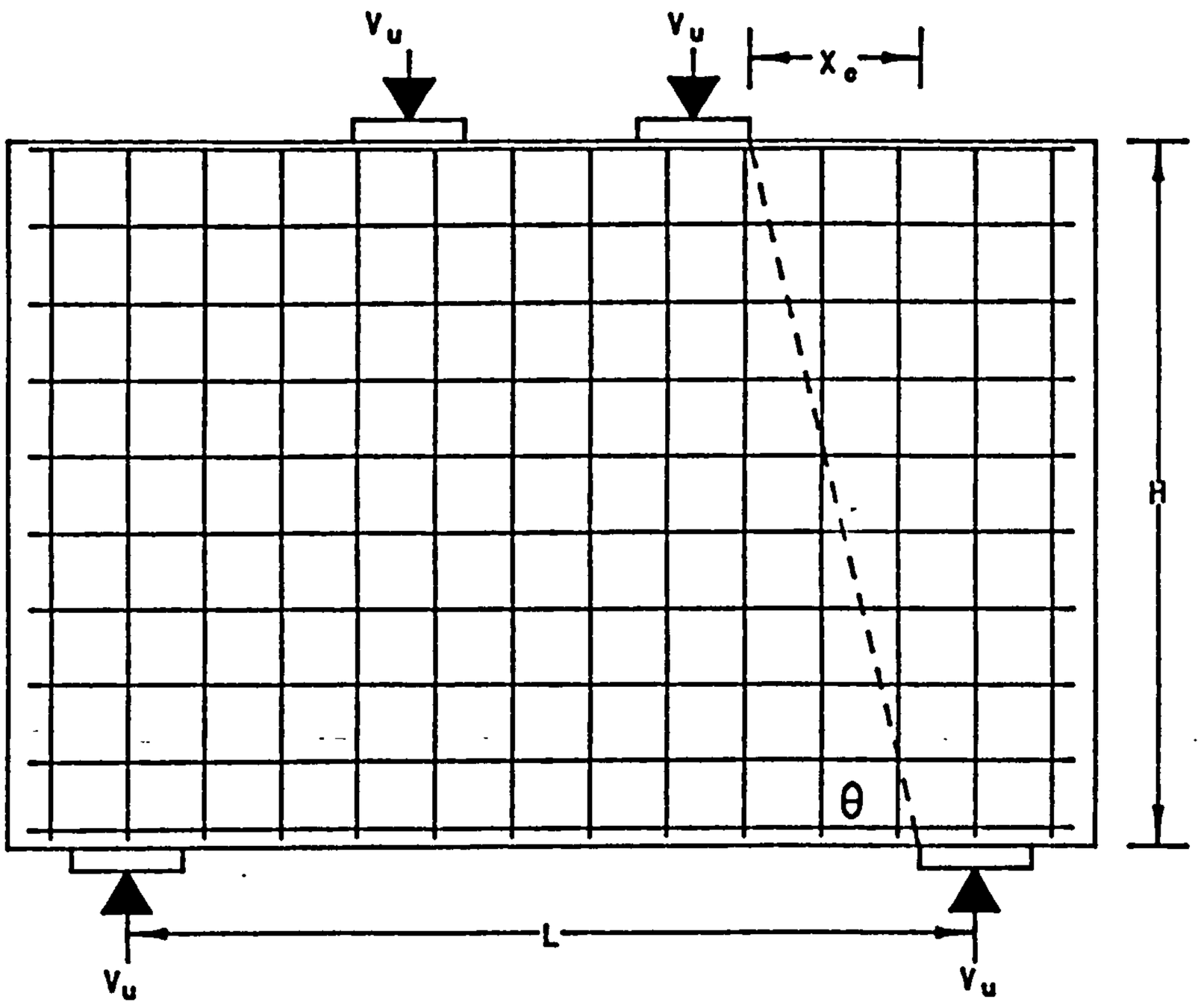

(d)

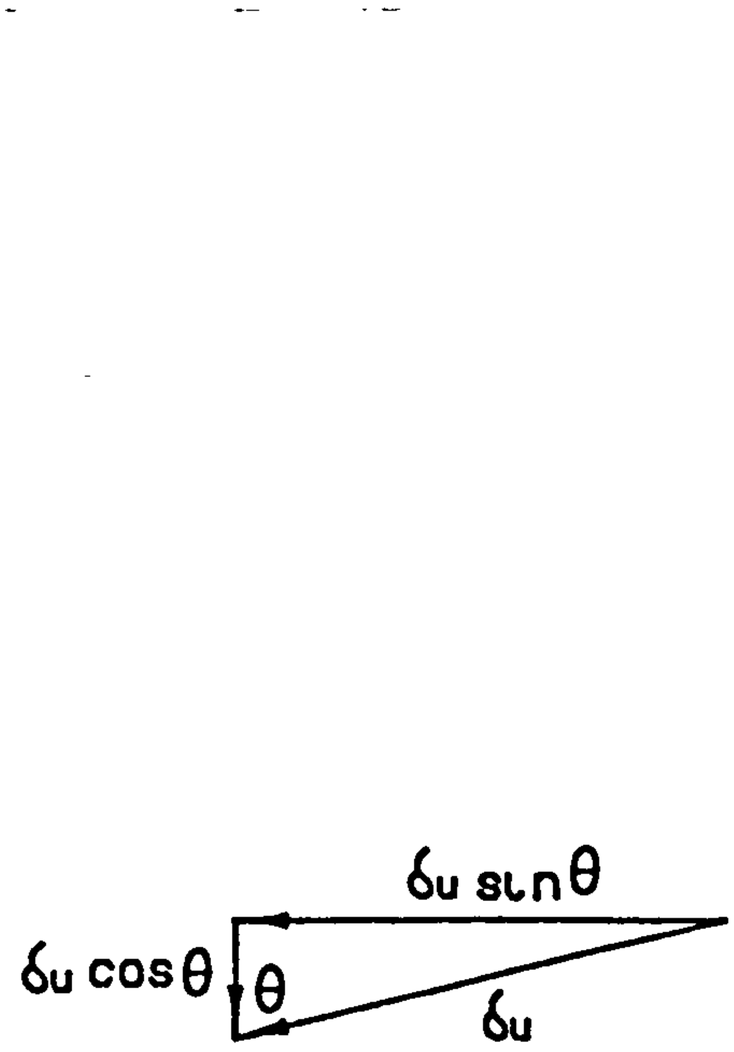

(d)

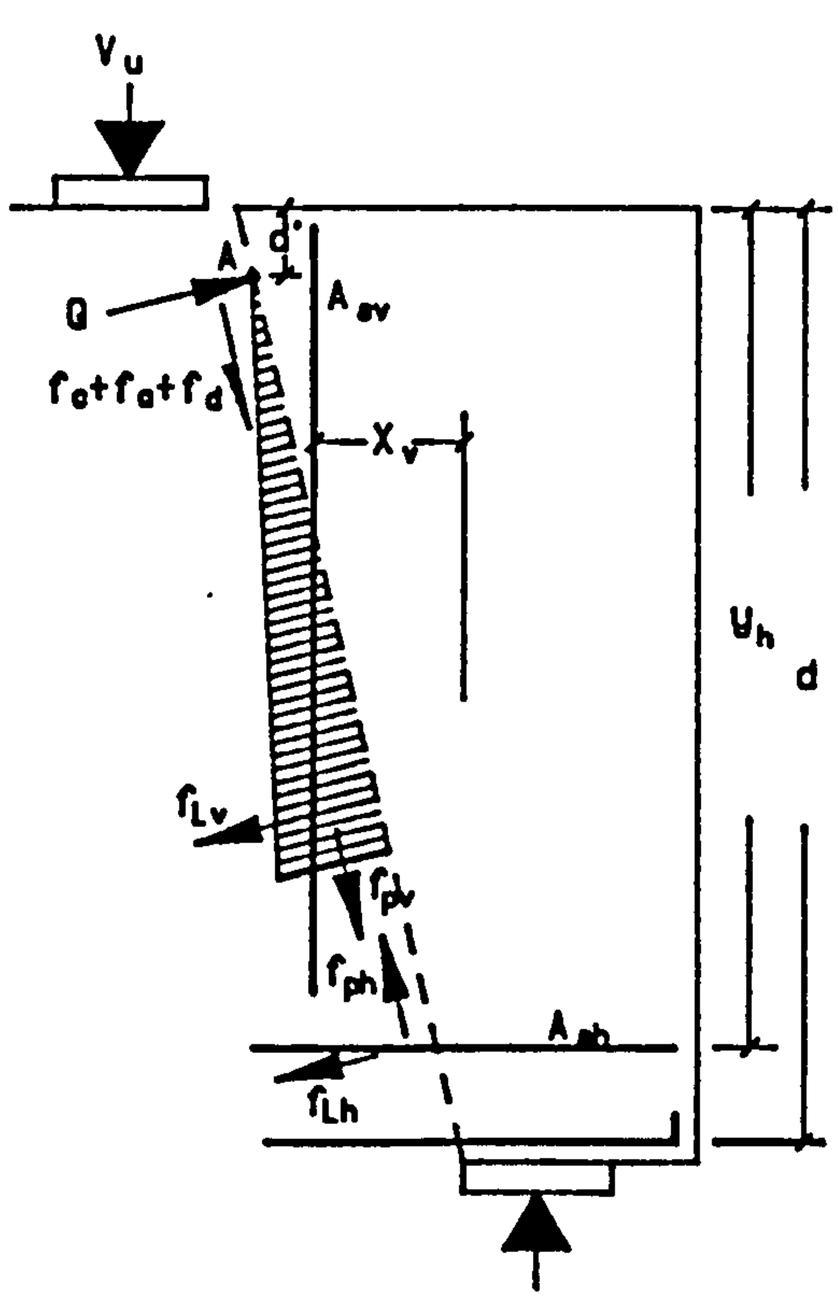

(b)

Fig.7.10 Proposed failure mechanism.

As shown in fig.7.10b, the shear crack is formed at an angle θ with the horizontal and according to the assumptions 3-5 above, we may write

$$\epsilon_{sh} = k \cdot \delta_u \cdot \sin\theta \qquad (7.18)$$

if when $\theta=90$ degs., $\epsilon_{sh}=\epsilon_{yh}$ $\therefore$ $\epsilon_{yh}=k \cdot \delta_u$

thus $$\epsilon_{sh} = \epsilon_{yh} \cdot \sin\theta \qquad (7.19a)$$

similarly, $$\epsilon_{sv} = \epsilon_{yv} \cdot \cos\theta \qquad (7.19b)$$

and $$f_{sh} = f_{yh} \cdot \sin\theta \qquad (7.20a)$$

$$f_{sv} = f_{yv} \cdot \cos\theta \qquad (7.20b)$$

where $\epsilon_{sh}, \epsilon_{sv}$ = Strain in the horizontal and vertical reinforcement respectively.

$\epsilon_{yh}, \epsilon_{yv}$ = Yield strain in the horizontal and vertical reinforcement respectively.

f_{sh}, f_{sv} = Stress in the horizontal and vertical reinforcement respectively.

f_{yh}, f_{yv} = Yield stress in the horizontal and vertical reinforcement respectively.

Assuming a triangular distribution of stresses in the reinforcement resulting from the rotation of the concrete block about the centre of compression in the compression zone (point A). Tensile force in the reinforcement can be calculated as

$$T_h = A_{sh} \cdot f_{sh} (y_h - d') / (d - d')$$
$$= A_{sh} \cdot f_{yh} \cdot \sin\theta (y_h - d') / (d - d') \qquad (7.21a)$$

$$T_v = A_{sv} \cdot f_{sv} (H - X_v \cdot \tan\theta - d') / (d - d')$$
$$= A_{sv} \cdot f_{yv} \cdot \cos\theta (H - X_v \cdot \tan\theta - d') / (d - d') \qquad (7.21b)$$

where T_h, T_v = Tensile force in the horizontal and vertical reinforcement respectively.

d' = Depth of the centre of compression in the

compression zone (point A) from the top of the beam.

y_h = Depth of the horizontal reinforcement from the top of the beam.

X_v = Distance of the vertical reinforcement from the inner edge of the support.

H = Total height of the beam.

Stresses due to the reinforcement perpendicular and parallel to the crack are

$$f_{Lh} = T_h \cdot \sin\theta / (b \cdot S_h \cdot \operatorname{cosec}\theta)$$

$$= \frac{A_{sh} \cdot f_{yh} \cdot \sin^3\theta}{b \cdot S_h} \cdot \frac{y_h - d'}{d - d'} \qquad (7.22a)$$

$$f_{ph} = T_h \cdot \cos\theta / (b \cdot S_h \cdot \operatorname{cosec}\theta)$$

$$= \frac{A_{sh} \cdot f_{yh} \cdot \sin^2\theta \cdot \cos\theta}{b \cdot S_h} \cdot \frac{y_h - d'}{d - d'} \qquad (7.22b)$$

$$f_{Lv} = T_v \cdot \sin\theta / (b \cdot S_v \cdot \sec\theta)$$

$$= \frac{A_{sv} \cdot f_{yv} \cdot \cos^3\theta}{b \cdot S_v} \cdot \frac{H - X_v \cdot \tan\theta - d'}{d - d'} \qquad (7.22c)$$

$$f_{pv} = T_v \cdot \sin\theta / (b \cdot S_h \cdot \sec\theta)$$

$$= \frac{A_{sv} \cdot f_{yv} \cdot \cos^2\theta \cdot \sin\theta}{b \cdot S_v} \cdot \frac{H - X_v \cdot \tan\theta - d'}{d - d'} \qquad (7.22d)$$

where f_{Lh}, f_{ph} = Stresses perpendicular and parallel to the crack due to horizontal reinforcement respectively.

f_{Lv}, f_{pv} = Stresses perpendicular and parallel to the crack due to vertical reinforcement respectively.

As shown in figs.6.7-12, flexural cracks extended to a depth of 0.7H from the top. It is reasonable to assume that the maximum tensile stress in the concrete is at the tip of the crack. Below this point, the tensile stress is zero and a triangular distribution of tensile stress is assumed above it. Therefore, the tensile stress in the concrete in the direction perpendicular to the crack can be written as

$$f_t' = \begin{cases} f_t \cdot y/(0.7H-d') & \text{---------} \quad y < 0.7H \\ 0 & \text{---------} \quad y > 0.7H \end{cases} \tag{7.23}$$

where f_t' = Tensile stress of concrete perpendicular to the direction of the crack.
f_t = Tensile strength of concrete.
y = Distance from the top of the beam.

Stresses perpendicular to the direction of the crack should be taken as the maximum of $(f_{Lh}+f_{Lv})$ and f_t (i.e.)

$$f_L = \max(f_{Lh}+f_{Lv}, f_t) \tag{7.24}$$

Two modes of failure of reinforced concrete deep beams are considered. They are (1) splitting failure along the crack and (2) shear failure along the crack.

MODE 1 — Splitting failure

Consider the rotation of the concrete block about point A (fig.7.10b) and failure of the beam is due to the splitting of the concrete block. By taking moments about point A, thus

$$\therefore \quad V_{u1} = \int_{J_0}^{H} \frac{f_L \cdot b \cdot \mathrm{cosec}^2\theta \cdot (y-d')}{X_c - d' \cdot \cot\theta}\, d(y) \qquad (7.25)$$

where X_c = Clear shear span,

V_{u1} = Ultimate shear capacity of the reinforced concrete deep beam estimated by failure mode 1.

MODE 2 -- Shear failure

Consider the forces acting along the direction of the crack. They include the components of forces of the reinforcement, shear stress in the compression zone, aggregate interlocking stress and dowel action of the reinforcement. By considering the equilibrium of these forces, the shear strength of the reinforced concrete deep beam can be found.

where v_c = Shear stress in the compressive zone,

f_a = Shear stress due to aggregate interlock effect,

f_d = Shear stress due to dowel action of the reinforcement,

V_{u2} = Ultimate shear capacity of the reinforced concrete deep beam estimated by failure mode 2.

However, estimation of v_c, f_a and f_d is necessary before the shear capacity of a deep beam can be found.

Shear stress in the compressive zone can be estimated by the recommendation of ACI-318 [2], Eq.5.22.

$$v_c' = (3.5-2.5M/V\cdot d)(1.9\sqrt{f_c'} + 2500p\cdot V\cdot d/M)$$

$$< 2.5(1.9\sqrt{f_c'} + 2500p\cdot V\cdot d/M) \qquad (5.22)$$

$$< 6\sqrt{f_c'}$$

Aggregate interlocking stress is dependent on the restraining stress (stress perpendicular to the direction of the crack). It was suggested by Paulay and Loeber [70] that

$$f_L = 0.473 f_a'^{1.03} \quad (psi) \qquad (7.1)$$

Fenwick and Paulay [24] stated that the aggregate interlocking stress was also proportional to the square root of the cylinder strength of concrete

$$f_a' = k\cdot\sqrt{f_c'} \qquad (7.27)$$

where k = proportional constant.

Eq.7.1 may be modified without much loss of accuracy to

$$f_L = 0.582\ f_a' \qquad (7.28)$$

Since Paulay and Leober [70] used an average concrete cube strength of 5300 psi. in their experiment, therefore, the appropriate proportional constant should be taken as k=0.165 . Thus, the aggregate interlocking stress can be estimated as

$$f_a' = 0.165\sqrt{f_c'}\cdot(f_{Lh}+f_{Lv})/0.582 \qquad (7.29)$$

It is recognized that the aggregate interlock effect can only happen in the region where the crack has formed, otherwise only shear stress of the concrete is effective. Therefore, the sum of the shear stress in the concrete and the aggregate

interlocking stress should be equal to the maximum of the aggregate interlocking stress in Eq.7.29 or the concrete shear stress in Eq.5.22 in any position of the crack, (i.e.)

$$f_a+v_c = \max(f_a', v_c) \qquad (7.30)$$

Stresses due to dowel action are considered to be proportional to the square of the sine of the angle between the reinforcement and the crack (Eq.7.16). A proportional constant of 0.45 is suggested by Kong's formula (Eq.5.23). He used a constant of 130N/mm^2 for plain steel bars with yield stress of 286N/mm^2. Therefore, dowel stress, f_d can be estimated as

$$f_d = 0.45(f_h.\sin^2\theta + f_v.\cos^2\theta) \qquad (7.31)$$

where f_h = Stress of the horizontal reinforcement,
f_v = Stress of the vertical reinforcement,
f_d = Dowel stress of the reinforcement.

Substituting Eqs.7.22, 30 and 31 into Eq.7.26, the shear capacity of the reinforced concrete deep beam with failure mode 2 can be found.

The shear capacity of the reinforced concrete deep beam should be the minimum of the values obtained by Eq.7.25 and 7.26. In the case of deep beams with uniformly distributed load, the shear crack is assumed to form along the line joining the inner edge of the support and the third span on the top of the beam.

7.7 COMPARISON WITH TEST RESULTS

Test results from various sources [44,42,47,73,69] are analysed with the proposed method and compared with methods given by Paiva and Siess [69], Ramakrishnan and Ananthanarayana [73], Kong [45] and Al-Najjim [63]. The effectiveness of different design guides; CP110 [19], CIRIA [68] and ACI-318 [1] are also discussed. The results are presented in table 7.1 as ratios of the ultimate load obtained during tests to the values given by different design guides and formulae. Figures with experimental ultimate loads varies the calculated values are given in figs.7.11-18 together with a diagonal line of 45 degrees which represents the calculated values equal to the experimental ones.

Among the design guides, CP110 gives the most conservative results. It gives an average safety factor of 6.5 and a high standard deviation of 4.4. Generally, beams with small shear span to depth ratio have a higher factor of safety. Fig.7.11 shows that none of the beams was over-estimated by British Code CP110 and most of its estimates lie within a 50kN range even for those with 600kN capacity. The CIRIA design guide gives much better results than CP110, in fact it is the best among the three codes: CP110, CIRIA and ACI-318. It gives an average value of experimental to calculated ultimate shear strength of 1.706 and a standard deviation of 0.38. Fig.7.12 shows that CIRIA design guide gives more conservative results for higher

strength deep beams and it under-estimates the shear strength for all the beams except for a few of Ramakrishnan and Ananthanarayana's single point loaded deep beams which failed in flexure rather than shear. An average factor of safety of 2.054 and a standard deviation of 0.995 are obtained with the recommendations for the design of deep beams in the ACI-318 Design Code. It gives slightly more scattered results than with the CIRIA design guide as shown in fig.7.13.

Paiva and Siess's empirical formula on average gives only a slight over-estimation of 2.2% and with a reasonable standard deviation of 0.215. Generally, this formula can predict Kong's beams quite well but it over-estimates Ramakrishnan and Ananthanarayana's beams with concentrated loads by 36% (standard deviation of 0.068) and under-estimates those with uniformly distributed load by 11% (standard deviation of 0.316). An average ratio of experimental to calculated ultimate shear strength of 0.969 and 0.671 (corresponding standard deviation of 0.103 and 0.127) is obtained with their beams which failed in shear and flexure respectively.

In the calculation with Ramakrishnan and Ananthanarayana's formula, k=1.57 is used and it is based on the use of the cylinder splitting test in the estimation of the tensile strength of concrete. This formula gives an excellent mean value of 1.007 in the ratio of experimental to calculated shear strength of deep beams, but the standard deviation is high at

0.26. The simplicity of this formula is one of its great advantages, and therefore, it can be used for a primary estimate of the shear strength of deep beams. However, it should be noted that the effect of reinforcement on the shear strength of deep beams is not taken into account by this formula.

The formula introduced by Kong and later adopted by CIRIA with modifications, as a design tool for reinforced concrete deep beams gives good results as shown in table 7.1 and fig.7.16. It has an overall average values of experimental to calculated shear strength of 1.037 (3.7% under-estimate) and a modest standard deviaton of 0.208.

Al-Najjim's theory was based on the compression of a curved strut which was deflected by the present of web reinforcement inside the beams. As shown in table 7.1, Al-Najjim's theory gives an average of 38% under-estimation and a high standard deviation of 0.354. Most of the points in fig.7.17 lie in the region where experimental ultimate load is greater than the estimated one, except for a few of Paiva and Ramakrishnan's data which fall outside this region. This method of assessing the ultimate shear strength is rather complicated and no particularly good results can be obtained, therefore, its practical use is of limited value. However, it has suggested an explanation of the behaviour of reinforced concrete deep beams after cracking.

Beam no.	L (mm.)	H (mm.)	L/H	X_o (mm.)	X_o/H	f_o N/mm^2	f_t N/mm^2	$P_{u\,(test)}$ (kN)	Ultimate shear strength ratio P_y (test) / P_y (cal.)													
									CP110		CIRIA Eq.5.27		ACI-318 Eq.5.23		Paiva Eq.5.7		Ramakrish. Eq.5.12		Kong Eq.5.23		Al-Najjim Eq.5.28, 36		Proposed Eq.7.25, 26		Proposed Design Guide	
TWO POINT LOADED -- Kong's (1970) normal weight concrete beams																										
1-30	762	762	1.0	178	0.23	21.5	2.83	477.7	1.10	x = 7.344 σ = 3.629	1.66	x = 1.751 σ = 0.163	1.49	x = 1.694 σ = 0.235	0.97	x = 1.011 σ = 0.118	0.93	x = 1.043 σ = 0.080	0.98	x = 1.046 σ = 0.063	1.67	x = 1.206 σ = 0.493	0.94	x = 0.992 σ = 0.083	1.39	x = 1.485 σ = 0.128
2-30	762	762		178		19.2	2.62	498.3	2.53		1.82		1.87		1.09		1.04		1.09		1.98		1.05		1.57	
3-30	762	762		178		22.6	2.85	553.3	9.36		1.65		1.59		0.89		1.06		0.99		0.77		0.96		1.45	
4-30	762	762		178		22.0	2.57	483.6	8.28		1.59		1.41		0.90		1.03		1.02		1.56		0.94		1.40	
5-30	762	762		178		18.6	2.50	478.7	1.98		1.65		1.52		0.95		1.05		1.02		1.70		1.00		1.47	
6-30	762	762		178		26.1	3.06	616.1	10.07		1.86		1.73		1.05		1.10		1.11		0.82		1.01		1.53	
7-30A	762	762		178		25.1	2.98	505.2	8.26		1.65		1.83		0.93		0.93		0.99		1.63		0.95		1.41	
7-30B	762	762		178		19.2	3.06	599.4	10.99		2.14		2.25		1.29		1.07		1.12		0.86		1.20		1.80	
7-30C	762	762		178		25.1	2.98	528.8	8.65		1.65		1.62		0.94		0.97		0.99		0.71		0.90		1.36	
7-30D	762	762		178		21.3	2.69	527.8	9.20		1.70		1.56		1.00		1.08		1.04		0.74		0.93		1.40	
7-30E	762	762		178		21.3	2.69	594.5	10.36		1.89		1.76		1.11		1.21		1.16		0.83		1.03		1.56	
1-25	762	635	1.2	178	0.28	24.6	2.97	448.3	1.23	x = 5.489 σ = 3.909	1.75	x = 1.765 σ = 0.152	1.58	x = 1.673 σ = 0.210	1.02	x = 1.030 σ = 0.112	0.99	x = 1.068 σ = 0.086	1.05	x = 1.062 σ = 0.093	1.46	x = 1.526 σ = 0.193	0.92	x = 0.968 σ = 0.083	1.38	x = 1.457 σ = 0.095
2-25	762	635		178		18.6	2.55	448.3	2.72		1.97		2.05		1.21		1.16		1.19		1.92		1.08		1.61	
3-25	762	635		178		21.0	2.76	451.3	9.04		1.64		1.63		0.91		1.08		0.99		1.43		0.94		1.43	
4-25	762	635		178		21.0	2.76	402.2	8.05		1.61		1.45		0.94		0.96		0.96		1.42		0.91		1.36	
5-25	762	635		178		19.2	2.61	415.9	2.04		1.69		1.57		0.99		1.05		1.02		1.49		0.96		1.43	
6-25	762	635		178		25.1	2.98	530.7	9.91		1.93		1.76		1.11		1.17		1.16		1.45		1.00		1.53	
1-20	762	508	1.5	178	0.35	21.4	2.79	378.7	1.32	x = 5.945 σ = 4.203	1.94	x = 1.988 σ = 0.208	1.85	x = 1.993 σ = 0.326	1.20	x = 1.208 σ = 0.138	1.12	x = 1.182 σ = 0.154	1.15	x = 1.178 σ = 0.143	1.47	x = 1.495 σ = 0.217	0.94	x = 1.015 σ = 0.098	1.42	x = 1.552 σ = 0.159
2-20	762	508		178		20.0	2.69	430.7	3.20		2.28		2.57		1.42		1.32		1.36		1.91		1.15		1.75	
3-20	762	508		178		19.2	2.61	415.9	10.05		2.01		1.99		1.24		1.31		1.22		1.50		1.09		1.68	
4-20	762	508		178		21.1	2.88	361.0	8.38		1.81		1.83		1.08		1.03		1.05		1.40		0.94		1.43	
5-20	762	508		178		20.1	2.88	345.3	2.10		1.73		2.62		1.04		0.99		0.99		1.28		0.91		1.38	
6-20	762	508		178		26.1	3.06	490.5	10.62		2.16		2.10		1.27		1.32		1.30		1.41		1.06		1.65	
1-15	762	381	2.0	178	0.47	21.2	2.79	328.6	1.53	x = 5.028 σ = 3.418	2.22	x = 1.850 σ = 0.282	2.48	x = 2.082 σ = 0.448	1.44	x = 1.142 σ = 0.194	1.29	x = 1.115 σ = 0.152	1.33	x = 1.115 σ = 0.155	1.60	x = 1.300 σ = 0.211	1.11	x = 0.972 σ = 0.131	1.53	x = 1.423 σ = 0.199
2-15	762	381		178		22.8	2.90	279.6	2.68		1.86		2.67		1.18		1.06		1.11		1.38		0.96		1.38	
3-15	762	381		178		21.9	2.89	318.8	8.83		1.94		1.92		1.14		1.21		1.15		1.33		1.03		1.65	
4-15	762	381		178		22.0	2.57	218.8	6.05		1.43		1.69		0.88		0.93		0.92		1.01		0.77		1.13	
5-15	762	381		178		21.9	2.89	254.1	2.03		1.63		1.53		0.99		0.96		0.96		1.11		0.87		1.27	
6-15	762	381		178		26.1	3.05	345.3	9.05		2.02		2.20		1.22		1.24		1.22		1.37		1.07		1.58	
1-10	762	254	3.0	178	0.70	21.7	2.83	178.5	1.28	x = 4.403 σ = 2.677	1.81	x = 1.832 σ = 0.203	2.94	x = 3.593 σ = 1.525	1.31	x = 1.238 σ = 0.172	1.04	x = 1.073 σ = 0.107	1.09	x = 1.123 σ = 0.118	1.39	x = 1.442 σ = 0.181	1.02	x = 1.100 σ = 0.104	1.28	x = 1.606 σ = 0.273
2-10	762	254		178		20.1	2.72	199.1	2.90		2.14		5.90		1.51		1.20		1.28		1.65		1.22		1.94	
3-10	762	254		178		22.6	2.70	172.7	6.34		1.69		2.54		1.09		1.05		1.07		1.37		1.07		1.78	
4-10	762	254		178		22.6	2.70	191.3	7.03		1.93		5.15		1.31		1.17		1.23		1.55		1.18		1.91	
5-10	762	254		178		22.6	2.85	156.0	1.87		1.56		2.42		1.05		0.90		0.95		1.19		0.95		1.42	
6-10	762	254		178		25.1	2.98	196.2	7.00		1.83		2.61		1.16		1.08		1.12		1.50		1.16		1.80	
								mean	5.887		1.825		2.134		1.109		1.089		1.097		1.367		1.007		1.516	
								standard deviation	3.567		0.206		0.943		0.166		0.118		0.116		0.334		0.101		0.186	

Table 7.1a P_u (test) / P_u (cal.) calculated by various researchers.

Beam no.	L (mm.)	H (mm.)	L/H	X_o (mm.)	X_o/H	f_c N/mm^2	f_t N/mm^2	P_u (test) (kN)	Ultimate shear strength ratio P_u(test)/P_u(cal.)													
									CP110		CIRIA Eq.5.27		ACI-318 Eq.5.29		Paiva Eq.5.7		Ramakrish. Eq.5.12		Kong Eq.5.23		Al-Najjim Eq.5.28,36		Proposed Eq.7.25,26		Proposed Design Guide	
TWO POINT LOADED -- Kong's (1971) Light weight concrete beams																										
L1-30	762	762	1.0	178	0.23	28.2	3.64	448.1	1.21	x = 10.89 σ = 5.893	1.45	x = 1.634 σ = 0.175	1.33	x = 1.578 σ = 0.134	0.78	x = 0.868 σ = 0.085	0.68	x = 0.839 σ = 0.123	0.90	x = 1.016 σ = 0.096	1.26	x = 1.361 σ = 0.145	0.87	x = 0.990 σ = 0.112	1.28	x = 1.488 σ = 0.170
L2-30	762	762		178		28.2	3.64	408.5	3.63		1.32		1.40		0.71		0.62		0.82		1.19		0.81		1.19	
L3-30	762	762		178		28.2	3.64	677.9	17.58		1.99		1.74		1.03		1.02		1.11		1.67		1.23		1.83	
L4-30	762	762		178		28.2	3.64	557.4	14.45		1.77		1.68		0.94		0.84		1.07		1.54		1.09		1.61	
L5-30	762	762		178		27.9	3.49	558.3	1.50		1.64		1.44		0.85		0.88		0.94		1.39		0.99		1.47	
L6-30	762	762		178		30.0	3.30	555.6	14.41		1.68		1.64		0.90		0.92		1.10		1.32		1.01		1.50	
L7-30A	762	762		178		27.9	3.49	478.7	12.41		1.56		1.72		0.84		0.75		1.00		1.42		0.95		1.40	
L7-30B	762	762		178		27.9	3.49	490.3	12.71		1.57		1.66		0.85		0.77		0.99		1.23		0.94		1.40	
L7-30C	762	762		178		30.0	3.30	512.1	13.28		1.57		1.59		0.83		0.85		1.05		1.22		0.94		1.40	
L7-30D	762	762		178		30.0	3.30	566.7	14.69		1.70		1.59		0.90		0.94		1.10		1.35		1.02		1.52	
L7-30E	762	762		178		30.0	3.30	580.1	15.04		1.72		1.55		0.92		0.96		1.10		1.38		1.04		1.55	
L1-25	762	635	1.2	178	0.28	28.6	3.58	418.7	1.35	x = 5.278 σ = 5.788	1.61	x = 1.695 σ = 0.093	1.50	x = 1.640 σ = 0.130	0.88	x = 0.908 σ = 0.028	0.77	x = 0.830 σ = 0.074	1.00	x = 1.018 σ = 0.220	1.41	x = 1.313 σ = 0.120	0.90	x = 0.988 σ = 0.062	1.33	x = 1.438 σ = 0.098
L2-25	762	635		178		28.6	3.58	419.6	4.32		1.62		1.76		0.89		0.77		1.01		1.42		0.93		1.38	
L3-25	762	635		178		28.6	3.58	-	-		-		-		-		-		-		-		-		-	
L4-25	762	635		178		28.6	3.58	-	-		-		-		-		-		-		-		-		-	
L5-25	762	635		178		31.7	3.79	532.1	1.71		1.79		1.56		0.92		0.92		1.01		1.23		1.03		1.53	
L6-25	762	635		178		31.7	3.79	497.8	13.73		1.76		1.74		0.94		0.86		1.05		1.19		1.01		1.51	
L1-20	762	508	1.5	178	0.35	27.0	3.48	377.8	1.52	x = 8.170 σ = 6.380	1.86	x = 0.898 σ = 0.235	1.88	x = 1.953 σ = 0.310	1.07	x = 1.048 σ = 0.143	0.89	x = 1.017 σ = 0.142	1.11	x = 1.150 σ = 0.107	1.63	x = 1.443 σ = 0.215	0.98	x = 1.057 σ = 0.139	1.44	x = 1.560 σ = 0.236
L2-20	762	508		178		27.0	3.48	356.9	4.43		1.77		2.18		1.01		0.84		1.06		1.55		0.96		1.43	
L3-20	762	508		178		27.0	3.48	497.8	15.30		2.26		2.01		1.23		1.18		1.24		1.48		1.30		1.96	
L4-20	762	508		178		27.0	3.48	417.8	12.84		2.04		2.25		1.15		1.99		1.20		1.62		1.13		1.68	
L5-20	762	508		178		33.6	3.05	379.6	1.53		1.57		1.38		0.81		1.02		1.01		1.08		0.93		1.29	
L6-20	762	508		178		33.6	3.05	437.8	13.38		1.89		2.02		1.02		1.18		1.28		1.30		1.04		1.56	
L1-15	762	381	2.0	178	0.47	34.3	3.53	274.7	1.49	x = 7.222 σ = 5.188	1.64	x = 0.832 σ = 0.111	2.00	x = 2.223 σ = 0.534	0.93	x = 1.027 σ = 0.058	0.85	x = 0.960 σ = 0.073	1.03	x = 1.082 σ = 0.080	1.62	x = 1.575 σ = 0.177	1.04	x = 1.513 σ = 0.085	1.28	x = 1.515 σ = 0.149
L2-15	762	381		178		34.3	3.53	296.0	4.75		1.79		2.84		1.00		0.92		1.14		1.77		1.15		1.45	
L3-15	762	381		178		34.3	3.53	344.9	12.63		1.95		1.75		1.04		1.07		1.14		1.55		1.29		1.71	
L4-15	762	381		178		34.3	3.53	318.7	11.67		1.92		2.89		1.06		0.99		1.20		1.76		1.24		1.58	
L5-15	762	381		178		28.1	3.43	301.8	1.64		1.82		1.61		1.03		0.97		0.99		1.34		1.11		1.47	
L6-15	762	381		178		28.1	3.43	298.7	11.15		1.87		2.25		1.10		0.96		1.05		1.41		1.09		1.60	
L1-10	762	254	3.0	178	0.70	29.6	3.84	179.1	1.50	x = 5.570 σ = 3.973	1.76	x = 1.770 σ = 0.181	3.17	x = 4.700 σ = 2.852	1.18	x = 1.123 σ = 0.105	0.77	x = 0.807 σ = 0.089	0.92	x = 0.985 σ = 0.094	1.69	x = 1.617 σ = 0.156	1.13	x = 1.203 σ = 0.123	1.39	x = 1.652 σ = 0.271
L2-10	762	254		178		29.6	3.84	150.2	3.54		1.53		5.49		0.99		0.64		0.82		1.48		1.00		1.38	
L3-10	762	254		178		29.6	3.84	184.5	9.04		1.84		3.83		1.14		0.79		0.97		1.58		1.25		1.91	
L4-10	762	254		178		29.6	3.84	196.0	9.60		2.01		10.29		1.29		0.84		1.09		1.87		1.32		1.96	
L5-10	762	254		178		33.5	3.45	184.0	1.53		1.68		2.13		1.05		0.88		0.95		1.44		1.20		1.46	
L6-10	762	254		178		33.5	3.45	193.4	9.29		1.80		3.29		1.09		0.92		1.05		1.64		1.32		1.81	
mean									8.147		1.750		2.338		0.981		0.886		1.045		1.455		1.068		1.523	
standard deviation									5.660		0.188		1.663		0.134		0.132		0.106		0.193		0.139		0.197	

Table 7.1b P_u(test)/P_u(cal.) calculated by various researchers.

Beam no.	L (mm.)	H (mm.)	L/H	X_o (mm.)	X_o/H	f_{o}^{2} N/mm^2	f_{t}^{2} N/mm^2	$P_{u\,(test)}$ (kN)	Ultimate shear strength ratio P_u (test)/P_u (cal.)													
									CP110	CIRIA Eq.5.27		ACI-318 Eq.5.23		Paiva Eq.5.7		Ramakrish. Eq.5.12		Kong Eq.5.23		Al-Najjim Eq.5.28,36		Proposed Eq.7.25,26	Proposed Design Guide
TWO POINT LOADED -- Kong's (1972) light weight concrete beams																							
1A-1/0.23	508	508	1.0	117	0.23	29.9	3.41	511.2	2.58	x = 8.350 σ = 8.780	2.18	x = 2.128 σ = 0.154	2.29	x = 2.065 σ = 0.212	1.19	x = 1.143 σ = 0.091	1.23	x = 1.215 σ = 0.111	1.30	x = 1.285 σ = 0.110	1.46	x = 1.350 σ = 0.141	0.87	x = 0.853 σ = 0.074	1.32	x = 1.243 σ = 0.134
2A-1/0.23	508	508		117		29.2	3.43	563.2	14.94		2.31		2.19		1.23		1.35		1.29		1.48		0.95		1.43	
3A-1/0.23	508	508		117		31.5	3.74	489.0	2.46		1.95		1.83		1.02		1.08		1.07		1.20		0.79		1.20	
4A-1/0.23	508	508		117		29.9	3.48	508.0	13.42		2.07		1.95		1.13		1.20		1.16		1.26		0.80		1.23	
1A-2/0.23	1016	508	2.0	117	0.23	29.9	3.41	483.6	2.44	x = 8.201 σ = 8.341	2.07	x = 2.087 σ = 0.117	2.03	x = 1.988 σ = 0.138	1.12	x = 1.107 σ = 0.070	1.17	x = 1.237 σ = 0.100	1.23	x = 1.198 σ = 0.088	1.38	x = 1.268 σ = 0.192	0.82	x = 0.813 σ = 0.072	1.24	x = 1.239 σ = 0.106
1B-2/0.23	1016	508		117		29.7	3.35	444.5	1.24		1.90		1.69		1.04		1.09		1.14		1.24		0.75		1.13	
1C-2/0.23	1016	508		117		29.7	3.35	506.7	2.56		2.17		2.14		1.18		1.24		1.30		1.45		0.86		1.30	
2A-2/0.23	1016	508		117		29.2	3.43	573.4	15.21		2.36		2.20		1.25		1.38		1.32		1.51		0.96		1.46	
2B-2/0.23	1016	508		117		31.8	3.38	549.0	14.35		2.06		2.02		1.05		1.34		1.13		1.27		0.77		1.19	
2C-2/0.23	1016	508		117		31.8	3.38	529.0	13.83		2.10		1.94		1.10		1.29		1.22		1.31		0.86		1.30	
3A-2/0.23	1016	508		117		31.5	3.74	511.2	2.58		2.04		1.89		1.07		1.12		1.12		1.25		0.83		1.24	
3B-2/0.23	1016	508		117		32.0	3.72	533.4	1.49		1.99		1.95		1.02		1.18		1.05		1.21		0.74		1.13	
3C-2/0.23	1016	508		117		32.0	3.72	515.6	2.60		2.04		1.89		1.06		1.14		1.13		1.25		0.82		1.25	
4A-2/0.23	1016	508		117		29.9	3.48	533.4	14.09		2.17		2.11		1.18		1.26		1.22		1.32		0.84		1.30	
4B-2/0.23	1016	508		117		33.3	3.54	533.4	13.93		1.99		1.92		1.06		1.24		1.10		0.73		0.68		1.05	
4C-2/0.23	1016	508		117		31.4	3.19	537.8	14.09		2.15		2.08		1.15		1.39		1.29		1.29		0.83		1.28	
1A-3/0.23	1524	508	3.0	117	0.23	29.9	3.41	509.0	2.57	x = 7.773 σ = 8.256	2.17	x = 2.038 σ = 0.145	2.02	x = 1.819 σ = 0.123	1.18	x = 1.081 σ = 0.087	1.23	x = 1.200 σ = 0.082	1.29	x = 1.143 σ = 0.113	1.45	x = 1.219 σ = 0.235	0.86	x = 0.784 σ = 0.069	1.30	x = 1.199 σ = 0.122
1B-3/0.23	1524	508		117		29.7	3.35	489.0	1.36		2.09		1.71		1.14		1.20		1.25		1.36		0.82		1.24	
2A-3/0.23	1524	508		117		29.2	3.43	554.3	14.70		2.28		2.00		1.21		1.33		1.27		1.46		0.93		1.41	
2B-3/0.23	1524	508		117		31.8	3.38	529.0	13.83		1.99		1.79		1.02		1.29		1.09		1.22		0.74		1.15	
3A-3/0.23	1524	508		117		31.5	3.74	514.3	2.59		2.05		1.74		1.07		1.13		1.12		1.26		0.83		1.25	
3B-3/0.23	1524	508		117		32.0	3.72	511.2	1.42		1.91		1.72		0.98		1.13		1.00		1.16		0.71		1.08	
4A-3/0.23	1524	508		117		29.9	3.48	445.8	11.78		1.82		1.81		0.99		1.05		1.02		1.11		0.70		1.08	
4B-3/0.23	1524	508		117		33.3	3.54	533.4	13.93		1.99		1.76		1.06		1.24		1.10		0.73		0.68		1.08	
1A-3/0.70	1524	508	3.0	356	0.70	30.5	3.38	351.2	1.77	x = 5.111 σ = 3.867	1.82	x = 1.711 σ = 0.207	2.43	x = 2.034 σ = 0.404	1.19	x = 1.094 σ = 0.144	0.85	x = 0.793 σ = 0.087	1.11	x = 0.995 σ = 0.106	1.46	x = 1.253 σ = 0.188	1.09	x = 1.003 σ = 0.107	1.33	x = 1.305 σ = 0.198
1C-3/0.70	1524	508		356		29.7	3.38	333.4	1.68		1.75		2.32		1.15		0.81		1.05		1.39		1.03		1.26	
2A-3/0.70	1524	508		356		29.9	4.17	375.6	9.92		1.92		2.19		1.20		0.74		0.99		1.42		1.09		1.77	
2C-3/0.70	1524	508		356		31.8	3.38	280.0	7.32		1.40		1.61		0.86		0.68		0.84		1.02		0.86		1.27	
3A-3/0.70	1524	508		356		30.5	3.38	388.9	1.96		1.94		1.70		1.23		0.95		1.13		1.37		1.14		1.48	
3C-3/0.70	1524	508		356		32.0	3.72	333.4	1.68		1.63		1.45		1.02		0.74		0.91		1.16		0.96		1.24	
4A-3/0.70	1524	508		356		27.4	3.32	340.0	9.11		1.80		2.53		1.19		0.84		1.04		1.23		1.00		1.59	
4C-3/0.70	1524	508		356		31.5	3.19	284.5	7.45		1.43		2.04		0.91		0.73		0.89		0.97		0.85		1.22	
1A-3/0.70Z	1524	508	3.0	356	0.70	30.5	3.38	277.8	1.40	x = 4.483 σ = 3.878	1.44	x = 1.555 σ = 0.096	2.68	x = 2.475 σ = 0.568	0.94	x = 1.003 σ = 0.048	0.68	x = 0.703 σ = 0.096	0.88	x = 0.895 σ = 0.025	1.41	x = 1.370 σ = 0.094	0.98	x = 1.023 σ = 0.056	1.20	x = 1.405 σ = 0.214
2A-3/0.70Z	1524	508		356		29.9	4.17	326.7	8.63		1.67		2.50		1.05		0.64		0.86		1.47		1.08		1.69	
3A-3/0.70Z	1524	508		356		30.5	3.38	317.8	1.60		1.58		1.69		1.01		0.77		0.92		1.35		1.06		1.29	
4A-3/0.70Z	1524	508		356		27.4	3.32	288.9	7.74		1.53		3.03		1.01		0.72		0.88		1.25		0.97		1.44	
								mean	7.063		1.938		2.023		1.091		1.068		1.103		1.247		0.876		1.289	
								standard deviation	5.527		0.250		0.327		0.197		0.238		0.143		0.186		0.125		0.162	

Table 7.1c P_u (test)/P_u (cal.) calculated by various researchers.

Beam no.	L (mm.)	H (mm.)	X_o (mm.)	f_c N/mm²	f_t N/mm²	$P_{u\,(test)}$ (kN)	Ultimate shear strength ratio P_u (test) / P_u (cal.)													
							CP110		CIRIA Eq.5.27		ACI-318 Eq.5.23		Pavia Eq.5.7		Ramakrish. Eq.5.12		Kong Eq.5.23		Al-Najjim Eq.5.28,36		Proposed Eq.7.25,26		Proposed Design Guide	
TWO POINT LOADED -- Ramakrishnan and Ananarayana's (1968) normal weight concrete beams																							
A1	686	381	140	24.0	2.27	113.3	5.84	x = 6.604 σ = 1.178	0.91	x = 1.028 σ = 0.083	1.57	x = 1.322 σ = 0.142	0.55	x = 0.596 σ = 0.040	0.55	x = 0.682 σ = 0.095	0.68	x = 0.794 σ = 0.065	1.94	x = 1.922 σ = 0.273	1.04	x = 0.972 σ = 0.048	1.33	x = 1.304 σ = 0.085
A2	686	508	140	20.4	2.03	161.4	6.35		0.99		1.27		0.59		0.65		0.76		1.84		0.96		1.23	
A3	686	572	140	23.4	2.22	212.9	7.16		1.05		1.26		0.59		0.68		0.79		1.95		0.94		1.22	
A4	686	762	140	27.3	2.47	324.5	8.33		1.13		1.30		0.59		0.72		0.83		2.32		1.00		1.43	
A4(R)	686	762	140	12.3	1.41	216.9	5.34		1.06		1.21		0.66		0.81		0.91		1.56		0.92		1.31	
B1	686	381	140	20.4	2.03	135.6	4.41	x = 5.800 σ = 1.510	1.01	x = 1.058 σ = 0.088	1.64	x = 1.343 σ = 0.201	0.64	x = 0.618 σ = 0.021	0.73	x = 0.748 σ = 0.035	0.76	x = 0.790 σ = 0.053	0.83	x = 0.913 σ = 0.137	0.58	x = 0.820 σ = 0.086	0.82	x = 0.913 σ = 0.135
B2	686	508	140	21.3	2.09	180.0	4.68		0.97		1.20		0.59		0.71		0.74		0.81		0.54		0.81	
B3	686	572	140	24.8	2.31	247.1	5.56		1.08		1.25		0.62		0.76		0.80		0.91		0.62		0.92	
B4	686	762	140	28.4	2.53	378.3	7.74		1.17		1.28		0.62		0.79		0.84		1.11		0.74		1.10	
C1	686	381	140	21.5	2.10	180.0	2.74	x = 2.715 σ = 0.343	1.25	x = 1.196 σ = 0.123	1.31	x = 1.135 σ = 0.187	0.77	x = 0.713 σ = 0.070	0.94	x = 0.905 σ = 0.088	0.93	x = 0.903 σ = 0.079	0.97	x = 1.055 σ = 0.109	0.71	x = 0.898 σ = 0.043	1.03	x = 1.030 σ = 0.065
C2	686	508	140	24.4	2.28	280.9	3.18		1.34		1.28		0.77		0.98		1.00		1.05		0.75		1.12	
C3	686	572	140	19.6	1.98	236.9	2.56		1.14		1.01		0.68		0.87		0.86		0.99		0.65		0.97	
C4	686	762	140	16.4	1.78	276.9	2.38		1.06		0.94		0.63		0.83		0.82		1.21		0.68		1.00	
						mean	5.098		1.089		1.271		0.639		0.771		0.826		1.345		0.779		1.099	
						standard deviation	1.995		0.117		0.186		0.068		0.118		0.087		0.511		0.171		0.197	

TWO POINT LOADED -- Pavia and Siess's (1965) normal weight concrete beams																								
G23S-11	610	330	102	24.6	Estimated by $f_t = 0.5\sqrt{f_c}$		179.7	8.96	x = 5.937 σ = 2.799	1.95	x = 1.811 σ = 0.246	1.94	x = 2.074 σ = 0.333	1.06	x = 0.969 σ = 0.103	1.38	x = 1.378 σ = 0.248	1.05	x = 0.833 σ = 0.121	1.36	x = 1.413 σ = 0.781	1.01	x = 0.872 σ = 0.156	1.43	x = 1.140 σ = 0.185
G33S-11	610	229	102	23.3			170.8	6.74		1.64		1.71		0.92		1.29		0.78		0.54		0.77		1.03	
G33S-12	610	229	102	19.9			169.0	7.03		1.71		1.72		0.98		1.38		0.80		0.58		0.77		1.10	
G33S-31	610	229	102	19.9			213.9	7.88		2.15		2.15		1.08		1.75		0.78		0.75		0.68		0.99	
G33S-32	610	229	102	20.1			202.8	1.15		2.03		2.03		1.02		1.66		0.71		2.96		0.64		0.88	
G34S-11	610	229	102	35.2			219.7	8.09		1.83		2.10		0.95		1.35		0.91		1.70		0.97		1.15	
G43S-11	610	178	102	24.2			153.9	6.00		1.54		2.43		0.89		1.10		0.75		1.89		0.99		1.28	
G44S-11	610	178	102	37.0			167.2	6.15		1.43		2.73		0.76		0.97		0.73		1.36		0.97		1.16	
F3S3	610	178	102	34.3			242.9	1.43		2.02		1.86		1.06		1.52		0.99		1.58		1.05		1.24	
G23S-21	610	330	102	23.6			106.7	6.71	x = 6.119 σ = 1.276	1.30	x = 1.243 σ = 0.238	1.65	x = 1.873 σ = 0.458	0.73	x = 0.671 σ = 0.127	0.83	x = 0.803 σ = 0.185	0.77	x = 0.704 σ = 0.125	0.85	x = 0.980 σ = 0.180	0.86	x = 0.909 σ = 0.062	1.16	x = 1.143 σ = 0.104
G24S-11	610	330	102	38.6			181.5	8.65		1.64		1.75		0.80		1.11		0.92		0.94		0.97		1.19	
G24S-21	610	330	102	36.1			100.5	6.26		1.01		1.34		0.51		0.63		0.61		0.70		0.76		0.94	
G33S-21	610	229	102	21.0			108.9	5.78		1.30		1.82		0.76		0.87		0.70		1.18		0.93		1.21	
G34S-21	610	229	102	34.2			112.1	5.34		1.10		1.72		0.58		0.70		0.62		0.92		0.88		1.07	
F3S2	610	229	102	24.3			122.8	6.13		1.39		2.03		0.79		0.91		0.76		1.19		0.99		1.24	
F4S1	610	178	102	34.3			94.3	4.50		0.96		2.80		0.53		0.57		0.55		1.08		0.97		1.19	
						mean	6.016		1.563		1.986		0.839		1.126		0.777		1.224		0.888		1.141	
						standard deviation	2.200		0.374		0.392		0.188		0.365		0.136		0.609		0.127		0.137	

Table 7.1d P_u (test) / P_u (cal.) calculated by various researchers.

Beam no.	L (mm.)	H (mm.)	X_o (mm.)	f_o N/mm^2	f_t N/mm^2	$P_{u\,(test)}$ (kN)	Ultimate shear strength ratio $P_u(test)/P_u(cal.)$								
							CP110	CIRIA Eq.5.27	ACI-318 Eq.5.23	Paiva Eq.5.7	Ramakrish. Eq.5.12	Kong Eq.5.23	Al-Najjim Eq.5.28,36	Proposed Eq.7.25,26	Proposed Design Guide
SINGLE POINT LOADED -- Ramakrishnan and Ananarayana's (1968)							normal weight concrete beams								
K1'	686	381	140	15.2	1.56	111.6	5.75	1.24	3.74	0.96	0.76	1.06	2.56	1.72	2.19
K1' (R)	686	381	140	13.7	1.46	78.7	4.05	0.91	2.77	0.72	0.57	0.79	1.81	1.24	1.61
K2'	686	508	140	14.0	1.52	123.6	4.65	0.96	1.62	0.68	0.64	0.82	2.05	1.29	1.65
K2' (R)	686	508	140	14.3	1.68	103.6	3.95	0.81	1.37	0.57	0.49	0.63	1.72	1.04	1.34
K3'	686	572	140	14.8	1.57	120.5	4.05	0.81	1.20	0.55	0.54	0.68	1.75	1.04	1.33
K4'	686	762	140	13.9	1.61	151.2	3.69	0.74	0.90	0.48	0.49	0.59	1.62	0.85	1.10
K4' (R)	686	762	140	10.6	1.27	132.5	3.29	0.75	0.91	0.50	0.55	0.66	1.46	0.83	1.06
						mean	3.421	0.889	1.787	0.637	0.577	0.747	1.853	1.144	1.469
						standard deviation	1.450	0.175	1.071	0.168	0.096	0.161	0.360	0.308	0.390
UNIFORMLY DISTRIBUTED LOADED -- Ramakrishnan and Ananarayana's (1968)							normal weight concrete beams								
K1	686	381	-	13.4	1.86	210.2	10.56	2.05	3.45	1.39	1.16	1.41	1.77	1.43	1.80
K1 (R)	686	381	-	11.2	1.56	211.1	10.86	2.30	3.86	1.59	1.44	1.71	1.79	1.54	1.93
K2	686	508	-	13.9	1.58	197.4	7.28	1.45	2.15	0.98	0.96	1.18	1.49	1.10	1.40
K2 (R)	686	508	-	12.3	1.52	184.0	7.01	1.47	2.19	1.01	0.96	1.17	1.39	1.05	1.34
K3	686	572	-	14.8	1.57	228.9	7.45	1.46	2.09	0.97	1.00	1.24	1.66	1.10	1.40
K4	686	762	-	14.8	1.54	224.0	5.46	1.10	1.47	0.73	0.76	0.95	1.50	0.74	0.96
						mean	8.103	1.706	2.535	1.112	1.047	1.277	1.600	1.160	1.472
						standard deviation	2.141	0.380	0.916	0.316	0.231	0.259	0.164	0.287	0.349
UNIFORMLY DISTRIBUTED LOADED -- Present tested beams							normal weight concrete beams								
DB1	1000	1000	-	46.9	3.57	1415	2.54	1.99	1.68	0.94	1.26	1.42	1.20	0.69	0.85
DB2	1100	1000	-	45.4	3.36	1400	2.52	2.09	1.94	1.06	1.33	1.59	1.17	0.72	0.89
DB3	1000	1000	-	50.9	3.57	1700	3.05	1.88	1.71	0.72	1.52	1.40	1.37	0.88	1.30
DB4	900	1000	-	50.2	4.03	1960	3.50	2.22	2.02	0.87	1.54	1.45	1.62	1.04	1.53
DB5	800	1000	-	47.5	3.82	1975	3.55	2.23	2.03	0.87	1.65	1.53	1.62	1.04	1.54
DB6	700	1000	-	49.8	3.77	1980	3.56	2.28	2.08	0.90	1.67	1.55	1.53	1.07	1.57
						mean	3.120	2.115	1.910	0.895	1.495	1.490	1.418	0.907	1.280
						standard deviation	0.495	0.157	0.173	0.111	0.167	0.077	0.203	0.170	0.332
Over-all mean and standard deviation															
						mean	6.504	1.706	2.054	0.978	1.007	1.037	1.381	0.966	1.375
						standard deviation	4.413	0.380	0.995	0.215	0.260	0.208	0.354	0.181	0.256

Table 7.1e $P_u(test)/P_u(cal.)$ calculated by various researchers.

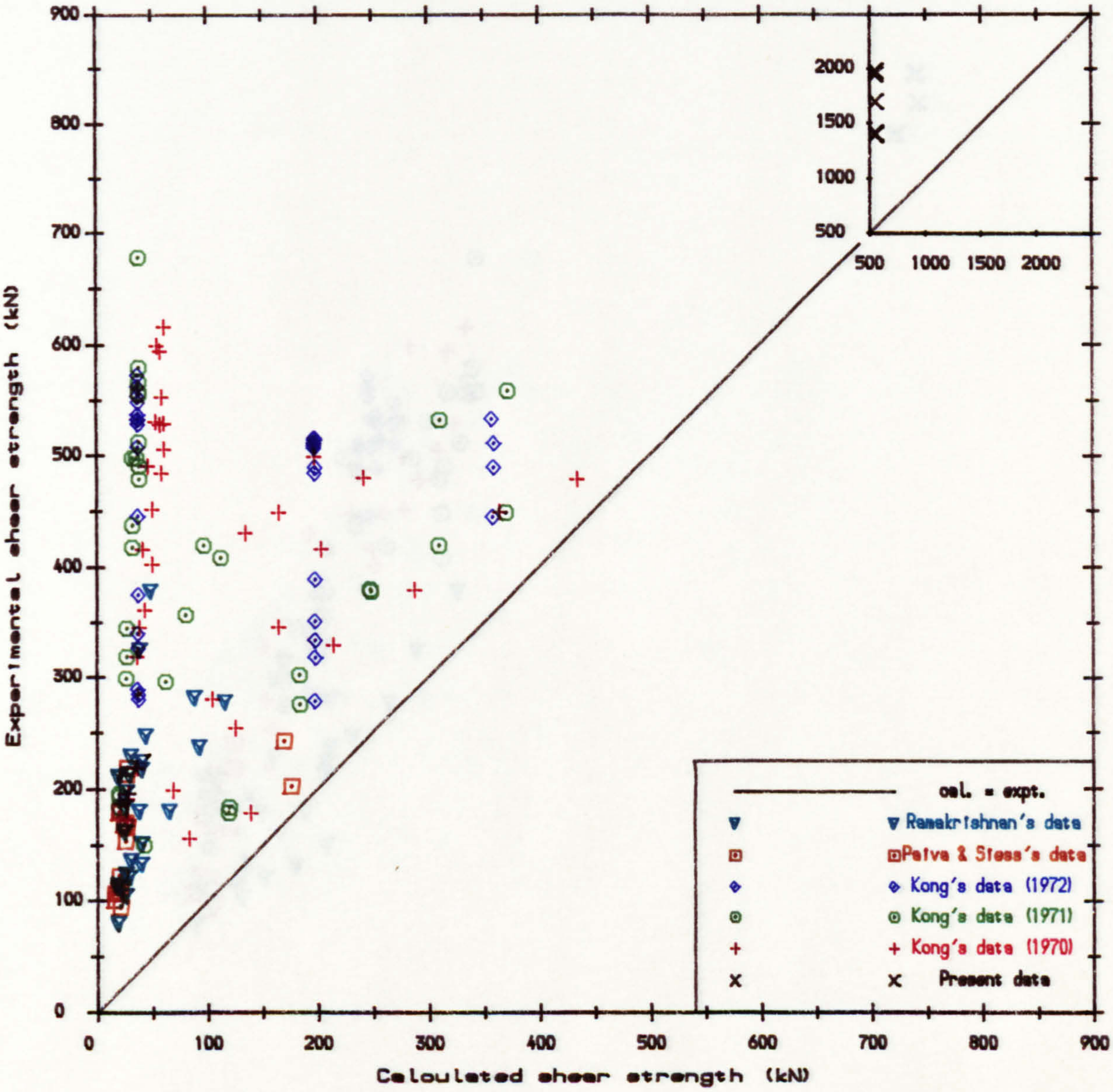

Fig. 7.11. Expt. vs cal. shear strength of deep beam. (CP110 design guide)

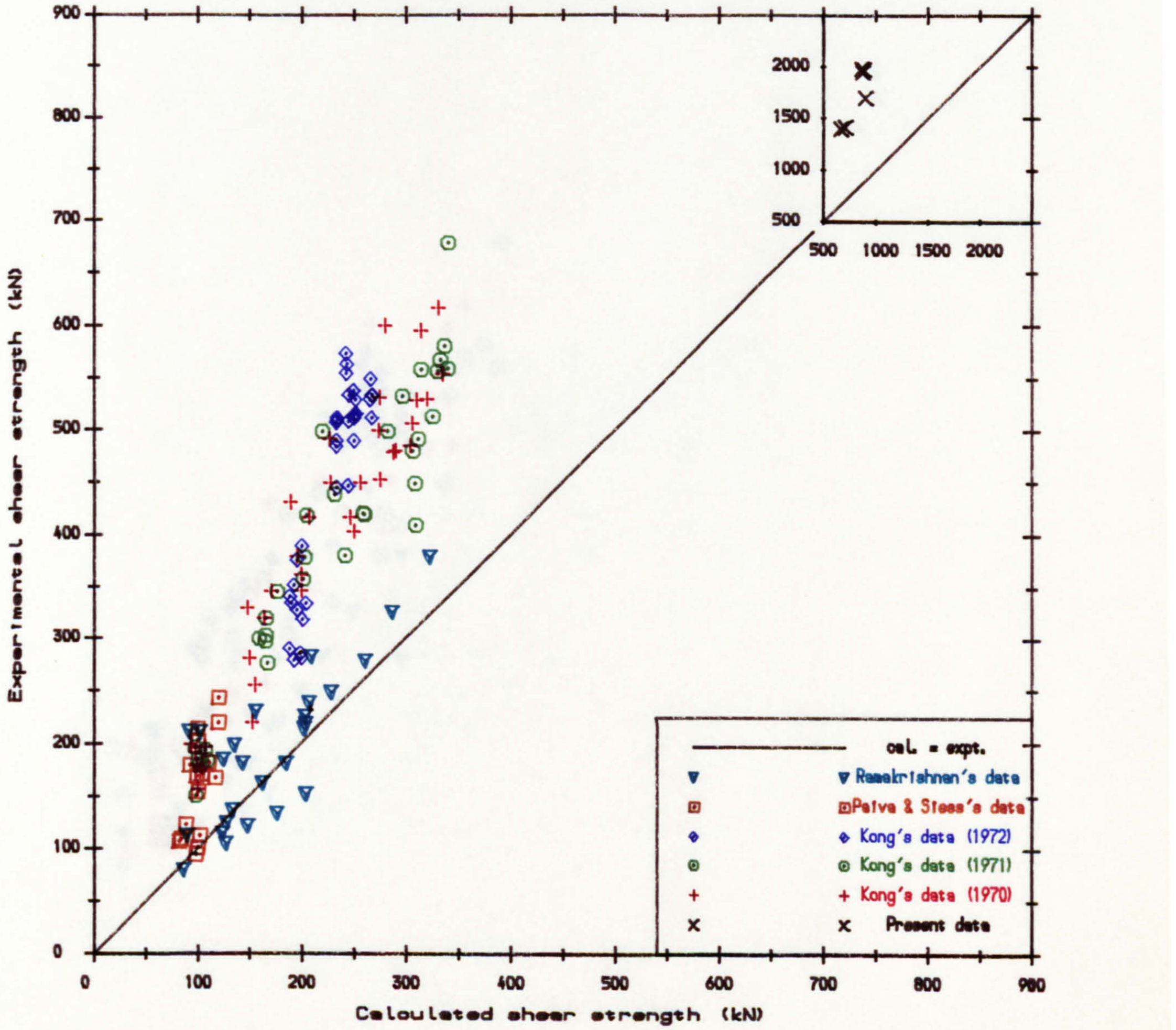

Fig. 7.12. Expt. vs cal. shear strength of deep beam. (CIRIA design guide)

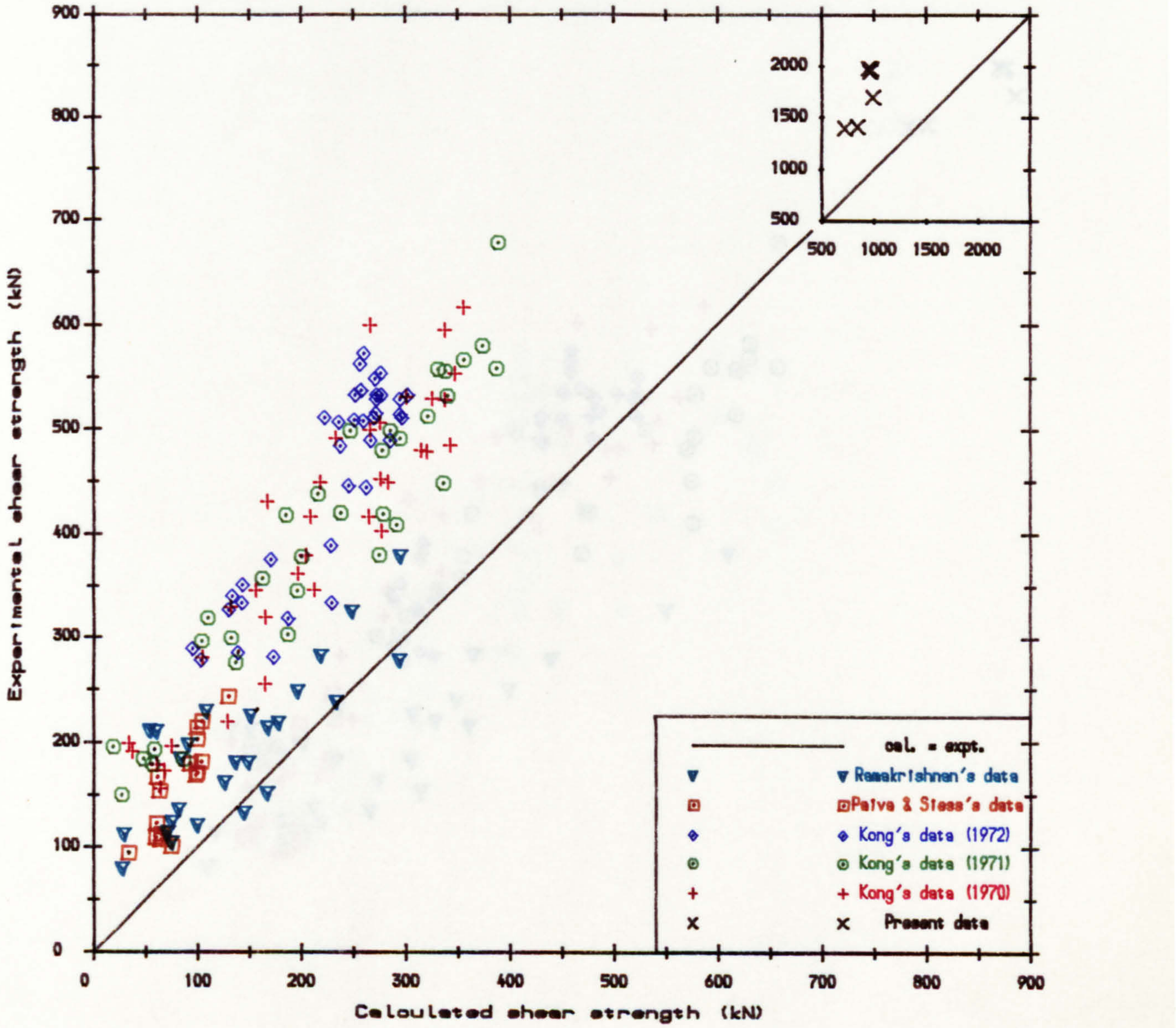

Fig. 7.13. Expt. vs cal. shear strength of deep beam. (ACI design guide)

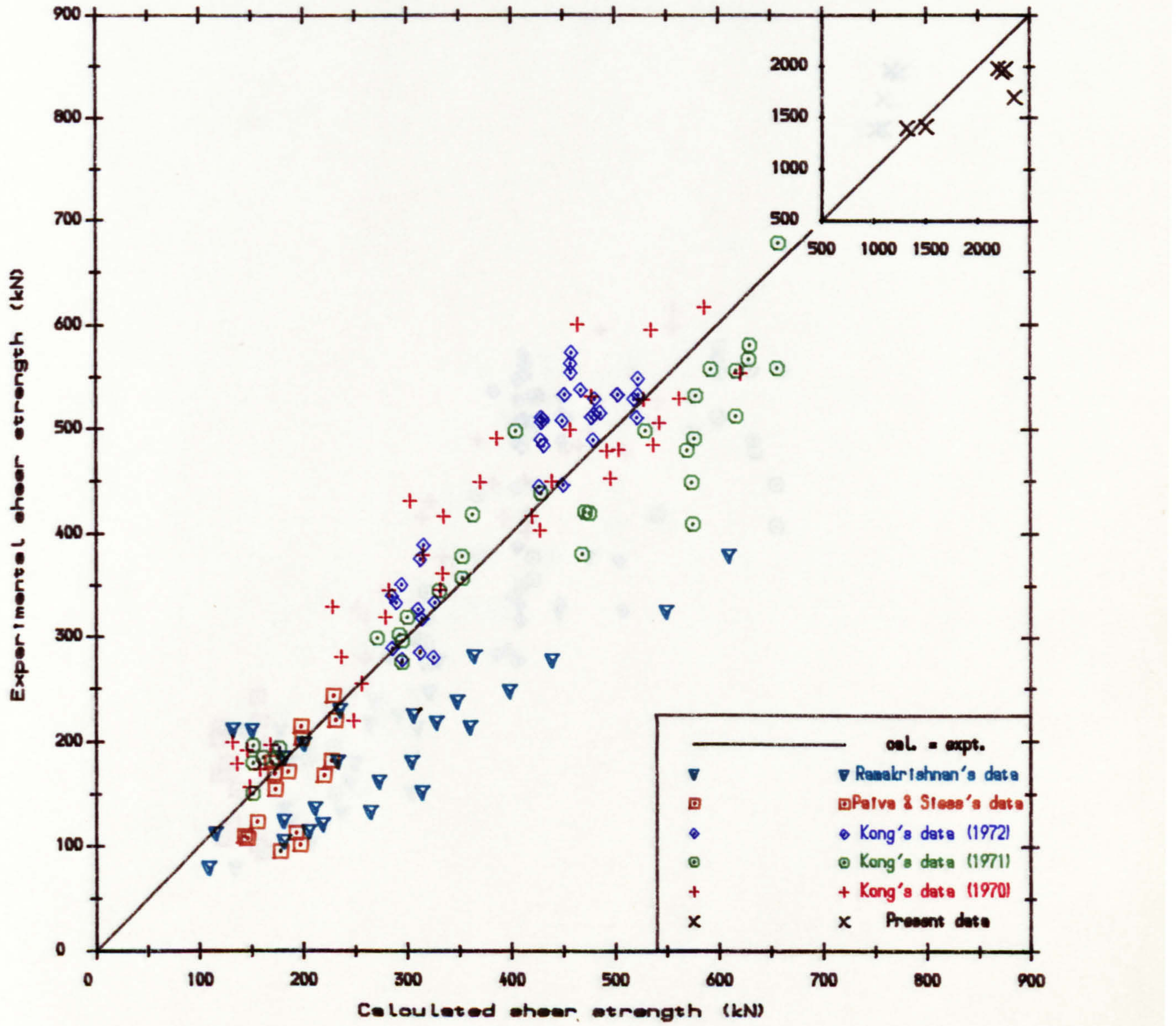

Fig. 7.14. Expt. vs cal. shear strength of deep beam. (Palva & Siess's formula)

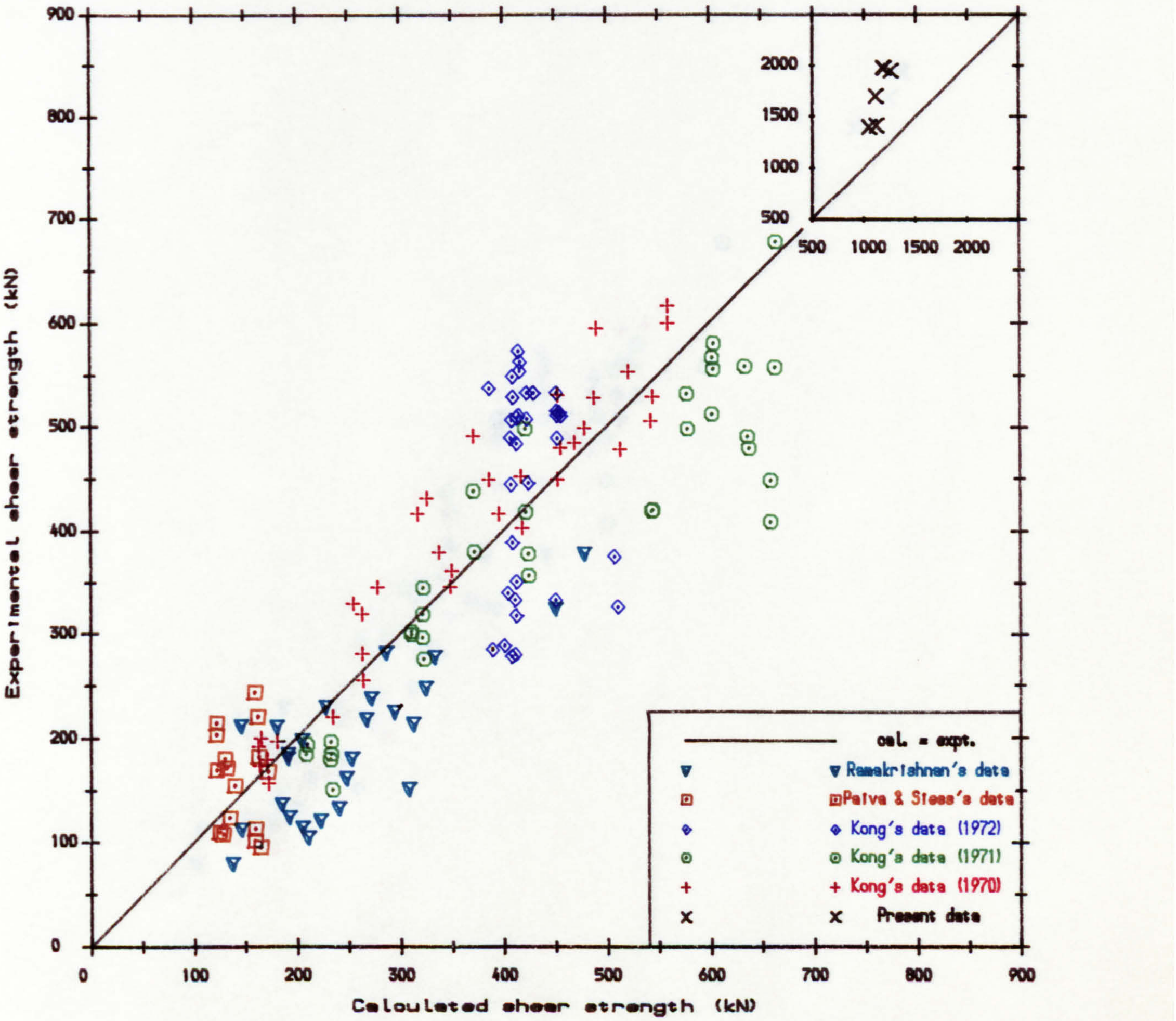

Fig. 7.15. Expt. vs cal. shear strength of deep beam. (Ramakrishnan's formula)

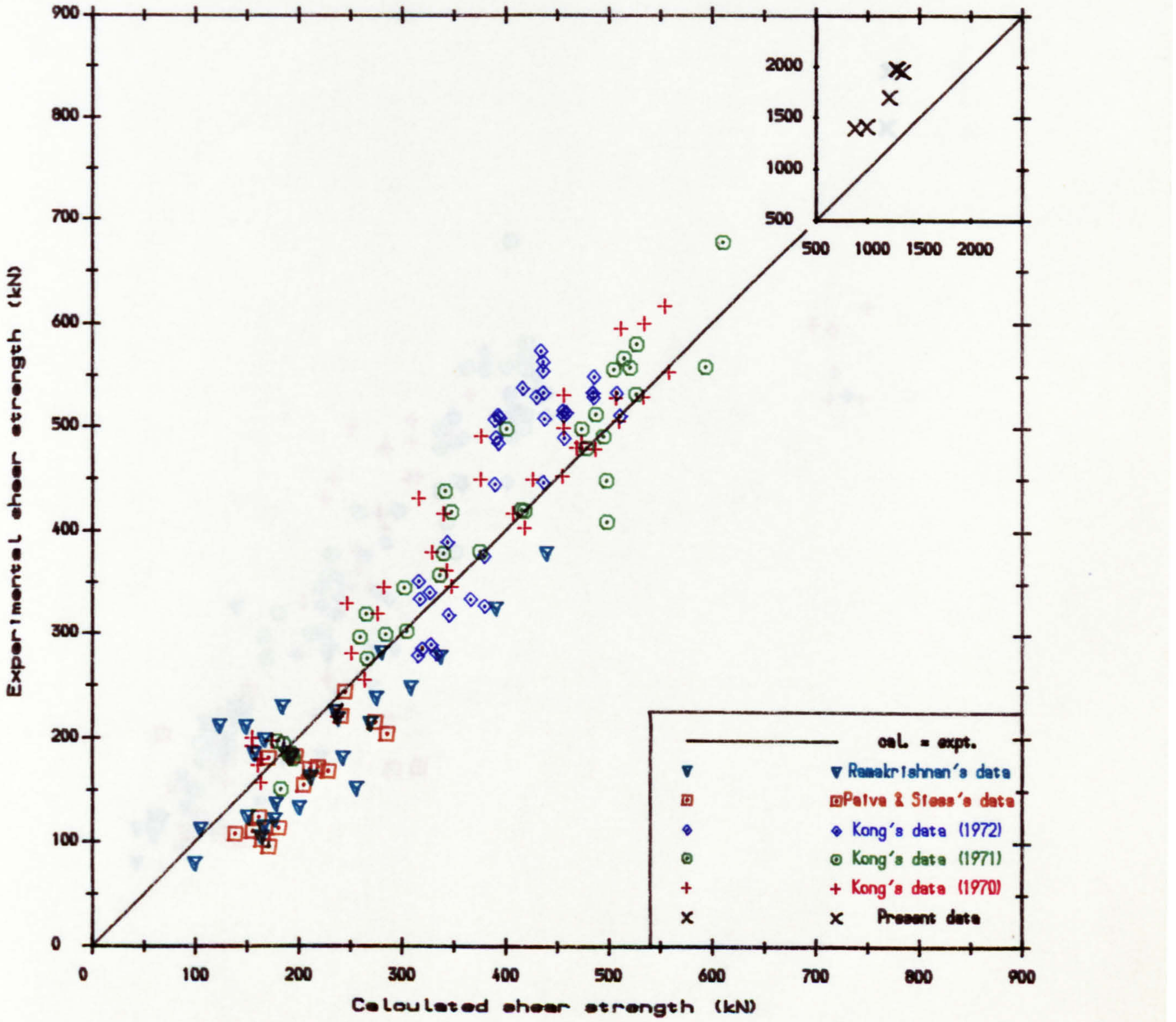

Fig. 7.16. Expt. vs cal. shear strength of deep beam. (Kong's formula)

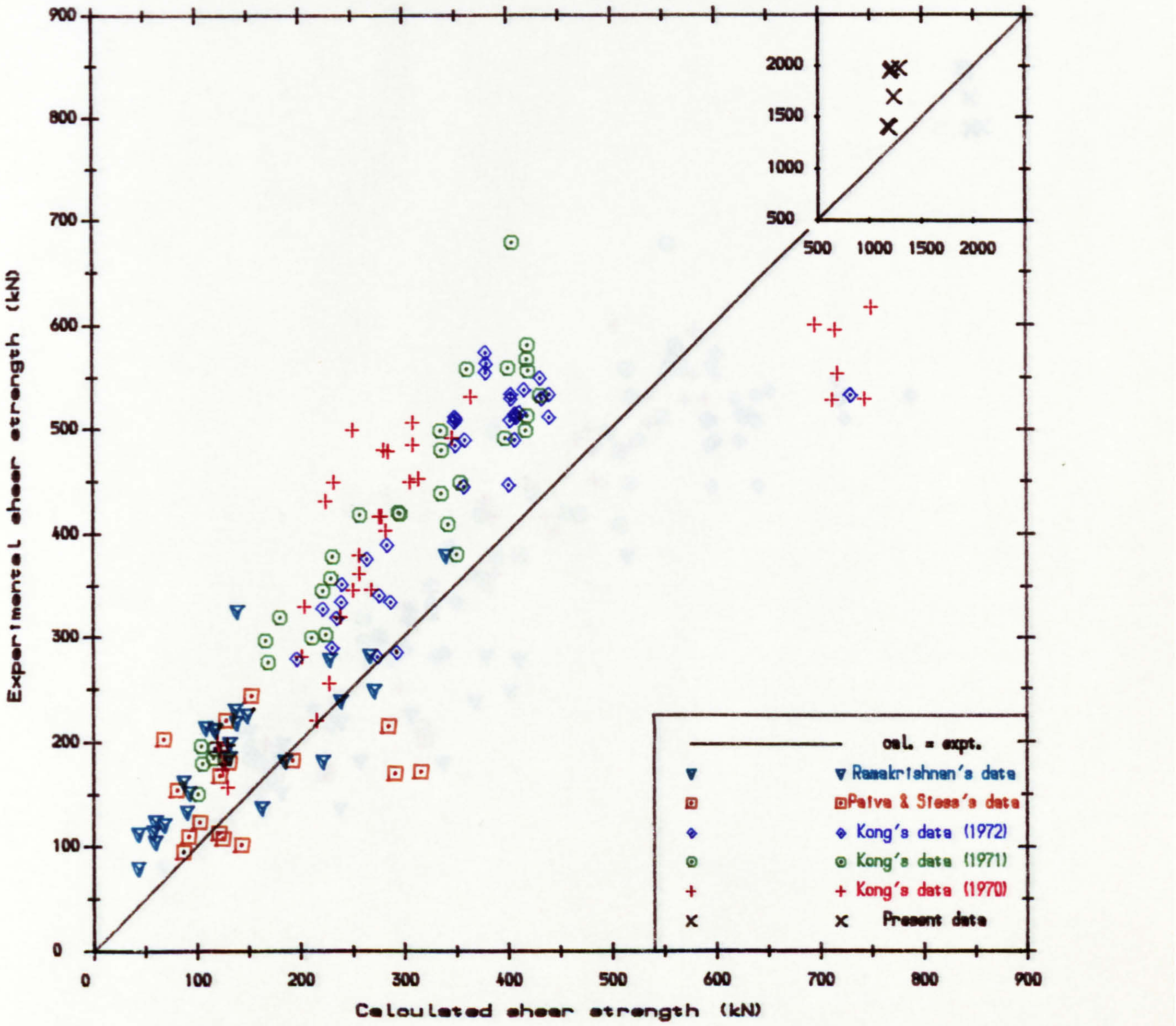

Fig. 7.17. Expt. vs cal. shear strength of deep beam. (Al-Najjim's model)

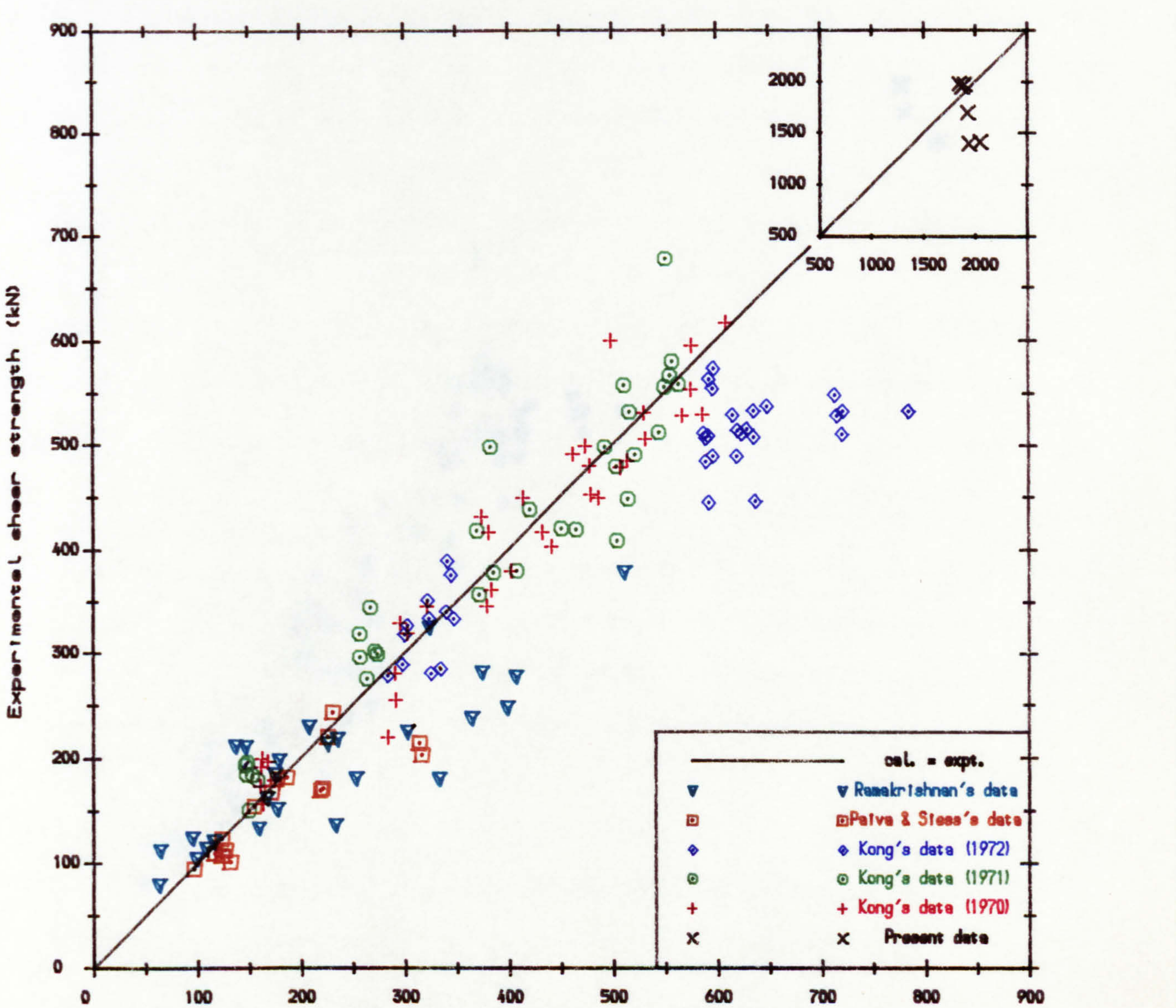

Fig. 7.18. Expt. vs cal. shear strength of deep beam. (Proposed model)

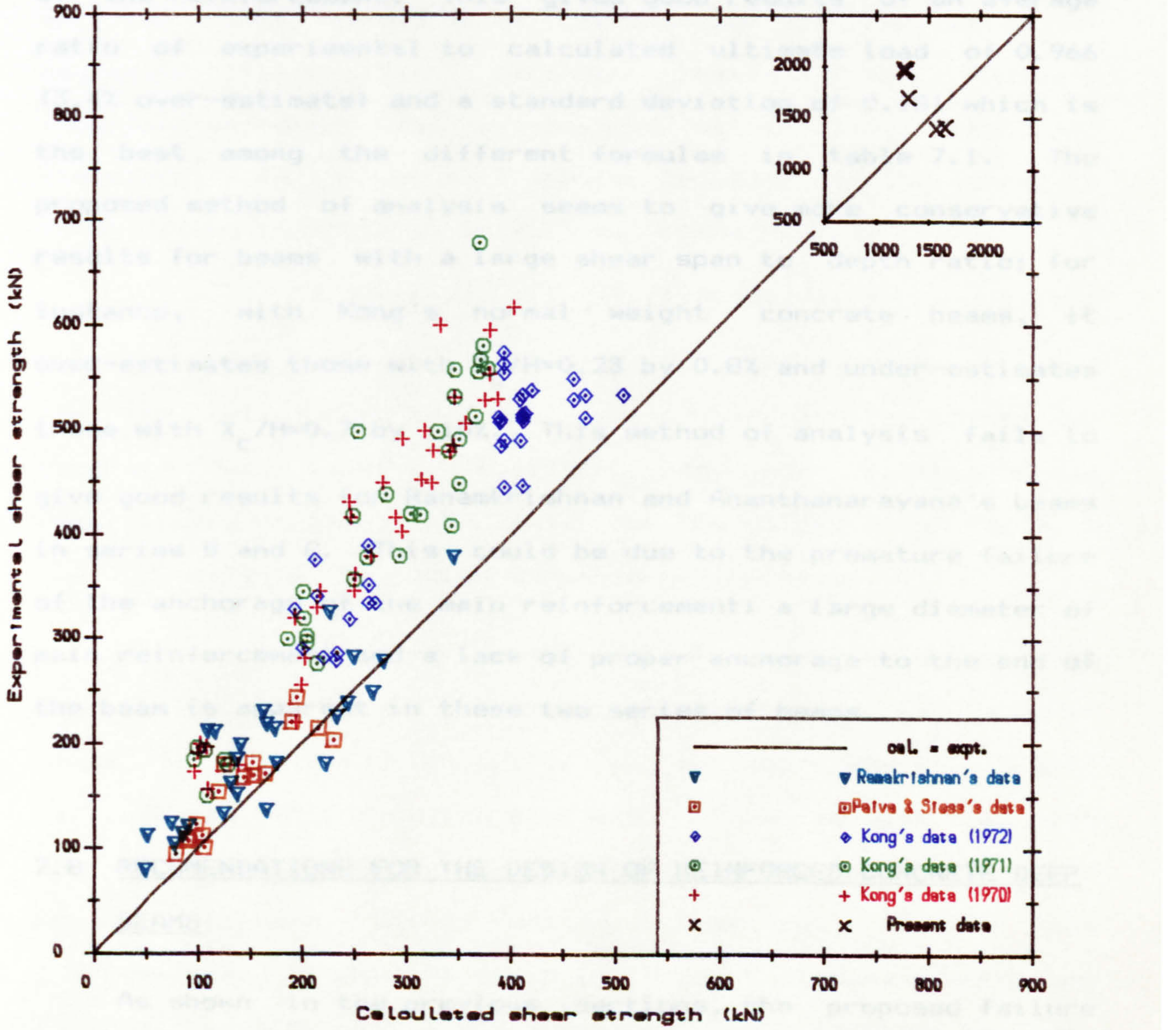

Fig. 7.19. Expt. vs cal. shear strength of deep beam. (Proposed design guide)

The proposed method of analysis is based on the calculation of shear along the crack which involved the shear in the compression zone, aggregate interlock and dowel action of the reinforcement. This gives good results of an average ratio of experimental to calculated ultimate load of 0.966 (3.4% over-estimate) and a standard deviation of 0.181 which is the best among the different formulae in table 7.1. The proposed method of analysis seems to give more conservative results for beams with a large shear span to depth ratio; for instance, with Kong's normal weight concrete beams, it over-estimates those with $X_c/H=0.23$ by 0.8% and under-estimates those with $X_c/H=0.7$ by 10%. This method of analysis fails to give good results for Ranamkrishnan and Ananthanarayana's beams in series B and C. This could be due to the premature failure of the anchorage of the main reinforcement: a large diameter of main reinforcement and a lack of proper anchorage to the end of the beam is apparent in these two series of beams.

7.8 RECOMENDATIONS FOR THE DESIGN OF REINFORCED CONCRETE DEEP BEAMS

As shown in the previous sections, the proposed failure mechanism for reinforced concrete deep beams gives excellent estimates of the ultimate strength. By introducing the appropriate factor of safty, Eqs.7.25 and 7.26 can be used for

the design.

Material factors recommended by CP110, are taken as 1.5 for both tensile and compressive strengths of concrete and 1.15 for the yield strength of reinforcement. Estimation of aggregate interlocking strength taken from Paulay's experimental datas [70] is bounded within 17%, (fig.7.4). Therefore, a factor of 1.17 should be added to the aggregate interlocking strength in Eq.7.29 to become Eq.7.32

$$f_a' = \left[0.165\sqrt{f_c'}\cdot(f_{Lh}+f_{Lv})/0.582\right]/1.17 \qquad (7.32)$$

With the above-mentioned factors, Eq.7.25 and 7.26 can be used for the calculation of the design strength of reinforced concrete deep beams in splitting and shear failure modes respectively. Again, the lesser of the values from Eqs.7.25 and 7.26 will be the design strength of the beam.

The ratios of experimental to calculated design strength for various reinforced concrete deep beams are tabulated in table 7.1. Fig.7.18 is plotted for the experimantal ultimate strength against the design strength. It can be seen that with the exception of nine values, all the rest are estimated safely by the proposed design method. Four out of the nine over-estimated beams are in series B and C of Ramakrishnan and Anathaanrayana's beams. As discussed in the previous section, their over-estimation is due to the premature failure of the anchorage of the main reinforcement. The other over-estimated

beams are DB1 and DB2 in the present investigation. They are over-estimated because of bearing failure at the supports; crushing of concrete due to the lack of bearing steel and instability of the beam as a result of the distortion of the supports due to small edge distances are found in beams DB1 and DB2 respectively. Generally, the proposed design formula gives an average factor of safety of 1.375 and a standard deviation of 0.256, which is better than CIRIA guide with an average of 70.6% over-estimate and a standard deviation of 0.38.

A check on the bearing strength of the supports is also neccessary, especially for beams with height greater than span. The bearing strength of the supports can be estimated by Eq.4.11 (Chapter 4) and bearing steel in form of closely spaced interlocking stirrups should be added where appropriate. Edge distances with $2W_a/a_1$ less than 3.5 should be avoided. Moreover, it is advised to used small diameters, closely spaced bar rather than larger diameters widely spaced steel as main or web reinforcement.

7.9 SUMMARY

(1) A shear crack is formed along the line joining the inner edge of the support and the outer edge of the loading plate in the case of deep beams with concentrated loads. With uniformly distributed load, a shear crack is formed

at an angle of 70 degrees from the inner edge of the supporting plate.

(2) Aggregate interlock and dowel action play important parts in the shear strength of reinforced concrete deep beams.

(3) Aggregate interlock and dowel action are interdependent and not easy to separate them from each other.

(4) Aggregate interlock is mainly dependent on crack width and is proportional to the square root of the cylinder strength of concrete. It is independent of aggregate size, shape and hardness.

(5) The restraining force required to maintain constant crack width was found to be a function of aggregate interlock stress [70]

$$f_L = 0.473\ f_a^{1.03} \quad \text{(psi)} \qquad (7.1)$$

(6) It was found that shear and kinking are the principal mechanisms of dowel action. The shear stress provided by dowel action of light reinforcement is proportional to the square of the sine of the angle between the direction of shear crack and the reinforcement times the steel stress.

$$v_u = k \cdot \sin^2\theta \cdot f_s \qquad (7.16)$$

(7) Based on aggregate interlock and dowel action, the shear strength of reinforced concrete deep beams can be

estimated by the lesser of the values given by Eq.7.25 and 7.26.

(8) Among the design guides, CIRIA gives the best estimate of shear strength of reinforced concrete deep beams with a safety factor of 1.7 and a standard deviation of 0.38.

(9) The simplicity of Ramakrishnan and Ananthanarayana's formula with reasonable accuracy (an average of 7% under-estimation, standard deviation of 0.26) enables its use as a primary estimate of the shear strength of reinforced concrete deep beams.

(10) The proposed model gives the best result (3.4% over-estimation, standard deviation of 0.181). It seems to gives more conservative results for beams with large shear span to depth ratio.

(11) By introducing appropriate material factors; 1.5 for concrete, 1.15 for steel and 1.17 for the aggregate interlocking strength, Eqs.7.25 and 7.26 can be used to calculated the design strength of reinforced concrete deep beams.

8 CONCLUSIONS AND SUGGESTION FOR FURTHER RESEARCH

8.1 BEARING CAPACITY

Bearing capacity is important in many cases, such as in the anchorage zone of a post-tensioned beam and at the supports of reinforced concrete deep beams. The prime factor affecting the bearing strength of concrete blocks is the value R; the footing to loading area ratio. Most researchers have adopted the cube root formula, Eq.4.7 but it has been shown to be to conservative, especially for those with large value of R. It is found that the square root formula would be more appropriate Eq.4.8.

$$f_b/f_c = k\cdot\sqrt{R} \qquad (4.8)$$

Restraint at the base of the concrete block can also affect the bearing strength. This restraint can be the frictional force between concrete and steel at the base. Higher specimens has the loading area further away from the base and there is a lesser effect but shorter specimens (H/a<0.5) are shown to have a 30% increase in strength. These effects have been neglected by many researchers except Muguruma [62], Eq.2.22. He was able to estimate well for specimens with H/a>1 but seriously over-estimated those with H/a<1. Specimens with larger bearing plates are affected more by the condition of the base, because a larger loading area

generates a deeper tension zone and thus can easily intercept the base. The size effect in this investigation is found to be proportional to

$$f_b/f_c' = 1.45\, e^{-a/80} + 0.9 \qquad (4.3)$$

Closely spaced (30 mm) small diameter (10 mm diameter in practice) interlocking stirrups provide the most effective form form of reinforcement in concrete blocks under concentrated bearing loads. Reinforcement should be maintained to the depth of the tension zone (0.75a below the loading surface) and extended at least to the width of and preferably to twice the width as the loading plate. Edge distances with $2W_a/a_1<3.5$ should be avoided.

In general, the cracking strength of reinforced concrete blocks and ultimate strength of plain concrete block can be estimated by

$$f_b/f_c' = \begin{cases} 0.47W_a/a_1 + 0.55 & 2W_a/a_1<3.5 \\ \left.\begin{array}{ll} 0.12W_a/a_1 + 1.16 & \text{(plain)} \\ 0.22W_a/a_1 + 1.01 & \text{(reinft.)} \end{array}\right\} & 2W_a/a_1>3.5 \end{cases} \qquad (4.4)$$

The proposed model of failure mechanism suggested that the bearing capacity of plain concrete blocks can be calculated by

$$r^3 - r - \left[16z_2 \cdot F_2 + 8(z_3 - z_1 + 2z_2) \cdot F_3\right]/3a_1^2 \cdot f_c' \qquad (4.11)$$

where $F_1 = F_2 + F_3 - F_4$ $\qquad$ $z_1 = 0.4a_1$

$$F_2 = f_t \cdot (z_2 - z_1)/2 \qquad z_2 = a_1$$
$$F_3 = f_t \cdot (z_3 - z_2)/2 \qquad z_3 = 0.75a$$
$$F_4 = 0 \qquad z_4 = H$$

and

$$r = f_b/f_c'$$

This gives excellent results for all higher specimens (H/a>1); average under-estimation of 0.5%, standard deviation of 0.098. For shorter blocks (H/a<1), it shows an exponentially increasing under-estimation with decreasing ratio of H/a as in Eq.4.12.

$$f_{b(test)}/f_{b(cal.)} = 0.657\ e^{-1.15H/a+0.9} \qquad (4.12)$$

By multiplying the reciprocal of this factor to the bearing capacity obtained from Eq.4.11, the modified model gives good estimates (average over-estimation of 1.6%, standard deviation of 0.085) for the full range of height of all the specimens.

8.2 DEEP BEAMS

After shear crack is formed along the line joining the inner edge of the support and the outer edge of the loading plate. For uniformly distirbuted loaded beams, shear cracks are formed at an angle of 70 degrees from the inner edge of the supporting plate. After cracking, the shear strength of reinforced concrete deep beams is maintained by aggregate interlock and dowel action along the crack.

The aggregate interlocking strength is found to be dependent on the restraining stress provided by the reinforcement and is proportional to the square root of the cylinder strength of concrete.

$$f_L = 0.473\ f_a^{1.03}\ (psi.)$$

Dowel action is taken to be proportional to the square of the sine of the angle between the crack and the reinforcement.

$$V_u = k \cdot \sin^2\theta \cdot f_s \qquad (7.16)$$

Based on the above two findings, a failure mechanism for reinforced concrete deep beams is proposed. The ultimate splitting and ahear strength for orthogonally reinforced concrete deep beams can be calculated by Eqs.7.25 and 7.26 respectively.

$$V_{u1} = \int_0^H \frac{f_L \cdot b \cdot \mathrm{cosec}^2\theta \cdot (y-d')}{X_c - d' \cdot \cot\theta}\, d(y) \qquad (7.25)$$

$$V_{u2} = \int_0^H \frac{(f_{pv} - f_{ph} + v_c + f_a + f_d) \cdot \mathrm{cosec}\theta}{\sin\theta}\, d(y) \qquad (7.26)$$

The ultimate strength will be the lesser of the two values found by Eqs.7.25 and 7.26. This gives the best result (average over-estimation of 3.4%, standard deviation of 0.181) among different formulae by recent researchers.

By introducing certain material factors, Eqs.7.25 and 7.26 can be used for the design of reinforced concrete deep beams. The appropriate factor for aggregate interlocking strength is taken as 1.17 (fig.7.4,[70]). The material factors, as recommended by CP110, are taken as 1.5 for concrete and 1.15 for steel. The design equation has been proved to be very effective with an average factor of safety of 1.375 and a standard deviation of 0.256. Only 9 beams out of 152 are over-estimated in strength by the design formula (table 7.1), of which 2 are due to premature failure of the bearing at supports and 4 have anchorage problems with the main reinforcement.

8.3 SUGGESTIONS FOR FURTHER RESEARCH

The effects of height and base friction on the bearing capacity of concrete blocks need further investigation. The mechanisms of aggregate interlock and dowel action are complicated in nature and need to be studied further. There is limited knowledge on the effects of openings and wall connections of deep beams and this subject should be further investigated.

APPENDIX A

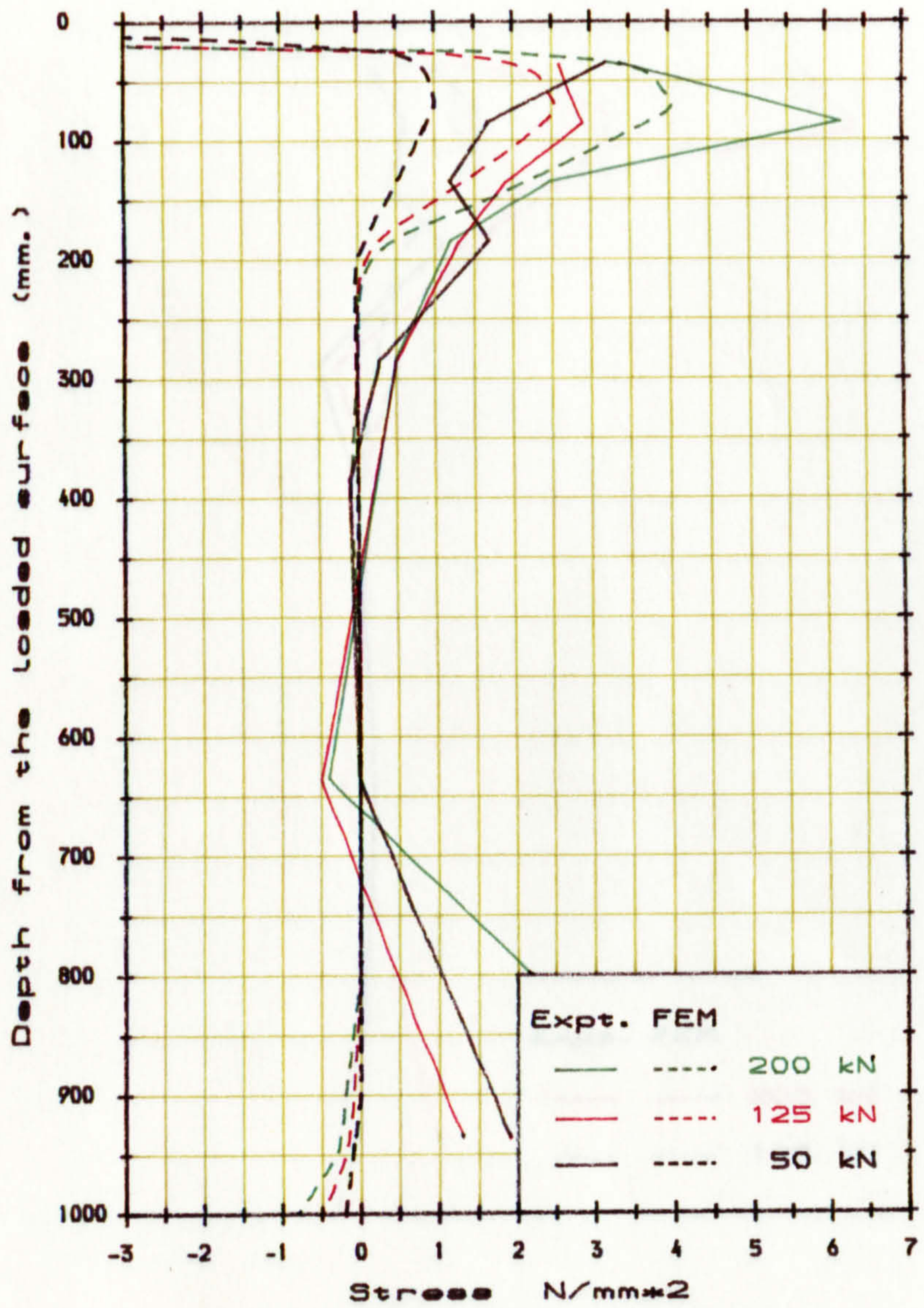

END 1

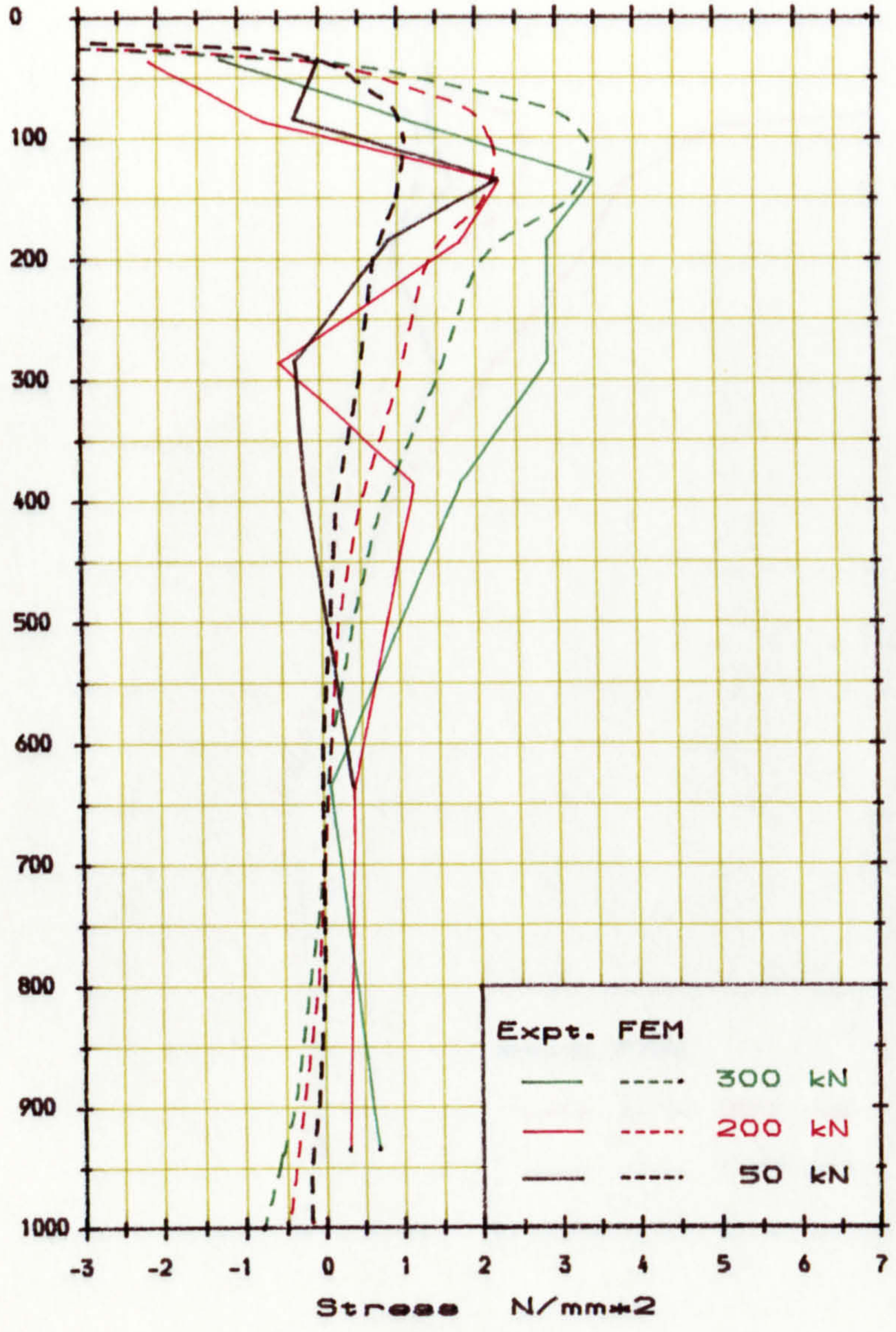

END 2

Fig. A. 1. Horizontal stress along the loaded line (Block E1).

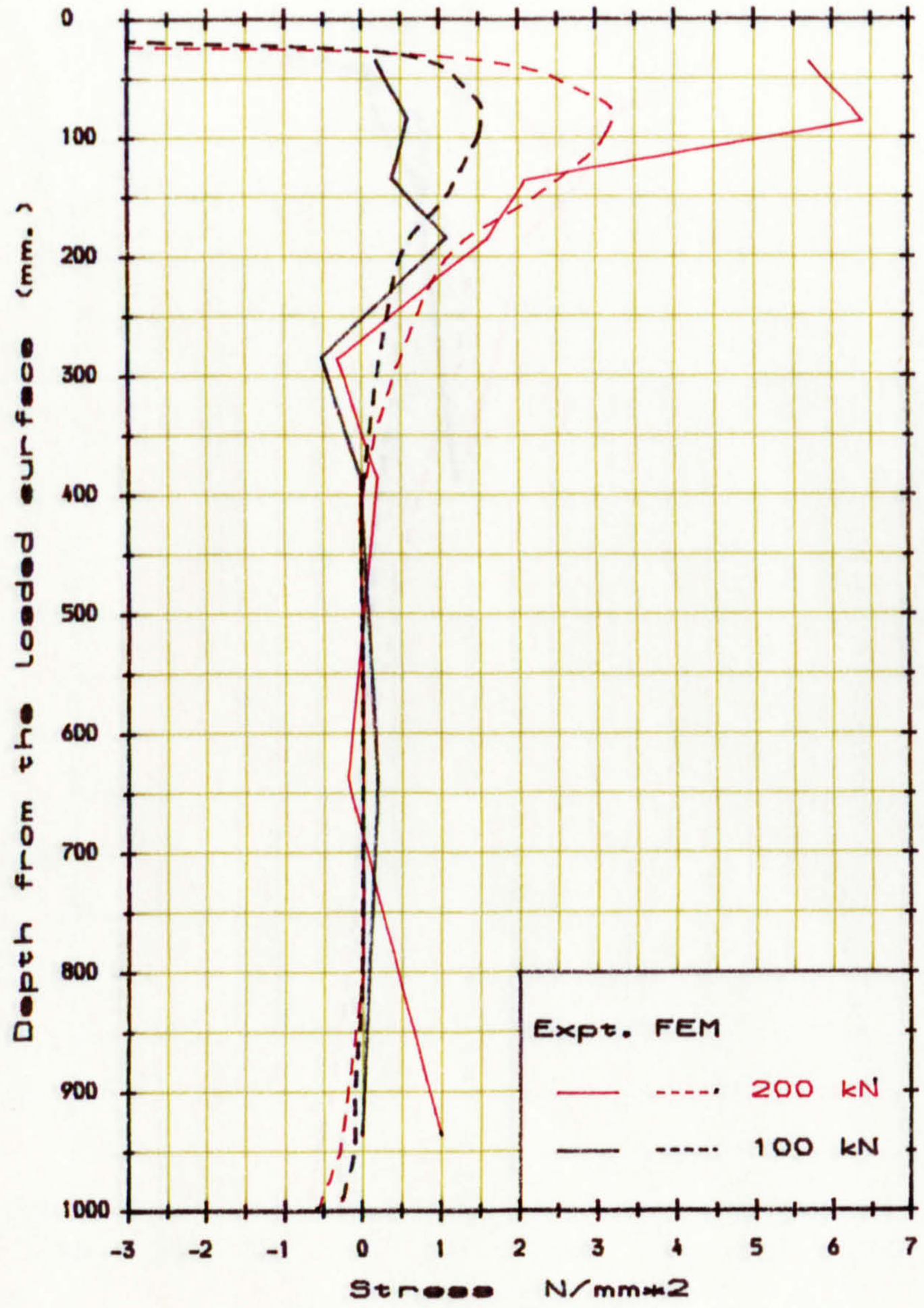

END 1

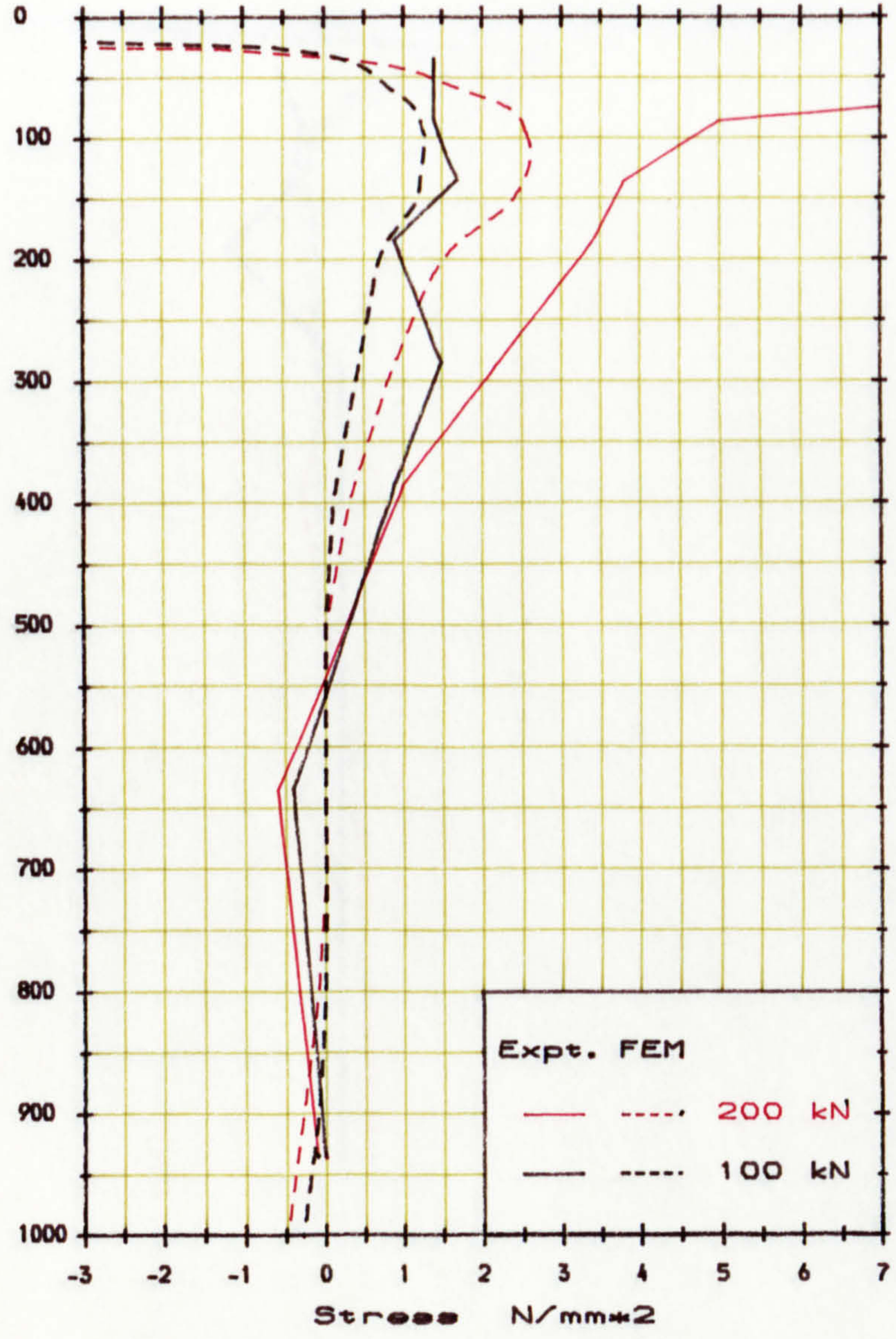

END 2

Fig. A. 2. Horizontal stress along the loaded line (Block E2).

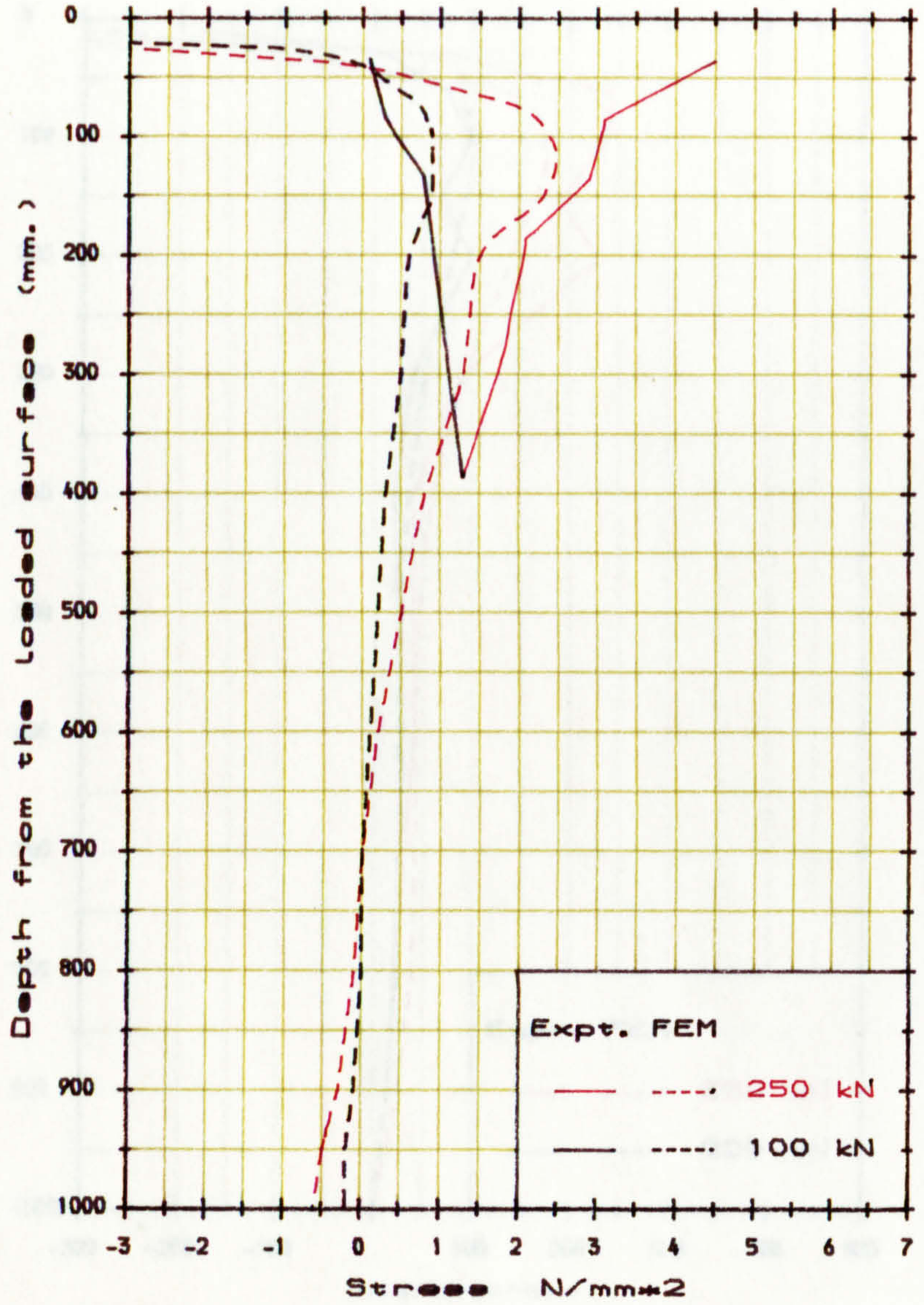

END 1

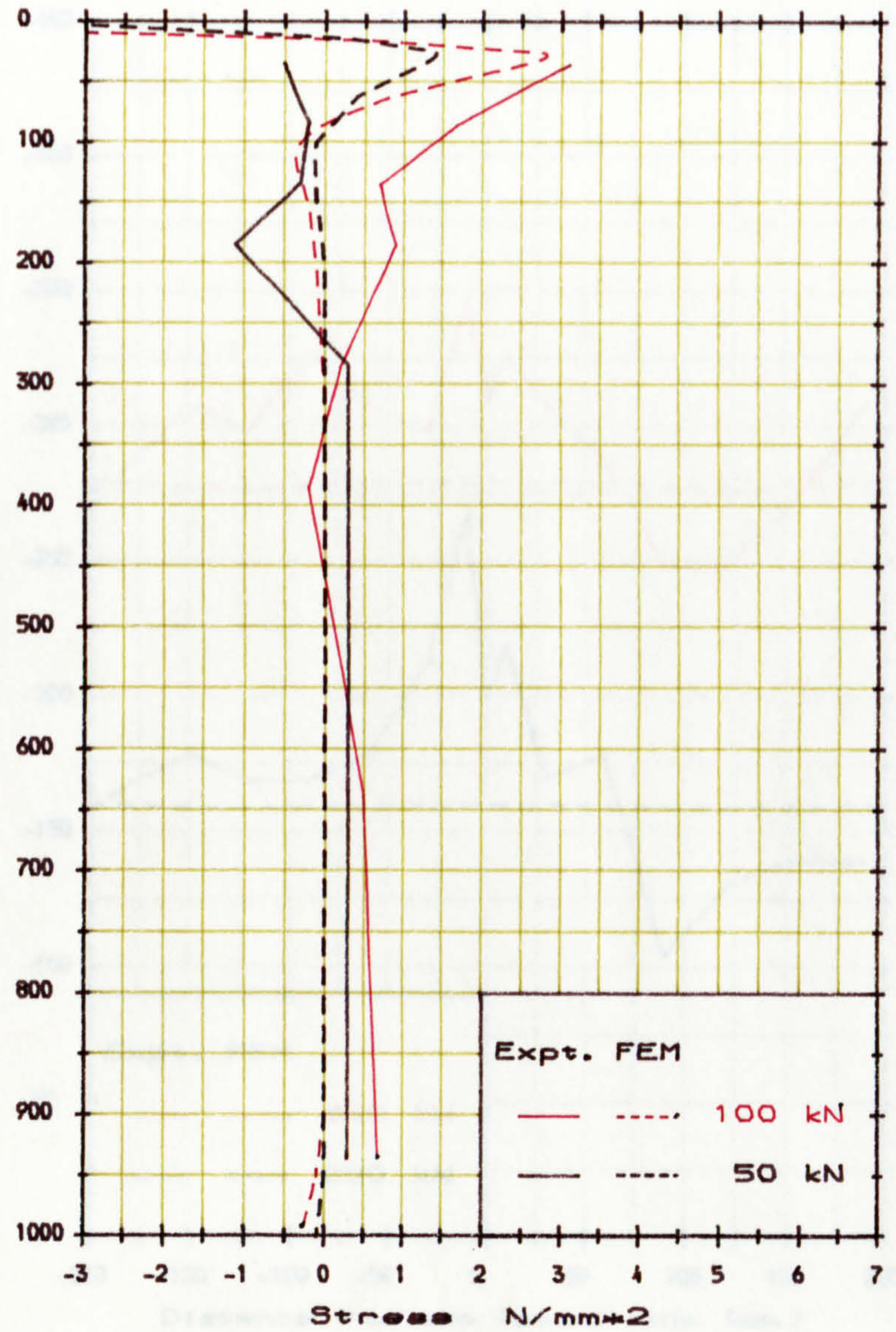

END 2

Fig. A. 3. Horizontal stress along the loaded line (Block E3).

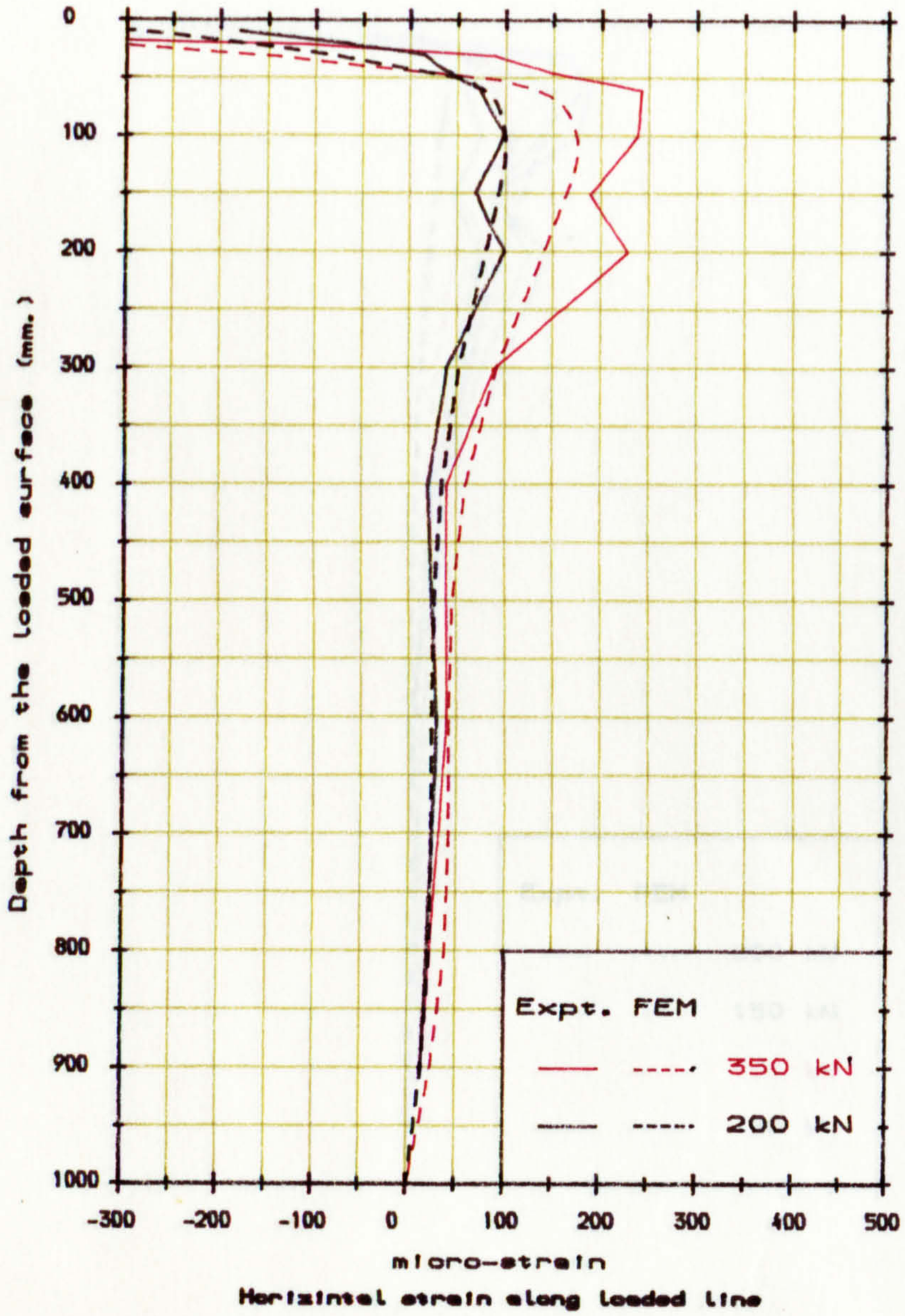

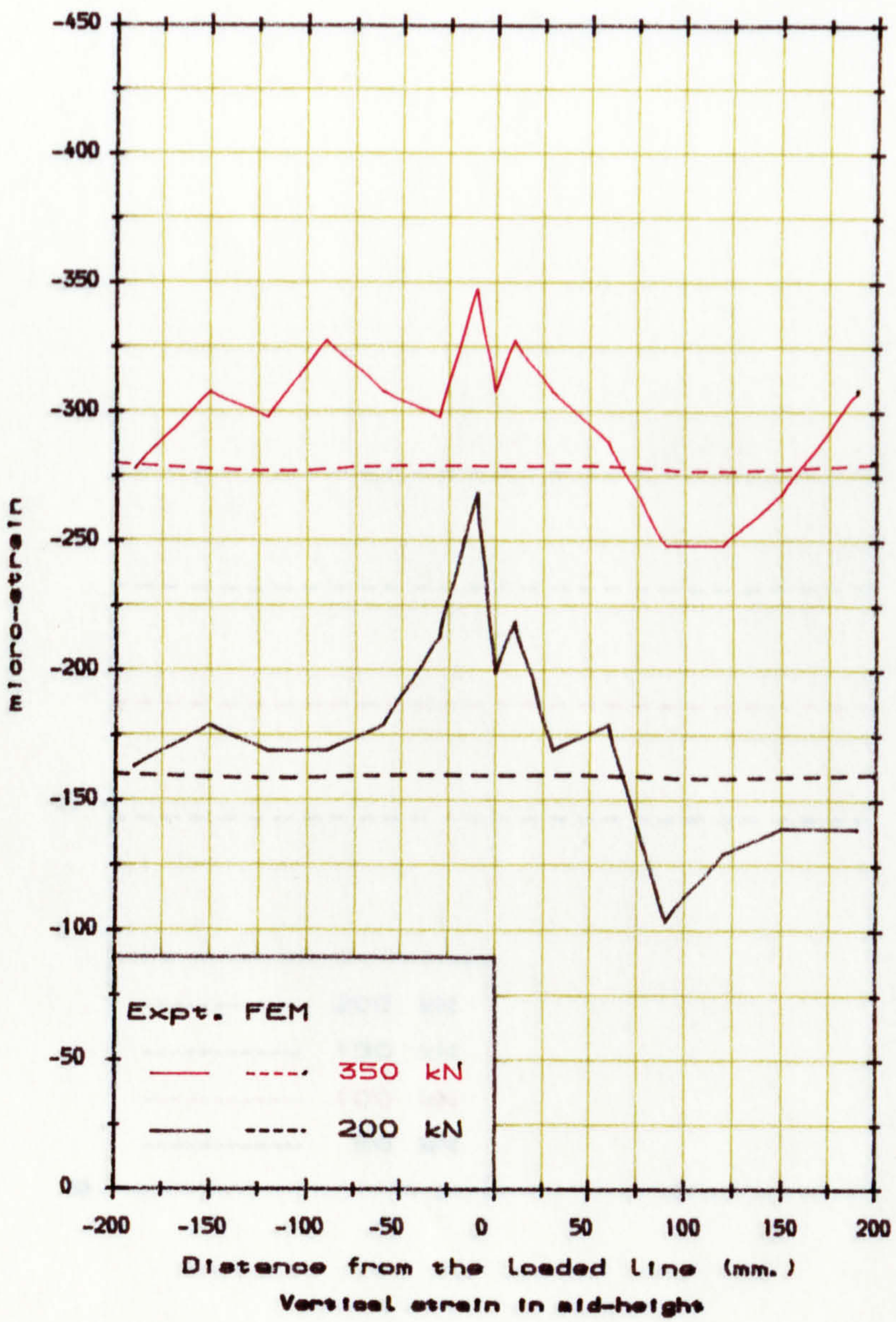

Fig. A. 4. Strain distribution of block R1-H1.

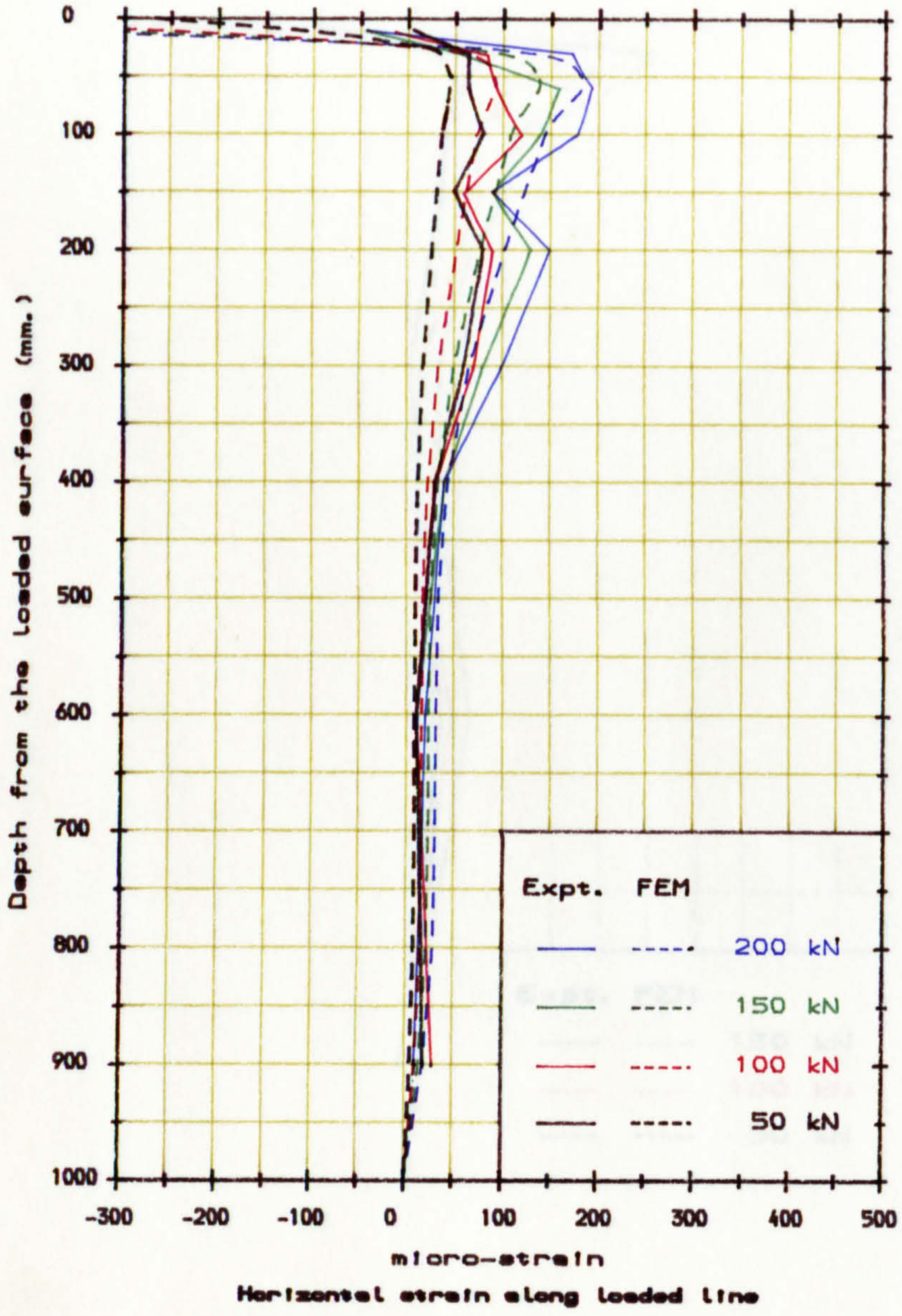

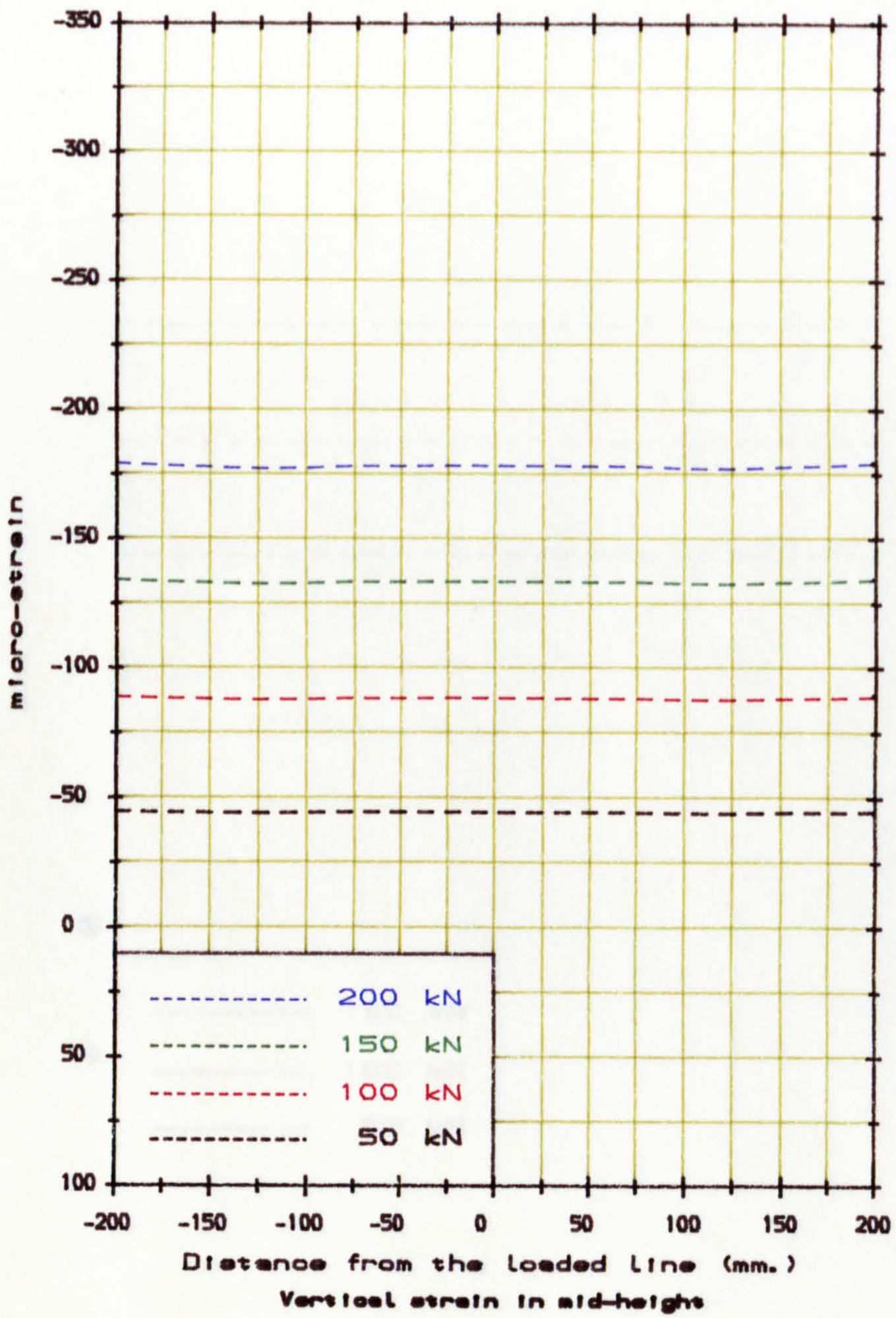

Fig. A. 5. Strain distribution of block R2-H1.

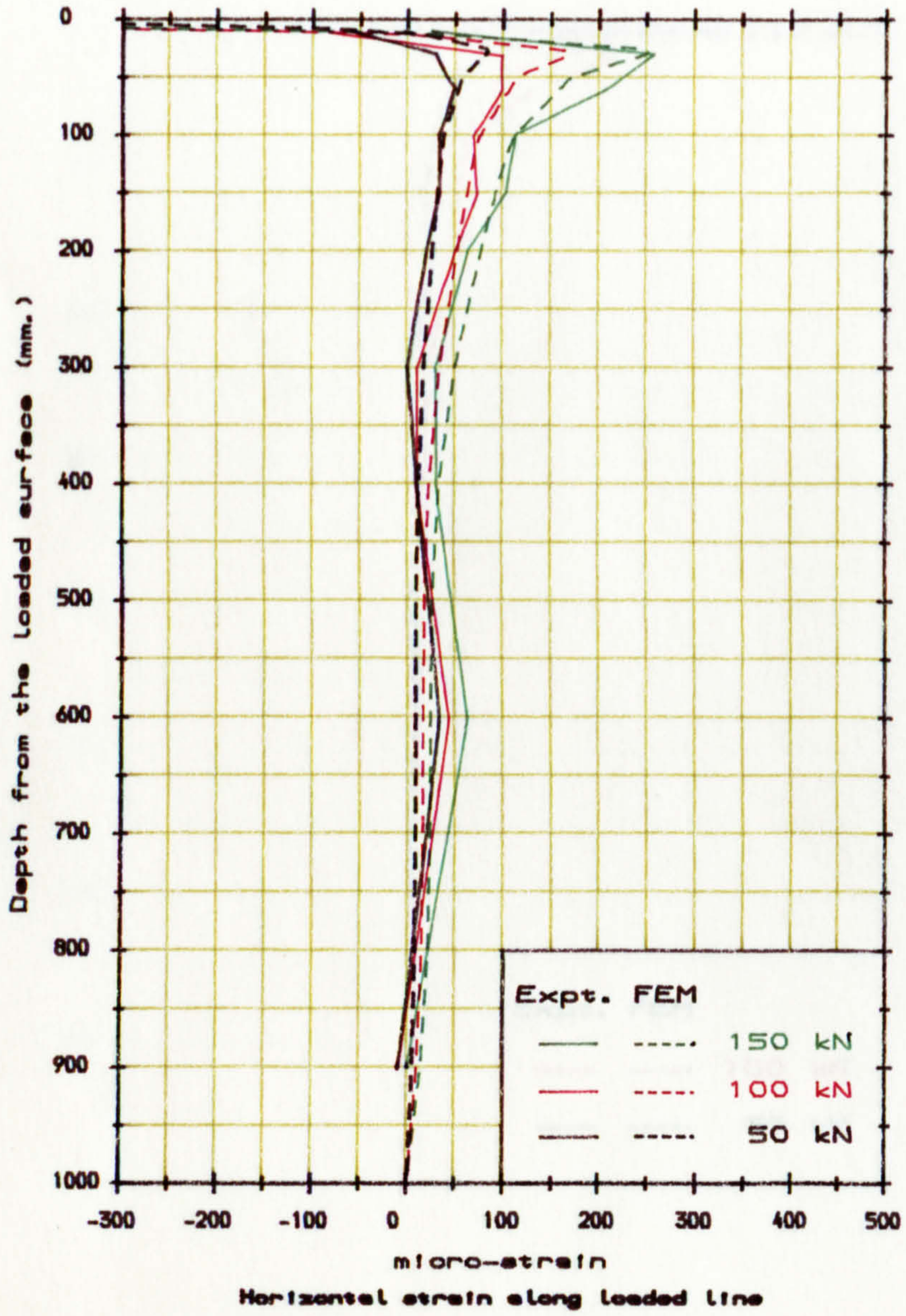

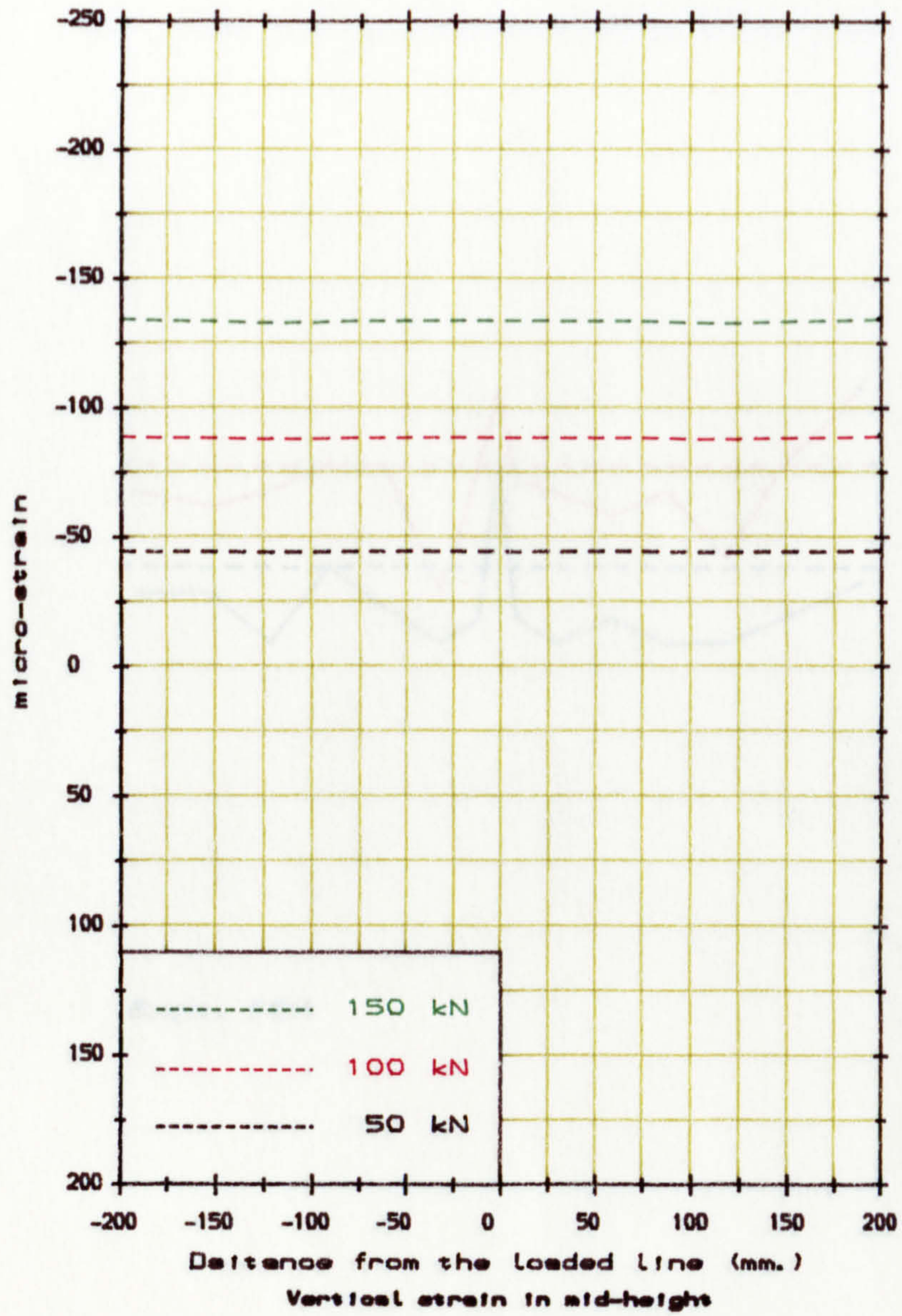

Fig. A. 6. Strain distribution of block R3-H1.

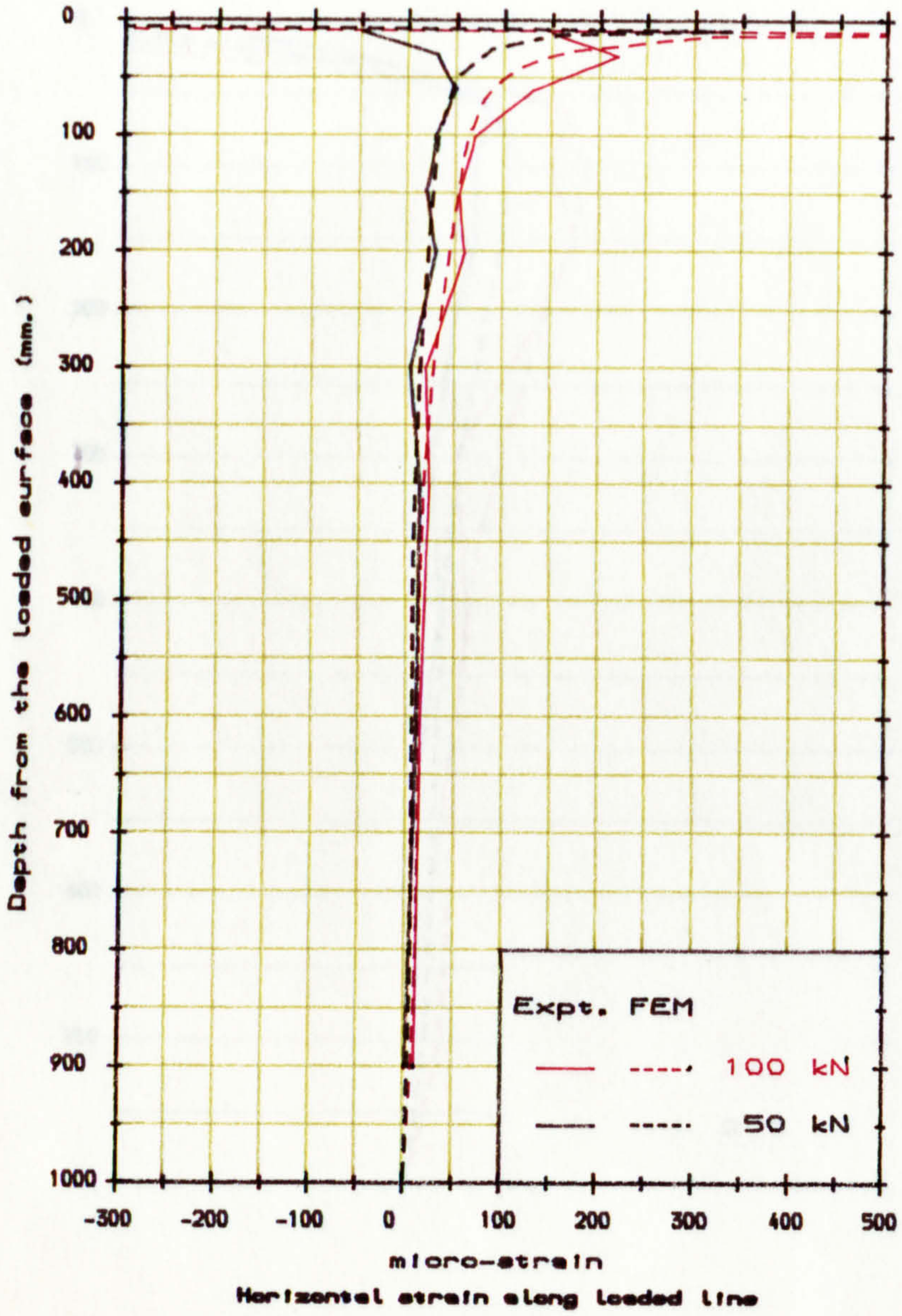

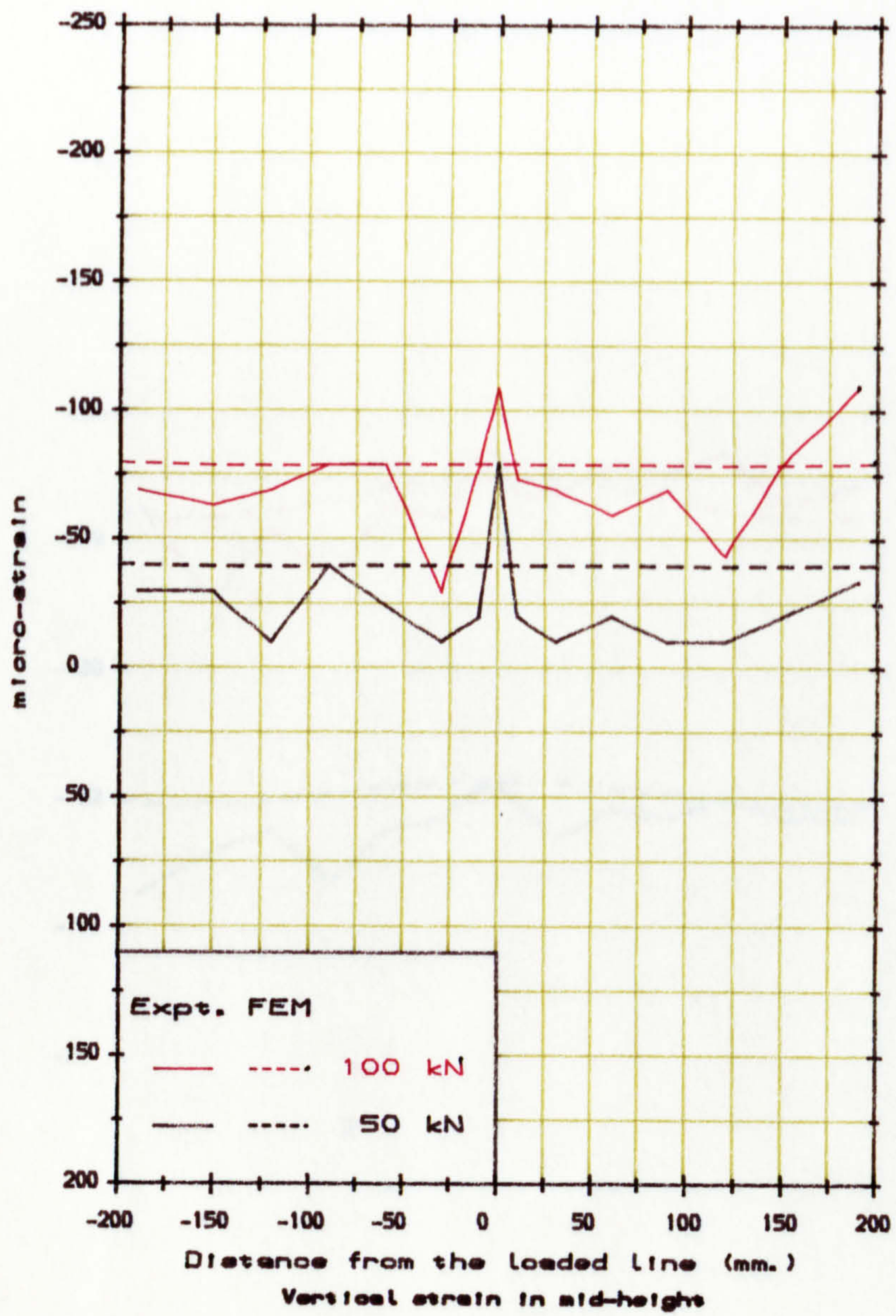

Fig. A. 7. Strain distribution of block R4–H1.

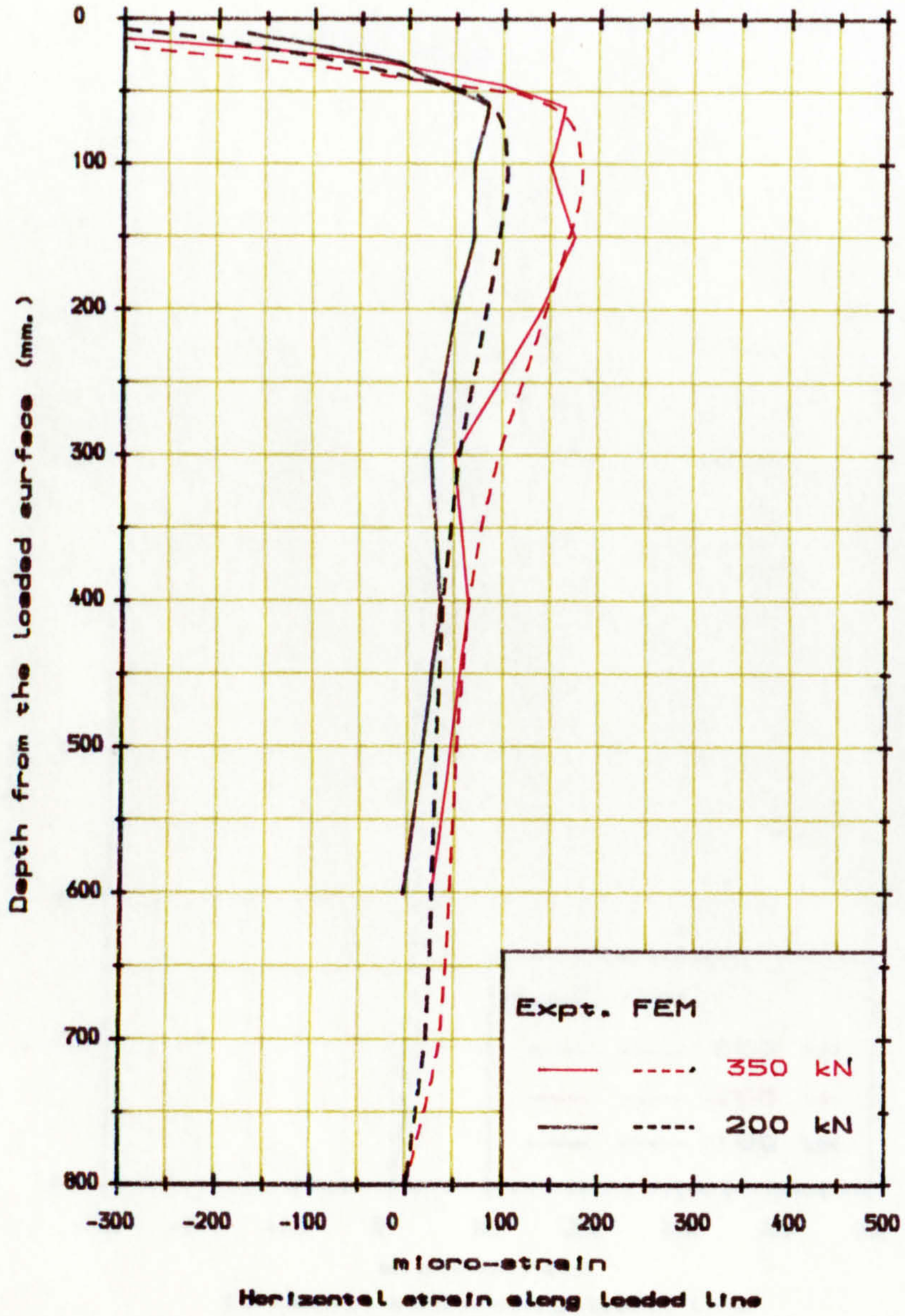

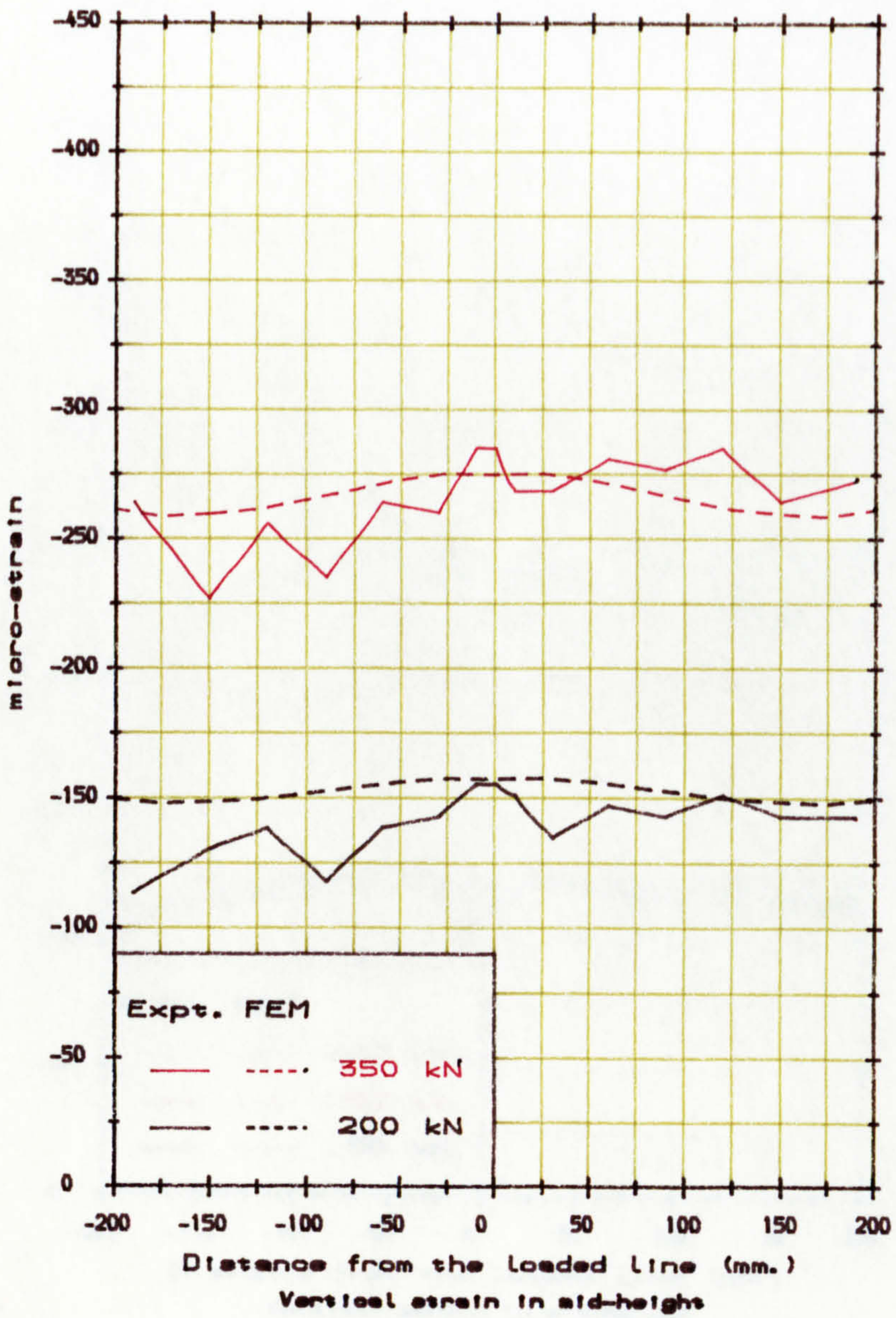

Fig. A. 8. Strain distribution of block R1-H2.

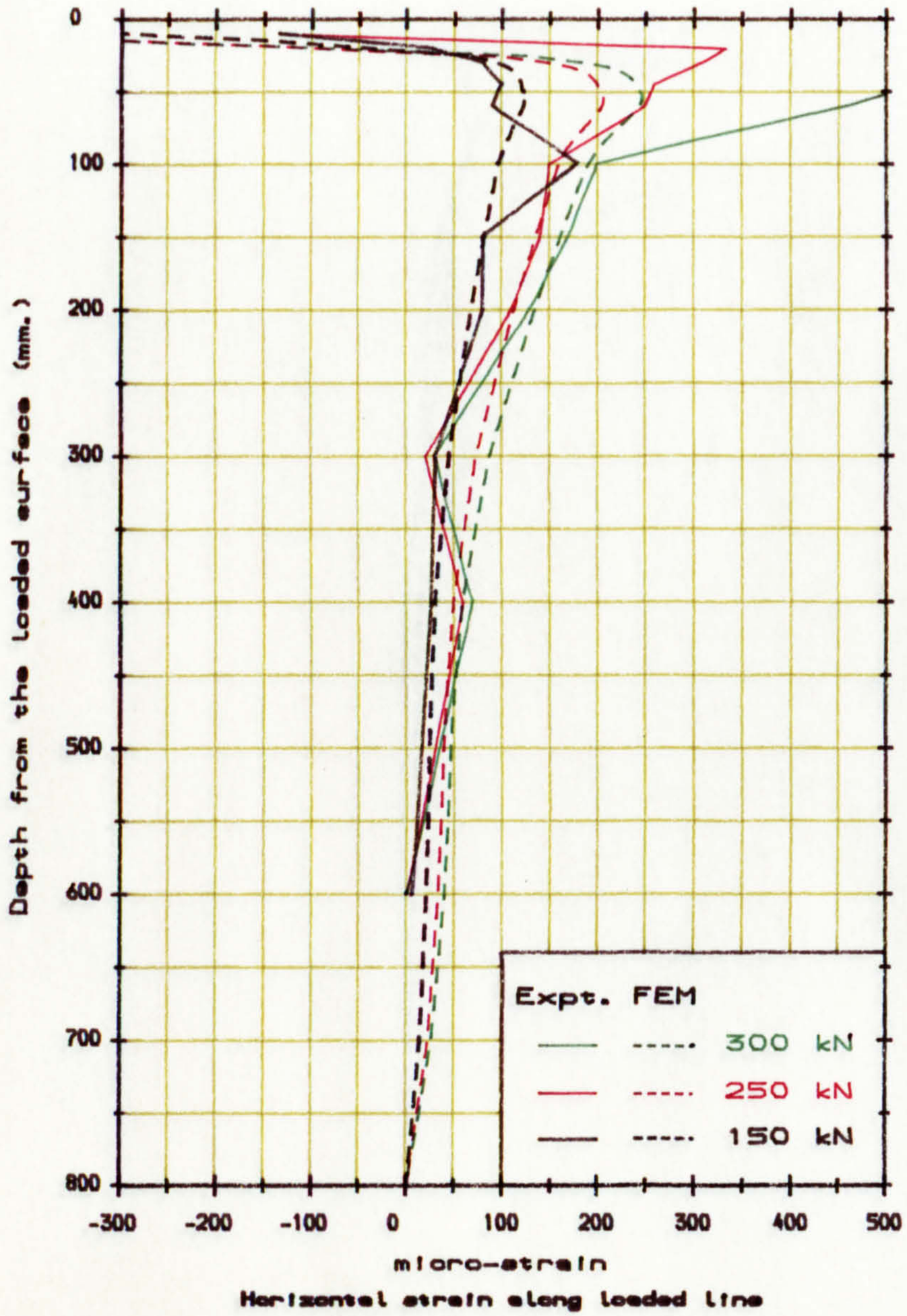

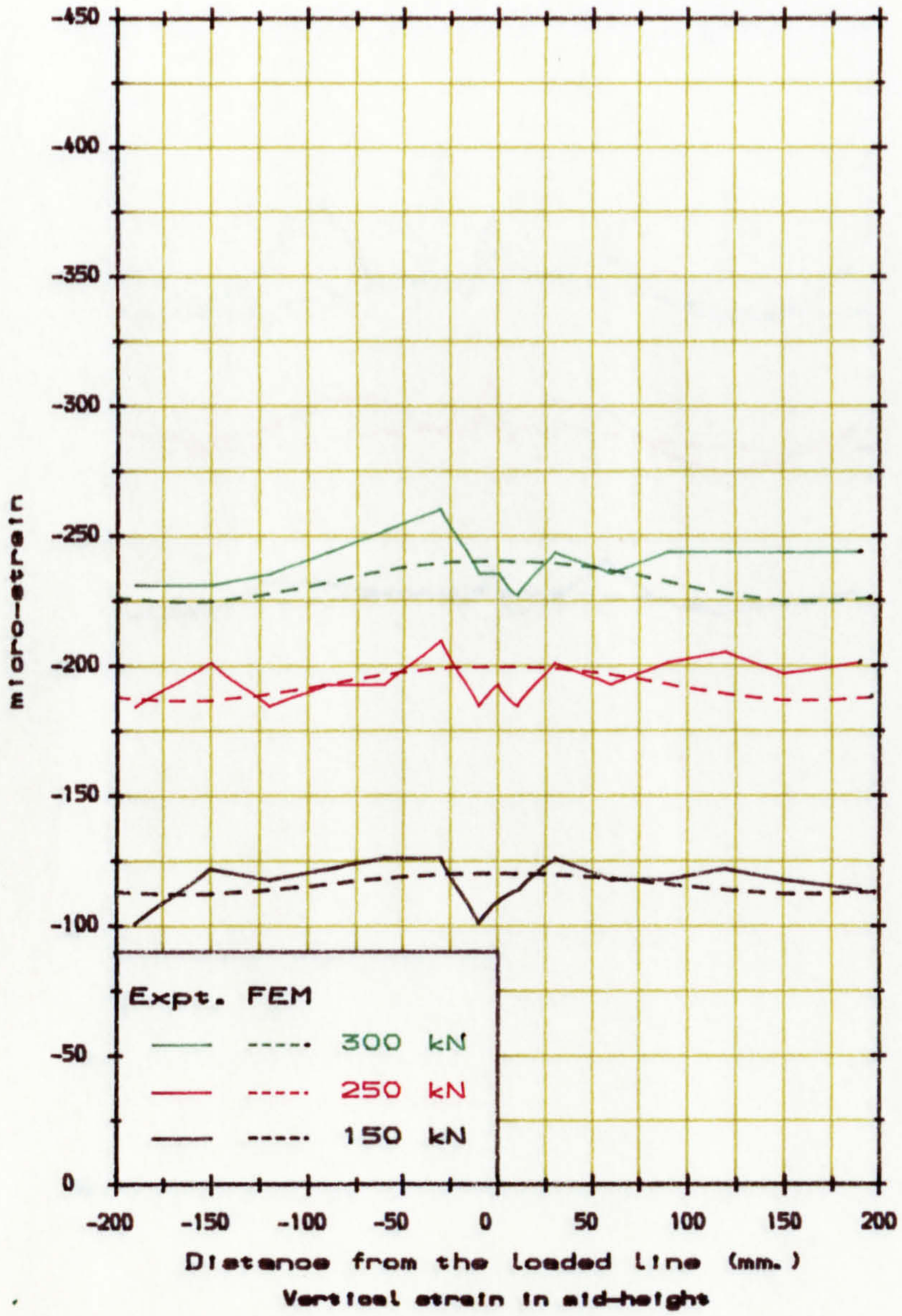

Fig. A. 9. Strain distribution of block R2-H2.

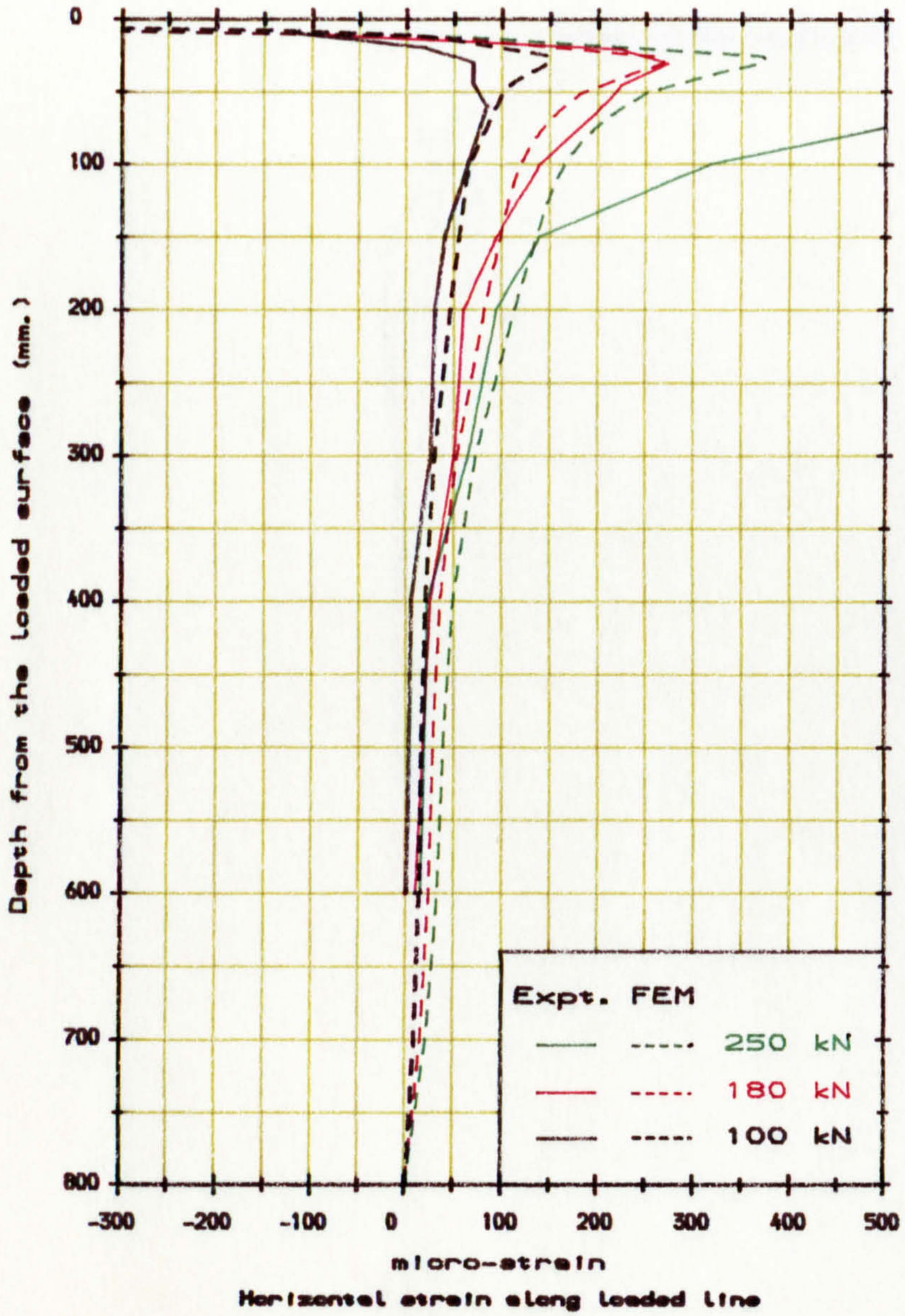

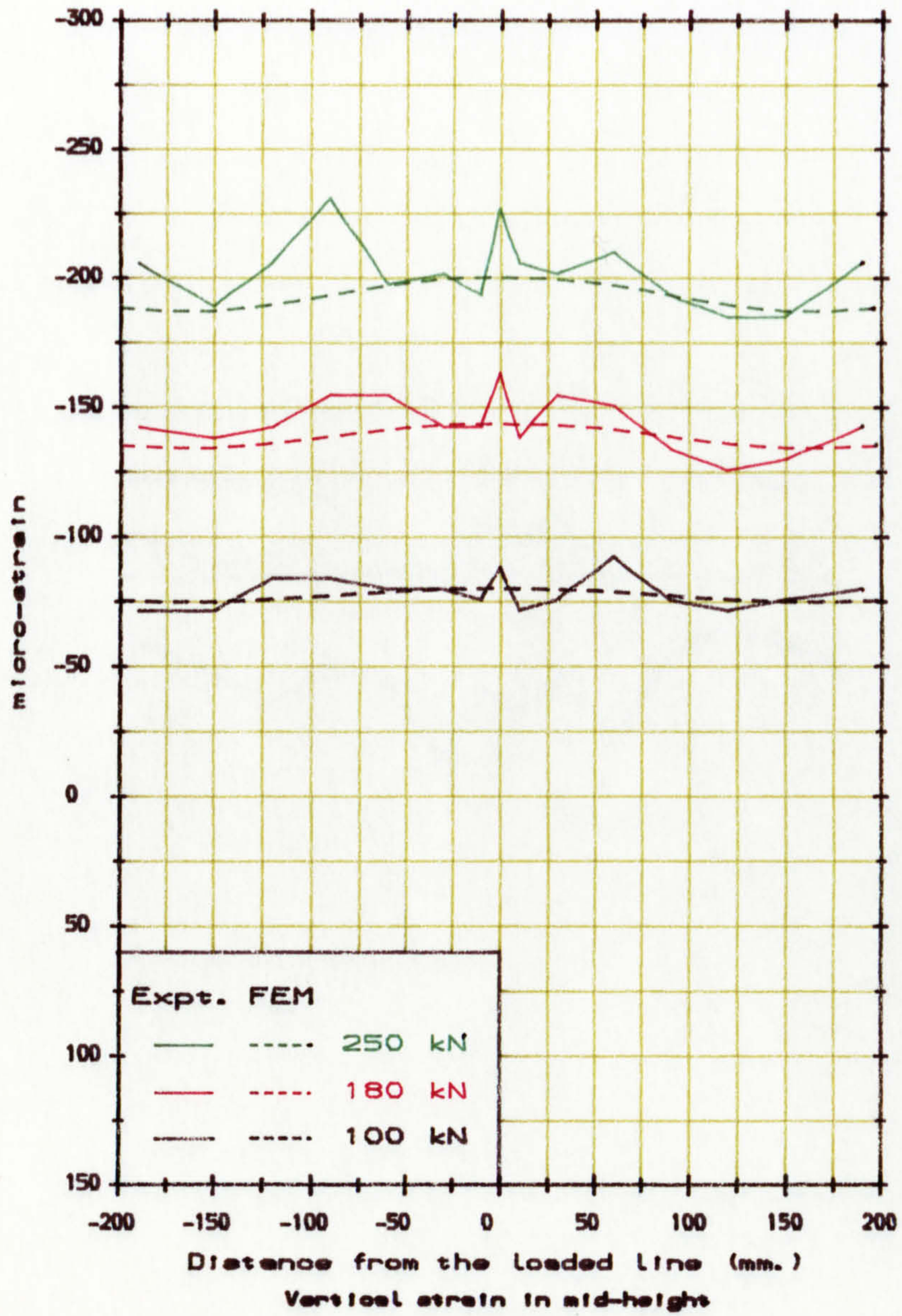

Fig. A. 10. Strain distribution of block R3-H2.

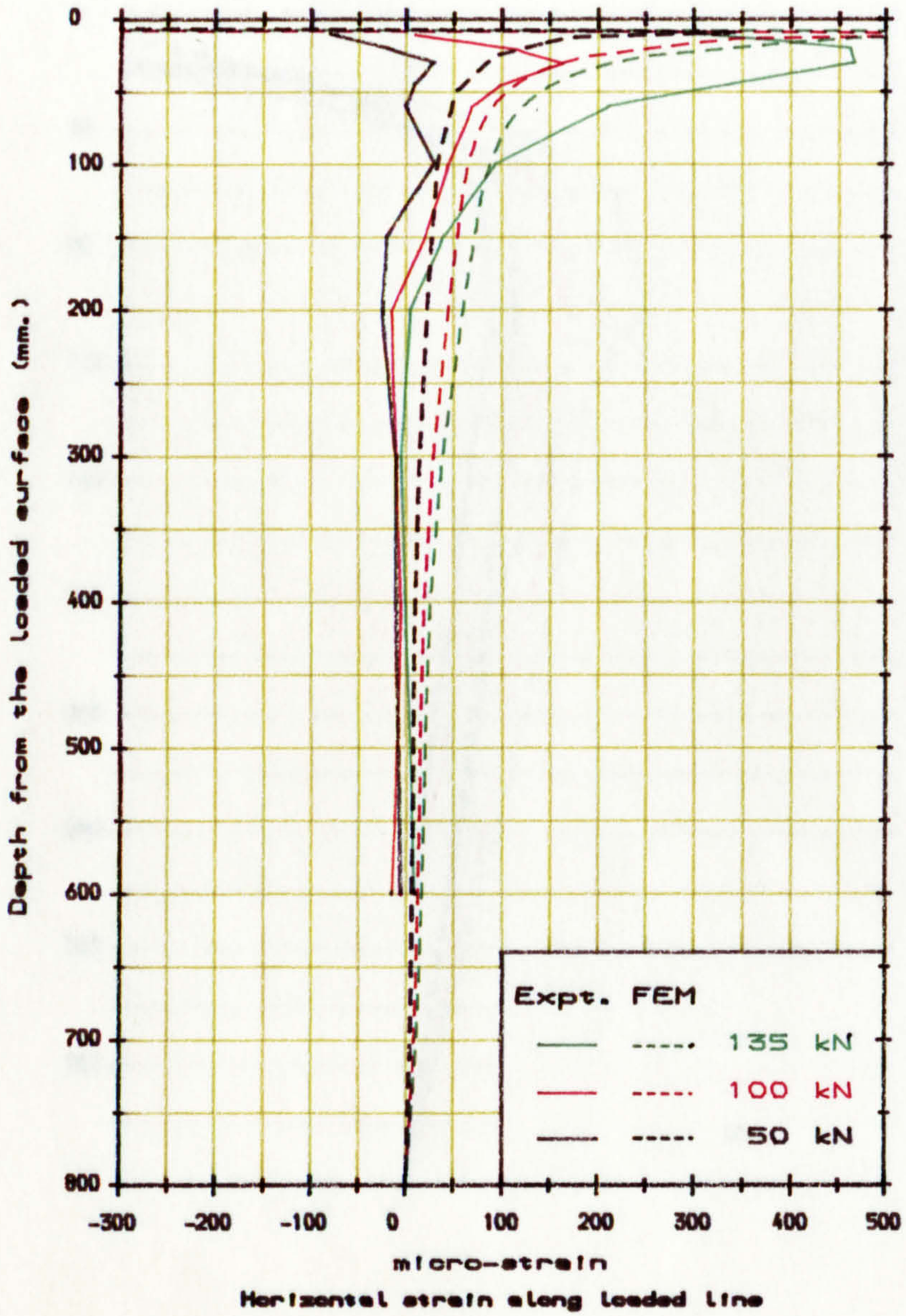

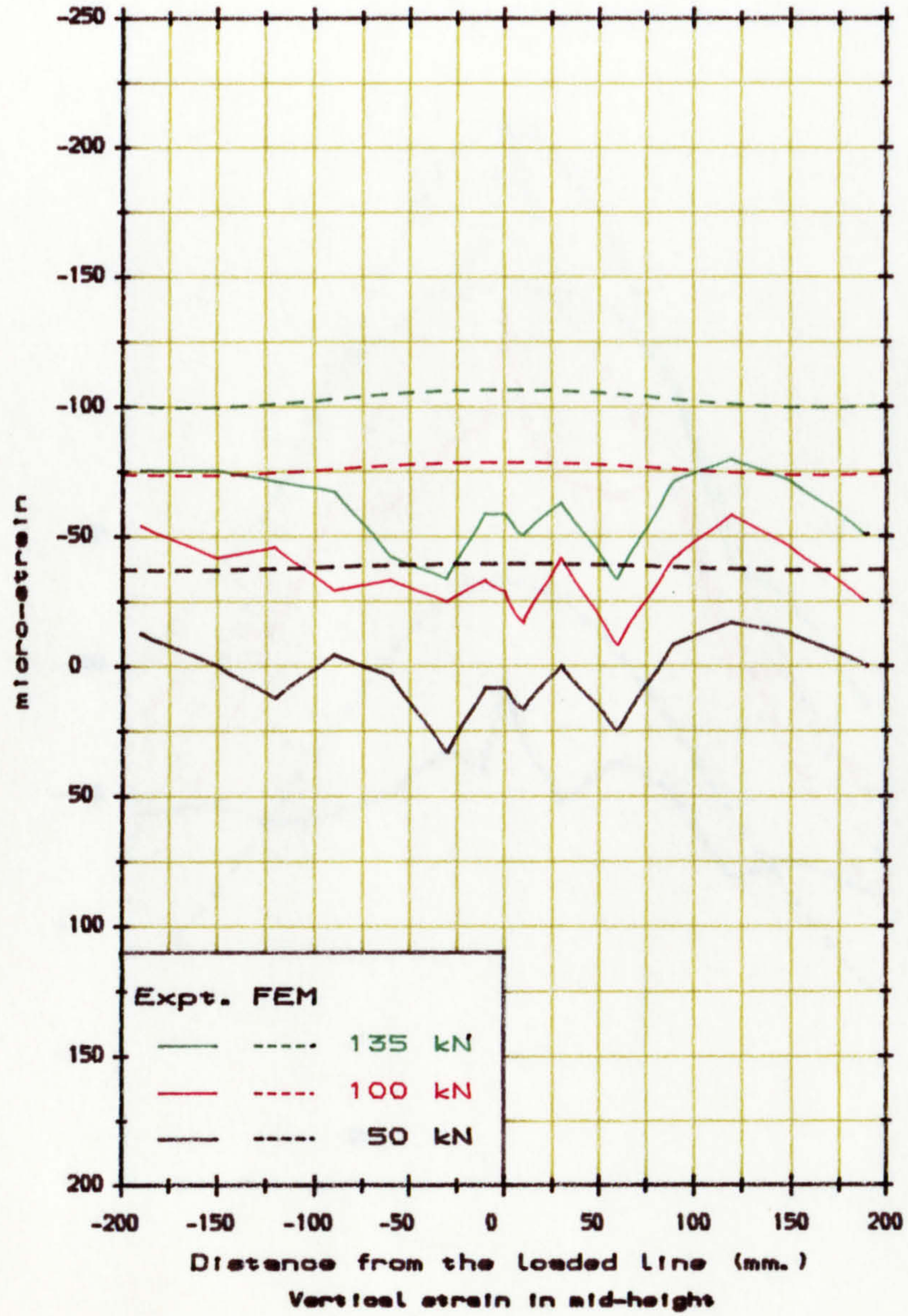

Fig. A. 11. Strain distribution of block R4-H2.

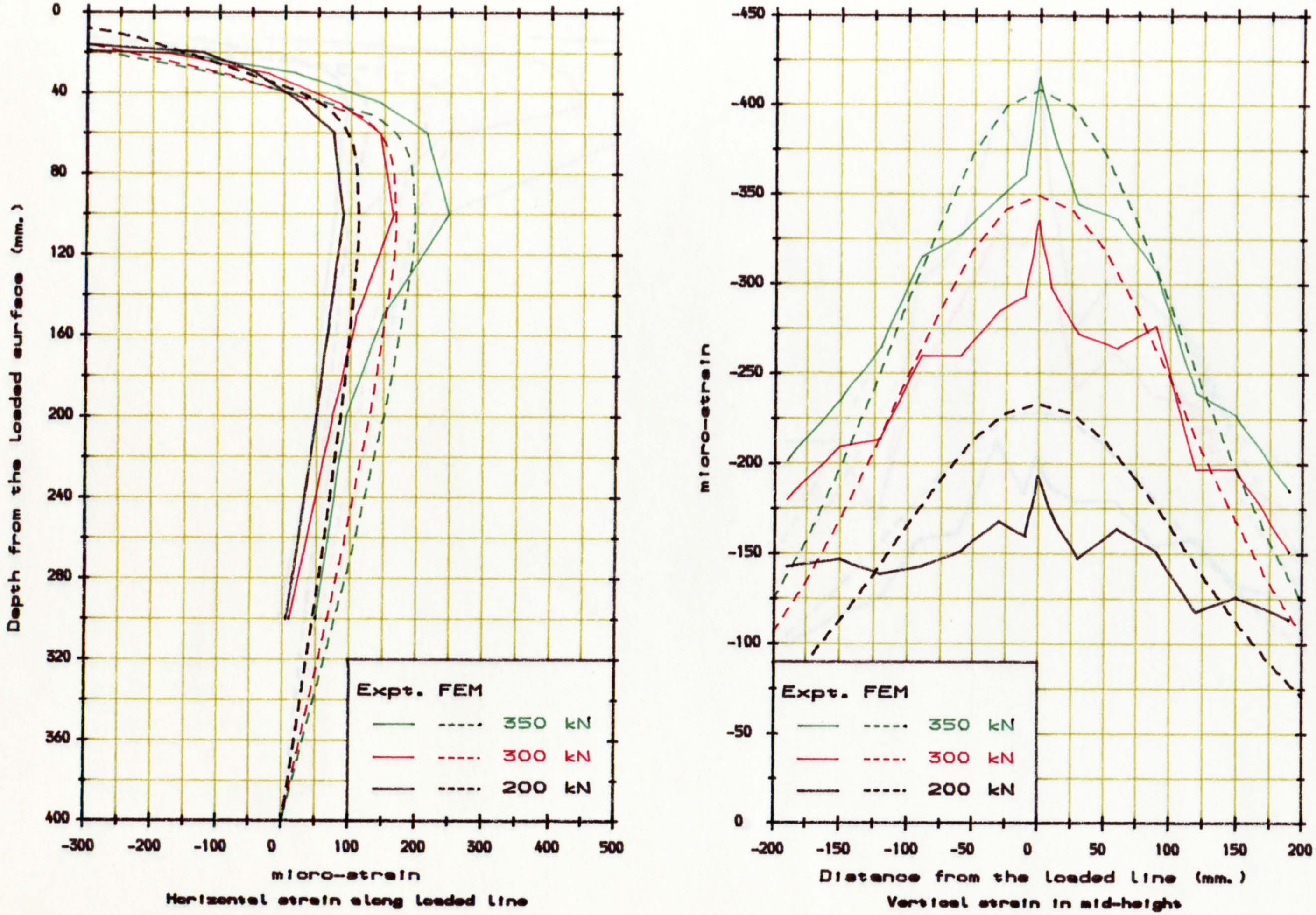

Fig. A. 12. Strain distribution of block R1-H3.

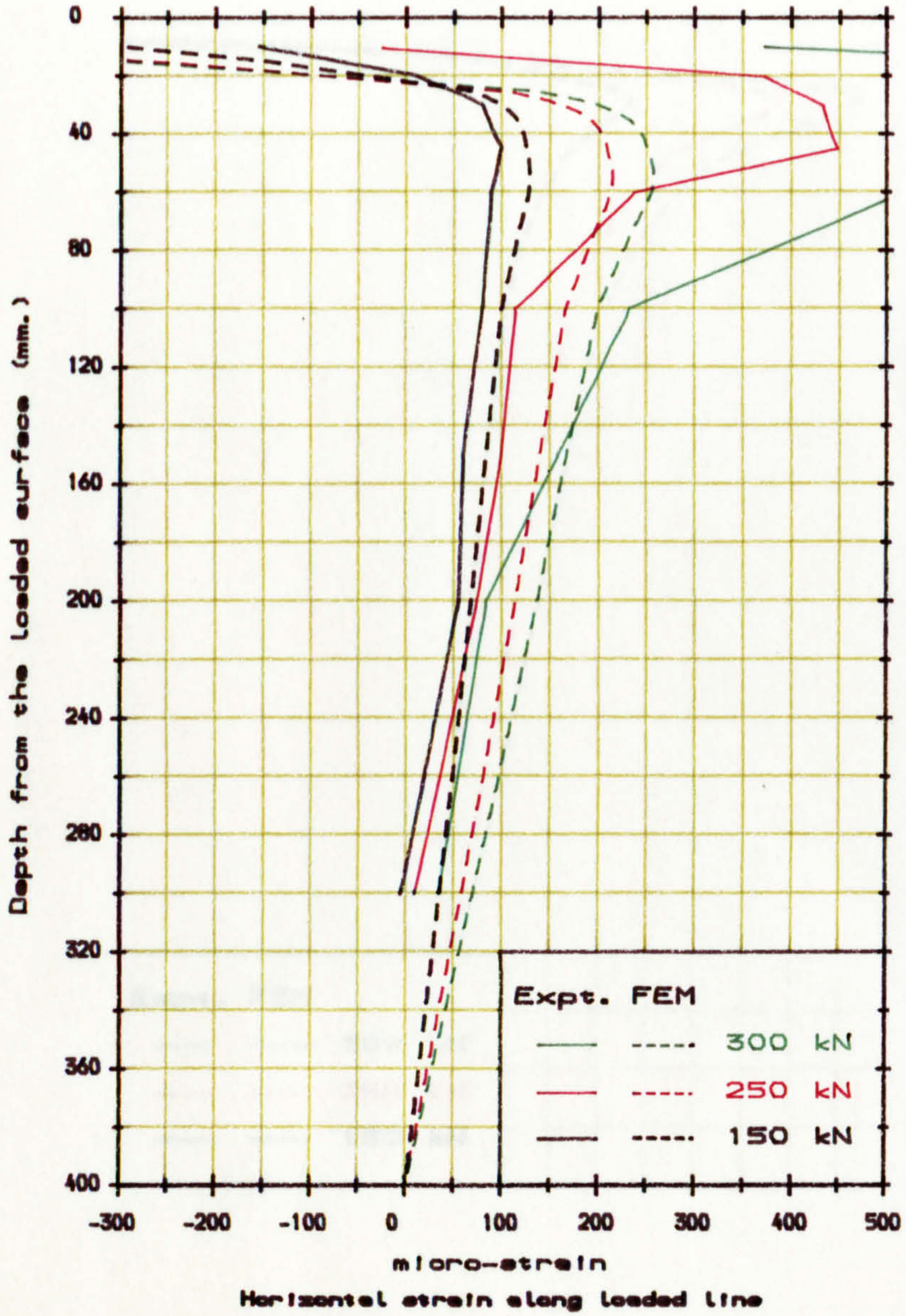

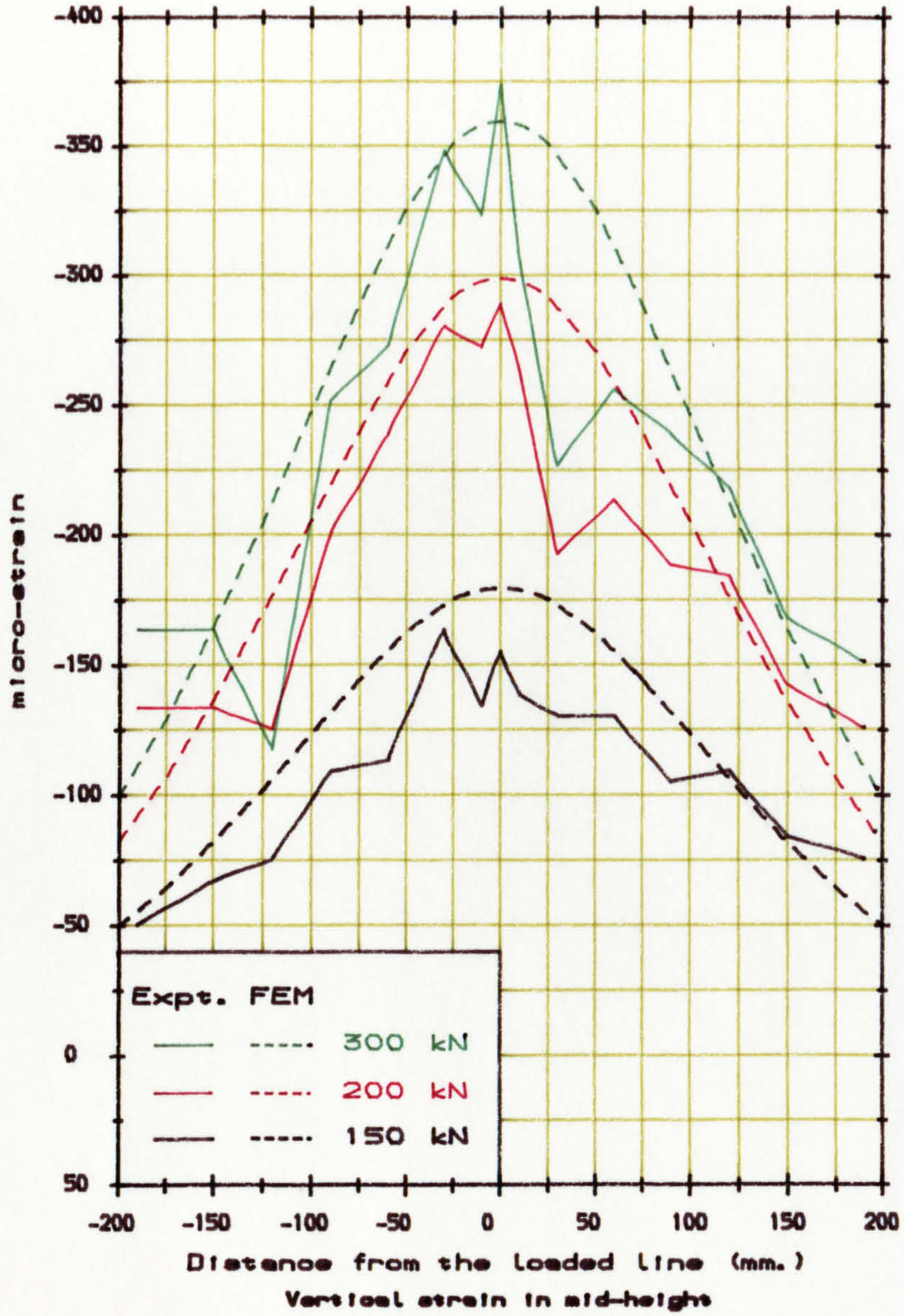

Fig. A. 13. Strain distribution of block R2-H3.

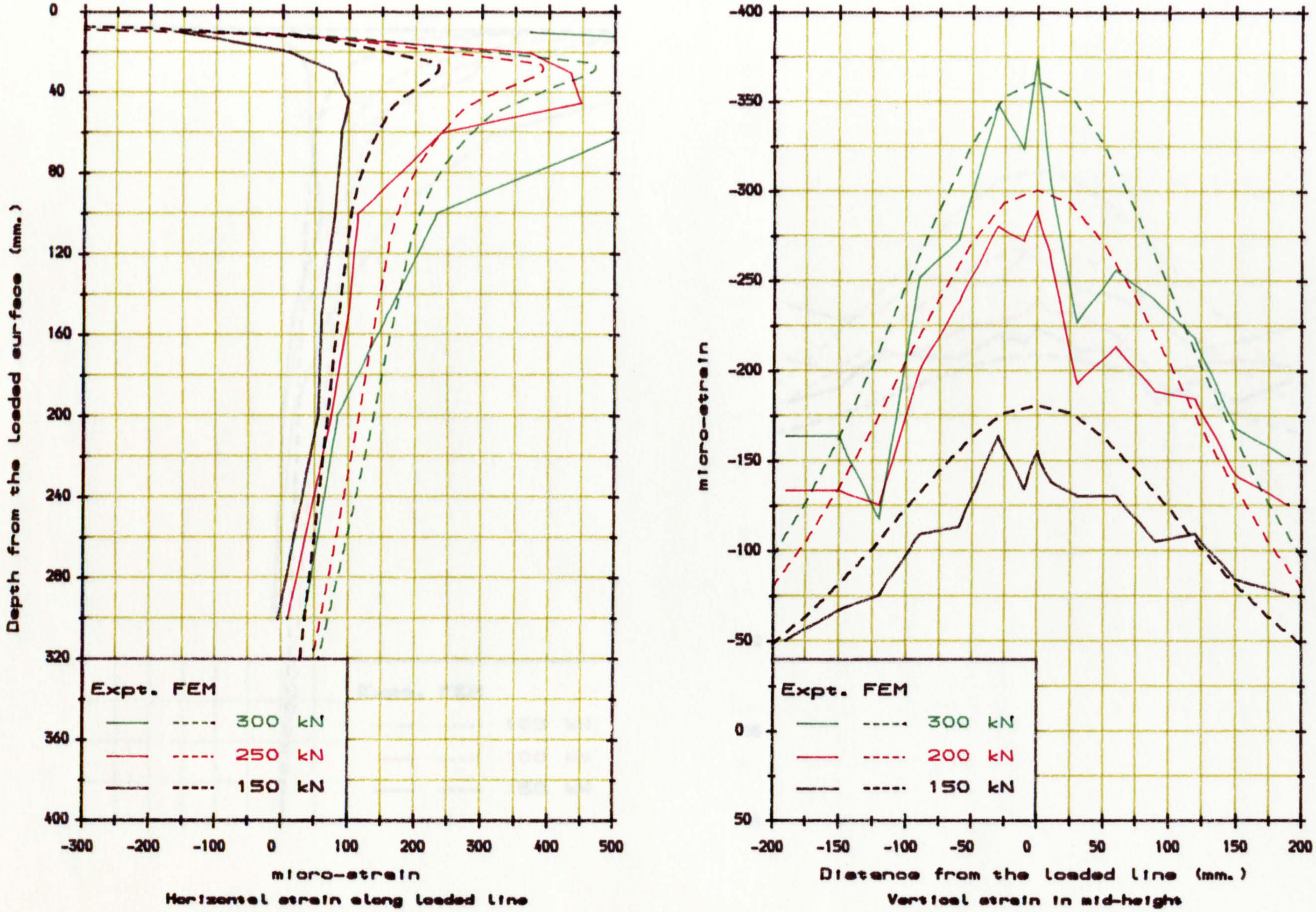

Fig. A. 14. Strain distribution of block R3-H3.

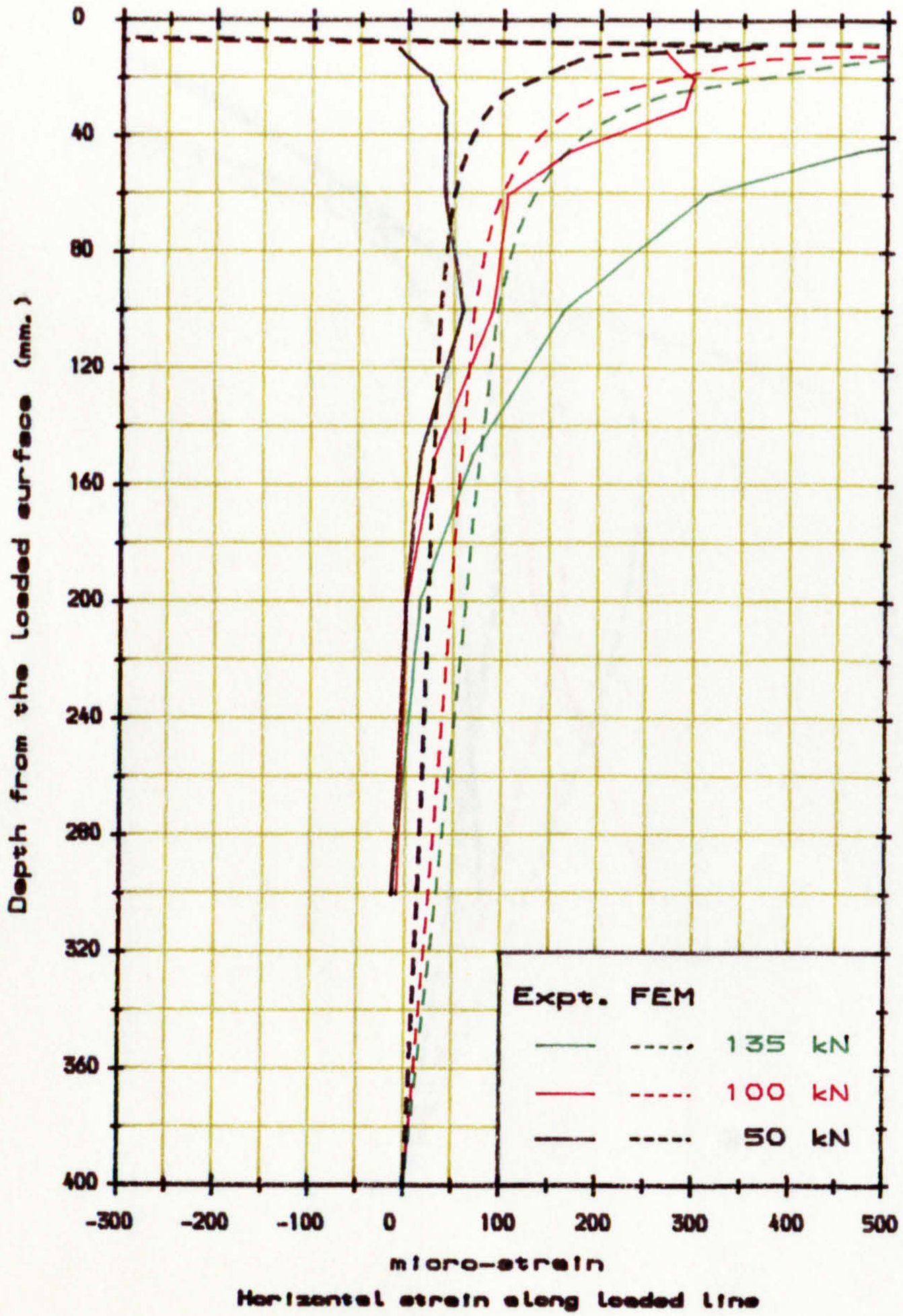

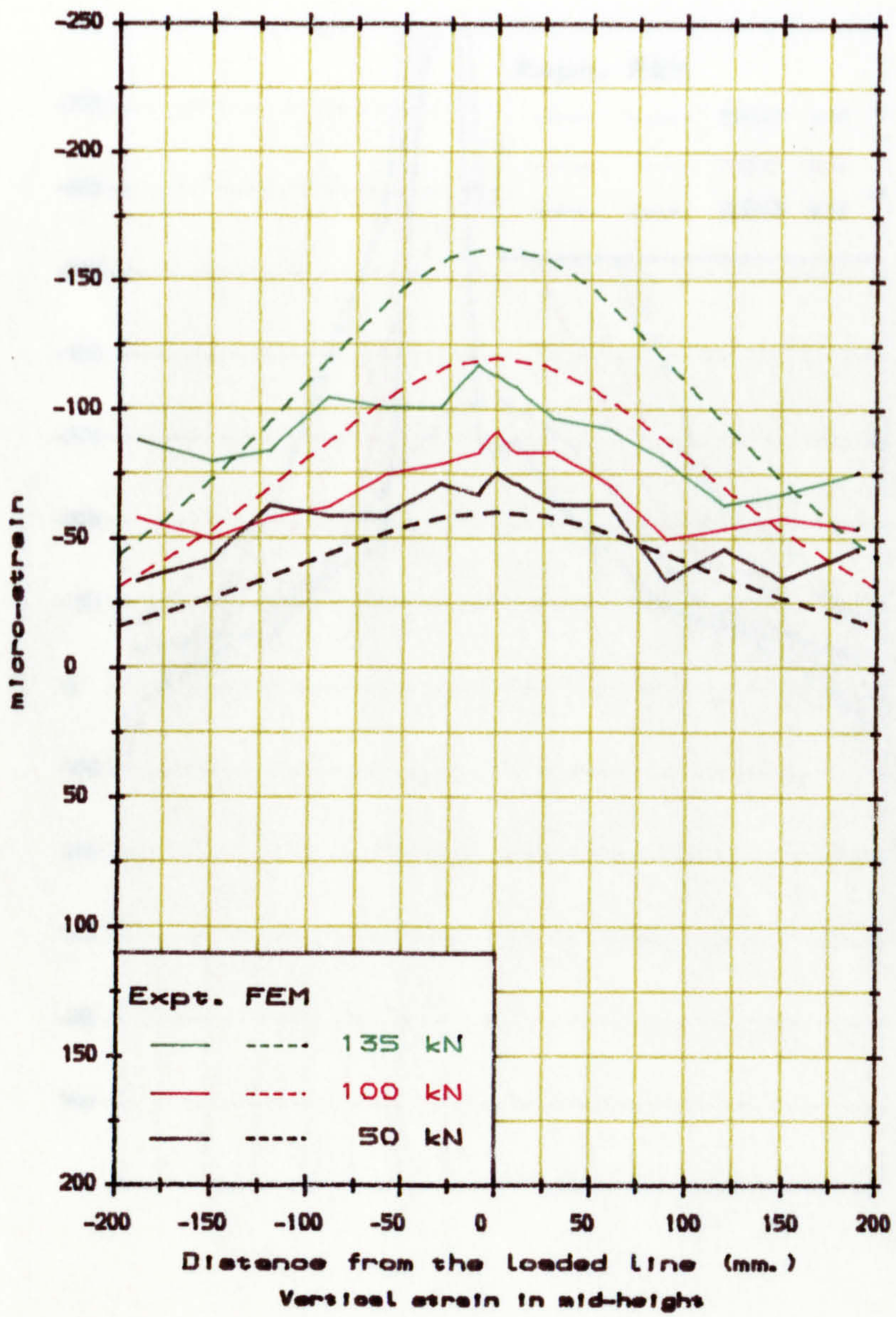

Fig. A. 15. Strain distribution of block R4-H3.

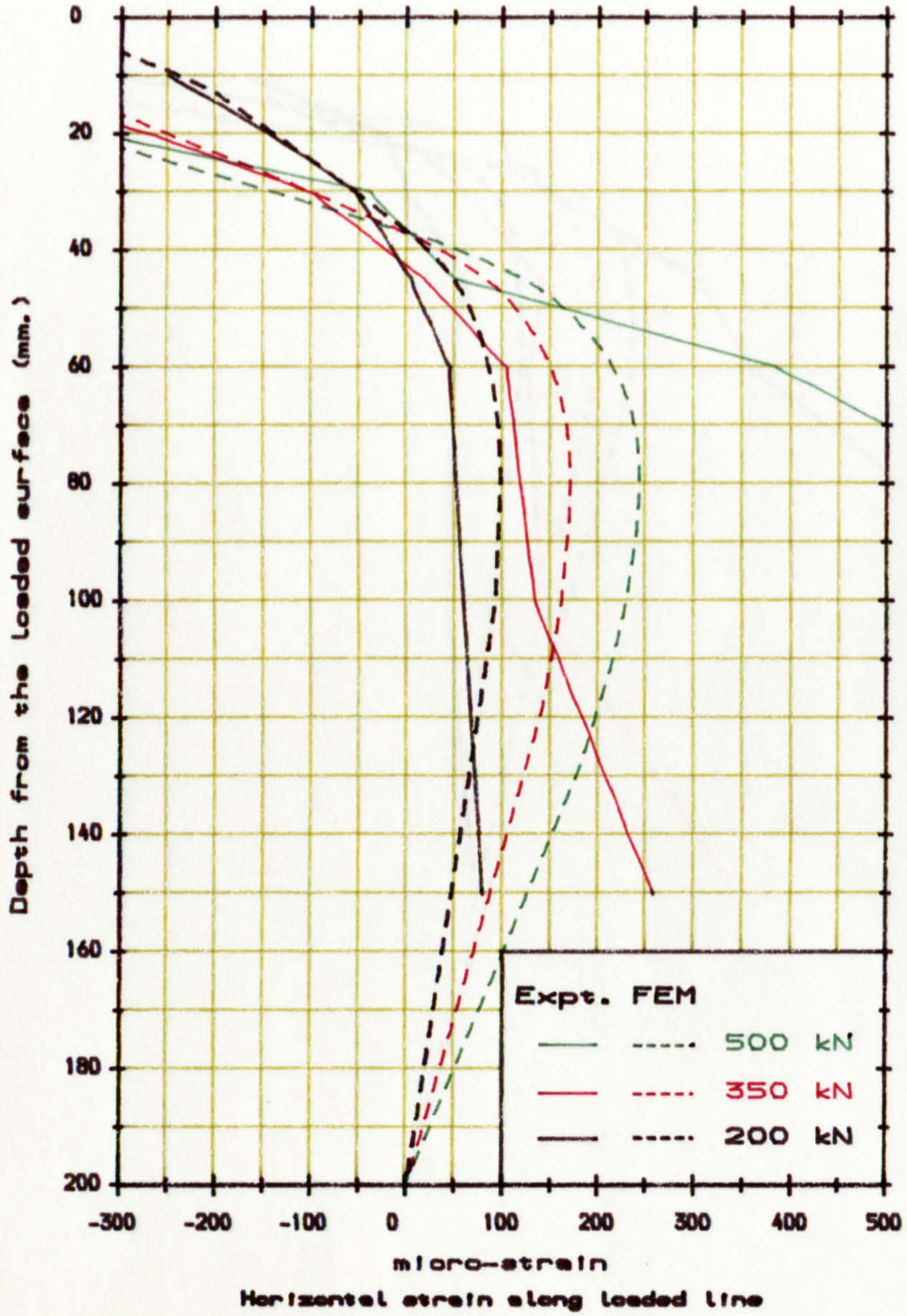

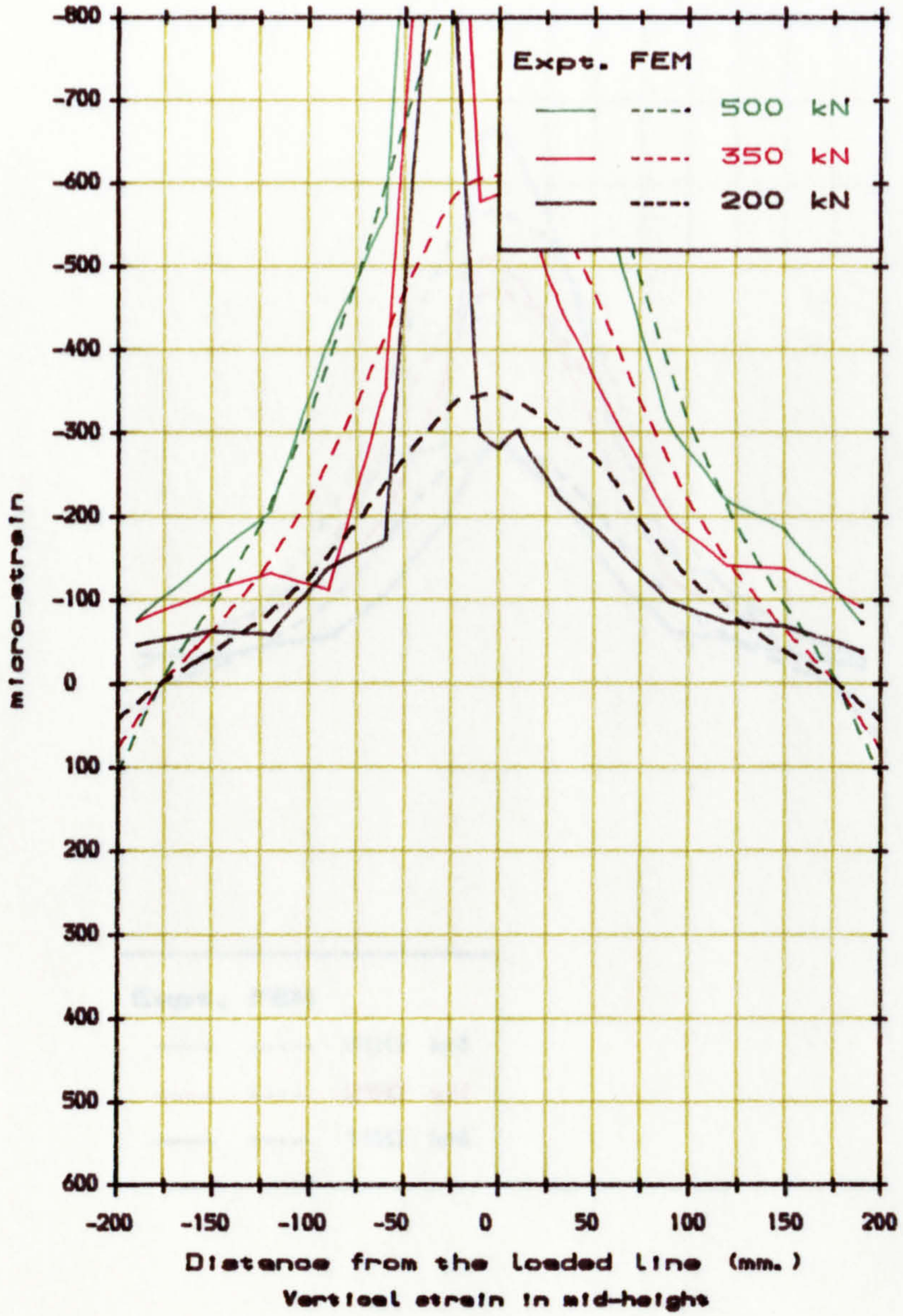

Fig. A. 16. Strain distribution of block R1-H4.

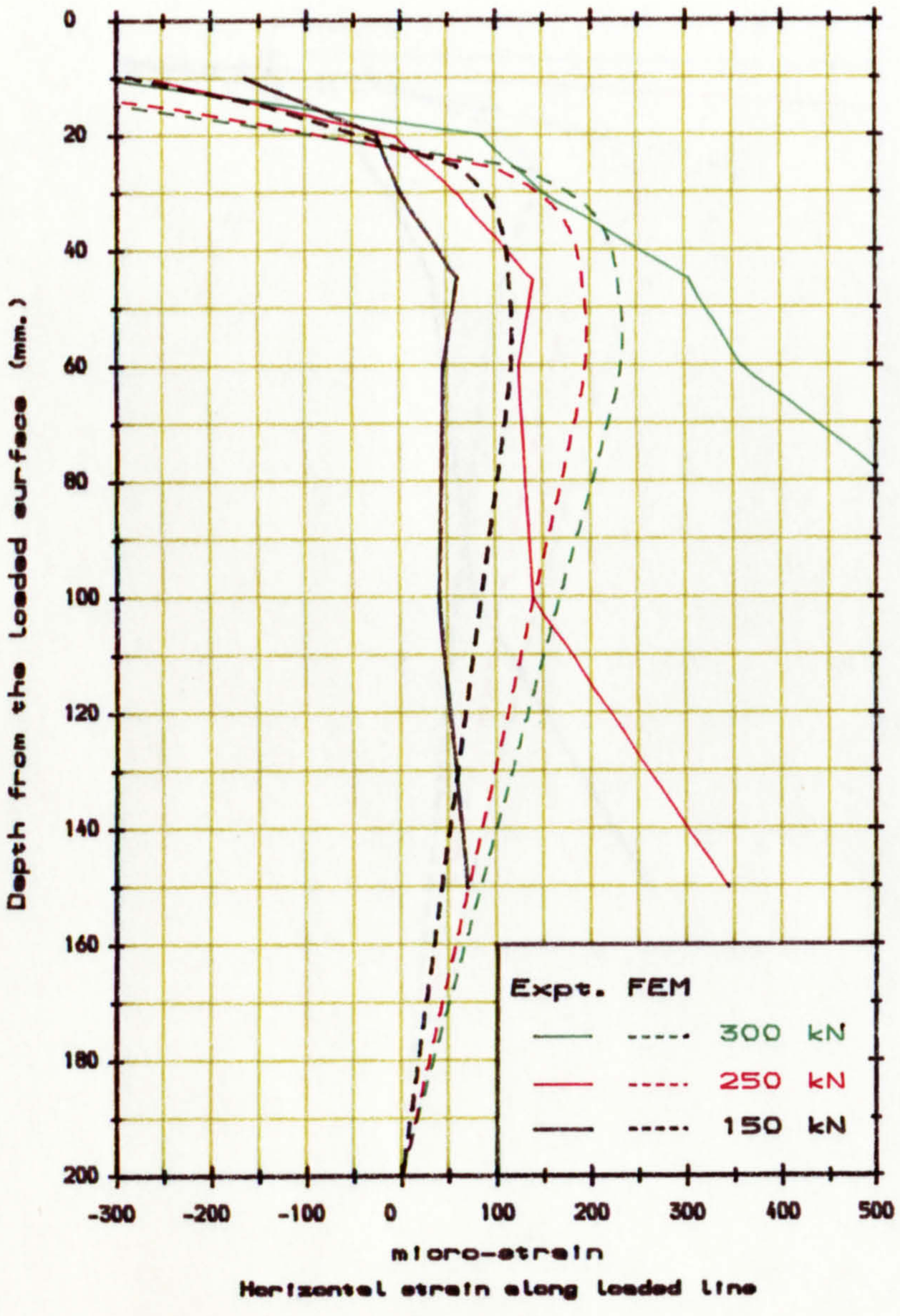

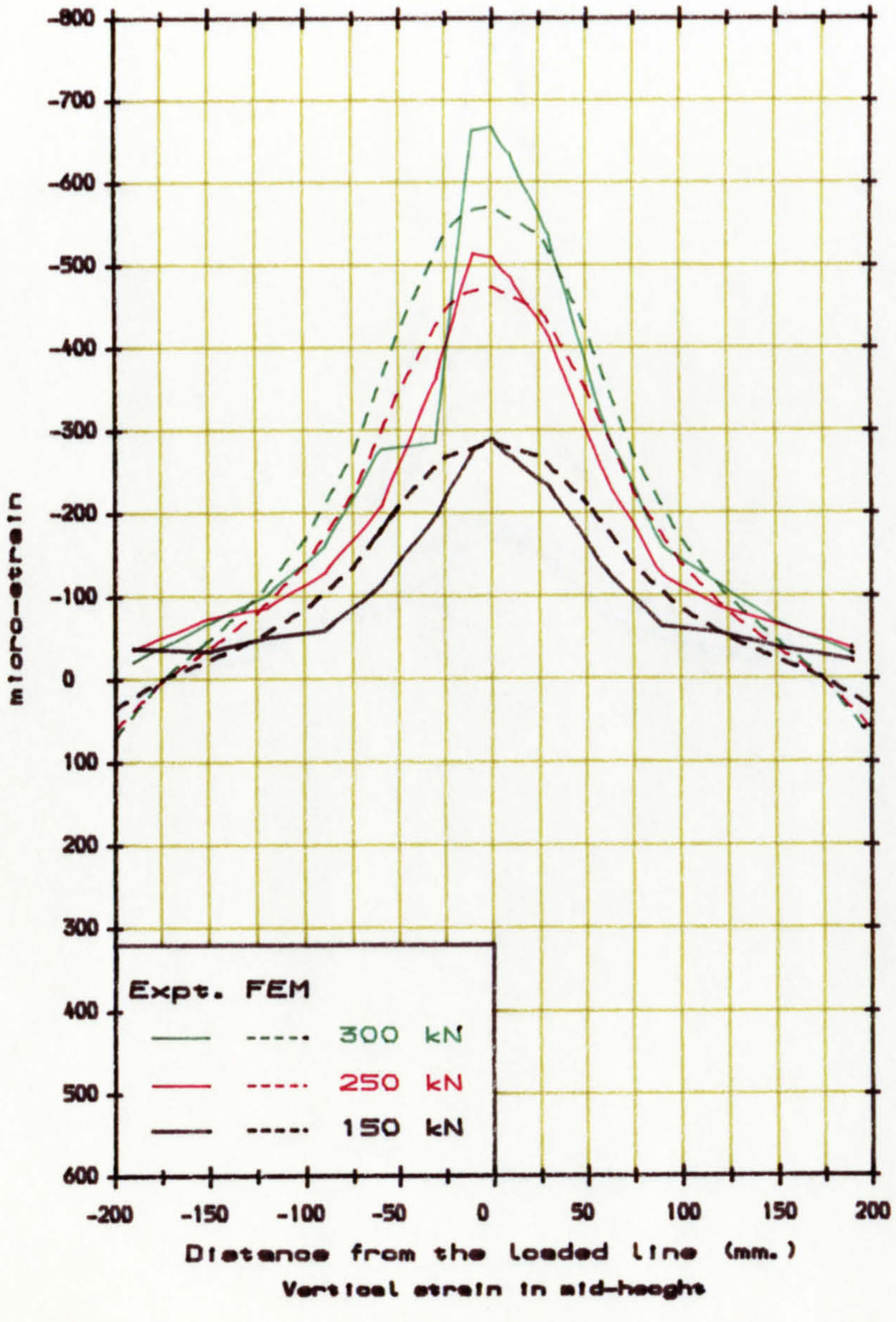

Fig. A. 17. Strain distribution of block R2-H4.

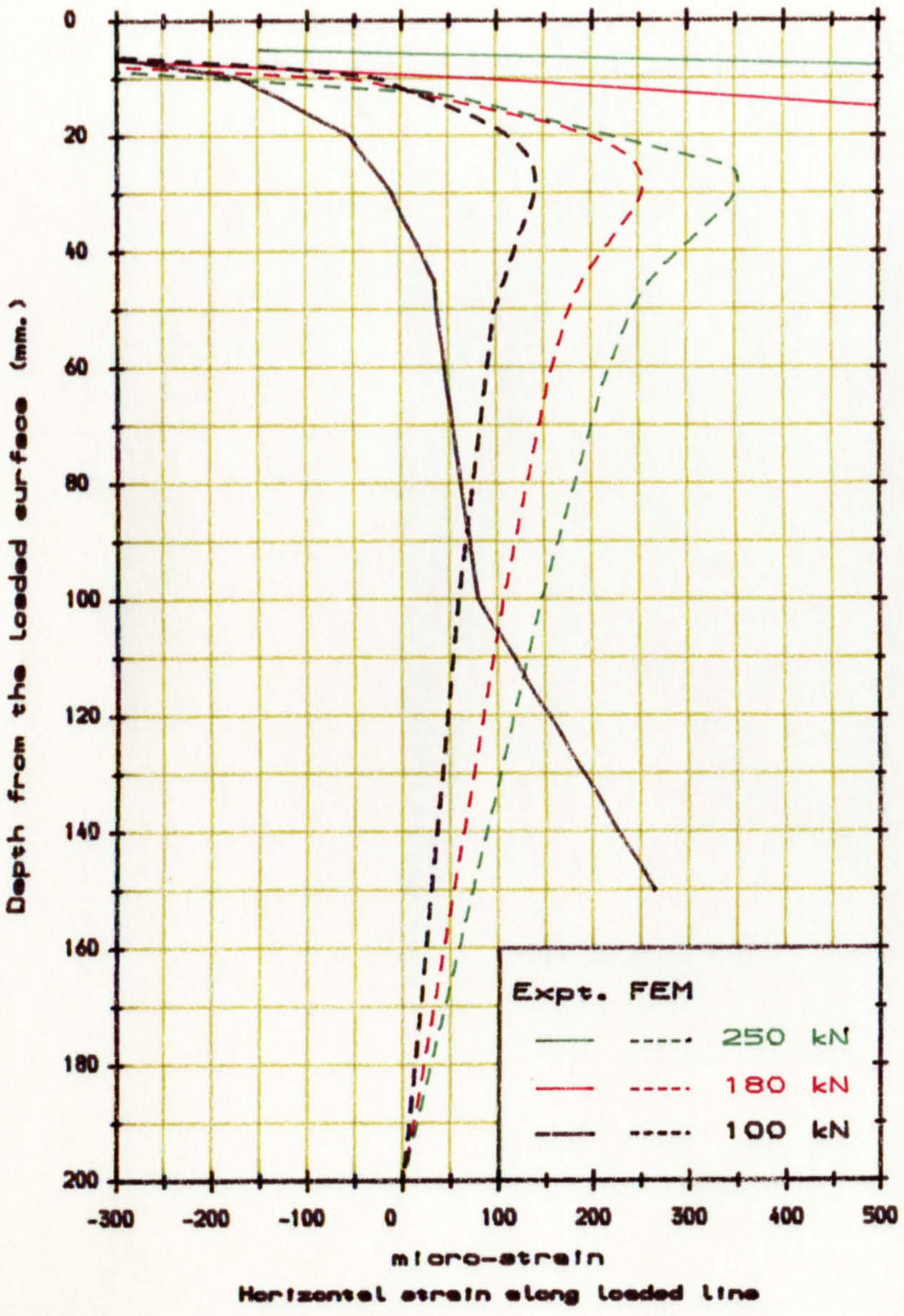

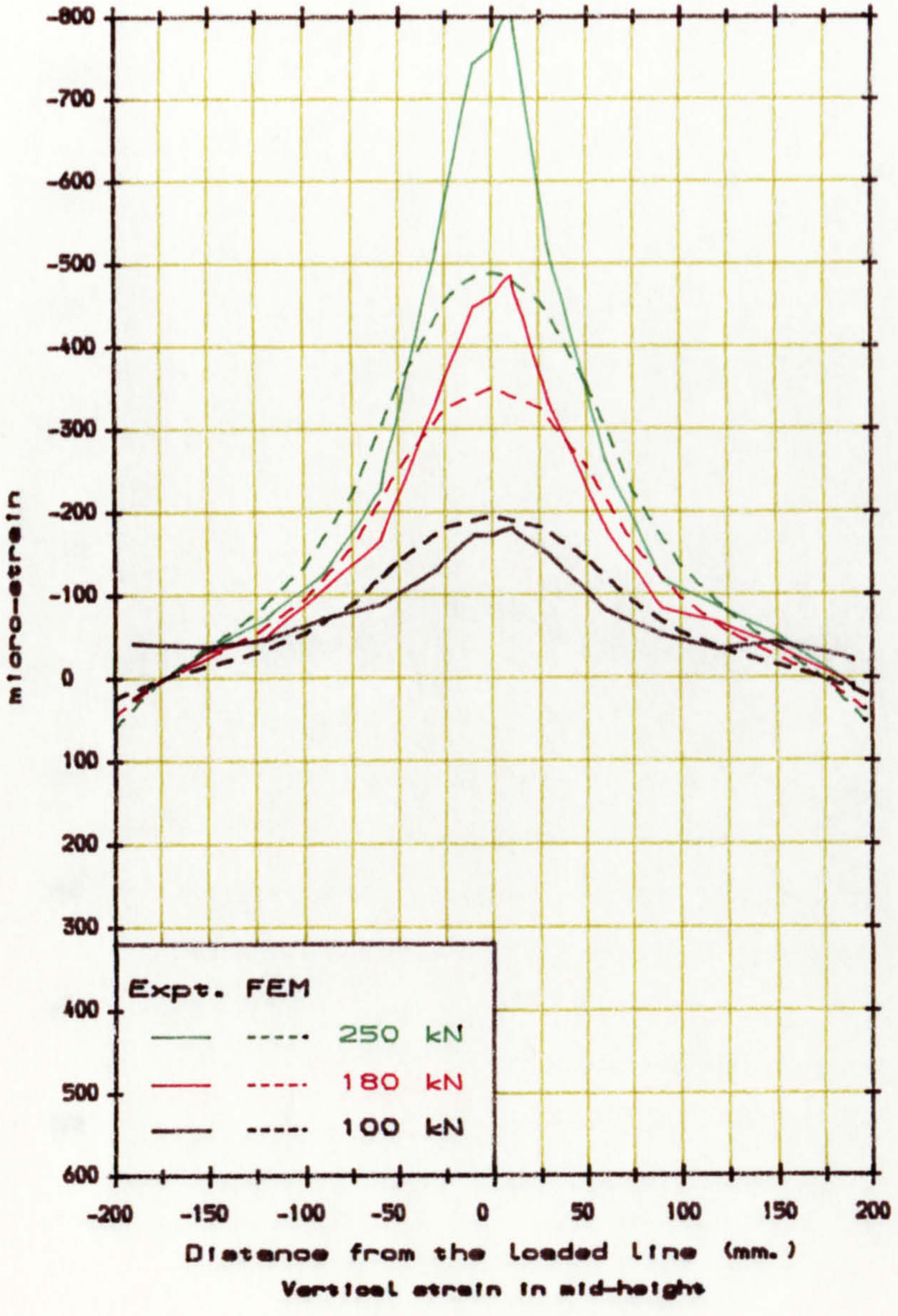

Fig. A. 18. Strain distribution of block R3-H4.

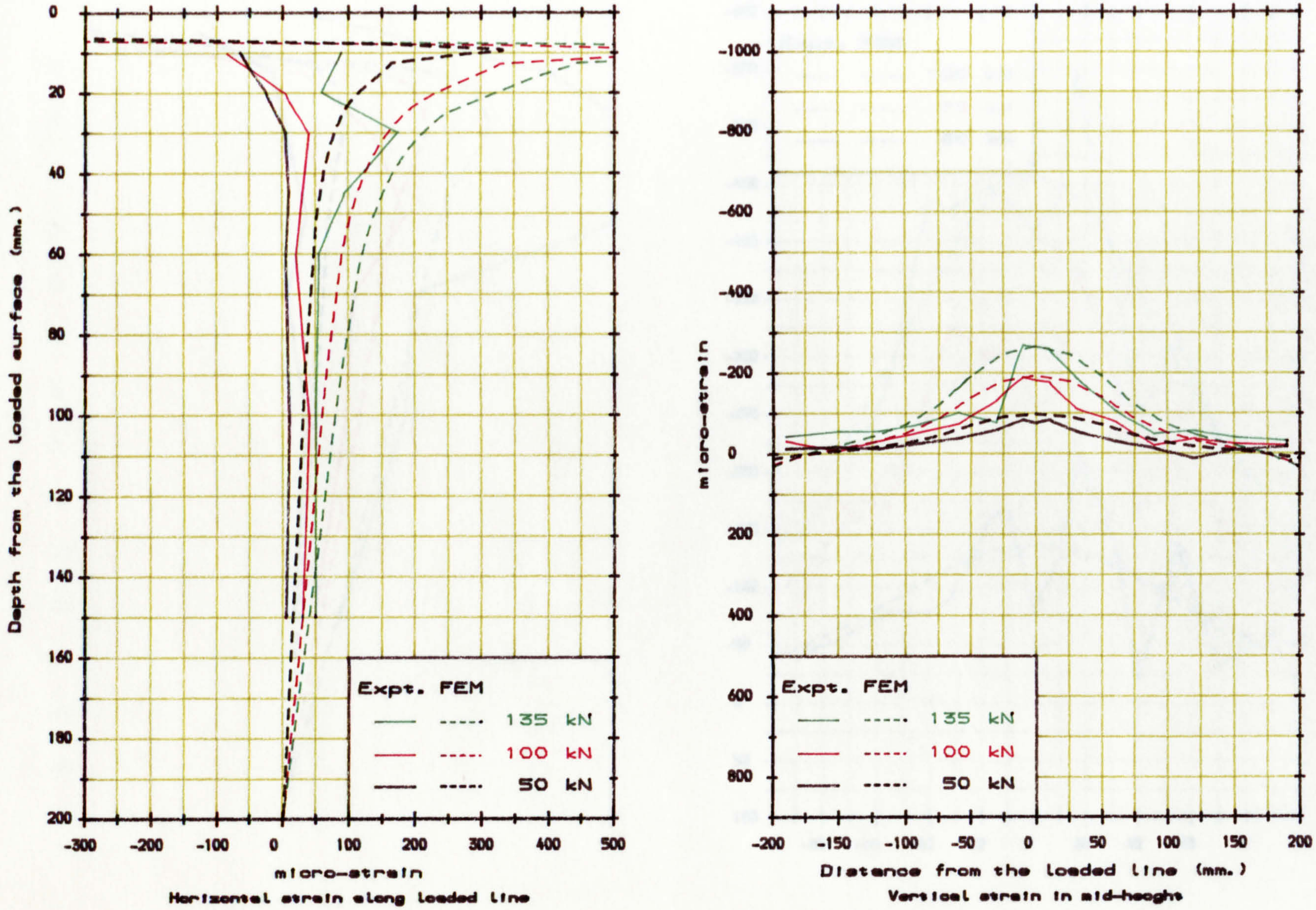

Fig. A. 19. Strain distribution of block R4-H4.

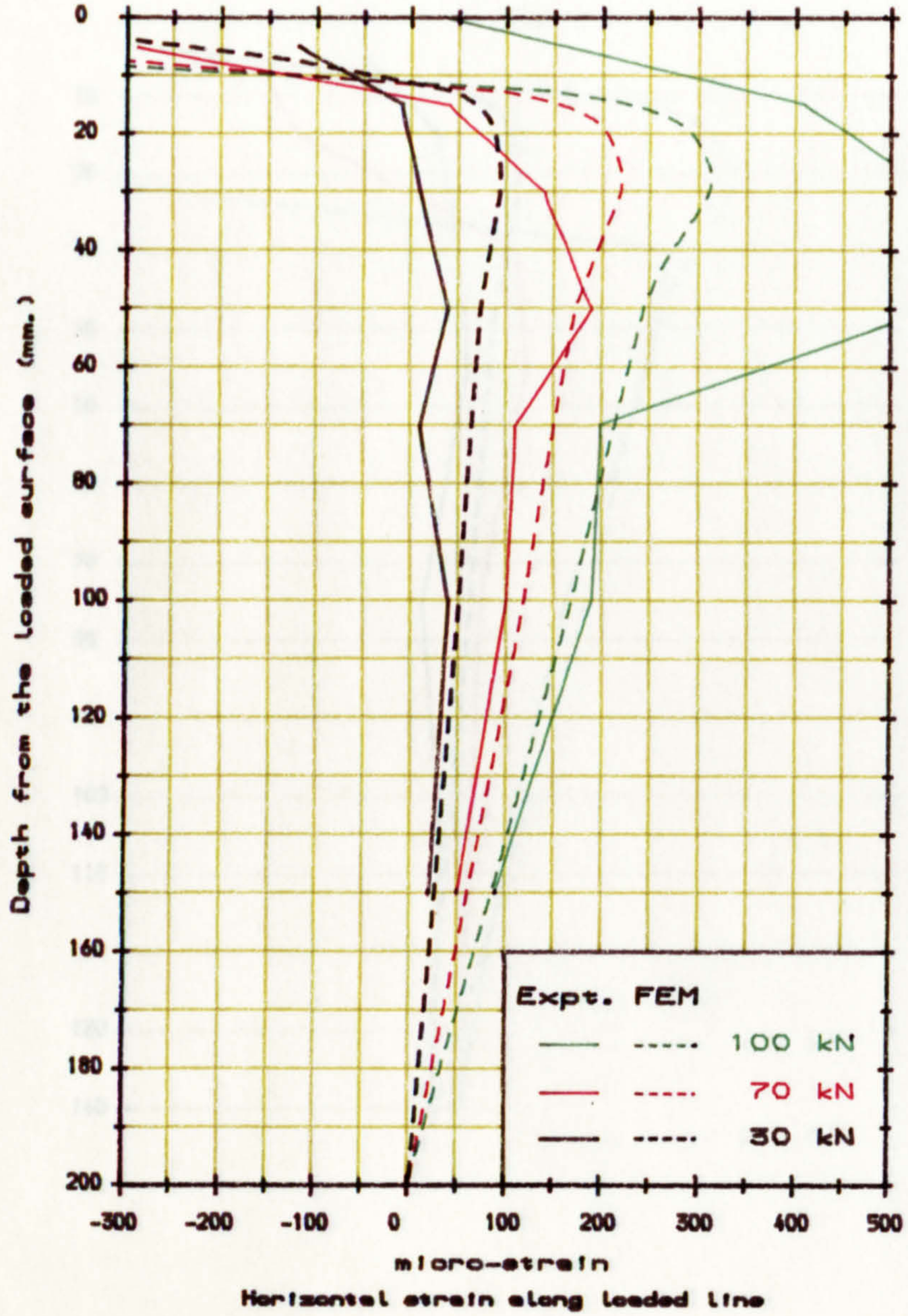

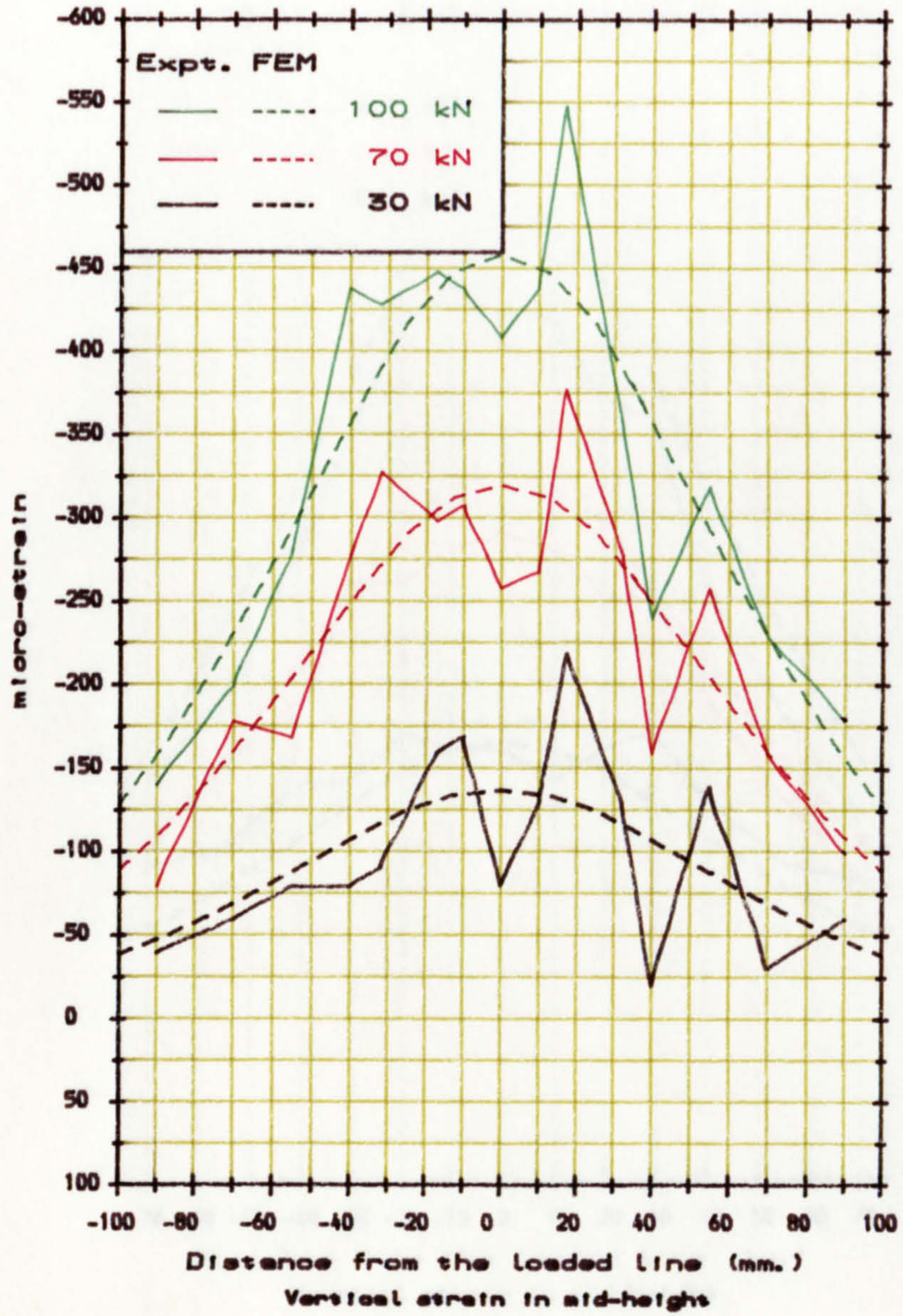

Fig. A. 20. Strain distribution of block S1.

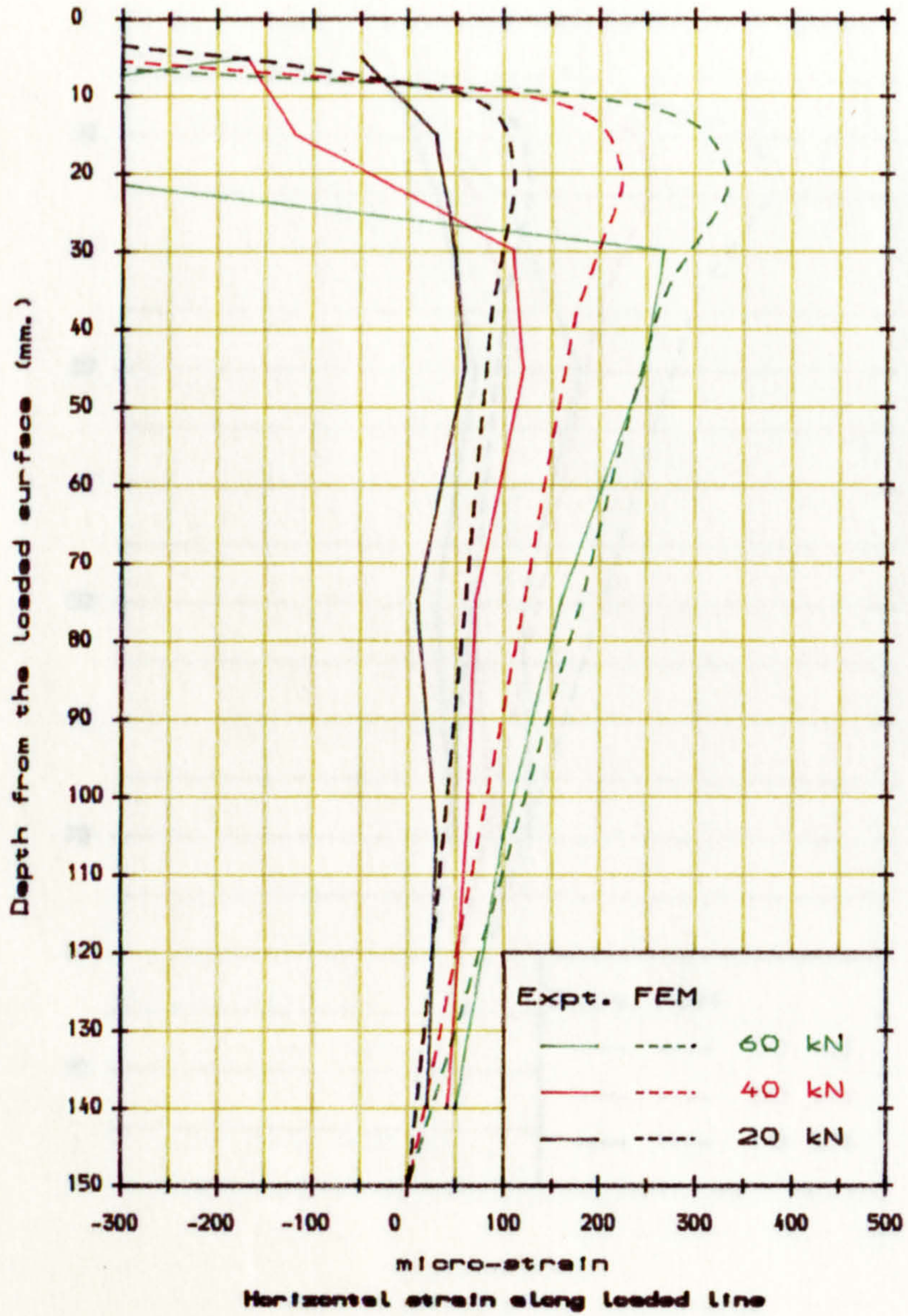

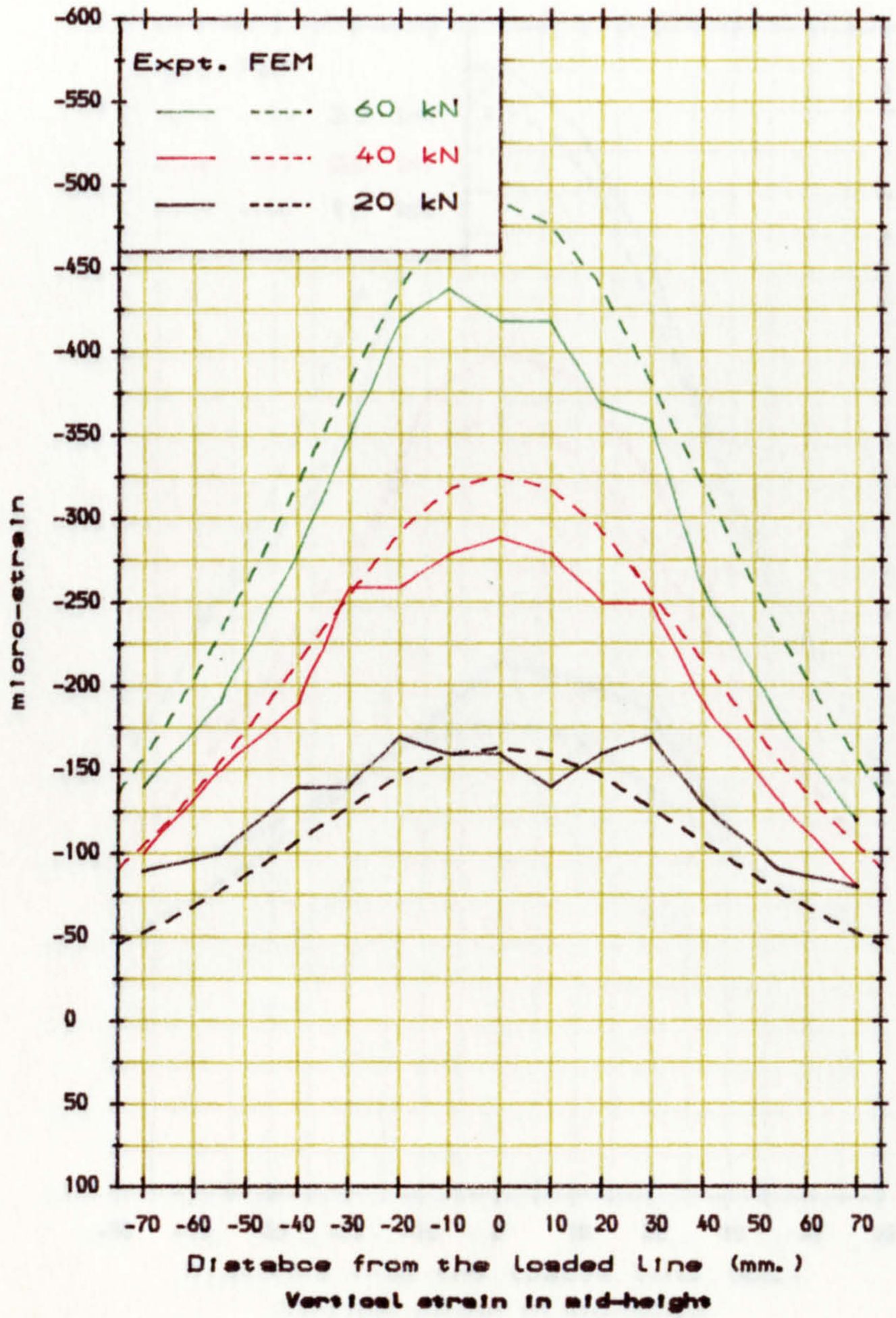

Fig. A. 21. Strain distribution of block S2.

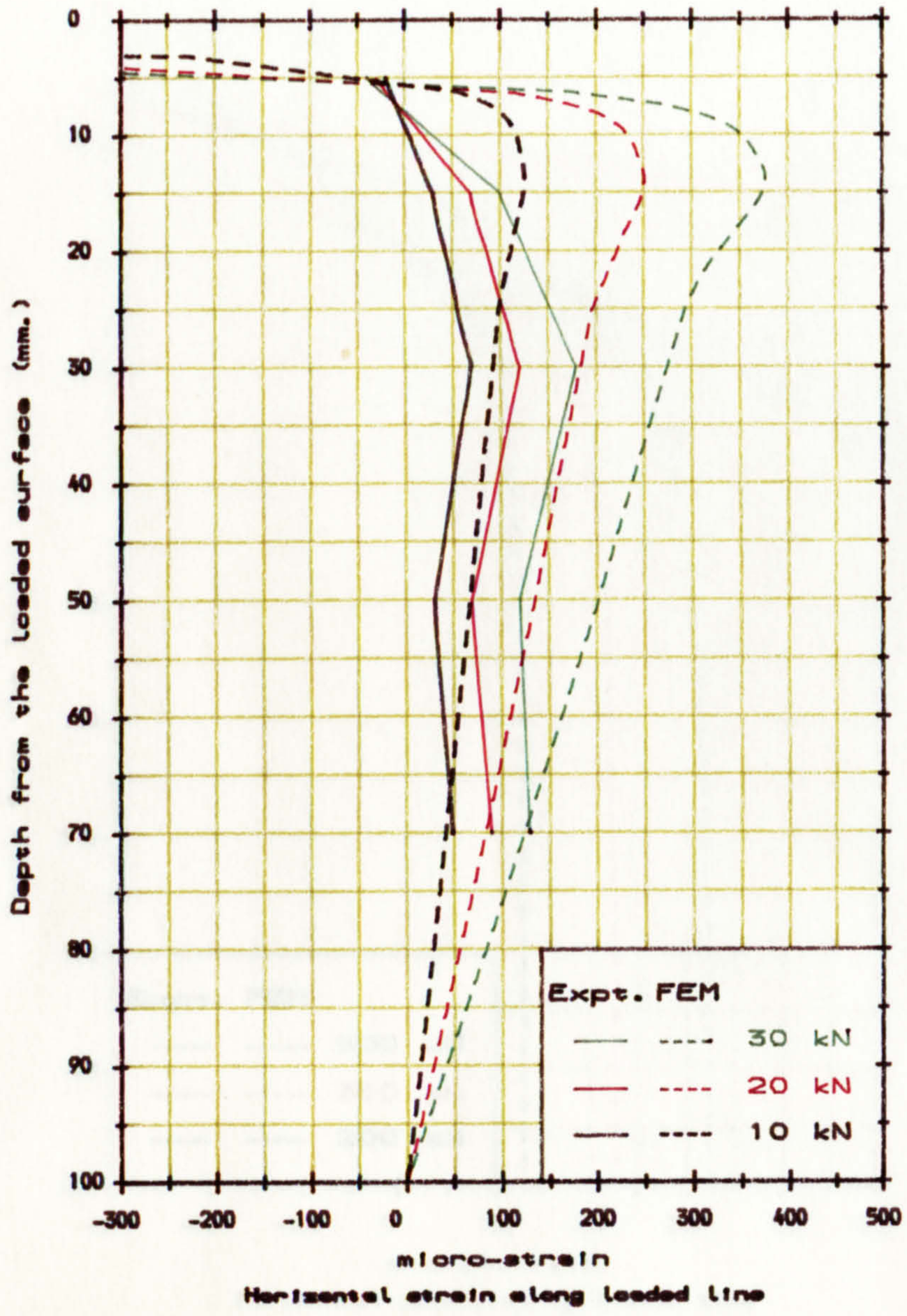

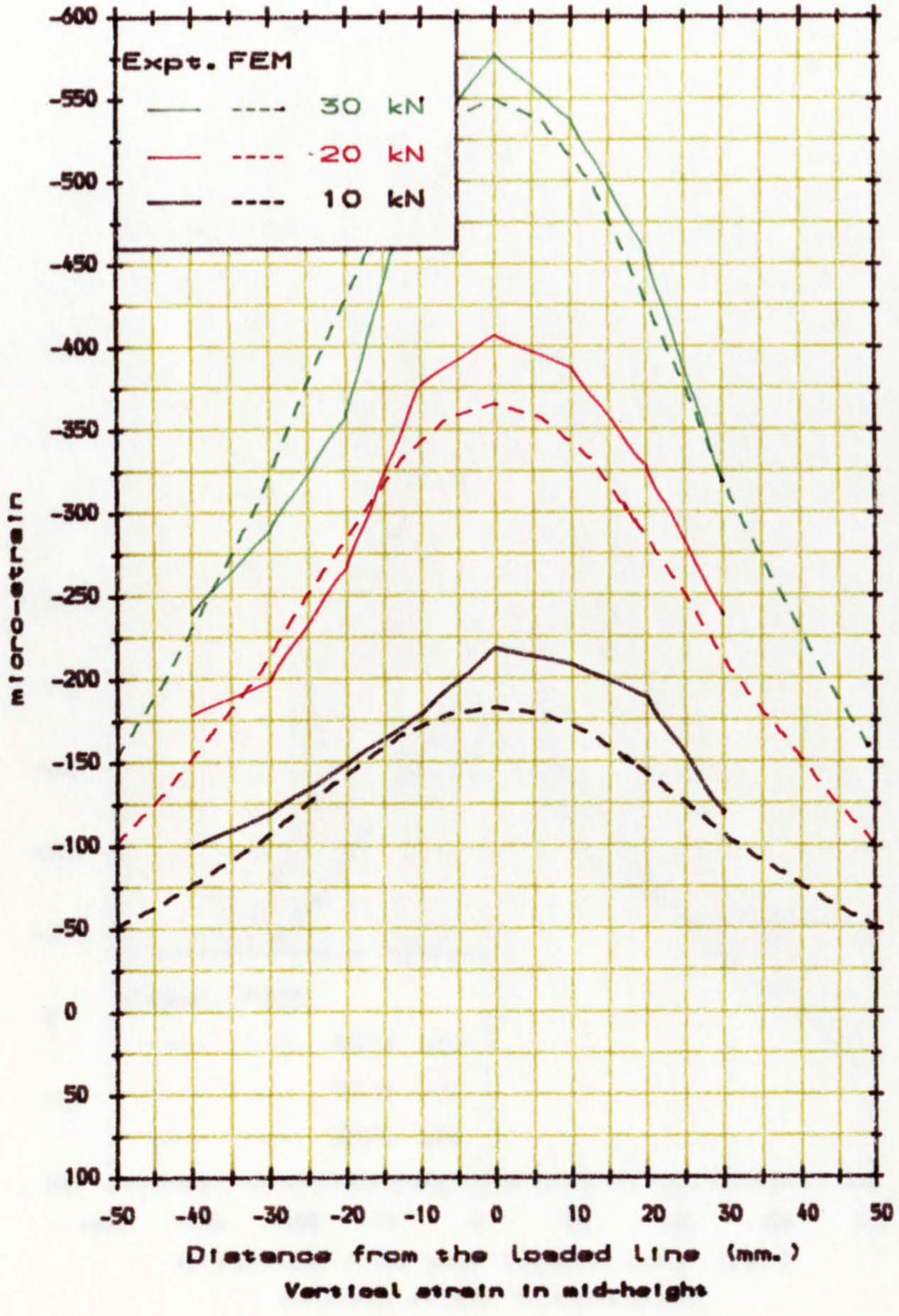

Fig. A. 22. Strain distribution of block S3.

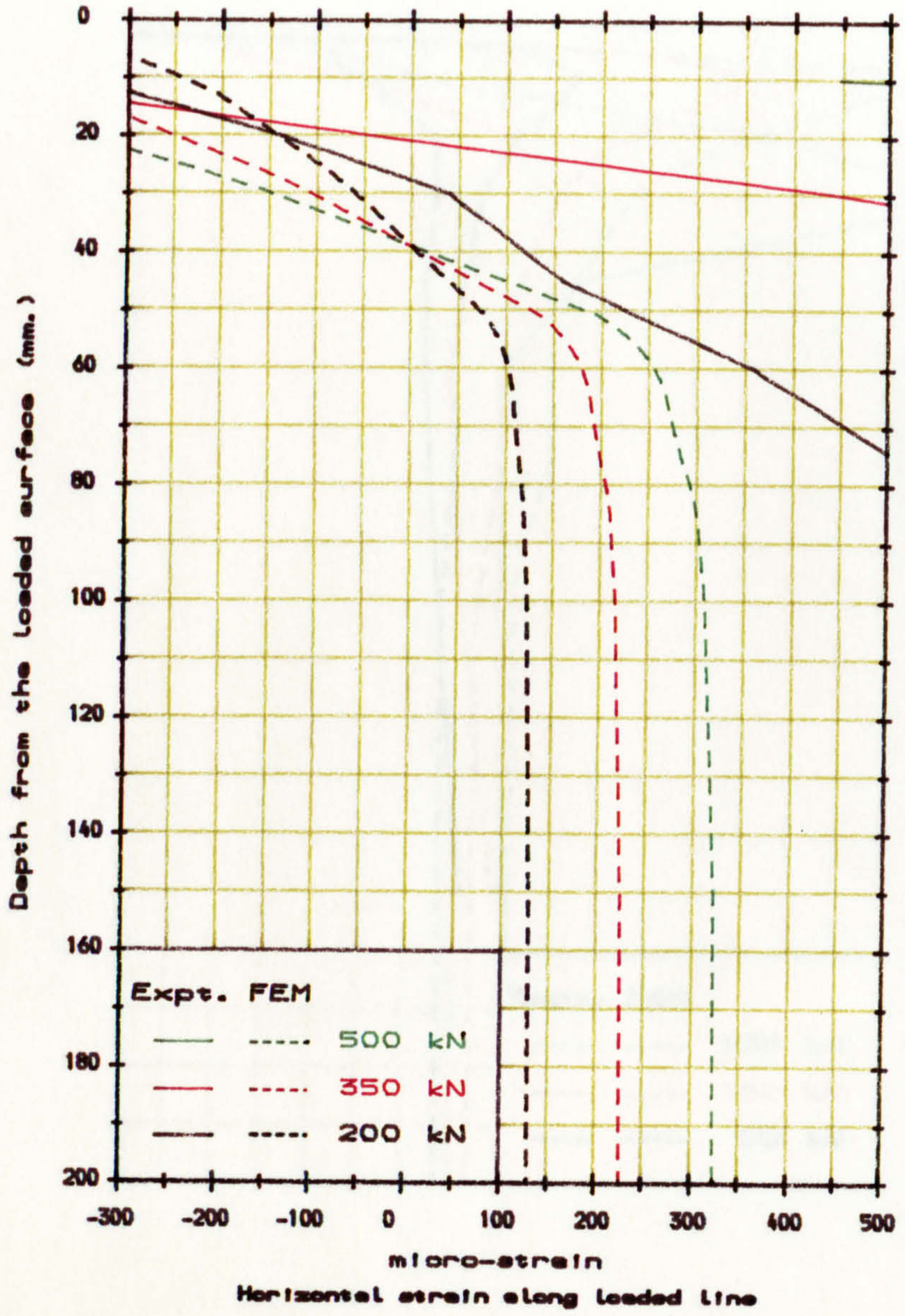

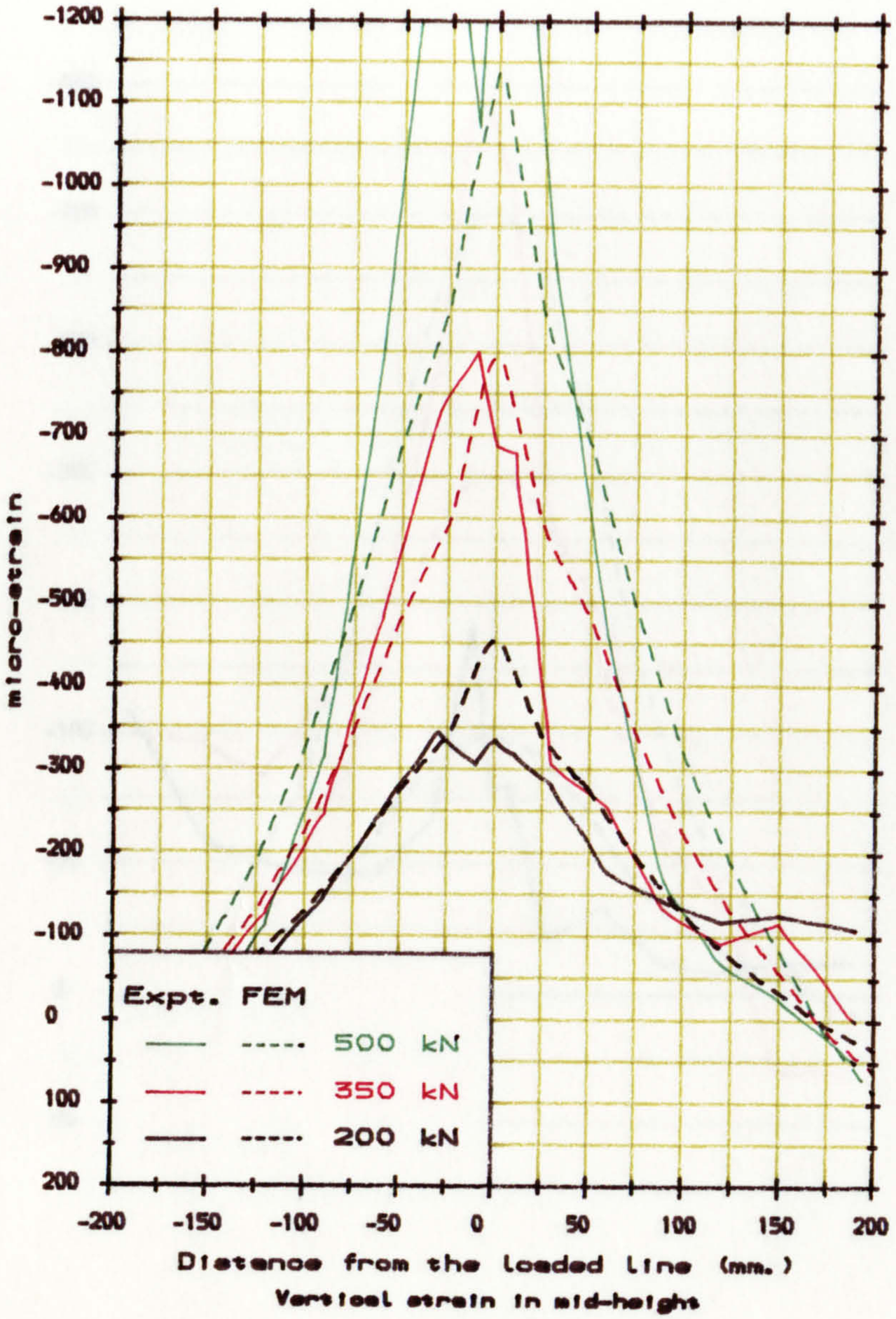

Fig. A. 23. Strain distribution of block B1.

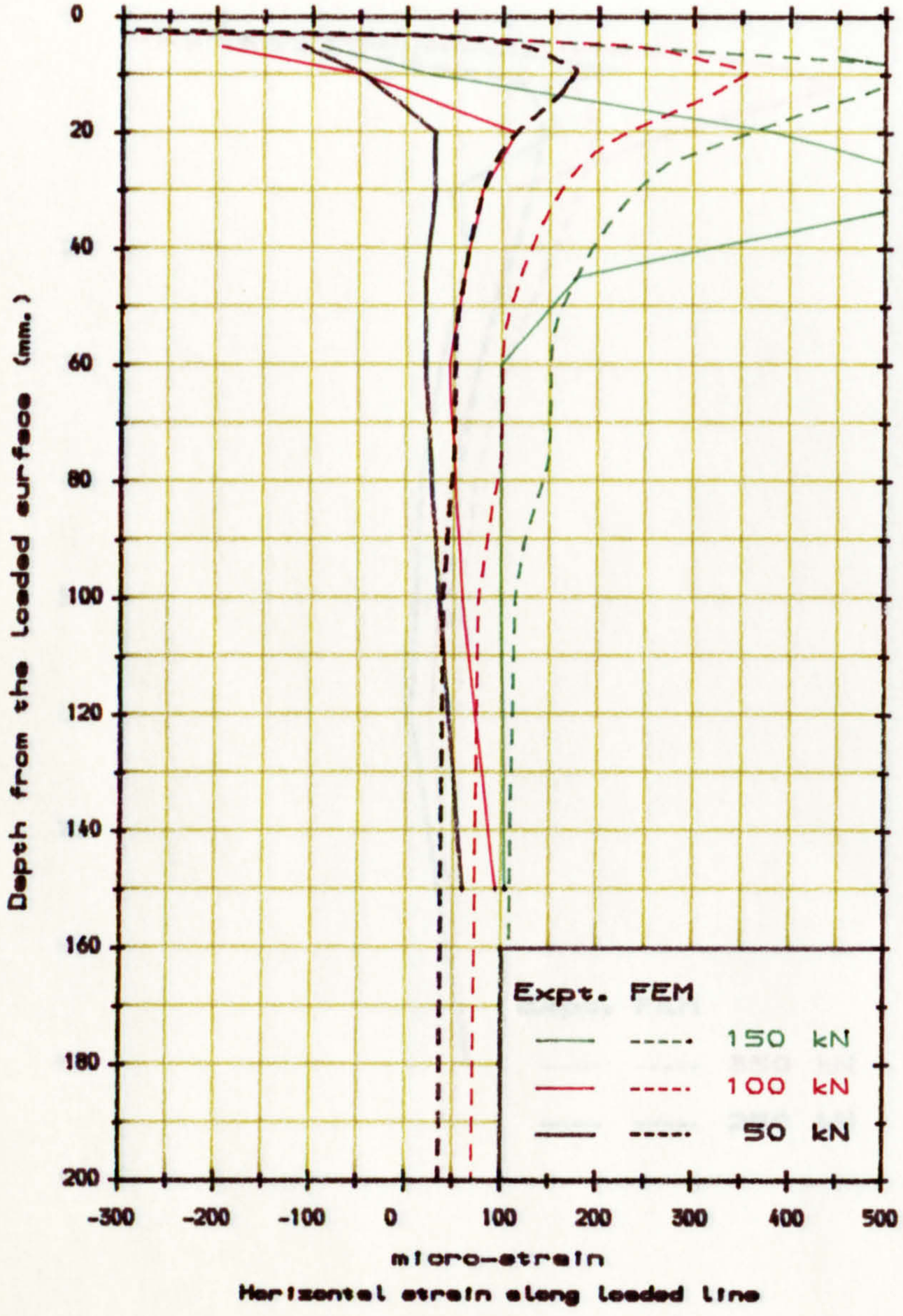

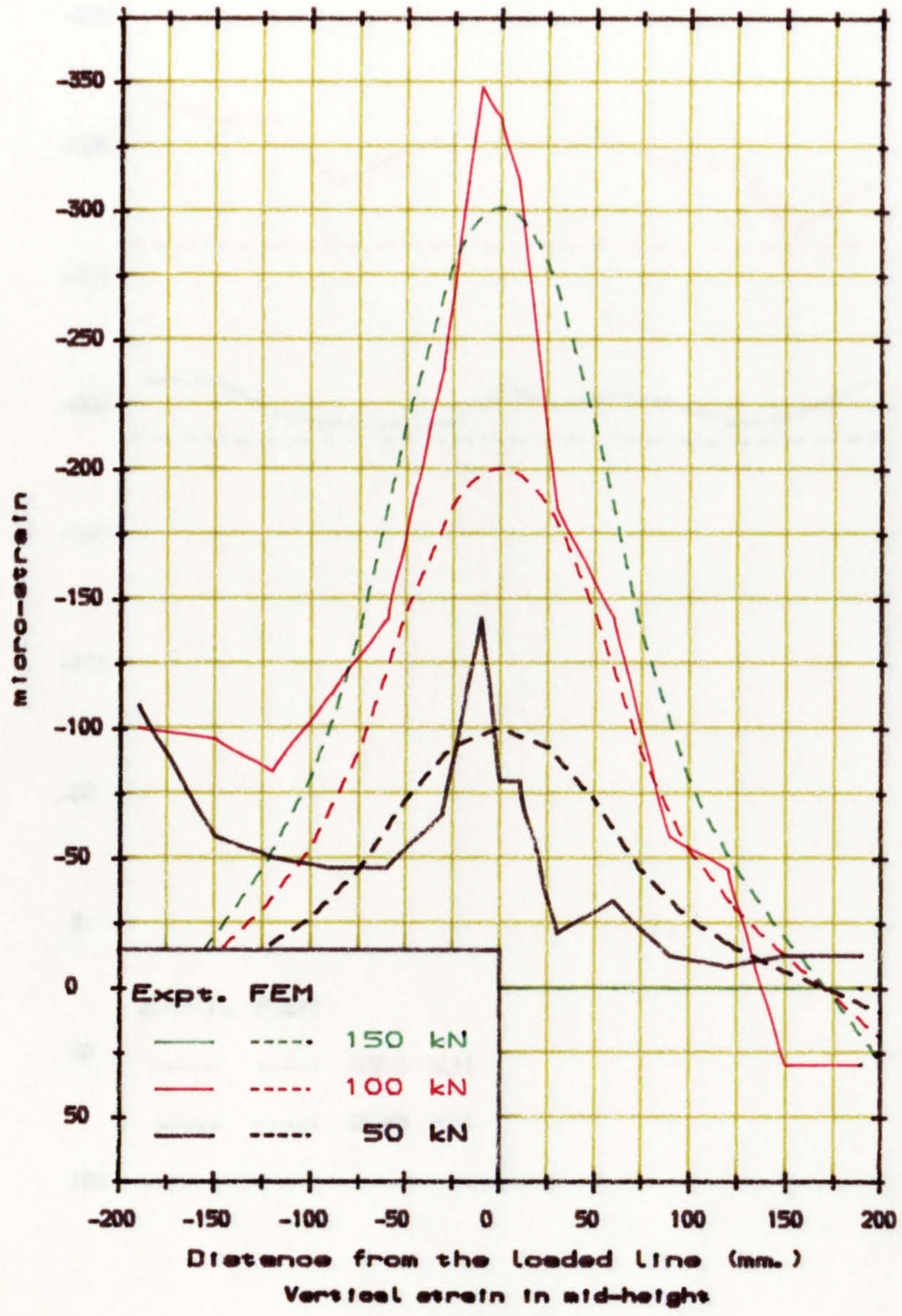

Fig. A. 24. Strain distribution of block B2.

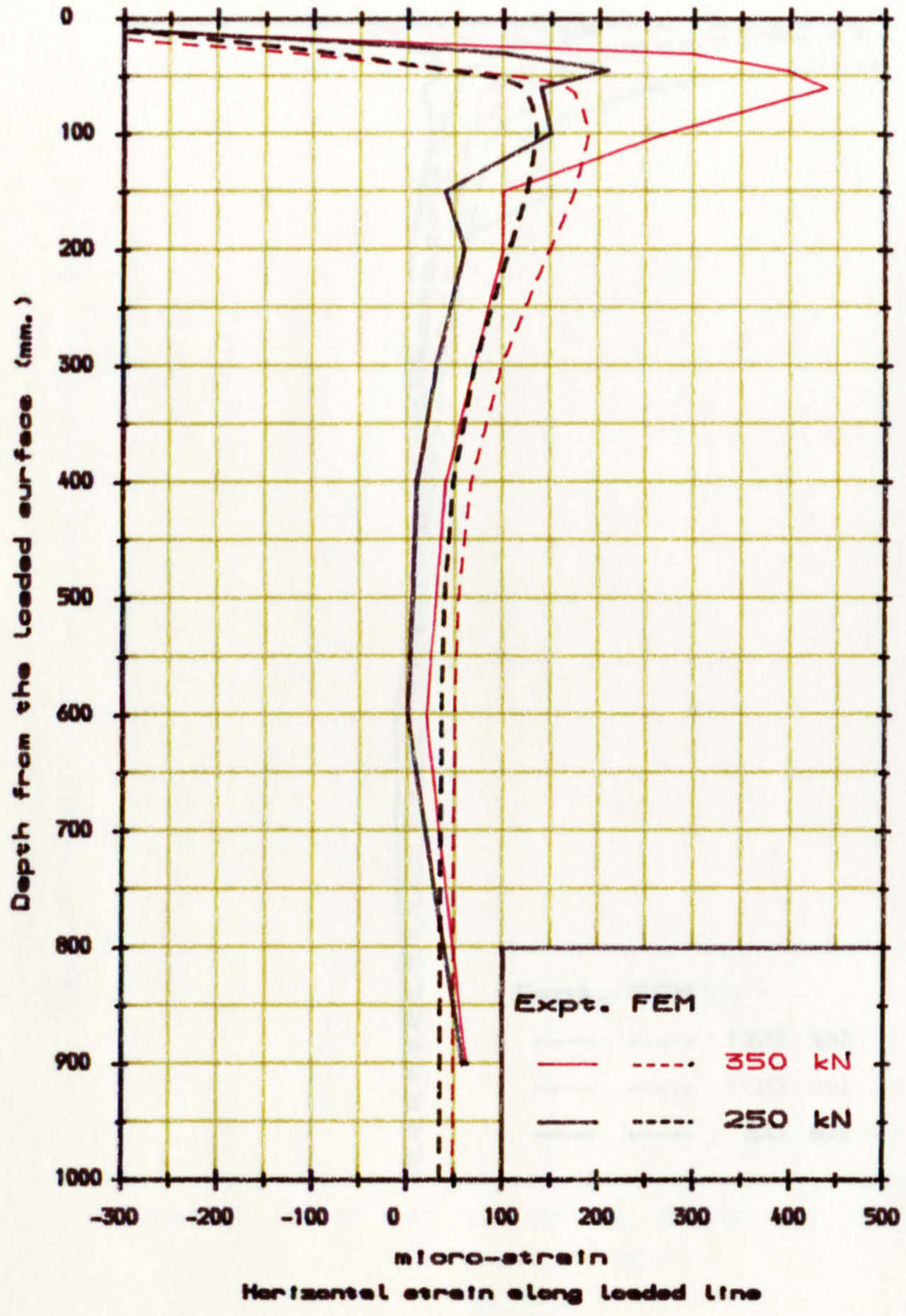

Horizontal strain along loaded line

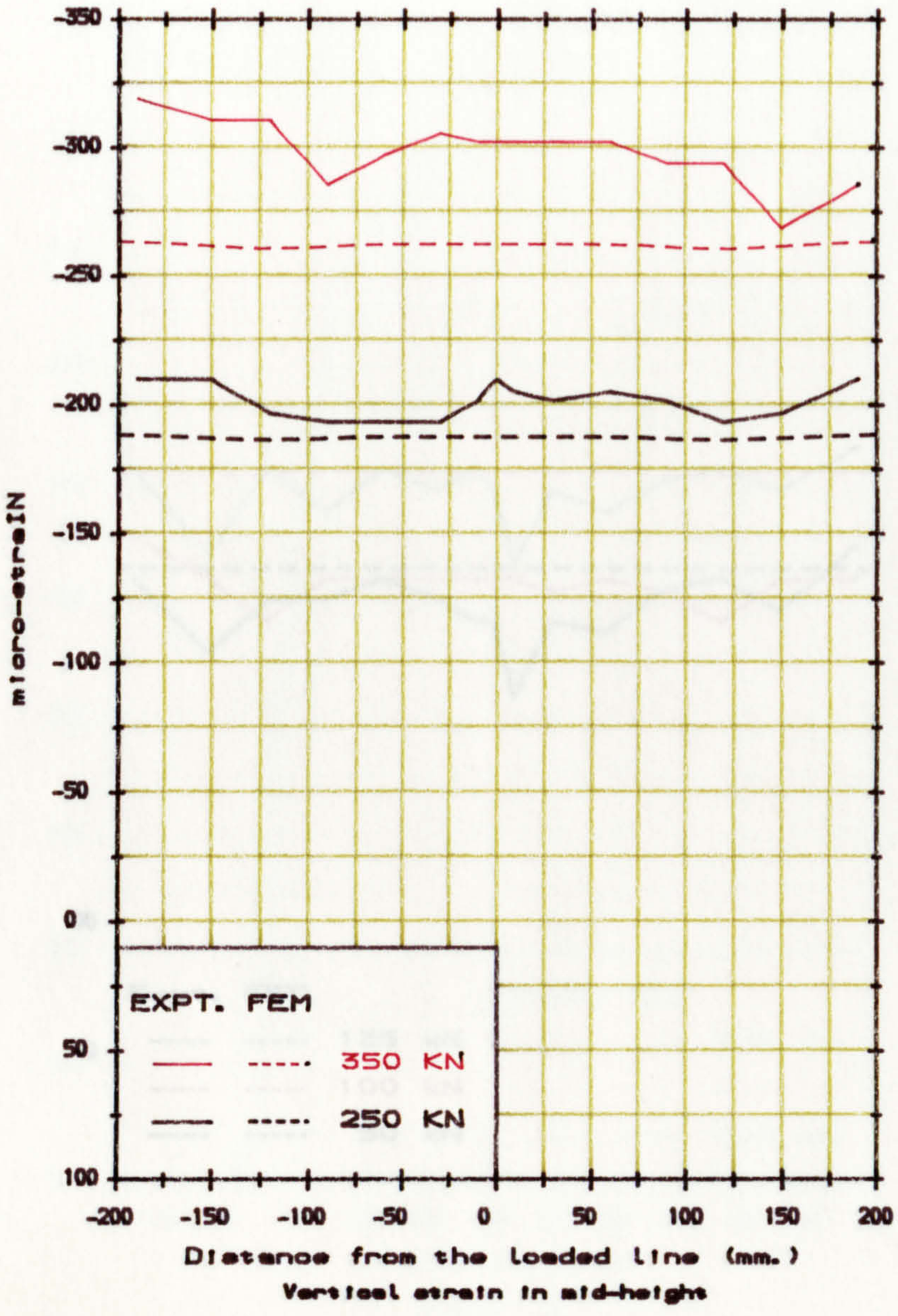

Vertical strain in mid-height

Fig. A. 25. Strain distribution of block B3.

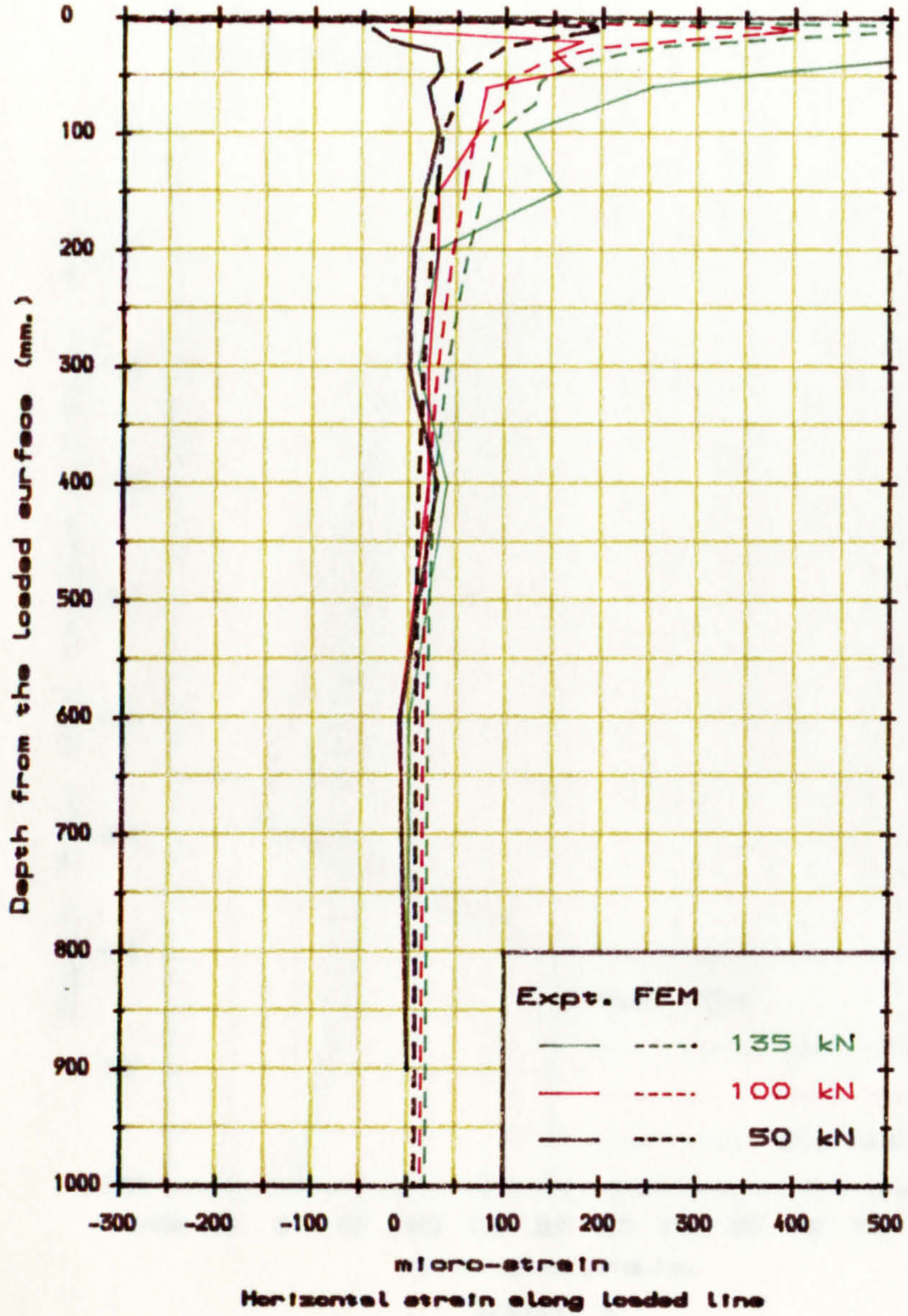

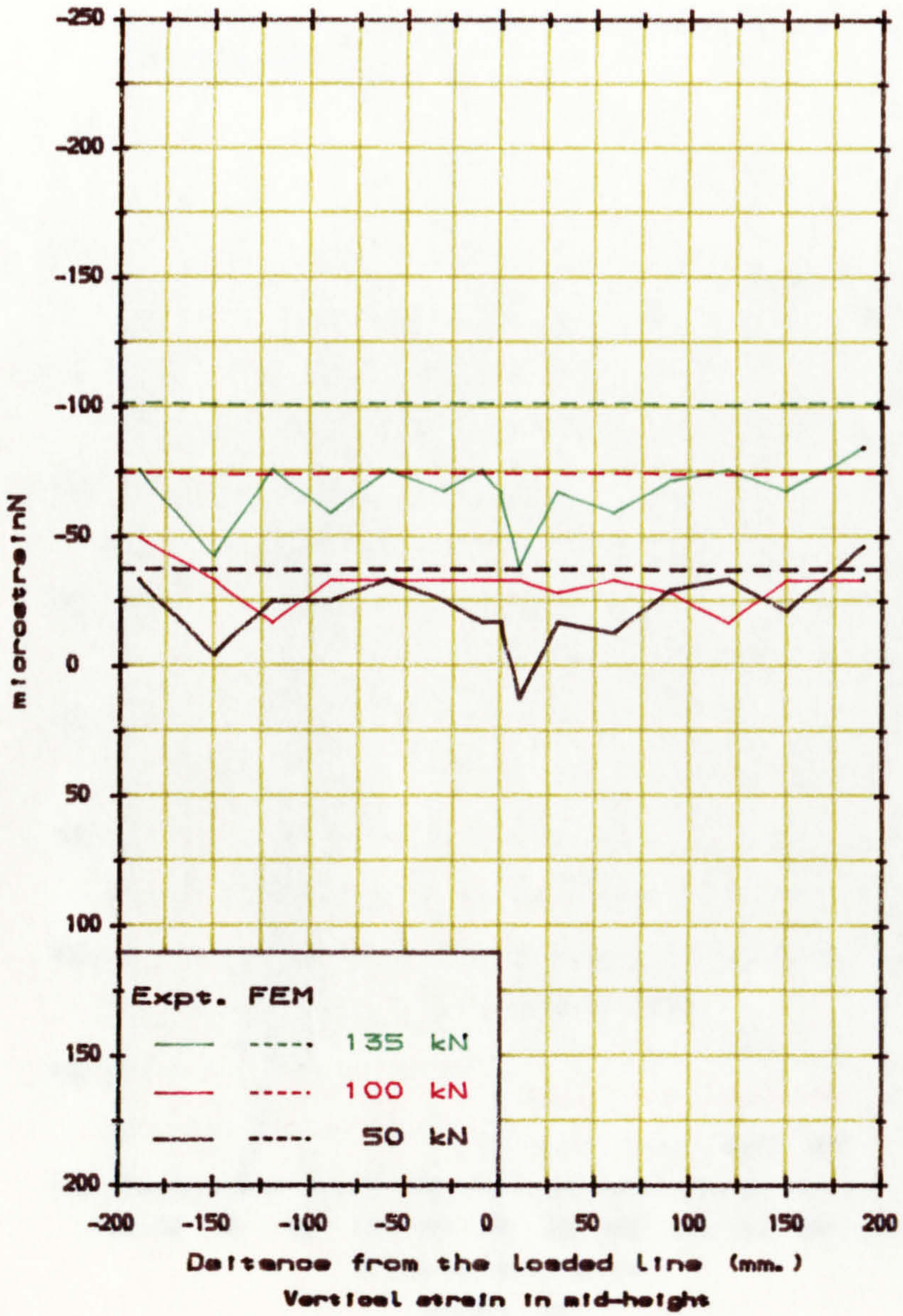

Fig. A. 26. Strain distribution of block B4.

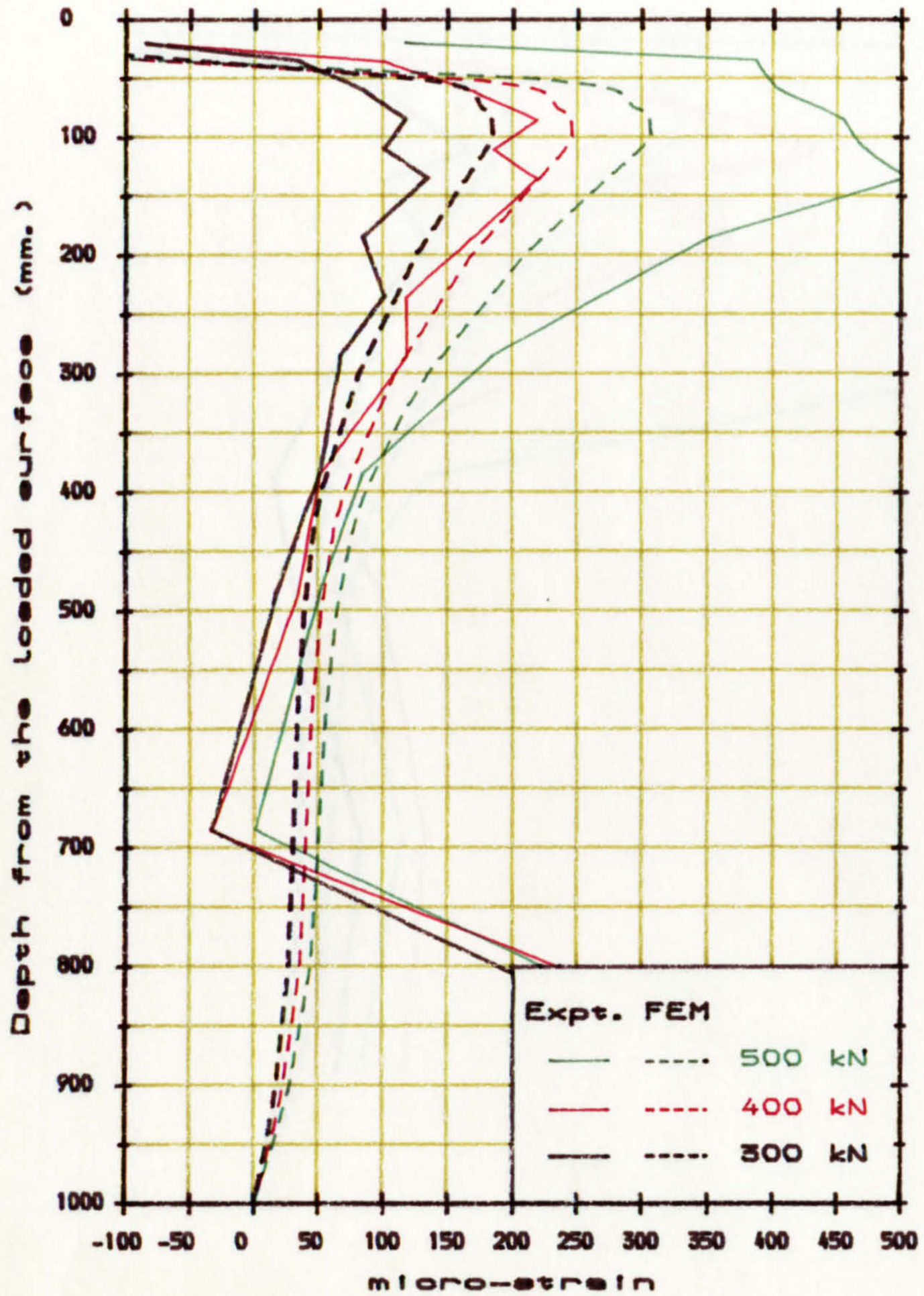

END 1

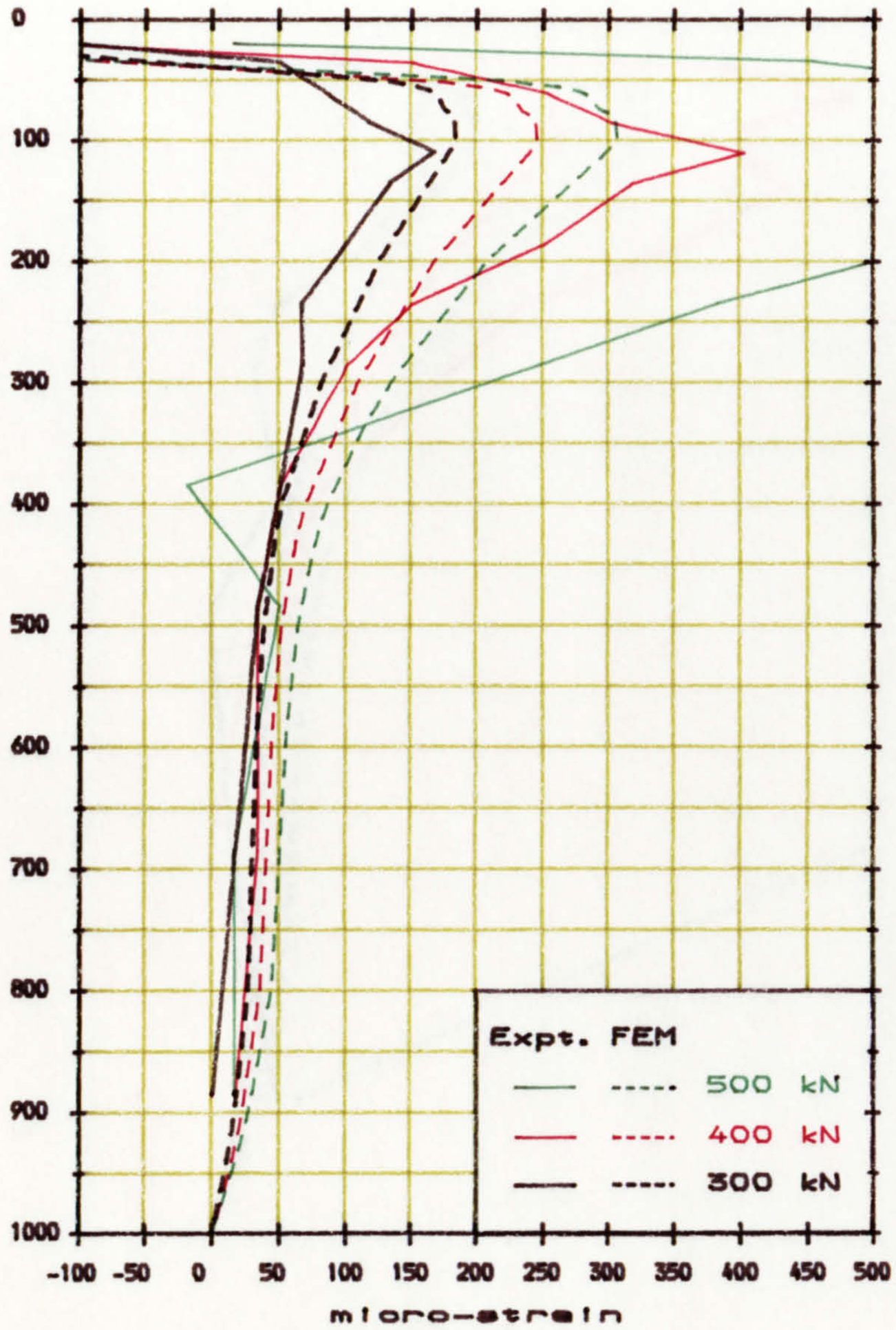

END 2

Fig. A. 27. Horizontal strain along the loaded line (Block R1).

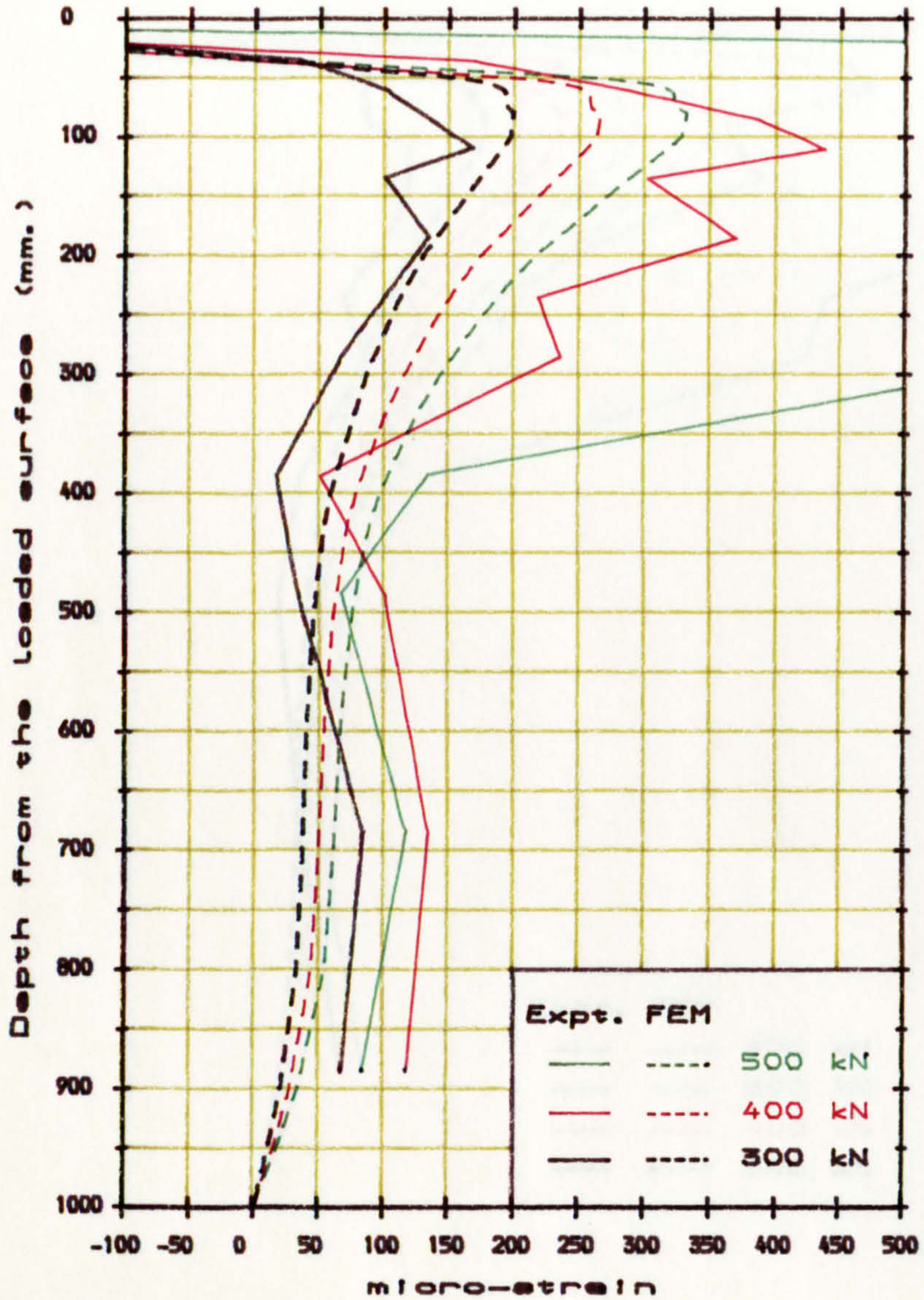

END 1

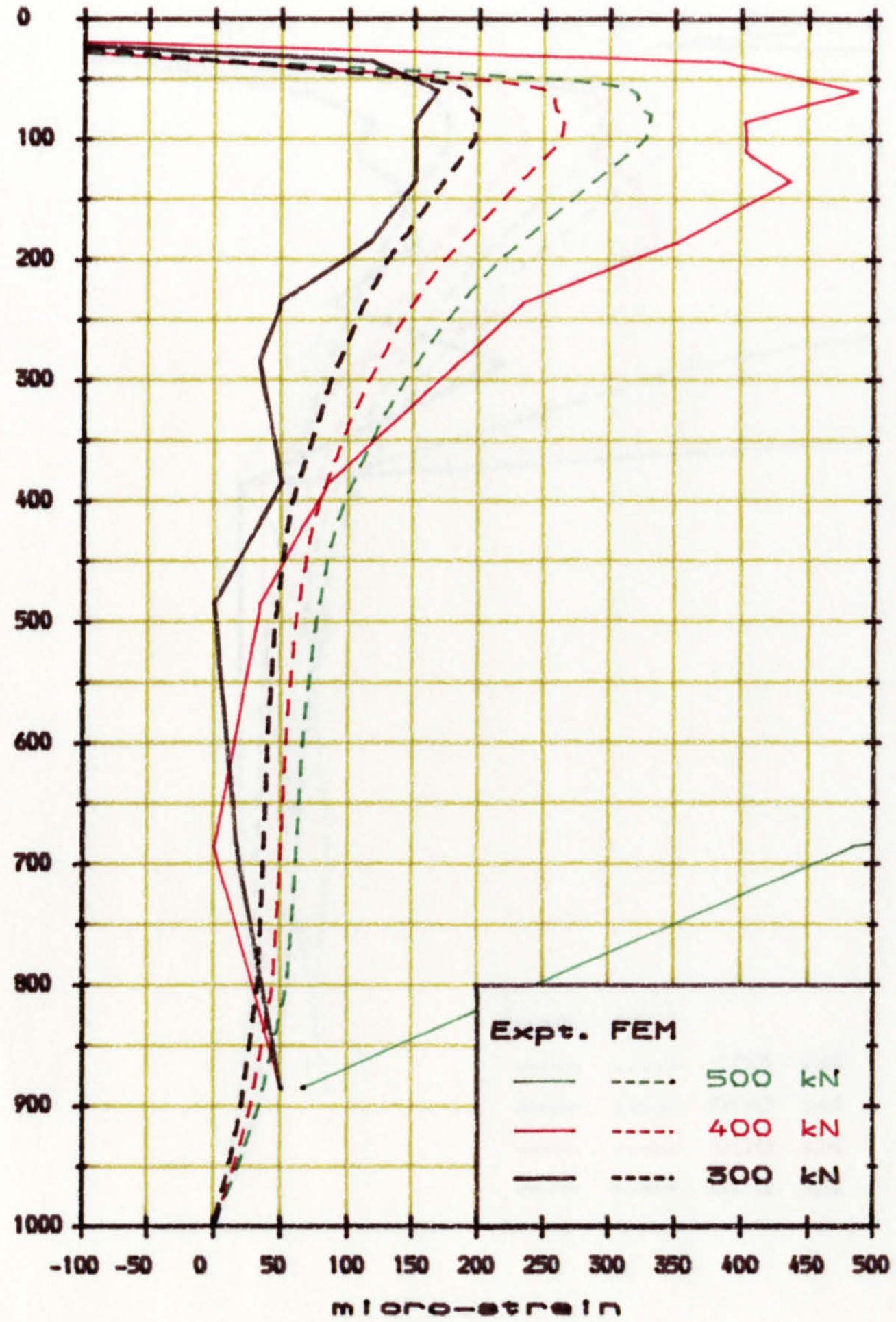

END 2

Fig. A. 28. Horizontal strain along the loaded line (Block R2).

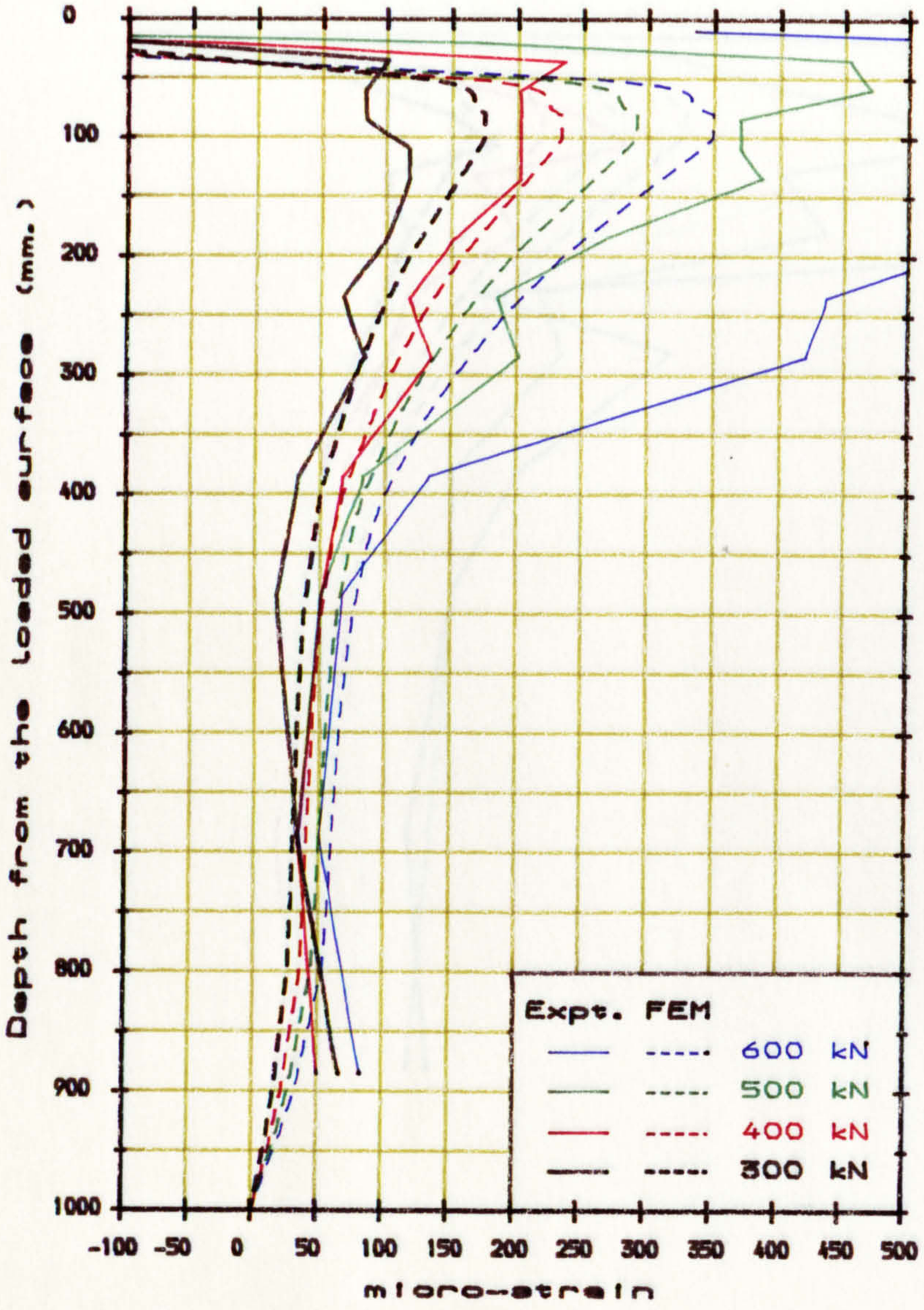

END 1

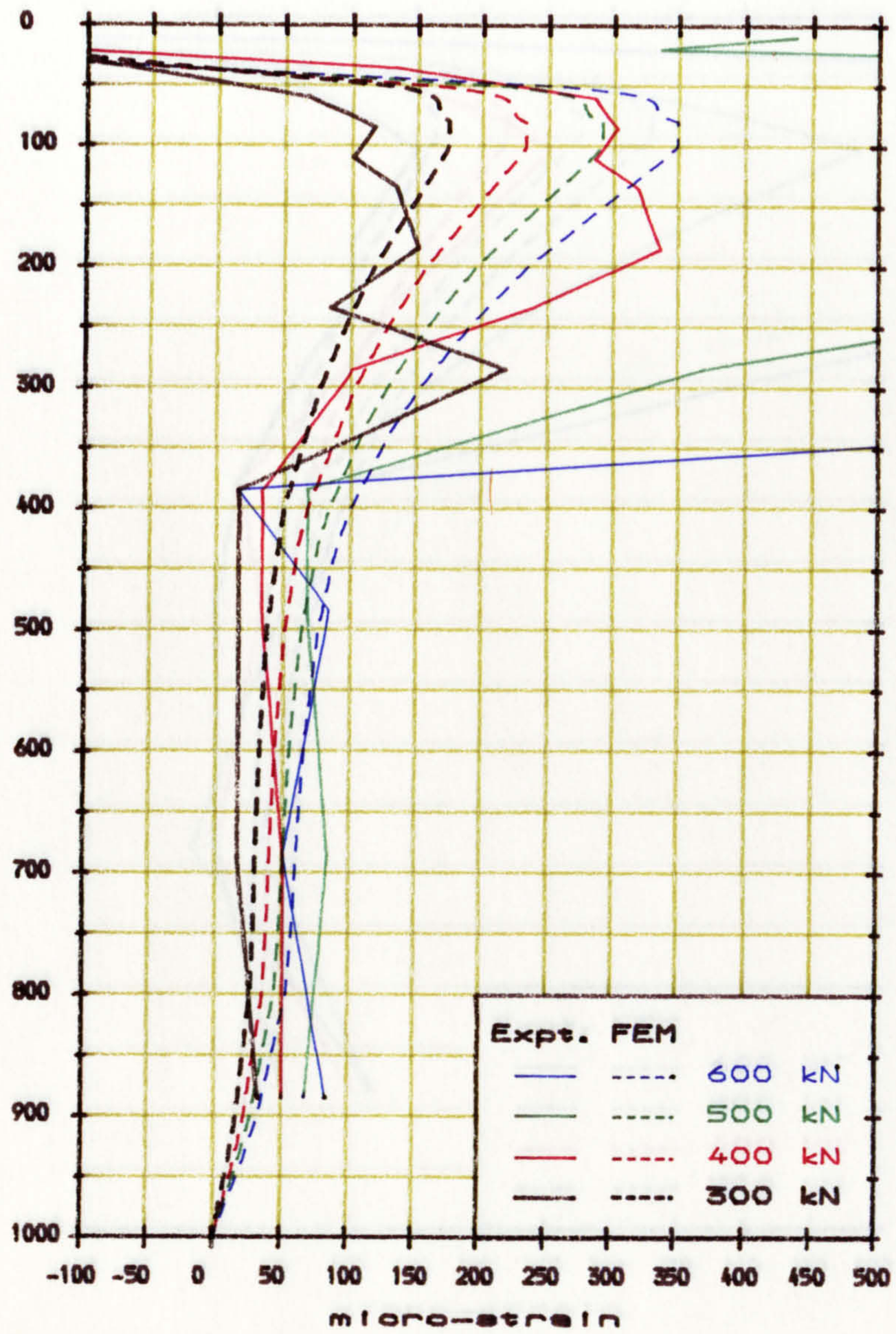

END 2

Fig. A. 29. Horizontal strain along the loaded line (Block R3).

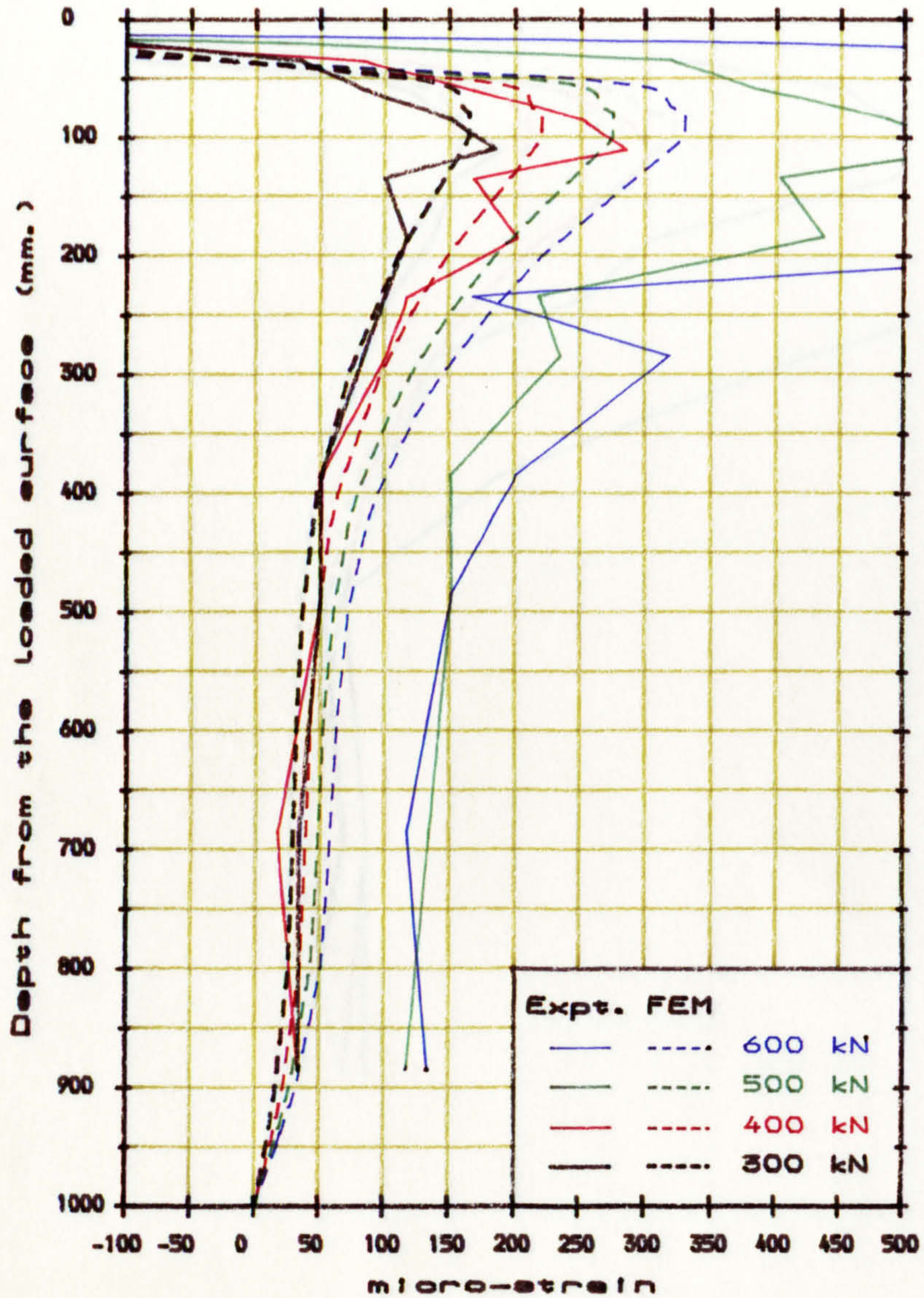

END 1

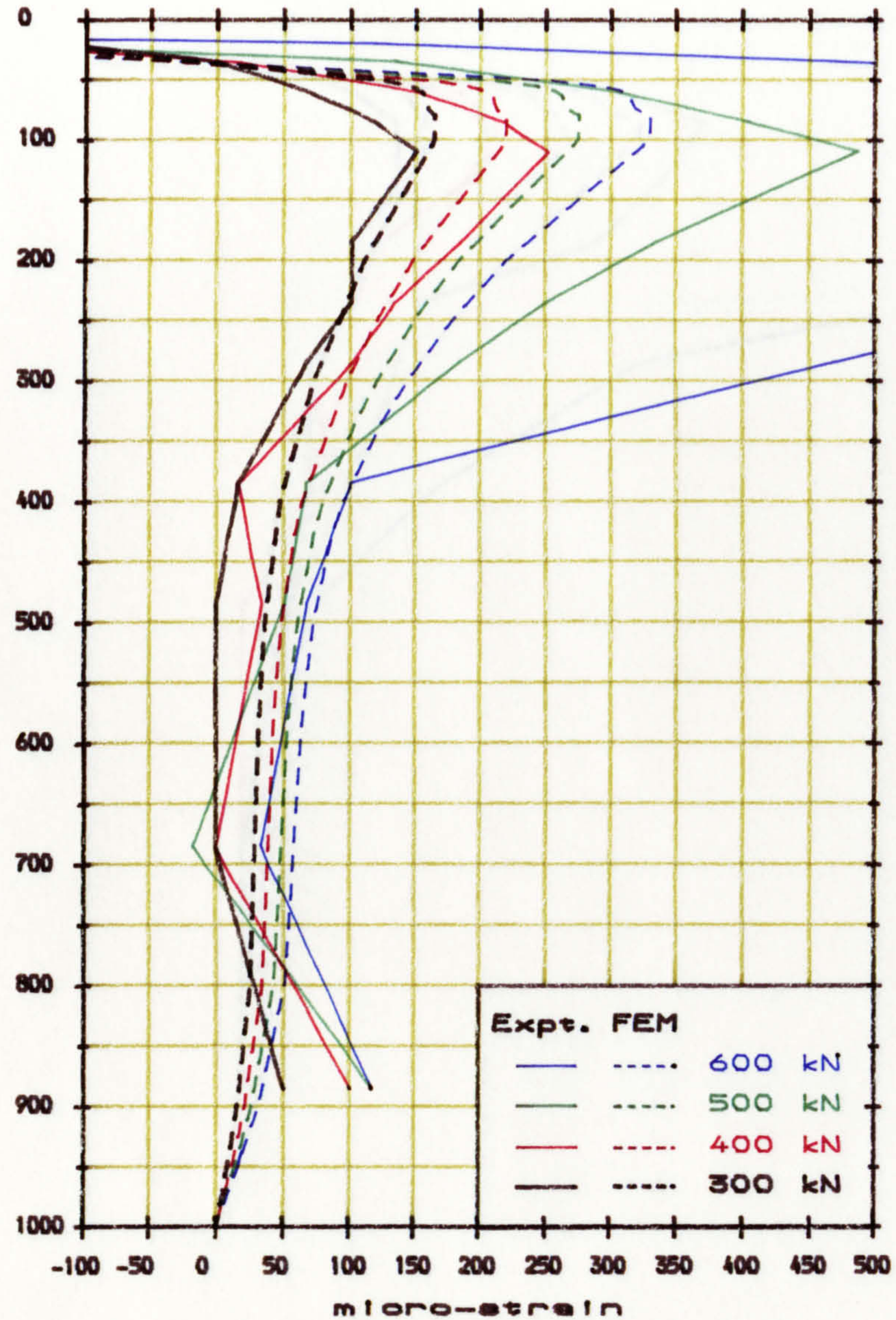

END 2

Fig. A. 30. Horizontal strain along the loaded line (Block R4).

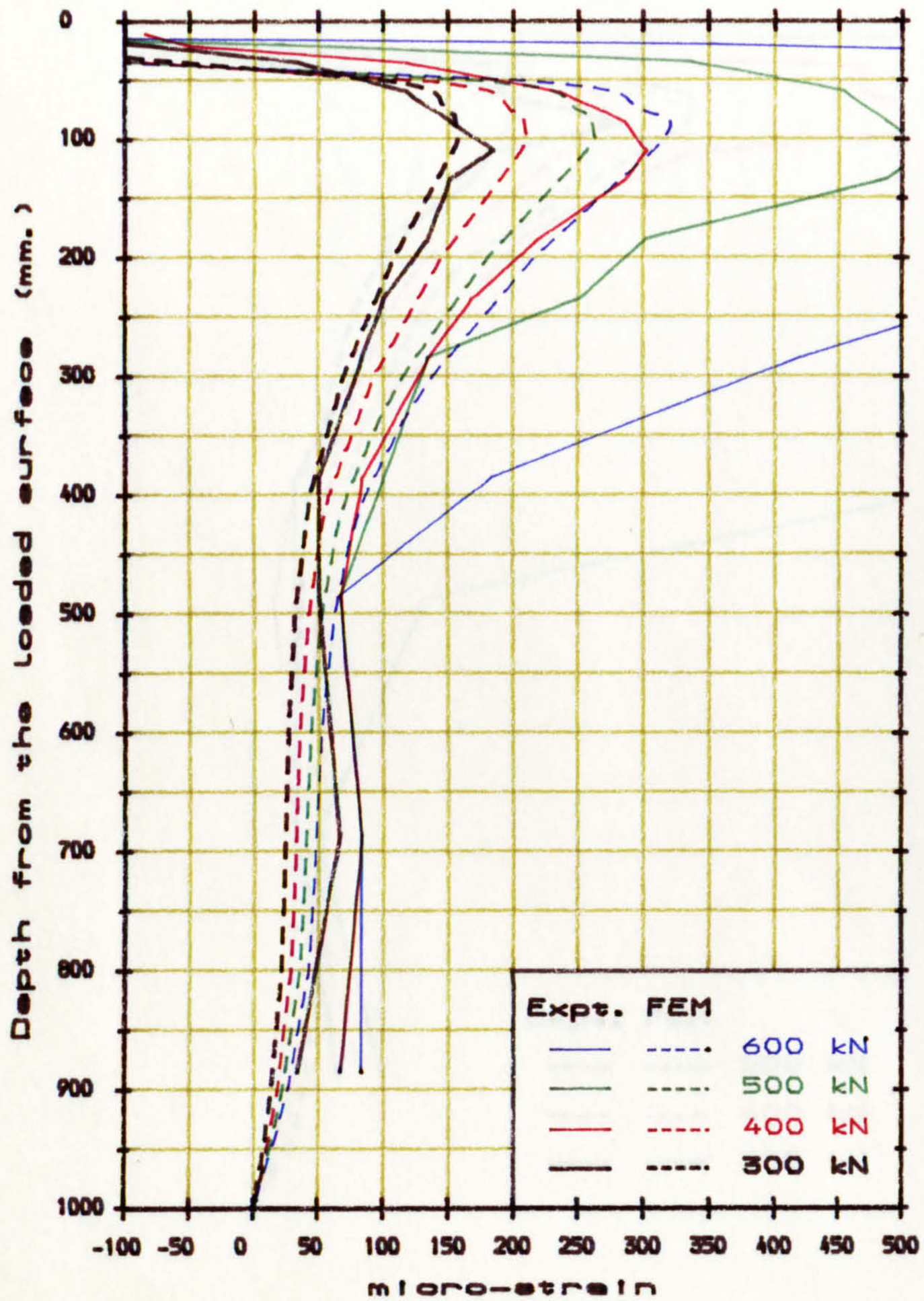

END 1

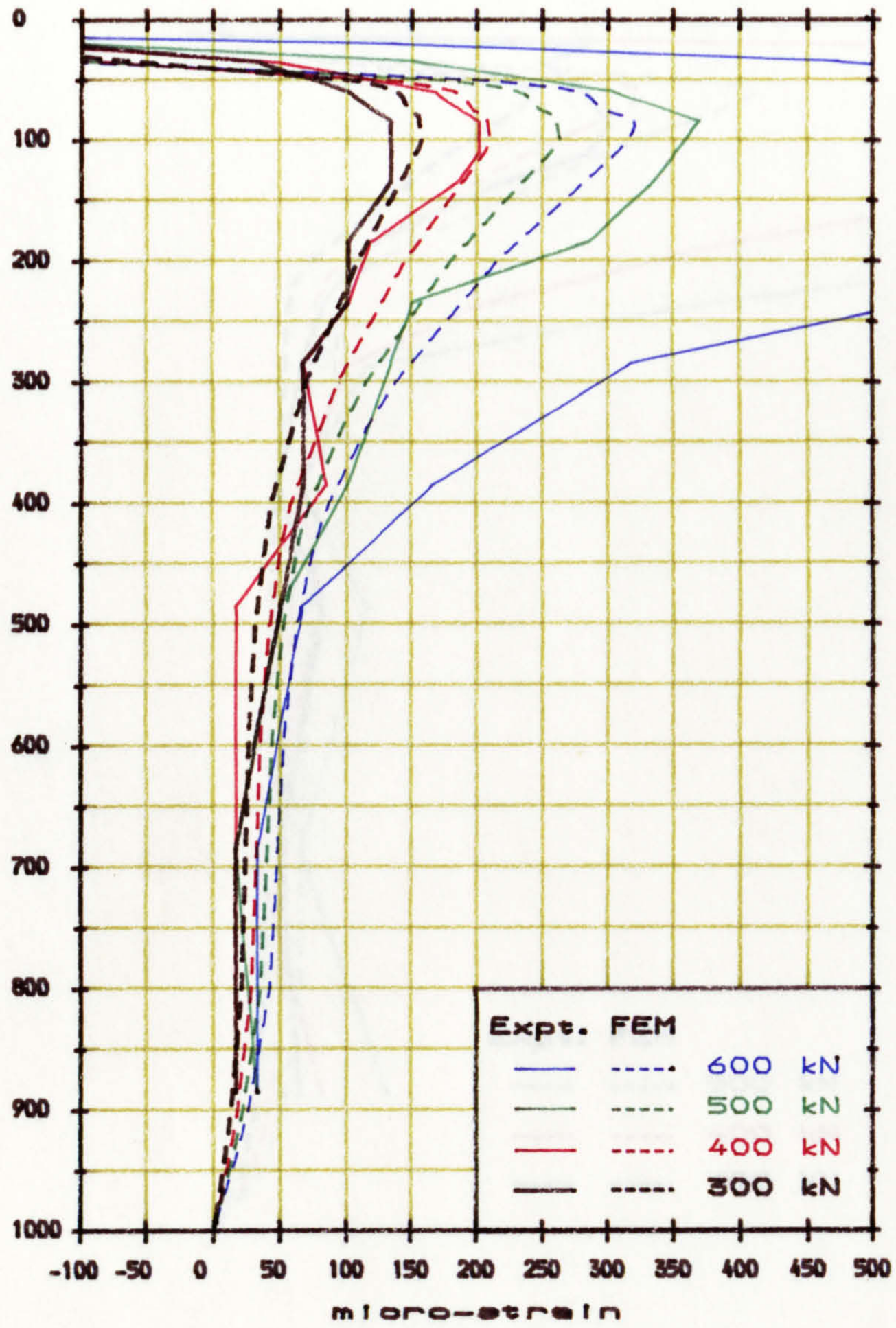

END 2

Fig. A. 31. Horizontal strain along the loaded line (Block R5).

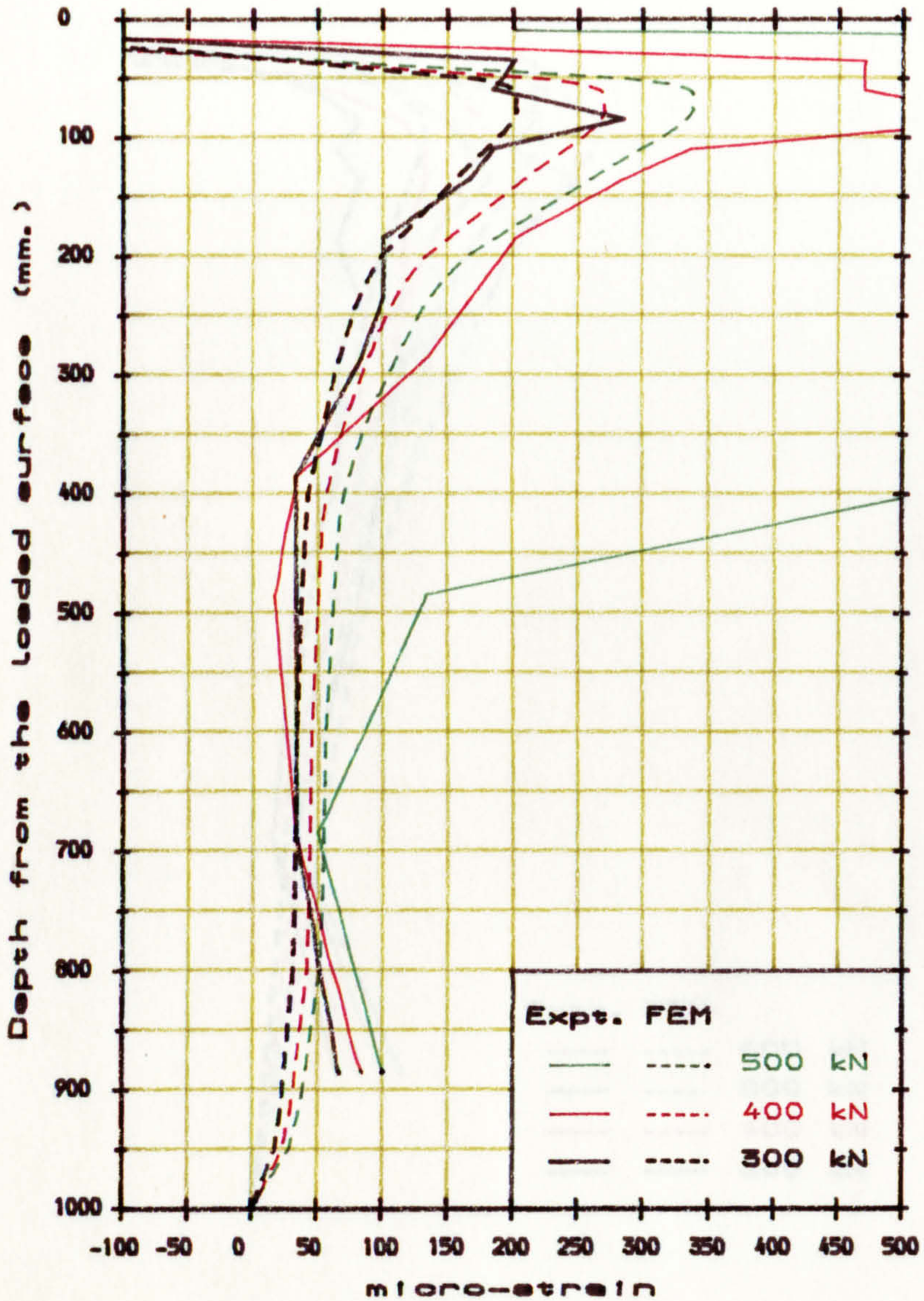

END 1

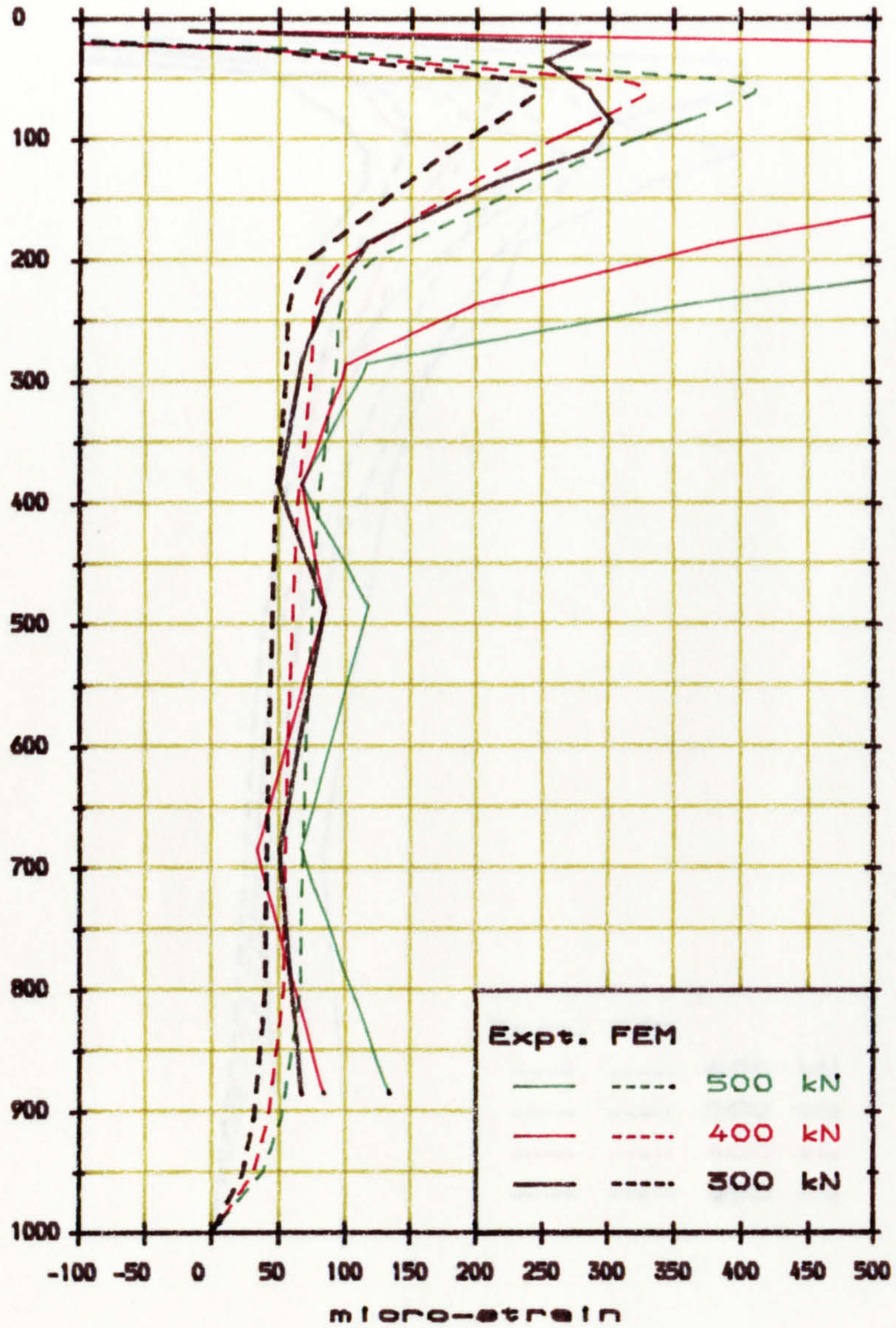

END 2

Fig. A. 32. Horizontal strain along the loaded line (Block R6).

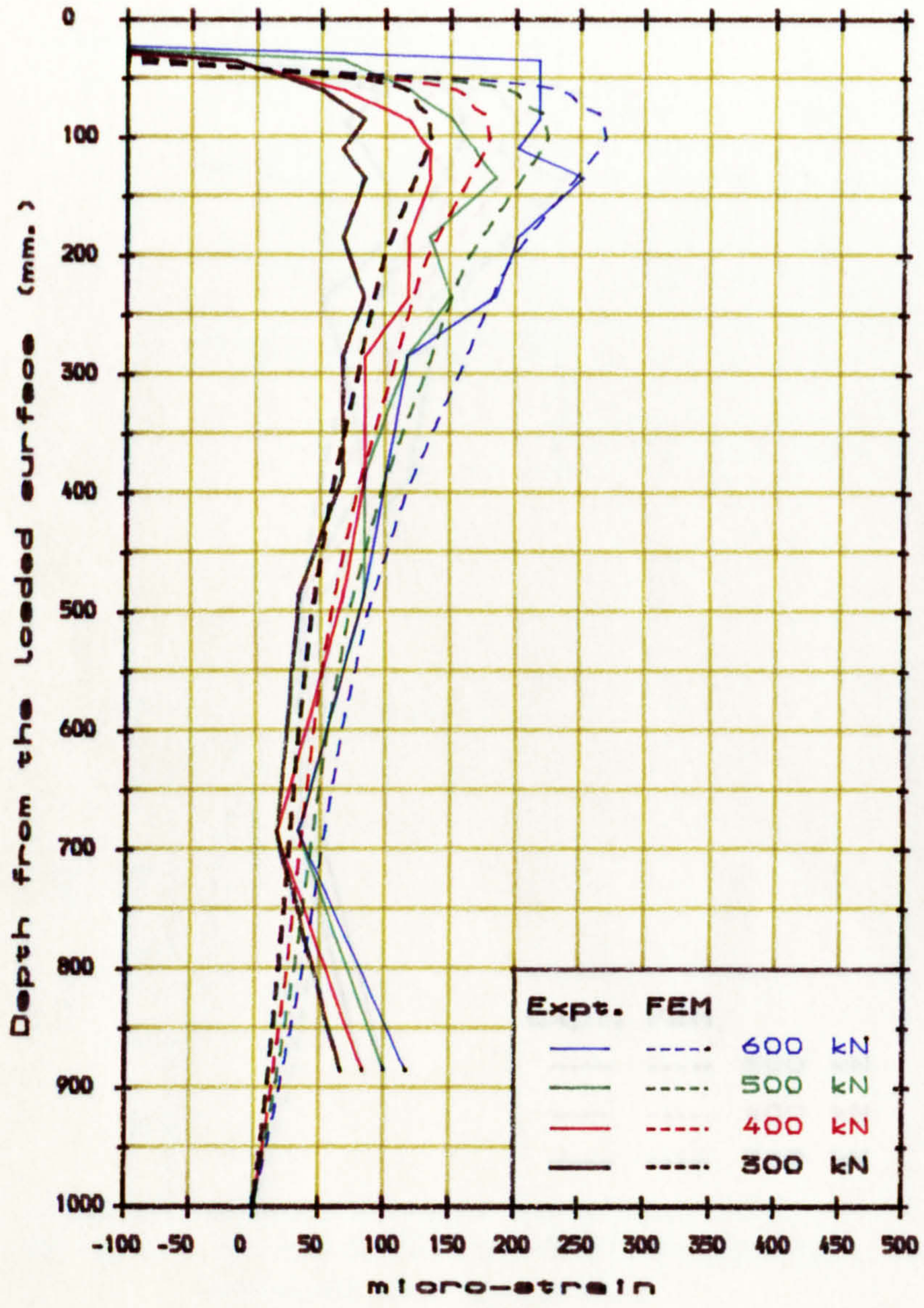

END 1

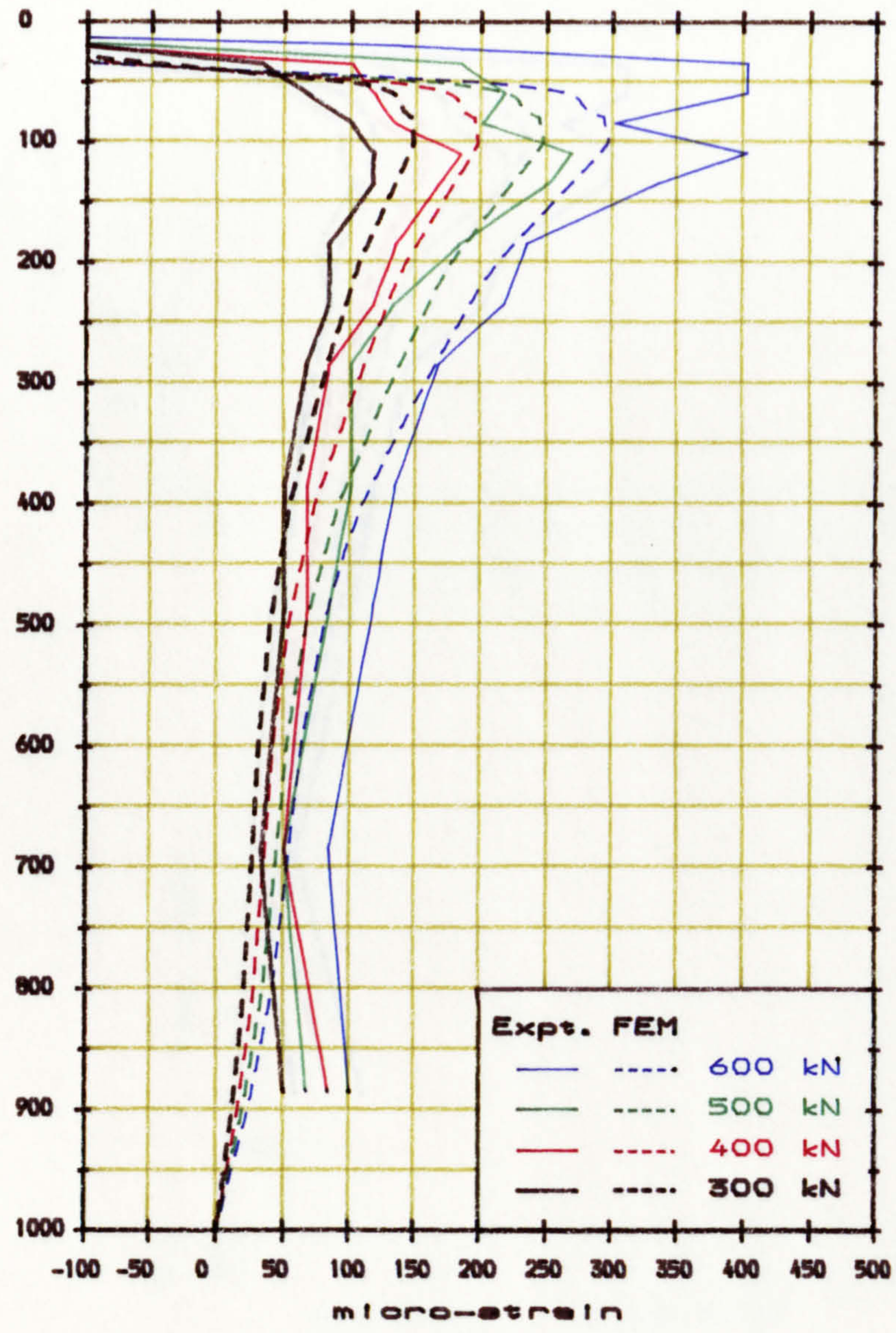

END 2

Fig. A. 33. Horizontal strain along the loaded line (Block R7).

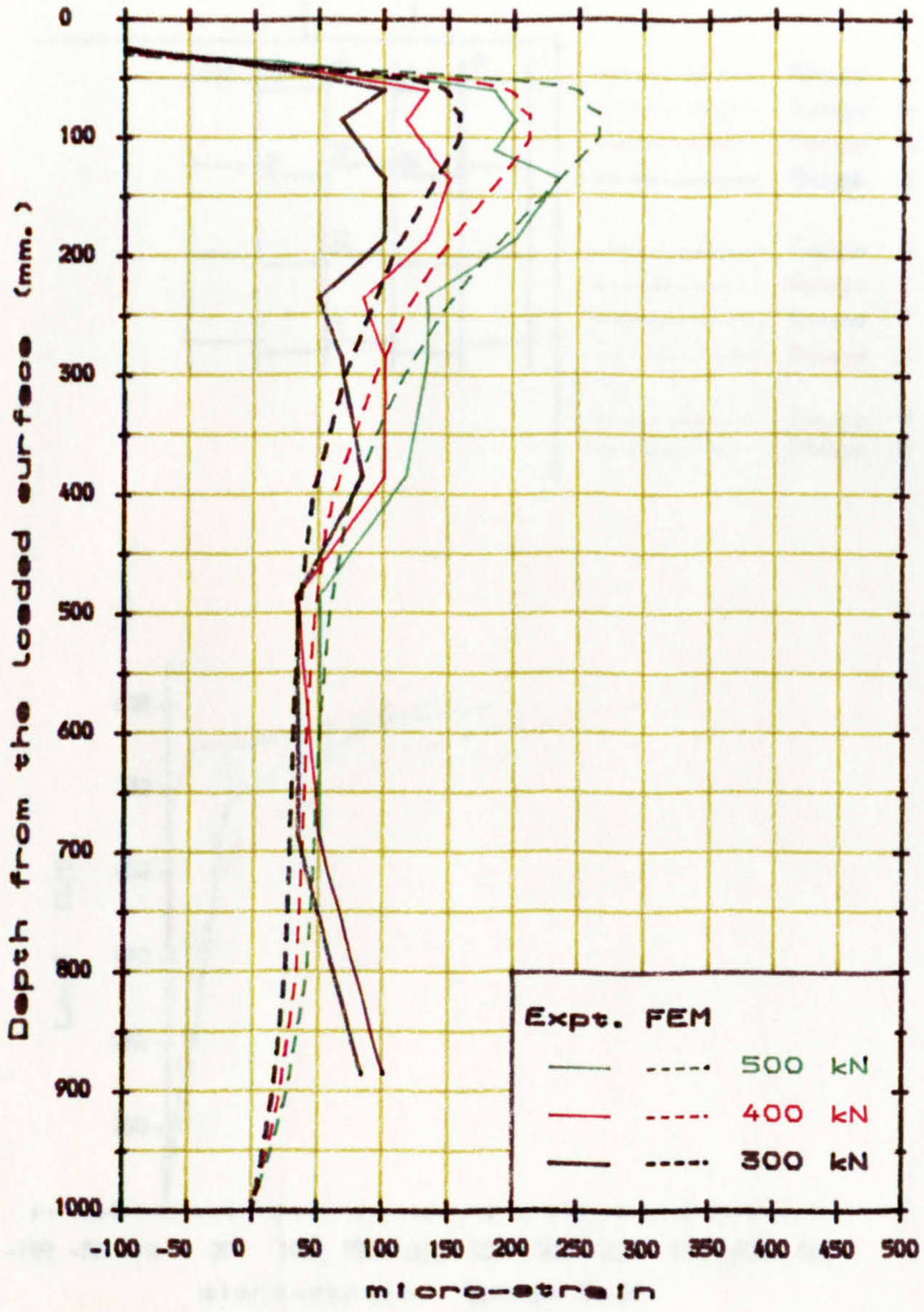

END 1

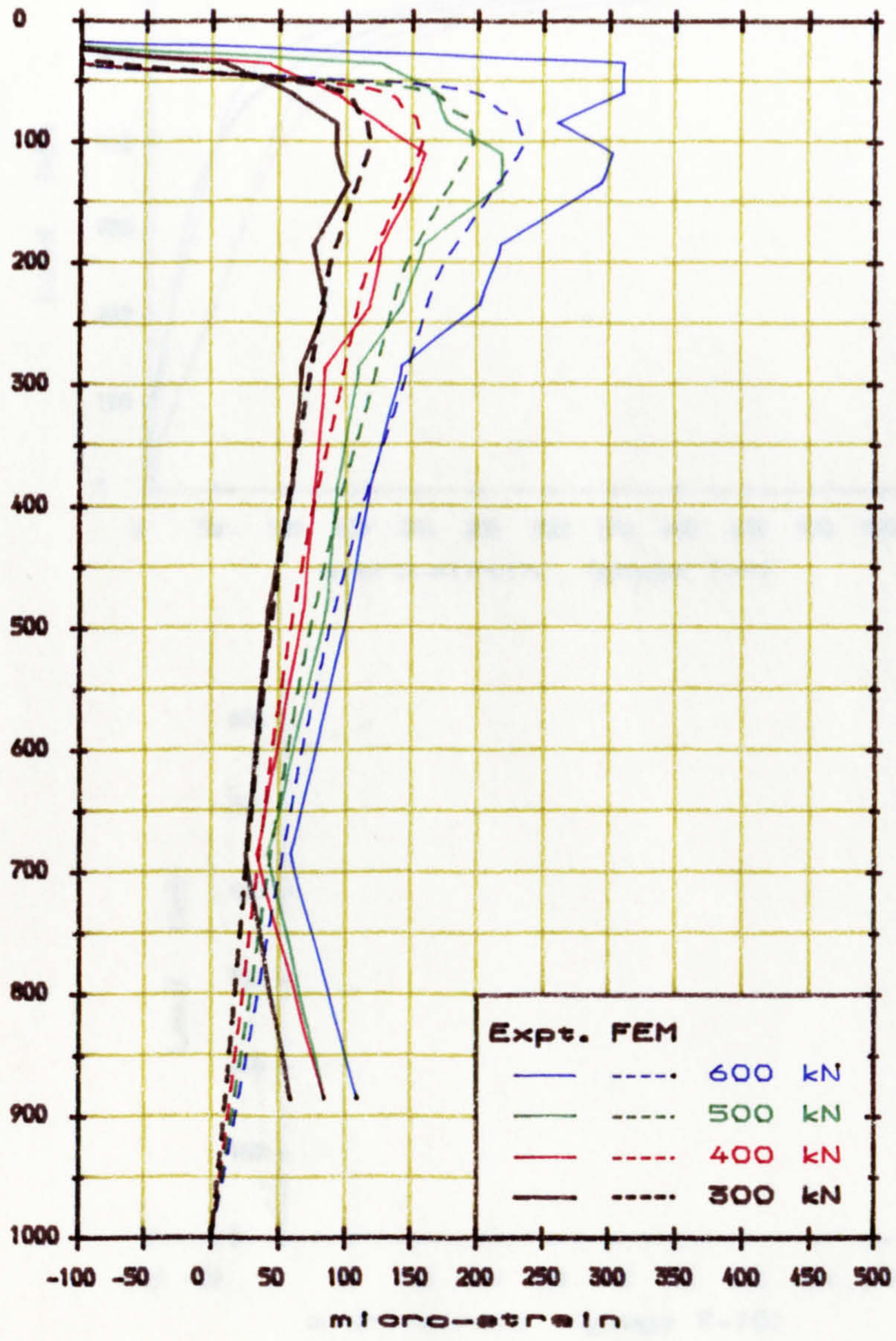

END 2

Fig. A. 34. Horizontal strain along the loaded line (Block R8).

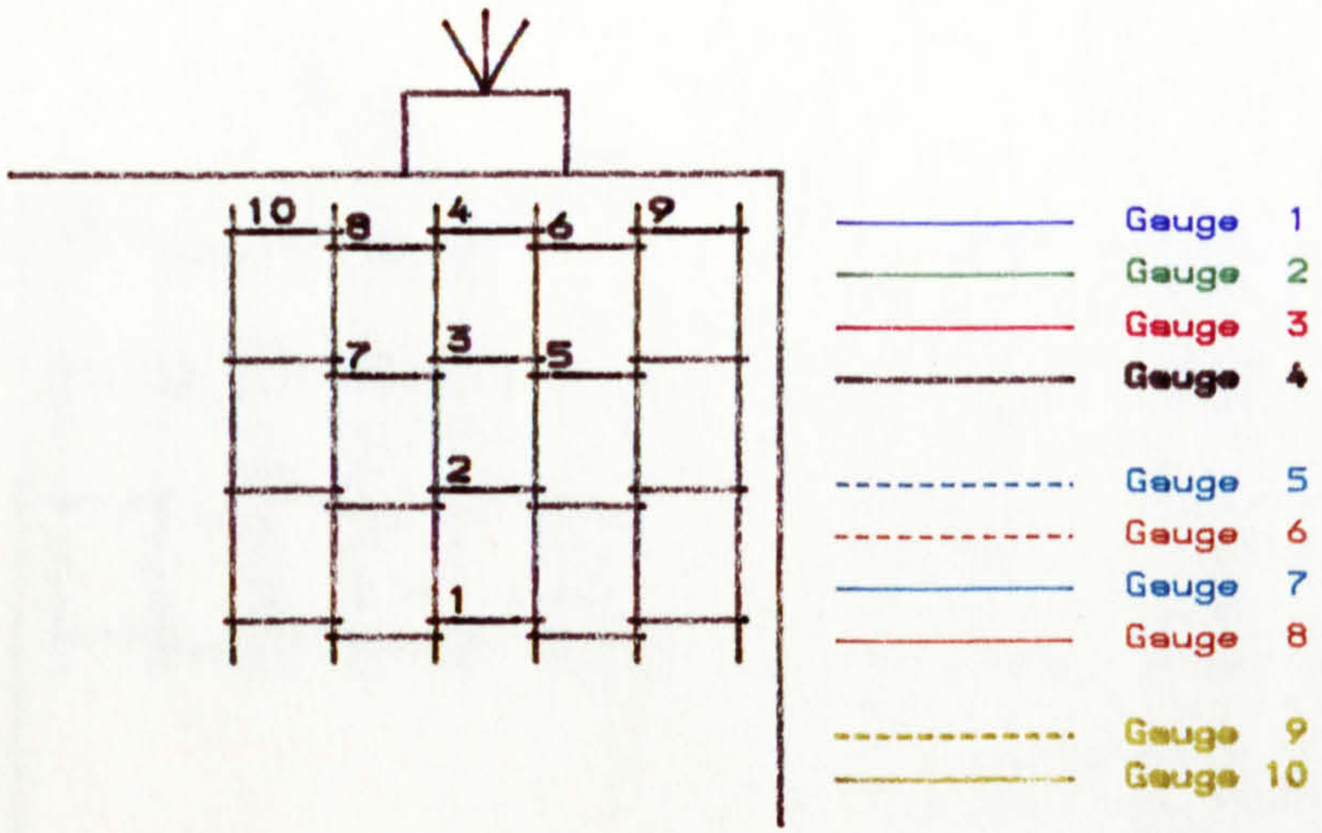

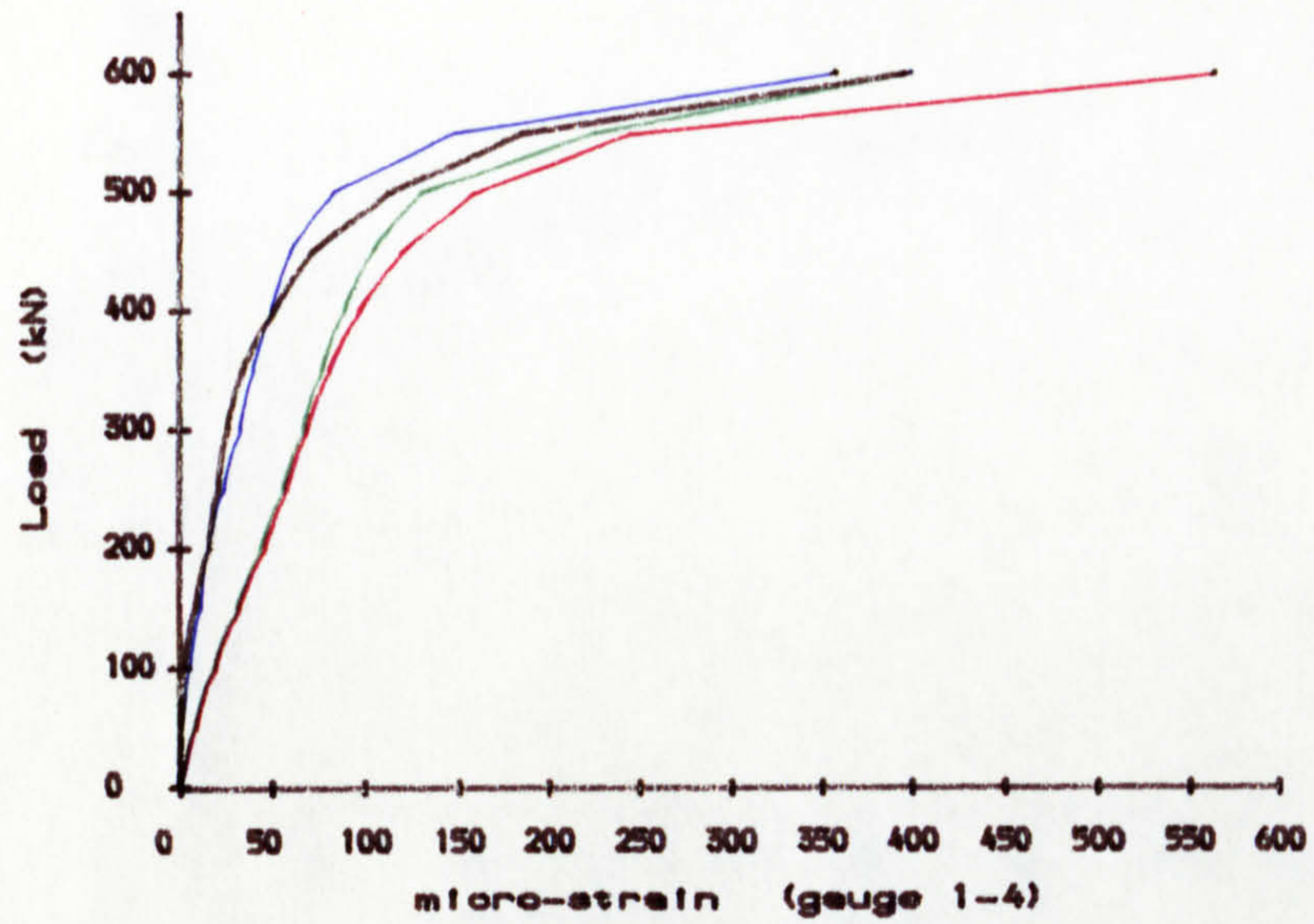

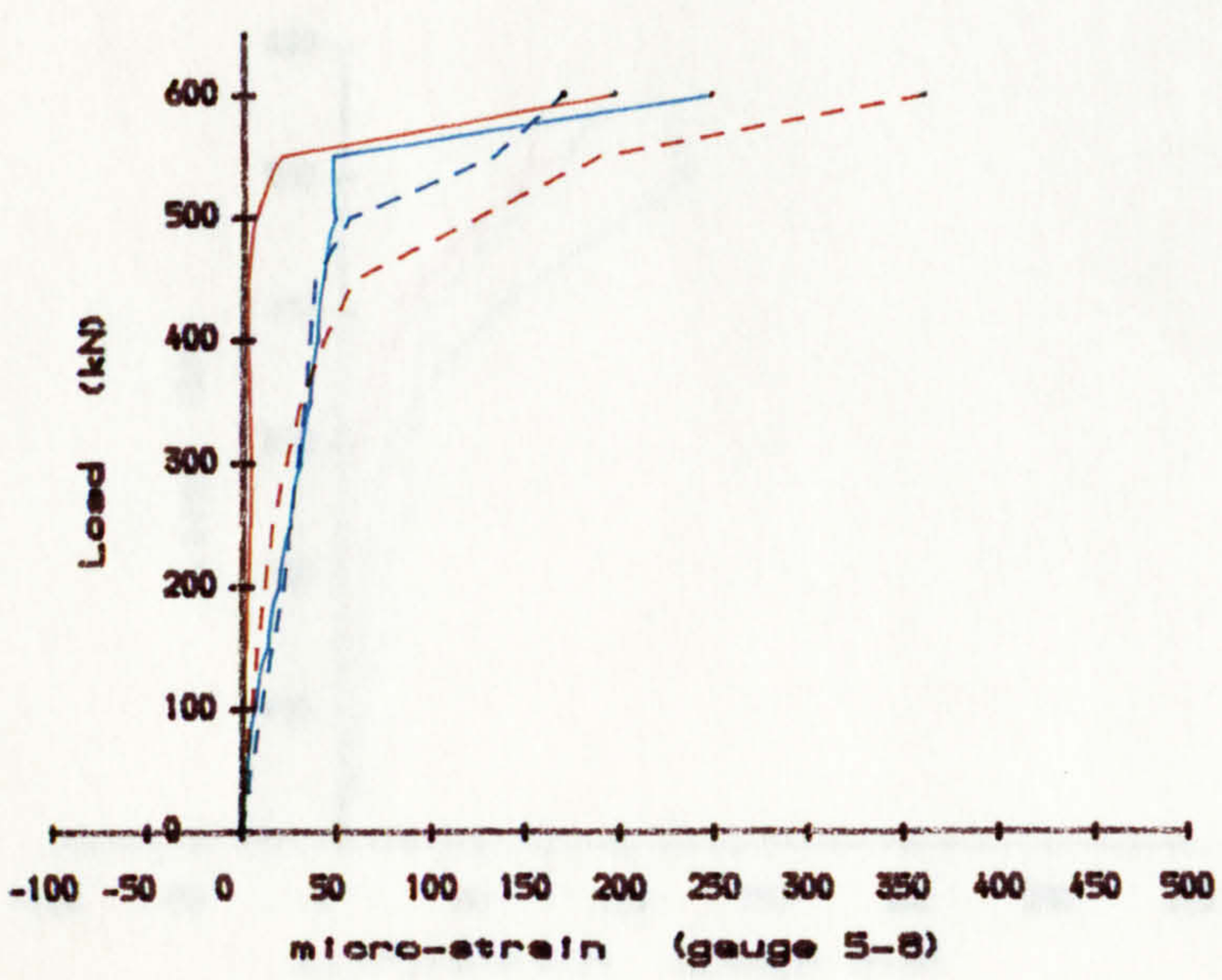

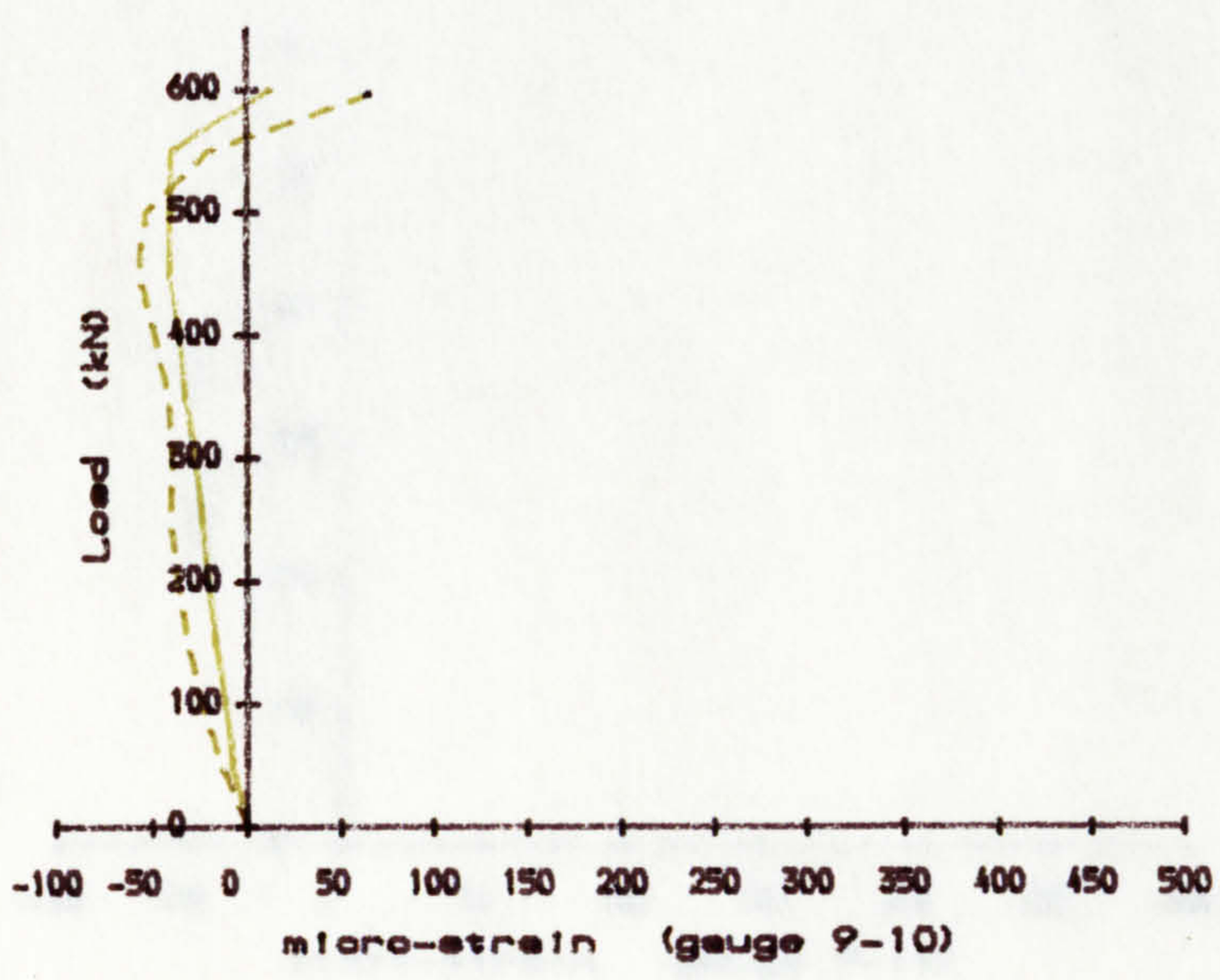

Fig. A. 35. Strain of steel in block R1/1.

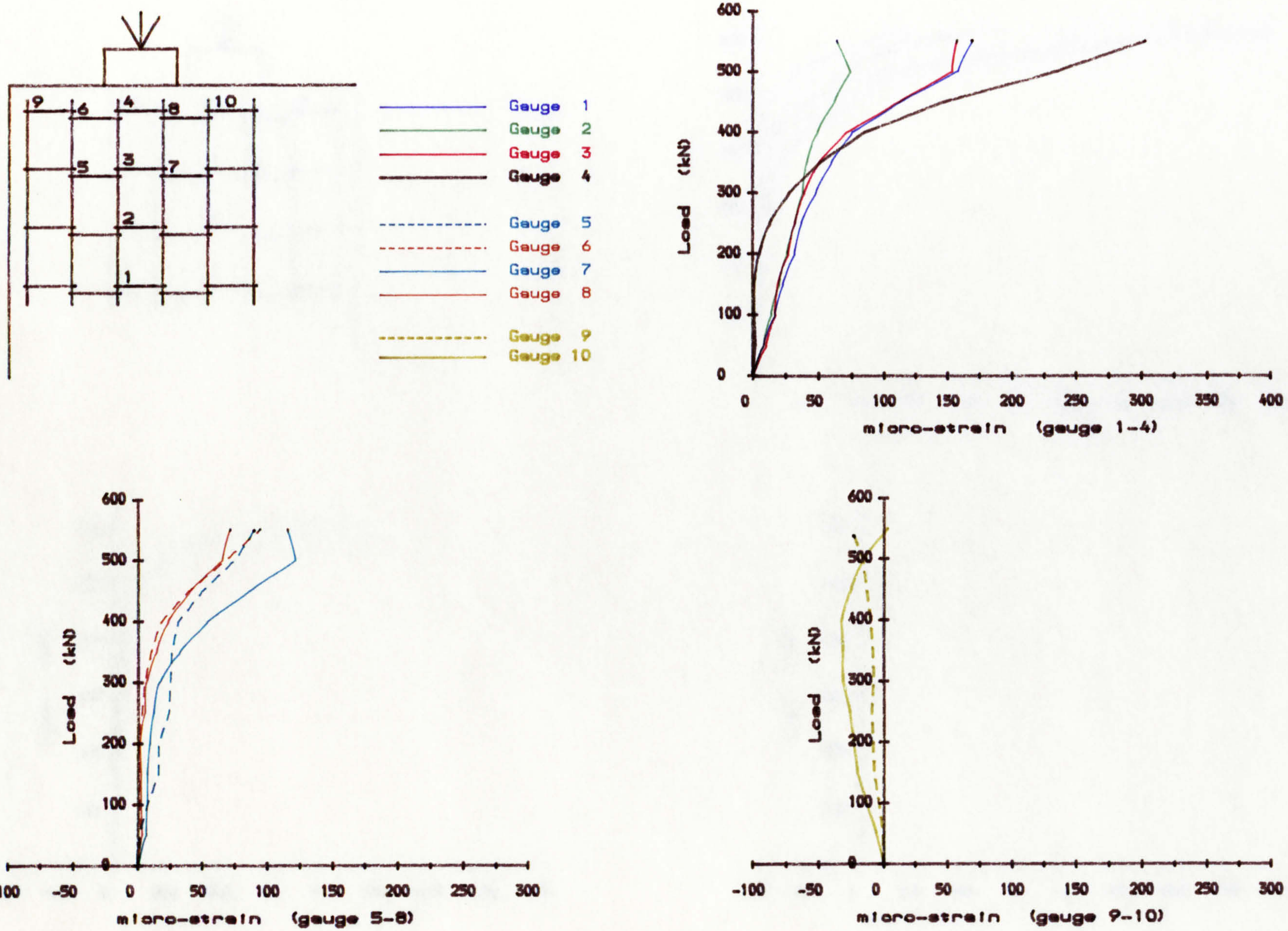

Fig. A. 36. Strain of steel in block R1/2.

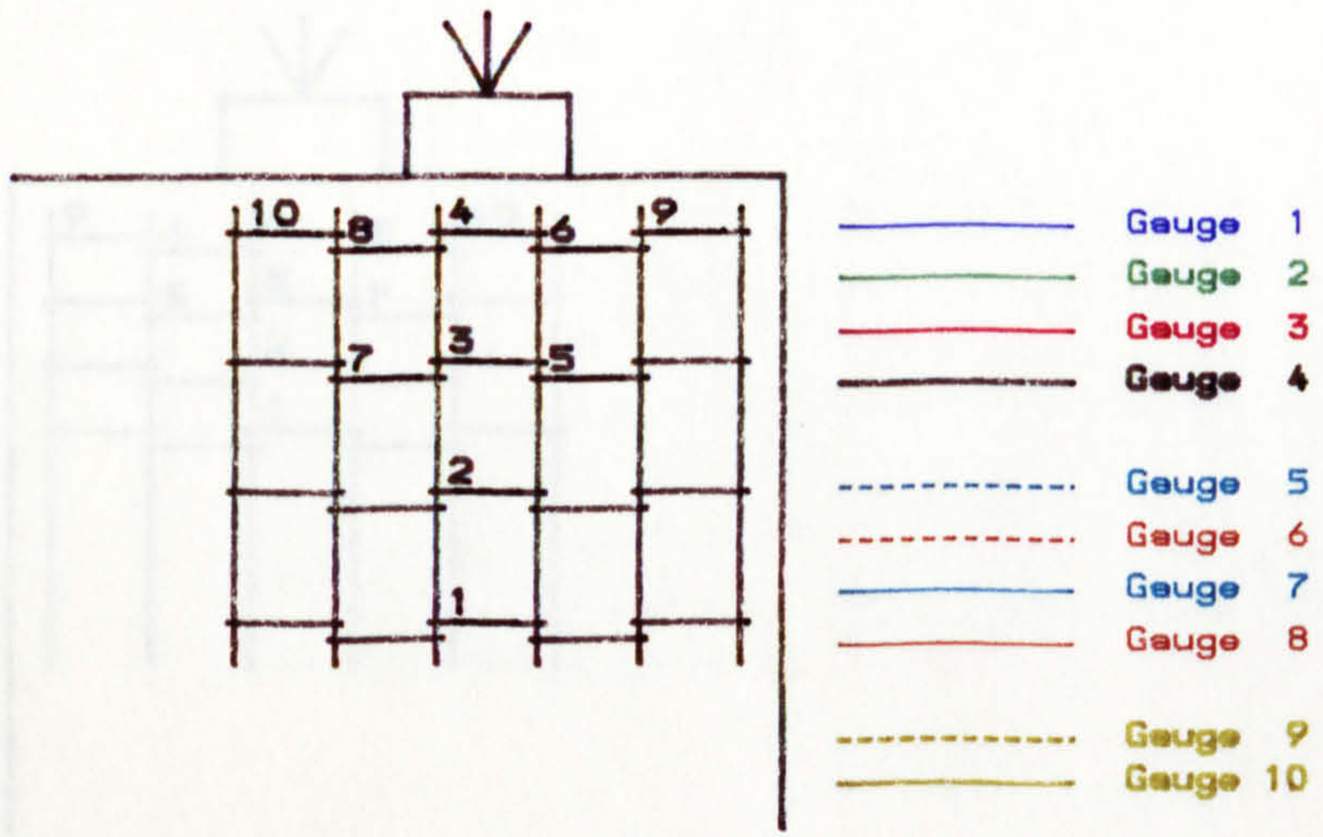

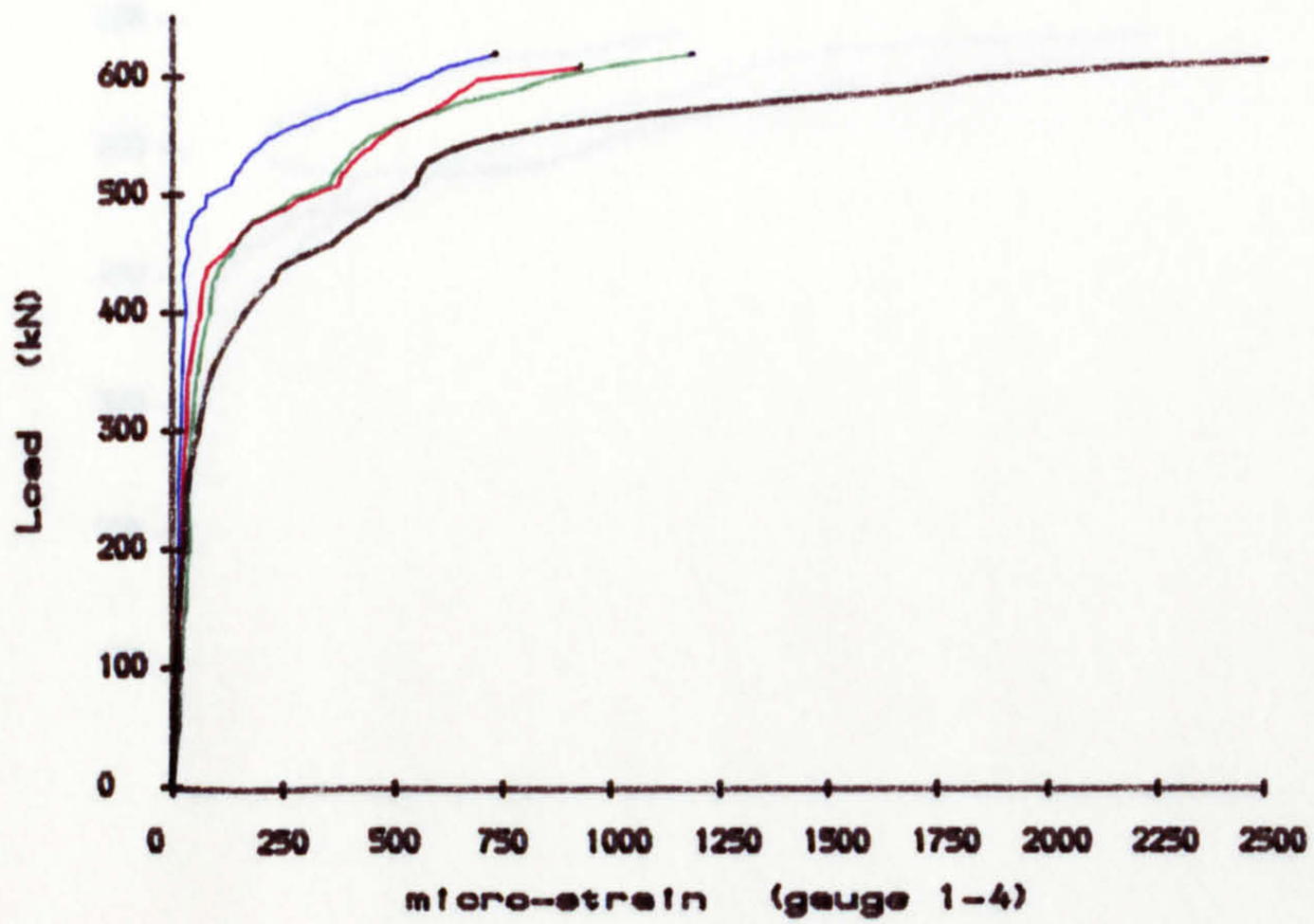

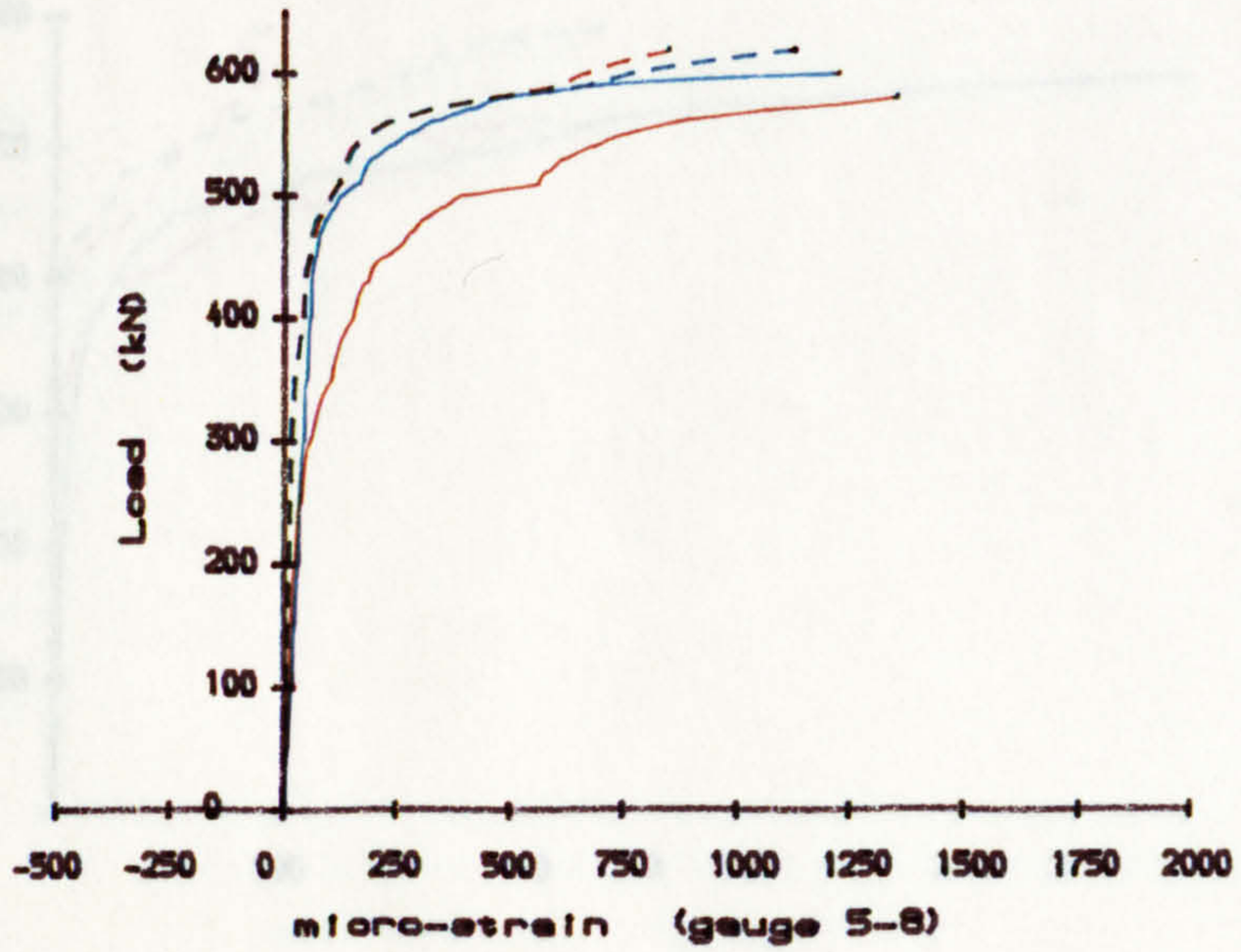

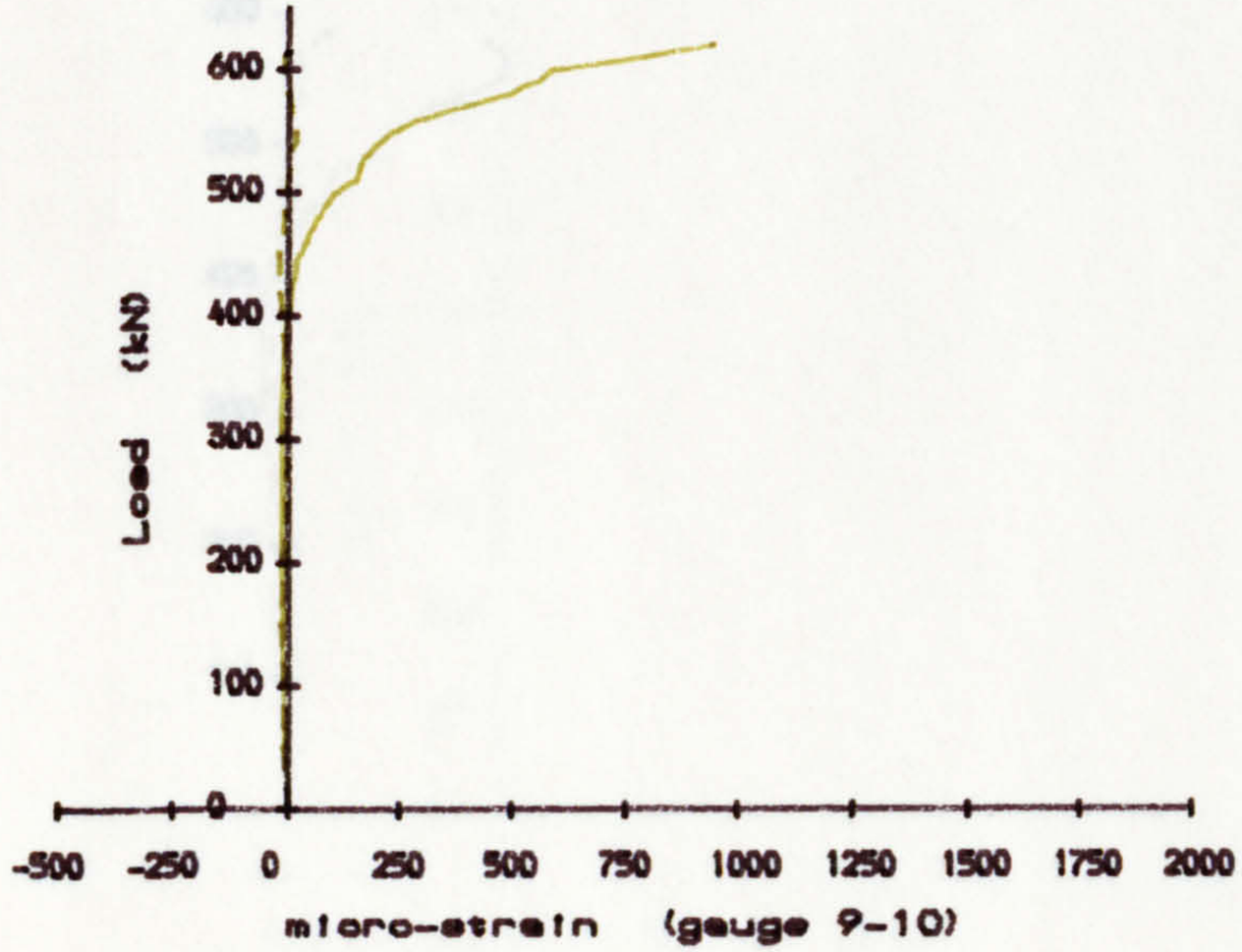

Fig. A. 37. Strain of steel in block R2/1.

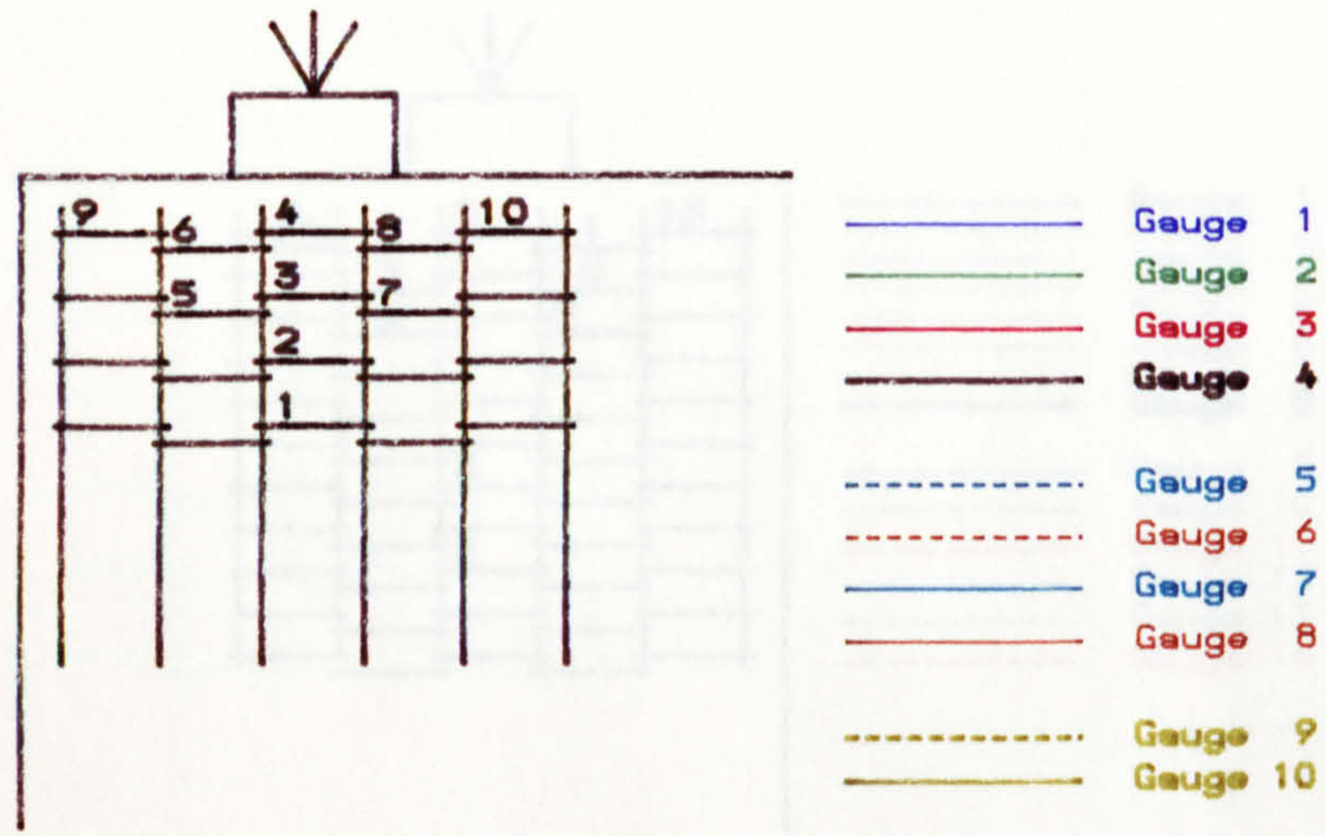

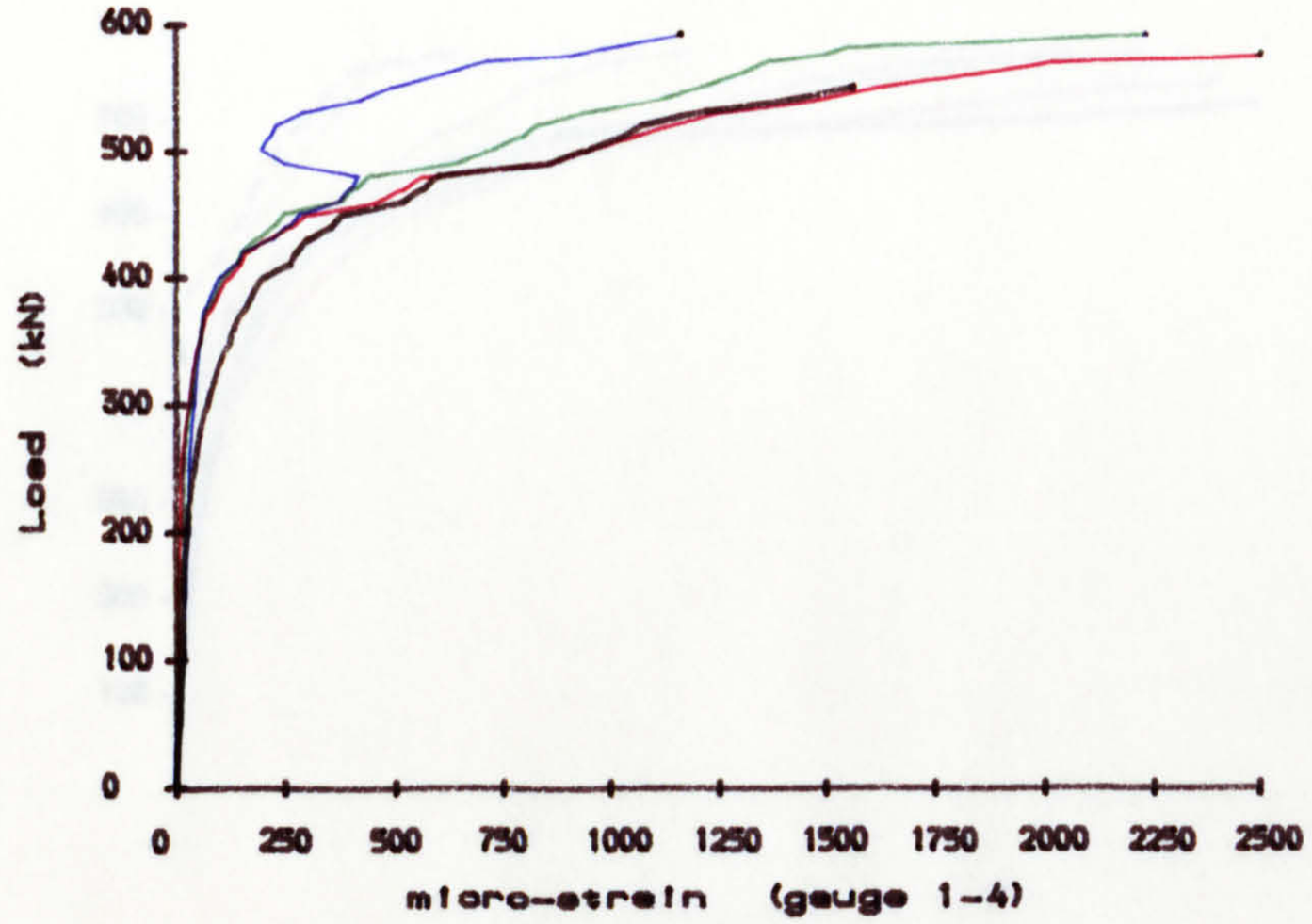

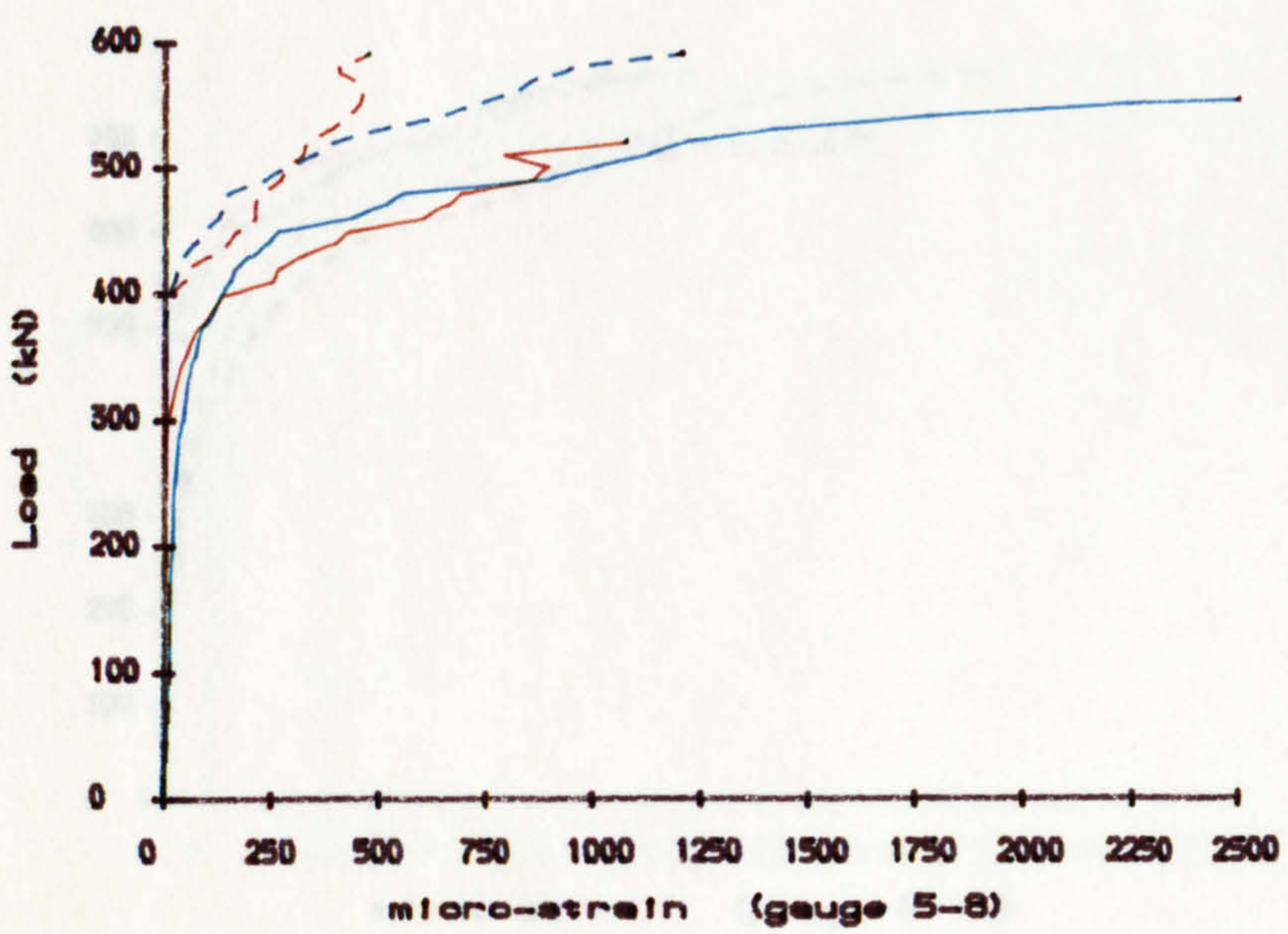

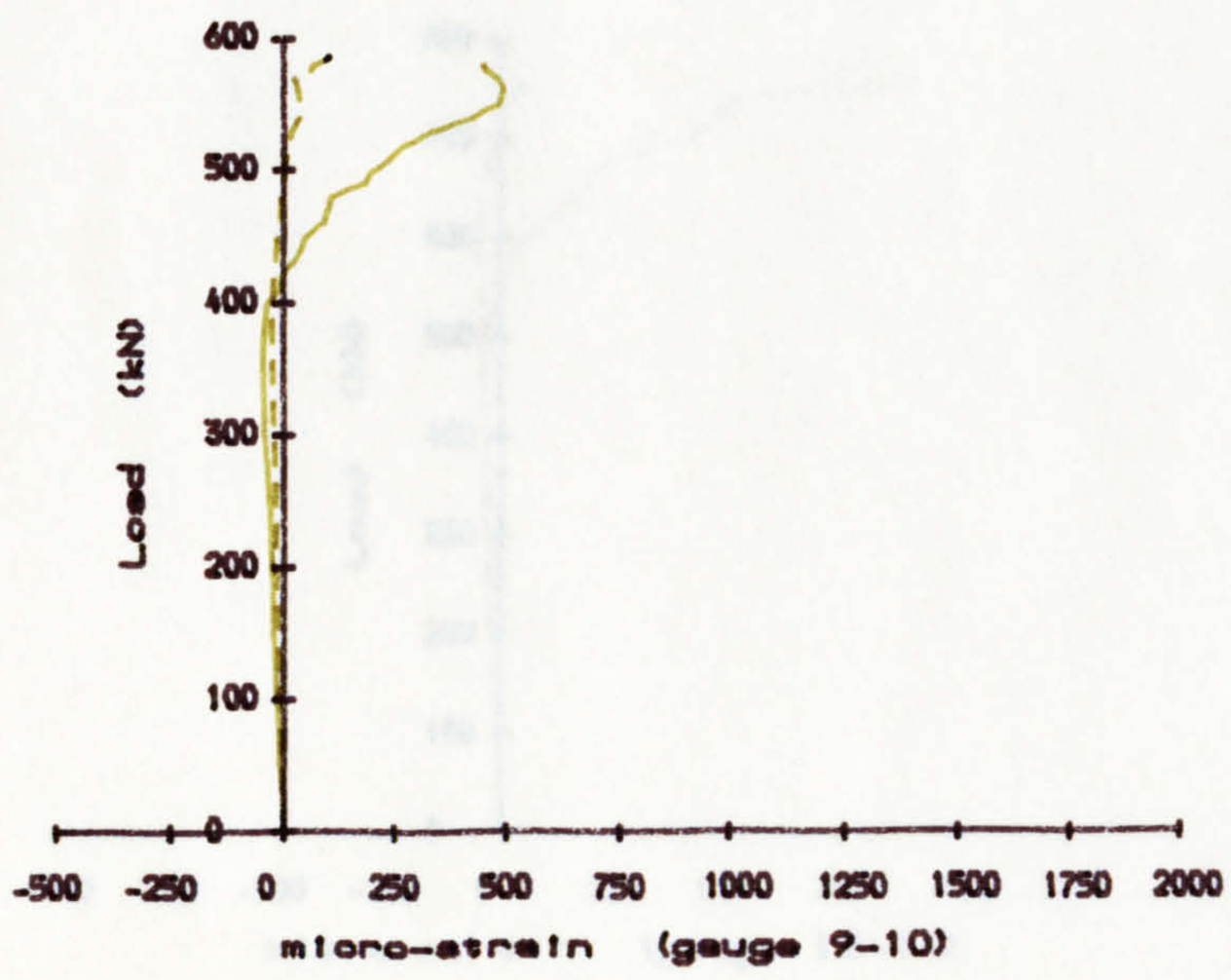

Fig. A. 38. Strain of steel in block R2/2.

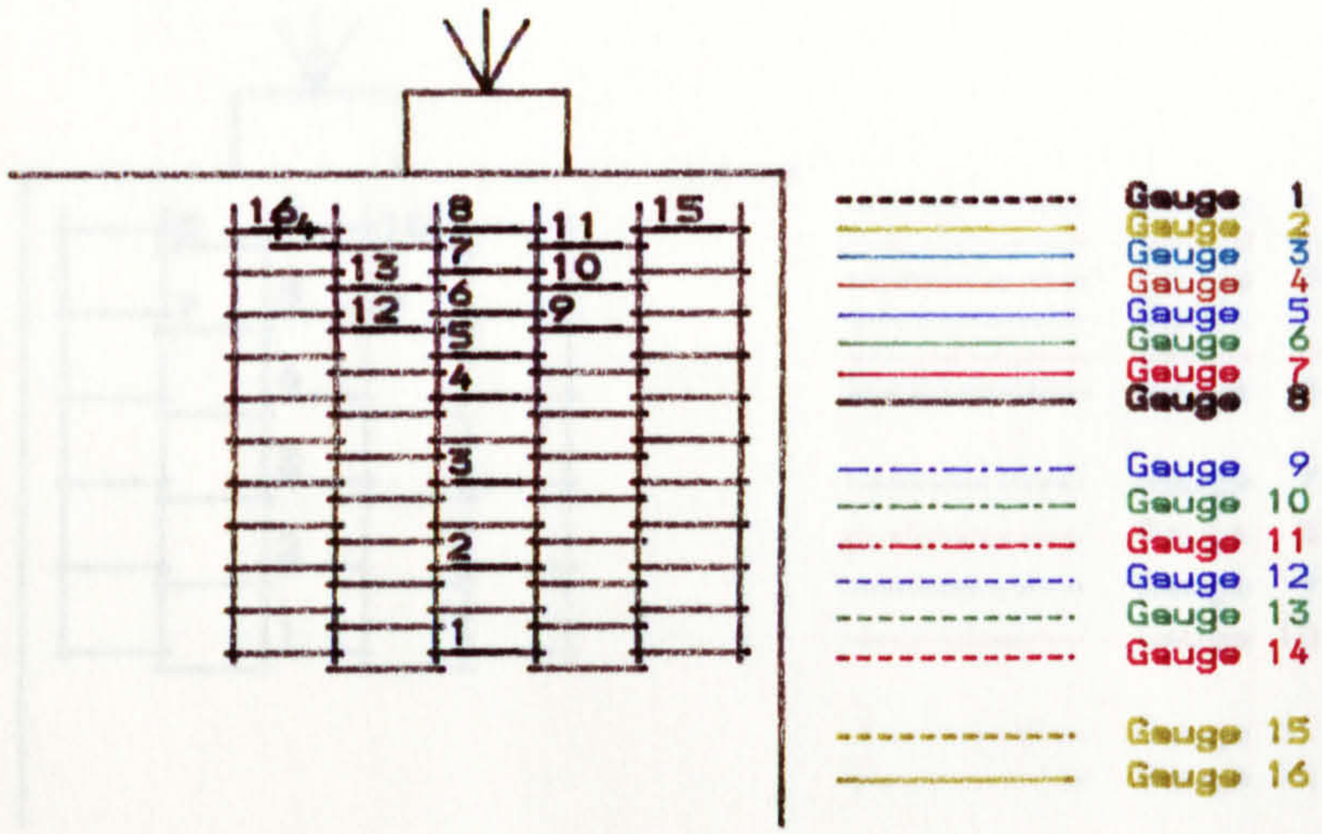

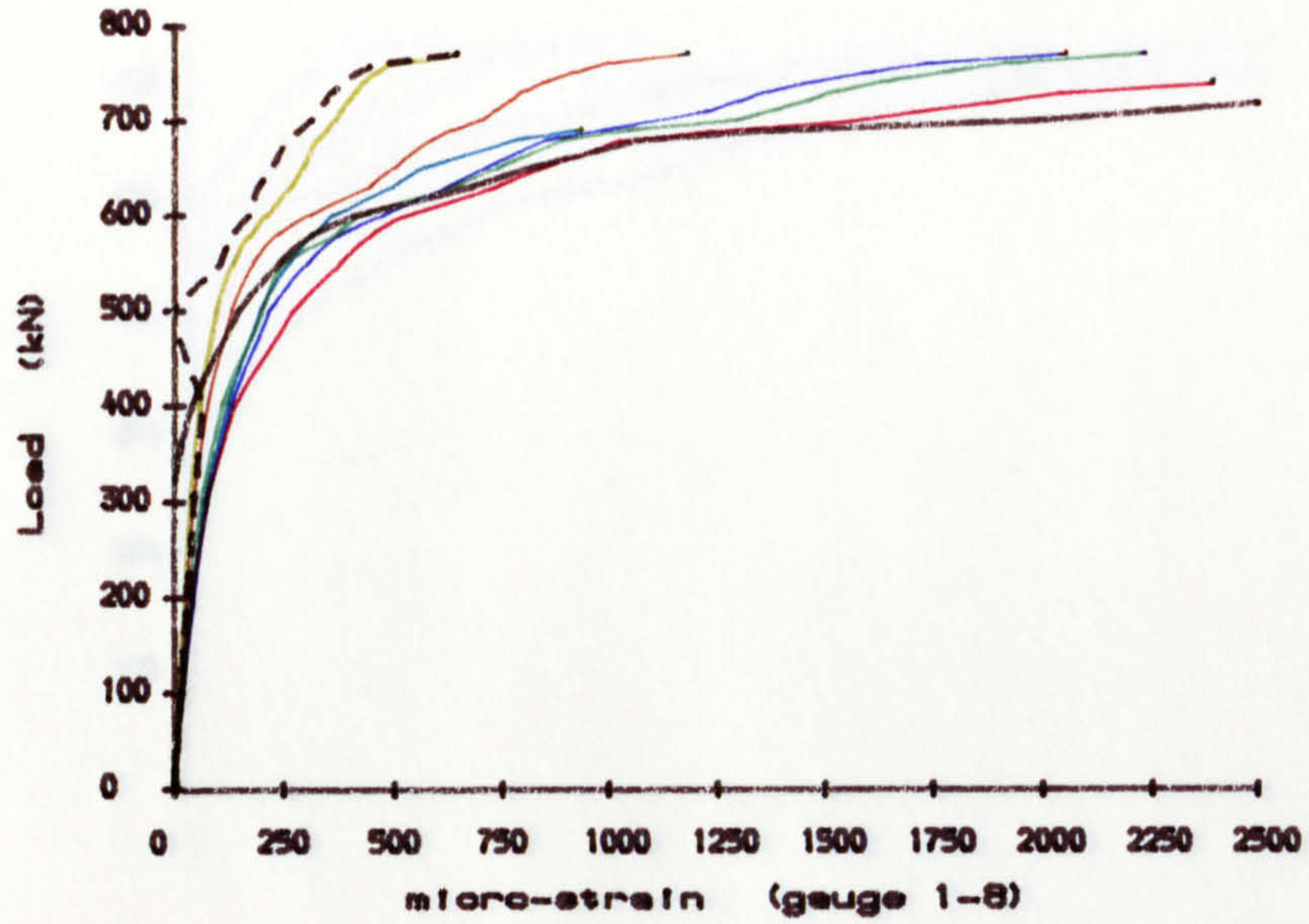

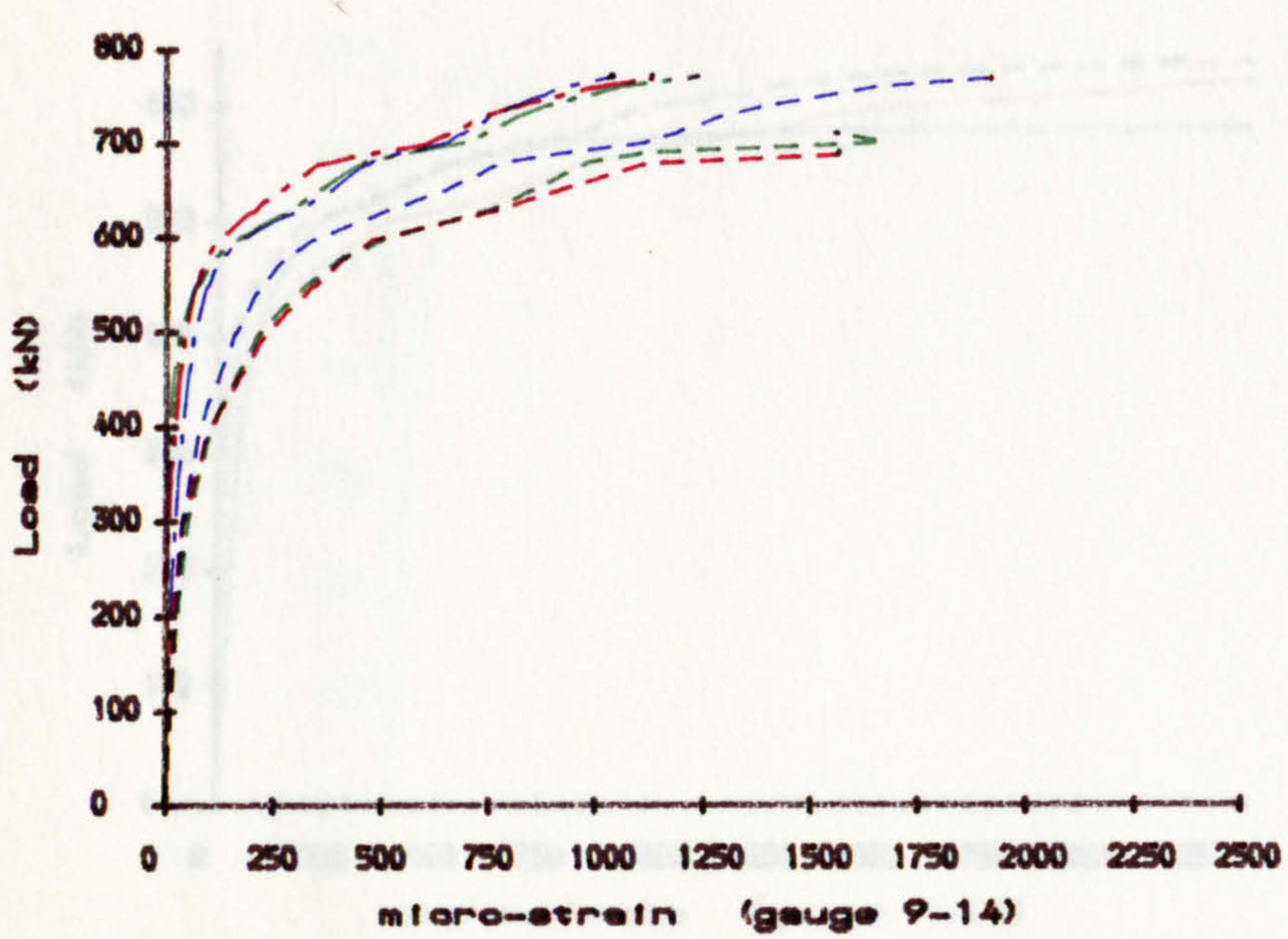

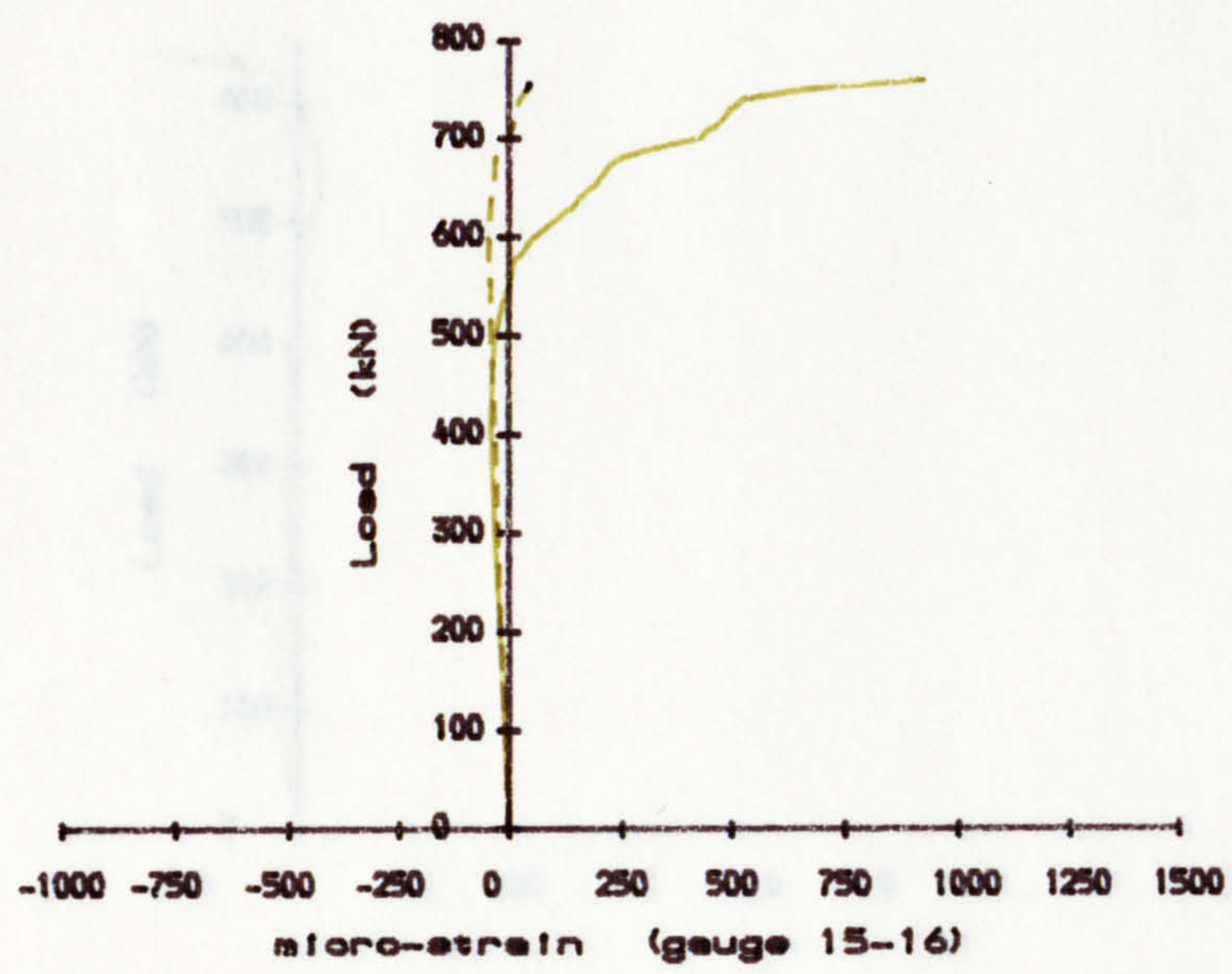

Fig. A. 39. Strain of steel in block R3/1.

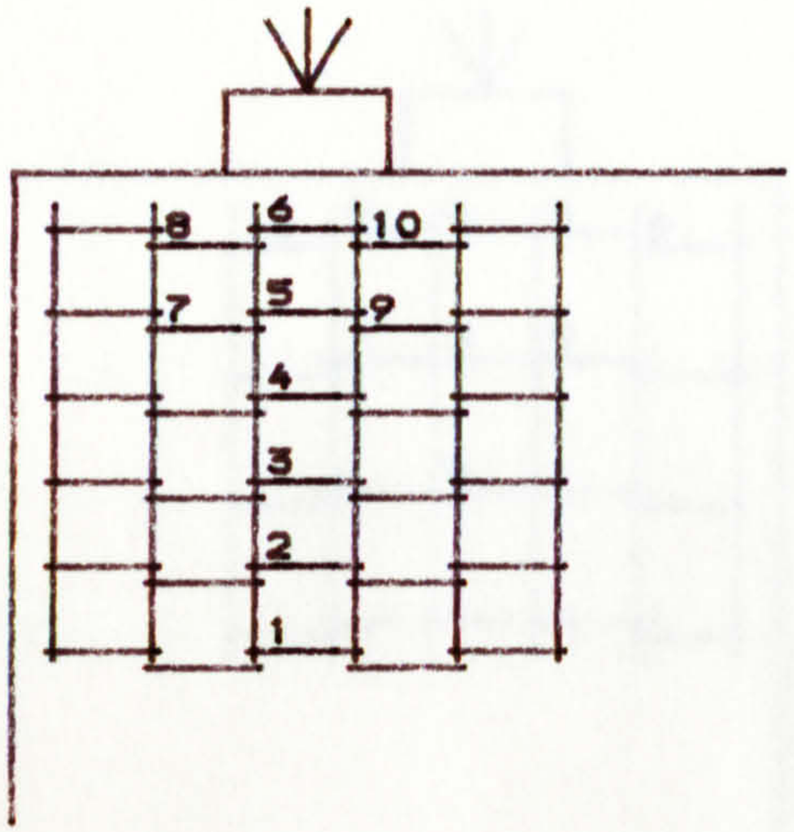

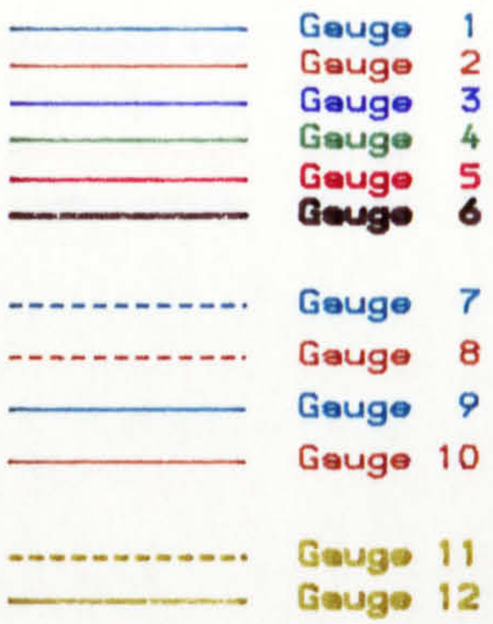

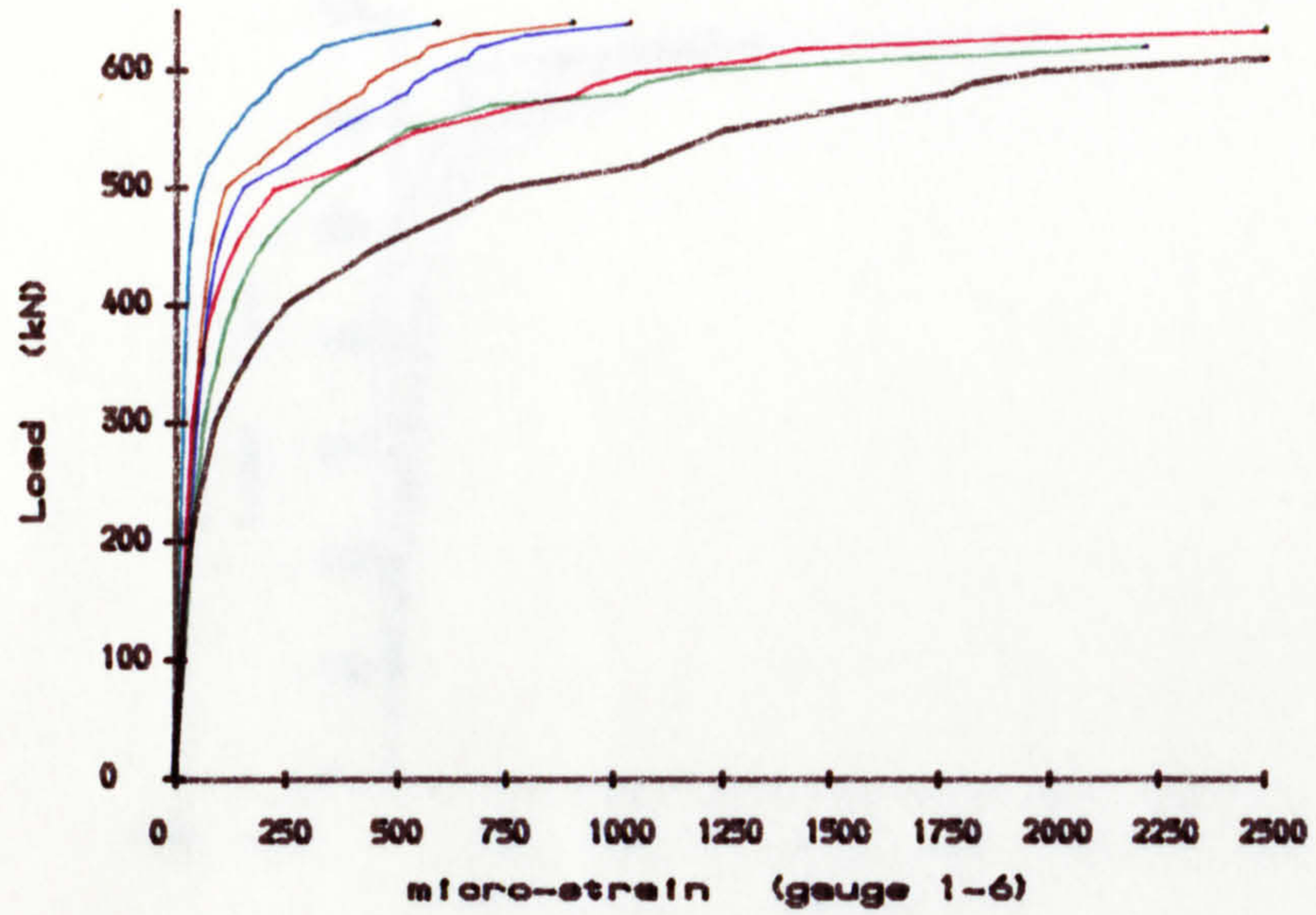

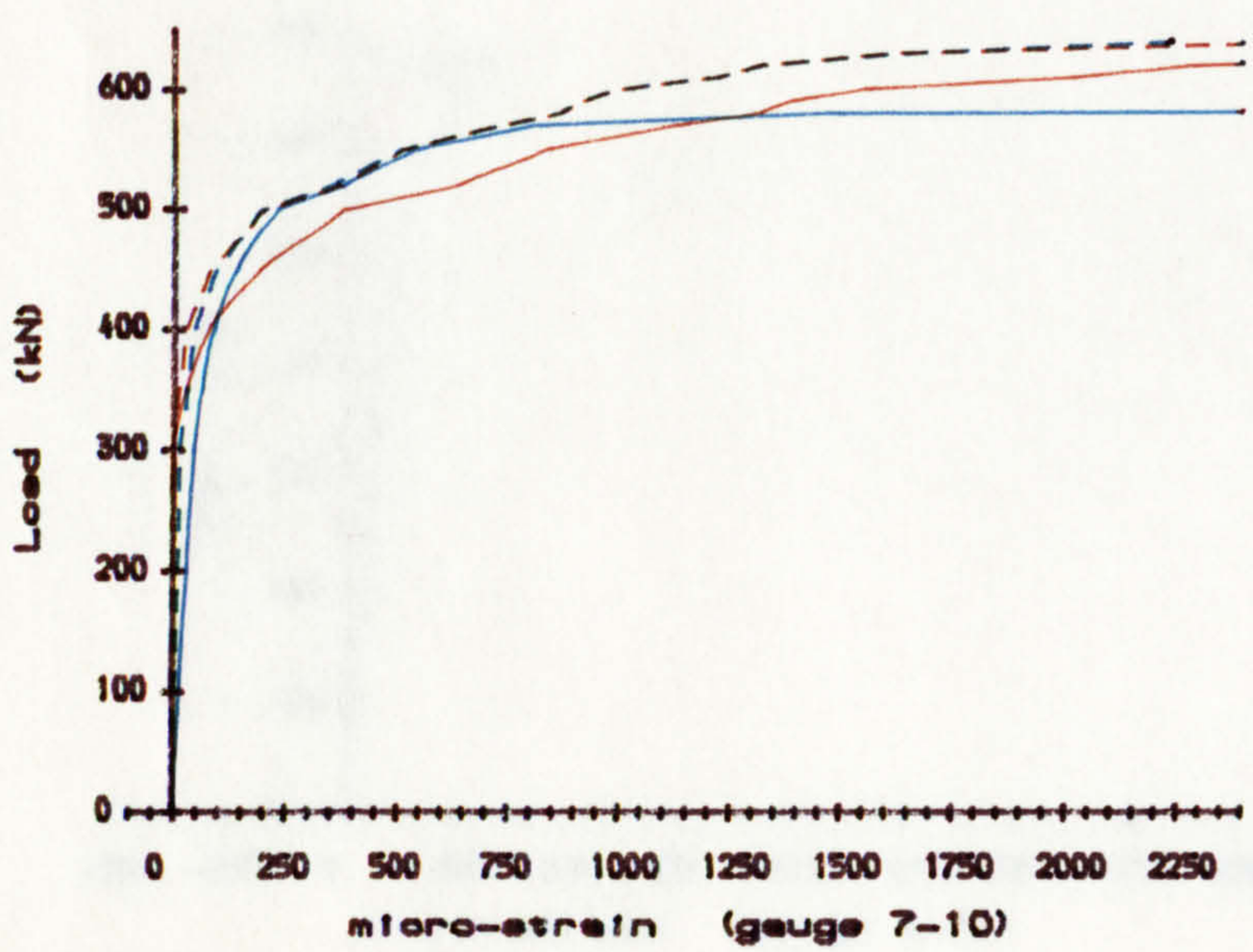

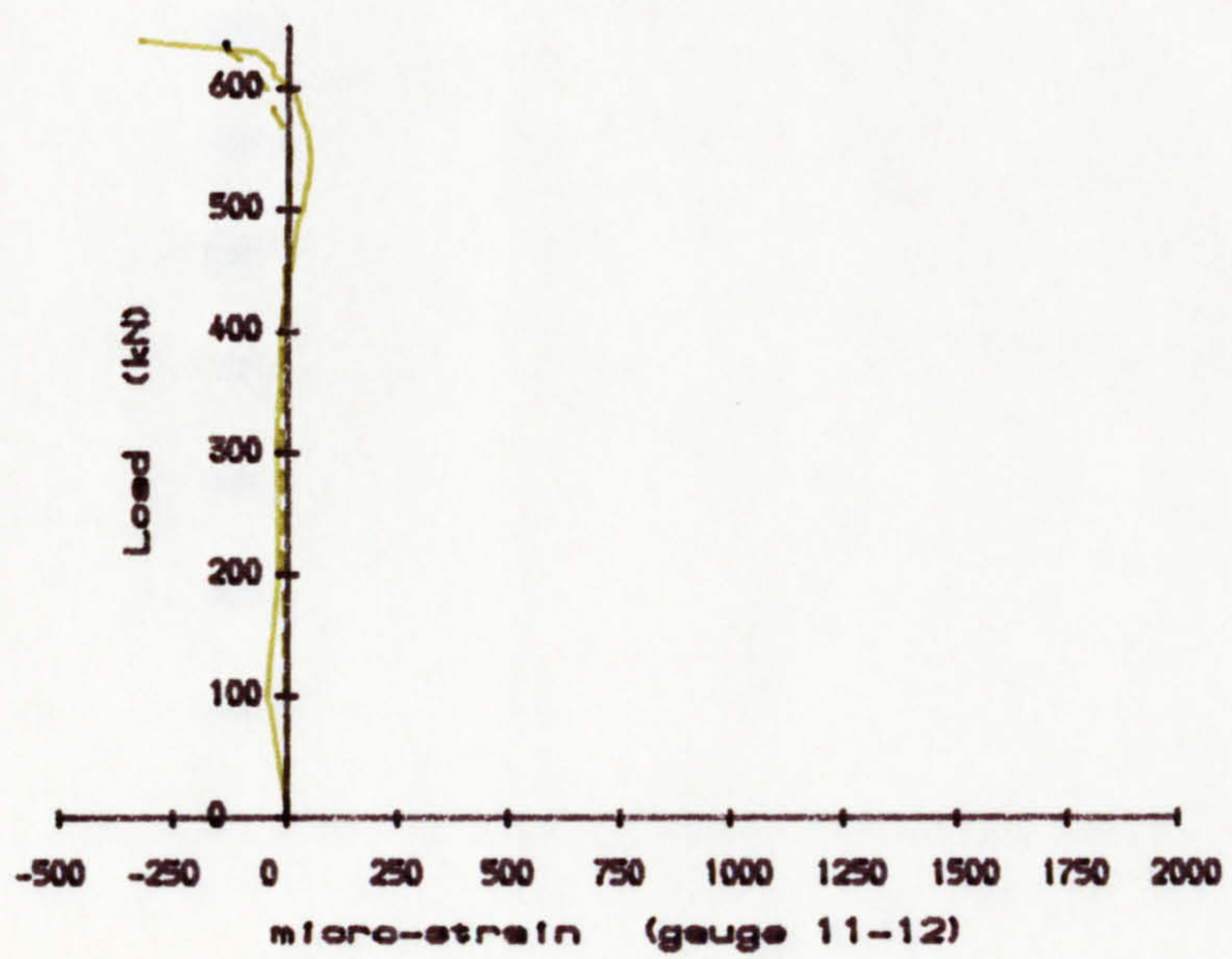

Fig. A. 40. Strain of steel in block R3/2.

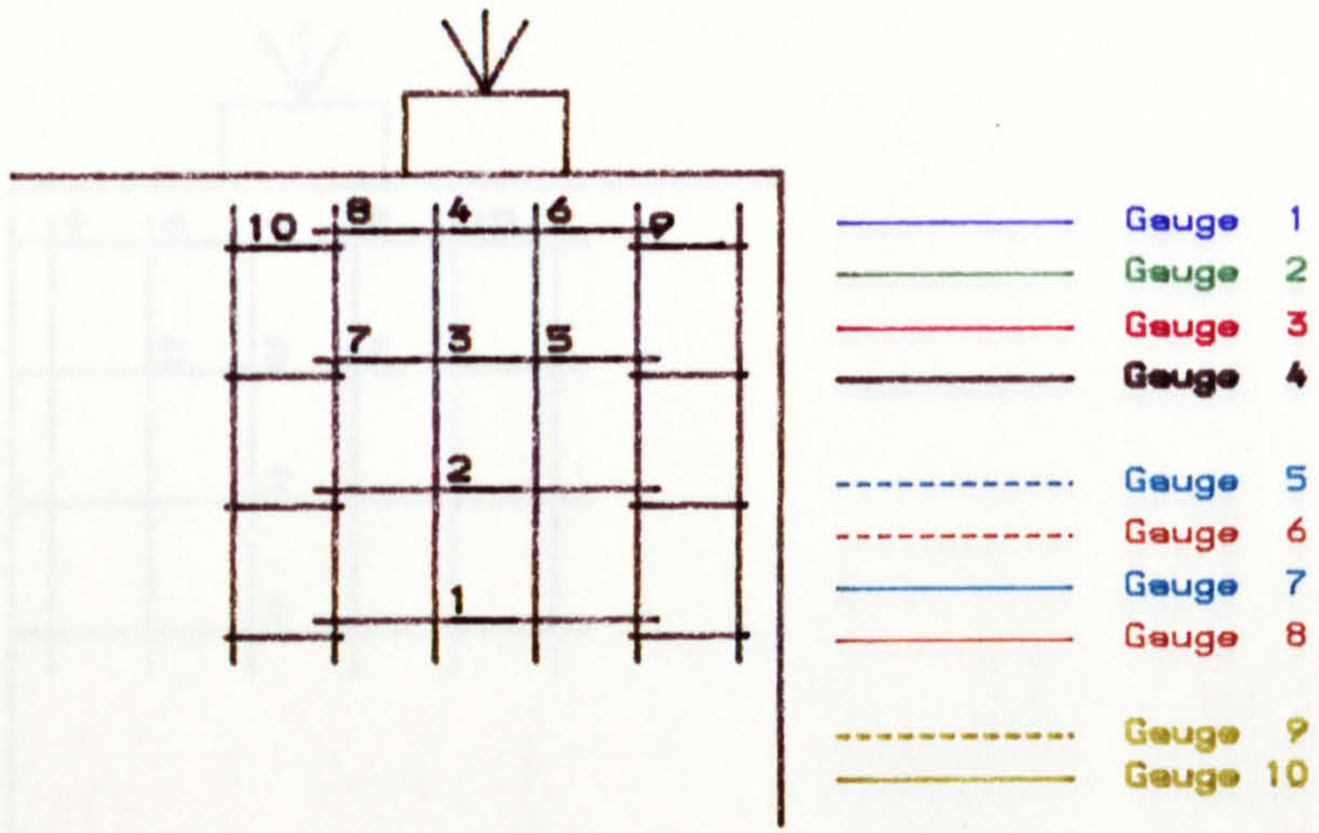

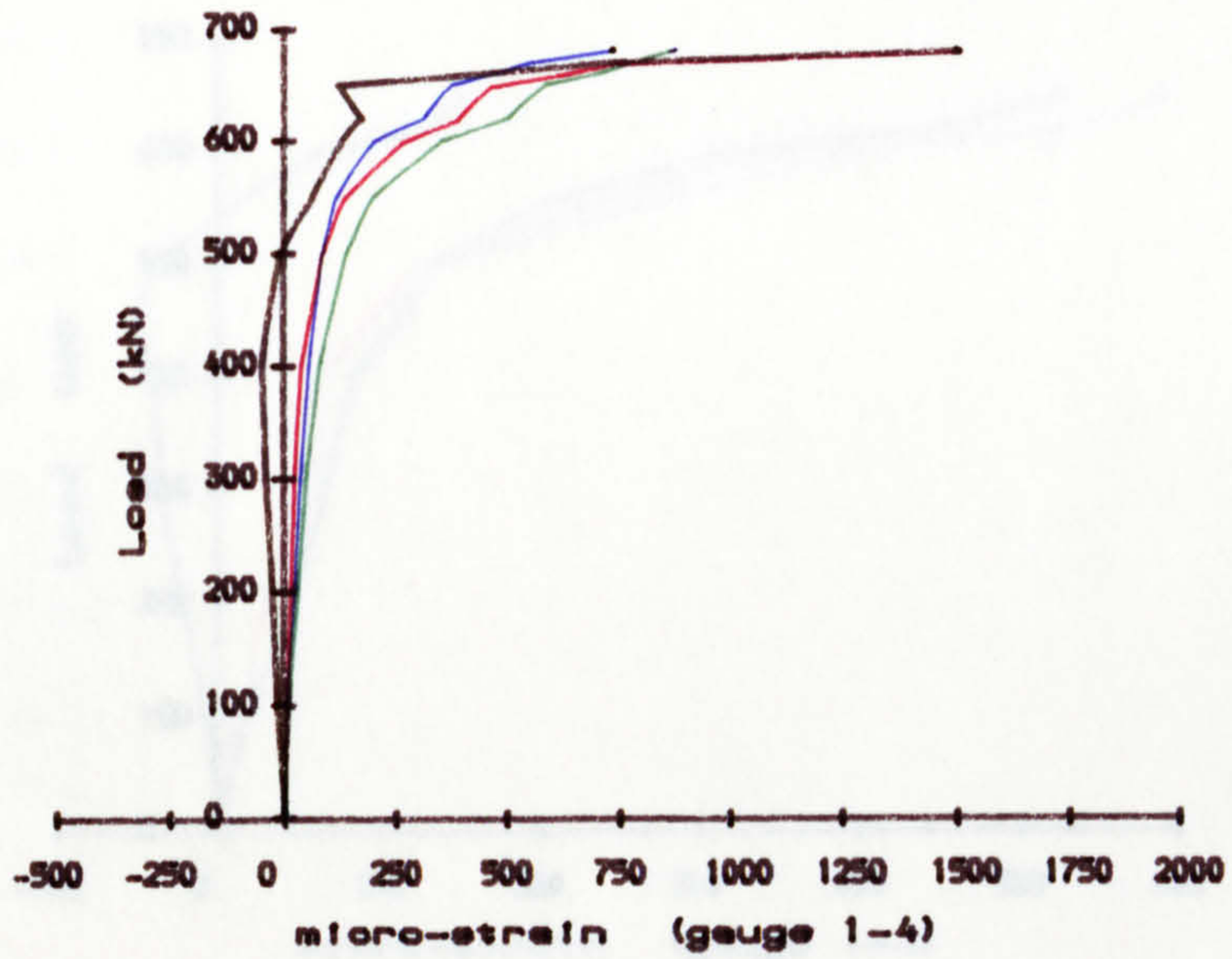

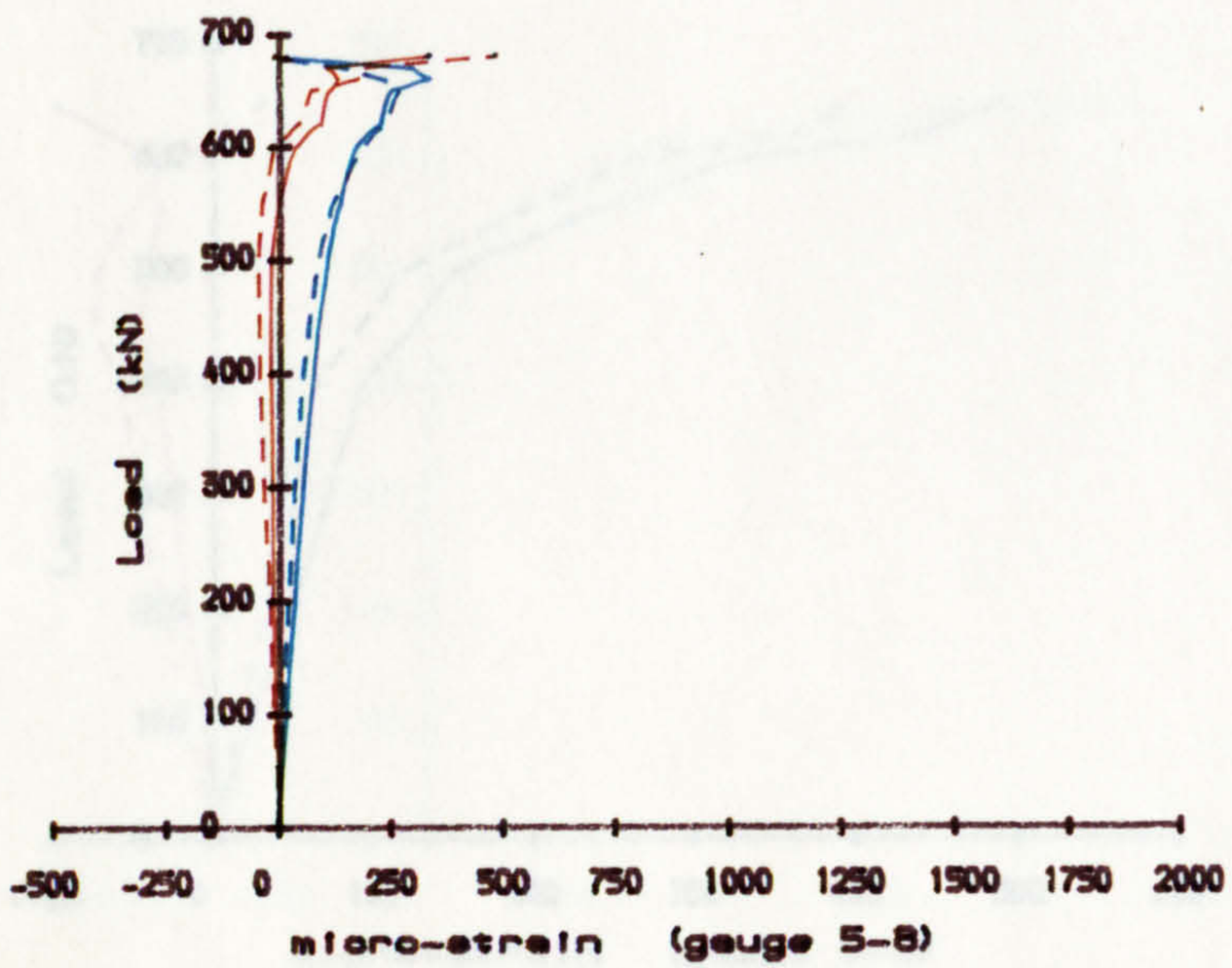

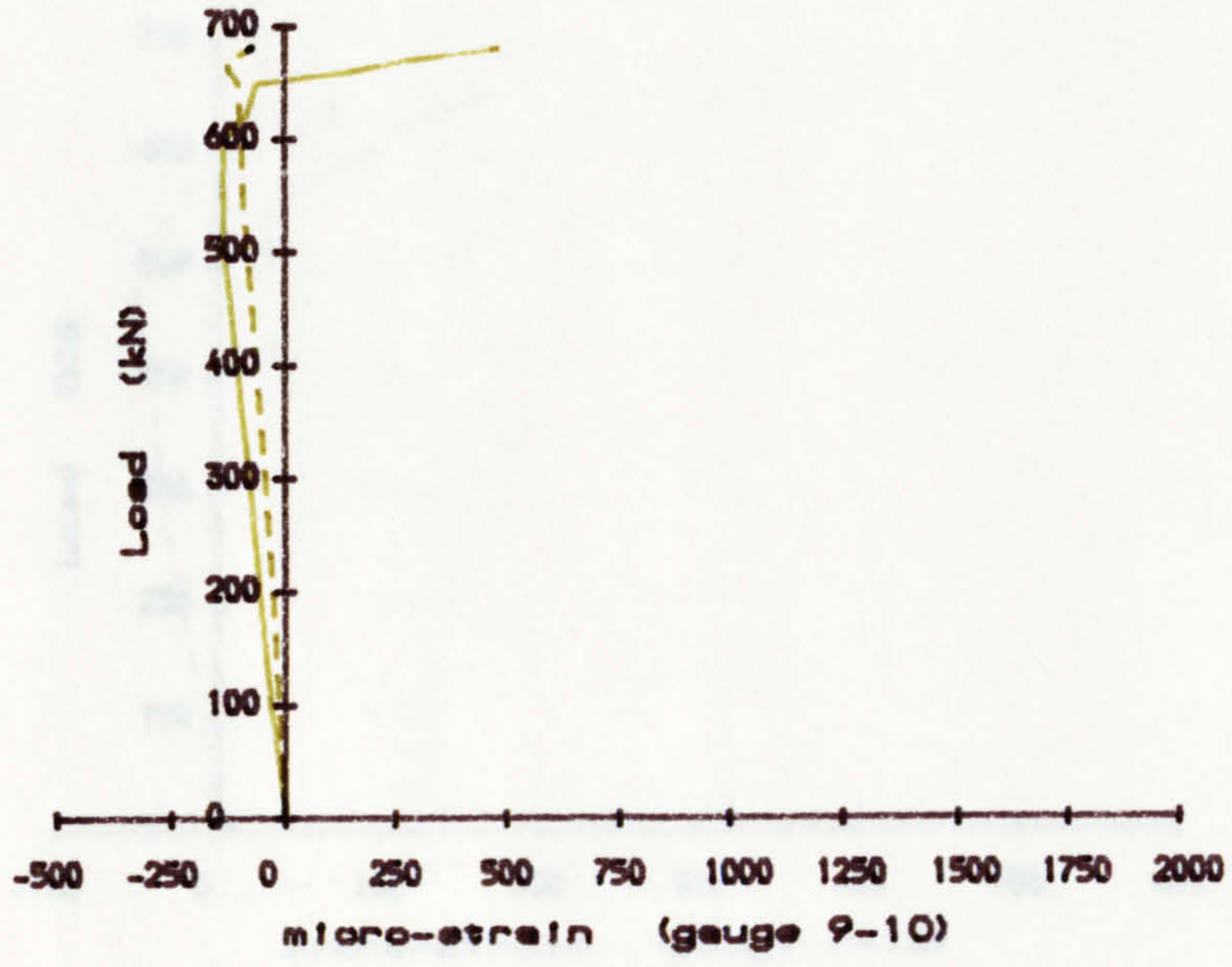

Fig. A. 41. Strain of steel in block R4/1.

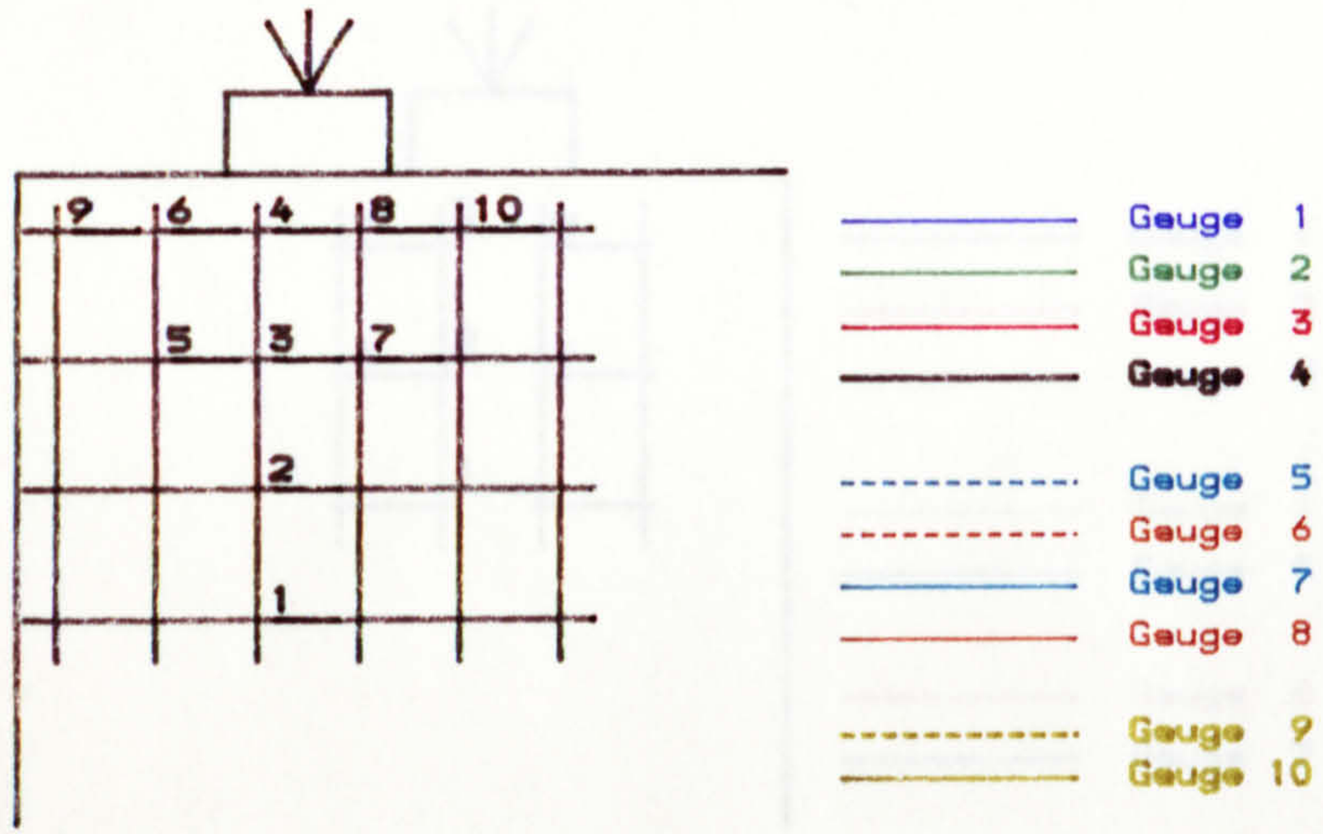

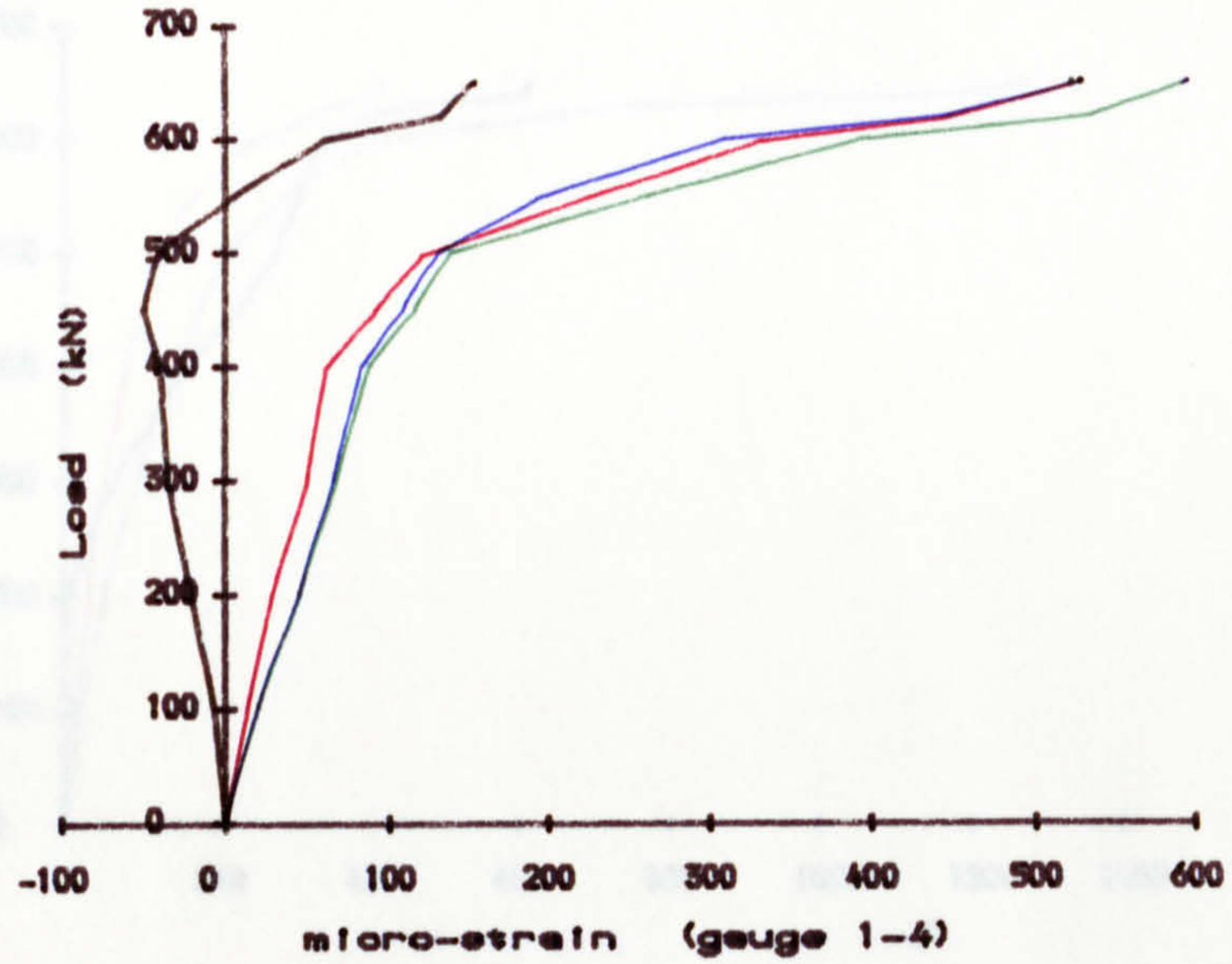

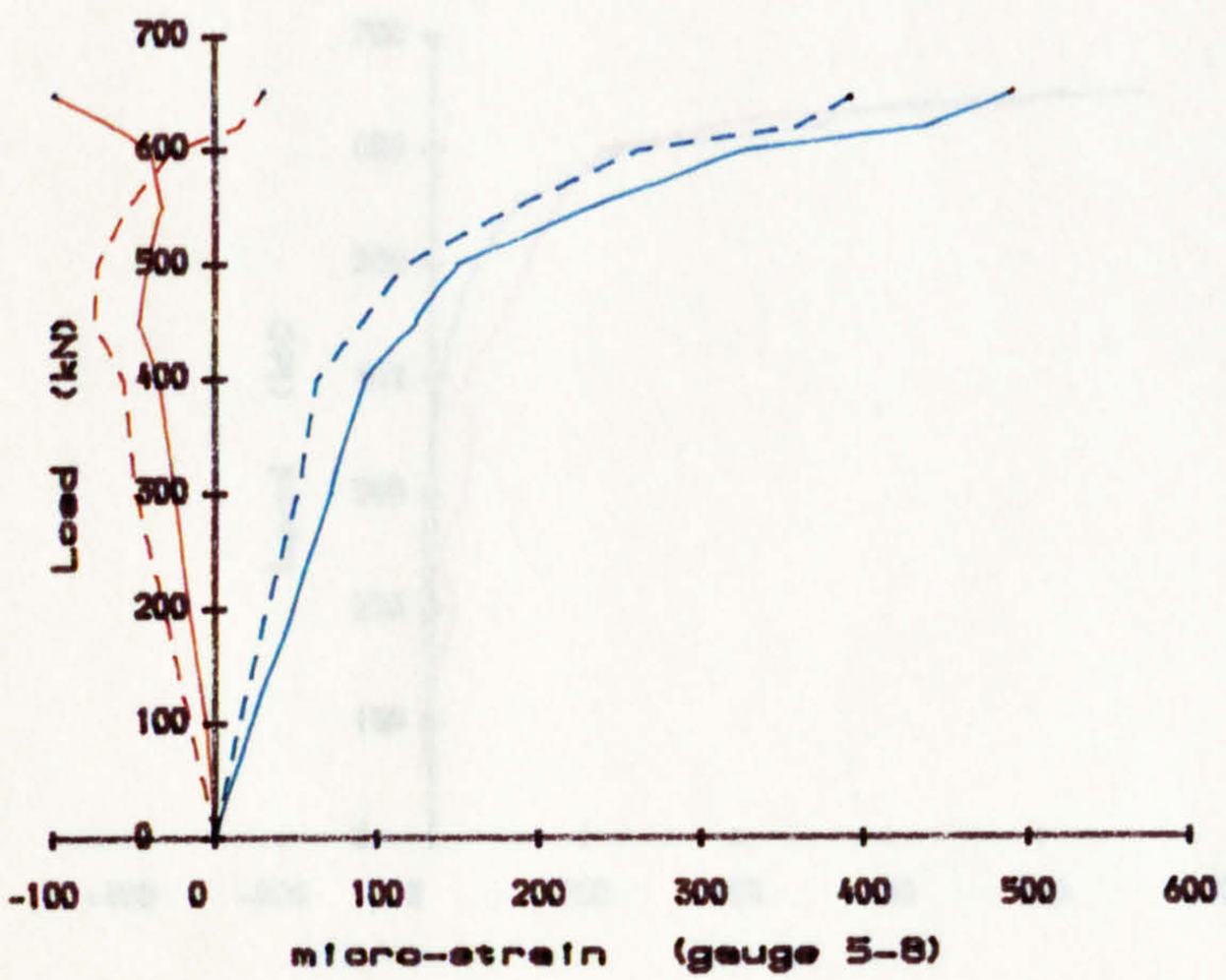

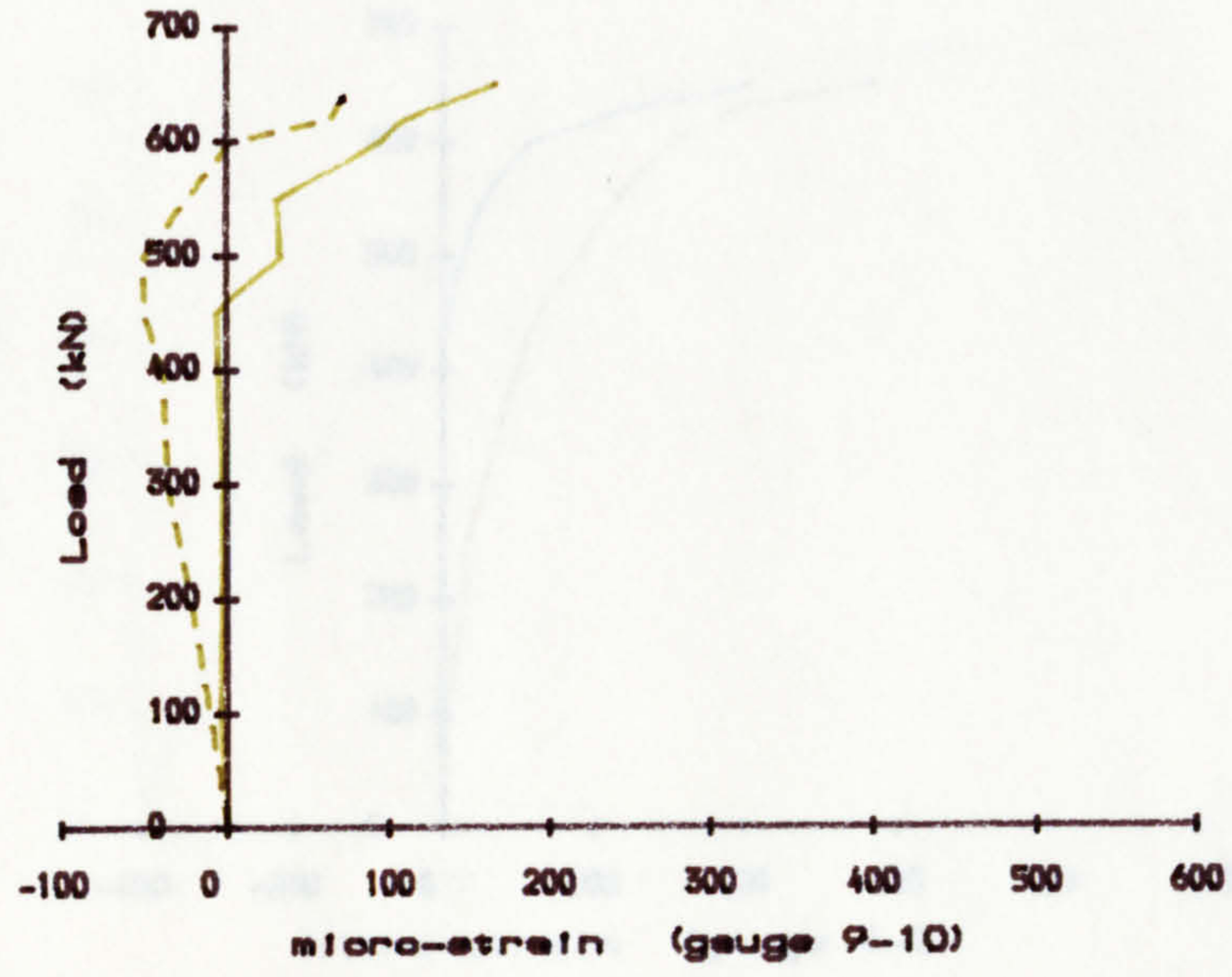

Fig. A. 42. Strain of steel in block R4/2.

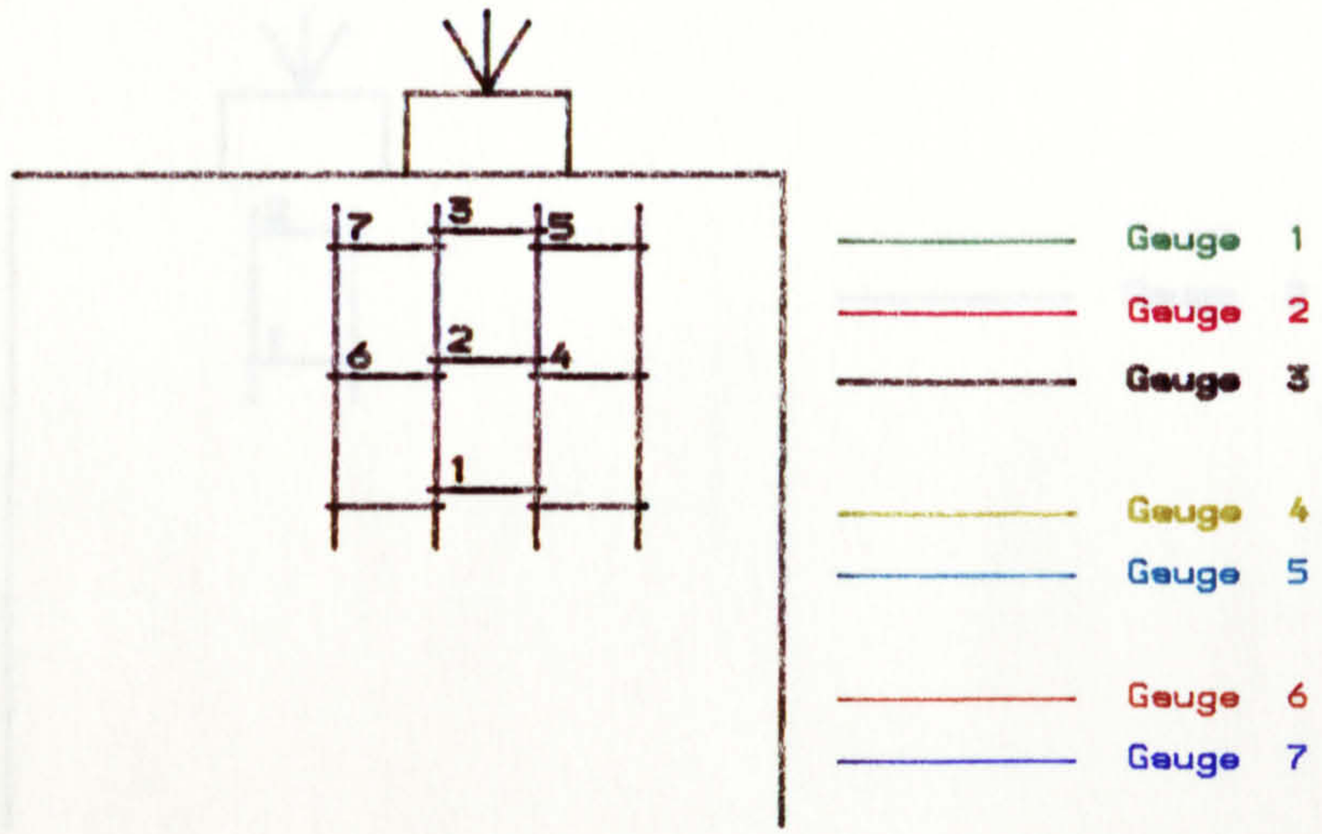

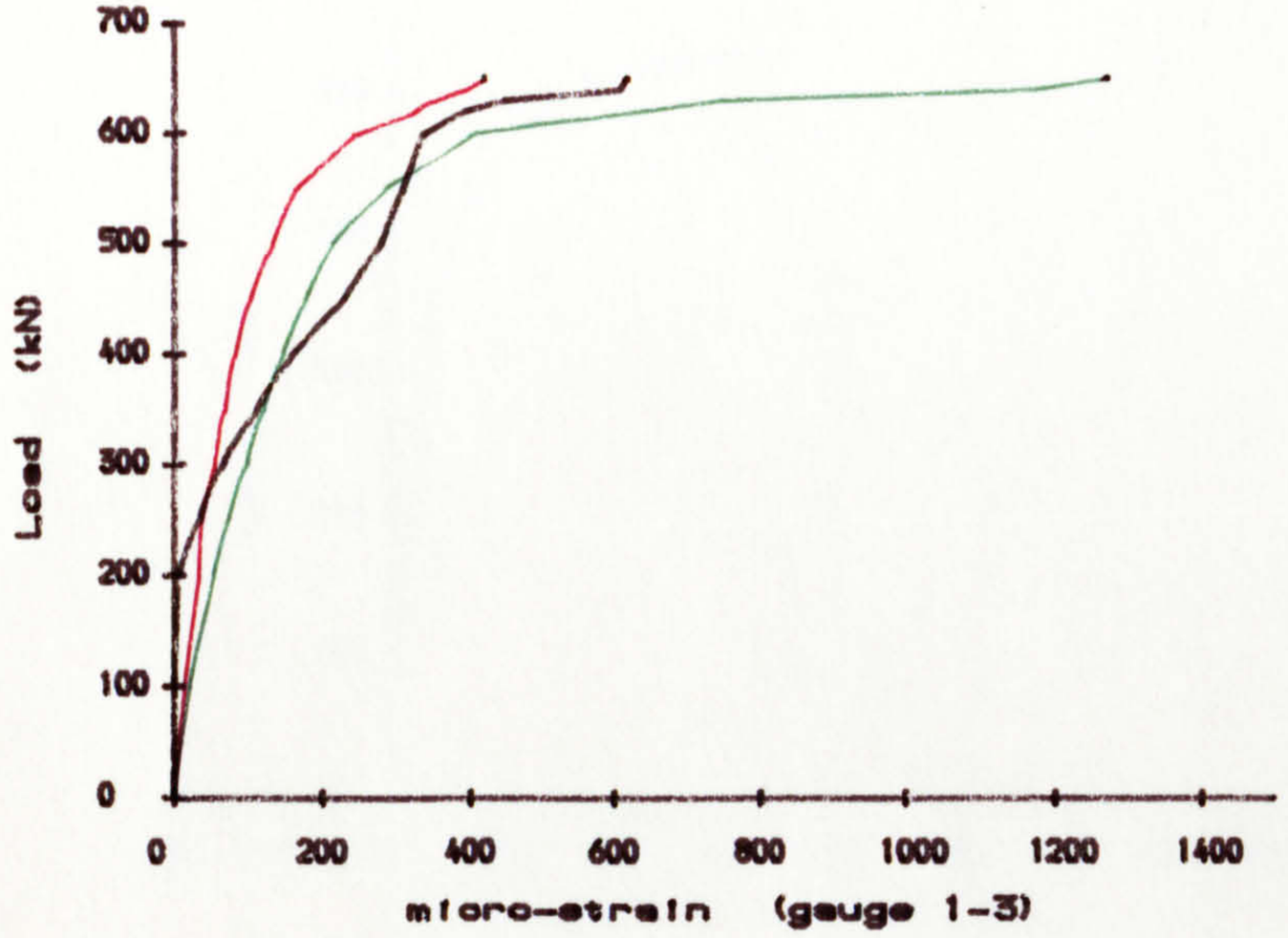

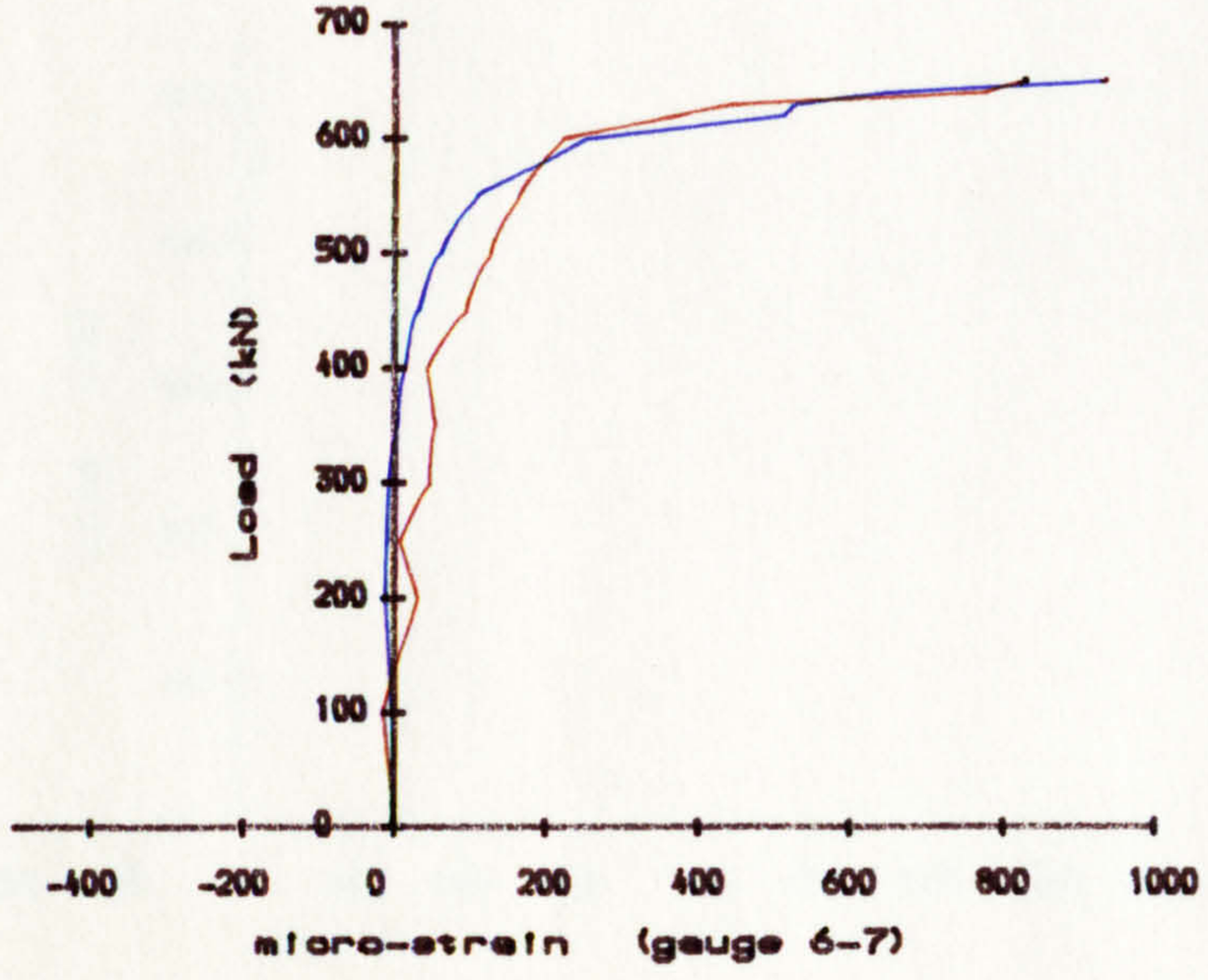

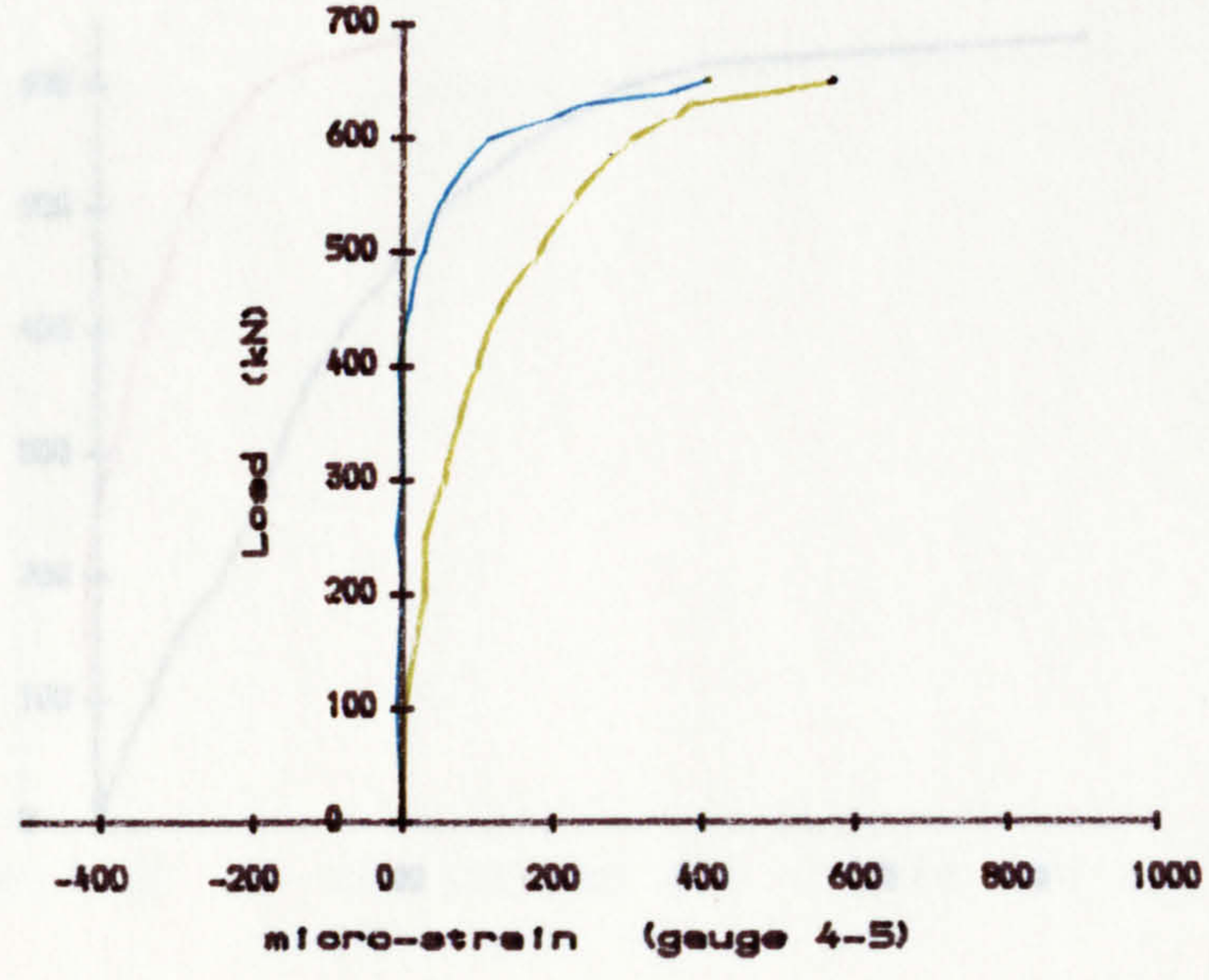

Fig. A. 43. Strain of steel in block R5/1.

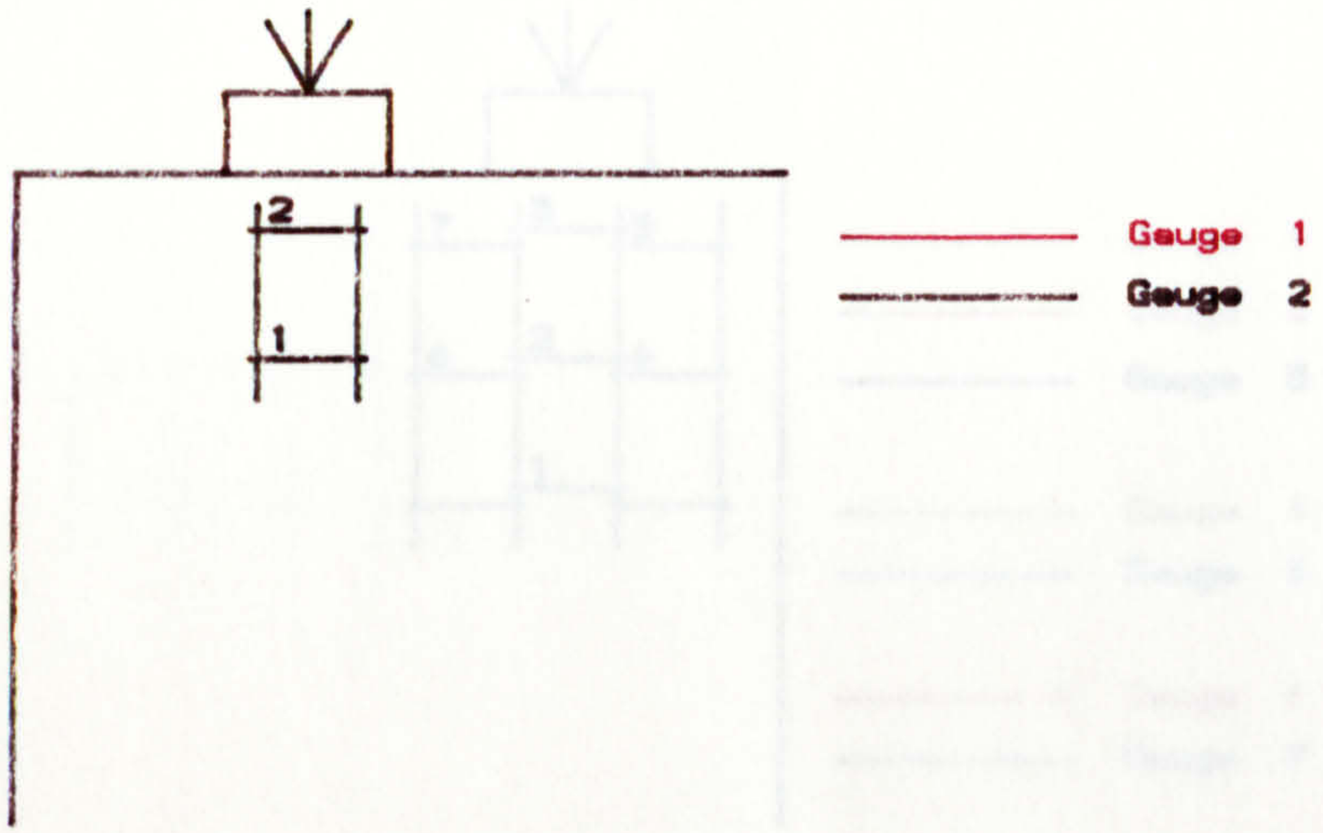

Gauge 1

Gauge 2

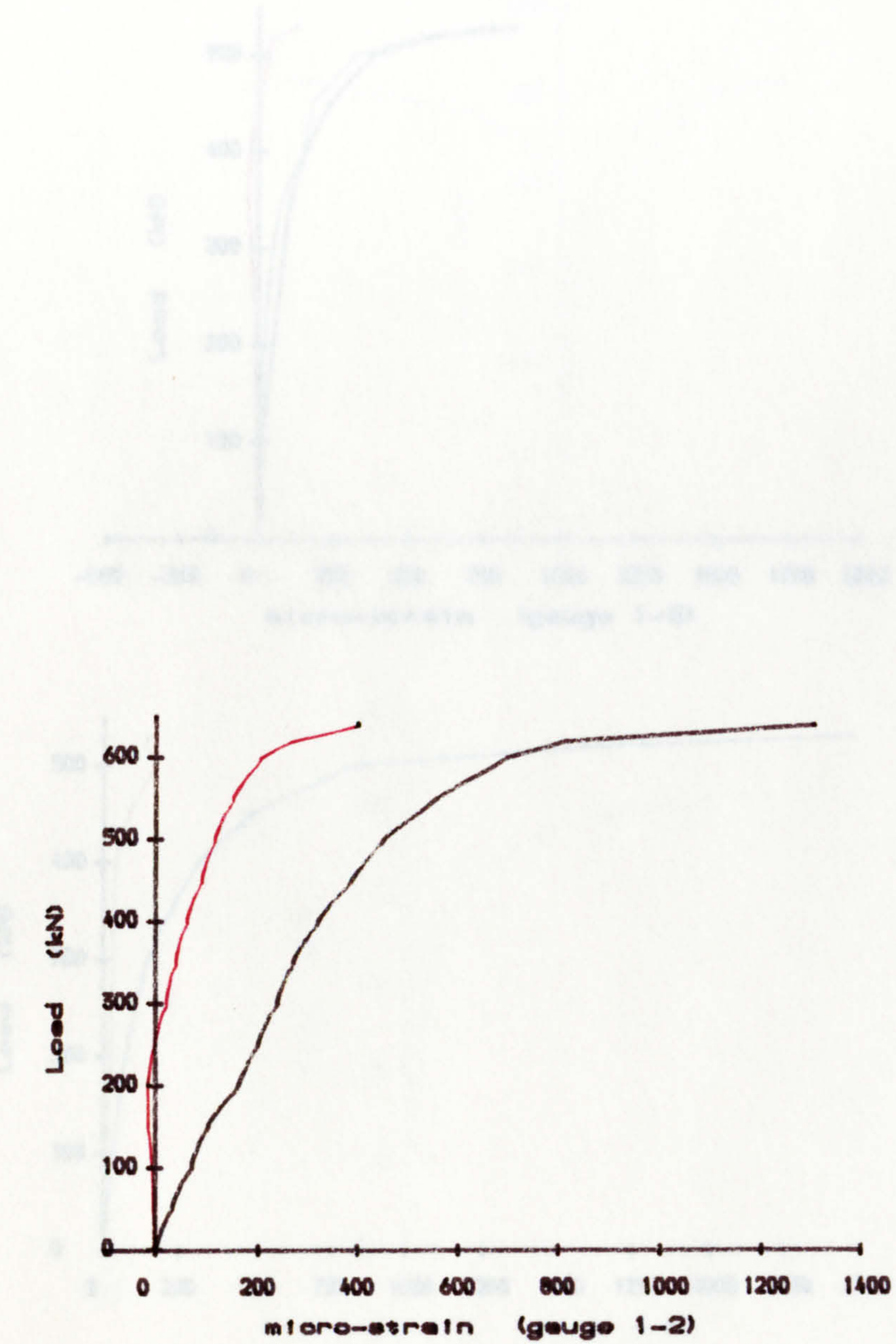

Fig. A. 44. Strain of steel in block R5/2.

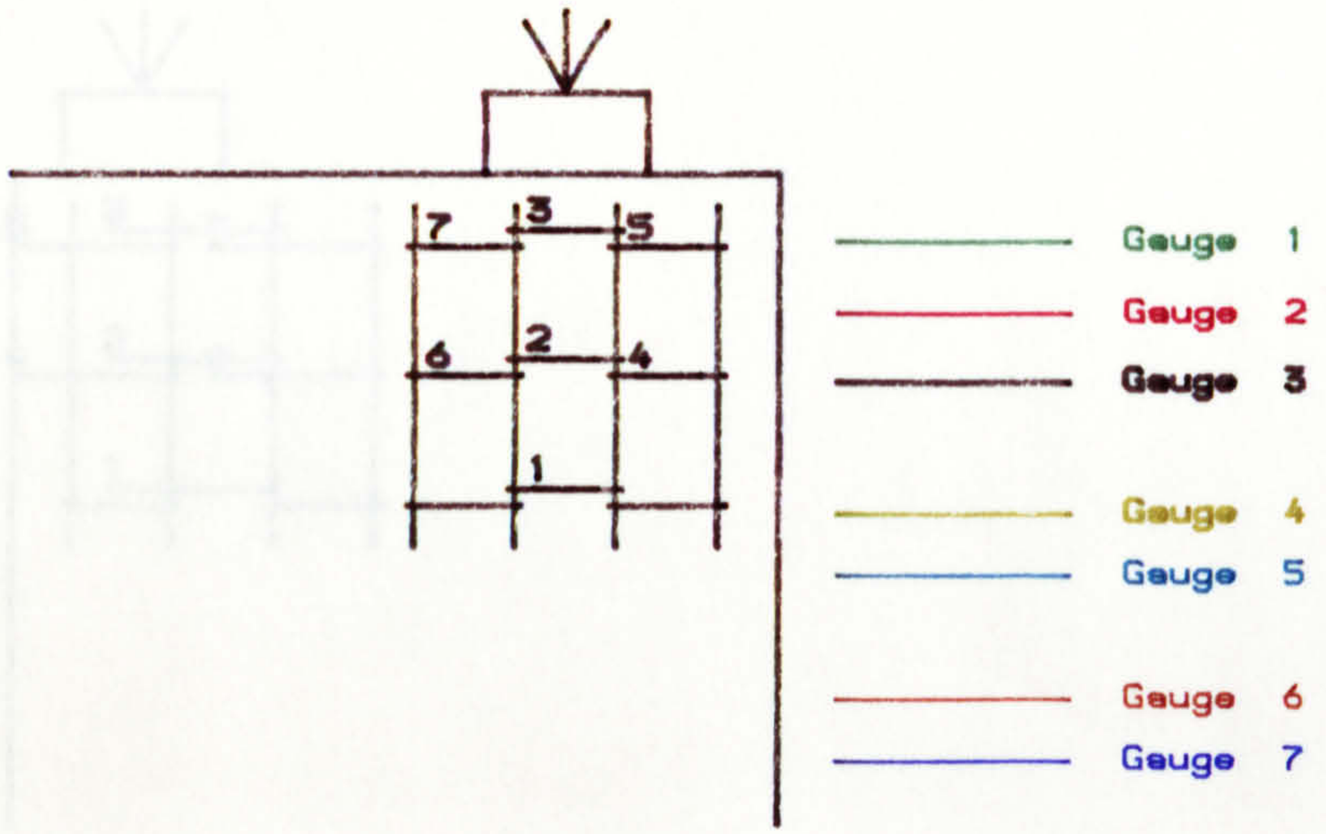

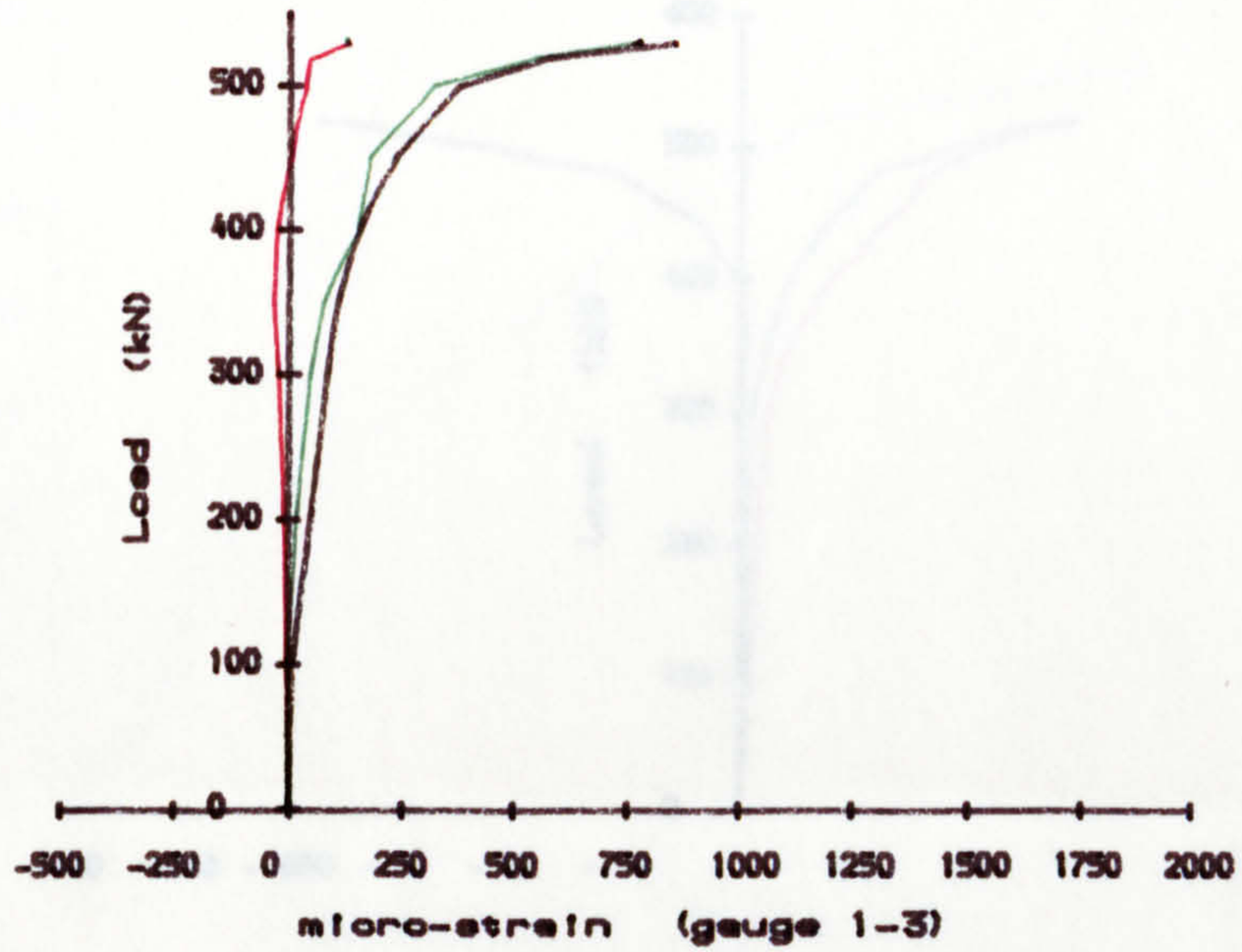

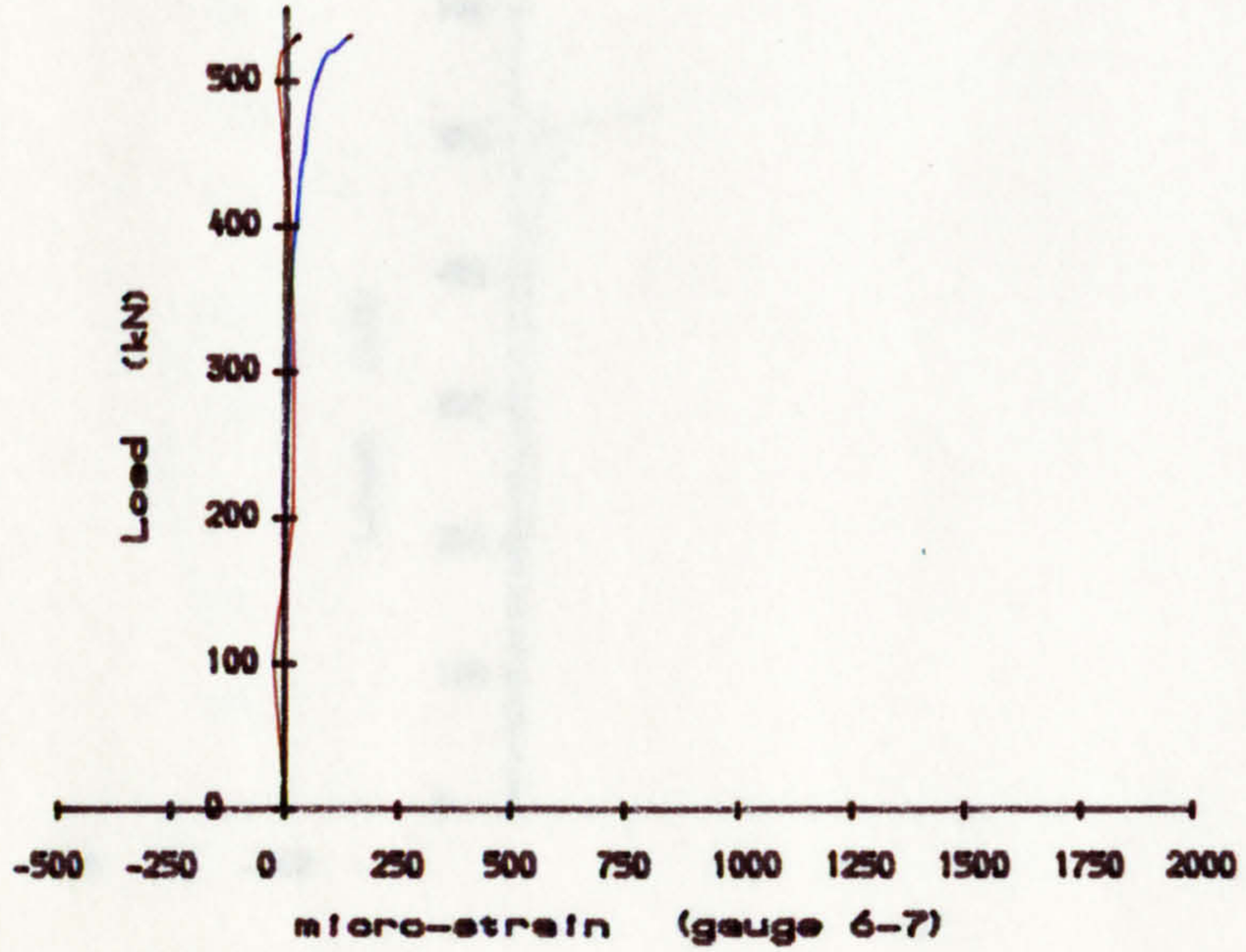

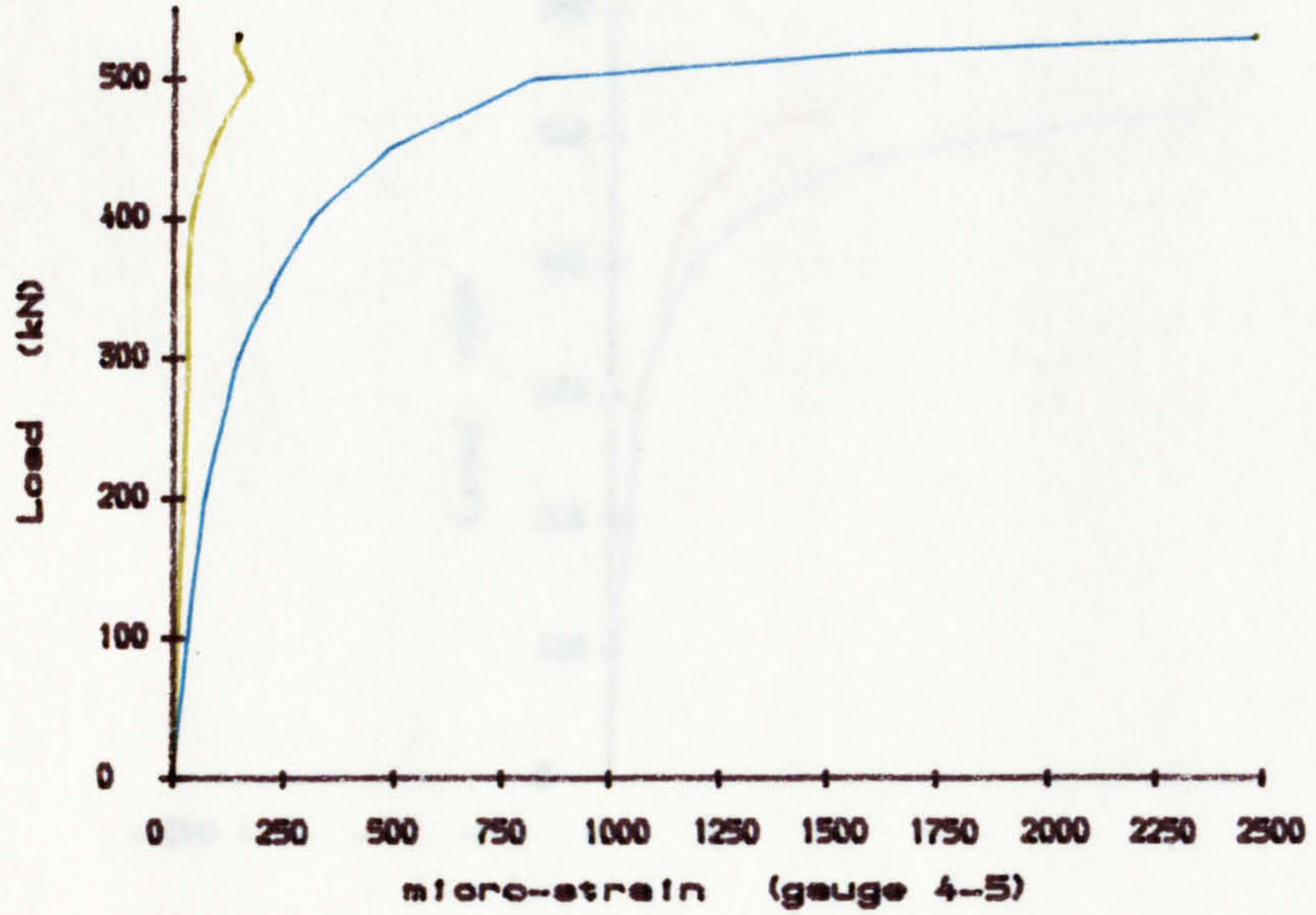

Fig. A. 45. Strain of steel in block R6/1.

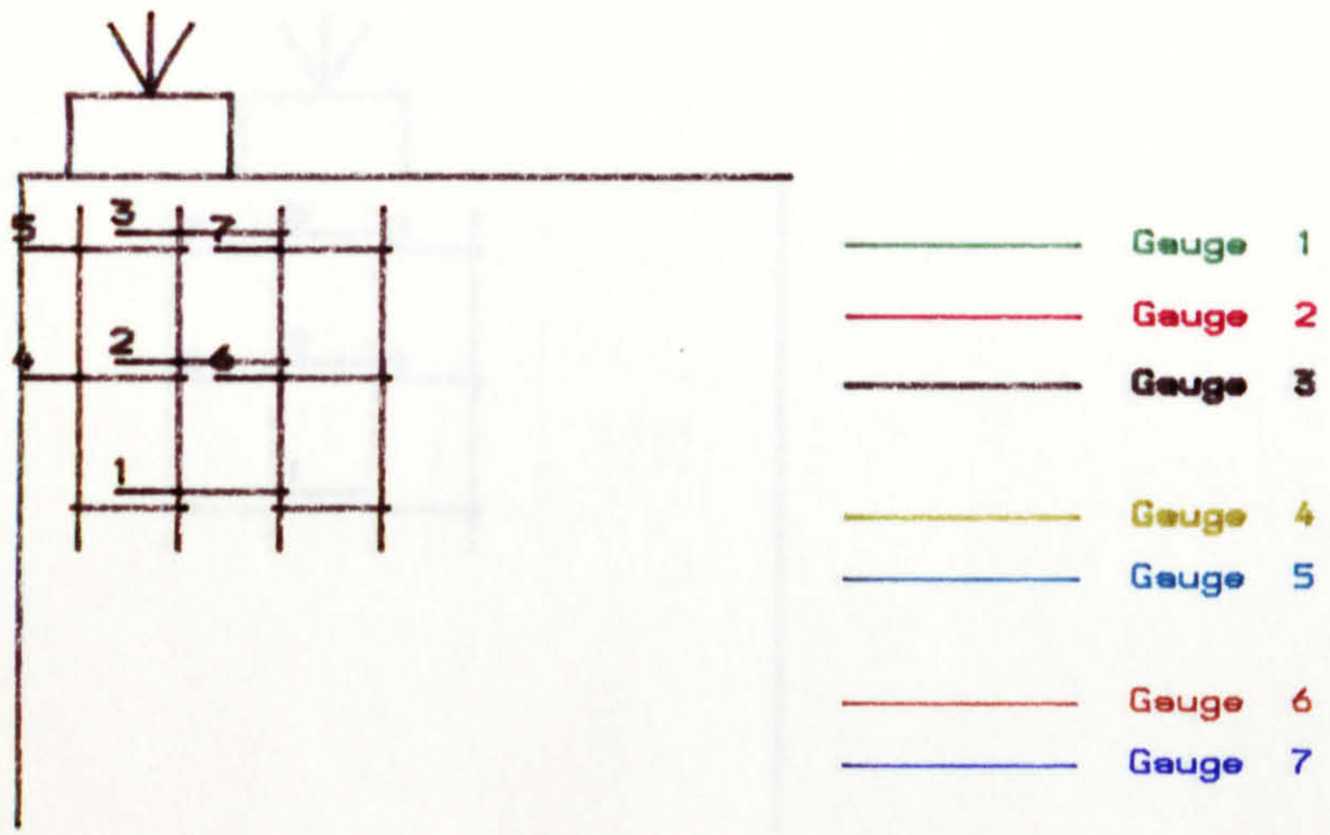

Gauge 1
Gauge 2
Gauge 3
Gauge 4
Gauge 5
Gauge 6
Gauge 7

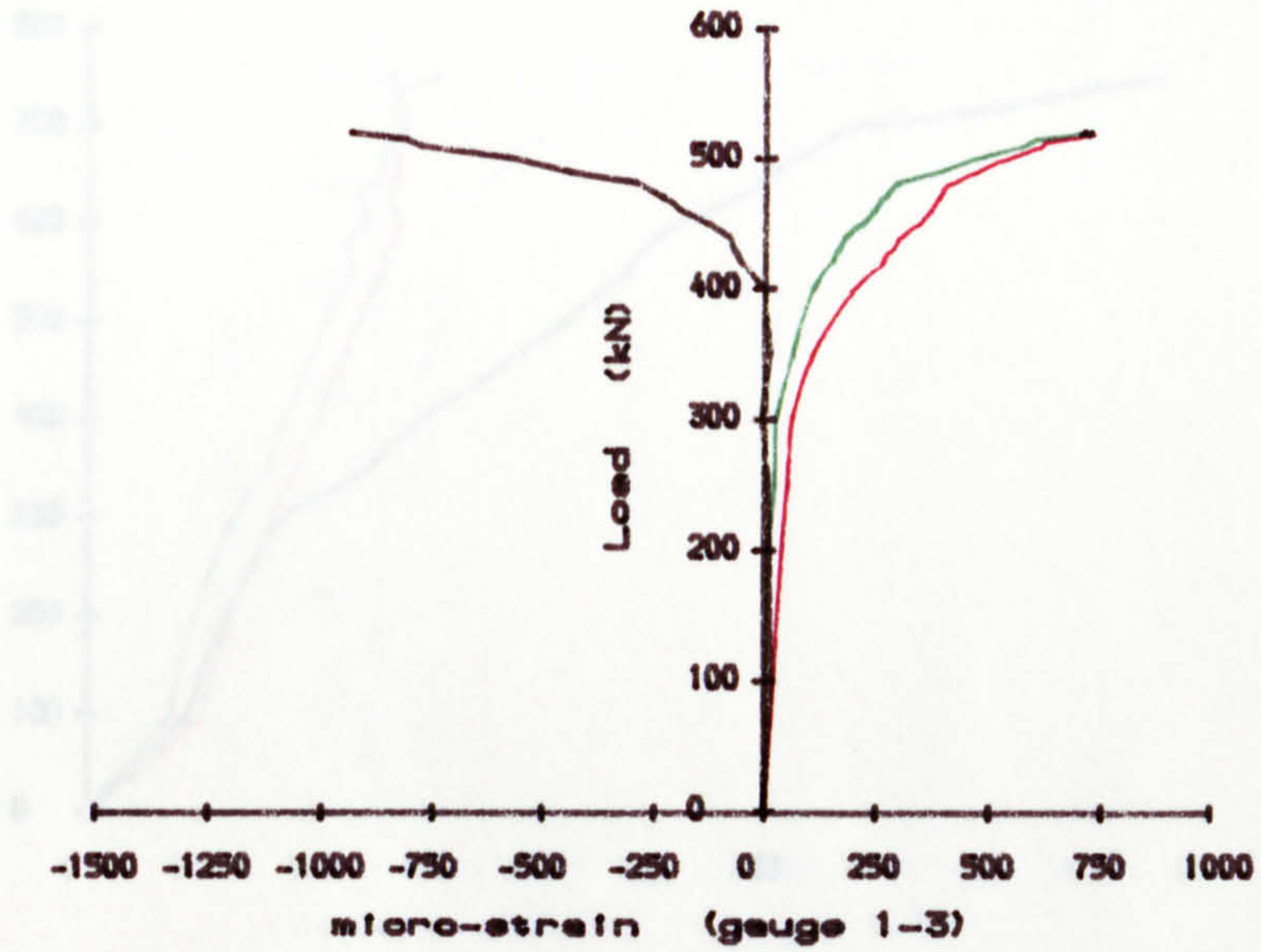

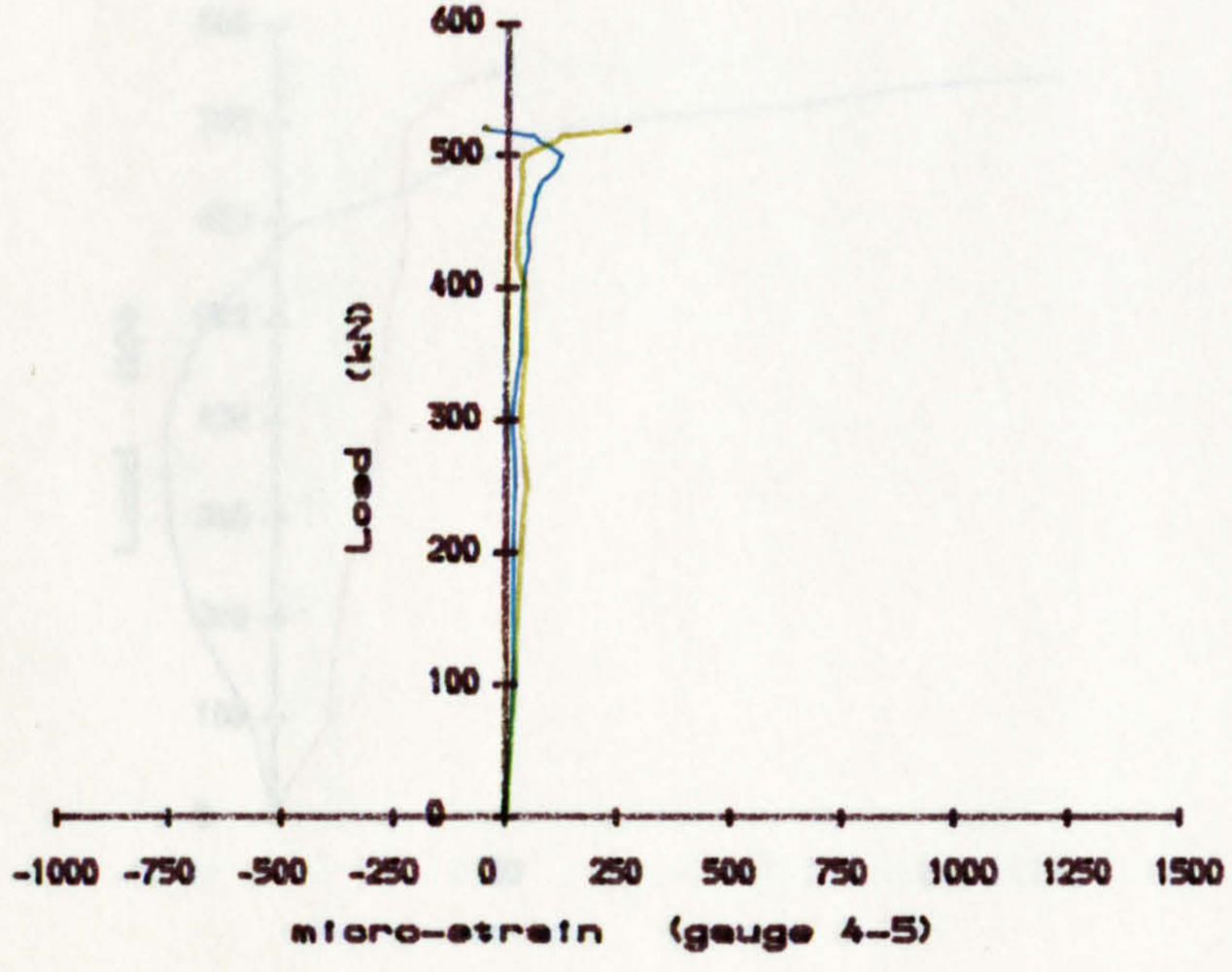

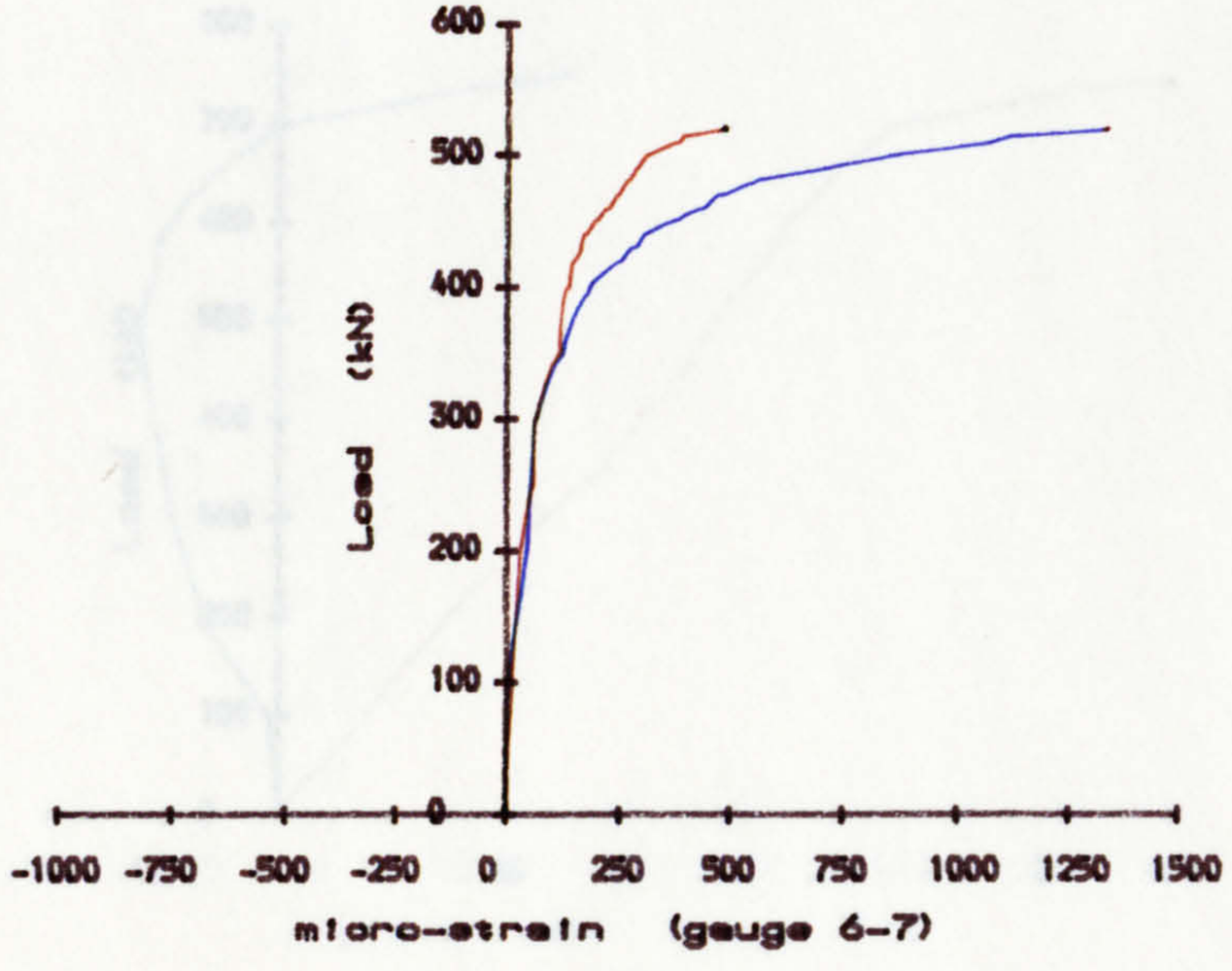

Fig. A. 46. Strain of steel in block R6/2.

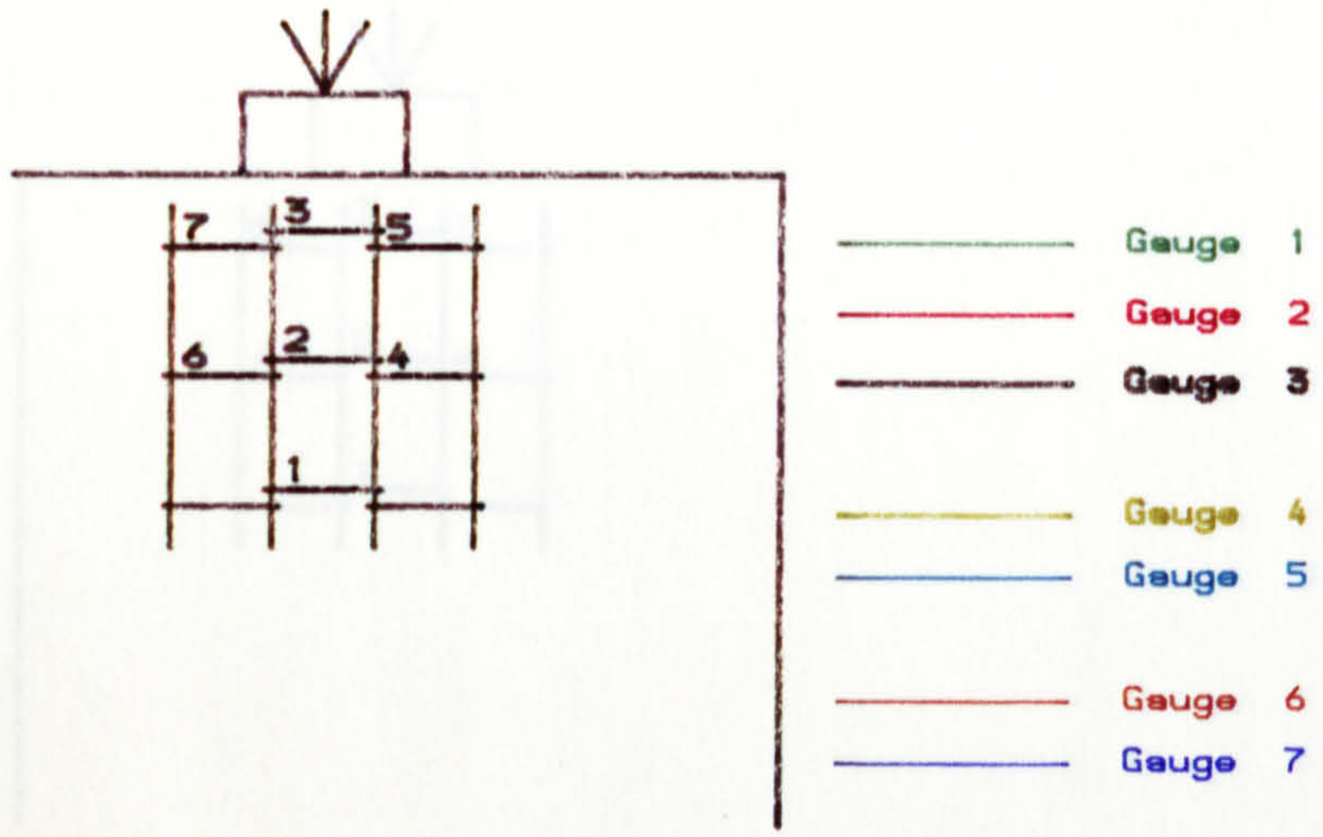

Gauge 1
Gauge 2
Gauge 3
Gauge 4
Gauge 5
Gauge 6
Gauge 7

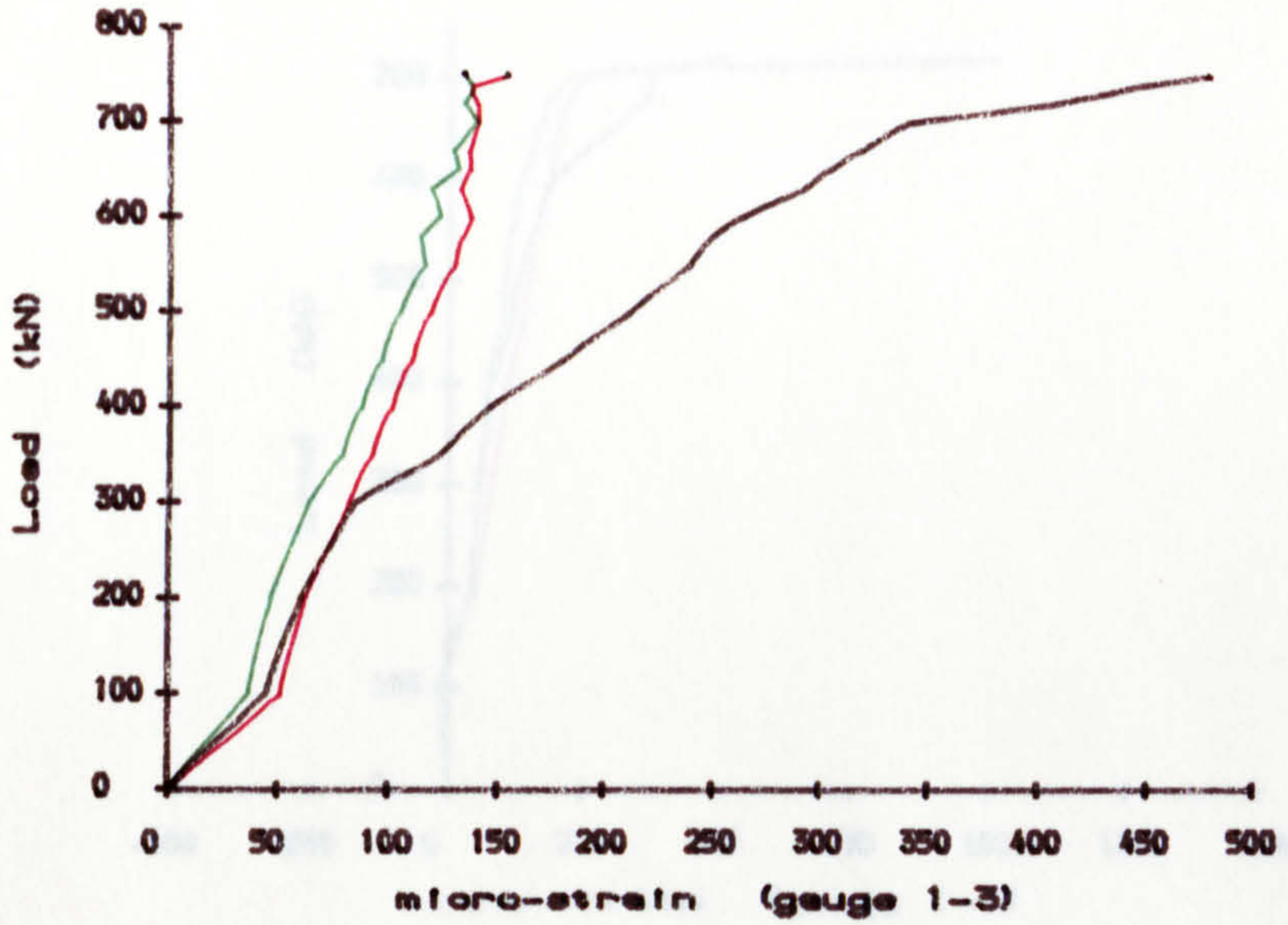

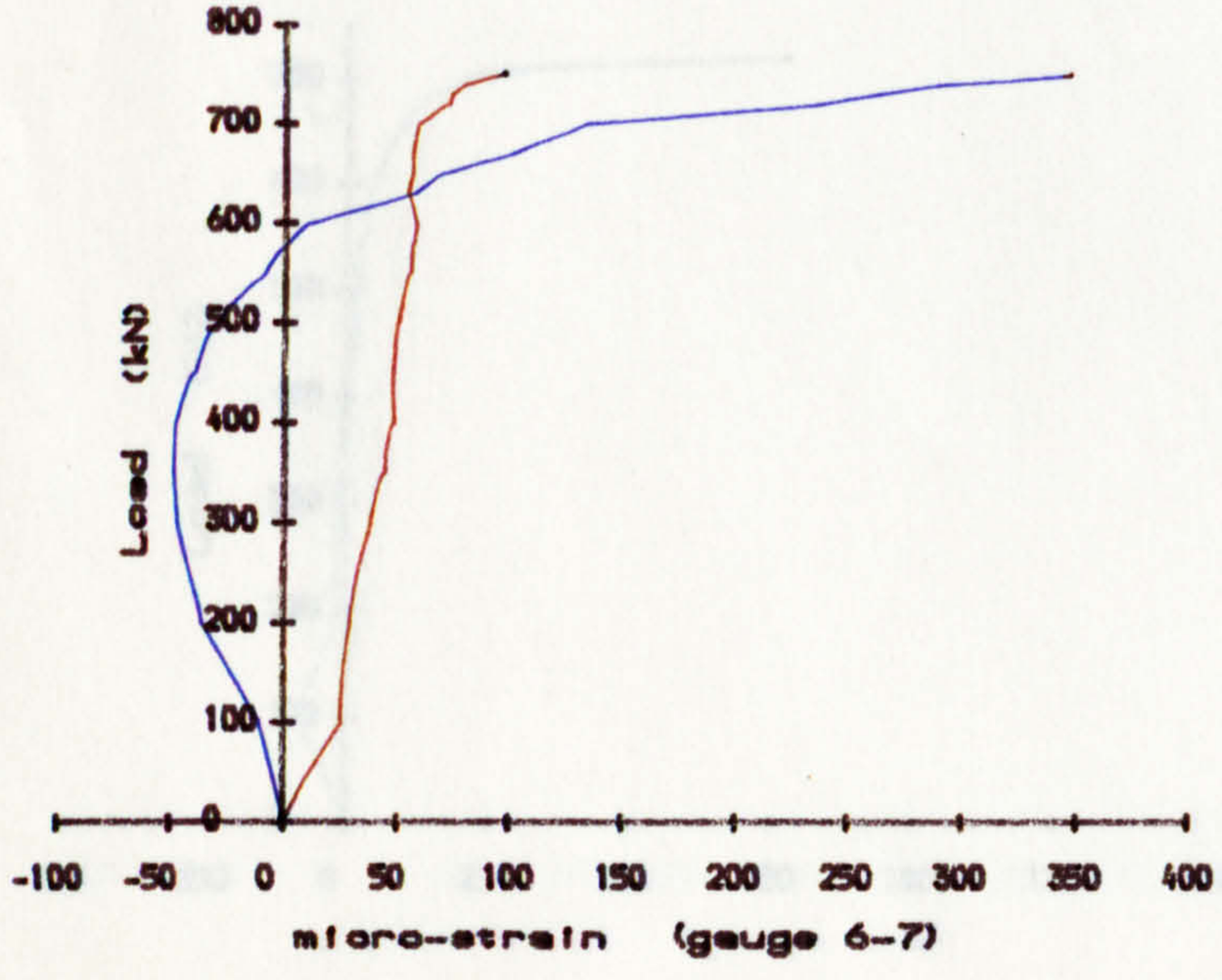

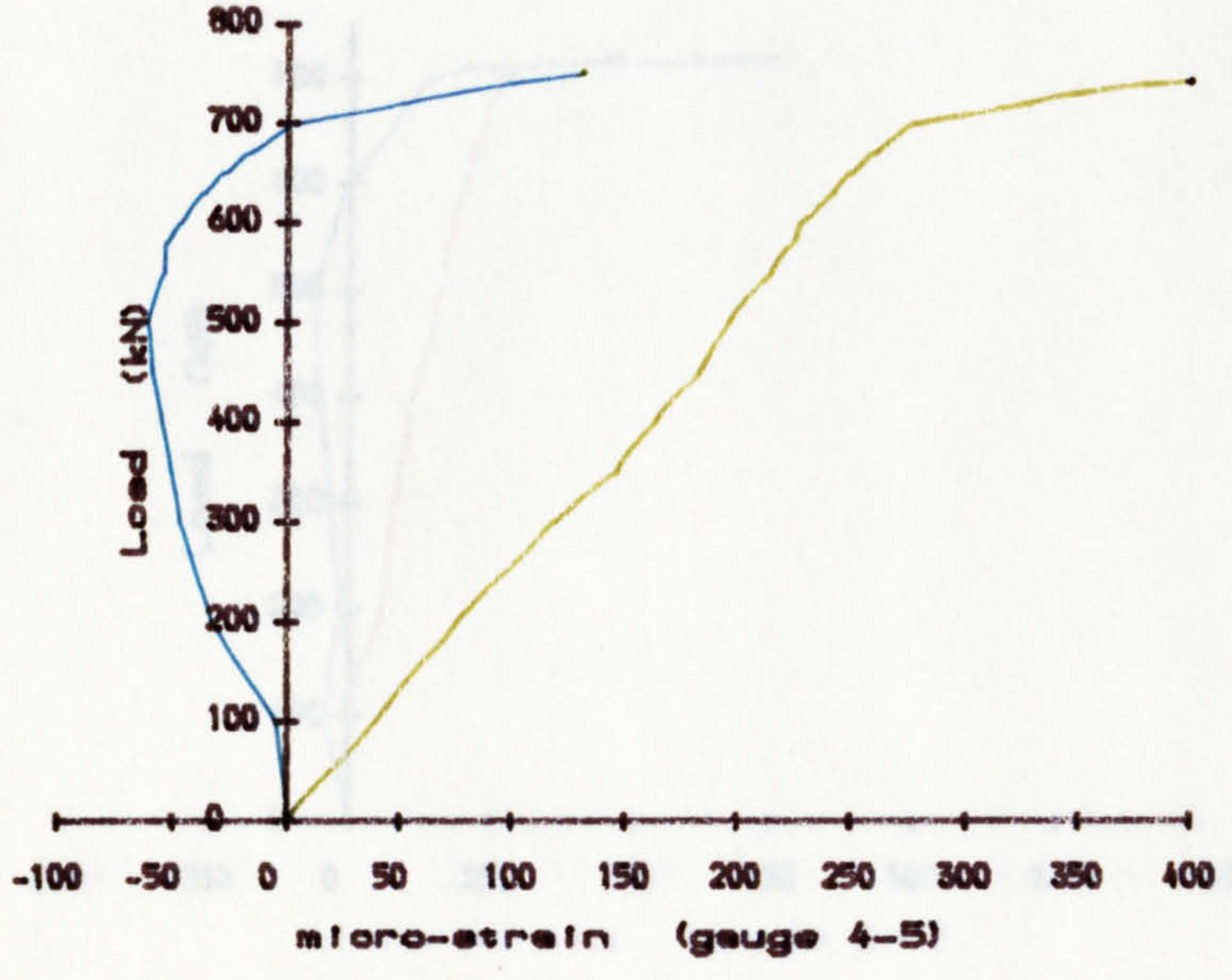

Fig. A. 47. Strain of steel in block R7/1.

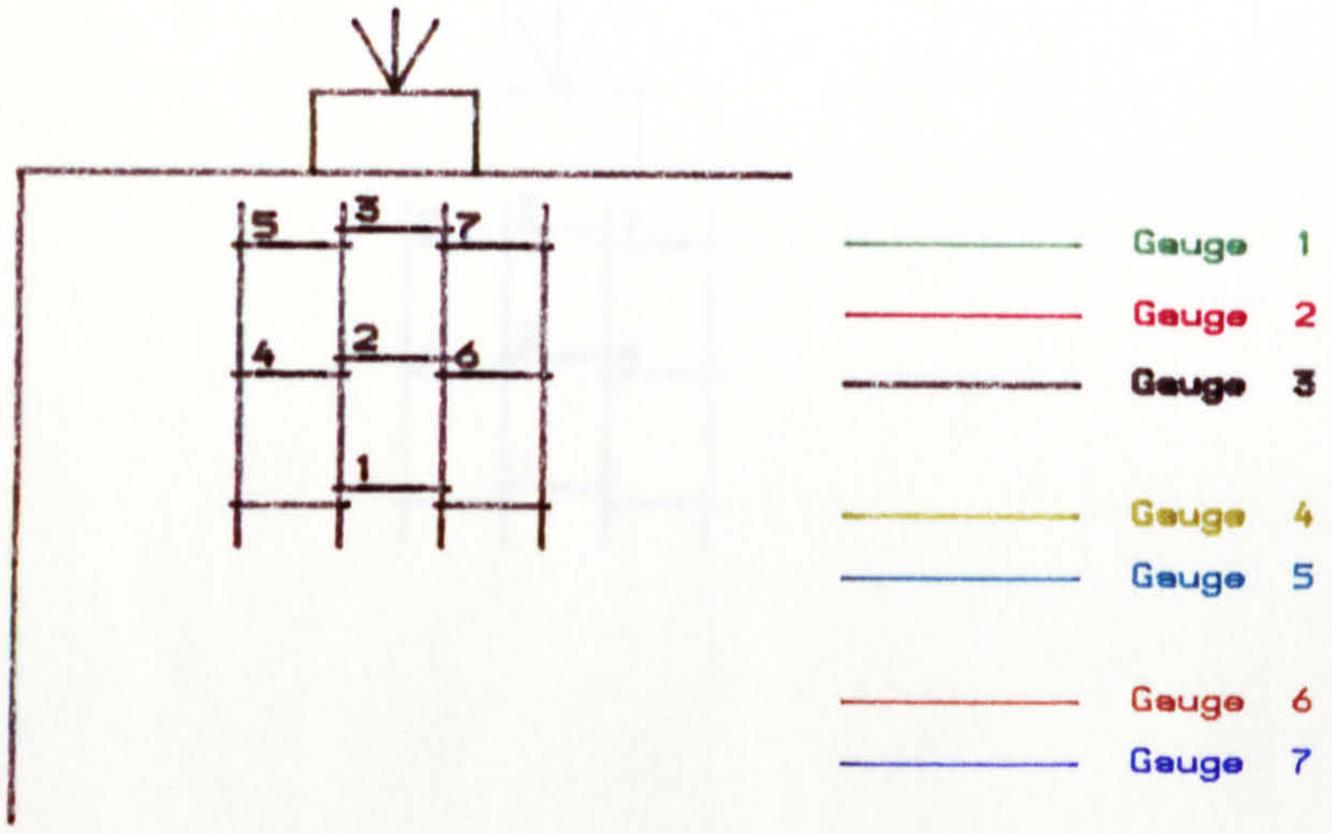

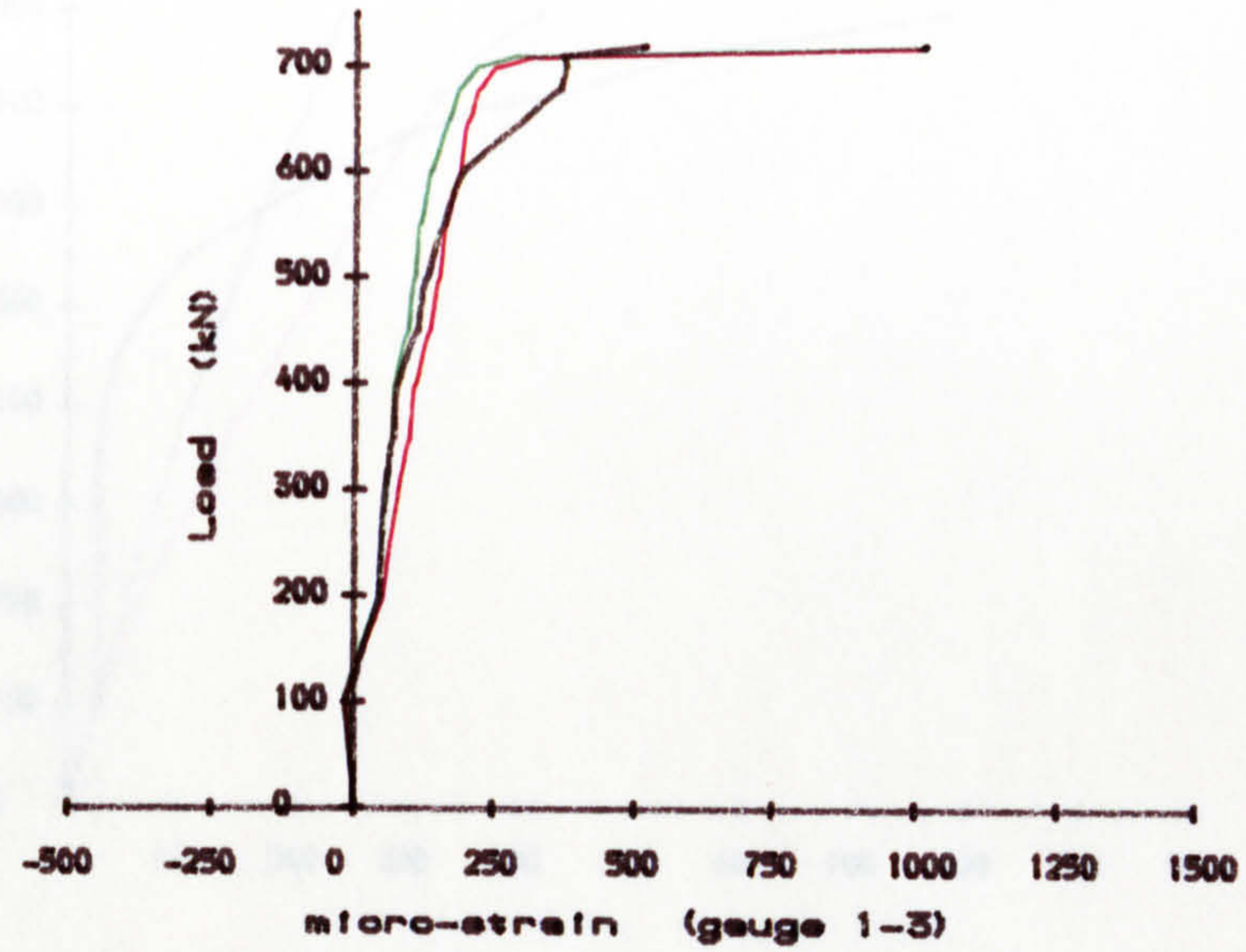

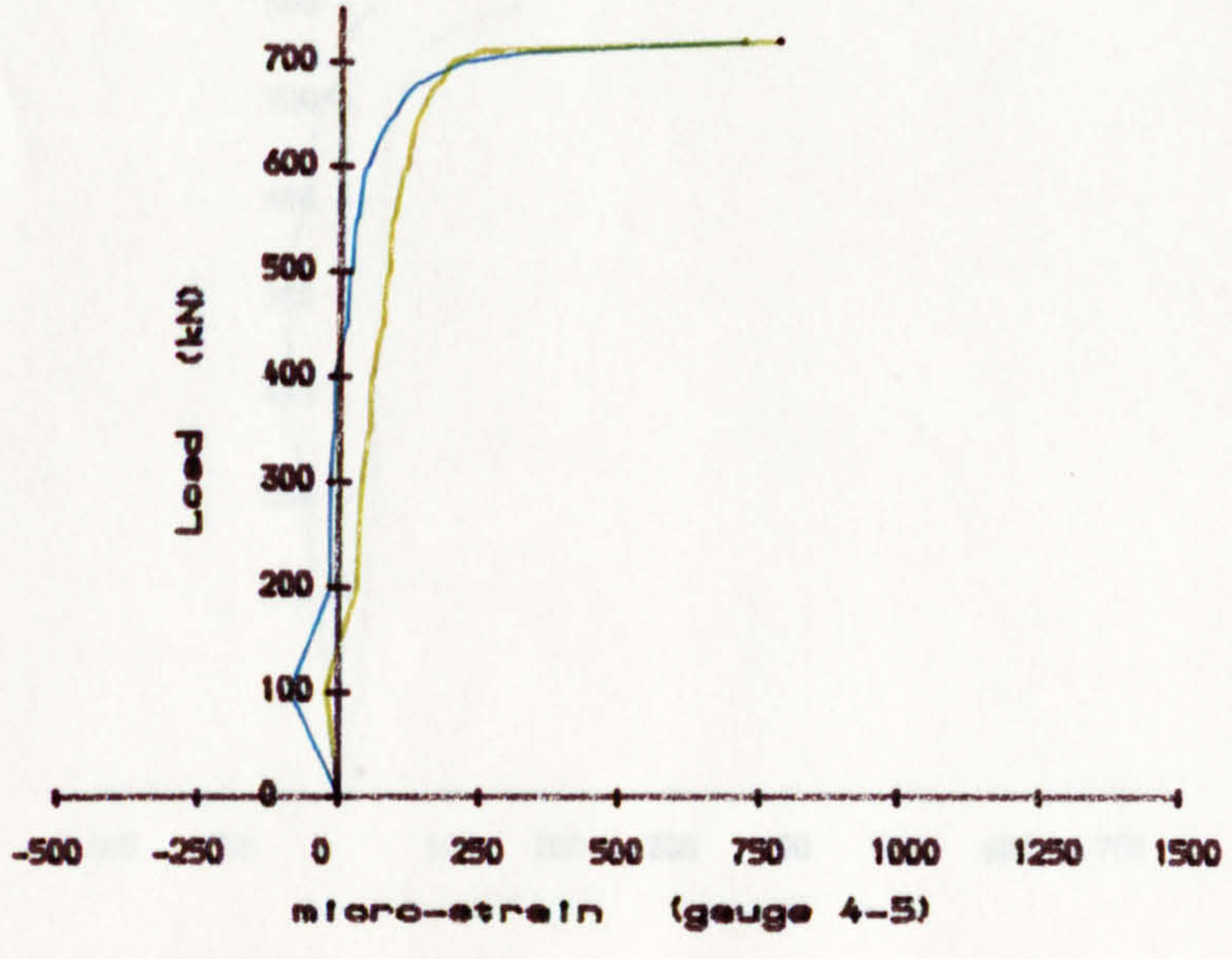

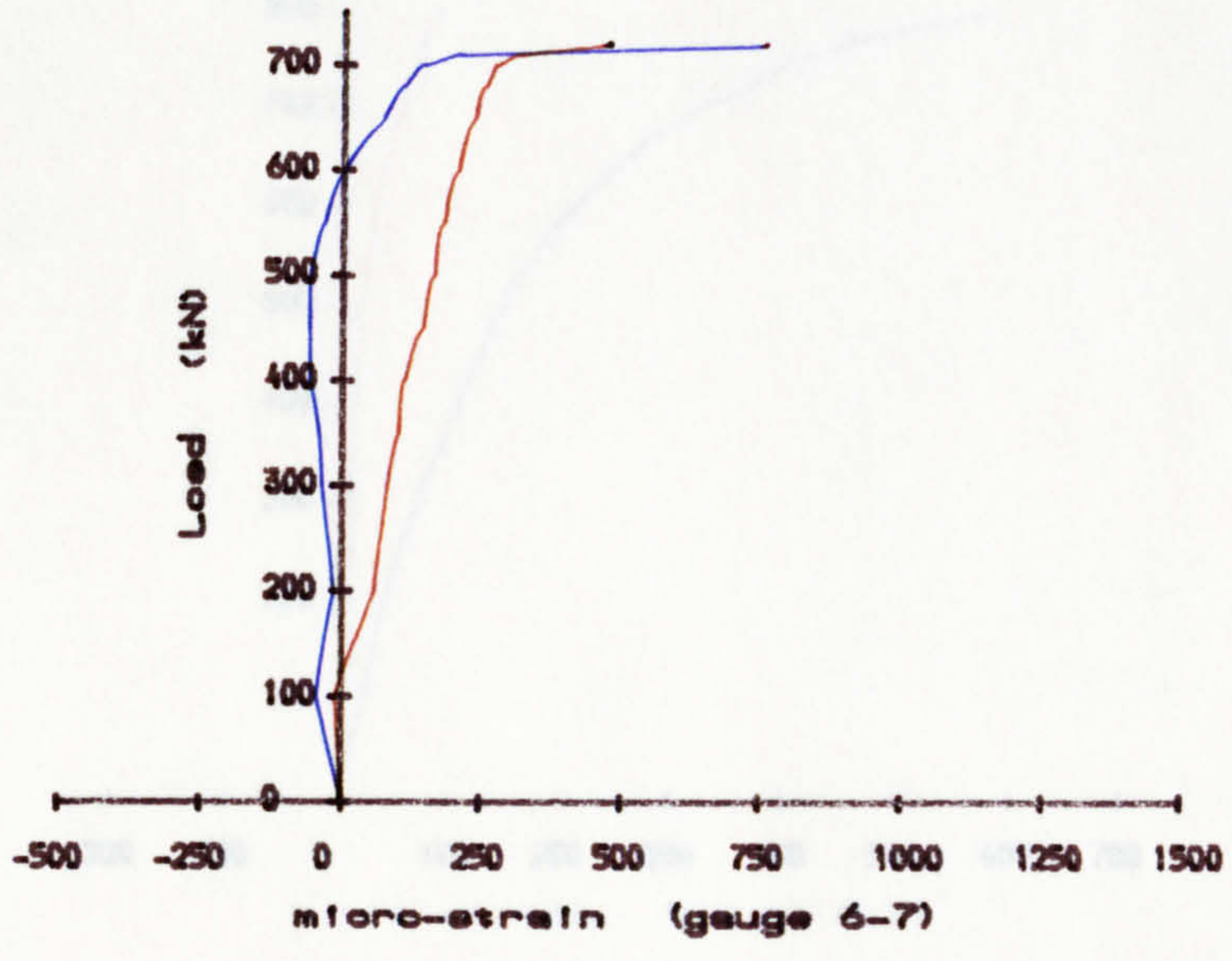

Fig. A. 48. Strain of steel in block R7/2.

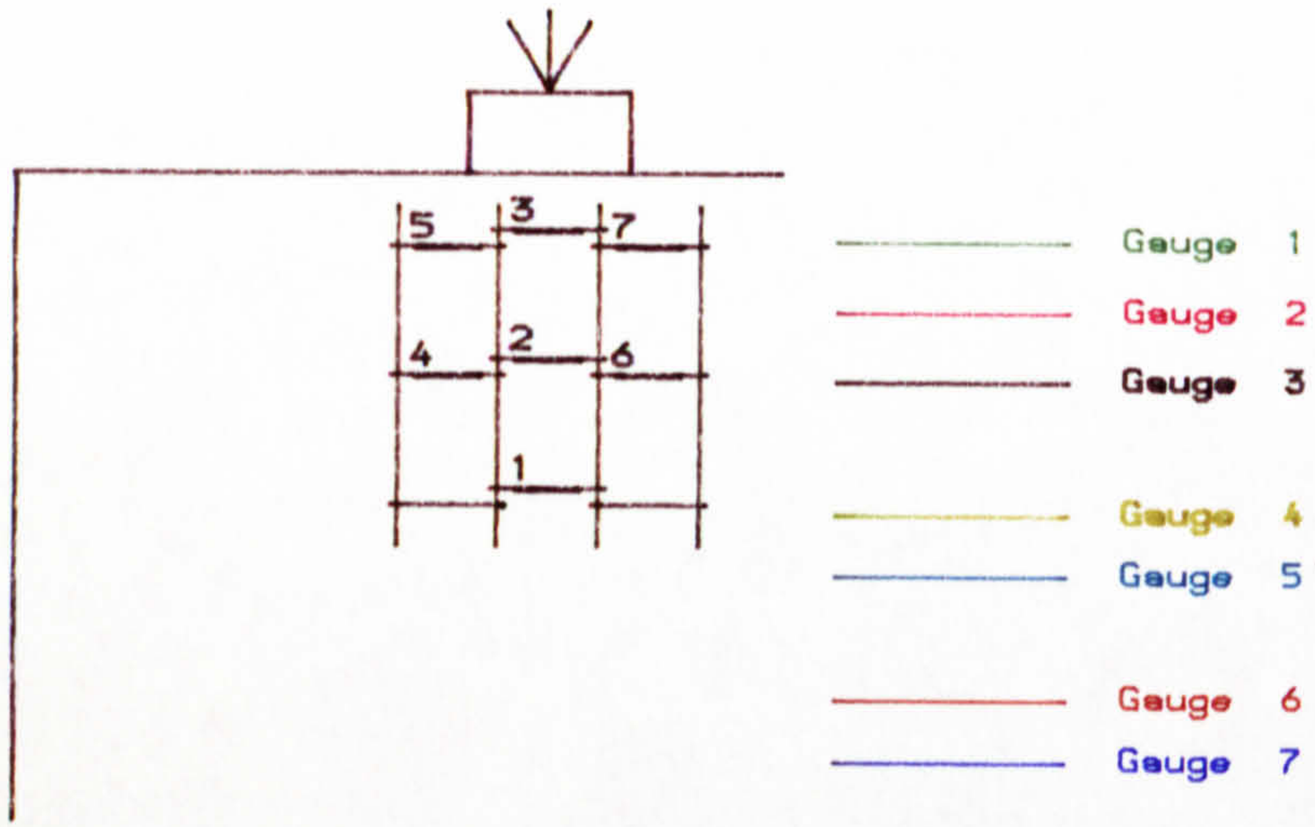

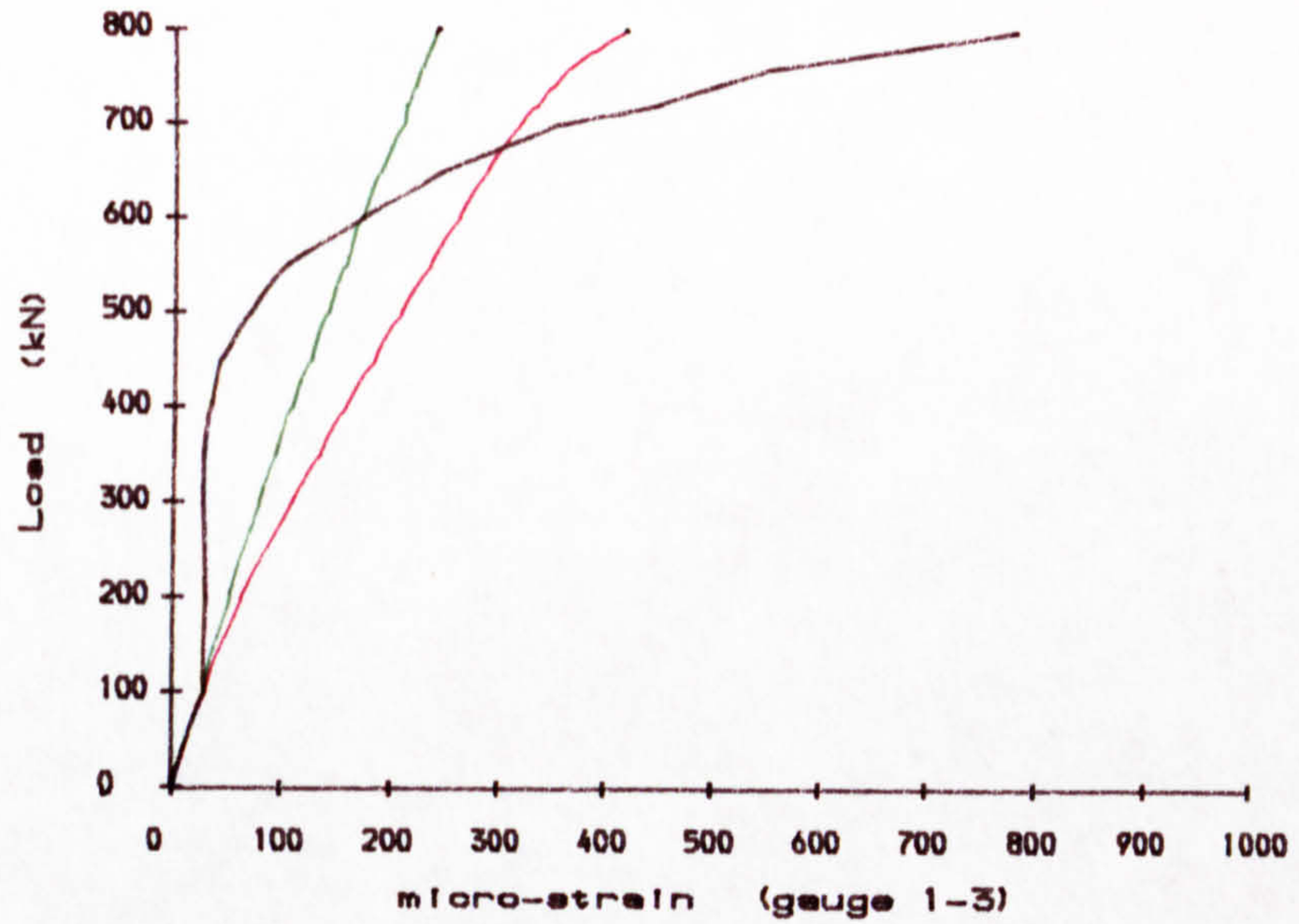

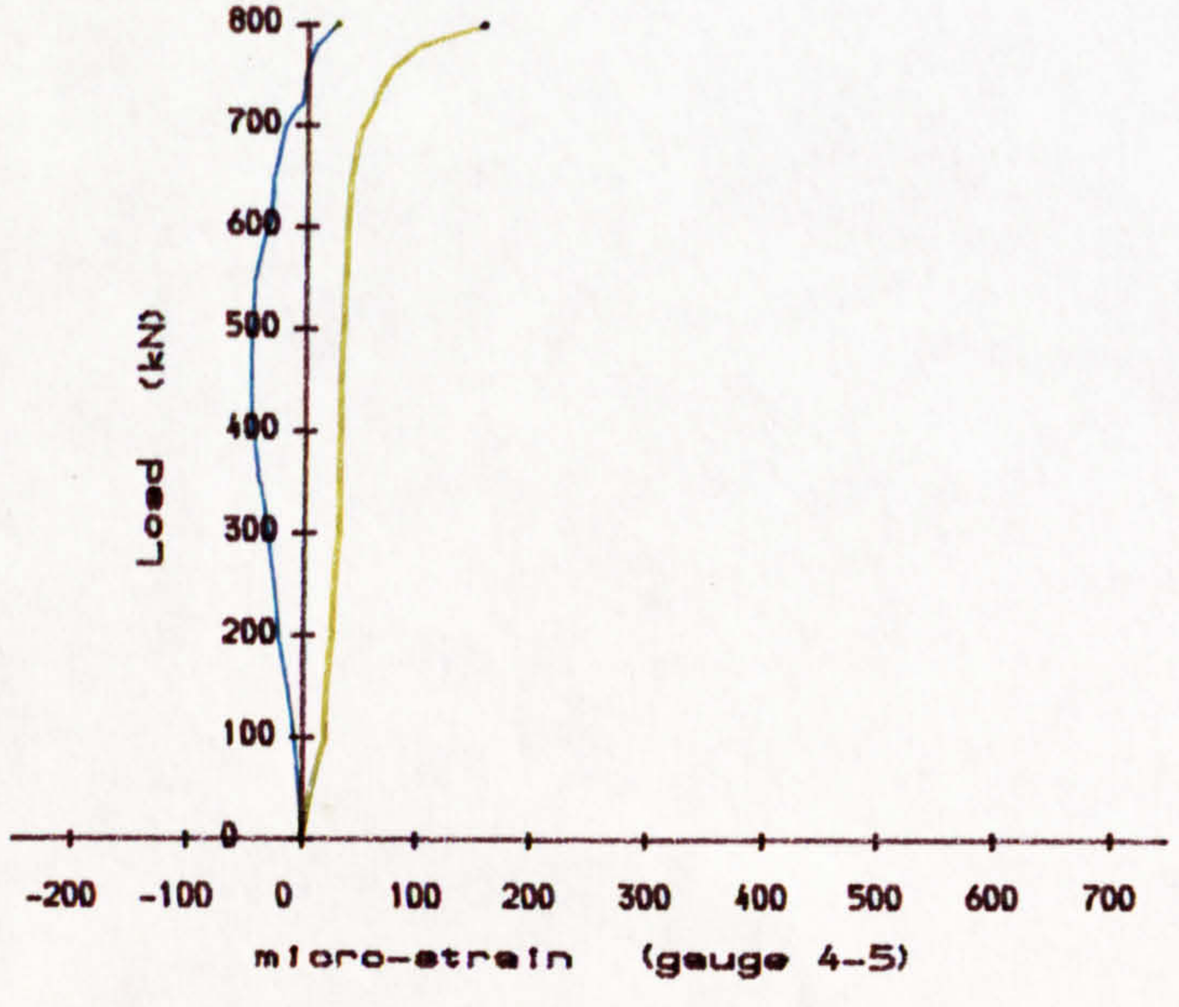

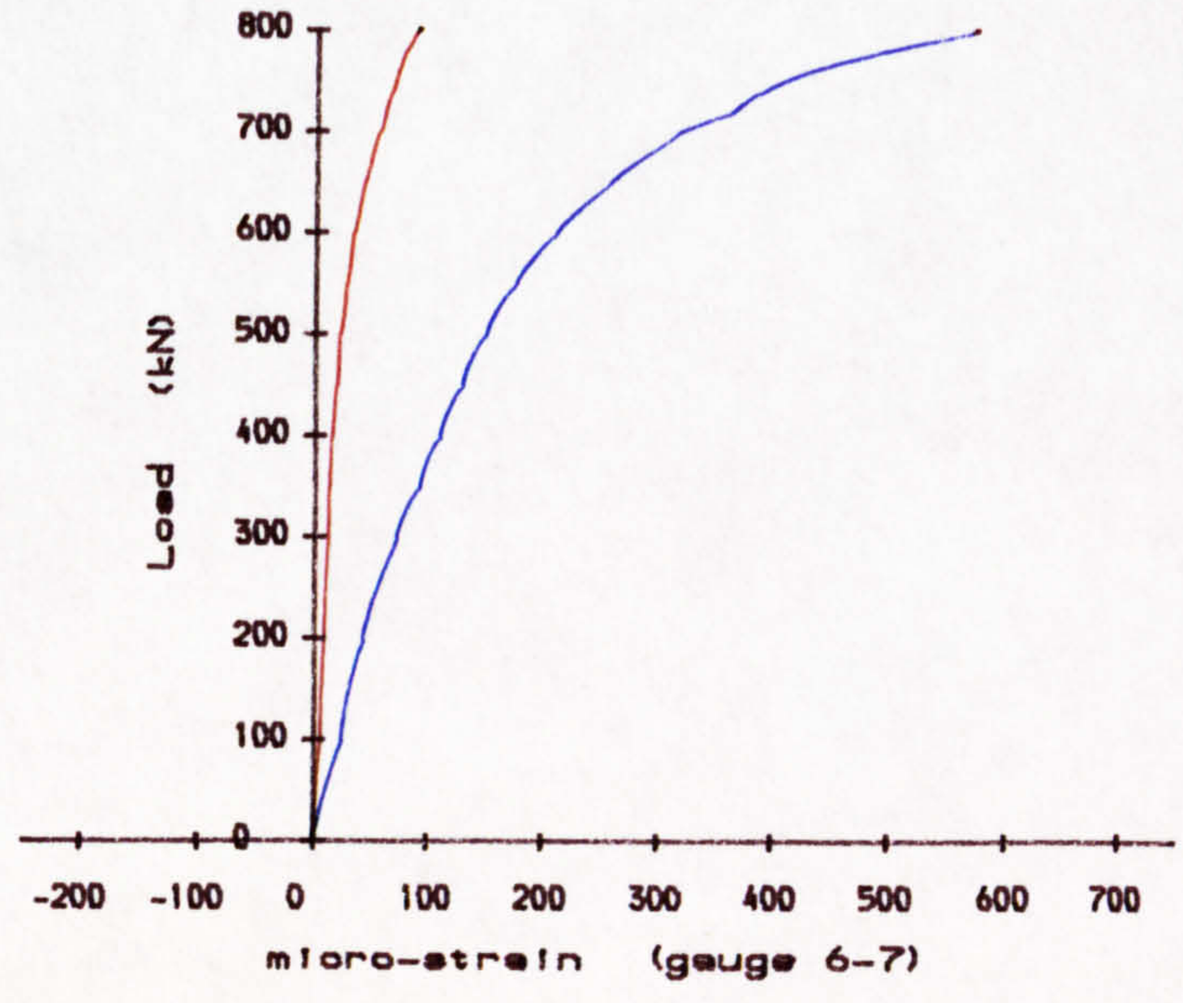

Fig. A. 49. Strain of steel in block R8/2.

APPENDIX B

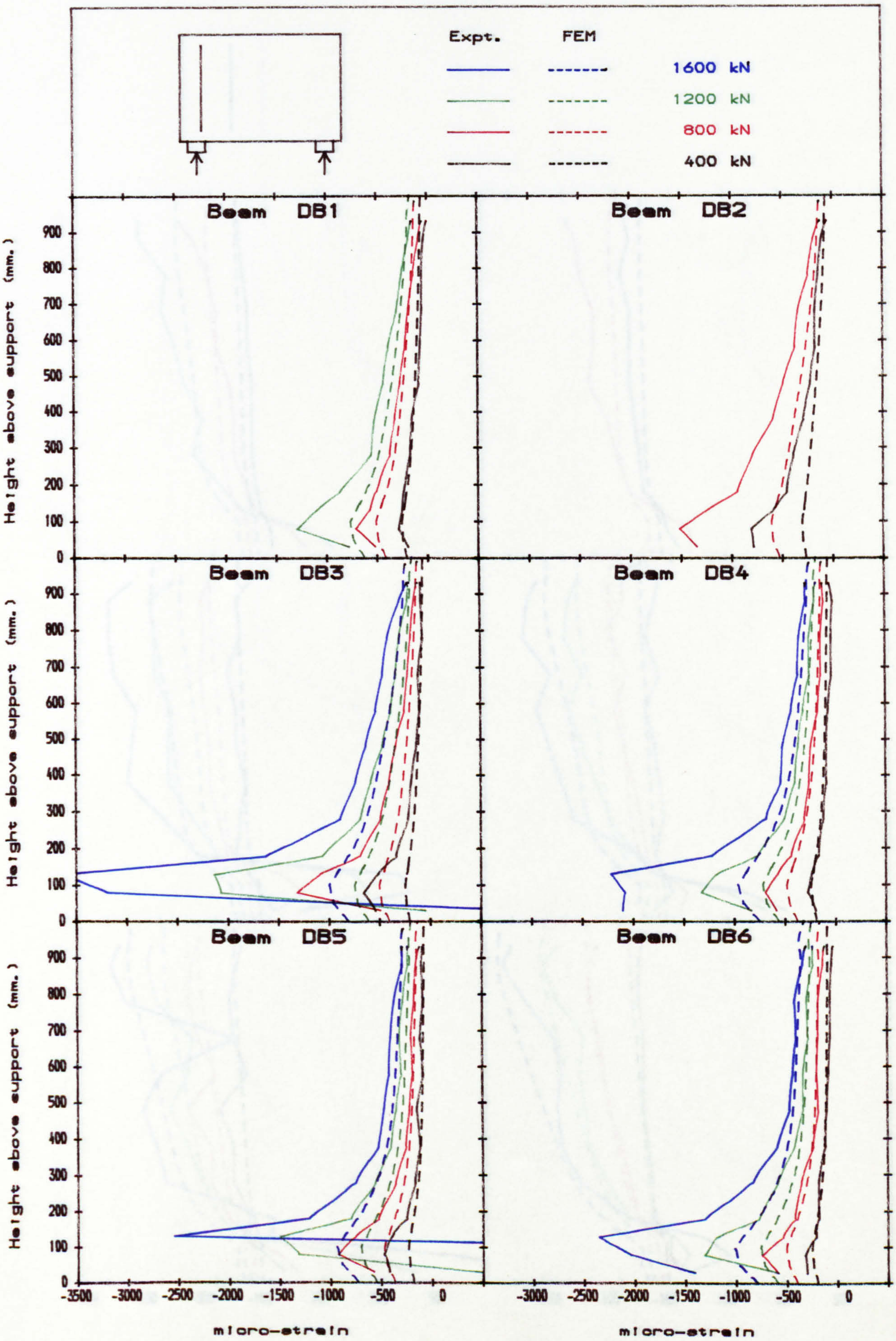

Fig. B. 1. Vertical strain in section 1.

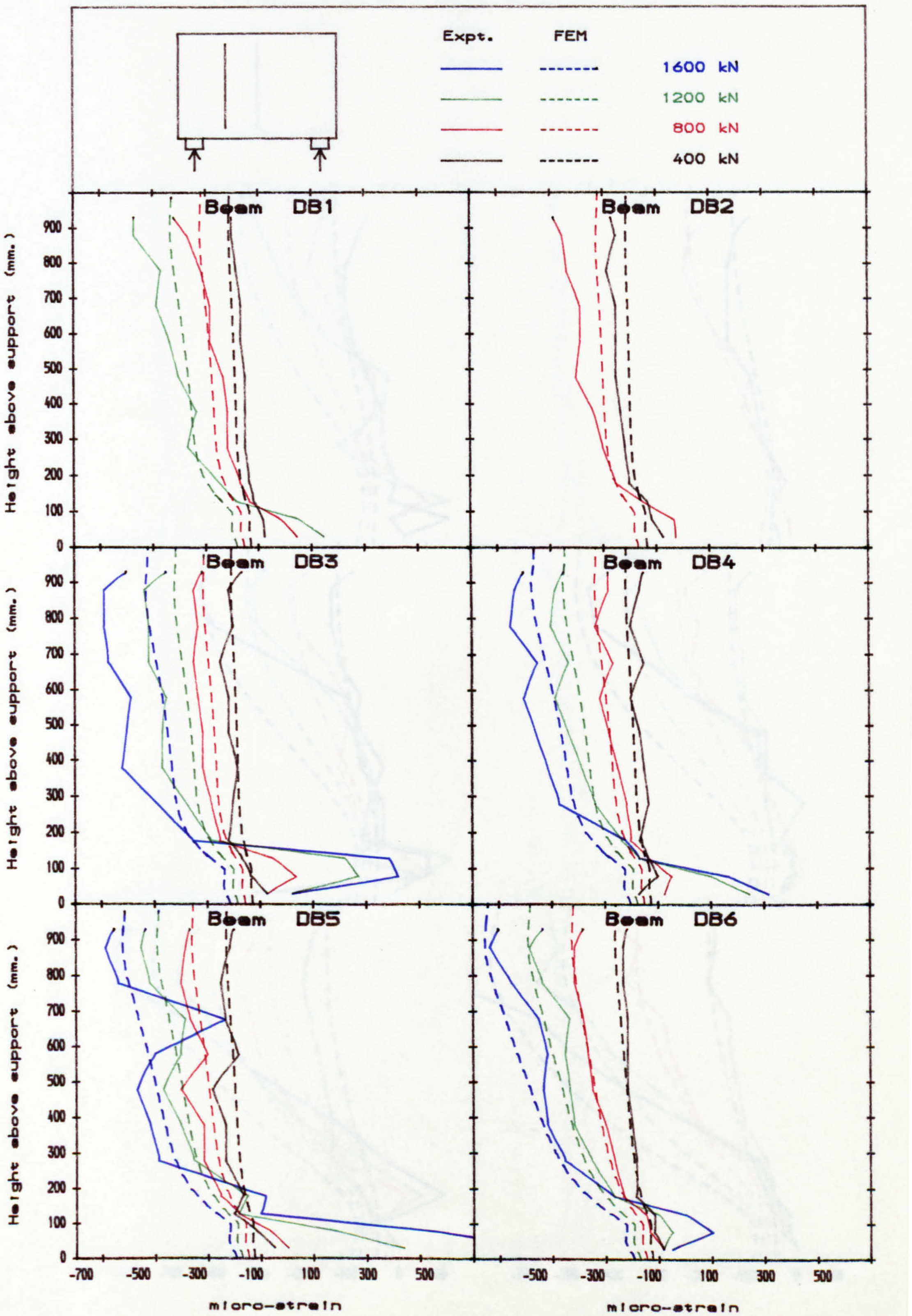

Fig. B. 2. Vertical strain in section 2.

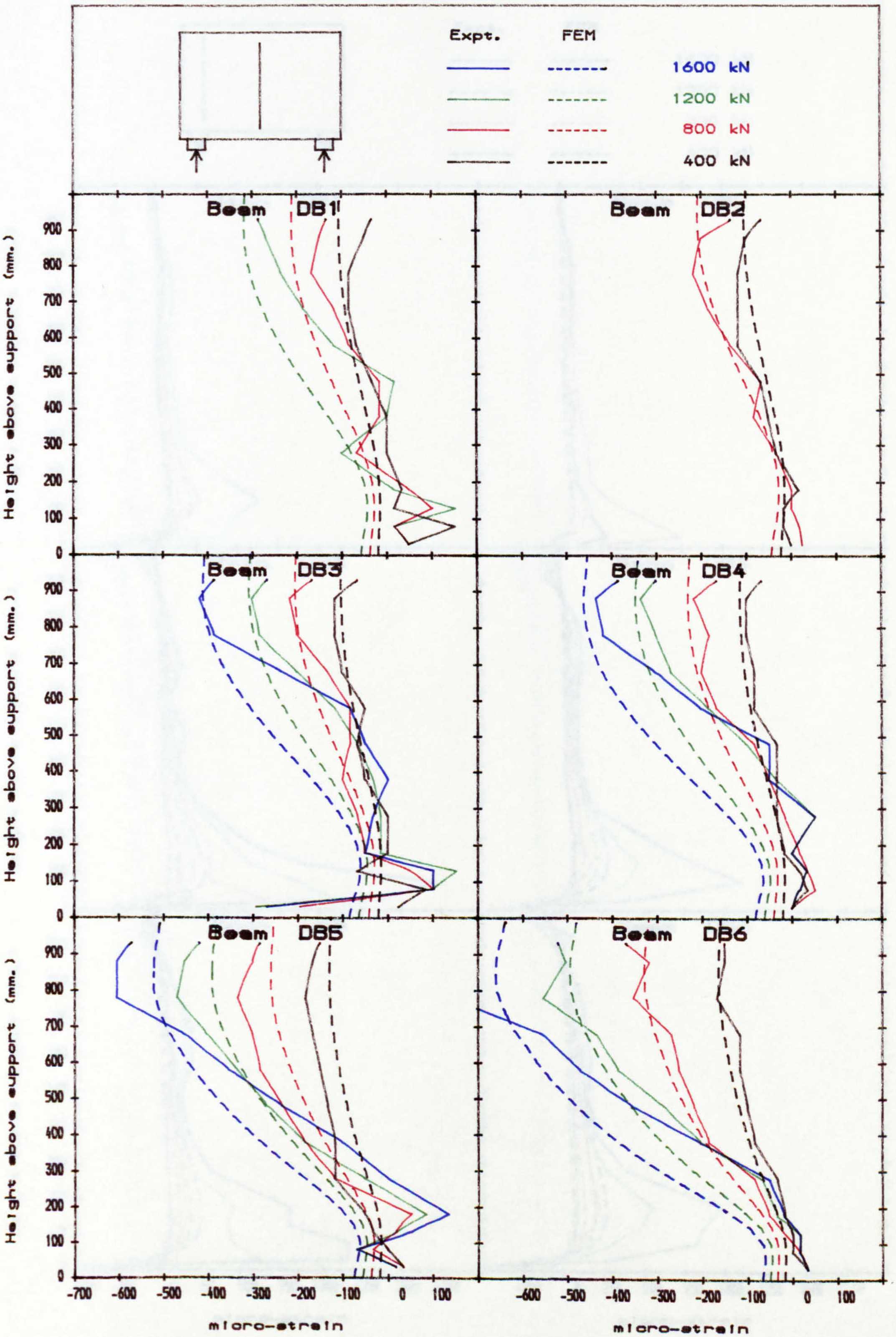

Fig. B. 3. Vertical strain in section 3.

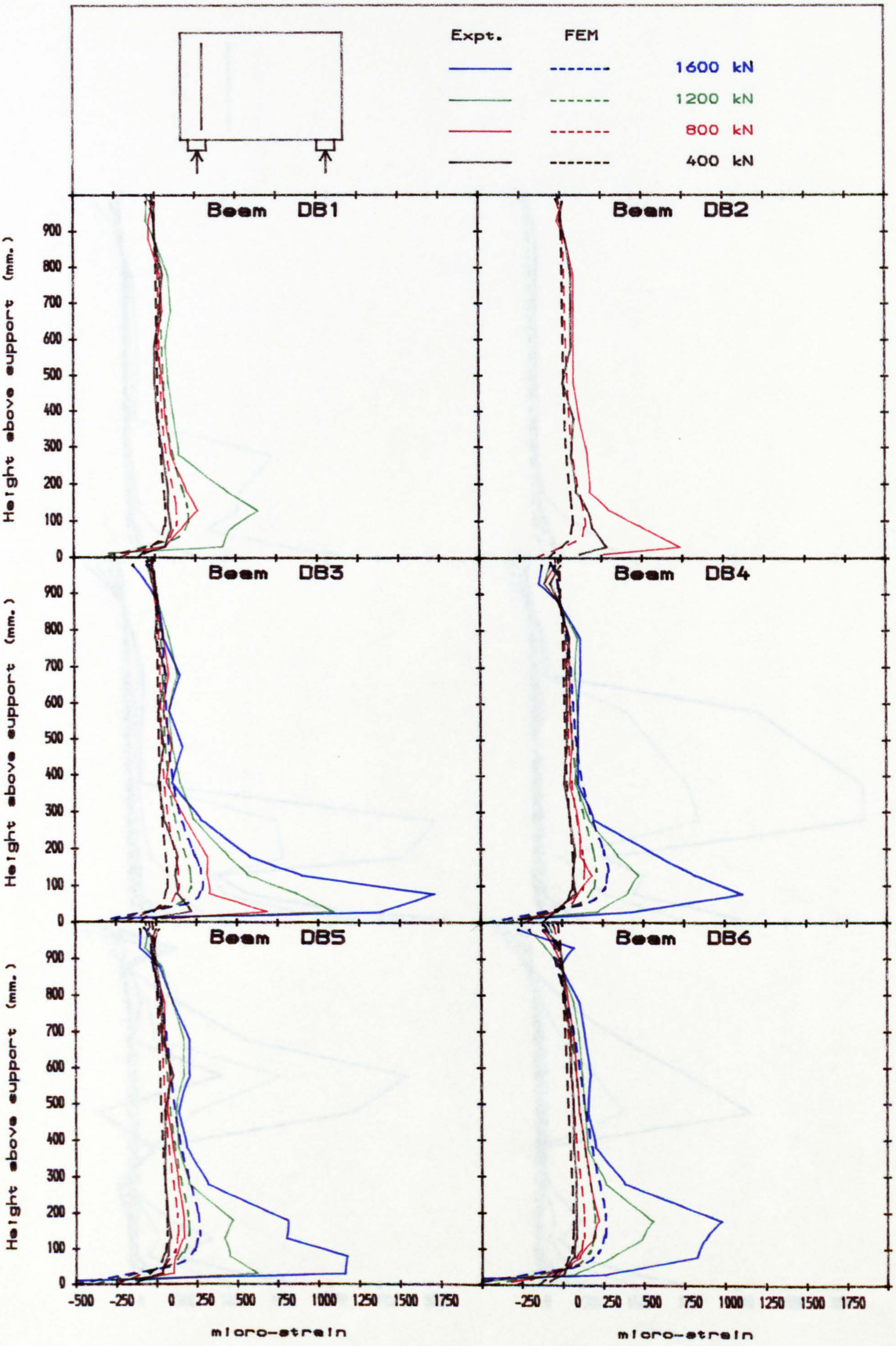

Fig. B. 4. Horizontal strain in section 1.

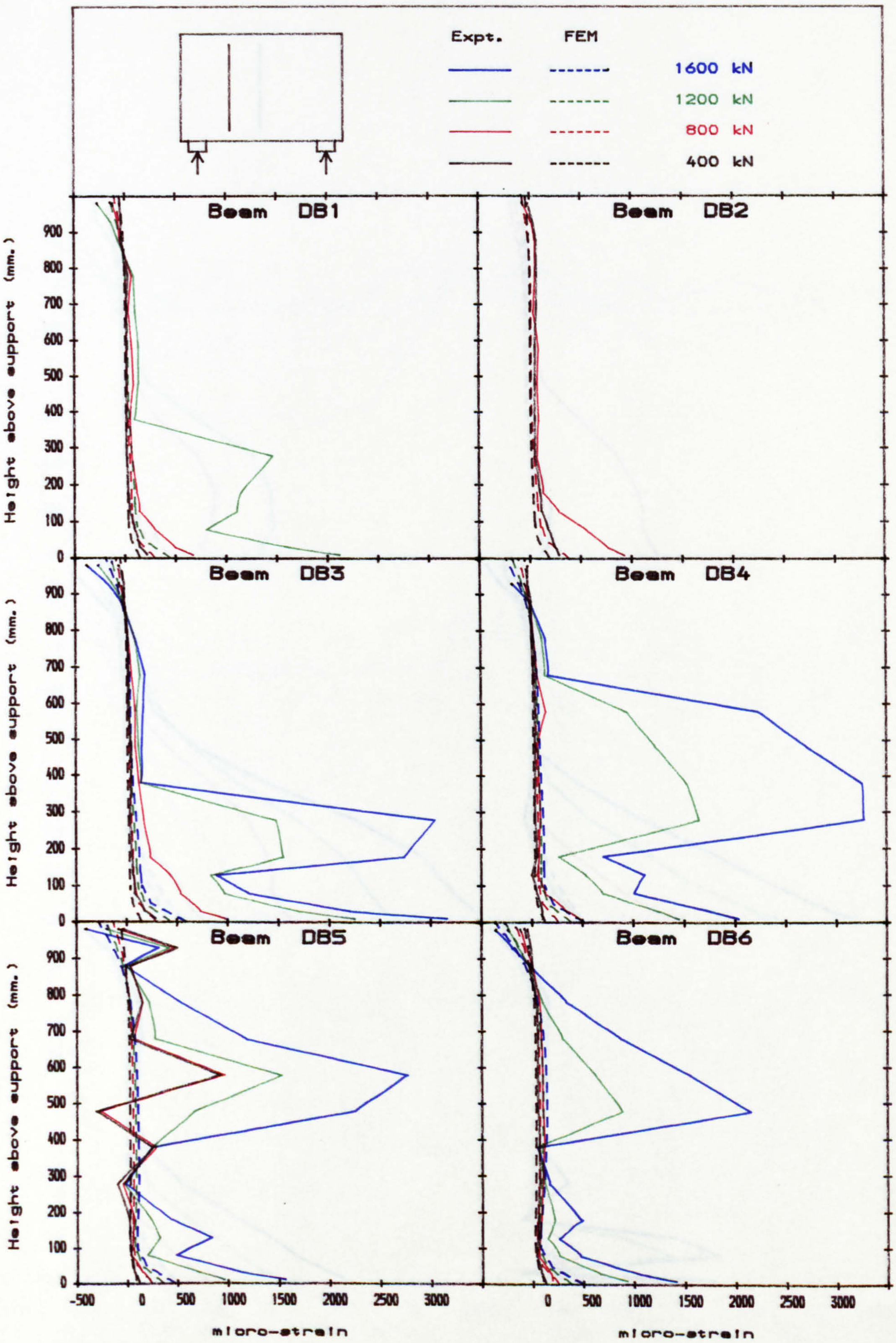

Fig. B. 5. Horizontal strain in section 2.

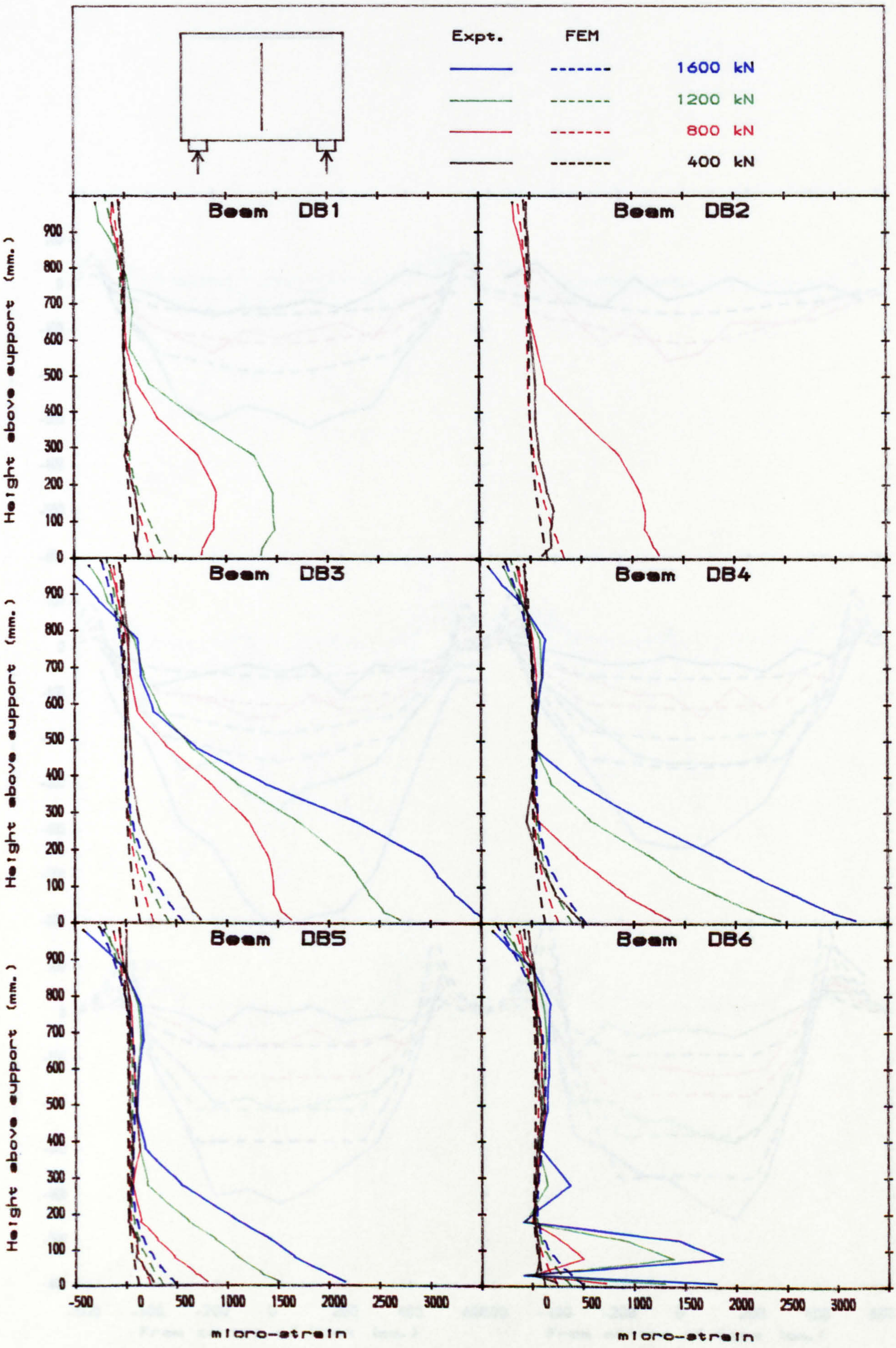

Fig. B. 6. Horizontal strain in section 3.

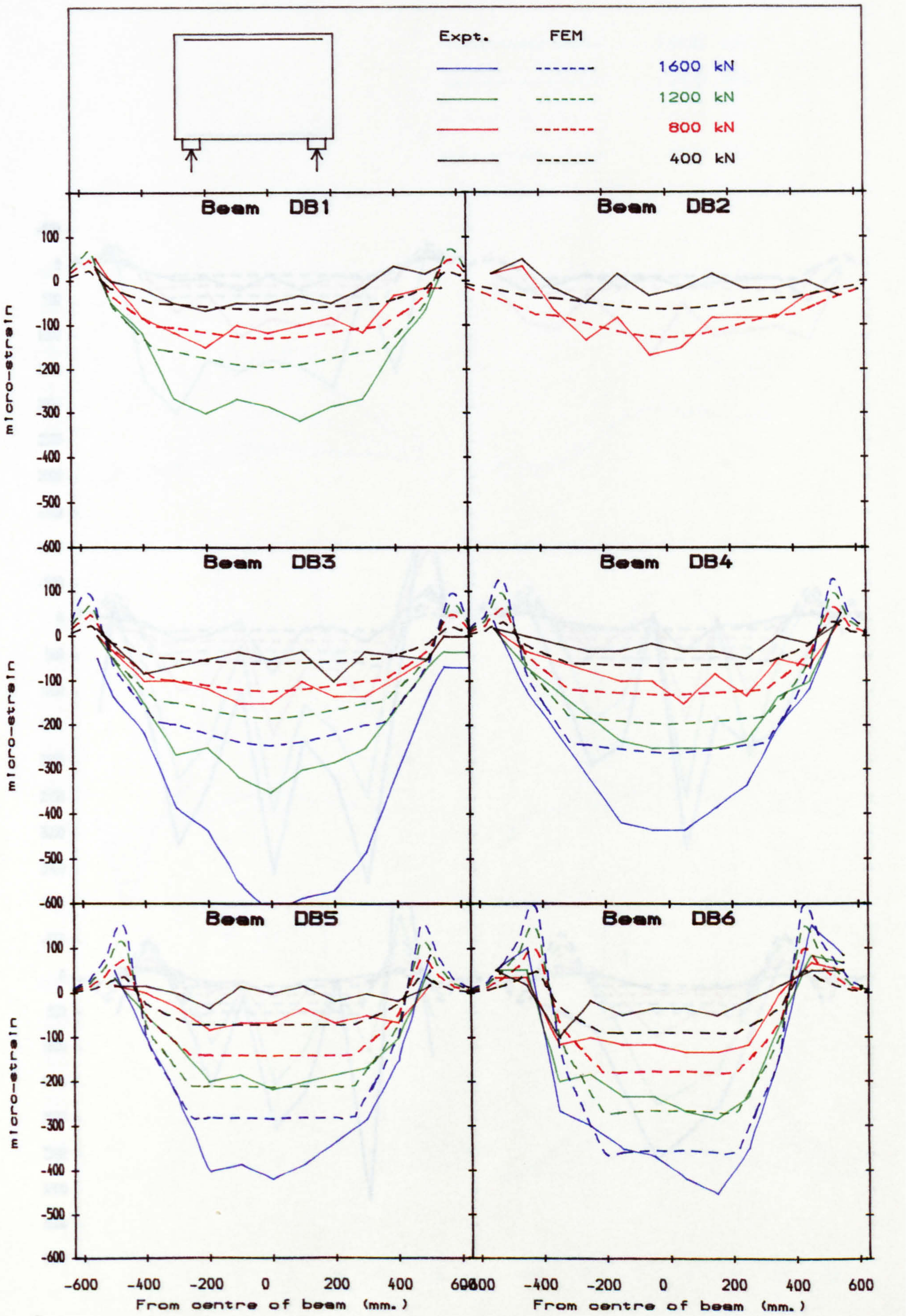

Fig. B. 7. Horizontal strain in section 4.

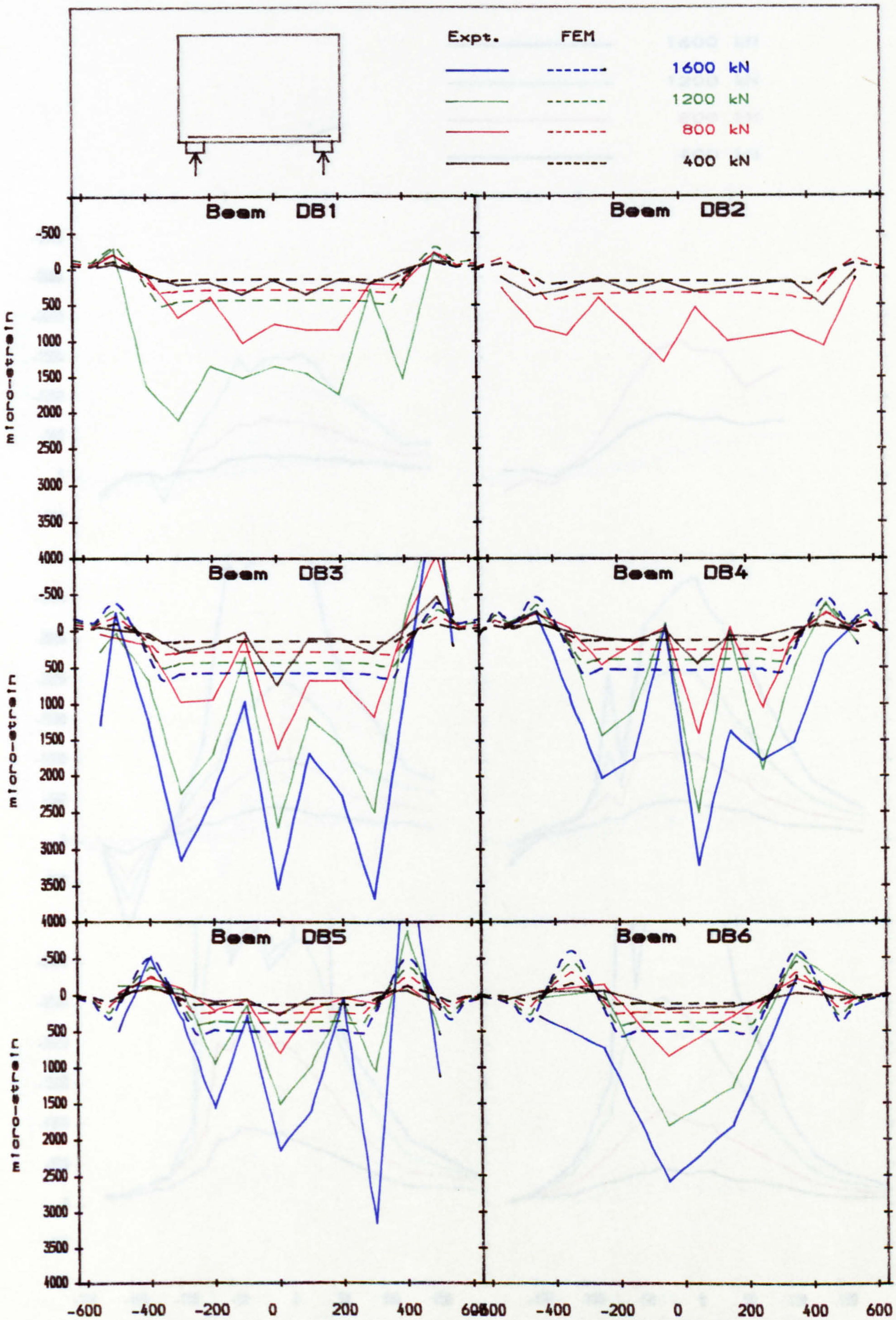

Fig. B. 8. Horizontal strain in section 5.

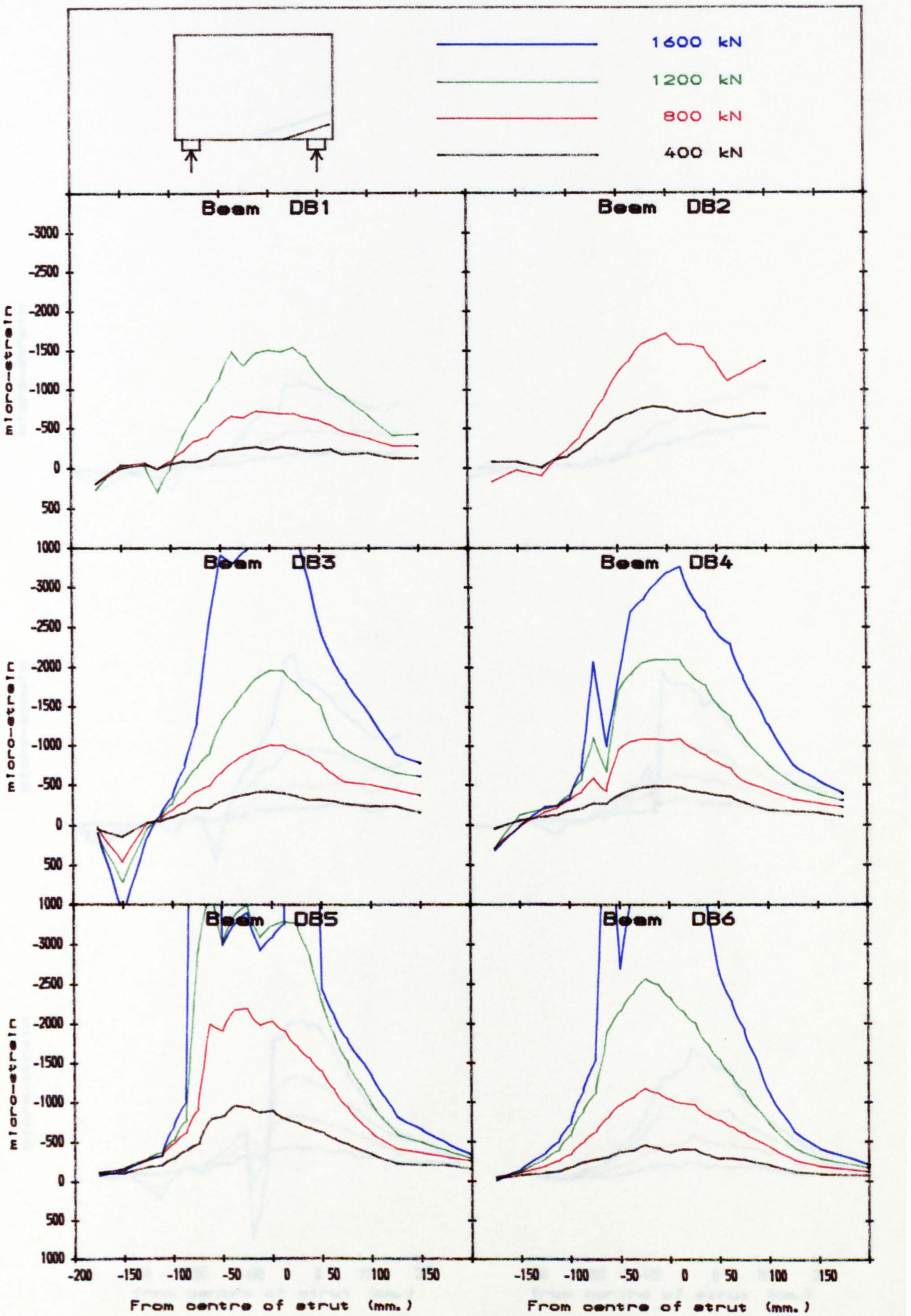

Fig. B. 9. Transverse strain in section 6.

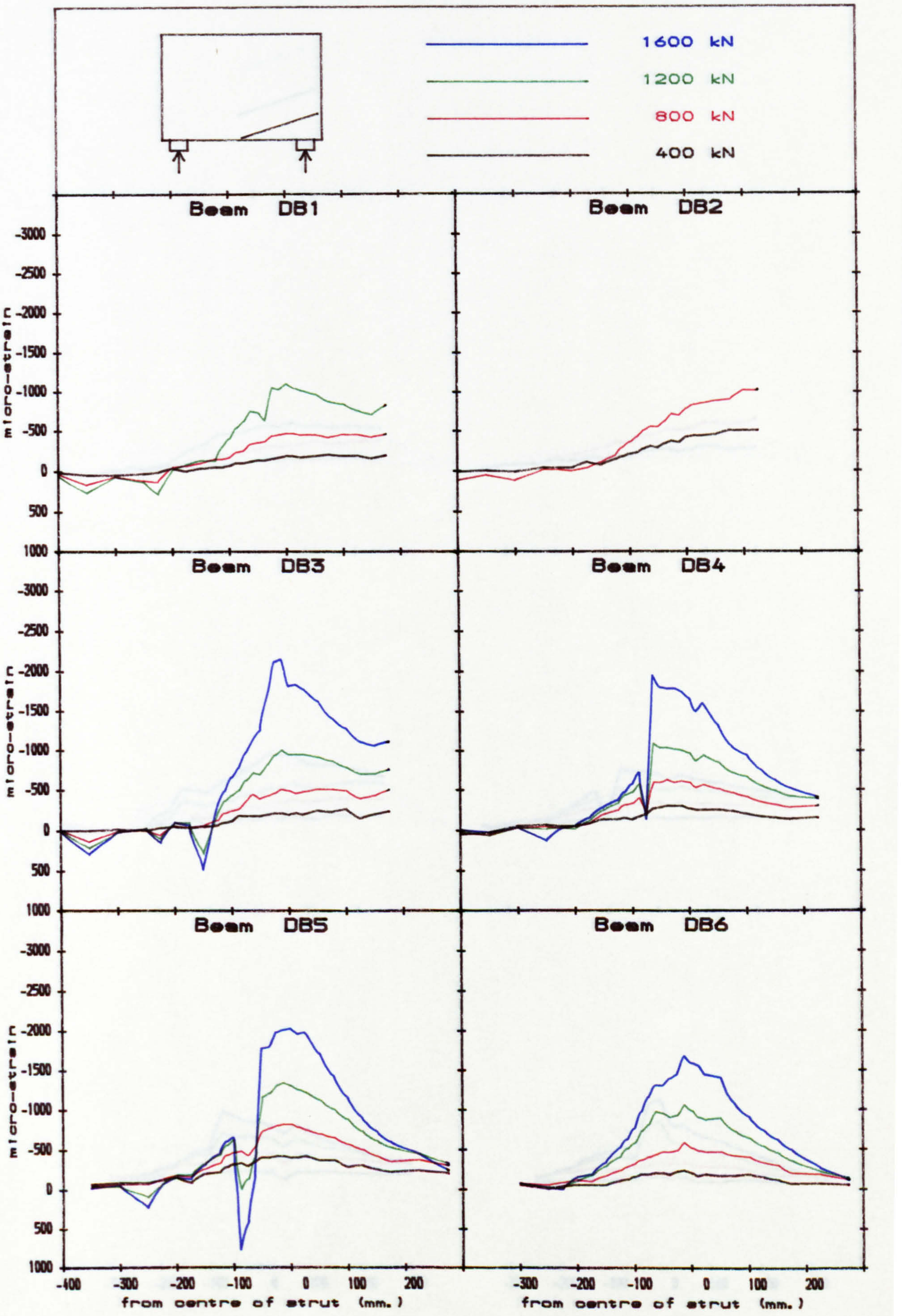

Fig. B. 10. Transverse strain in section 7.

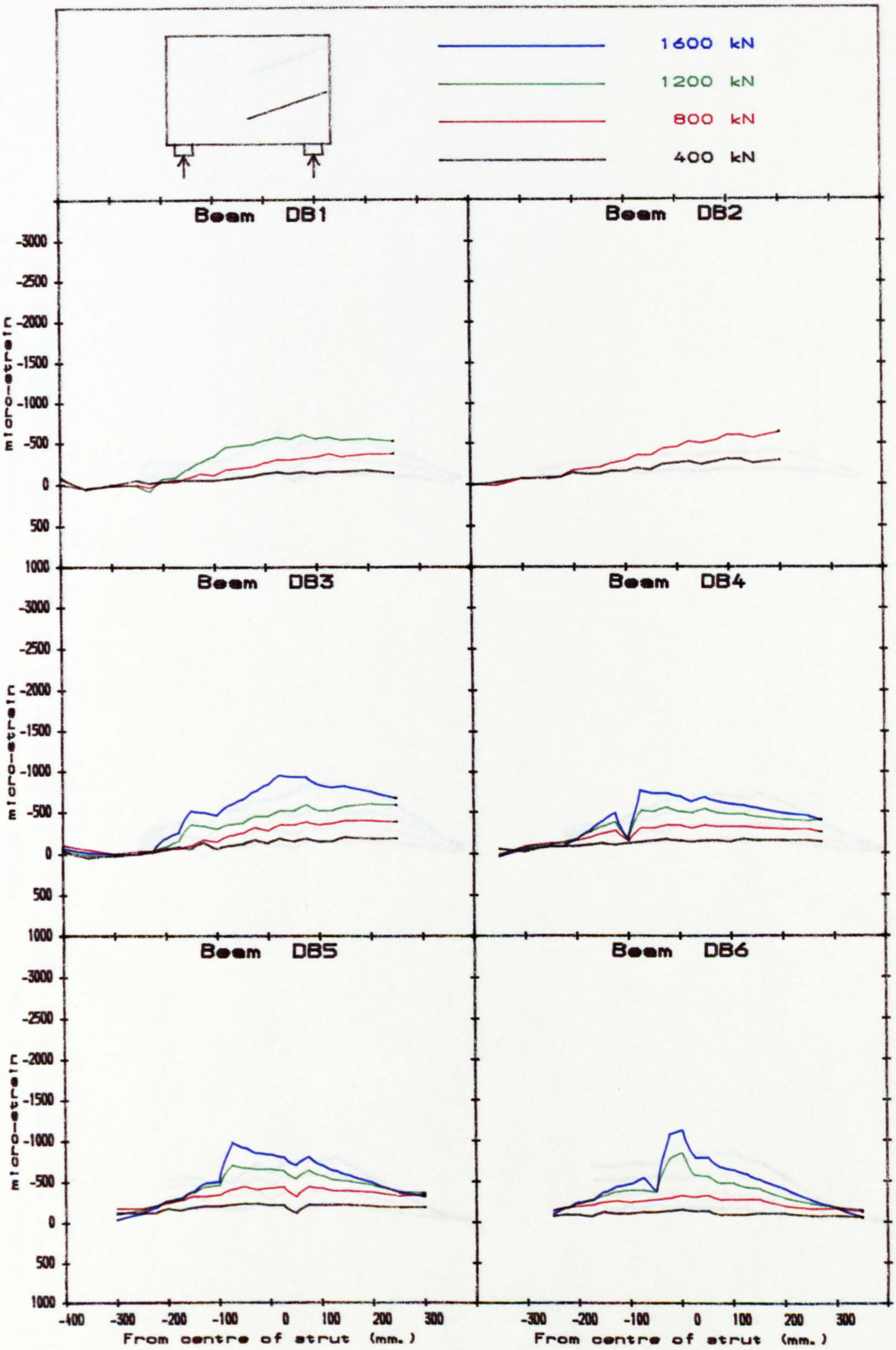

Fig. B. 11. Transverse strain in section 8.

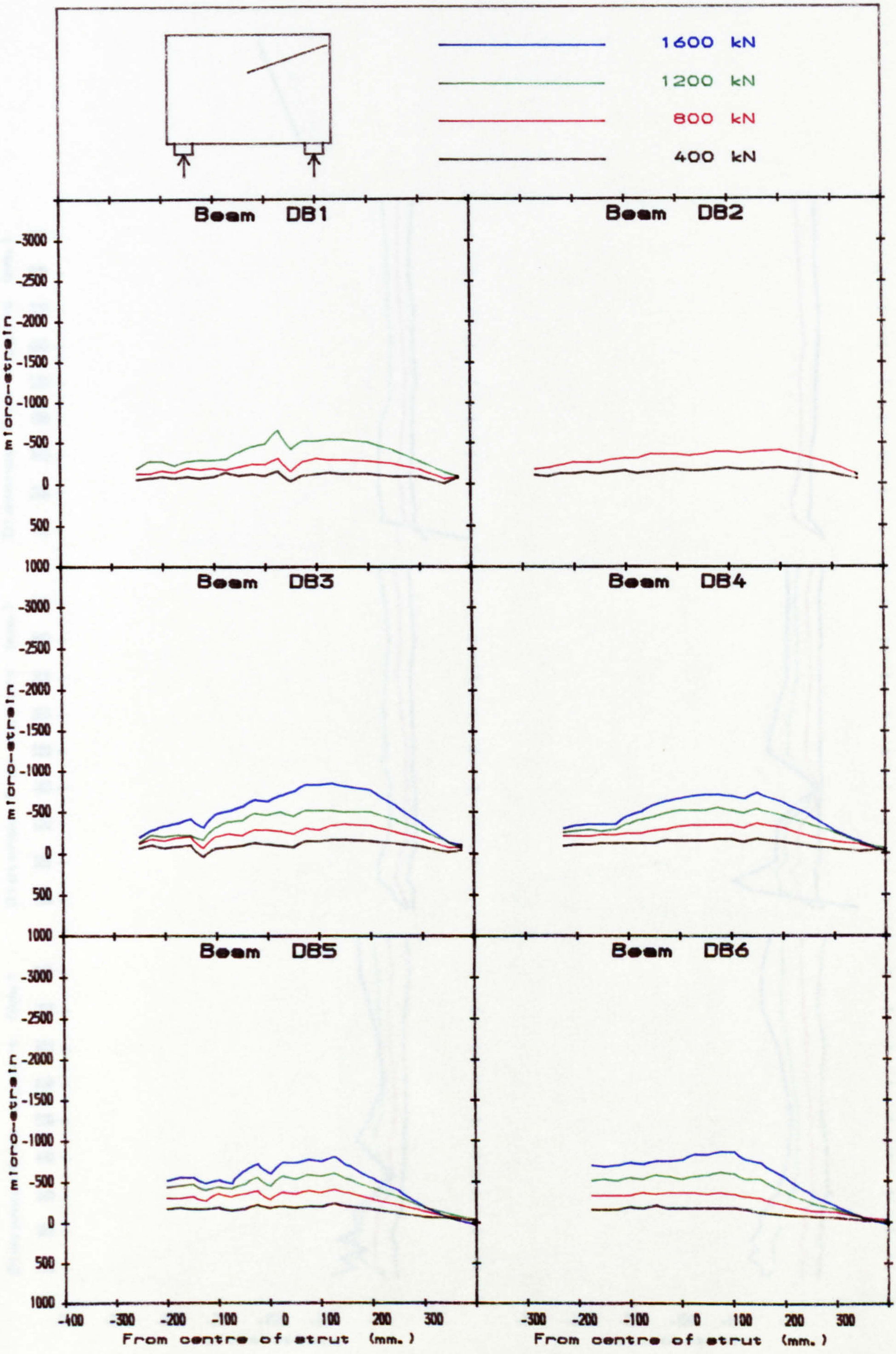

Fig. B. 12. Transverse strain in section 9.

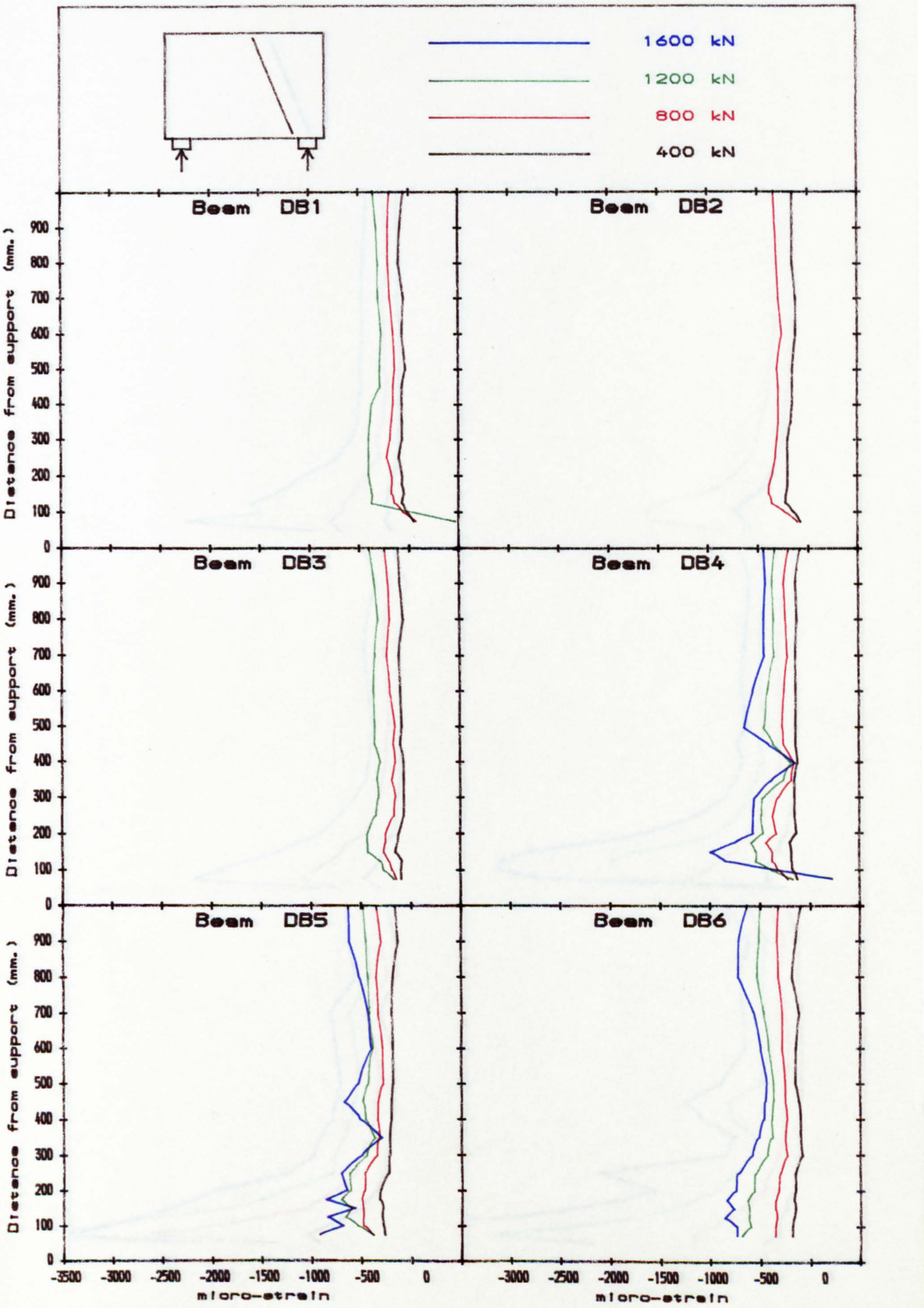

Fig. B. 13. Longitudinal strain in section 10.

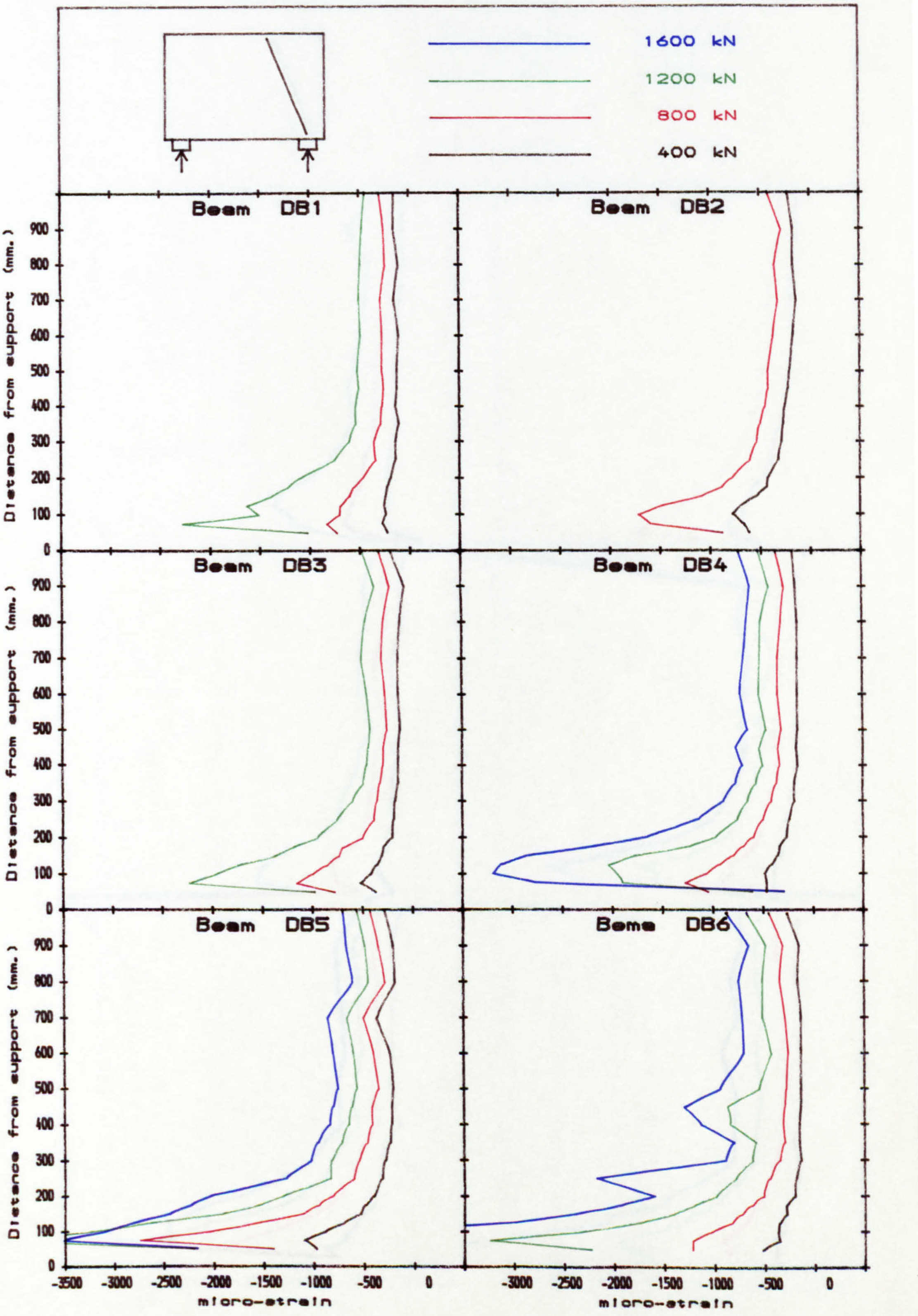

Fig. B. 14. Longitudinal strain in section 11.

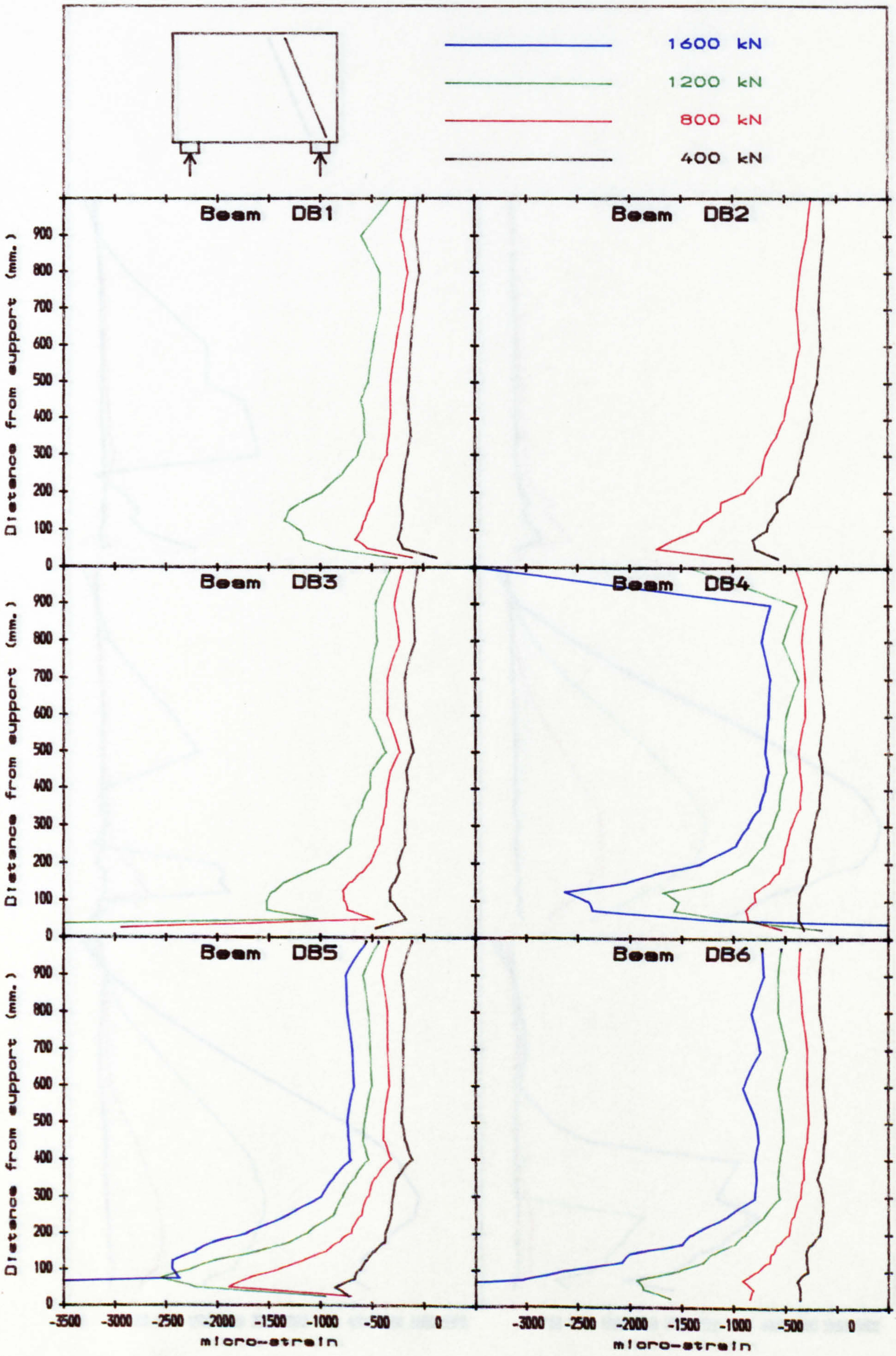

Fig. B. 15. Longitudinal strain in section 12.

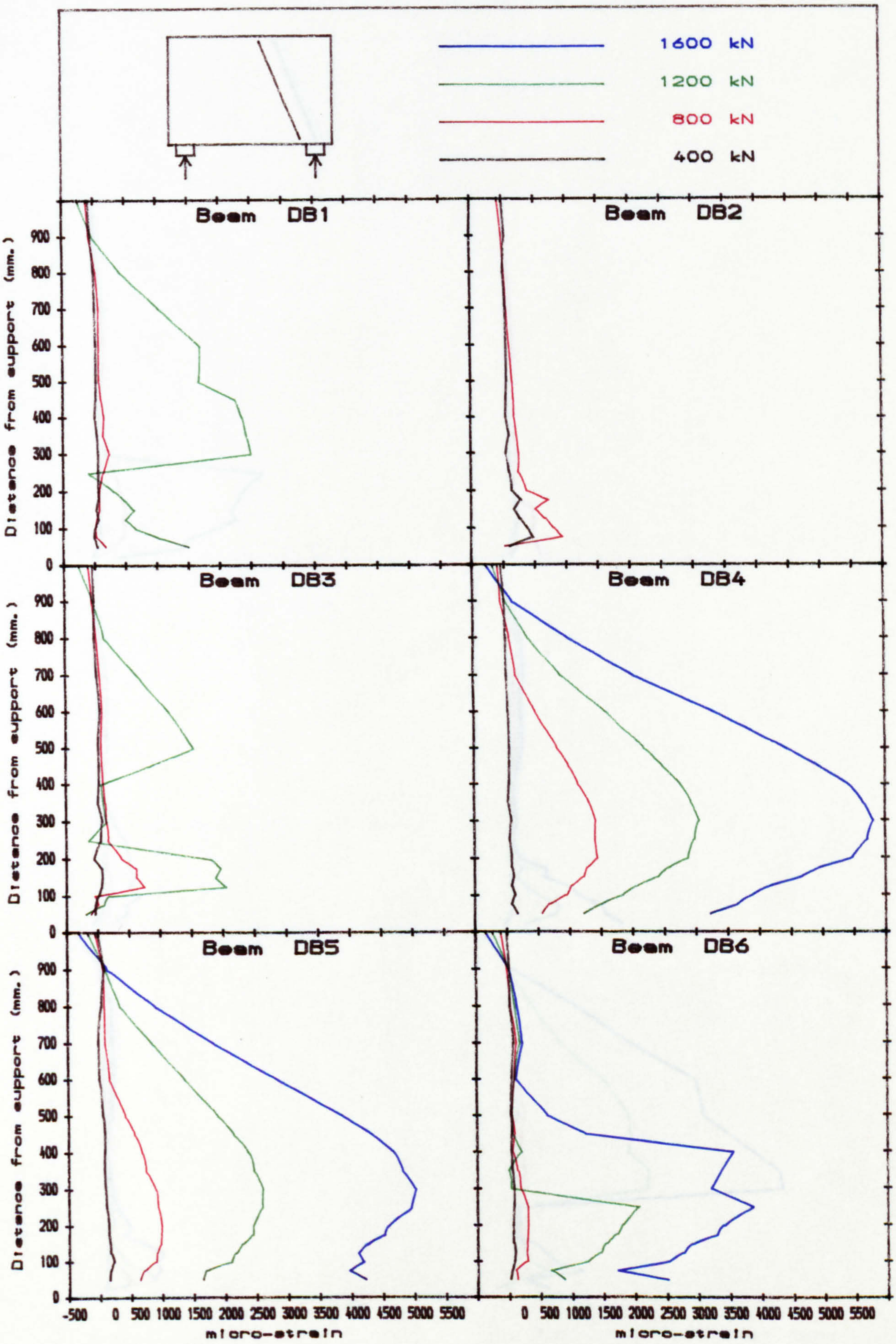

Fig. B. 16. Transverse strain in section 10.

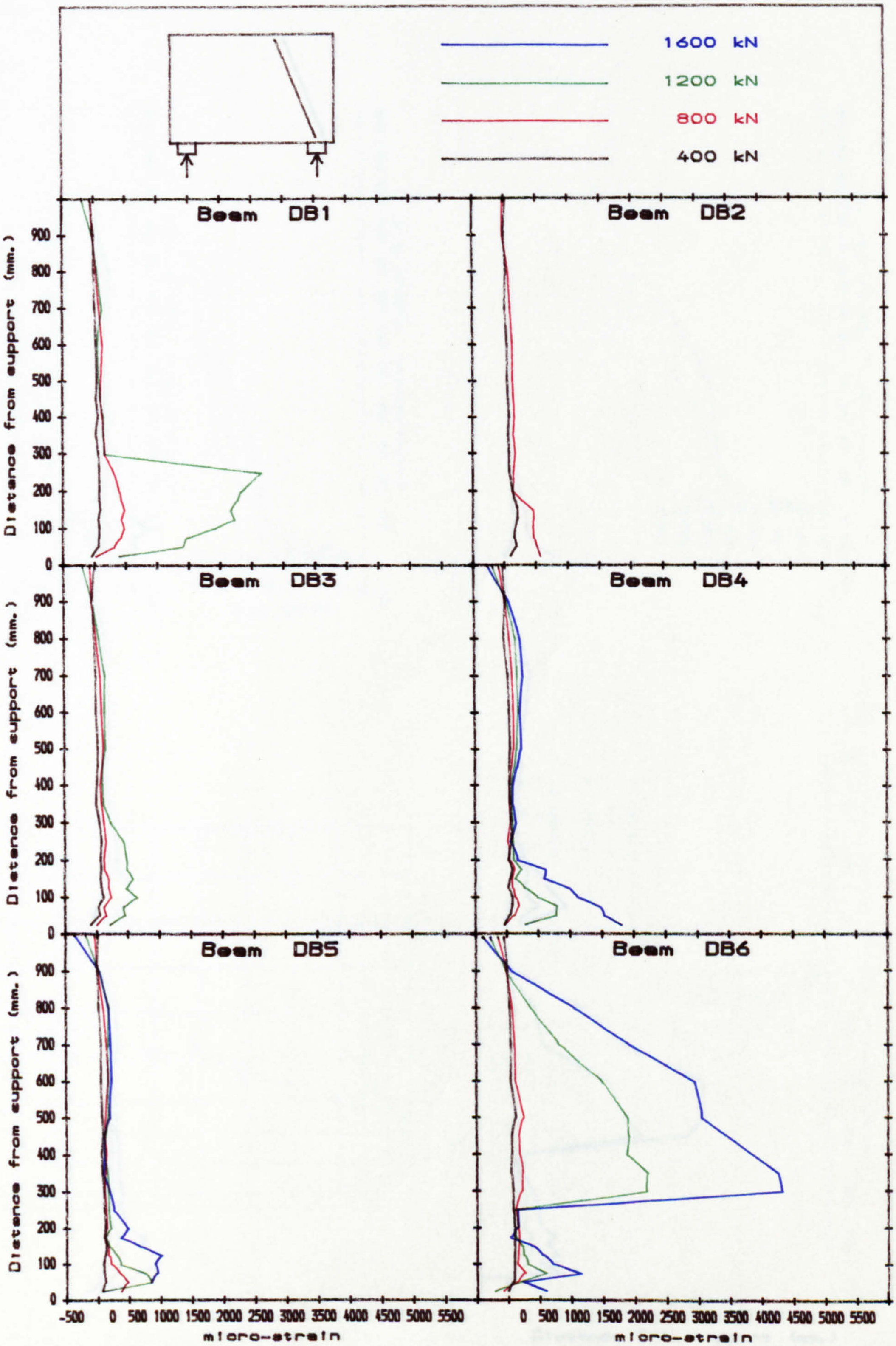

Fig. B. 17. Transverse strain in section 11.

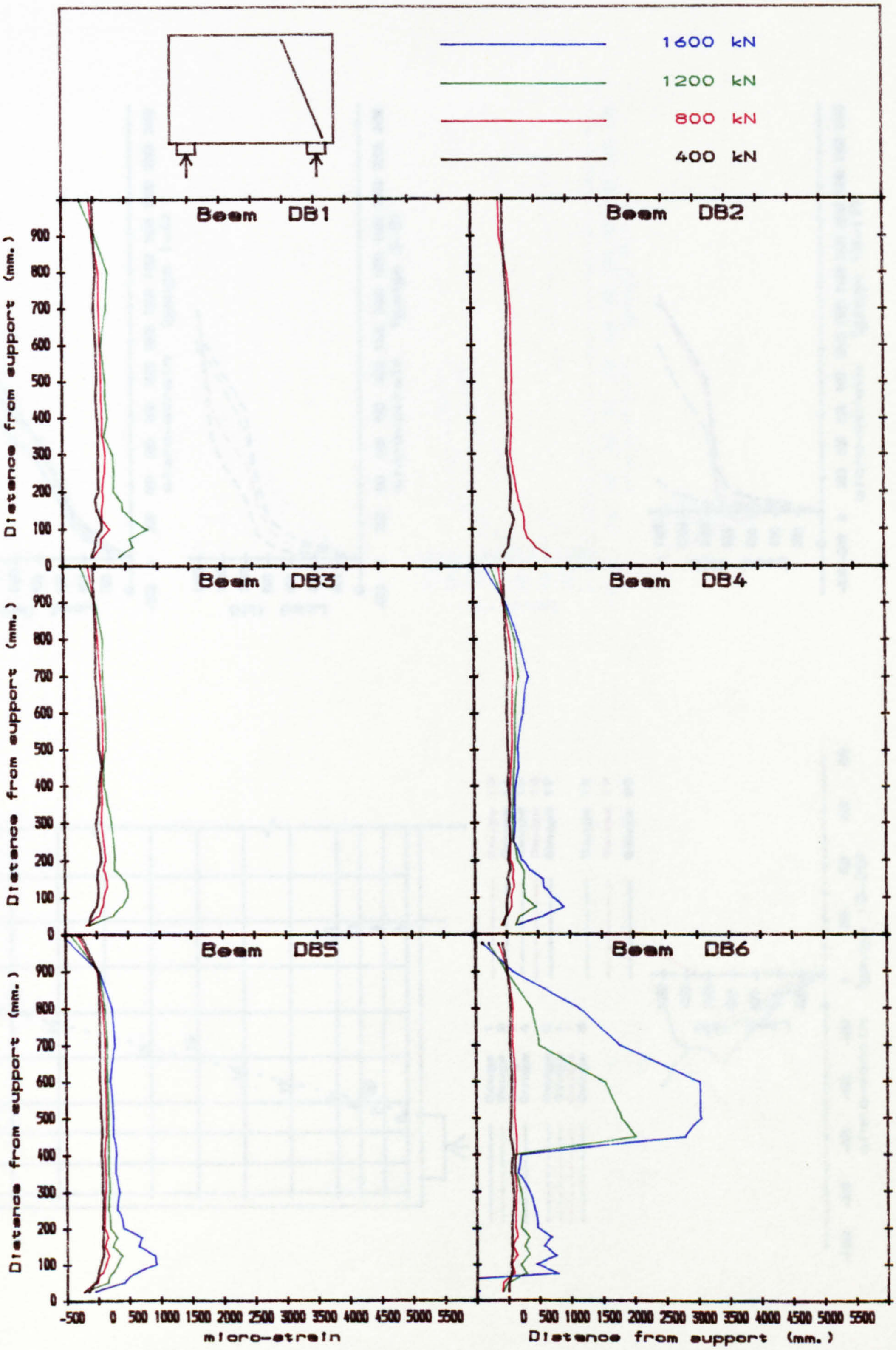

Fig. B. 18. Transverse strain in section 12.

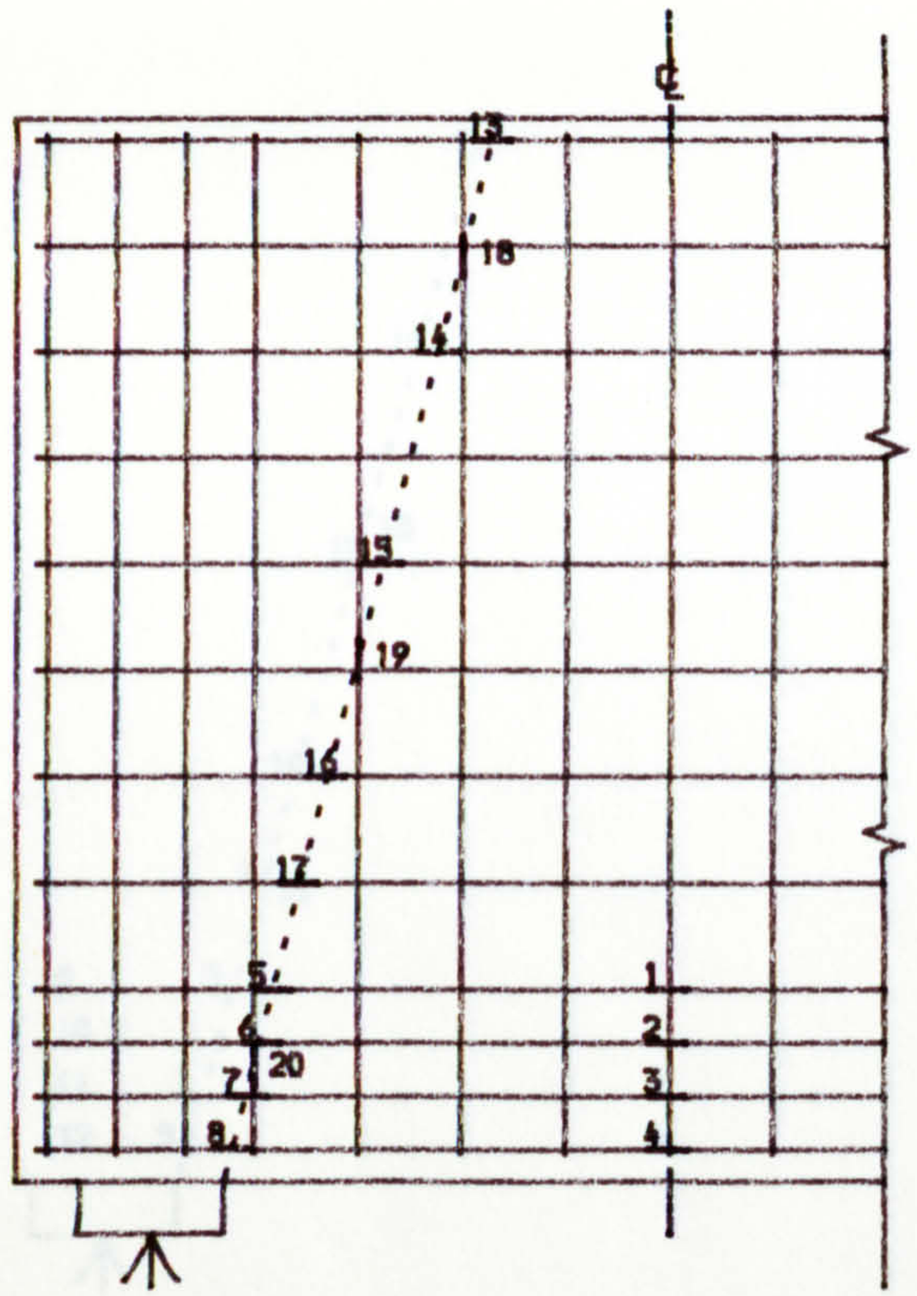

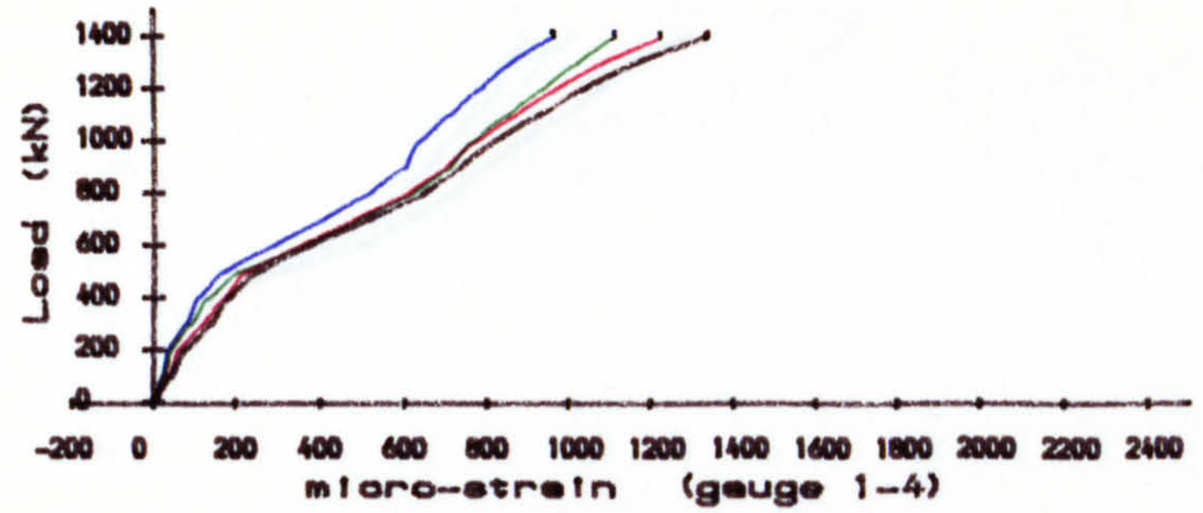

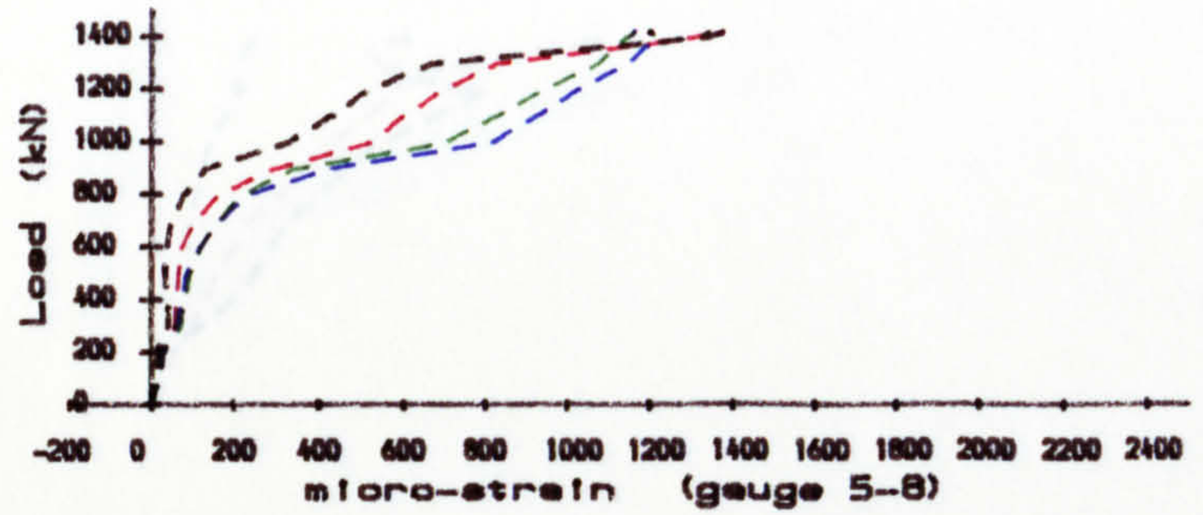

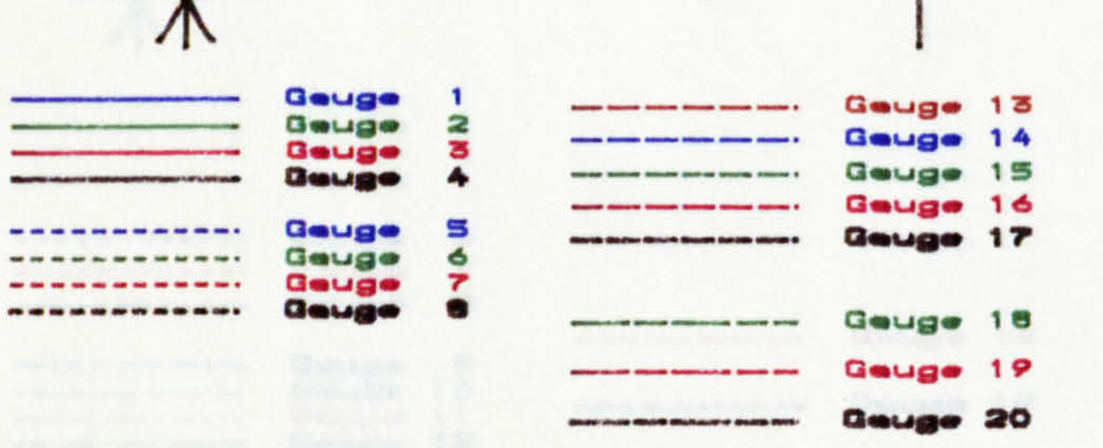

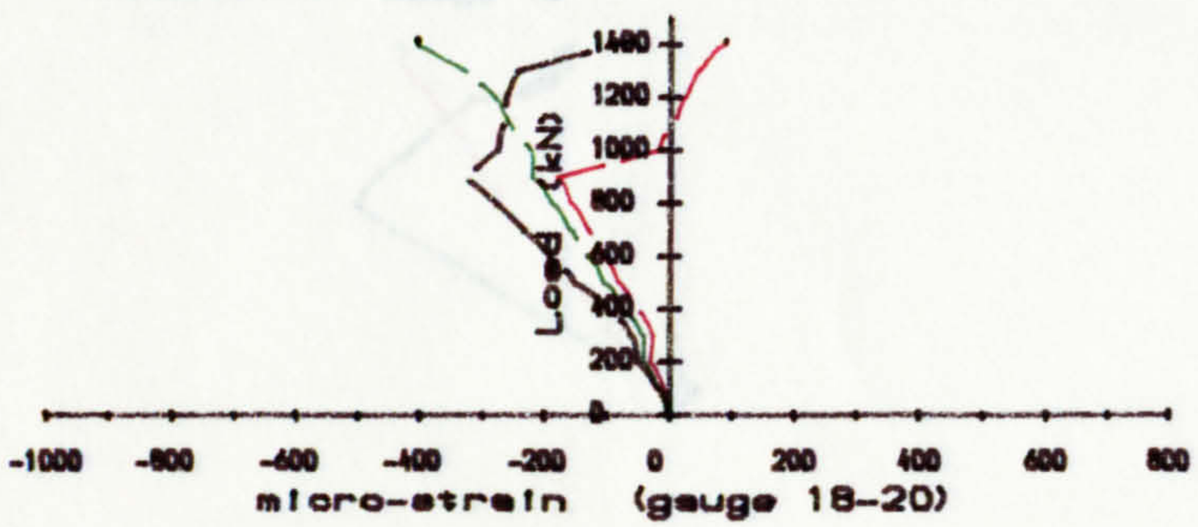

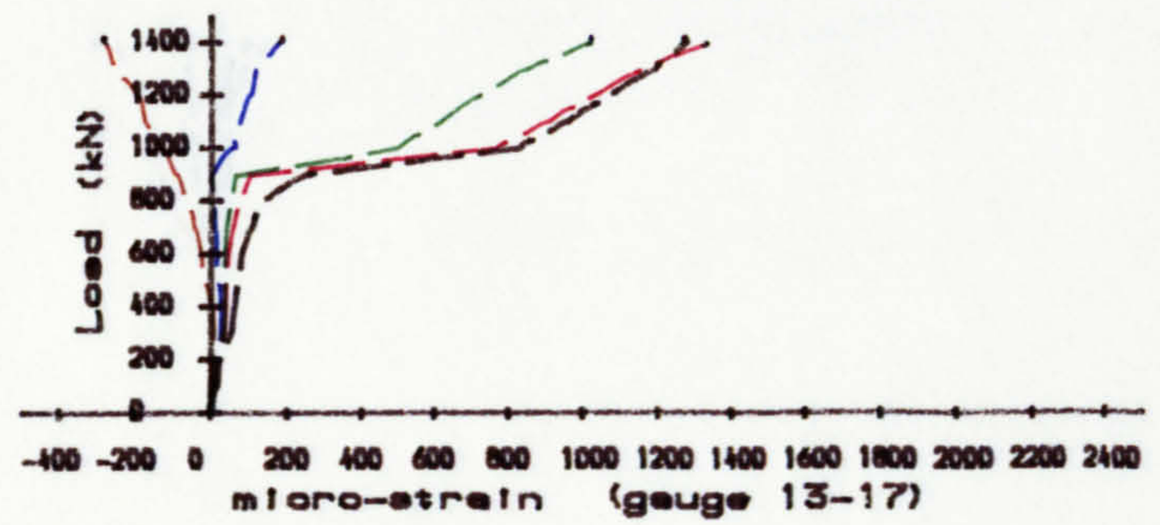

Fig. B. 19. Strain of reinforcements in beam DB1.

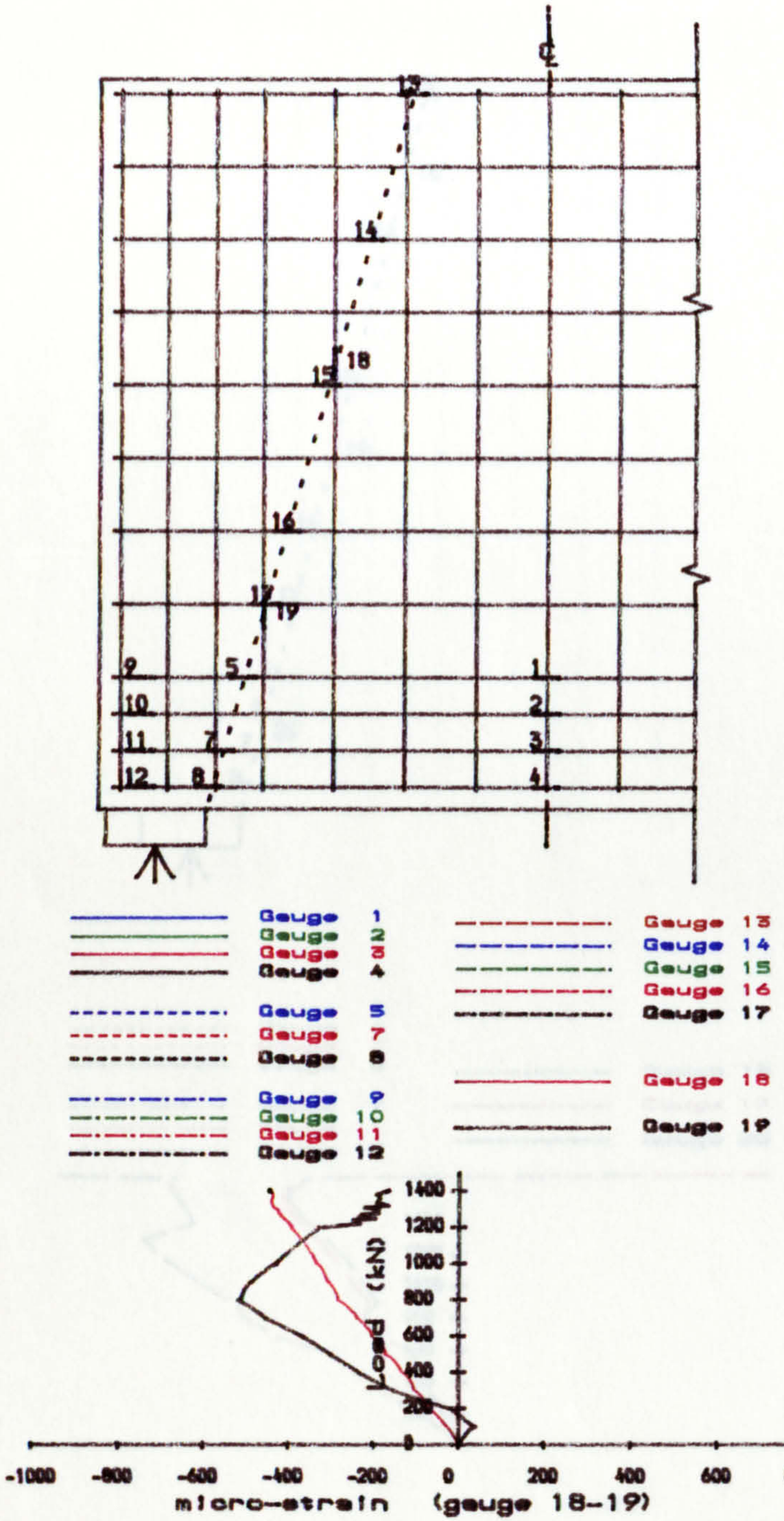

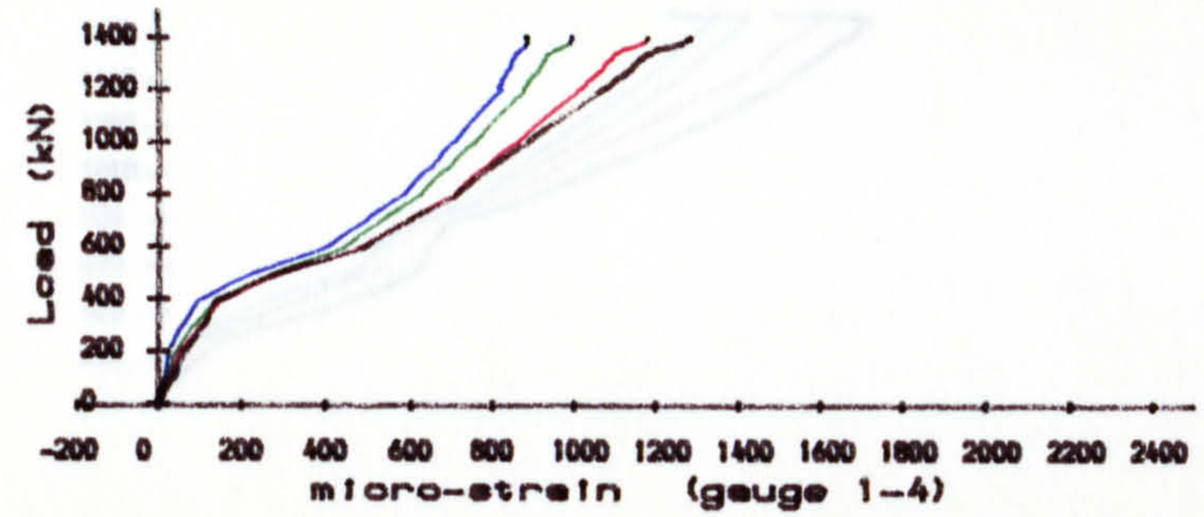

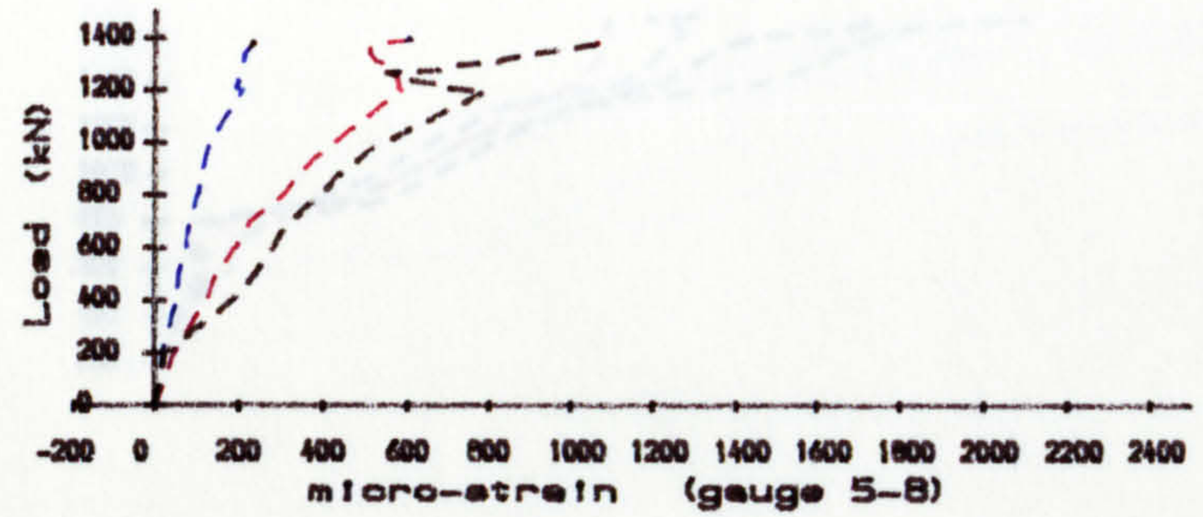

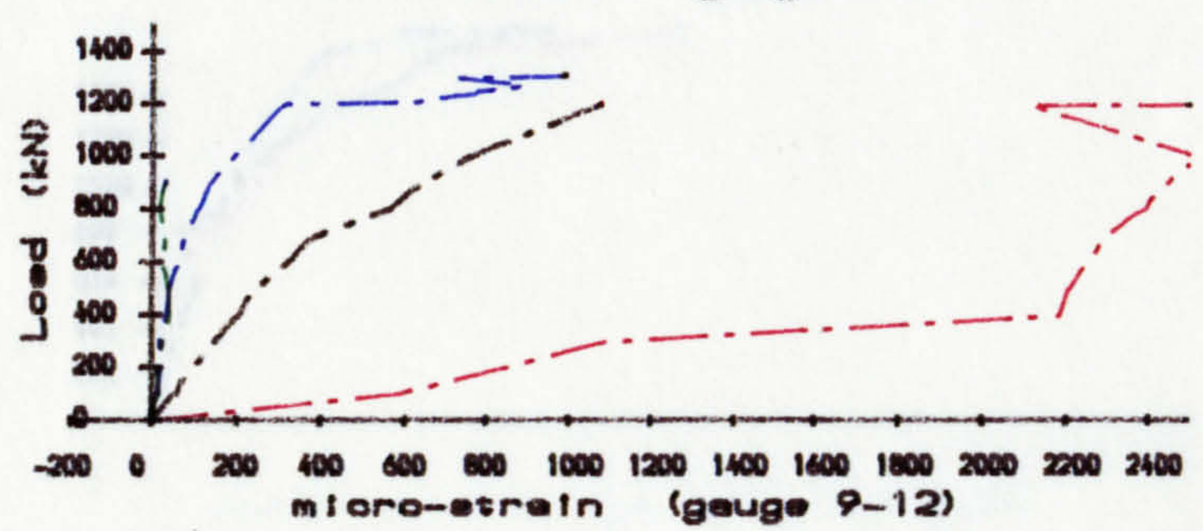

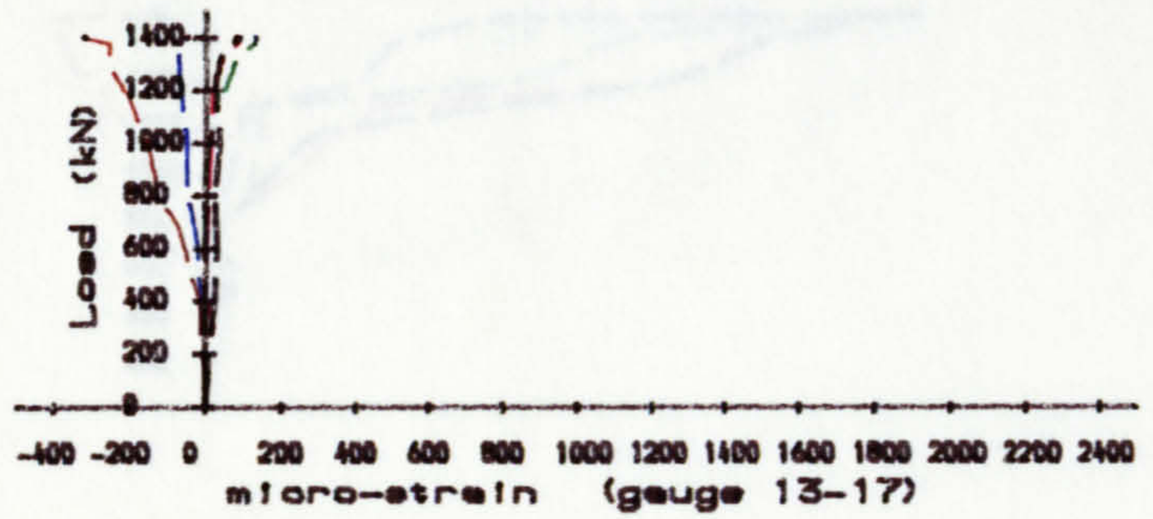

Fig. B. 20. Strain of reinforcements in beam DB2.

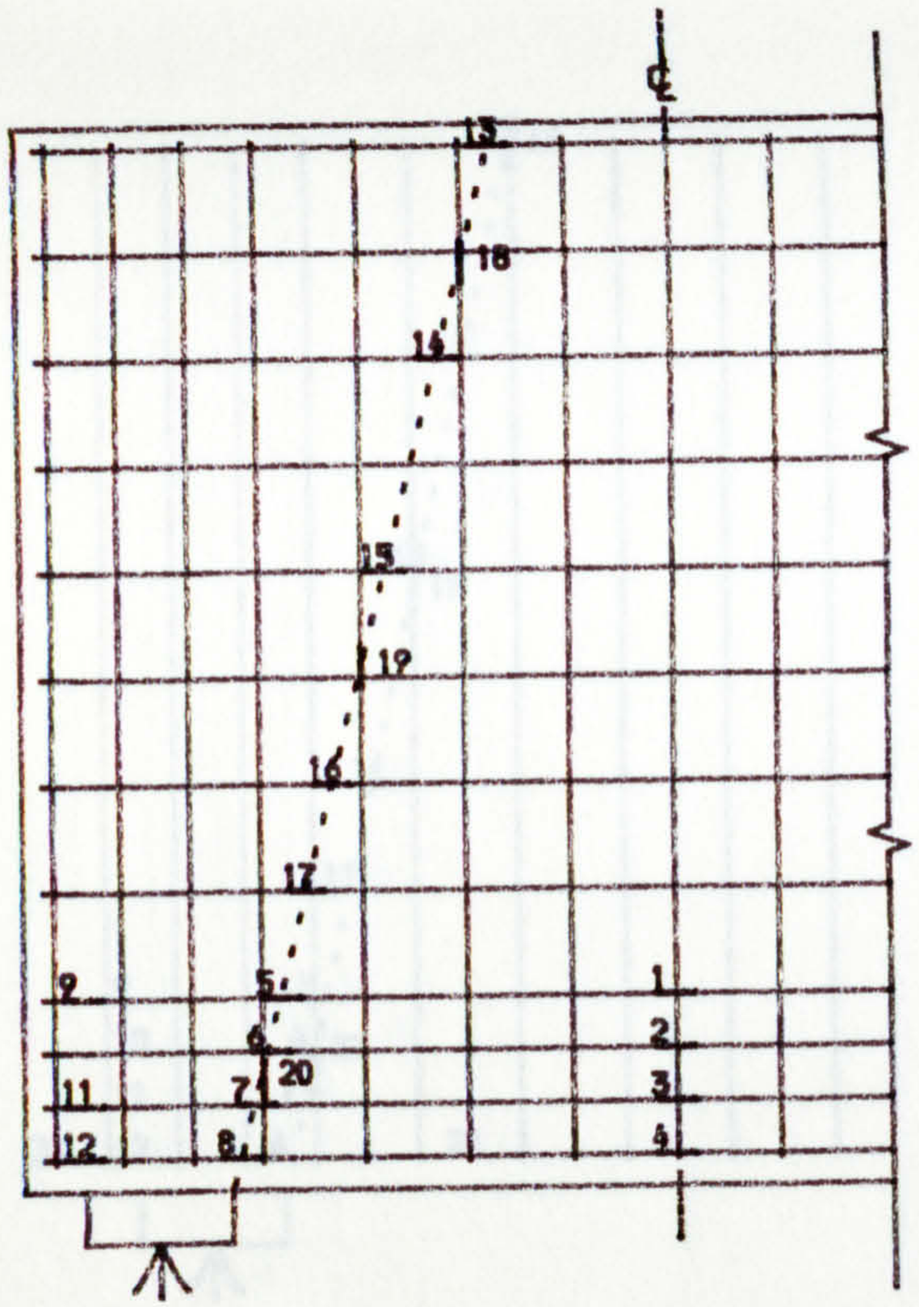

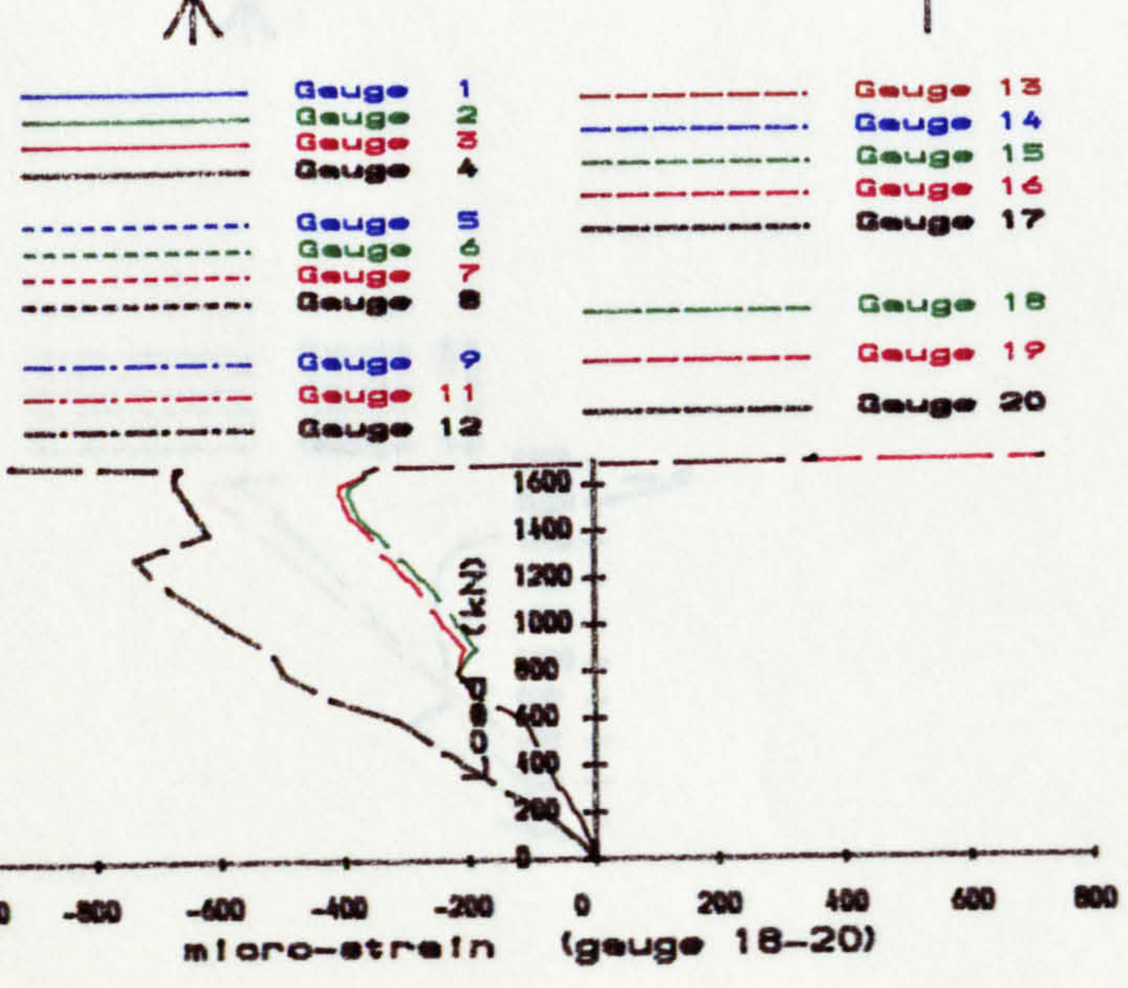

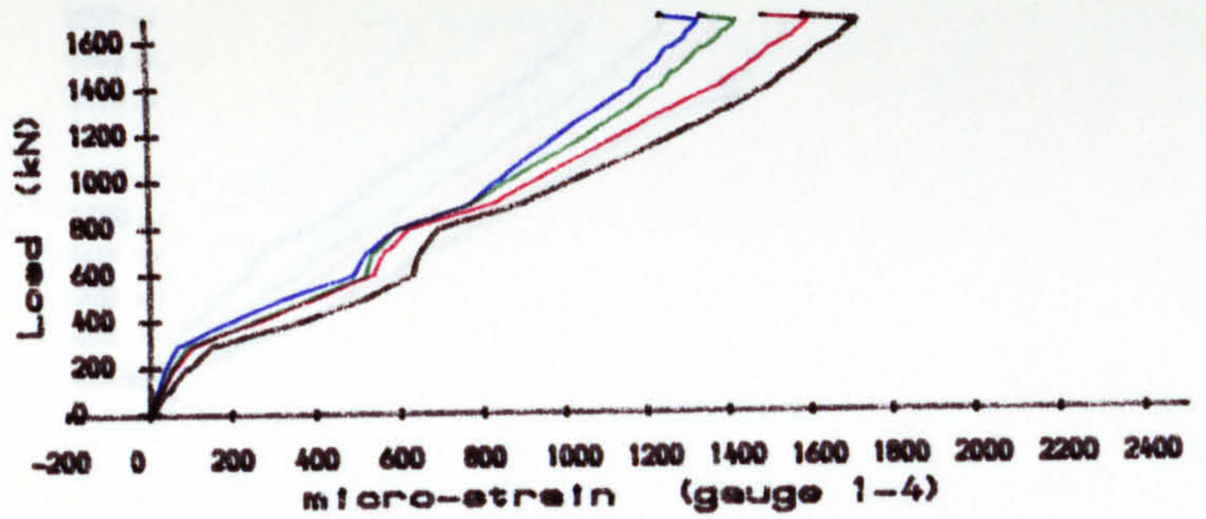

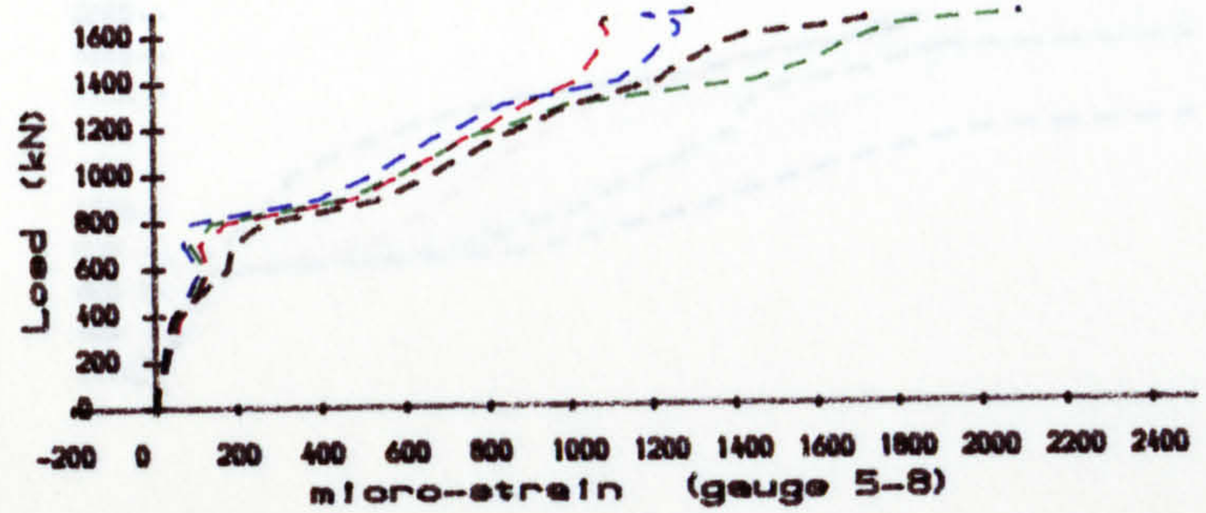

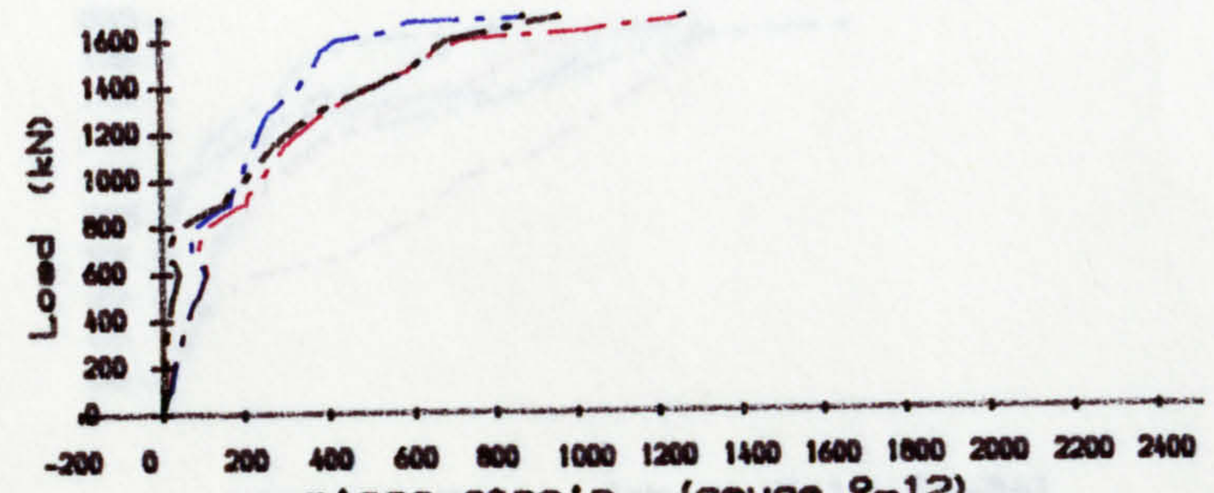

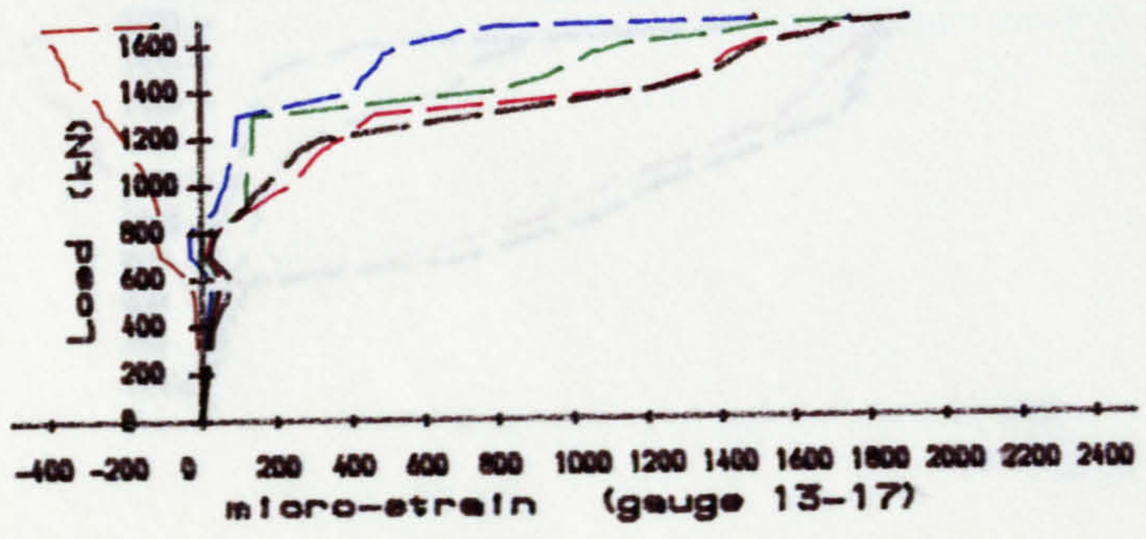

Fig. B. 21. Strain of reinforcements in beam DB3.

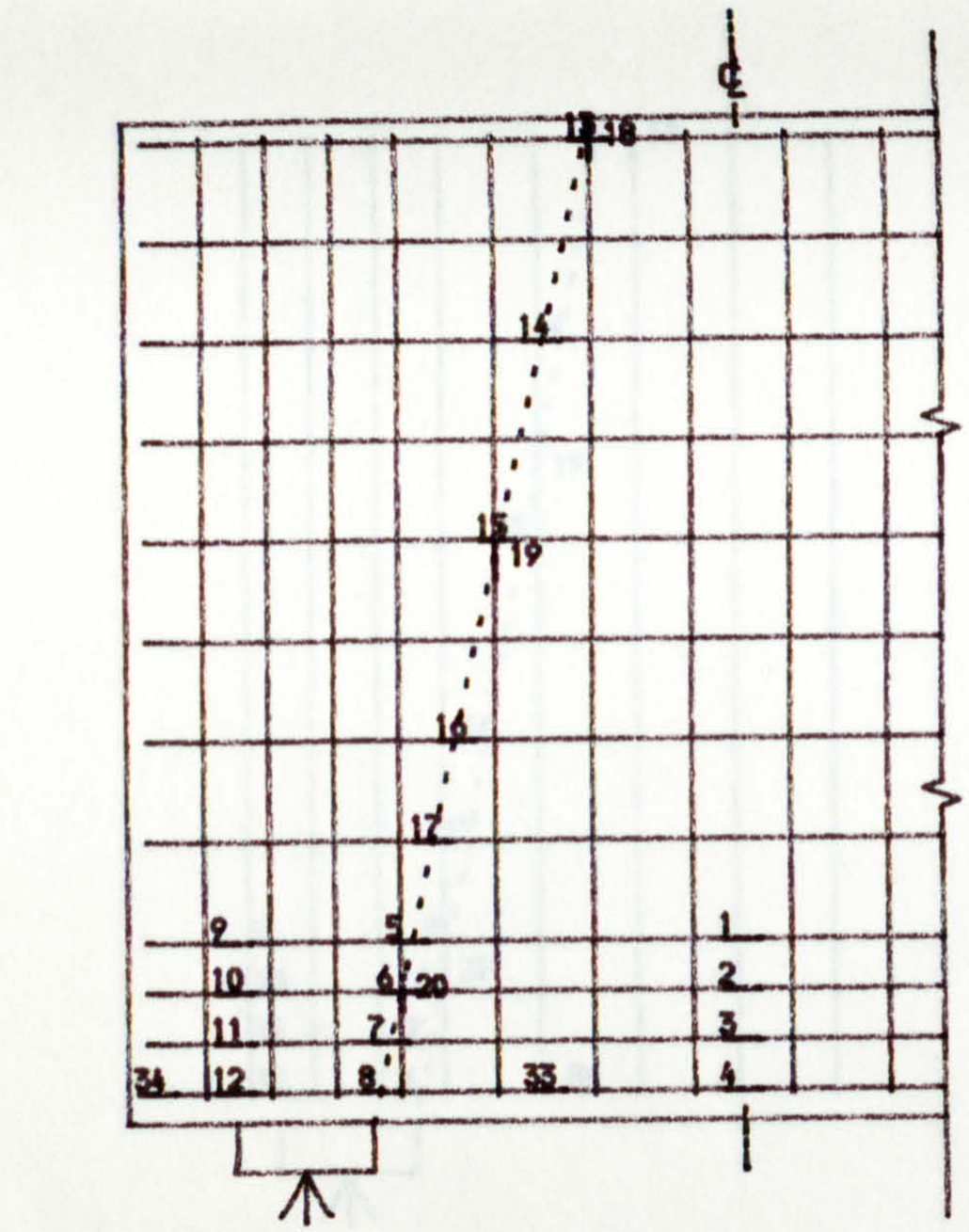

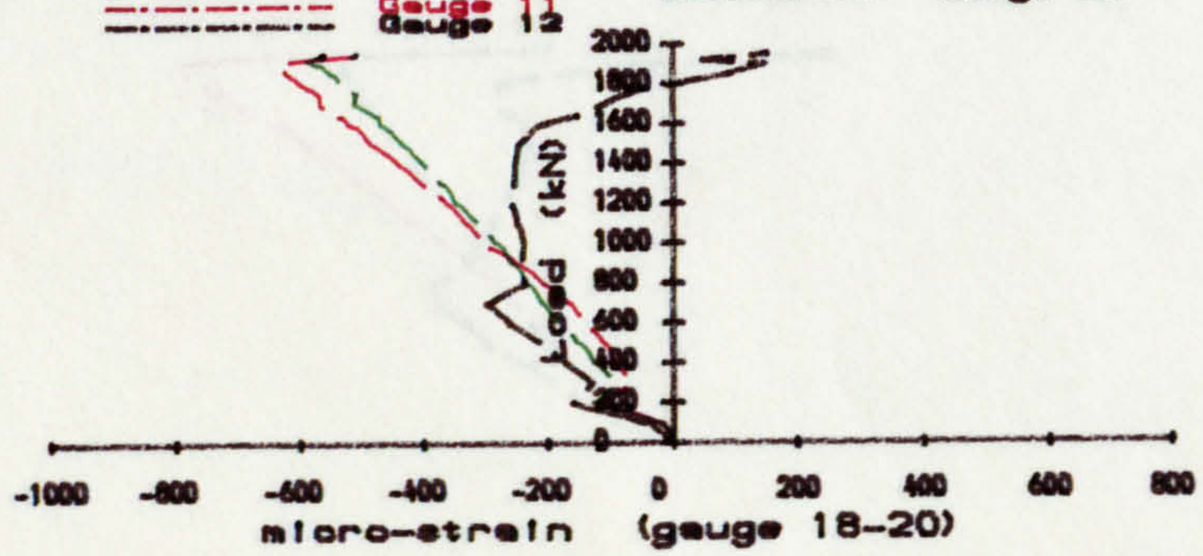

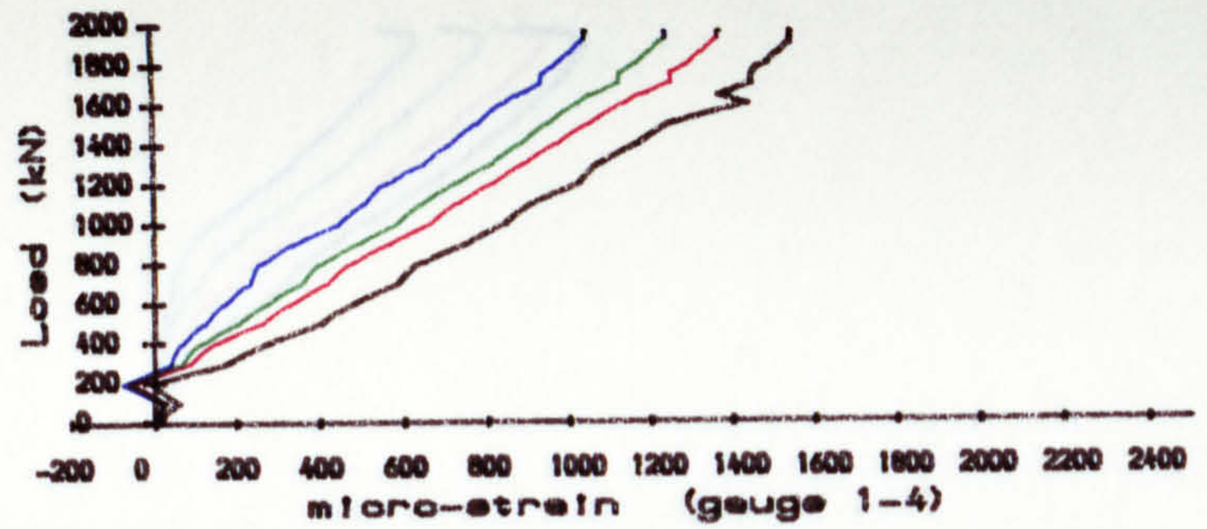

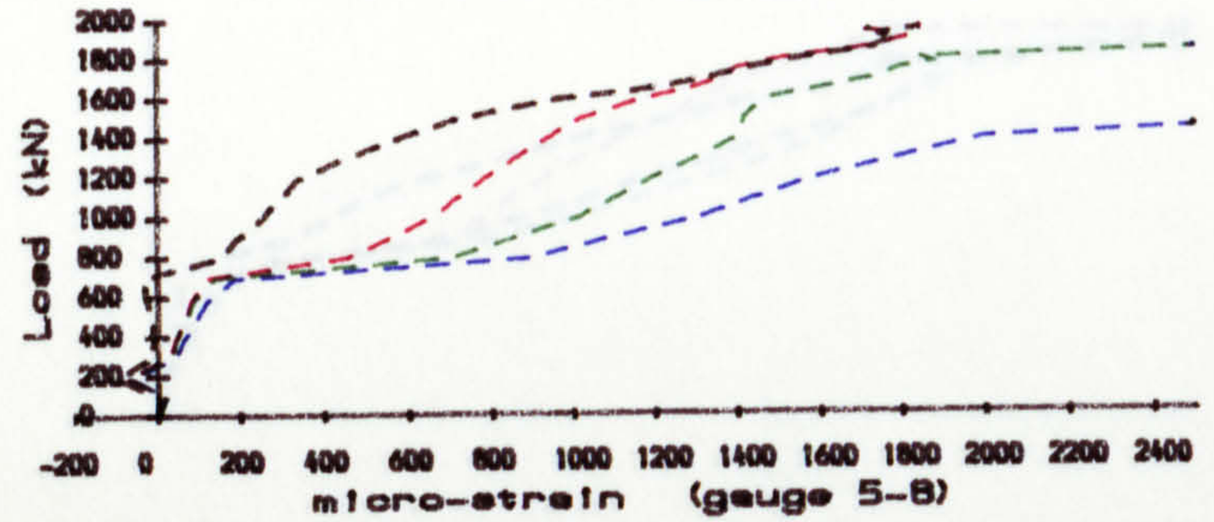

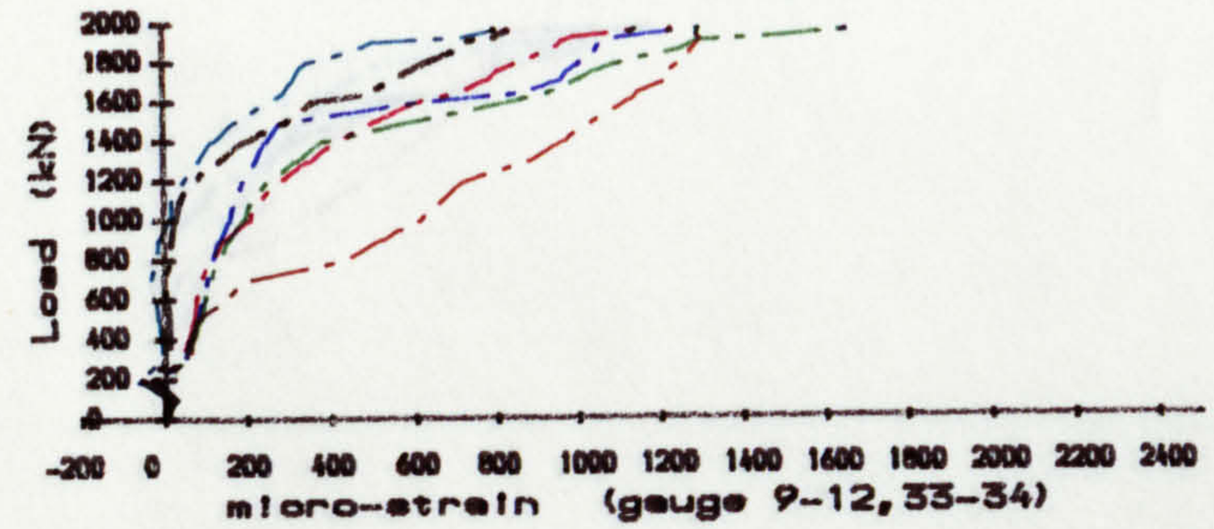

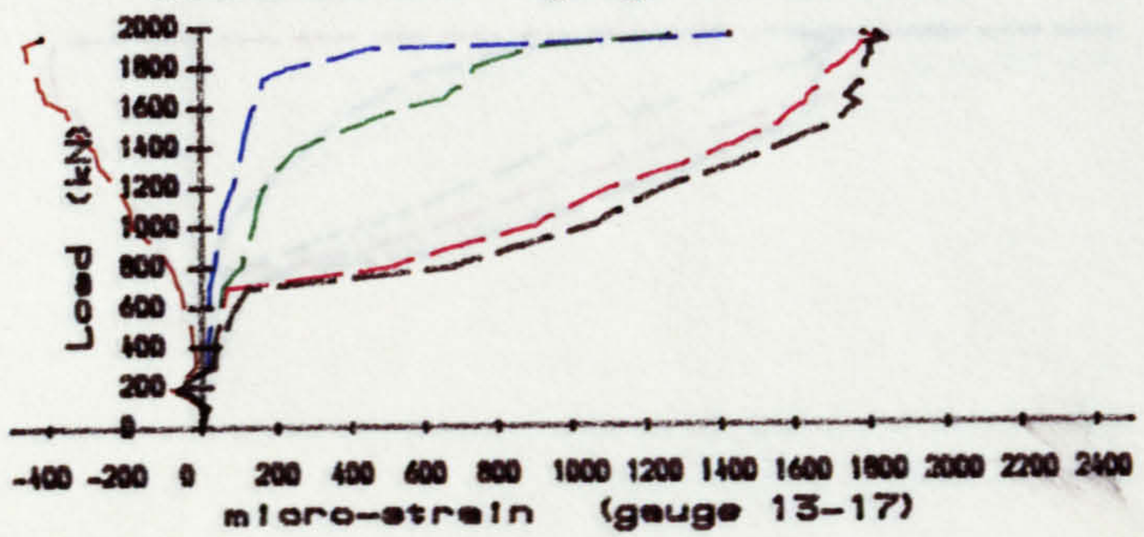

Fig. B. 22. Strain of reinforcements in beam DB4.

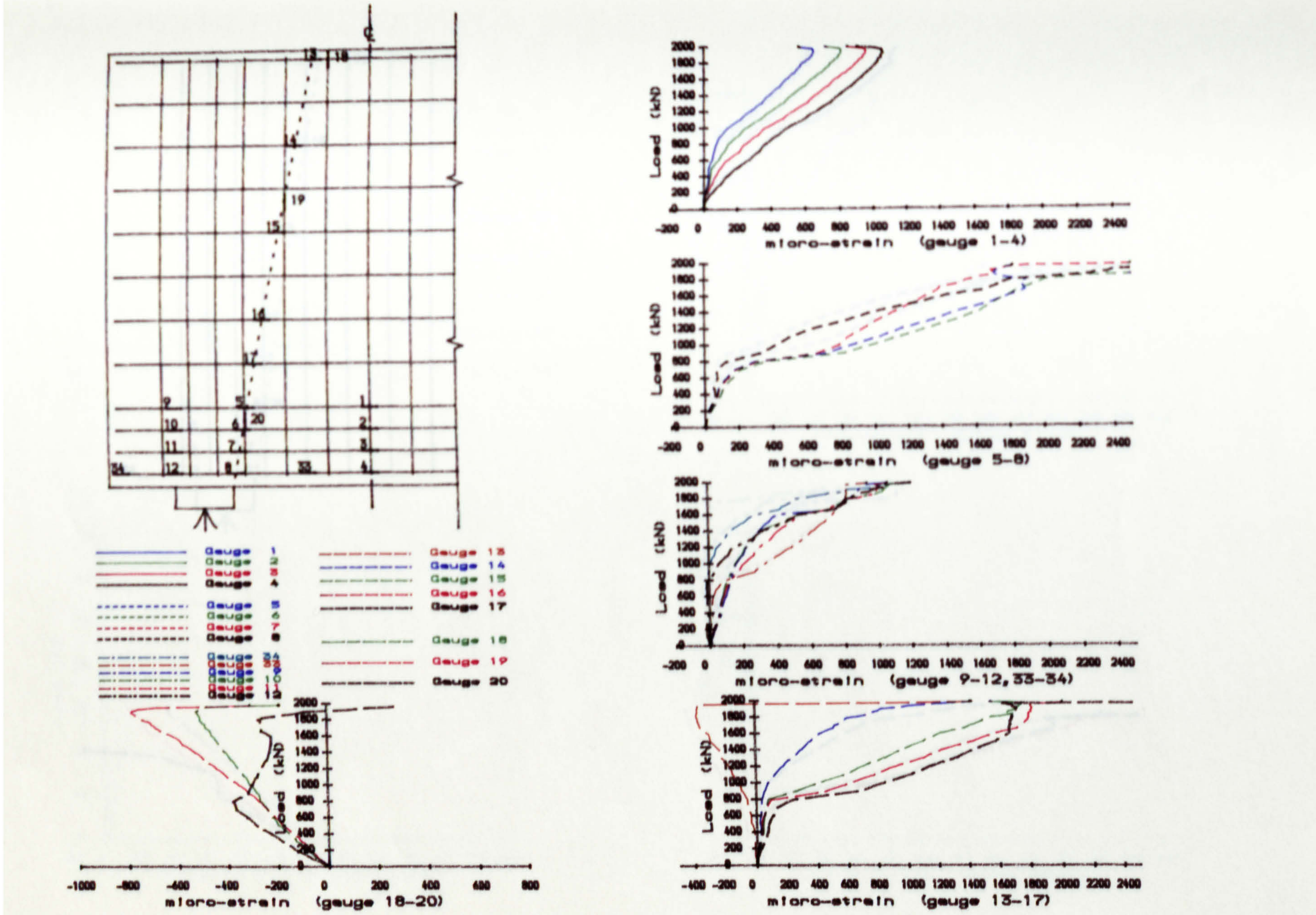

Fig. B. 23. Strain of reinforcement in beam DB5.

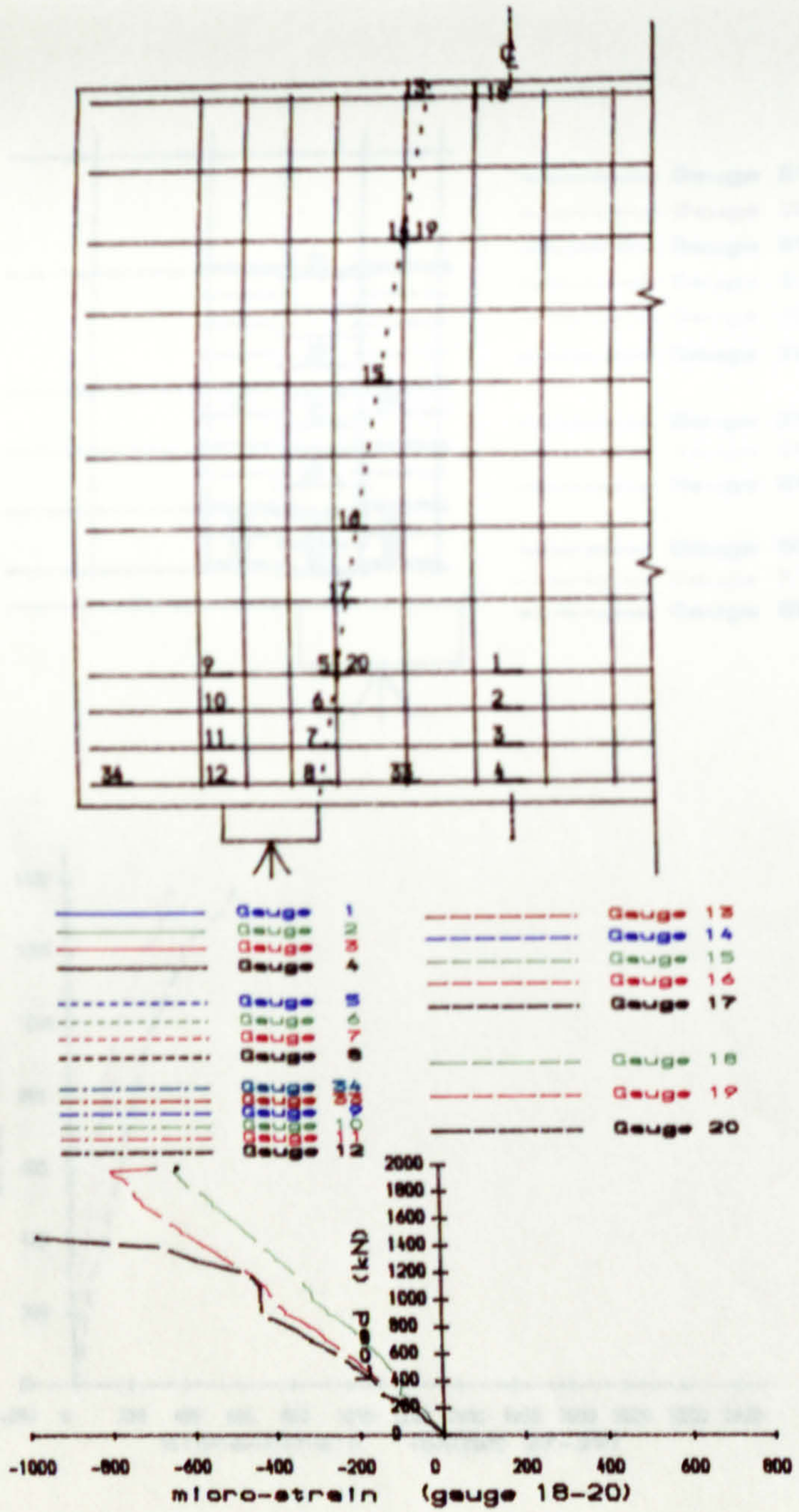

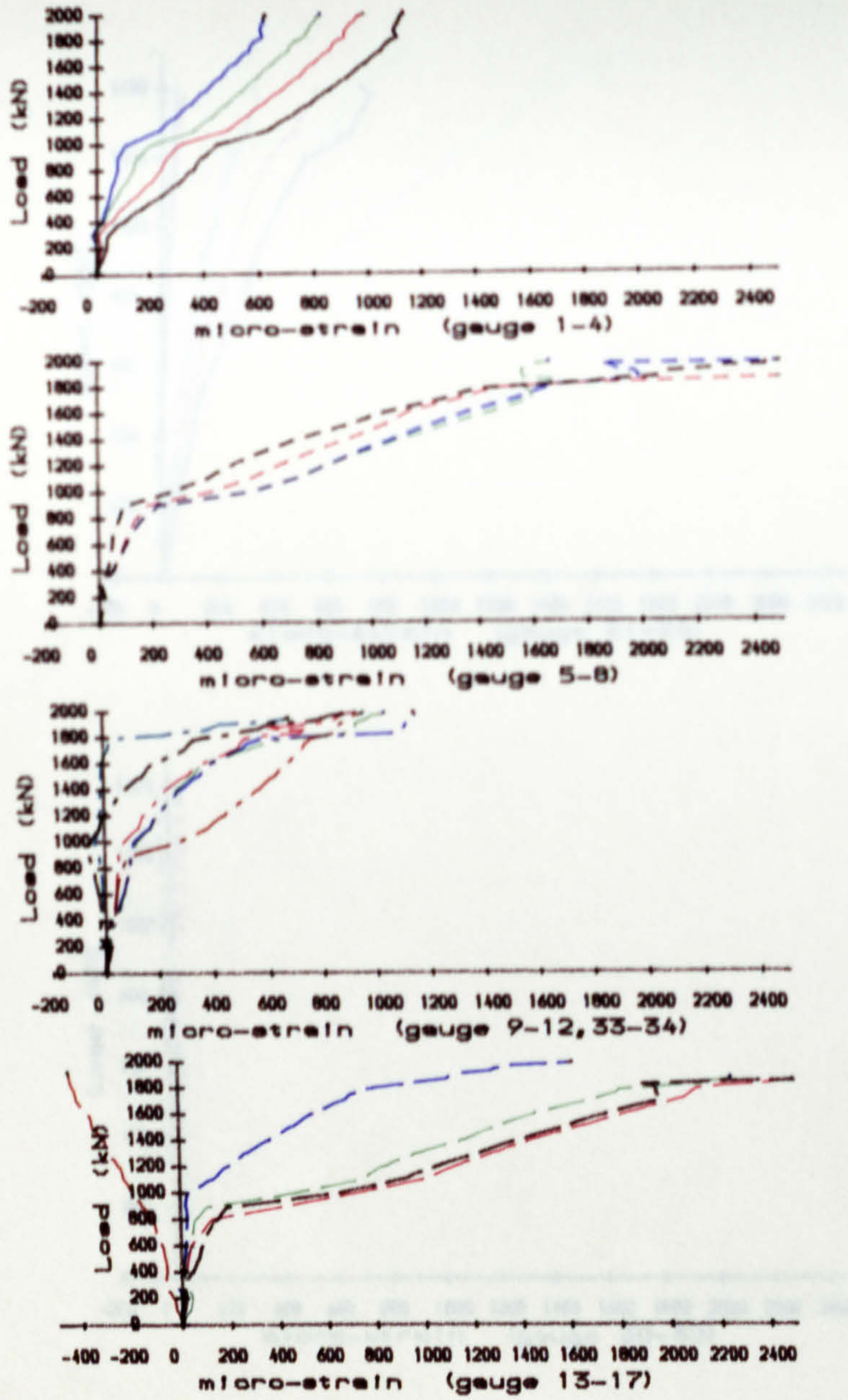

FIG. B. 24. Strain of reinforcements in beam DB6.

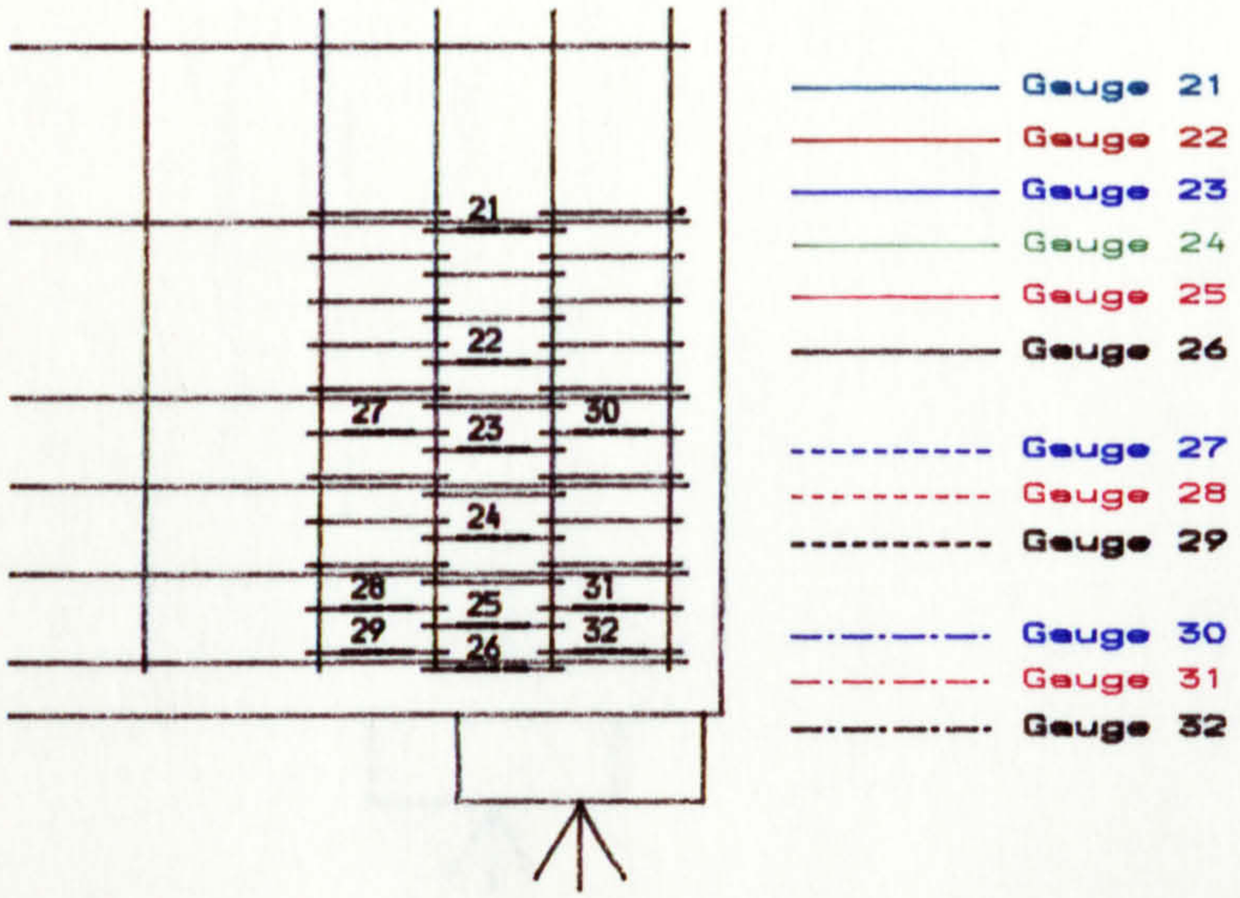

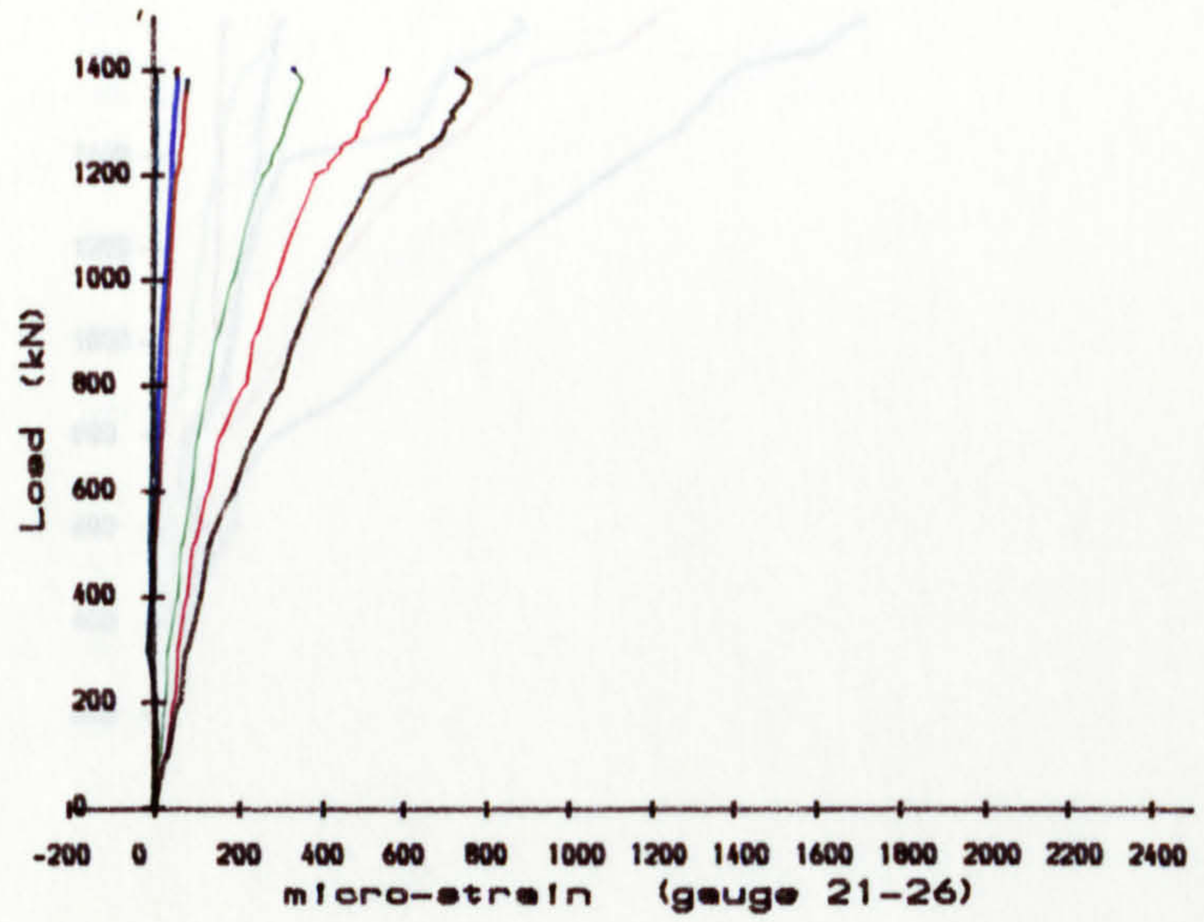

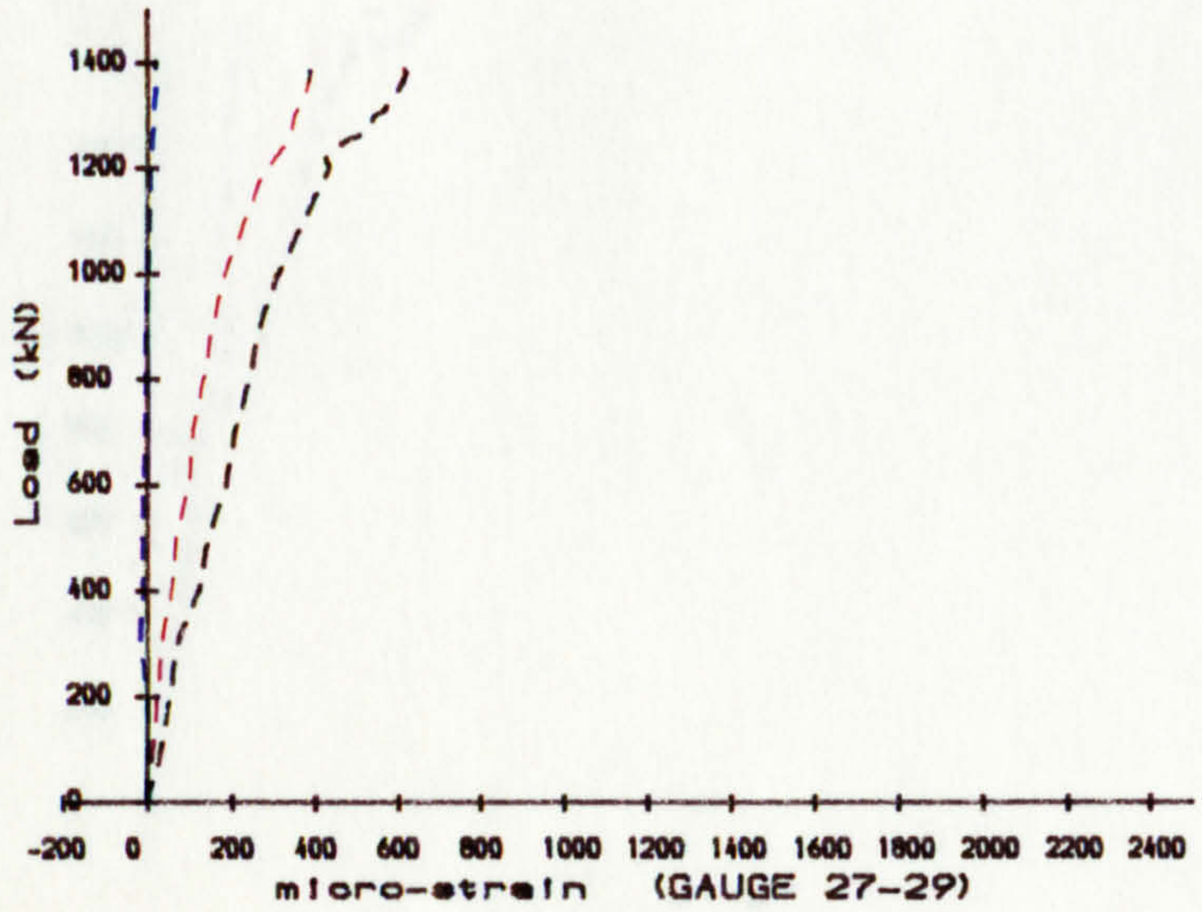

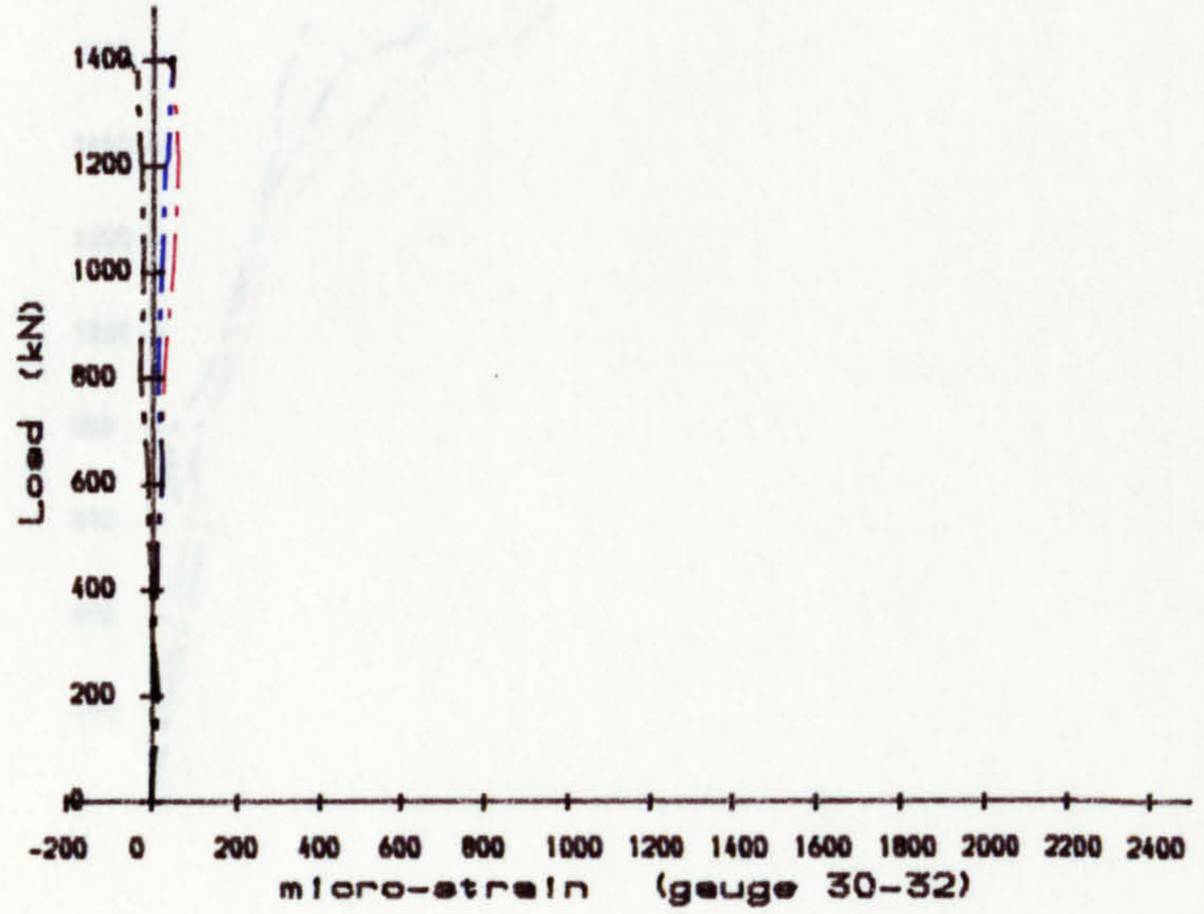

Fig. B. 25. Strain of bearing steel in beam DB2.

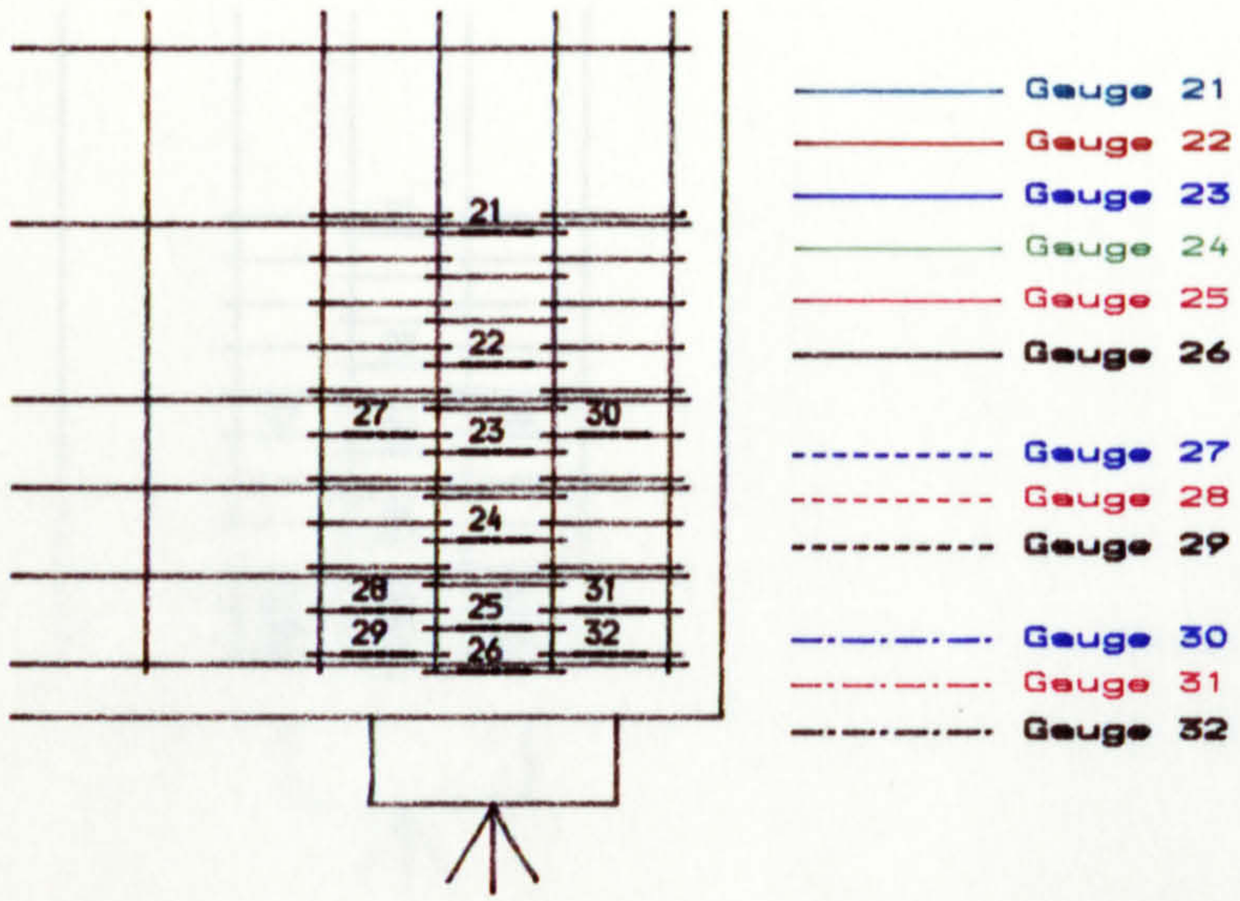

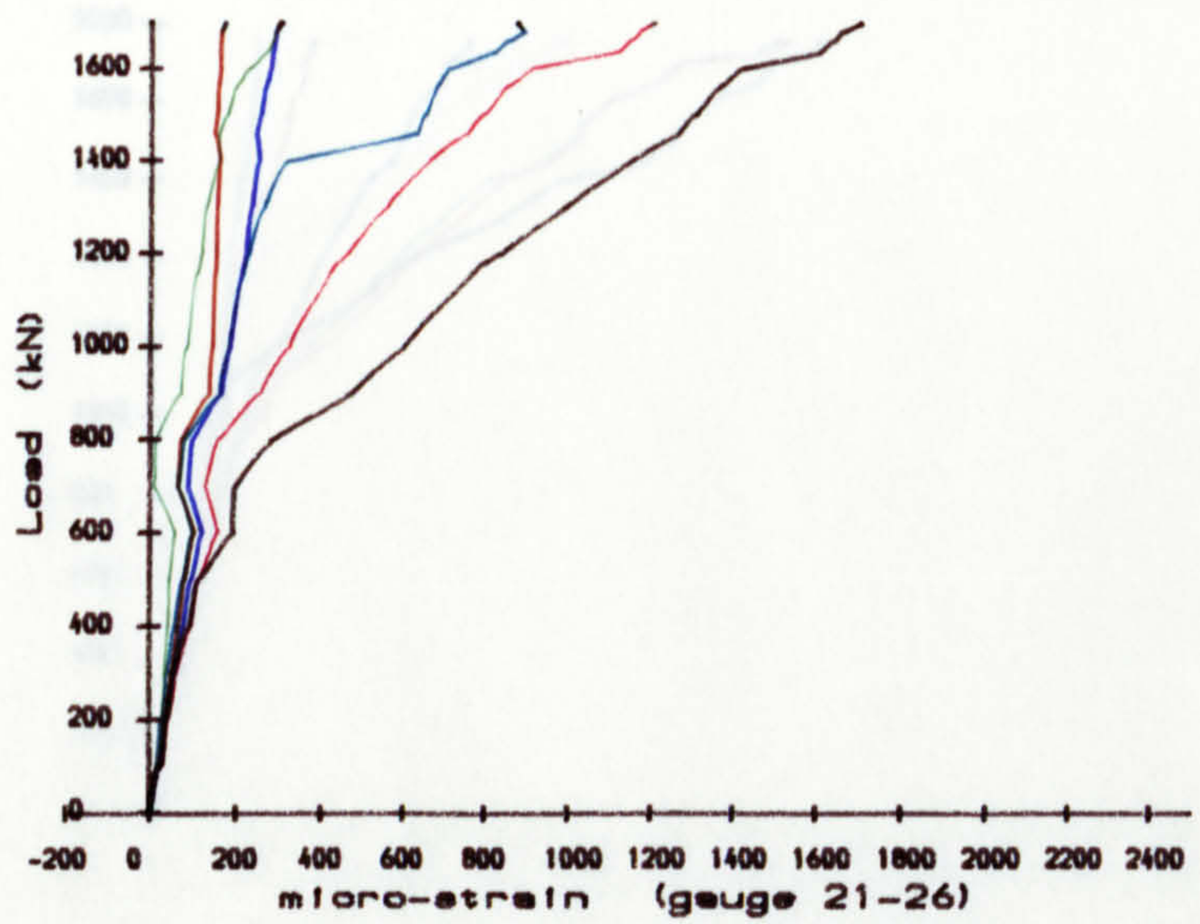

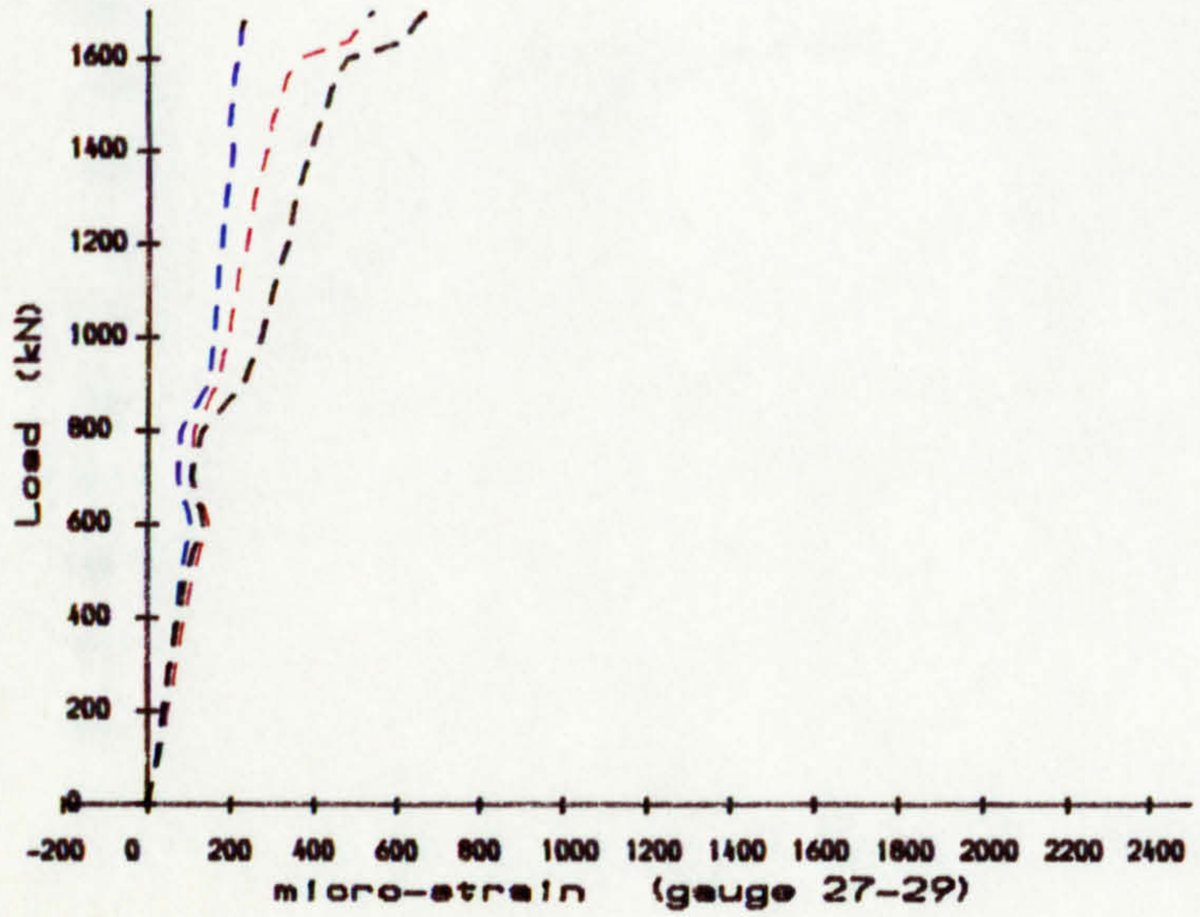

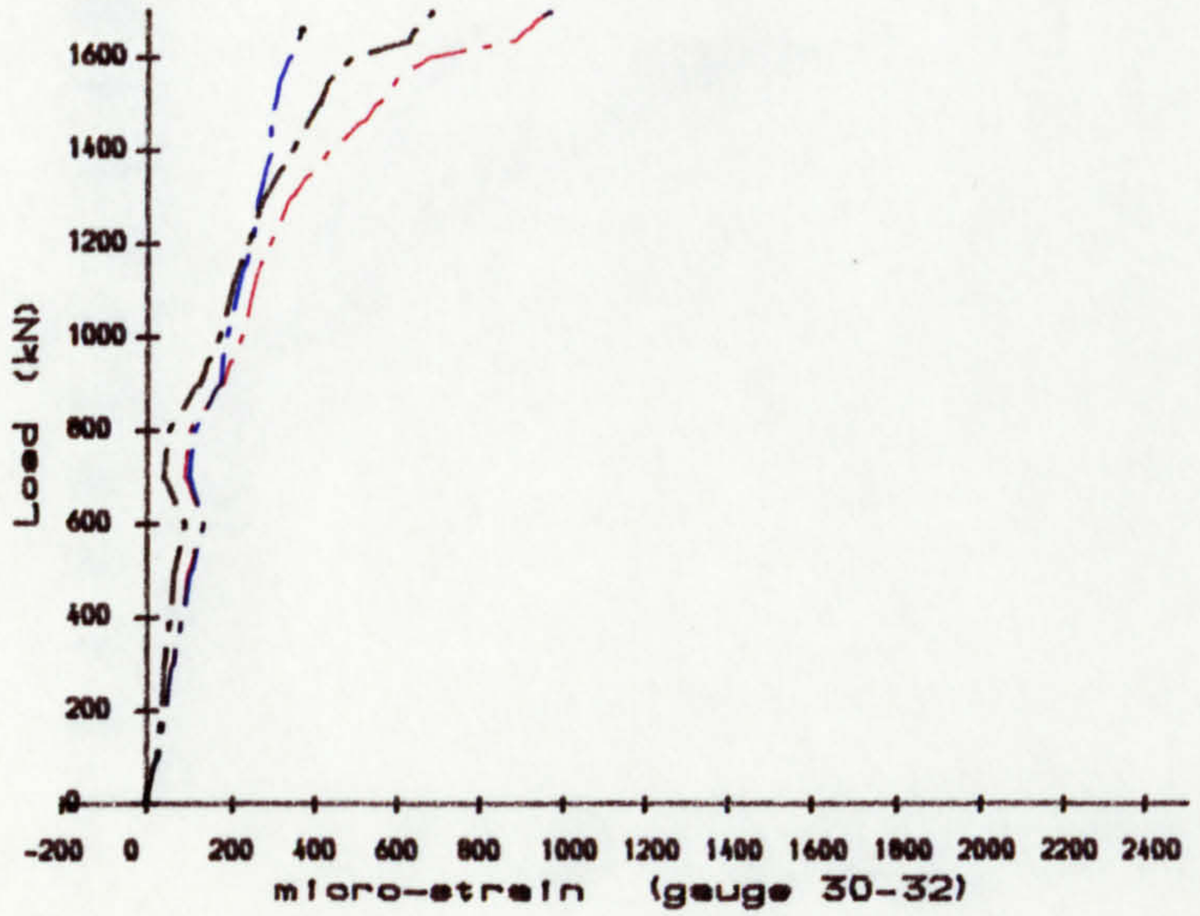

Fig. B. 26. Strain of bearing steel in beam DB3.

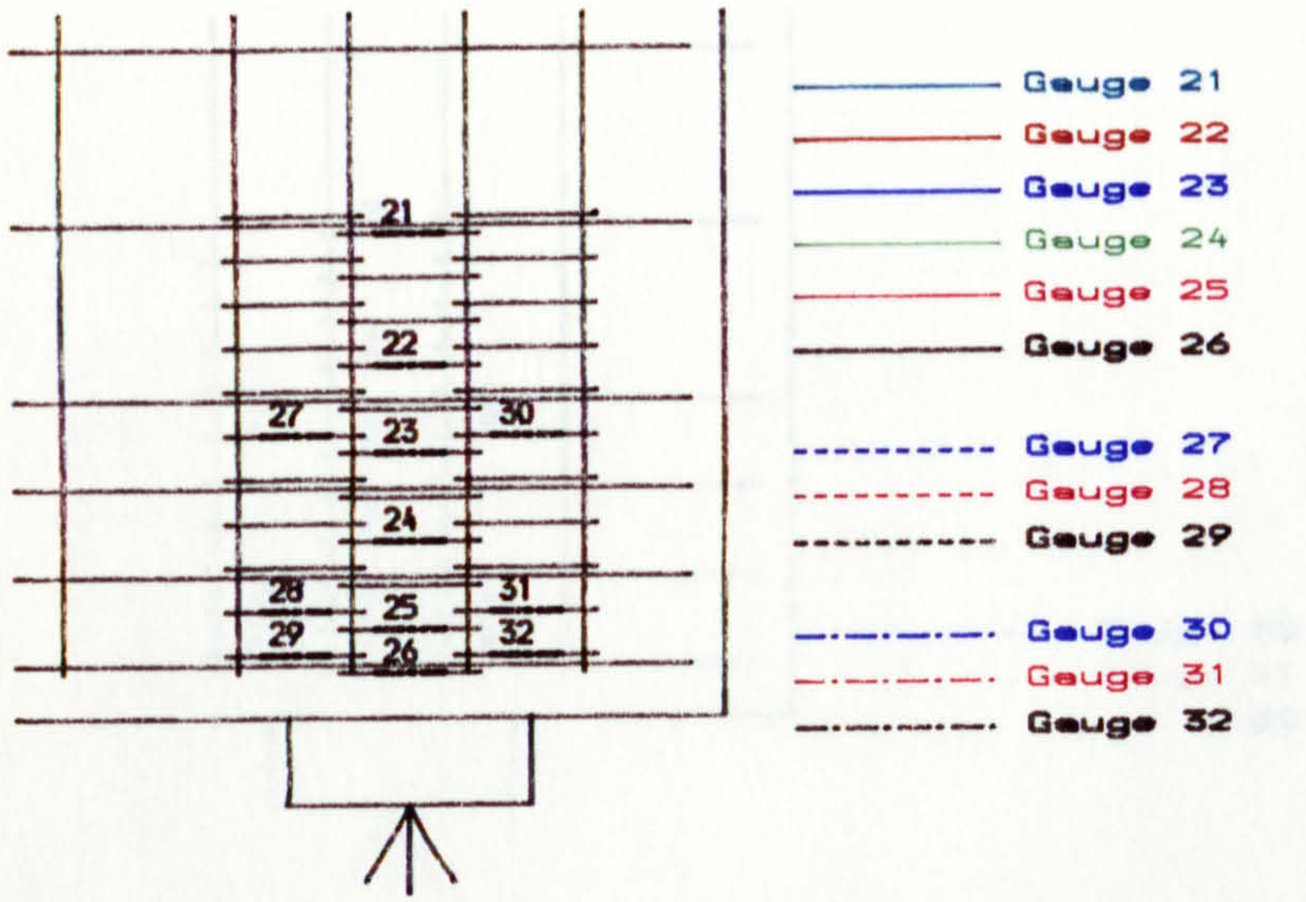

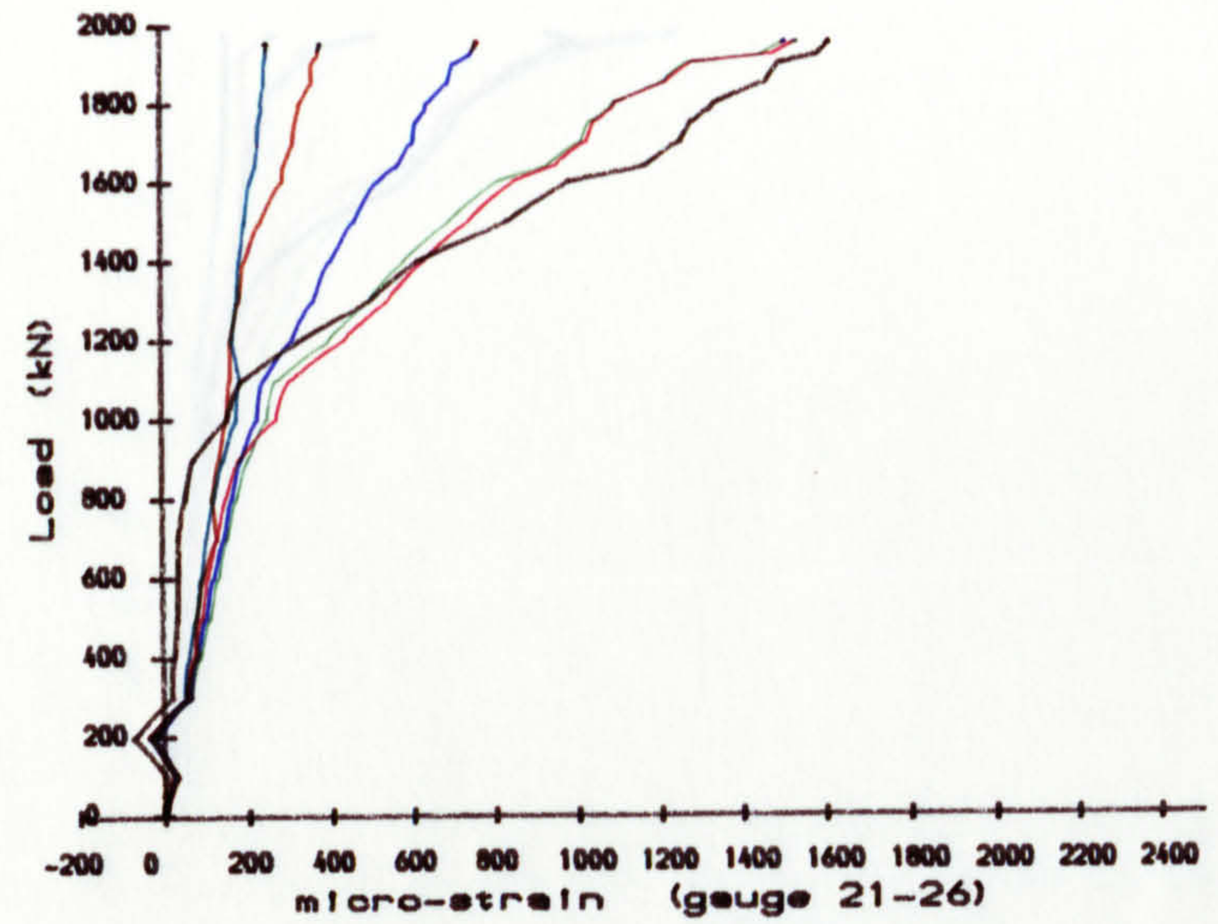

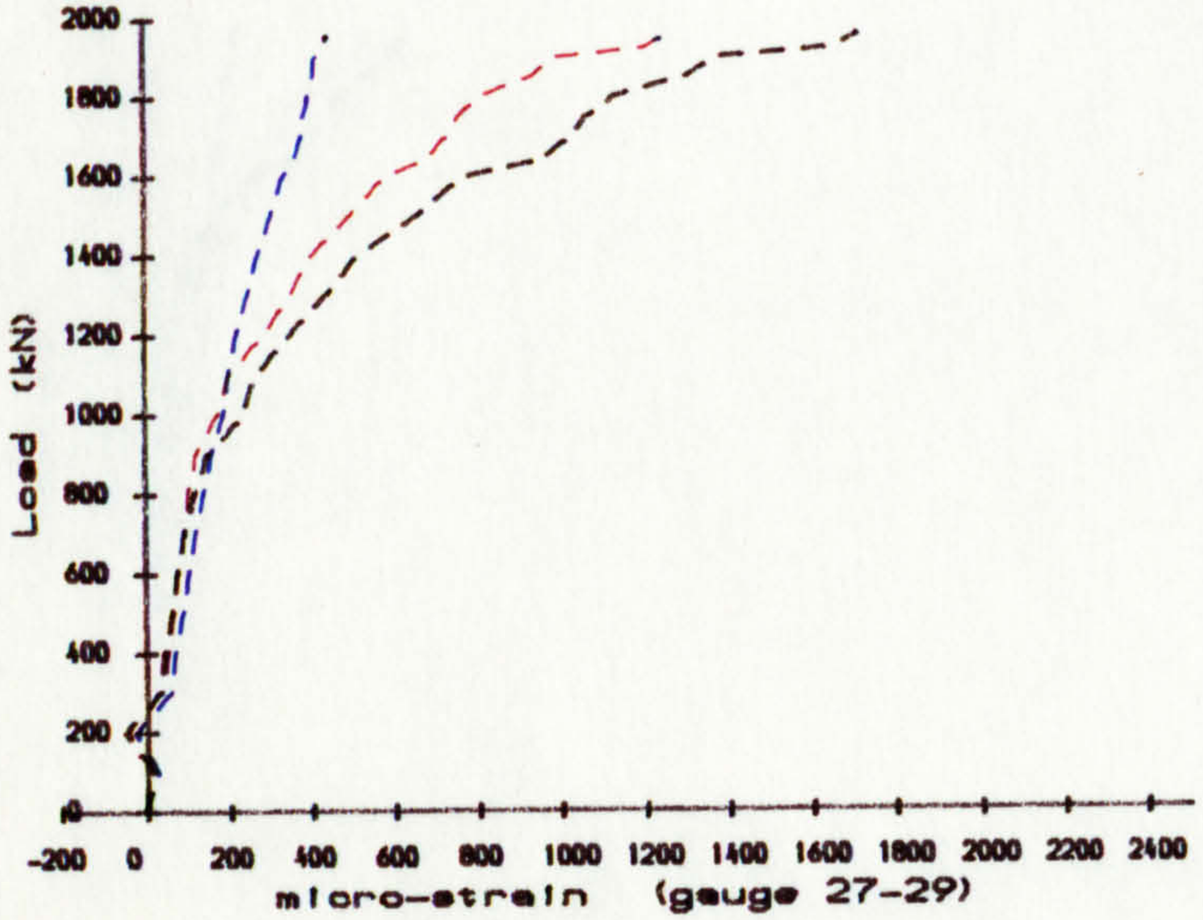

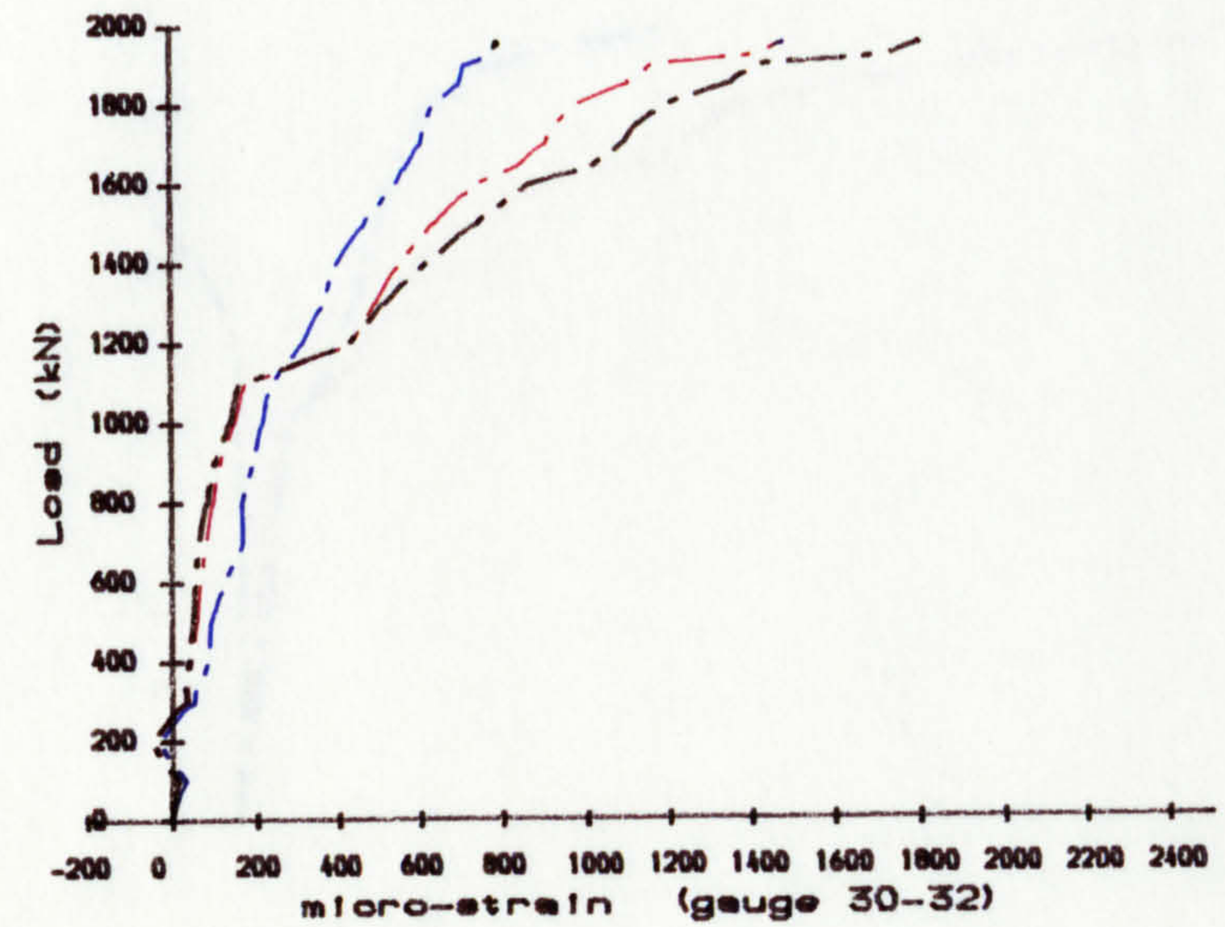

Fig. B. 27. Strain of bearing steel in beam DB4.

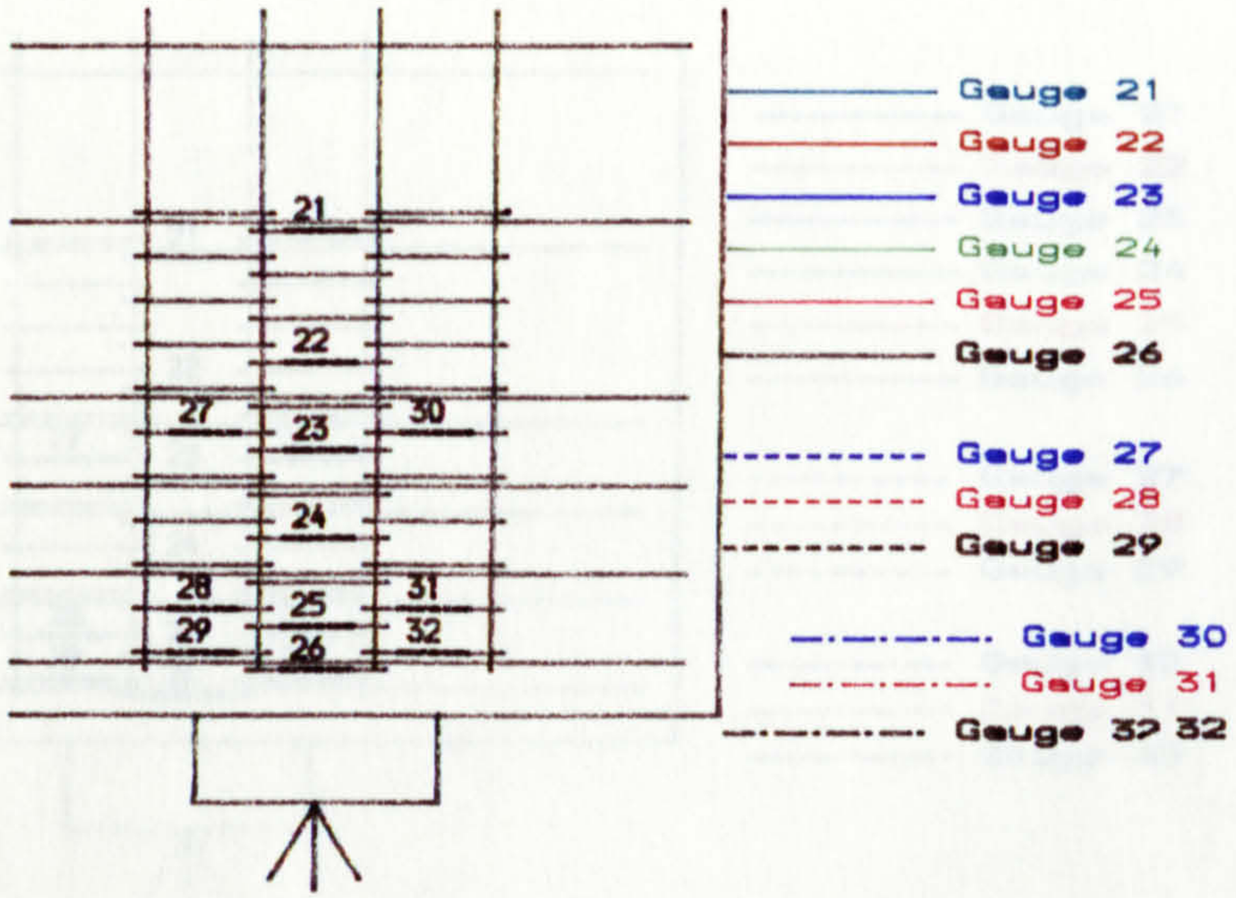

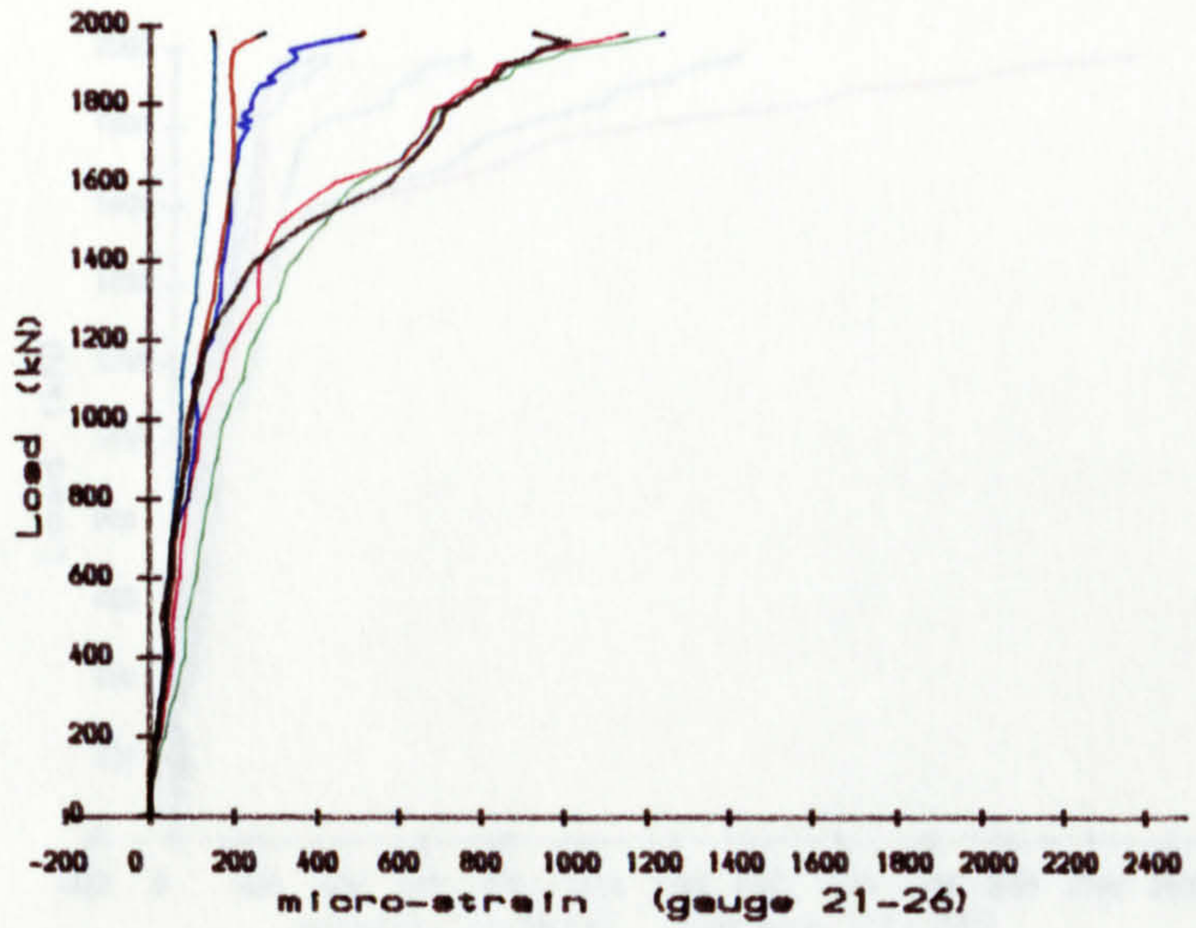

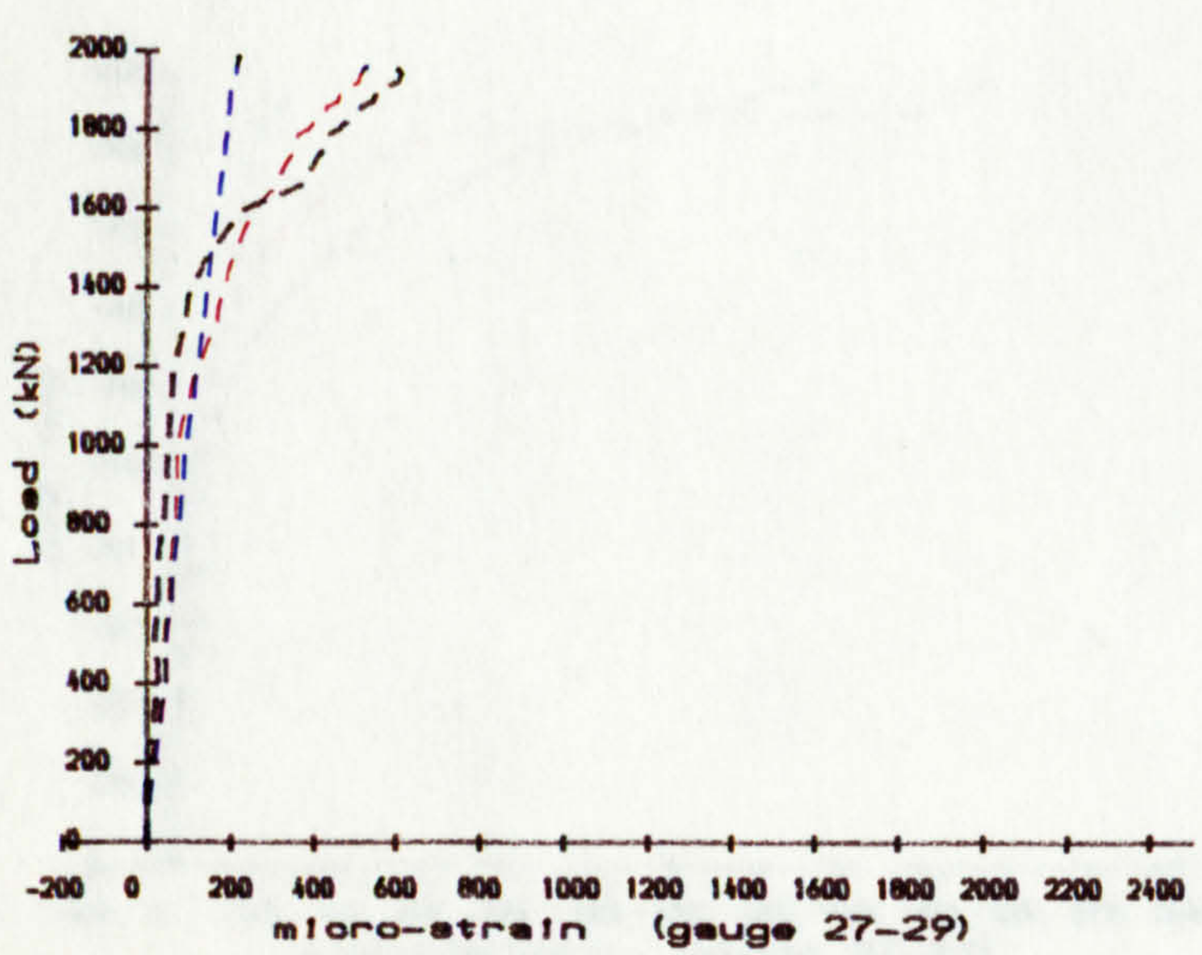

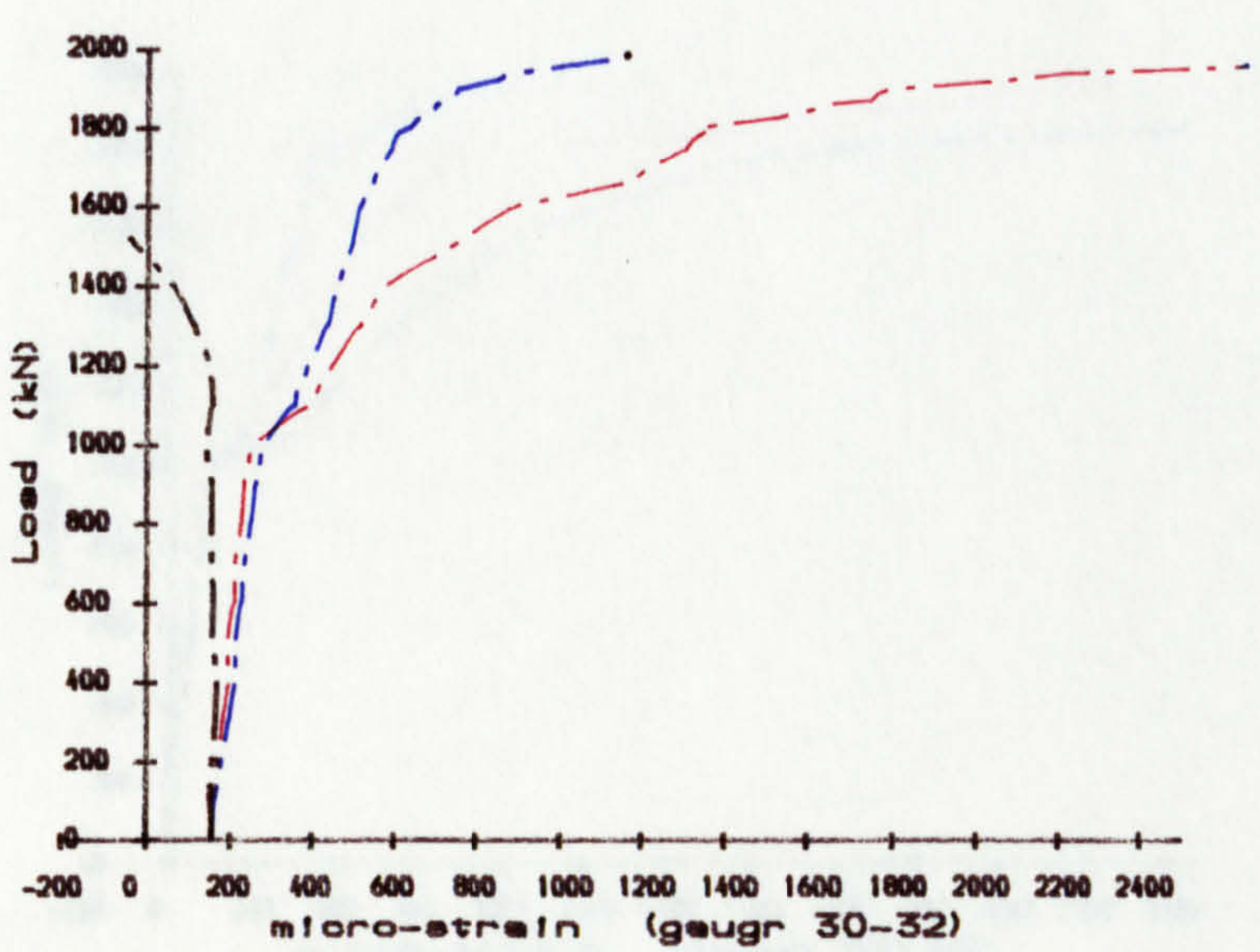

Fig. B. 28. Strain of bearing steel in beam DB5.

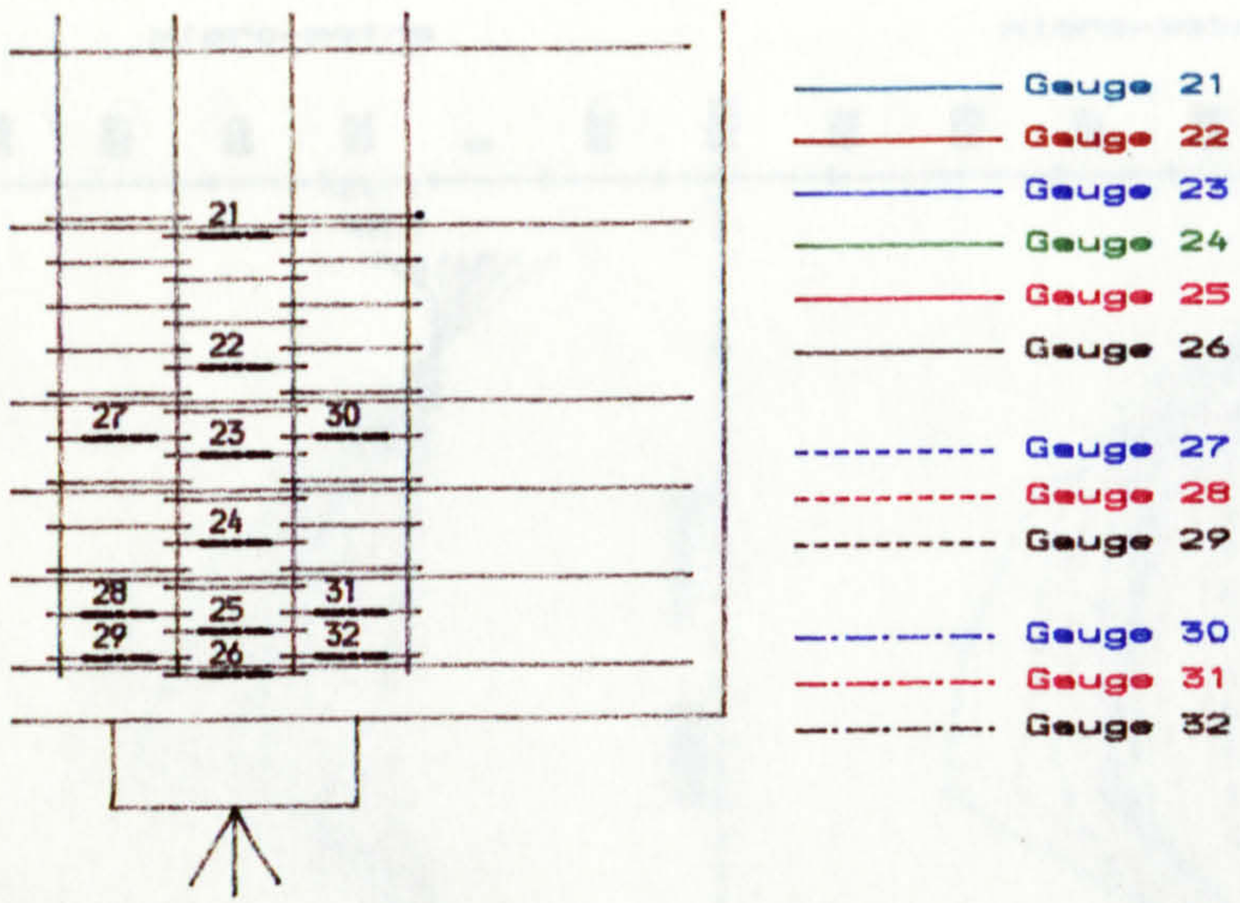

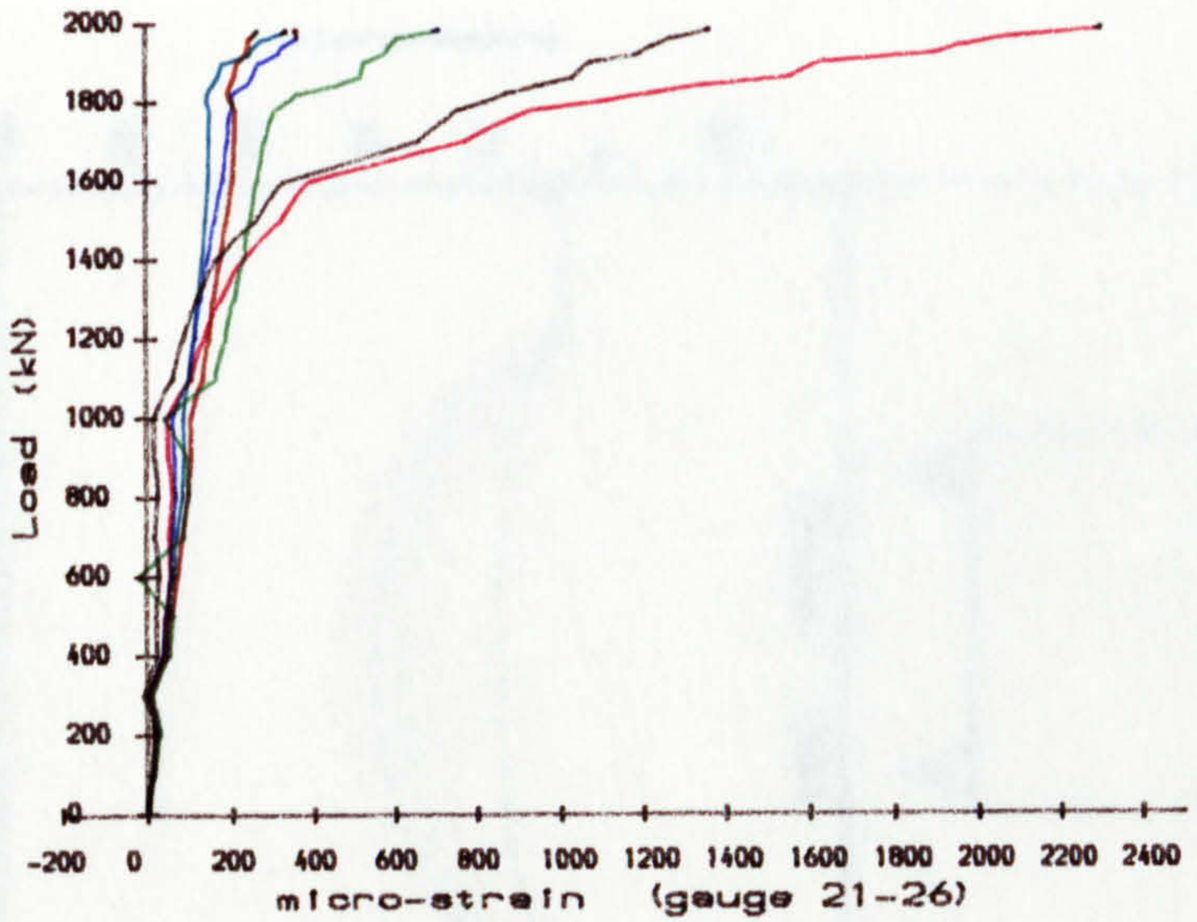

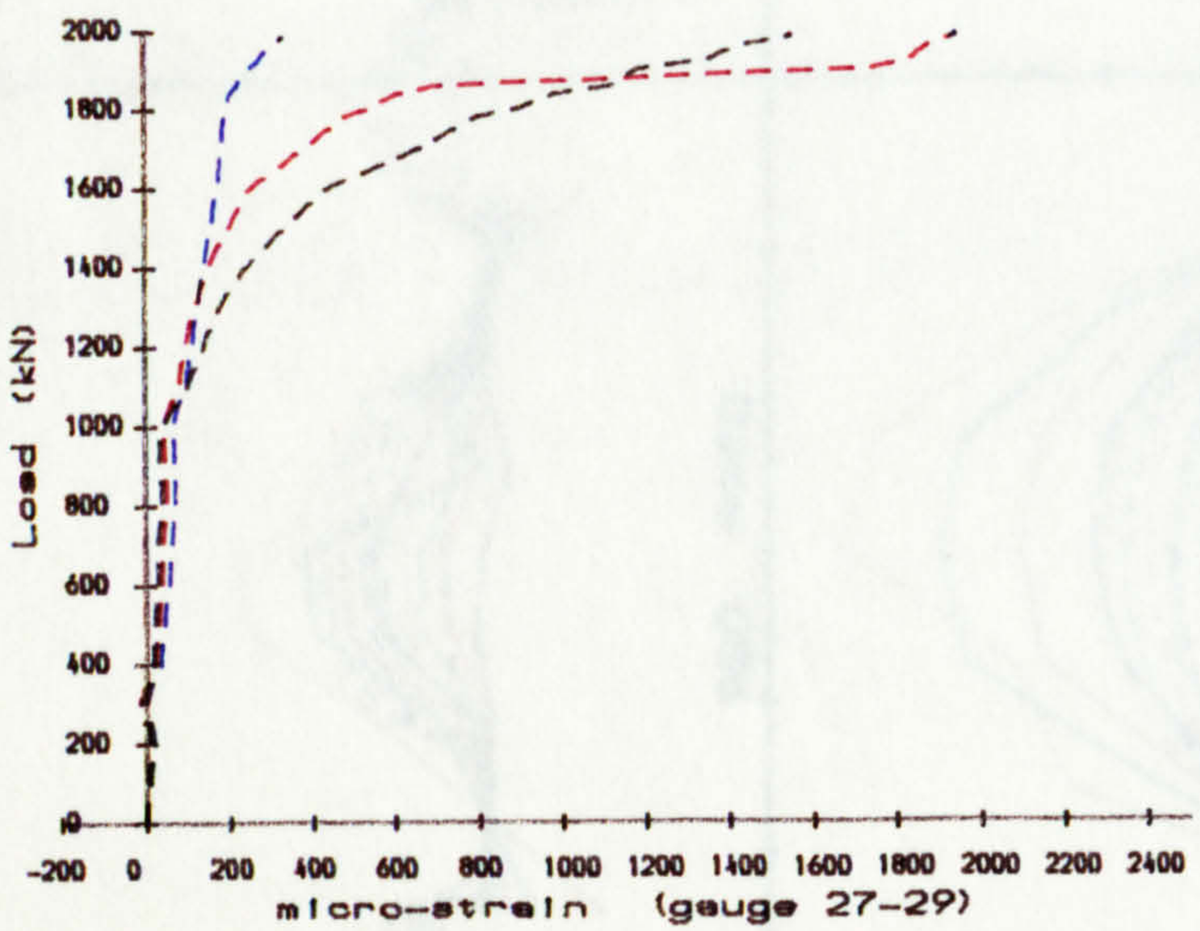

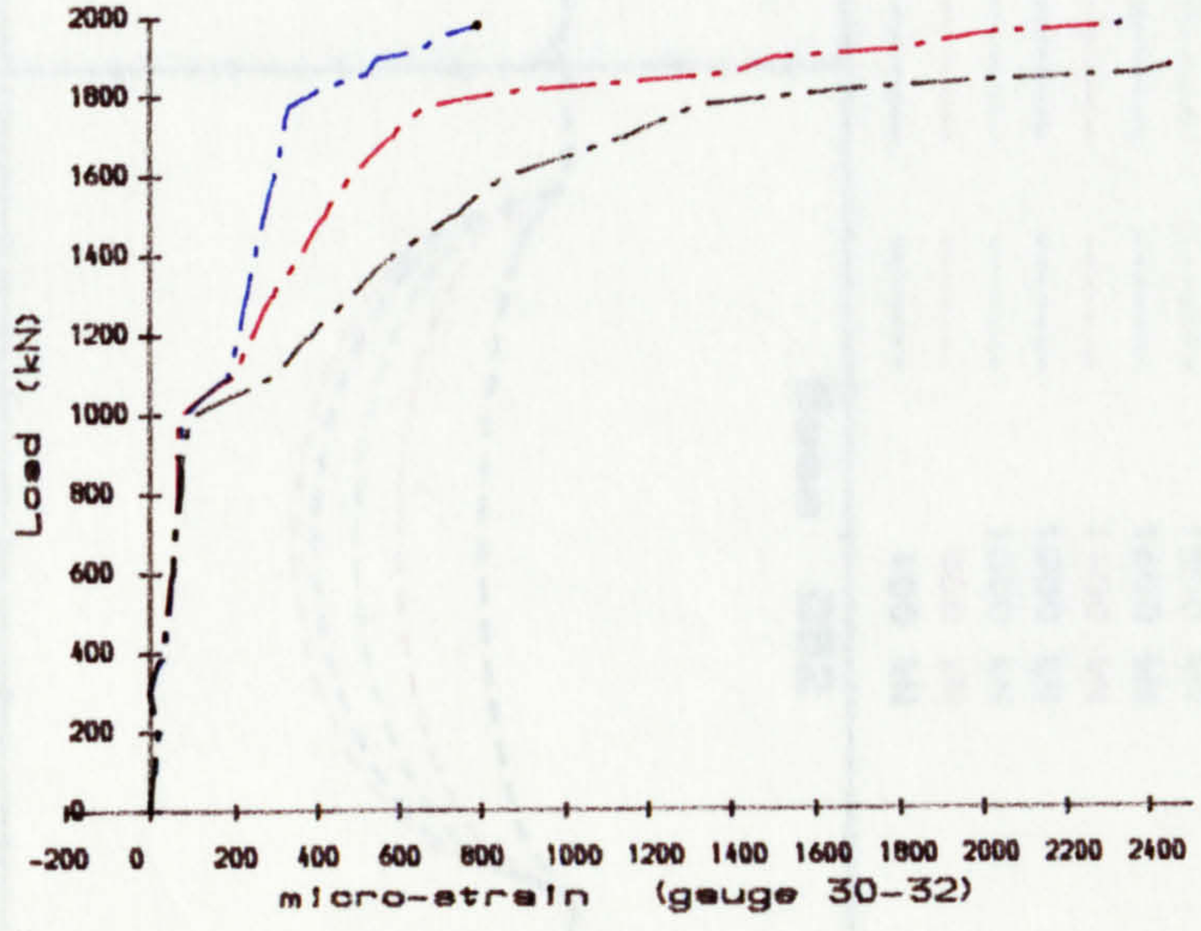

Fig. B. 29. Strain of bearing steel in beam DB6.

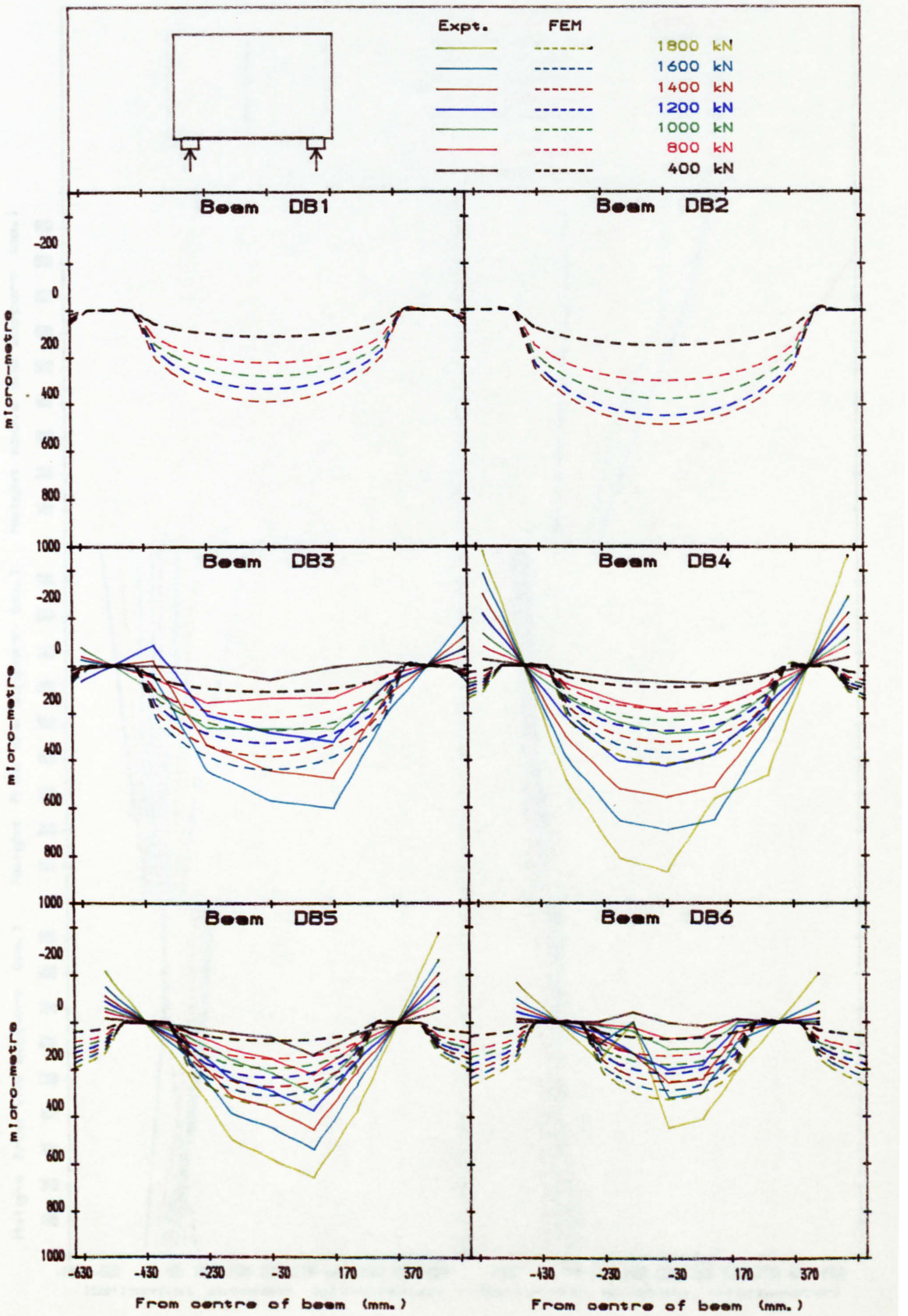

Fig. B. 30. Deflection of the beams.

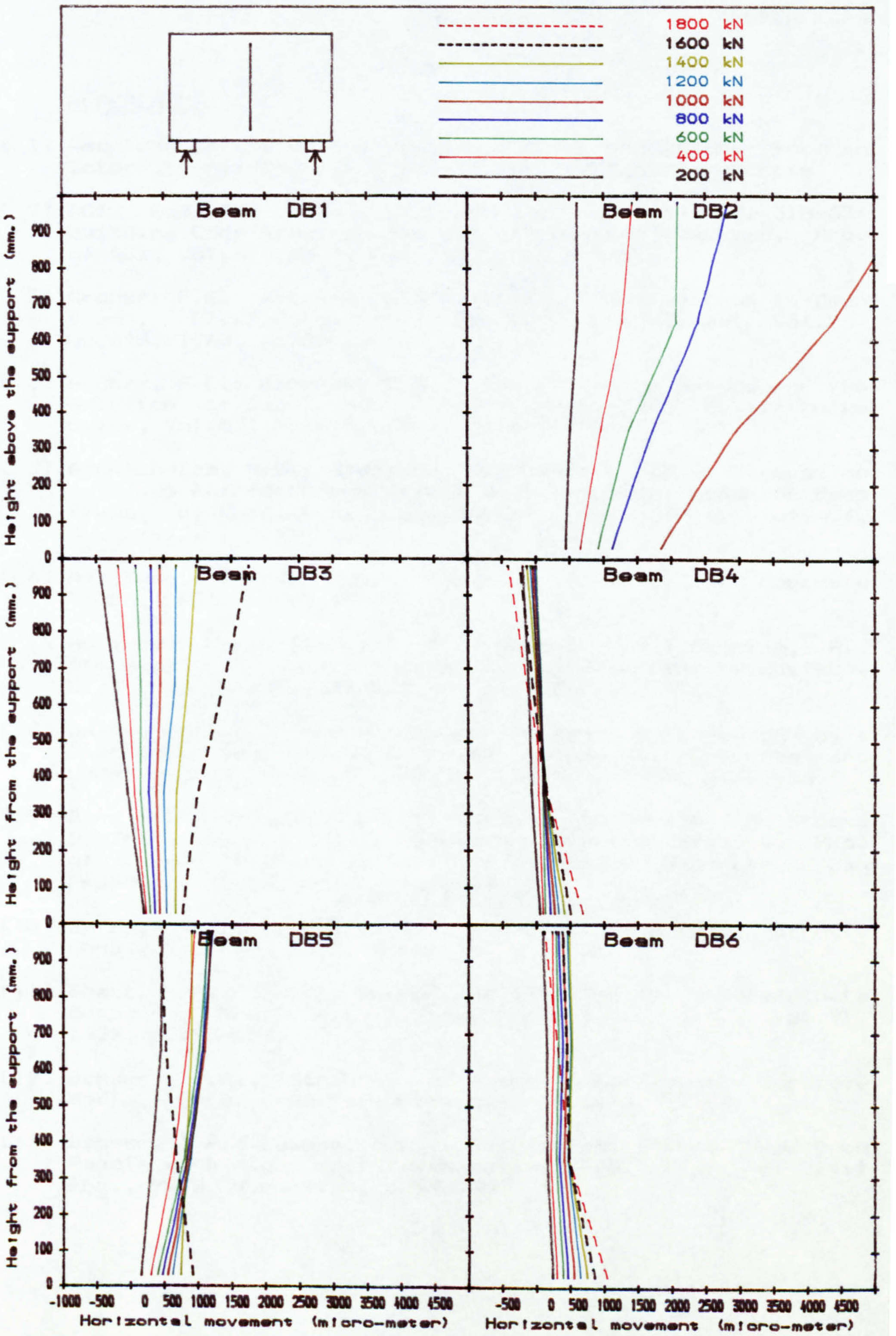

Fig. B. 31. Horizontal movement of the beam.

REFERENCES

[1] American Concrete Institution, 'Recommendations for an International Code of Practice for Reinforced Concrete'

[2] ACI Committe 318, 'Proposed Revision of ACI 318-63: Building Code Requirements for Reinforced Concrete,' Pro. of ACI, Vol.67, No.2, Feb. 1970, p.77-146.

[3] Archer, F.E.; Kitchen, E.M., 'Stress Distribution in Deep Beams,' Civil Engg. and Public Works Review, Vol.55, No.643, 1960, p.230-234.

[4] Archer, F.E.; Kitchen, E.M.; 'Strain Energy Method for the solution of Deep Beams,' Civil Engg. and Public Works Rview, Vol.52, No.618, 1957, p.1375-78.

[5] Arunachalam, N.V.; Aldridge, G.; Pandit, G.S., Discussion on 'Web Reinforcement Effect on Lightweight concrete Deep Beams, by Kong, F.K. and Robins, P.J.,' Pro. of ACI, Jan. 1972.

[6] Au Tung; Baird, D.L., 'Bearing Capacity of Concrete Block,' ACI, March 1960.

[7] Au Tung; Campbell-Allen, D; Plewes, W.G.; Maurice, R., Discussion of 'Bearing Capacity of Concrete by Shelson, W.,' Pro. of ACI, June 1958, p.1185-87.

[8] Baker, A.L.L., 'Shear Failure in Beams Represented by a Statically Indeterminate Truss Mechanism,' Concrete and Construction Engg., Vol.58, No.11, Nov. 1963, p.423-28

[9] Ban, S.; Muguruma, H.; Ogaki, Z., 'Anchorage Zone Stress Distributions in Post-tensioned Concrete Members,' Pro. of World Conference on Prestressed Concrete, San Francisco, July 1957, p.16/1-14.

[10] Barry, J.E.; Ainso, H., 'Single-Span Deep Beam,' Struct. Engg., Vol.109, No.3, March 1983.

[11] Bhatt, P., 'Deep Beams on Statically Indeterminate Supports,' Pro. ASCE, Engg. Mechanics Div., Vol.99, 1973, p.793-801.

[12] Besser, I.A., 'Strength of Slender Reinforced Concrete Walls,' Ph.D. thesis, University of Leeds, 1983.

[13] Besser, I.A.; Cusens, A.R., 'Reinforced Concrete Deep Beam Panels with high depth/span ratio,' Pro. Inst. of Civil Eng., Pt.2, June 1984, p265-278.

[14] BS 812 (1975) 'Method for Sampling and Testing of Mineral Aggregate, Sands and Fillers,' British Standard Institute, London.

[15] BS 1881 (1970) 'Method for Testing Concrete,' British Standard Institute, London.

[16] Caswell, J.S., 'Stresses in Short Beams,' Engineering, Vol.178, 1954, p.625-28 & p.656-58.

[17] Comite' Europe'en du Be'ton, 'International ecommendation for the Design and Construction of Concrete Structure,' Cement and Concrete Association, June 1970.

[18] Chow, L.; Conway, H.D.; Winter, G., 'Stresses in Deep Beams,' Trans. of ASCE, Vol.118, 1953, p.686-708.

[19] CP110 (1972) 'Code of Practice for the use of Concrete,' British Standard Institute.

[20] Deutsche Bauzeitung, 1906 Paper 263.

[21] Diaz de Cossio; Roger and Siess, C. P., 'Behavior and Strength in Shear of Beams and Frames without web reinforcement,' Pro. of ACI, Vol.56, No.8, Feb. 1960, p.695-735.

[22] Dischinger, F., 'Contribution to the Theory of the Half Plate and Wall-type Beams,' Int. Asso. for Bridge and Structural Eng., Zurich, Vol.1, 1932, p.69-93.

[23] Dulacska,H, 'Dowel Action of Reinforcement Crossing Cracks in Concrete,' Pro. of ACI, Dec. 1972, p.754-7.

[24] Fenwick, R.C.; Paulay, T., 'Mechanisms of Shear Resistance of Concrete Beams,' Pro. of ASCE, Struct. Div., Oct. 1968, p.2325-50.

[25] Geer, E., 'Stresses in Deep Beams,' Journal of ACI, Vol.31, No.7, 1960, p.651-61.

[26] Guyon, Y., 'Prestressed Concrete,' Contractors Record and Municipal Eng., 1953, p.127-74.

[27] Guyon, Y., 'Prestressed Concrete,' New York, John Wiley and Sons, 1955, Vol.1.

[28] Hawkins, N.M.; Ersoy, U., Discussion of 'Bearing Capacity of Concrete Block, by Au, T.; Baird, D.L.,' Proc. of ACI, Sept. 1960.

[29] Hawkins, N.M., 'The Behaviour and Design of End Blocks for Prestressed Concrete Beams,' Civil Eng. Transaction, Institute of Engineers, Australia, Vol.CE8, No.2, Oct. 1966, p.193-202.

[30] Hawkins, N.M., 'The Bearing Strength of Concrete Load through Rigid Plates,' Magazine of Concrete Research, March 1968.

[31] Hawkins, N.M., 'The Bearing Strength of Concrete Loaded through Flexible Plates,' Magazine of Concrete Reseach, June 1968.

[32] Hawkins, N.M., 'The Bearing Strength of Concrete for Strip Loadings,' Magazine of Concrete Research, June 1970.

[33] Hofbeck, F.A.; Ibrahim, I.O.; Mattock, A.H., 'Shear Transfer in Reinforced Concrete,' Pro. of ACI, Feb. 1969, p.119-128.

[34] Holmes, M.; Mason, P.M., 'Stress in Deep Beams,' Building Science, Vol.7, 1972, p.225-232.

[35] Houde, J.; Mirza, M.S., 'A Finite Element Analysis of Shear Strength of Reinforced Concrete Beams,' Shear in Reinforced Concrete, ACI SP42-5, Vol.1, p.103-28.

[36] Jensen, B.C., 'Some Applications of Plastic Analysis to Plain and Reinforced Concrete,' Institute of Buliding Design, Technical University of Denmark, Lyngby, Report 103, July 1977, p.119.

[37] Kaar, P.H., 'Stresses in Centrally Loaded Deep Beams,' Pro. Soc. for Experimental Stress Analysis, Vol.13, No.1, 1957, p.77-84.

[38] Kaar, P.H., 'Stresses in Centrally Loaded Deep Beams,' Portland Cement Asso., Vol.XV, No.1, Chicoga III.

[39] Kong, F.K., 'Deep Beams with Inclined Web Reinforcement,' Pro. of ACI, March 1972, p.172-176.

[40] Kong, F.K., 'Shear Analysis and Design of Reinforced Concrete Deep Beams,' Struct. Engr., Oct. 1972, p.405-409.

[41] Kong, F.K.; Kubik, L.A., Discussion of 'Collapse Load of Deep Reinforced Concrete Beams, by Kumar,' Magazine of Concrete Research, Vol.29, 1977, p.42.

[42] Kong, F.K.; Robins, P.J., 'Web Reinforcement Effect on Lightweight Concrete Deep Beams,' Pro. of ACI, July 1971, p.514-20.

[43] Kong, F.K.; Robins, P.J., 'Modified Finite Method Applied to Reinforced Concrete Deep Beams,' Civil Engg. and Public Works Review, Nov. 1973. p.963-66.

[44] Kong, F.K.; Robins, P.J.; Cole, D.F., 'Web Reinforcement Effect on Deep Beams,' Pro. of ACI, Dec. 1970, p.1010-17.

[45] Kong, F.K.; Robins, P.J.; Sharp, G.R., 'The Design of Reinforced Concrete Deep Beam,' Struct. Eng ., Vol.53, No.4, April 1975, p.173-180.

[46] Kong, F.K.; Sharp, G.R., 'Shear Strength of Lightweight Reinforced Concrete Deep Beams with Web Openings,' Struct. Engr., Aug. 1973, p.267-275.

[47] Kong, F.K.; Singh, A., 'Diagonal Cracking and Ultimate Loads of Lightweight Consrete Deep Beams,' Proc. of ACI, Aug. 1972, p.513-21.

[48] Kong, F.K.; Singh, A., 'Shear Strength of Lightweight Concrete Deep Beams subjected to Repeated Load,' Shear in Reinforced Concrete, ACI, SP.42, Vol.2, p.461.

[49] Kriz, L.B.; Raths, C.H., 'Connections in Precast Structures — Bearing Strength of Column Heads,' PCI Journal, Dec. 1963.

[50] Kumar, P., 'Collapse Load of Deep Reinforced Concrete Beams,' Magazine of Concrete Research, Vol.28, March 1976.

[51] Laupa, A; Siess, C.P.; Newmark, N.M., ' Shear Strength of Reinforced Concrete Beams,' Bulletin of the Expt. Station, No.428, University of Illinois, Urbana, March 1959.

[52] Lenschow, R.J.; Sozen, M.A., 'Practical Analysis of the Anchorage Zone Problem in Prestressed Beams,' Pro. of ACI, Nov, 1965, p.1421-39.

[53] Leonhardt, F., ' Report on Test on Deep Beams with Different Load and Suport Conditions and Reinforcement Arrangement including conclusion,' German Reinft. Concrete Comission, Tchnical University of Stuttgart, English Translation Version, p.26-71 and p.115-157.

[54] Leonhardt, F., Discussion on 'Strength and Behavior of Deep Beams in Shear,' Pro. of ASCE, Struct. Div., April 1966.

[55] Magnel, G., 'Design of the Ends of Prestressed Concrete,' Concrete and Constructional Eng., Vol.44, No.5, May 1949, p.141-8.

[56] Magnel, G., 'Prestressed Concrete,' McGraw Hill Books Co., Inc. New York, 3rd Edition, 1954.

[57] Mattock, A.H., 'Shear Transfer in Concrete having Reinforcement at an angle to the Shear Plane,' Shear in Reinforced Concrete, ACI SP42, p.17.

[58] Mattock, A.H.; Hawkins, N.M., 'Shear Transfer in Reinforced Concrete — Recent Research,' Journal of Prestressed Concrete Inst., Vol.17, No.2, March/April 1972, p.55-75.

[59] Meyerhof, G.G., 'The Bearing Capacity of Concrete and Rock,' Magazine of Concrete Research, April 1953.

[60] Millard, S.G.; Johnson, R.P., 'Shear Transfer across Cracks in Reinforced Concrete due to Aggregate Interlock and Dowel Action,' Magazine of Concrete Research, March 1984, p.9-21.

[61] Millard, S.G.; Johnson, R.P., 'Shear Transfer in cracked Reinforced Concrete,' Magazine of Concrete Research, Vol.37, No.130, March 1985.

[62] Muguruma, H.; Okamoto, S., 'Study on Bearing Capacity of Concrete,' The 8th Japan Congress on Testing Materials, Non-metallic Materials.

[63] Najjim-Al, A.G., 'Post Cracking Behaviour of Reinforced Concrete Deep Beams,' Ph.D. thesis, Central London Polytechnic, 1981.

[64] Nielsen, M.P., 'On the Strength of Reinforced Concrete Disc, Acta Polytechnica Scandinavica,' Civil Engg. and Building Construction Series, NO.70, Copenhagen, 1971, p.261.

[65] Niyogi, S.K., 'Bearing Strength of Concrete — Geometric Variations,' ASCE-Struct., July 1973.

[66] Niyogi, S.K., 'Concrete Bearing Strength — Support, Mix, Size Effect,' ASCE-Struct., August 1974.

[67] Niyogi, S.K., 'Bearing Strength of Reinforced Concrete Blocks,' ASCE-Struct., May 1975.

[68] Ove Arup and Partners, 'The Design of Deep Beam in Reinforced Concrete,' CIRIA Publication, Jan. 1977.

[69] Paiva, H.A.R.; Siess, C.P., 'Strength and Behavior of Deep Beams in Shear,' Pro. of ASCE, Struct. Div., Vol.91, ST5, Oct 1965, p.19-41.

[70] Paulay, T.; Loeber, P.T., 'Shear Transfer by Aggregate Interlock in Reinforced Concrete,' Shear in Reinforced Concrete, ACI SP42-1, Vol.1, p.1-15.

[71] Paulay, T.; Park, R.; Phillips, M.H., 'Horizontal Construction Joints in cast-in-plane Reinforced Concrete,' Shear in Reinforced Concrete, ACI SP42, Vol.2, p.599-616.

[72] Portland Cemenet Association, 'Design of Deep Girders,' Concrete Information Structural Bureau, Pamphlet No.ST66, Chicago III.

[73] Ramakrishnan, V.; Ananthanarayana, Y., 'Ultimate Strength of Deep Beams in Shear,' Pro. of ACI, Vol.65, No.2, Feb. 1968, p.87-98.

[74] Saad, S.; Hendry, A.W., 'Stresses in Deep Beams with a Central Concentrated Load,' Expt. Mech., Vol.1, 1961, p.192-98.

[75] Saad, S; Hendry, A.W., 'Gravitational Stresses in Deep Beams,' Struct. Engr., Jun 1961, p.185-194.

[76] Selson, W., 'Bearing Capacity of Concrete,' Proc. of ACI, Nov. 1957.

[77] Smith, K.N.; Vantsiotis, A.S., ' Shear Strength of Deep Beams,' Proc. of ACI, No.3, 1982, p.201-213.

[78] Swamy, R.N.; Andriopoulos, A.D., 'Contribution of Aggregate Interlock and Dowel Forces to the Shear Resistance of Reinforced Beams with Web Reinforcement,' Shear in Reinforced Concrete, ACI SP42, p129.

[79] Taylor, H.P.J., 'Investigation of the Forces Carried Across in Reinforced Concrete Beams by Interlock of Aggregate,' Cement and Concrete Ass., Technical Report 42.447, London, 1970, p.22.

[80] Uhlman, .L., 'The Theory of Girder walls with Special Reference to Reinforced Concrete Design,' Struct. Engr., Vol.XXX, No.8, April 1952, p.172-181.

[81] Zielinski, J.; Rowe, R.E., 'An investigation of the Stress Distribution in the Anchorage Zones of the Post-tensioned Concrete Members,' Research Report No.9, Cement and Concrete Association, Sept. 1960.

[82] Zielinski, J.; Rowe, R.E., 'The Stress Distribution Associated with Groups of Anchorages in Post-tensioned Concrete Members,' Research Report No.13, Cement and Concrete Association, Oct. 1962.